UNIMOLECULAR REACTION DYNAMICS OF LARGE POLYATOMIC MOLECULES

BY

THOMAS DAN SEWELL

Bachelor of Science

Hardin-Simmons University

Abilene, Texas

1986

Submitted to the Faculty of the
Graduate College of the
Oklahoma State University
in partial fulfillment of
the requirements for
the Degree of
DOCTOR OF PHILOSOPHY
December, 1991

UNIMOLECULAR REACTION DYNAMICS OF

LARGE POLYATOMIC MOLECULES

Thesis Approved:

Donald L. Thompson

Thesis Adviser

Lionel M. Raff

J. Paul Devlin

Paul W. Harland

Ben J. Anderson

Thomas C. Collins

Dean of the Graduate College

PREFACE

The work contained in this dissertation addresses a number of problems of current interest in the field of chemical dynamics. The topics are principally dealt with using classical trajectory techniques (with semiclassical overlays in some cases), and Monte Carlo transition-state theory. Our goal was to at least partially answer the following questions:

1. Can we predict the presence or absence of statistical behavior in polyatomic molecules and, in either case, explain why?
2. To what degree can we model the detailed, full-dimensional unimolecular reaction dynamics of large molecules (where "large" refers to molecules of up to twenty-one atoms)?
3. Are the vibrational dynamics of highly excited polyatomic molecules really chaotic (as has often been asserted)?
4. Can the "zero-point energy problem" in classical trajectory calculations be "corrected"?
5. Is there any possibility of observing mode specificity in the tunneling splitting associated with symmetric double-well molecules?

In the following pages we describe work we have performed over the past four-and-a-half years and attempt to relate it to other studies (both experimental and theoretical) in the literature. Finally, some problems that are worthy of attention are outlined in the CONCLUSIONS chapter.

There are a number of people that are deserving of thanks for their support while I've been riding this chaotic trajectory through graduate school. First and foremost

among these are my wife, Susie, and our two children, Jamie and Bryson. Their companionship and love made the good times even better and the not-so-good times at least bearable. They provide me with the greatest things in life, without which there would be no purpose: unquestioning love, caring affection, support and, of course, someone with whom to play "horsey" and "hold-me-upside-down-and-tickle-me monster!"

My parents, Phyllis and Holt Sewell, have made an enormous contribution over the years and I don't know of any way to thank them sufficiently for all they have done. I have been in school continuously now for some twenty-four years. Yet, when I stop and think about what I've learned, I cannot help but conclude that the most important things were learned by watching the examples provided by them. They gave me a practical course in living Life! Although it cannot compare with all that they have done for me, I dedicate this Dissertation to them.

My research adviser, Professor Donald L. Thompson, has provided me with guidance, advice, and support. If I've learned a tenth of what he taught, I should be pleased. His approach to advising, that is, to make the student think matters through without interference, has sometimes been difficult; but it has hopefully made a scientist out of me and, as my time under his tutelage comes to an end, I am grateful to have had the opportunity to study under him.

Thanks are also due the members of my examining committee: Professors Raff, Westhaus, Ackerson, and Devlin. In particular, I consider myself luck to have had the privilege of attending courses presided over by Drs. Raff, Westhaus, and Devlin; and the interactions between myself and the committee were, without exception, positive and (somewhat to my surprise!) enjoyable experiences.

I made a number of friends while pursuing my degree at OSU. There are too many to list them all. However, it is only fitting that I record the names of some of them

since they contributed (each in his or her own way), either directly or indirectly, to the successful completion of this work. Whether it was haggling (shouting, in some cases!) over some detail of a scientific problem that one of was was working on or enjoying a lunch at Mexico Joe's, I am thankful to have known and worked with Eric Wallis, Karen Bintz, Harry Schranz, Qin Yue, Huadong Gai, Dave Sahm, Jim Peploski, Alison Marks, Candee Chambers, Jeff Fuson, and Mel Zandler.

Certain individuals at the OSU computer center are also deserving of explicit acknowledgement: Konrad Brandemuhl, Dan Carlile, Lorraine Goff, and Terry Klarich. They helped me in a variety of ways and I am thankful. Also, the computer center granted me essentially free reign over the RS/6000 and DEC 5500 workstations that were at OSU for several months. This computer time made an indispensable contribution towards the completion of the work that is described in this Dissertation.

Financial support during my graduate career at OSU came primarily from the Army Research Office. Other support was provided by the Air Force Office of Scientific Research and Conoco, Inc.

TABLE OF CONTENTS

Chapter Page

Chapter Page

LIST OF TABLES

LIST OF FIGURES

CHAPTER I

INTRODUCTION

Chemical dynamics is the general area of study concerned with elucidating the microscopic details of processes occurring within and between molecules and, ultimately, explaining macroscopic chemistry in terms of these fundamental chemical and physical interactions. Experimentalists are continuously devising new techniques that allow them to make increasingly detailed inquiries into the spectroscopy and dynamics of highly excited chemical species,[1-4] and recent years have seen substantial advances in our theoretical understanding of several fundamental chemical processes.[5-8] The current level of agreement between experiment and theory in some areas of chemical dynamics suggests that, for these particular areas, the goal of chemical dynamics studies given in the opening sentence has been effectively realized.

A case in point is provided by experimental and theoretical studies of reactive scattering in the H_3 system (and isotopomers).[9-12] Sophisticated experiments have yielded product-state distributions for state-resolved reactants,[9-11] and the results of recent quantum scattering calculations in three dimensions are in excellent agreement with the experiments.[12] The completeness of the theory for reactive scattering in H_3 is such that experimentalists and theorists are pushing each other to provide more and more detailed information and are doing so on nearly equal footing. This is not to imply, however, that the problem is solved -- quantum scattering calculations are as yet restricted to considering only a few initial states (e.g., the $v = 0$, 1, and (perhaps) 2 vibrational states; and low rotational states). Increasing the number of channels quickly makes the problem computationally intractable.

Classical Trajectory Calculations

The fact that high-level quantum scattering calculations can only be performed for a very limited class of problems underscores a more general problem with approaching chemical dynamics from the full-blown quantum mechanical point of view. As the complexity of the problem increases, the work required to obtain the solution rapidly increases, eventually eclipsing the knowledge that can be gained. Of course, the benchmark quantum calculations are very important in that they allow us to evaluate whether or not the underlying theory is correct and could therefore be used, in principle, to solve other problems "exactly."

Since quantum mechanical solutions to most problems are excruciatingly difficult (or impossible) to obtain, recourse is usually made to approximate methods that, if chosen judiciously, yield "satisfactory" results. These methods most often correspond to making simplifying assumptions that render the problem solvable quantum mechanically (e.g., neglect[13-17] or restricted treatment[18-23] of "unimportant" degrees of freedom), or to employ semiclassical[24-32] or classical[33-36] techniques in *lieu* of quantum mechanical ones. Of these three possibilities, the most widely chosen one is classical mechanics.

The classical trajectory method assumes the validity of the Born-Oppenheimer approximation[37] and treats all nuclei as classical particles interacting under the influence of forces due to the electronic attraction/repulsion at a given nuclear configuration. The method is expected to work particularly well in cases where quantum effects such as tunneling,[38-40] nonadiabatic transitions,[41-42] and flow of zero-point energy[43-47] are minimized or can be accounted for (e.g., through some semiclassical "overlay" or *post facto* use of a correction factor). In favorable circumstances, classical trajectories can be expected to yield results in reasonable accord with experiments.[48-51] Additionally, if a suitably accurate representation of the potential-energy surface is available, classical

trajectory calculations can provide results that are unavailable experimentally or help illuminate ambiguous experimental results.

Calculation of classical trajectories is a fairly straightforward procedure. In the simplest implementation, a classical trajectory calculation can be broken down into roughly four parts: construction of the potential-energy surface, selection of initial conditions from which to initiate trajectories, numerical solution of the classical equations of motion, and analysis of the results.[33-36] A discussion of each of these components is given (within the framework of the studies that comprise this Dissertation) in Chapter II.

Difficulties associated with the construction of suitable potential-energy surfaces aside, the major impediment to classical trajectory studies (of large systems) is the significant investment of computer time required for the calculation of ensembles of trajectories. Trajectories provide a sort of "brute force" approach to solving a problem. However, with recent advances in computer technology and drastic reductions in the cost per CPU cycle, trajectory methods have become more and more attractive to theorists. Calculations are now routinely done on the dynamics of biomolecules,[52] liquids,[53] and solids[54-55].

Description of the Dissertation Problems

In the following Chapters, work that we have done over the past five years is summarized.[56-62] The primary thrust of the work is directed towards gaining a greater understanding of the detailed dynamics (both reactive and nonreactive) of "large" polyatomic systems containing between five and twenty-one atoms.[56-60] In addition, some calculations on model two degree-of-freedom systems were performed in an effort to address specific aspects of the dynamics of semiclassical treatments of tunneling processes[61] and zero-point energy flow[62] in classical calculations.

Unimolecular Decomposition of 2-chloroethyl Radical

A problem of long-standing interest in chemical dynamics is that of trying to understand why some systems behave statistically while others do not.[4,45,56-57,59-60,62-177] (By "statistical system" we mean one that exhibits reaction rates in accordance with the predictions of classical phase-space theory[178-179] or RRKM theory[180-181].) The problem of nonstatistical behavior is addressed directly in Chapters IV and V where calculations treating the unimolecular dissociation dynamics of 2-chloroethyl radical are described.

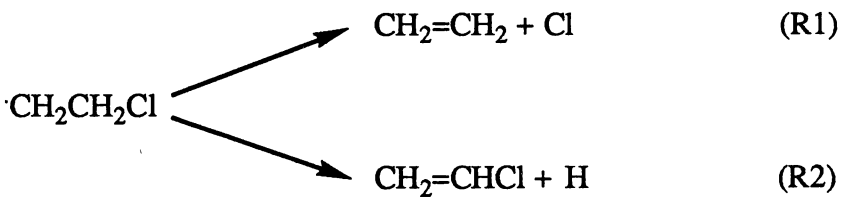

Classical trajectory calculations were performed using various types of initial conditions and the results were compared to those obtained using Monte Carlo transition-state theory[182-184] on the same potential-energy surfaces.[56-57] Energies ranging from 70 to 131 kcal/mol were considered. The lower end of this range corresponds to the upper energies accessible in the laboratory using single-photon overtone excitation techniques.[2,4]

Our results indicate that 2-chloroethyl radical behaves statistically for all energies in this range. The computed rate coefficients do not indicate a dependence on the initial conditions. Further, the statistical behavior is "robust" in the sense that the computed results are qualitatively unaffected by non-negligible variations of parameters in the potential-energy surface. Based on our work on the 2-chloroethyl radical,[56-57] and consideration of experimental[74-77,80,106] and theoretical[170-173] work done by others, we advance possible explanations for the observed behavior and suggest guidelines

which hold the promise of allowing predictions of whether or not systems will behave statistically.

Unimolecular Reaction Dynamics of RDX

In the past, most theoretical studies of unimolecular reaction dynamics were concerned with systems comprised of ten or less atoms.[33-36,45,56-57,85-89,102-103,110,114,129,149-177,184-211] However, recent increases in computational power have made it feasible to study the full-dimensional classical reaction dynamics of large gas-phase molecules.[48,175] We have performed a trajectory study of the unimolecular decomposition of the twenty-one atom hexahydro-1,3,5-trinitro-1,3,5-triazine molecule (RDX);[58] the results are given in Chapter VI. Our primary goal was to try to corroborate conclusions drawn by experimentalists concerning the initial steps of RDX dissociation in the gas phase. Another goal was to evaluate the utility of classical trajectories in studying the reactive dynamics of such a large polyatomic molecule. To our knowledge, RDX is the largest molecule for which the full-dimensional, multichannel reaction dynamics have been simulated.

A potential-energy surface that incorporates much of the available experimental[212-217] and theoretical[217-221] information (while retaining a reasonably simple functional form) was constructed. We explicitly considered the two chemically distinct reaction channels identified as being the principal (primary) reactions following infrared multiphoton excitation in a molecular beam.[222] These are simple N-N bond fission (R3) and a concerted triple dissociation (R4):

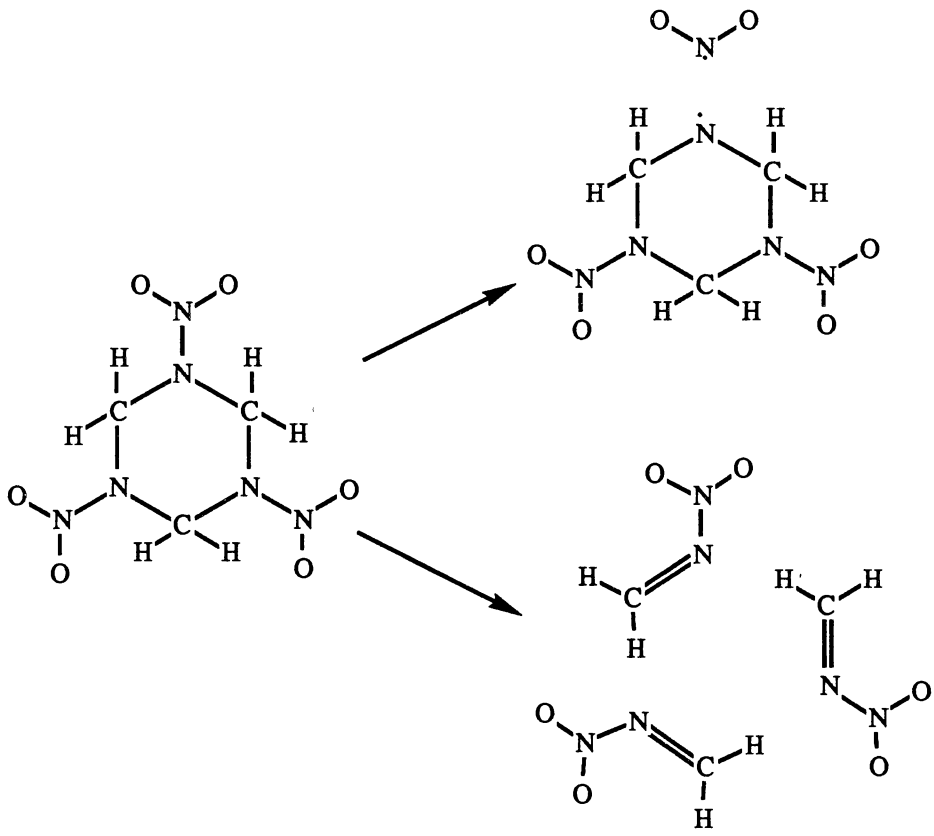

(R3)

(R4)

First-order rate coefficients, branching ratios, and product-energy distributions were calculated. The results were found to be in reasonable accord with the experimental data. (More work is probably warranted, however, in order to bring the calculated results into closer agreement with experiment.) The correspondence between the calculated and experimental results suggests that classical trajectories provide a viable means for studying the reaction dynamics of really large molecules.

Nonchaotic Dynamics in Excited Polyatomic Molecules

The role of chaos in the dynamics of *small* molecules is well known.[144,165-166,223-239] It is not as clear whether the classical dynamics of *large* molecules excited to total energies above the threshold for reaction will be strongly influenced by chaotic behavior.[171-174,203] We (and others[130,132]) think that this is not generally true. In fact,

simple considerations suggest that the vibrational dynamics of large molecules should *not* be chaotic.

The material presented in Chapter VII addresses this question. We present power spectra for five different molecules: C_2H_4, CH_3ONO, SiF_4, 2-chloroethyl radical, and RDX. Spectra were computed for individual and ensembles of trajectories as a function of the total energy and, for some cases, with and without angular momentum. The energies ranged from (essentially) the classical ground state to levels in excess of the dissociation thresholds. Our findings indicate that C_2H_4 and 2-chloroethyl radical undergo a comparatively early transition to chaos, compared to the other three molecules we considered. We discuss possible ramifications for unimolecular reaction dynamics.

Zero-point Energy Constraints in Classical Mechanics

A major issue in chemical dynamics is the problem of how to deal with the zero-point energy in classical trajectory calculations.[43-47] Quantum mechanically there is a minimum allowed energy for bound oscillators.[37] There is no corresponding classical analog. Among the consequences of this are reports of significantly different relaxation pathways for excited-state quantum and classical systems.[14,241] Additionally, there exists the possibility of contribution of zero-point energy to the reaction rates of chemical reactions.[45,195,203]

Constraints on the flow of zero-point energy are considered in Chapter VIII. In particular, two recently published methods[46-47] that serve to maintain (at least) zero-point energy in a set of zeroth-order harmonic modes are applied to the Hénon-Heiles Hamiltonian.[242] We also present an alternative method for constraining the energy in harmonic modes to have exactly the zero-point level.[61] The effects of the various methods are examined in some detail. Configuration-space projection and power spectra

of individual trajectories are used to draw direct comparisons among the three methods and also to the unconstrained classical dynamics.

Each of the methods for constraining the zero-point energy introduces serious aphysical behavior into the dynamics. We are led to question whether it is possible to constrain the classical energy flow without introducing unacceptable artifacts into the dynamics.

Mode-specific Tunneling Splitting in Malonaldehyde

There have been many investigations of tunneling in the malonaldehyde molecule.[20,22,30,243-248] The geometry of the molecule suggests that the tunneling may be modeled in terms of a symmetric double well.[37-38] Indeed, the splitting of some of the bands in the far-IR and microwave bands reveals that this is the case.[243-244,246,248] There have been several measurements of the splitting, and the reported values are in good agreement; a value of roughly 21 cm^{-1} is generally accepted.

An interesting suggestion is that it should be possible to influence the value of the splitting *via* low-energy, mode-selective excitations. If one excites fairly slowly decaying states that involve motions that are involved in the "tunneling coordinate", then it would seem quite likely that there should be some effect on the tunneling splitting. We discuss this possibility in Chapter VIII, where we describe a calculation that

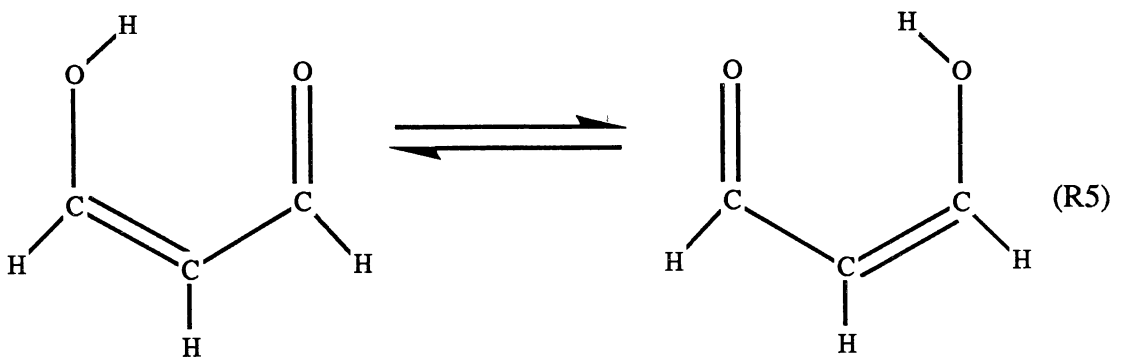

(R5)

incorporates a semiclassical tunneling model into a classical trajectory calculation. A model potential-energy surface (due to Hutchinson[249]) designed to model the hydrogen transfer in malonaldehyde is used in conjunction with a "classical plus tunneling" model.[30,144-145] We compute the tunneling splittings for various initial distributions of the available energy. There is a substantial dependence of the computed splitting on the initial conditions. Possible extensions of the calculation to more realistic models are discussed.

CHAPTER II

COMPUTATIONAL METHODS

The computational techniques used in this work are thoroughly described in the literature.[30,33-38,46-47,186,250-261] Most of the methods are standard and have been used successfully by many others. The general classical dynamics computer code, GenDyn[261], was used (with some modification) for trajectory calculations involving polyatomic molecules. Separate computer codes were written for the analysis of trajectory results, and for the calculations dealing with model systems. In this chapter, methods that were used in more than one calculation are detailed. Procedures specific to individual problems are presented in the chapter describing that work.

Potential-energy Surfaces

In order to perform classical trajectory calculations it is necessary to have values of the gradient of the potential energy for arbitrary molecular configurations.[33-36,262-264] These calculations can be done in the absence of a global analytic functional form for the potential (e.g., by using spline-fitting techniques to connect a grid of computed potential energies in the neighborhood of an arbitrary configuration).[265-266] Also, some semiempirical molecular-orbital theory codes are available in which the local energy and gradient are computed and a trajectory can be generated "on the fly".[267] However, in the vast majority of cases, an analytic form for the potential-energy surface is developed in such a way as to hopefully encompass the major features of the chemistry being studied.[262-264,] We have chosen, without exception, to use the latter method for the work described in this Dissertation.

A number of potential-energy surfaces describing the full-dimensional reaction and intramolecular vibrational relaxation (IVR) dynamics of polyatomic molecules were developed in the course of the work described here. They are based on equilibrium force fields for 2-chloroethyl radical, ethene, chloroethene, RDX, methylenenitramine, and silicon tetrafluoride. Some of the force fields were taken either in whole or in part from works (both published and unpublished) by others, while some were completely devised during the course of the current work. Varying degrees of detail were included in the potential-energy surfaces, with more attention generally being afforded the reactants.

In addition to the potential-energy surfaces developed for the full-dimensional studies, some model potential-energy surfaces were taken from the literature in order to study specific processes. Specifically, a restricted model that nominally describes the symmetric keto-enol tautomerization in the malonaldehyde molecule was borrowed from work published by Hutchinson[249] in order to investigate the possibility of evidence for mode specificity in the tunneling splitting[243-248] associated with the tautomerization, and the Hénon-Heiles Hamiltonian[242] was employed as a simple model for studies of the effects of various zero-point energy constraints[46-47] on classical dynamics. Since the forms of these two model potentials deviate significantly from those used to describe the full-dimensional processes, the description of the potential-energy surfaces in the following paragraphs will be limited to the forms used in the full-dimensional studies and the details of the model Hamiltonians will be deferred to the appropriate chapters.

Basic Functional Forms

There are a number of possible ways to describe the potential-energy surfaces for molecular systems in closed form.[262-264] Two of the more common choices are to write the potential in terms of valence internal coordinates (e.g., bond lengths, bond

angles, wag angles, and dihedral angles) or to expand the potential energy in a multidimensional Taylor series of n-body terms (where n = 2, 3, ..., N, and N is the number of atoms in the molecule). The latter approach becomes very difficult for anything but small ($N \leq 4$) systems.[262] Since we are focusing our attention on "large" molecules (five to twenty-one atoms), we have chosen to take the former approach in our work.

The potential-energy surface for a given molecule (or radical) was written as a sum of terms describing the energetics associated with displacement of individual bonds, angles, wag angles, and dihedral angles from the corresponding equilibrium values. Definitions of these coordinates are provided in Chapter 4 of Wilson, Decius, and Cross.[257] In addition to these "valence" coordinates, non-bonded interactions describing the forces between atoms separated by three (or more) intervening atoms were included (in some cases) using Lennard-Jones 6-12 potentials.

Thus, for small oscillations about the equilibrium geometry, the overall potential-energy function was written as:

$$V(\mathbf{r}, \theta, \gamma, \tau, \mathbf{r}_{LJ}) = \sum_{\text{bonds}} V(r_i) + \sum_{\text{angles}} V(\theta_i) + \sum_{\text{wags}} V(\gamma_i) + \sum_{\text{torsions}} V(\tau_i) + \sum_{\text{L-J}} V(r_{LJ}) + \frac{1}{2} \sum_{\text{bonds}} \sum_{\text{bonds}}{}' V_c(r_i,r_j) + \frac{1}{2} \sum_{\text{angles}} \sum_{\text{angles}}{}' V_c(\theta_i,\theta_j) + \frac{1}{2} \sum_{\text{bonds}} \sum_{\text{angles}} V_c(r_i,\theta_j). \qquad \text{(II.1)}$$

Bond-stretching terms were treated as anharmonic oscillators by using Morse potentials,[33-34]

$$V(r) = D_e \left\{ e^{-2\alpha(r - r^o)} - 2e^{-\alpha(r - r^o)} \right\}, \qquad \text{(II.2)}$$

where D_e is the well depth of the bond, α is the range parameter, and r^o is the equilibrium bond length. The range parameter α is given by

$$\alpha = \sqrt{\frac{k_r}{2D_e}}, \tag{II.3}$$

where k_r is the harmonic force constant describing the bond.

Harmonic oscillator functions were used for both the valence angle bending and wag-angle bending terms (denoted by θ and γ, respectively), and to describe nondiagonal bond-bond, angle-angle and bond-angle interactions:

$$V(q) = \frac{1}{2} k_q (q - q^o)^2 \quad (q = \theta \text{ or } \gamma) \tag{II.4}$$

and

$$V(q_i,q_j) = k_{qi,qj}(q_i - q_i^o)(q_j - q_j^o); \quad q_i, q_j = r, \theta \text{ and } q_i \neq q_j. \tag{II.5}$$

The torsional potentials were represented by six-term cosine series

$$V(\tau) = \sum_{j=0}^{5} a_j \cos(j\tau), \tag{II.6}$$

where $\{a_j\}$ are Fourier coefficients and τ is the dihedral angle. The Fourier coefficients were adjusted to give agreement with available experimental and/or theoretical data.

The Lennard-Jones 6-12 potentials were written as

$$V_{L\text{-}J}(r) = 4\varepsilon\left\{\left(\frac{\sigma}{r}\right)^{12} - \left(\frac{\sigma}{r}\right)^{6}\right\}. \tag{II.7}$$

The parameter ε is equal to the well depth and σ is related to the position of the minimum in the potential by

$$\sigma = \frac{r^o}{\sqrt[6]{2}}. \tag{II.8}$$

In the majority of the calculations, explicit bond-bond, angle-angle, and bond-angle interactions were neglected. There are two main reasons for doing so. First, for most sizeable systems, there simply is not enough information (e.g., detailed spectroscopic measurements or reliable *ab initio* results describing the relevant stationary points) to accurately specify the force fields for the reactant, transition state(s), and product(s). Given this frequent limitation, it would seem prudent to include only as many terms in the force field as are necessary to adequately reproduce the available information. Thus, if most of the known features of the equlibrium force fields can be reasonably well reproduced without recourse to nondiagonal terms, such terms should not be used. Finally, from a practical standpoint, inclusion of nondiagonal terms in the potential-energy surface sometimes leads to aphysical behavior in the classical dynamics for large-amplitude vibrations.[114,268-269]

For example, interaction terms of the form given by Eq. II.5 involving displacements of a bond and an angle can lead to significant spurious minima for configurations far removed from equlibrium. (It should be noted parenthetically that there are cases in the literature where the spurious behavior is associated with nondiagonal terms having *negative* force constants.[114] Since the displacements appearing in Eq. II.5 may be either positive or negative, this would seem to be an incorrect conclusion.) However, if sufficient data are available for the stationary points (the reactant in particular), it may be deemed necessary to include some nondiagonal terms in the potential-energy surface. In such cases, the potentially deleterious effects of the nondiagonal terms may be minimized by attenuation of the appropriate force constants using switching functions. (Switching functions are described below and in Refs. 36, 56-58, 99, 207, 270-275.)

Fitting the Force Fields

Given a physically motivated form for the force field, it is necessary to somehow adjust the parameters to give the best fit to whatever information is available. Since there are many more parameters appearing in Eq. II.1 than can normally be supplied by experiment, and *ab initio* data are in most cases not available, several approximations are made.

First, the equilibrium coordinates in Eq. II.1 are set equal to the experimental (or *ab initio*) values. Next, a set of trial force constants is inserted into Eq. II.1 and the normal-mode frequencies are obtained, either analytically[257,261,276-277] or from a power spectrum[258-260] of a low-energy trajectory. (Power spectra are discussed later in this Chapter.) The initial set of force constants may be chosen based on known values for similar molecules (if such data is available). Otherwise, "generic" values may be found in various references and used as a starting point.[257,276] The frequencies obtained using the trial force-constant matrix are compared with a set of reference frequencies and, if possible, the symmetry ordering of the normal-mode vectors from the empirical force field is compared to that obtained from experiment or an *ab initio* calculation. The parameters are then adjusted so as to optimize the fit between the empirical force field and the reference data. In many cases normal-mode assignments of the vibrational frequencies are not available. Under such circumstances, the frequencies are the principal basis for judgment of the quality of the force field.

One can minimize the discrepancy between the reference and calculated normal-mode frequencies using a least-squares scheme (a recently-added option in GenDyn[261]). The procedure is straightforward: Compute a set of normal-mode frequencies and sum the squares of the differences between the calculated and reference values. Change one of the force constants (or group of force constants, if appropriate) and repeat the

calculation, retaining the set of force constants that gives the smaller sum over the squares. This process can be incorporated into a loop so that thousands of possible force constant matrices can be considered and (usually) a good fit to the reference data can be achieved.

It is important when using this method to make sure that chemically equivalent coordinates are forced to have identical force constants, i.e., that the force field be symmetric. For instance, a diagonal, in-plane force field for ethene (C_2H_4) can be written in terms of five bonds and six angles. The four C-H bond stretching force constants should all have the same value, as should the two HCH angle-bending force constants and the four CCH angle-bending force constants. One should be aware that force fields generated in this way are not guaranteed to yield normal modes that are correctly ordered with respect to symmetry. All that is being optimized is the numerical values of the frequencies.

Dasgupta and Goddard[268] have published a method that combines the (assumed correct) experimental vibrational frequencies and the (assumed correct-in-form) *ab initio* Hessian matrix to yield an optimized fit to a given a potential-energy surface. This procedure, which generates so-called "Hessian-biased" force fields may prove to be quite useful in fitting force fields in cases where *ab initio* data are available. In a sense, the method hearkens back to ideas used earlier by others,[278-280] in that *ab initio* theorists often use scaling factors to adjust the computed force constants to give better agreement with experimental frequencies.

Switching Functions

The potential-energy surface described by Eq. II.1 is only suitable for small excursions about the equilibrium geometry of a molecule. In practice, a potential-energy

surface that adequately describes the vibrational motion of the reactant will usually result in a poor representation of the forces present in the product(s).

As a simple (but illustrative) example, consider the dissociation of a hypothetical nonlinear triatomic molecule, ABC --> AB + C. A diagonal potential-energy surface describing the ABC system would include two bond-stretching terms and one angle-bending term. Assume that the bond stretches are Morse oscillators and, for simplicity, that the strength of the AB bond is unaffected by the photodissociation process. Let the bending term be harmonic. As the B--C bond begins to break, the restoring force for displacement of the angle should diminish, eventually reaching zero for sufficiently large AB--C bond distances. Also, it may be that the "equilibrium angle" undergoes variation along the reaction profile for B-C bond fission. Finally, the vibrational frequency and equilibrium bond length of AB may vary as a function of the AB---C reaction coordinate, requiring changes in the Morse curvature parameter, α, and equilibrium bond length, r^o, for AB. Thus, the parameters k_θ, θ^o, α_{AB} , $r_{AB}{}^o$ must be written as functions of the BC bond length.

This attenuation of the parameters in the potential-energy surface can be accomplished through the use of "switching functions" that depend on the variables associated with the motion of the system along the reaction coordinate.[36] The switching functions must be continuous and have continuous first derivatives, and are usually involve combinations of exponential and/or hyperbolic functions.[56-58,270-275]

In most cases, there is little or no information regarding potential-energy surface features in regions far removed from the equilibrium structures of the reactants and products. Under such circumstances, it is most common to use switching functions that vary monotonically between asymptotic limits.[36, 57-58,99] In some instances, data concerning saddle points are available and can be used as an aid in constructing the switching function and adjusting the parameters.

Occasionally, there are *ab initio* data along a reaction path leading from the transition state to reactants and product(s).[48,270-273] In such cases, fairly accurate fitting of the potential-energy surface to points along the reaction coordinate can be obtained (for small-amplitude vibrations in the modes orthogonal to the reaction coordinate. Examples where this is the case include $CH_4 \rightarrow CH_3+H$,[271] $C_2H_5 \rightarrow C_2H_4 + H$,[270,281] $H_2CCH_3 \rightarrow H_3CCH_2$,[270,281] $H_2O_2 \rightarrow 2\ OH$,[198] pseudorotation of $(SiH_5)^-$,[282] $ClCH_3 + Cl^- \rightarrow Cl^- + CH_3Cl$,[273] $HO_2 \rightarrow O + OH$,[272] $HCN \rightarrow HNC$,[283] and methylnitrosamine.[48] In some cases, switching functions that were carefully fit to *ab initio* results for one system have been applied to others under the assumption that the functions do not change significantly from one system to another.[103,284] This is somewhat akin to transferral force constants between molecules.[285-286]

The question naturally arises as to how sensitive the results of dynamics calculations are to the details of switching functions. Several workers have investigated this aspect of the problem .[8,157,197-199,287-290] In some cases, the qualitative behavior is relatively insensitive to the presence or absence of the switching functions.[103] However, in most cases, a sensitive dependence of the results for a given process upon the switching is observed.[8,157,197-199,287-290] (Some *preliminary* calculations were done on the 2-chloroethyl radical in order to determine how important the switching functions in that system are. The calculations consider the two extreme cases of i) full attenuation of the potential-energy surface and ii) no attenuation of the potential-energy surface. The results indicate approximately a factor of seven decrease in the overall first-order rate coefficient when the attenuation is included for trajectories computed at 118 kcal/mol.)

The switching functions used in the studies that comprise this Dissertation are of either hyperbolic tangent or exponential form. The precise forms vary from system to

system. Therefore, they will be developed more fully in the appropriate sections of subsequent chapters.

Selection of Initial Conditions

Much time and work has been invested in trying to decide how best to select initial conditions for classical trajectories.[33-36,87,188,254-256, 291] The type of initial conditions to be used is to some extent determined by the type of problem being studied. However, for a given calculation (i.e., mode selective or random microcanonical sampling) there are a number of possibilities to be chosen from.

Quasiclassical Approach

One commonly used procedure for initiating classical trajectories is to generate what are known as "quasiclassical" initial conditions.[34] The method is based on the assumption that normal modes[257,276-277] can be used as a basis for partitioning the energy into a molecule and, more specifically, that the appropriate way of doing so is in accordance with the quantum-mechanical harmonic oscillator energy levels[37].

Quasiclassical initial conditions are obtained by first performing a normal-mode analysis of the potential-energy surface to obtain the eigenvalues Ω and eigenvectors L_k of the potential-energy surface in terms of the (mass-weighted) Hessian matrix. (Normal-mode analysis is thoroughly discussed in Wilson, Decius, and Cross[257] as well as in a number of other references[277]. The GenDyn[261] dynamics code uses the GIVENS algorithm to diagonalize the second-derivative matrix of the potential-energy surface.)

The normal-mode solutions are of the form[257]

$$Q_i(t) = \sqrt{\frac{2E_i}{\lambda_i}} \sin(2\pi\nu_i t + \delta_i), \qquad \text{(II.9)}$$

where E_i is the energy of normal mode i, λ_i is the "force constant", ν_i is the fundamental frequency, and δ_i is a phase factor determined by the phase of the normal mode at time t=0. It follows that the values of Q_i at the turning points are

$$Q_{\pm,i} = \pm\sqrt{\frac{2E_i}{\lambda_i}} \; . \tag{II.10}$$

The quasiclassical energy levels of the normal modes are

$$E_i = \left(v_i + \frac{1}{2}\right) h\nu_i = \frac{1}{2}\dot{Q}_i^2 + \frac{1}{2}\lambda_i Q_i^2, \tag{II.11}$$

where v_i is the "quantum number" for the ith normal mode and h is Planck's constant. Phases of the normal modes are selected from the distribution function[34]

$$Q_i = Q_i^o - (Q_i^o - Q_{<,i})\sin\left[\, \pi\left(\zeta + \frac{1}{2}\right)\right], \tag{II.12}$$

where ζ is a random number uniformly distributed on (0,1). The potential energy associated with this normal-mode phase is obtained by projecting the normal coordinate onto the Cartesian coordinates using the linear transformation equations

$$\mathbf{q} = \mathbf{L}_k^{\dagger}\mathbf{Q}_k, \tag{II.13}$$

where $\mathbf{q}$ is the vector of mass-weighted Cartesian displacements

$$q_i = \sqrt{m_i}\,(x_i - x_i^o), \tag{II.14}$$

$\mathbf{Q}$ is the matrix of normal coordinates, and $\mathbf{L_k}^{\dagger}$ is the transpose of the transformation matrix that yields the normal coordinates in terms of the mass-weighed Cartesian coordinates.

Since the actual potential is anharmonic, it is possible for the potential energy resulting from the projection of normal mode "i" onto the Cartesian coordinates to be greater than the total normal-mode energy E_i. Under such circumstances, the set of initial conditions for that normal mode are rejected and a new set is chosen.

The kinetic energy for normal mode "i" is just the difference between E_i and the potential due to displacement of mode "i" from equilibrium. The magnitude of the normal velocity can now be solved for. The sign of the velocity is chosen randomly.

This procedure is repeated independently for each of the normal modes. The net displacement of the Cartesian coordinates are a direct superposition of the individual displacements for each normal mode,

$$x_i = x_{i,o} + \sum_{j=1}^{3N-6} \Delta x_{ji} \qquad (i=1, 2, ..., 3N). \qquad \text{(II.15)}$$

The sum runs from j=1 to 3N-6 by virtue of the fact that, for systems at equilibrium, six of the eigenvalues are zero (three rotations and three translations). A similar procedure is used to project the kinetic energy of each normal mode onto the Cartesian velocities.

The total energy resulting from this procedure will, in general, be slightly different from the sum of the normal-mode energies. Also, there may be a small angular momentum following this initial energy partitioning. Therefore, the angular momentum is removed by vectorial subtraction[169]

$$\mathbf{p} = \mathbf{p_o} - \mathbf{p_{rot}}, \qquad \text{(II.16)}$$

where $\mathbf{p_0}$ is the initial momentum vector (including angular momentum) and $\mathbf{p_{rot}}$ is the vector of atomic momenta that correspond to net angular momentum.

Finally, the total energy $E(\mathbf{p},\mathbf{x})$ is then adjusted to the desired value (based on the sum of the normal-mode energies),

$$E_0 = \sum_{i=1}^{3N-6} E_i(\dot{Q}_i,Q_i), \tag{II.17}$$

using the relations[169]

$$\mathbf{x'} = \mathbf{x_0} + \sqrt{\frac{E_0}{E(\mathbf{p},\mathbf{x})}}\,(\mathbf{x} - \mathbf{x_0}) \tag{II.18}$$

and

$$\mathbf{p'} = \sqrt{\frac{E_0}{E(\mathbf{p},\mathbf{x})}}\,\mathbf{p} \tag{II.19}$$

If only normal modes are to be excited, this last step completes the selection of initial conditions for a given trajectory. The initial conditions are the 3N Cartesian coordinates $\mathbf{x'}$ and the 3N Cartesian momenta $\mathbf{p'}$.

In some cases, it is desired to assign an anharmonic X-H local mode a quantity of energy corresponding to an allowed energy level of the nonrotating Morse oscillator,[34]

$$E_M = \left(v + \frac{1}{2}\right) h\nu + \frac{\left(v + \frac{1}{2}\right)^2 h^2\nu^2}{4\,D_e}. \tag{II.20}$$

In such instances, zero-point energy is first partitioned along the normal modes using Eqs. II.10 to II.19. Then, a random phase for the X-H bond is selected from[34]

$$r = r^o + \frac{1}{\alpha} \ln\left[\frac{1 - \sqrt{E_M/D_e}\cos(2\pi\zeta)}{1 - (E_M/D_e)}\right] \tag{II.21}$$

and the coordinates of the H atom are adjusted accordingly. The kinetic energy is calculated as the difference between E_M and $V(r)-D_e$ (Eqs. II.20 and II.2, respectively). This energy is projected onto the H atom, with the sign of the momenta being chosen randomly. A net displacement of the center-of-mass coordinate and momentum generally result from excitation of the local mode, as well as a net angular momentum. These quantities are removed and the total energy is once again scaled to the desired value.[169]

Initial conditions obtained using the quasiclassical selection scheme approximate state-selected initial conditions. However, the precision of this initial state selection procedure is not high. This is due to the neglect of anharmonicity in choosing the initial phases of the oscillators (which necessitates scaling of the energy prior to trajectory integration). As a result, there is some spread in the individual mode energies from one trajectory to another. While the quasiclassical energy partitioning is useful for most purposes, it is not suited for work where precisely defined initial states are required, e.g., studies of state-specific decay.[141-143] In such cases, more sophisticated methods such as adiabatic switching[28,292-297] are required.

Random Microcanonical Sampling

Another commonly used technique for choosing initial conditions for trajectories is to generate a Markov chain in either the phase space[34,184,253-254], or configuration space[255-256] of the molecule, in order to sample a classical distribution of phase space. Methods have been developed in order to allow for both unrestricted angular momentum[253-254,255] and preselected angular momentum[184,256] sampling. In cases where totally random initial conditions for trajectories were required in this work, the EMS sampling algorithm was used.[255-256] Both the restricted[256] and unrestricted[255] angular momentum cases can be treated using this method.

The EMS procedure consists of a random walk through the configuration space of the reactant followed by selection of the atomic momenta so as to ensure a microcanonical ensemble of trajectories. Specifically, a Markov chain is generated in the reactant configuration space using a weight function of the form[255]

$$W(E,J) = [\, E - V(\mathbf{q}) \,]^{(3N-5)/2} \qquad \text{(II.22)}$$

or[256]

$$W(E,0) = \sqrt{\frac{1}{I_A\, I_B\, I_C}}\, [\, E - V(\mathbf{q}) \,]^{(3N-8)/2}, \qquad \text{(II.23)}$$

where E is the desired energy of the microcanonical ensemble, $V(\mathbf{q})$ is the potential energy associated with some configuration $\mathbf{q}$, N is the number of atoms in the molecule, and I_A, I_B, and I_C are the eigenvalues of the moment-of-inertia tensor.[277] Equation II.22 is for the case of no restriction on the total angular momentum and Eq. II.23 is for the case J=0. Both assume a nonlinear molecule vibrating in three dimensions.

Starting from a configuration $\mathbf{q}_k$, one or more of the position coordinates is (are) moved to yield a trial configuration $\mathbf{q}_{k+1}$. The trial configuration $\mathbf{q}_{k+1}$ is accepted or rejected on the basis of the following criteria:

1. The random walk is restricted to configurations corresponding to the "reactant". If the trial configuration $\mathbf{q}_{k+1}$ results in a configuration that is inconsistent with this restriction, then the trail configuration $\mathbf{q}_{k+1}$ is rejected and the configuration for state k+1 is taken to be the same as for state k.
2. Otherwise, if the statistical weight (Eq. II.22 or II.23) for trial configuration $\mathbf{q}_{k+1}$ is greater than that of configuration state k then the trial

configuration is accepted as state k+1.

3. Otherwise, the ratio W_{trial}/W_k is compared with a random number $0 \leq \zeta \leq 1$. If $W_{trial}/W_k > \zeta$ then the trial configuration q_{k+1} is accepted as state k+1.
4. Otherwise, trial configuration q_{k+1} is rejected and the configuration for state k+1 is taken to be the same as that for state k.

Periodically, a set of momenta are selected in order to completely specify the initial conditions for a trajectory. The momenta are selected according to[256]

$$p_i^o = \sqrt{m_i}\,\xi, \qquad (i=1, 3N) \qquad \text{(II.24)}$$

where ξ is a normally distributed random number having zero mean and unit variance. The center-of-mass momentum resulting from this selection is removed and, in the case of J = 0 sampling, the angular momentum is subtracted.[169] The momenta are then scaled to give the desired total energy using[255]

$$p_i = \sqrt{\frac{E - V(q)}{T(p^o)}}\,p_i^o, \qquad (i=1, 3N). \qquad \text{(II.25)}$$

At this point, a trajectory is computed.

In practice, an initial configuration is chosen (typically the equilibrium geometry or some other convenient configuration) and a fairly large number of states (*ca.* 10^6) are sampled in order to allow the system to "lose memory" of the initial configuration. Then, at periodic intervals, the random walk is suspended, a set of atomic momenta will be selected, and a trajectory computed. After calculation of the trajectory, the random walk will be continued. This procedure is repeated until the desired number of trajectories are computed.

Integration of Trajectories

Once a set of initial conditions are selected, classical trajectories are propagated by numerically solving Hamilton's equations of motion[34,277]

$$\dot{x}_i = \frac{\partial H(\mathbf{x},\mathbf{p})}{\partial p_i} \qquad (i=1, 2, ..., 3N) \qquad \text{(II.26)}$$

and

$$\dot{p}_i = -\frac{\partial H(\mathbf{x},\mathbf{p})}{\partial x_i}. \qquad (i=1, 2, ..., 3N) \qquad \text{(II.27)}$$

Equations II.26 and II.27 comprise a set of 6N coupled first-order differential equations. These are solved using a fourth-order Runge-Kutta-Gill integrator.[34] Trajectories are integrated in a space-fixed Cartesian coordinate system using a fixed stepsize. The stepsize varies somewhat from system to system (and with energy) but is typically of the order of 10^{-16} s. Starting from the initial conditions, trajectories are computed for some maximum integration time or, in the case of reaction dynamics studies, until reaction occurs.

Analysis of the Results

The analysis of the trajectories consists primarily of calculation of first-order rate coefficients, IVR curves for local and normal modes, and final-state analysis of the products of chemical reaction. In some cases, configuration-space projections of individual trajectories were used to study mechanisms for some of the reactions. Power spectra of the internal coordinates were computed in order to make qualitative conclusions about the nature of the vibrational dynamics and, in some cases, the role of angular momentum on energy transfer.

Endtests

In most of the work described here, one of the primary goals was to study the unimolecular *reaction* dynamics. Therefore, some means of determining when reaction had occurred was necessary. The bond-length criteria used were in the range 2.25 to 8.0 Å. The ratio $|V(r)|/D_e$ was greater than 0.96 in all cases. The time of reaction was taken to be that of the last inner turning point in the dissociating bond prior to that particular coordinate achieving the predetermined critical extension.[186]

First-Order Rate Coefficients

The first-order rate coefficient for an ensemble of N_0 trajectories is obtained from the first-order rate expression[34]

$$\ln\left(\frac{N_t}{N_0}\right) = -kt, \qquad \text{(II.28)}$$

where N_t is the number of undissociated trajectories at time t and k is the first-order rate coefficient. Although there are alternative ways of obtaining lifetimes,[153-154] this simple method has been used many times before[98,102-103,114] and seems to give good results. There are also methods for fitting lifetime data to a sum of exponentials[87] but such techniques were not necessary here due to the high-quality fits of Eq. II.48 to the data.

The branching ratio for two chemically distinct reactions (R_i) and (R_j) is[209]

$$\text{Branching ratio} = k_i/k_j, \qquad \text{(II.29)}$$

where

$$k_i = k - k_j \qquad \text{(II.30)}$$

and

$$k_j = k/(1+N_i/N_j). \qquad \text{(II.31)}$$

N_i and N_j are the numbers of trajectories in the ensemble that led to reactions (R_i) and (R_j), respectively.

We employed the "bootstrap method"[298] in an effort to determine the degree of variability in the rate coefficients, based on the set of computed lifetimes for a given ensemble of trajectories. Several thousand sample data sets were generated by selecting at random from the pool of computed trajectory outcomes, i.e., either a lifetime corresponding to reaction, or a trajectory that did not lead to dissociation within the imposed time cutoff. First-order rate coefficients were computed for each sample data set and the standard deviation in the computed rate coefficients was calculated. Branching ratios at each energy were computed as the quotient of the mean value of k_1 to k_2, with appropriate propagation of uncertainties. This procedure yields an estimate of the precision of the rate coefficients and branching ratio for a particular set of trajectory results.

Mode Energies

Following the flow of energy through an excited molecule is not a simple problem. The origin of the difficulty is that one would like to map the energy flow through various "modes" as though they are separable when, in fact, they are not. Several different methods have been proposed to do this.[98,162,199,250-252,299] We have used two simple approximations to monitor IVR, specifically, the normal- and local-mode energies, defined as[162]

$$E_{nm} = \frac{1}{2}\dot{Q}_i(t)^2 + \frac{1}{2}\lambda_i Q_i(t)^2 \qquad \text{(II.32)}$$

and[250]

$$E_{lm} = \frac{\mathbf{p_H \cdot p_H}}{2\mu_{XH}} + V(r_{XH}) \qquad \text{(II.33)}$$

for the normal and local modes, respectively.

Due to the quadratic form of the potential in normal coordinates, the normal-mode approximation is exact only for infinitesimal displacements from equilibrium. If one of the normal coordinates undergoes large-amplitude motion then the normal-mode energy associated with that coordinate will become very large. However, the normal-mode energies are useful for examining the short-time dynamics of the IVR. It is very important that there be no residual rotational or translational momentum when monitoring normal-mode energies since the normal coordinates are calculated relative to the space-fixed equilibrium Cartesian coordinates of the reactant molecule.

Local-mode energies are more generally useful, particularly if one is interested in the relaxation of a high-frequency oscillator. There is considerable experimental[2,4] and theoretical[300-301] evidence that, for sufficiently high intensity lasers, the absorption bands resulting from overtone pumping studies correspond closely to excitation of single bonds.

The major flaws with the local-mode approximation (as written in Eq. II.33) are that the expression assumes that the heavy X atom is "infinitely" heavy and does not project the momentum of the light atom onto the unit vector connecting the two atoms. This means that the local-mode energies so computed will provide an upper limit to the actual energy "in" the X-H bond.[302]

Power Spectra

The vibrational frequencies of a real molecule are functions of the total energy due to anharmonicity in the potential-energy surface. Thus, normal-mode analysis does not necessarily provide a realistic picture of the vibrational dynamics of the system

except for very low energies. Power spectra can be used to provide qualitative information about the vibrations, regardless of the energy.[258,260] For instance, in a quasiperiodic system, the power spectrum will consist of highly resolved peaks at the fundamental vibrational frequencies and, perhaps, at overtones and combinations of the fundamentals.[260] As the system increases in energy and (ultimately) becomes chaotic, the peaks will become increasingly broadened and shifted relative to a low-energy spectrum. The shifting and broadening are due to anharmonicity and energy transfer among the various modes. If the system is completely chaotic, the peaks will become essentially unidentifiable. Another tell-tale signature of chaos in the power spectrum is broadband "noise" over all frequencies.[258]

Power spectra were computed by recording the time histories of the internal coordinates and computing the Fourier transform of the autocorrelation functions:[258]

$$I(\nu) = \int_{-T}^{T} C_{qq}(\tau)\, e^{-\iota 2\pi\nu\tau}\, d\tau, \qquad \text{(II.34)}$$

where ν is the frequency, T is the length of the trajectory, and $C_{qq}(\tau)$ is the autocorrelation function of the time history of the variable q(t) (= bond length, angle, dihedral, etc.)

$$C_{qq}(\tau) = \frac{\int_{0}^{T\to\infty} \langle q(t)\rangle \langle q(t+\tau)\rangle\, dt}{\int_{0}^{T\to\infty} \langle q(t)\rangle \langle q(t)\rangle\, dt}. \qquad \text{(II.35)}$$

The variables <q(t)> and <q(t+τ)> are the values of the time history (with the mean removed) at times t and t+τ respectively. Since C(τ) is even, the integral in Eq. 1 can be

replaced by the corresponding cosine Fourier transform, with the result being multiplied by two to yield the one-sided power spectrum:[258]

$$I(\nu) = 2 \int_{-\infty}^{+\infty} C(\tau) \cos(2\pi\nu\tau)\, d\tau. \qquad \text{(II.36)}$$

The resolution of the power spectrum is inversely proportional to the length of the trajectory[258]

$$\text{Resolution} = \frac{1}{2T}, \qquad \text{(II.37)}$$

(for a two-sided autocorrelation obtained from a trajectory of length T) and the cutoff frequency (the so-called Nyquist frequency) is given in terms of the spacing between sampled points in q(t):[258]

$$\nu_C = \frac{1}{2\Delta t}, \qquad \text{(II.38)}$$

where Δt is the separation in time between data points being transformed.

In practice, the autocorrelation function for an individual trajectory was approximated by the "sample autocorrelation function",[259]

$$C_{qq}(\tau=m\Delta t) \approx \frac{\sum_{j=0}^{N-m} [q(t_j)-\langle q\rangle][q(t_{j+m})-\langle q\rangle]}{\sum_{j=0}^{N} [q(t_j)-\langle q\rangle]^2}, (m = 0, 1, 2, ..., N) \qquad \text{(II.39)}$$

where $(j+m) \leq N$. The approximation to $C_{qq}(\tau)$ was inserted into the cosine transform and the integral was evaluated numerically using a Simpson's rule algorithm.[303]

CHAPTER III

REVIEW OF EXPERIMENTAL AND THEORETICAL STUDIES OF MODE-SPECIFIC BEHAVIOR IN UNIMOLECULAR PROCESSES FOLLOWING SINGLE-PHOTON OVERTONE EXCITATION

Mode-selective chemistry has been an area of active research for roughly the past three decades.[4] Both experimentalists and theorists have been actively working in an attempt to understand the basic processes that may lead to mode specificity in chemical reactions. Mode specificity is generally considered to include all effects on the rate of a chemical process that originate from selective excitation of some mode or group of modes within a molecule. There are three major types of mode-specific effects that are likely candidates for observation, either experimentally or theoretically. They are i) a non-monotonically increasing rate of some chemical process as a function of the energy of the reacting molecule, ii) a dependence (at an approximately fixed energy) of the rate of reaction upon the means of imparting energy to the reactant molecule, and iii) an enhancement (relative to the predictions of statistical theories) of the rate of one chemical process over another in a reactant system capable of reacting through two or more available channels, with the observed enhancement resulting from selective excitation of one mode or group of modes of the reactant. Evidence has been observed, either experimentally[82-84,90,100-101,107] or theoretically[85-87,89,98,102-103,114,163-165,167,171,175,195-196,304], for each of the categories listed.

There are at least three reasons that the search for mode specificity in chemical reactions has spawned so much interest. The most immediately obvious reason is that an understanding of the circumstances under which mode-specific effects are likely to occur and, if they do, why, would require a thorough knowledge of the microscopic processes which govern intramolecular reaction dynamics.[4] Perhaps, for many scientists, the largest single motivation for investigating mode-specific processes resides in the fact that they provide a means of determining under what circumstances RRKM theory is applicable to chemical reactions. One of the main assumptions of RRKM theory is that the rate of a unimolecular reaction is dependent only upon the total energy possessed by an activated molecule, and not upon the mechanism by which this energy is imparted to it.[180] Implicit in this assumption is the further supposition that, in a hypothetical case for which a quantity of energy sufficient to induce reaction is added to a molecule in such a way as to localize the excitation to a single mode or small combination of modes, the subsequent intramolecular vibrational relaxation (IVR) occurs on a time scale that is much shorter than that corresponding to the actual chemical reaction. Hence, an understanding of mode-specific chemistry is inextricably tied to an understanding of IVR. The development of laser techniques suitable for single photon excitation of X-H bonds (X = C, N, O) to overtone levels high enough to overcome barriers to chemical reaction has provided experimentalists with an incisive tool for investigating this fundamental requirement of RRKM theory.[4,305] Finally, from a more practical standpoint, the ability to selectively induce one chemical reaction over another in systems capable of yielding multiple reaction products could conceivably prove to be very useful in situations for which the normal distribution of products disfavors production of a desired compound. There are no examples to date where this has been achieved, however.

There is now a fairly widely used scheme for classifying chemical systems with respect to their amenability to statistical treatment.[33,87] Molecules that yield rates of reaction that are consistent with the predictions of RRKM theory under all conditions are known as intrinsically RRKM molecules. Systems for which the rate of reaction under thermal conditions is inconsistent with the predictions of RRKM theory are regarded as being intrinsically non-RRKM, and those which yield RRKM behavior for thermal conditions but exhibit mode-specific characteristics for nonrandom excitation are classified as apparent non-RRKM molecules.

General Characteristics of Chemical Systems Likely to Exhibit Mode Specificity

The question naturally arises as to when mode-specific behavior might be expected to occur in unimolecular reactions. Considerable effort has been devoted to unravelling this problem and some tentative rules are now becoming available. However, the rules to be given below are not intended to be absolute in any sense, but rather, to simply provide qualitative guidance in selection of systems to be studied.

Although a number of scenarios for which mode specificity may be observed are to be discussed, a common thread between them is that they are all dependent (to a greater or lesser degree) on the dynamics of the intramolecular vibrational redistribution (IVR). For many systems that have been investigated it is seen that energy localized in one mode or group of modes tends to initially transfer to the rest of the molecule along fairly well-defined pathways.[89,98,102,166-167,175,164,193,299,306,320] Thus, the ability to identify these pathways is an important tool that should be exploited in the search for mode specificity. The fewer the number of internal degrees of freedom possessed by a molecule the greater the likelihood that IVR will occur along identifiable pathways and that the dissemination of energy will occur in such a way as to channel significant

amounts of energy into a critical mode corresponding to the reaction coordinate. Furthermore, as the number of internal degrees of freedom increases it quickly becomes more likely that the initially localized energy will become effectively randomized on a time scale that is significantly smaller than that corresponding to unimolecular reaction. Thus, as the number of "bath" modes in a molecule increases there is an accompanying decrease in the probability of observing mode-specific behavior. A notable exception to this generalization is sometimes found in the experimental and theoretical studies of systems in which energy transfer through the molecule is seen to be strongly inhibited by the presence of a heavy central atom separating different regions of the molecule.[71,117-122]

Most chemical reactions involving the rupture of one or more chemical bonds require a large investment of excitation energy relative to amounts conveniently supplied by way of single photon excitation methods. While other methods (e.g. multiphoton excitation, internal conversion, or chemical activation resulting from radical addition to stable species) are readily able to effect reaction, they do so with a concomitant loss of localization of energy.[4] In light of this difficulty it would seem that an important factor in determining whether a molecule will exhibit mode-selective behavior is the height of the barrier to reaction in the system. A class of reactions which frequently avoids this complication is *cis-trans* isomerization, and indeed, mode specificity has been observed for these systems, both experimentally[100-101,107] and theoretically[89,102-103,114,163-165].

One of the greatest difficulties in finding systems that are demonstrably mode specific resides in the already mentioned fact that IVR often occurs much more quickly than does chemical reaction, resulting in reaction rates that are consistent with predictions based on statistical distributions of energy within the reactant molecule. If a molecule could be found in which the selectively excited mode was strongly coupled to or was an integral part of the reaction coordinate then perhaps energy that was

selectively deposited in this mode could induce mode-specific reaction by virtue of rapid energy transfer directly into the reaction coordinate. Examples of such processes are reactions involving intramolecular rearrangements, e.g., transfer of hydrogen atoms. To date there have been multiple investigations of such processes[74,175], with one of these studies indicating the possibility of mode-specific enhancement in the rate of hydrogen transfer.[175]

In light of the fact that in many cases energy flow from initial sites of selective excitation occurs much more rapidly than does unimolecular reaction, the possibility of observing mode-specific effects might at first seem to be completely contingent upon reaction occurring before relaxation of the excited mode is complete. However, there is some recent evidence suggesting that mode specificity can exist even on time scales that are relatively long compared to the time scale for initial relaxation of the excited mode, so long as the resultant energy transfer tends to channel preferentially into identifiable modes and remain there for reasonably long periods of time before complete energy redistribution takes place. In at least one case this behavior has been observed in a study of a relatively large molecule for which the potential-energy surface is highly coupled.[171]

Review of Experimental and Theoretical Work

Considerable effort has been expended by both experimentalists and theorists in the search for chemical systems capable of displaying mode-specific reactivity. The work done to date has encompassed a wide variety of molecules and experimental techniques. However, for most of the cases to be discussed below the means by which energy is deposited in the reactant molecule involves the selective excitation of overtones of X-H stretching transitions. It is frequently feasible to excite X-H stretching modes to relatively high states (v = 4 - 7) *via* absorption of a single photon of infrared or visible

radiation. These levels of excitation are, in some cases, sufficient to induce chemical reaction.[4,305] Moreover, empirical fitting of the spectra resulting from these excitations suggests that the energy absorbed in such transitions is highly localized in single local-mode oscillators.[307-310] Thus, the absorption of a single photon possessing sufficient energy to excite a high-frequency X-H overtone is thought to largely correspond to excitation of an individual X-H bond, rather than a normal-mode vibration involving simultaneous energization of all or several of the "local" oscillators in the molecule.

The format of the following literature review will be as follows: Experimental and theoretical results will be discussed together on a molecule by molecule basis where possible. Attempts to induce mode-specific behavior will be considered, irrespective of the outcome of the experiment, since negative results are of comparable significance to positive observations of mode-specific behavior. Molecular systems will be classified according to the chemical environment of the site of excitation, with molecular species grouped by the type of oscillator excited and by the primary structure of the molecule in the neighborhood of the excitation site, e.g. H-C-, H-C≡, H-N=, H-O, etc. Molecules containing X-H linkages in two or more chemical environments (e.g. ethylenic and methylenic groups in the same molecule) will be discussed together in an independent section. An exception to this convention will be made for the case of methyl and polymethyl peroxides. Discussion for a given set of molecules will be presented in approximately chronological order. Suggestions for further work will be made in the course of discussion of these systems and will be restated in a final summary.

Molecules Containing XH_3 Moieties

Methyl Isocyanide. A series of experiments on the isomerization of methyl isocyanide to acetonitrile

$$CH_3NC \rightarrow CH_3CN \qquad (R6)$$

was carried out in the later 1970's by Reddy and Berry.[82,83] In these provocative experiments Reddy and Berry employed an intracavity continuous-wave dye laser excitation technique to selectively excite high C-H overtone levels by single-photon absorption in the gas-phase molecule, and measured the resulting spectra using photoacoustic detection methods. The excitations were to v = 4, 5, and 6 with high state selectivity due to separation of the absorption bands corresponding to each of the overtones. Product analysis following irradiation was performed using gas chromatographic techniques. For the v = 4 and v = 5 experiments, the pressure dependence of the reaction rates is linear when represented by a plot of the reciprocal of the appearance rate coefficient versus pressure (Stern-Volmer plot), indicating that the behavior at these levels is probably in accordance with RRKM predictions. The results for the v = 6 overtone excitation yield a result somewhat in disagreement with RRKM theory, but, as Reddy and Berry noted, the results of their RRKM calculations were very sensitive to the choice of parameters used in the model RRKM calculation. Consequently, Reddy and Berry were hesitant to state unequivocally that methyl isocyanide behaves in a non-RRKM fashion.

Part of the reason Reddy and Berry were motivated to suggest that the reaction was, perhaps, occurring in a nonstatistical fashion was some early classical trajectory results of Bunker and co-workers.[85-87] The earliest of these calculations was carried out for a tritium-substituted model of the methyl isocyanide molecule in which they were attempting to simulate experiments studying tritium substitution reactions.[85] The primary result of this early calculation was that energy relaxation in the methyl isocyanide molecule is highly dependent upon the means by which initial conditions are selected. A subsequent calculation by Bunker and Hase considered more complex models for the methyl isocyanide molecule and included more realistic selection of initial

conditions approximately simulating thermal conditions.[87] The distribution of reactive lifetimes in these calculations exhibited relatively low sensitivity to the details of the potential energy surface but a pronounced dependence upon the method of selecting initial conditions was once again observed. The energy dependence of the isomerization rate coefficients was not in good agreement with theoretical energy-dependence curves as calculated from RRKM theory for a wide range of energies (70 - 200 kcal/mol). Bunker and Hase concluded that methyl isocyanide is an intrinsically non-RRKM molecule.

More recently, Sumpter and Thompson revisited the methyl isocyanide isomerization reaction.[89] Their calculations were based on selection of initial conditions more in accord with the experiments of Reddy and Berry.[82,83] Sumpter and Thompson investigated the energy dependence of the system in the range 75 - 200 kcal/mol by computing trajectories for two qualitatively different kinds of initial conditions. The first method was carried out by choosing the total system energy and then subtracting out an amount of energy equal to that of the v = 6 local mode. The remaining energy was allowed to randomize among the vibrational degrees of freedom using Metropolis sampling techniques, afterwhich the remaining energy was projected onto a C-H local mode. Initial conditions corresponding to uniform distributions of energy were obtained using Metropolis sampling on the energy shell corresponding to the total energy of the previous case. They investigated the dynamics for a total of seven potential-energy surfaces, including the Bunker and Hase surfaces (but for zero total angular momentum; the calculations performed by Bunker *et al.* included rotational energy). For a total energy of 200 kcal/mol they observed a factor of three enhancement in the rate of isomerization for the C-H excitation on a potential-energy surface for which the only potential couplings were stretch-stretch terms between C-H and C-N bonds. Introduction of more coupling terms resulted in no isomerizations but led to elimination

of hydrogen atoms. Their results indicate that energy from an initially excited C-H bond relaxes into the methyl bending modes and remains there for at least 5.4 ps.

At this point it is probably not possible to state with complete confidence whether the isomerization of methyl isocyanide is or is not well treated by statistical theories of reaction. Experimental results are not without ambiguity and the discrepancies observed by different groups regarding the sensitivity of the trajectory results to details of the potential energy surface do not lend themselves to strong statements as to what the situation in the actual molecule is.

Ethane. The competing dissociation reactions of the ethane molecule

$$C_2H_6 \rightarrow 2CH_3 \qquad \text{(R7.a)}$$

$$C_2H_6 \rightarrow C_2H_5 + H \qquad \text{(R7.b)}$$

have been investigated using classical trajectories by Grant and Bunker.[167] This study was carried out as an explicit test of the assumption of rapid redistribution of energy following energization of polyatomic molecules. Grant and Bunker evaluated this assumption through the use of four different excitation schemes corresponding to qualitatively different distributions of energy within the molecule. One of these methods approximated thermal distributions of energy in the same fashion as the work on methyl isocyanide carried out previously by Bunker and Hase (progressive sampling).[87] The second method consisted of excitation of all the normal mode vibrations to the same energy. The two remaining methods were designed so as to localize energy either in one of the C-H bonds or in the C-C bond. This was accomplished by excitation of small combinations of normal modes. The results of these trajectory studies were compared for three total system energies (180, 210, and 240 kcal/mol). The C-C and C-H mode sampling techniques were only used for a total energy of 210 kcal/mol. Were the assumption of rapid energy redistribution correct then each of the four techniques for

selecting initial conditions would be expected to yield approximately the same behavior. The results of their calculations indicate that the distribution of lifetimes and branching ratio of products is not independent of the initial energy distribution. Excitation of the C-H stretching mode leads preferentially to elimination of H atoms while C-C excitation increases the relative rate of CH_3 formation. In contrast to the high sensitivity of the results as a function of the scheme for approximating thermal conditions observed by Bunker and Hase in their investigation of methyl isocyanide,[87] Grant and Bunker observed good agreement between the two methods they used in their calculations for the ethane molecule. The rates calculated for unimolecular decomposition through both reaction channels were consistently lower than the results obtained from a carefully tailored RRKM calculation. As a consequence of the disagreement between $k(E)_{traj}$ and $k(E)_{RRKM}$ and the observation that k(E) was (at least for E_{tot} = 210 kcal/mol) dependent on the initial distribution of energy within the molecule, Grant and Bunker concluded that ethane is not a RRKM molecule. They suggested that a possible explanation of their result could be found in the relatively weak interaction between the C-H and C-C stretching motions of the molecule.

Si_2H_6. The dynamics of chemical vapor deposition of silicon compounds are of considerable interest to many segments of the high-tech society (for example, industries concerned diamond-film growth processes and degradation of semiconductor surfaces). As part of an ongoing series of studies on the dynamics of silicon-containing systems, Agrawal, Thompson, and Raff[211] have developed a potential-energy surface for the Si_2H_6 system, incorporating a large body of experimental and *ab initio* data into an analytic form. In addition to simple bond fissions, the potential-energy surfaces includes H-migration, and three- and four-center elimination channels. Agrawal *et al.* employed this potential-energy surface to study the unimolecular dissociation of Si_2H_6. Initial conditions were by initially partitioning zero-point energy into the normal modes

and allowing the system to evolve for a randomly chosen period of time (less than or equal to the median vibrational frequency of Si_2H_6). After this inital warm up, the excitation energy was projected onto the normal modes and the trajectory was integrated for 0.611 ps or until dissociation occurred. The range of total energies considered was 5.31 to 9.31 eV. Over the entire range of energies considered, Si-Si bond fission dominated Si-H fission. At the lower end of the energy range, hydrogen transfer followed by Si-Si cleavage to yield SiH_4 + SiH_2 was the dominant channel, followed by Si-Si bond cleavage. For higher energies, Si-Si bond cleavage became the most likely channel for dissociation. Agrawal *et al.* rationalized the results in terms of competing entropy and energy effects and semi-quantified their arguments using classical RRK theory.

Recently, Schranz, Raff, and Thompson[172] studied the unimolecular dissociation of Si_2H_6 using an efficient implementation of Monte Carlo transition-state theory. The calculations were constructed so as to only consider the seven simple bond-fission channels. If the system is statistical then the rates calculated using the transition-state theory will define upper bounds to the classical trajectory results. Schranz *et al.* discovered that, rather than yielding larger rates than the trajectory results, *the statistical calculations gave rate coefficients that were roughly one to two orders of magnitude smaller than the trajectories*. Thus, Si_2H_6 is clearly an intrinsically nonstatistical molecule.

Schranz *et al.* went one step further in their investigations of Si_2H_6.[173] They computed ensembles of trajectories at five energies in the range 5.31 to 9.31 eV using four different excitations schemes: Microcanonical excitation using the EMS algorithm,[255] random energization using projection methods,[171] and local energization of Si-H and Si-Si stretches, respectively. The results showed considerable mode specificity, with the overall rate coefficients varying by nearly an order of magnitude

depending on the initial conditions selection used. Microcanonical sampling and random distributions of energy gave nearly the same results for the overall rate of decomposition. Si-H mode excitations gave larger rates. The rate coefficients for individual processes were also quite mode specific (rates spanning nearly five orders of magnitude!). In general, excitation of the Si-Si and Si-H modes gave larger rates for the Si-Si and Si-H rate coefficients, respectively. This is not entirely unexpected due to earlier energy transfer results.[172] However, extensive mode specificity is also present for the multicenter reaction. Si_2H_6 is clearly an example of a molecule which is both intrinsically nonstatistical and capable of exhibiting mode-specific behavior.

SiH_2. NoorBatcha, Raff, Thompson, and Viswanathan have investigated the SiH_2 system.[170] They constructed a closed-form potential-energy surface that yielded fair agreement with the reported experimental data. Rate coefficients were computed for various initial conditions designed as a probe for mode specificity. The results indicated that the rates were a monotonically increasing function of energy and were insensitive to initial energy partitioning. The rate-coefficient data were well represented by RRK theory. Recently, Schranz, Raff, and Thompson reported the results of statistical calculations on SiH_2.[172] They found that the statistical calculations yielded upper bounds to the trajectory results over the entire energy range considered. Thus, SiH_2 appears to behave statistically.

Ethyl Radical. The unimolecular reaction dynamics of the ethyl radical $\cdot CH_2CH_3$ have received considerable attention from Hase and co-workers.[168,203,270,281] A global potential-energy surface was constructed for the ethyl radical system, based on an analytical fit of internal coordinate potential energy terms to small basis set *ab initio* molecular orbital calculations.[270,281] The potential-energy surface included elimination of H atoms to yield $C_2H_4 + H\cdot$, as well as intramolecular migration of H from one carbon center to the other. Potential energy terms were

attenuated appropriately through the use of switching functions as the radical underwent fragmentation or rearrangement.

Initial conditions employed in the work on the ethyl radical consisted of progressive and orthant sampling to yield random initial conditions for studies of all possible reaction channels, and barrier sampling techniques to investigate the C-H dissociation dynamics in particular. In the barrier sampling techniques one of the C-H bonds was extended to 2.0Å, which corresponds to the C-H dissociation saddle point on the potential energy surfaces used in this series of calculations. The relative velocity of the hydrogen atom was assigned a positive or negative relative velocity with equal probability. The remaining degrees of freedom were then energized using orthant sampling. Angular momentum was required to account for less than 1% of the total energy for trajectories begun with barrier excitation and less than 2% for trajectories begun with random excitation.

Random excitation calculations were performed at total energies of 100 and 150 kcal/mol. For the case of 150 kcal/mol, both progressive and orthant sampling were employed. Only orthant sampling was employed at 100 kcal/mol. Barrier sampling was used in the energy range 50 - 150 kcal/mol. Dissociation lifetimes, the angular momentum distribution of the eliminated hydrogen atom, and final impact parameter of the hydrogen atom were computed and the results were compared to theoretical predictions of RRKM theory.

The results at 150 kcal/mol using random excitation yielded dissociation rate coefficients that were roughly 10 times smaller than the RRKM calculations, but the authors attributed this effect to the use of a RRKM code that assumed harmonic behavior. At an energy of 100 kcal/mol the calculated rates are in good agreement with RRKM theory. Moreover, the ratio of k_{CH}/k_{mig} obtained from trajectory results were in reasonable agreement with the RRKM predictions. The trajectory lifetime distributions

yielded different results at different energies. For the 150 kcal/mol case the lifetime distribution was observed to be random whereas for 100 kcal/mol it was observed to be nonrandom. This effect was not significantly affected by substitution of a deuterium atom for one of the hydrogen atoms.

Comparison of translational-energy distribution for random versus barrier excitations showed that the average relative translational energies of eliminated hydrogen atoms corresponding to random excitation were approximately equal for large C-H internuclear separation, but that at the barrier (r_{CH} = 2.0Å) the barrier sampling method resulted in much lower relative translational energies than did random sampling. The authors attributed this to strong coupling between the H atom and C_2H_4 in the range r_{CH} = 2.0 - 3.0Å.

On the basis of this work on this system the authors concluded that, for energies of 100 kcal/mol, the ethyl radical is an intrinsically non-RRKM molecule. The behavior observed for E = 150 kcal/mol was taken as evidence for intrinsic RRKM behavior, although the question could not be completely resolved due to the aforementioned harmonic approximation used in their RRKM code. However, in a subsequent publication, an error in the initial conditions selection procedure of the earlier work was pointed out.[203] Correcting this error and repeating the calculations reduced the disparity in dissociation rate coefficients between trajectory and RRKM results at E = 150 kcal/mol to within a factor of four, which the authors claimed was within reason allowing for anharmonic corrections to harmonic RRKM calculations. Comparison of both sets of results indicated that the error had no effect on translational energy and angular momentum distributions of the products.

Dimethylnitramine. Dimethylnitramine, $(CH_3)_2N\text{-}NO_2$ (DMNA), is a molecule belonging to the class of systems mentioned previously for which local-mode excitation of a C-H stretch could potentially enhance the rate of a chemical process due to intimate

coupling of the C-H stretching mode to the reaction coordinate. There exist five distinct chemical decomposition reactions for the DMNA molecule. These are elimination of NO_2, scission of C-H bonds, C-N bond rupture, N-O rupture, and concerted elimination of HONO. It is this latter reaction that is of particular interest with respect to enhancement of reaction probability as a result of mode-specific excitation. The HONO elimination is thought to occur by a simultaneous lengthening of a C-H bond and shortening of the O-H internuclear separation along with a simultaneous fission of the N-N bond. By selectively depositing a large quantity of energy in a C-H local mode it may be possible to increase the rate of elimination of HONO since the C-H motion is presumably of considerable importance in the concerted elimination process.

Sumpter and Thompson[175,320] have carried out a series of studies on DMNA in which they investigate this possibility. In the first paper of the series they investigated the energy transfer in the molecule for harmonic and anharmonic potential energy functions.[28] Of primary interest to this work is the observation that energy initially deposited in a C-H local stretch transferred preferentially to both methyl groups, with the methyl group containing the initially excited C-H bond receiving the energy before the other one. Energy flow out of the initially excited C-H bond was complete within about 0.25 ps and energy flow from the methyl modes to the rest of the molecule was complete within approximately 0.5 ps. There were minor differences in the rates of initial relaxation depending upon the anharmonicity of the potential energy surface but within 0.5 ps the behavior was seen to be relatively insensitive to the form of the potential. The final paper in the series dealt with the unimolecular reaction dynamics of DMNA.[175] Fission of the N-N bond was observed to be the primary dissociation channel. However, for a potential energy surface that included the possibility of concerted HONO elimination, it was observed that local-mode excitation of a C-H bond did lead to elimination of HONO whereas an initially random distribution of energy

(obtained from Metropolis sampling) did not. Although the authors were quick to point out that the HONO elimination was a rather minor reaction channel and that their conclusions were based on a small number of trajectories, the observation of a dependence on energy localization for HONO elimination does suggest that depositing enough energy into a mode that is directly associated with the reaction coordinate can, in some cases, induce mode-specific reaction.

There is one remaining intramolecular reaction channel in DMNA which has not been treated. This is the internal isomerization resulting from internal rotation of the NO_2 group to yield the structure $(CH_3)_2N\text{-}O\text{-}N{=}O$. Subsequent work on the unimolecular dynamics of the DMNA molecule should, perhaps, include this potentially interesting reaction as it could conceivably be quite competitive with the HONO elimination channel.

Methyl Nitrite. Methyl nitrite, CH_3ONO, has been studied both experimentally[107,113] and theoretically[114]. It has a low barrier to *cis-trans* isomerization and contains methyl hydrogen atoms. For systems which possess low barriers to internal isomerization there exists the possibility that the density of states in the real molecule is low enough to hinder intramolecular relaxation and, by extension, unimolecular reaction. These characteristics make methyl nitrite an interesting candidate for investigating mode specificity.

Experiments performed to investigate the possibility of nonstatistical behavior in methyl nitrite have been carried out by Bauer and co-workers.[107,113] Bauer and True used nuclear magnetic resonance techniques to measure the rate of internal isomerization in the gas-phase molecule under thermal conditions and deduced that methyl nitrite did yield rates of isomerization that were consistent with statistical behavior.[113] They did, however, leave open the possibility that large impact parameter collisions could lead to enhancement of intramolecular relaxation over what would be observed for molecules

under collision-free environments. Indeed, in a subsequent study Lazaar and Bauer carried out experiments at low pressures and presented a pressure-dependent model that predicted second-order behavior for high pressures but first-order behavior at low pressures.[107] They then suggested that, for systems consisting of small numbers (2 - 4) of degrees of freedom, the intramolecular relaxation may not completely satisfy the RRKM assumption concerning rapid energy transfer due to weak coupling between the phase space correlating to the reaction coordinate and the "remaining" regions of phase space.

Preiskorn and Thompson have carried out a theoretical study of intramolecular energy transfer and unimolecular isomerization in the methyl nitrite molecule.[114] They presented first-order rate coefficients for both *cis* -> *trans* and *trans* -> *cis* isomerization on three different potential energy surfaces. The calculations were designed to investigate the influence of various aspects of the potential energy surfaces used (anharmonic versus harmonic, harmonic with or without coupling terms) on the rates of energy transfer and unimolecular reaction and to search for mode-specific effects arising from various kinds of initial conditions.

Selection of initial conditions was accomplished in four ways: either zero-point energies were assigned to the normal modes of vibration and a single C-H local mode was excited to a quasiclassical state, zero-point energies were assigned to the normal modes and each of the three C-H bonds were assigned energies corresponding to a quasiclassical state, all of the normal modes of vibration (except for torsion) were excited so as to partition approximately the same energy into each normal mode, or all of the excess excitation energy was assigned to the normal mode corresponding to the O-N=O bending motion.

The energy transfer results indicated that relaxation of an excited C-H local mode occurs more rapidly from anharmonic stretches than from harmonic ones, but that the

effects due to the initial conformation of the molecule (i.e. *cis* or *trans*) were minor.[114] The effect of initial conformation on the rate of isomerization was found to be of considerable significance, however, with *cis* -> *trans* isomerization occurring approximately four to five times as fast as the reverse process. Inclusion of anharmonicity in the potential led to consistently larger first-order rate coefficients at a given energy for both isomerization directions. Interestingly, the effect of nondiagonal harmonic coupling terms on the rate of isomerization in both directions (as compared to a diagonal harmonic force field) was quite small, even though exclusion of the nondiagonal force constants changed some of the normal-mode frequencies considerably.

Calculations designed to probe mode specificity as a function of initial energy distribution indicated the presence of some interesting effects. First, excitation of all of the normal modes (except torsion) yielded somewhat lower rates than did the more localized excitation schemes. Excitation of the O-N-O bending modes and excitation of C-H local modes led to rate coefficients that were similar, both being 2 - 3 times as large as those calculated for the case of excitation of all normal modes. Comparison of results obtained for excitation of a single C-H local mode to those resulting from simultaneous excitation of all three C-H local modes does not indicate any strong dependence of the behavior of rate for the harmonic potentials, but for the case of anharmonic potentials simultaneous excitation of all three C-H bonds appears to lead to somewhat smaller rates relative to excitation of a single C-H local mode. Thus, in the methyl nitrite molecule there appears to be some evidence for mode-specific rate enhancement resulting from excitation of modes that are presumably strongly coupled to the reaction coordinate (O-N=O bends) and, perhaps, as a result of excitation of single C-H local modes to high levels.

Molecules Containing Substituted Methyl Groups

1,2-Difluoroethane. In a series of recent papers, Raff and co-workers have investigated the intramolecular energy redistribution and unimolecular decomposition of the 1,2-difluoroethane system using classical trajectories.[171,209,275,299] Raff has formulated a global potential-energy surface using available experimental and theoretical data and has obtained a functional form that reproduces many known characteristics of the 1,2-difluoroethane system quite well.[275] While Raff and Graham have also considered the $C_2H_4 + F_2$ van der Waals system using this global potential energy surface,[209] this work will focus only on the unimolecular results.

The unimolecular decomposition studies were carried out in the energy range 6.0 - 9.0 eV using various methods of initial conditions selection. In the first paper on decomposition of 1,2-difluoroethane Raff employed Metropolis sampling in order to simulate a random distribution of energy over the degrees of freedom of the reactant molecule.[209] Trajectories were allowed to continue until reaction occurred or for 2.548 ps. At all energies studied, four-center elimination of HF was found to be the reaction of principal importance, although C-C and C-H bond fission were observed starting at 7.5 and 9.0 eV, respectively. RRK plots of the computed rate coefficients yielded linear behavior.

Another study of 1,2-difluoroethane dealt explicitly with mode-specific dependence of the rates of the individual processes contributing to the overall decomposition of the reactant.[171] By comparing the rates of reaction at a constant energy of 7.5 eV for trajectories begun with different initial energy distributions, Raff was able to demonstrate that initial distributions of energy play an important role in determining rates of chemical reaction in the 1,2-difluoroethane system. This was accomplished by comparing the results of the earlier work, in which the sampling of initial conditions had been totally random, with results based on two methods which

simulated i) random distribution of all energy in excess of the zero-point energy and ii) depositing zero-point energy in all normal modes followed by addition of all of the excess energy to a single mode. Examination of both the overall rate of decomposition and the rates for the individual processes indicates considerable mode specificity in the system. While the dominant process is, under all cases investigated, elimination of HF, the overall rate of reaction varies between 0.642 - 0.970 ps^{-1} depending on the means of excitation of the molecule.

On the basis of a method that precisely monitors the flow of kinetic energy in order to follow IVR in polyatomic systems, Raff has found evidence for considerable specificity in the redistribution of (initially localized) energy throughout the various vibrational modes of the 1,2-difluoroethane molecule.[299] Moreover, this relaxation-path specificity appears to be sufficiently pronounced to manifest itself in mode-specific reaction dynamics, even though the rates of mode-to-mode energy transfer are much greater than the rate of actual chemical reaction. This appears to be possible because, while energy transfer from the site of initial excitation is fast compared to chemical reaction, the energy remains in a small subset of modes of the molecule thereby allowing mode-specific effects to become theoretically observable.

Raff has shown that the 1,2-difluoroethane molecule can be made to exhibit apparent non-RRKM behavior through selective excitation of various vibrational modes. The work presented in his studies of this relatively large polyatomic system provides an example of mode-specific behavior resulting from channeling of energy into specific groups of vibrational modes for relatively long periods of time, in spite of the highly coupled nature of the potential energy surface chosen to represent the chemical system.

2-Chloroethyl Radical. Experimentalists are currently attempting to study the unimolecular decomposition of the 2-chloroethyl radical.[311] The system is of interest, in part, due to the expectation that the dissociation energies of the C-Cl and C-H bonds

on the saturated carbon have been estimated to be approximately 20 and 40 kcal/mol, respectively.[312,321] These barriers are sufficiently low that it may be experimentally possible to induce photodissociation of the radical through absorption of a single photon excitation of a C-H vibration on the radical end of the system to v = 4 or v = 5. Moreover, as the frequencies of the all of the C-H vibrations are thought to be in the usual range, the anharmonicities of the C-H bond potentials on different carbons must be considerably different, allowing for even greater selectivity.[311]

Reinhardt and Duneczky have carried out some calculations on a model of the 2-chloroethyl radical system.[304] They have attempted to determine whether mode-specific lifetime distributions can be obtained for the decomposition of the 2-chloroethyl radical as a result of selective excitation of C-H local modes on opposite ends of the system. Trajectories were calculated for excitation of individual C-H stretches to v = 5 and v = 6 and lifetimes distributions were obtained. They observed a propensity for more rapid Cl elimination when the C-H bond excited was on the same end of the molecule as the C-Cl bond, suggesting apparent non-RRKM behavior.

Sewell and Thompson have carried out calculations on the 2-chloroethyl radical system in which they investigate the effects of qualitatively very different initial conditions on the overall rate of decomposition, as well as the branching ratio of decomposition products over a wide range of energies.[56] The initial conditions employed were chosen so as to allow a comparison between results obtained for an initial distribution of energy in which i) all of the normal modes of vibration were assigned zero-point energies and a single C-H local mode on the radical end of the system was excited to an overtone state and ii) an initial distribution achieved by distributing the same total energy (as in the local-mode excitation case) uniformly over all of the normal modes of the reactant. The results of these calculations indicated that the initial distribution has virtually no effect on either the overall rate of decomposition

or the branching ratio between the decomposition products. This result, while different than that obtained by Reinhardt *et al.*, is not entirely unexpected due to the extensive potential coupling required due to the large differences in geometries and potential energy surfaces of the reactant and products.

Comparison of the work done by Reinhardt and Duneczky[304] with that of Sewell and Thompson[56] is not directly possible for two reasons. First, Sewell and Thompson did not consider excitation of C-H local modes on the chloro end of the radical, and second, details of the potential energy surface employed by Reinhardt and Duneczky were not reported. Perhaps a worthwhile calculation to allow at least partial reconciliation of these possibly disparate results would be calculation of first-order decomposition rate coefficients for excitation of C-H local modes on the chloro end of the 2-chloroethyl radical i) to v = 5 and v = 6 and ii) to energies corresponding more closely to those obtained by excitation of the C-H local mode on the non-chloro end of the system to v = 5 and v = 6 on the potential energy surface of Sewell and Thompson.

Molecules Containing Acetylenic Linkages

There have been numerous theoretical studies based on molecules containing acetylenic linkages.[126,161-162,306,313-314] One motivation for these studies is the idea that the relatively stiff carbon-carbon triple bond may act as an effective inhibitor to IVR.[126] Among the studies carried out on acetylene and its substituted derivatives there have been a few studies devoted explicitly to determining whether dissociation lifetimes are influenced by initial energy partitioning.[161-162]

Two studies on acetylenic molecules were carried out by Hase and co-workers.[161-162] The papers dealt with relative rates of energy redistribution in acetylene, chloroacetylene, and dichloroacetylene, as well as on the effects of random versus nonrandom energy distributions on the reactive lifetimes. The results indicate

that energy flow from dichloroacetylene is the fastest of three molecules considered in the work, with acetylene being the least efficient at redistributing the excitation energy. This effect, which might at first seem rather surprising, can be partially reconciled with recent work by Holme and Levine on acetylene and its deuterated derivatives.[313] They, too, observed that the acetylenic species with the heavier substituents were more effective at transferring energy between the vibrational modes of the system. This result was attributed to a more effective frequency match between the majority of the vibrational modes of the molecule as a consequence of replacing hydrogen atoms with deuterium.

The second paper dealt in detail with chloroacetylene.[162] In this work, Sloane and Hase investigated three qualitative types of initial conditions designed to probe the details of energy redistribution in chloroacetylene for total energies of approximately 133.5 kcal/mol. All initial conditions were couched in terms of the normal mode description.

In the first case energy was partitioned so as to place most of the energy in the normal mode corresponding primarily to C-C stretching. The results obtained are in accord with RRKM predictions of the percent dissociation within 1 ps.

The second distribution of energy was such that most of the energy was localized in the C-H stretching motion, with zero-point energy in the remaining normal modes (Somewhat more than zero-point energy was also allocated to the C-C mode). For this initial energy distribution the results exhibit nonstatistical behavior, with more C-H bond rupture and less C-Cl dissociation than estimated using the RRKM model employed in these studies.

In light of the result obtained for the second set of initial conditions a third set was examined. In this case 10.0 kcal/mol of the 100.0 kcal/mol localized in the C-H stretching mode was moved to the C-C-H bend in hopes of enhancing energy transfer as

a result of nonlinear motions. As a consequence of this attempt at controlling the dissociation dynamics, the authors were partially successful. They reported a decrease in the number of C-H bond dissociations (as anticipated) but no effect whatsoever on the probability of reaction through the C-Cl decomposition channel.

The potential-energy surfaces employed by Hase and co-workers[161-162] were probably over-simplifications of the potential in the real molecule. For example, they did not include any stretch-bend interaction terms in their potential, nor did they attenuate the bending interaction terms as the molecule underwent dissociation. The effect of excluding these two factors in their potential energy surface is likely to be a decrease in the rate of energy transfer and unimolecular decomposition, respectively. Nonetheless, the results obtained by these workers indicated considerable initial specificity for the propensity of one reaction to occur over another in the very early stages of relaxation (< 1 ps). However, based on the computed RRKM lifetime for chloroacetylene at 134 kcal/mol (3.3×10^{-11} sec) these workers concluded that it would be highly unlikely to observe apparent non-RRKM behavior in the chloroacetylene system.

Molecules Containing Multiple C-H Linkages
in Different Chemical Environments

The ability to selectively excite more than one C-H bond in a polyatomic molecule to levels high enough to induce chemical reaction provides the experimental physical chemist with a potentially powerful means of interrogating molecular systems in an effort to discover mode-specific effects. In such a system the possibility arises of observing a dependence of the rate of some chemical process upon spatial factors (i.e. excitation of a C-H stretching mode near to or far removed from the reaction

coordinate). A number of experiments have been carried out in an effort to ascertain whether such behavior can be effected.[74-77,90-91,304]

Allyl Isocyanide. The previously discussed overtone excitation experiments of Reddy and Berry on the methyl isocyanide molecule were followed by similar experiments by the same workers on the isomerization of allyl isocyanide.[90]

$$CH_2=CHCH_2NC \rightarrow CH_2=CHCH_2CN \qquad (R8)$$

The allyl isocyanide molecule possesses C-H bonds of three distinctly different and spectroscopically resolvable kinds. These are terminal olefinic, non-terminal olefinic, and methylenic C-H bonds, each with different fundamental vibrational frequencies (methylenic < methyl < olefinic, aryl < acetylenic).[77]

Using the same techniques as employed in the experiments on methyl isocyanide,[82] Reddy and Berry measured the overtone excitation spectra in the v = 4, 5, and 6 region for each type of C-H present in allyl isocyanide and investigated the overtone induced isomerization for each of these bands. The results of the experiments were partially in accord with statistical predictions. The calculated ratio of $k(E)_{exp}/k(E)_{RRKM}$ was approximately unity for the methylenic and non-terminal olefinic C-H modes corresponding to the v = 4 overtone state, for the terminal olefinic C-H corresponding to v = 5, and for two wavelengths for the methylenic C-H stretch in the band corresponding to v = 6. However, there appeared to be some disagreement between the prediction of the statistical treatment and the experimentally observed results for the remaining bands, with the experimentally observed rates for the methylenic and non-terminal olefinic C-H stretches being too high by a factor of approximately two for overtone excitation to v = 5, and the non-terminal olefinic stretch being too high by a factor of approximately three for excitation of the v = 6 overtone. Thus, the rates

displayed a non-monotonic increase as a function of energy and an apparent dependence (at approximately equal energies) upon the site of excitation.

All of the calculated ratios were presented on the basis of the results of a model RRKM calculation whose accuracy is uncertain within a factor of 2 - 5 over the energy range of the experiments, but an error in this aspect of the determination would only shift the assessment of which excitations lead to mode-specific isomerization rates and not the presence or absence of a mode-specific effect. On the basis of comparison of their experimental results with theoretical predictions, Reddy and Berry concluded that allyl isocyanide is probably an apparent non-RRKM molecule.

Allyl isocyanide isomerization has recently been re-investigated by Segall and Zare.[91] In their experiments, which were carried out in a manner similar to that of Reddy and Berry,[90] Segall and Zare noted that variation of the frequency of radiation within a given overtone absorption band resulted in a factor of up to 1.8 difference in the observed rate of isomerization. Segall and Zare obtained results that were in reasonable agreement with those of Reddy and Berry in that they reproduced the general behavior observed in the latter's experiments and calculated rates that were in fairly good agreement (after making a correction required due to use of a different numerical value of a parameter required in the data analysis). However, unlike Reddy and Berry, Segall and Zare were able to rationalize their data without invoking an argument involving nonstatistical behavior. Segall and Zare were able to effectively model the data for the isomerization of allyl isocyanide by assuming inhomogeneous broadening in the overtone bands. This explanation is reasonable based on the observation of significant variation of the isomerization rate within a given excitation band. Although they were not able to explain the results for the data corresponding to excitation of the $v = 5$ overtone band (due to lack of information concerning the exact value of the critical energy required for isomerization, E_0), Segall and Zare state that they do not expect

minor variations in the value of E_0 to have a significant effect on their conclusion based on the v = 6 data. Thus, Segall and Zare conclude that allyl isocyanide is probably not a non-RRKM molecule.

There have been no reported classical trajectory calculations for the allyl isocyanide system. Such calculations would be difficult to execute due to the large size of the system (10 atoms) and lack of knowledge concerning the potential energy surface. However, calculations based on a simple model of allyl isocyanide should be worthwhile as they would allow comparison between the rates of isomerization resulting from local-mode excitation of three kinds of C-H bonds present within a single molecule.

Cyclobutene. A series of experiments conceptualized with the expressed purpose of attempting to influence the rate of reaction as a consequence of excitation of various C-H local modes in polyatomic molecules was undertaken by Jasinski, Frisoll, and Moore.[74-77] The first of these experiments was directed at the isomerization of cyclobutene to yield 1,3-butadiene following single-photon excitation of C-H overtones.[76]

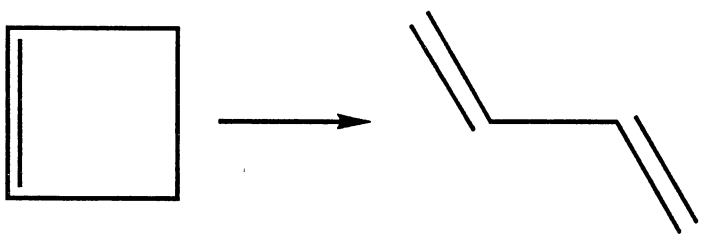

(R9)

Cyclobutene has two distinctly different types of C-H bonds with overtone transitions sufficiently separated to be selectively excited. The C-H bonds correspond to methylenic and olefinic linkages.

Jasinski *et al.* investigated the photo-induced isomerization at eight wavelengths within the v = 5 and v = 6 overtone bands. They observed only very minor deviations

in the behavior of the rate of isomerization as a function of the photon energy; the rates were observed to increase monotonically within the reported experimental uncertainty. Moreover, the reported results were well described by a RRKM calculation. Thus, Jasinski *et al.* reported no evidence for mode specificity in the ring opening isomerization of cyclobutene.

2-Methylcyclopentadiene. Following the cyclobutene study, Jasinski, Frisoll, and Moore investigated the isomerization of 2-methylcyclopentadiene.[74]

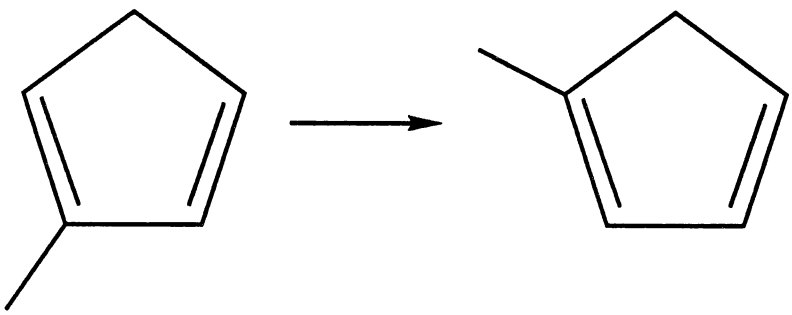

(R10)

This isomerization reaction involves the migration of a hydrogen atom from one carbon atom to another and thus, it was conjectured, excitation of the C-H stretching mode associated with the migrating hydrogen atom might result in deposition of energy in modes directly associated with the reaction coordinate with sufficient localization so as to enhance the rate of isomerization relative to that obtained for the other two types of C-H linkages present in the molecule. By selectively exciting the three types of C-H linkages (methyl, methylenic, and olefinic) to the v = 5 state Jasinski *et al.* attempted to ascertain if such mode specificity existed in the 2-methylcyclopentadiene system. Their data was consistent with statistical predictions and thus Jasinski *et al.* were forced to report another negative result in their search for mode-specific chemistry.

The result of the experiment on 2-methylcyclopentadiene deserves additional comment. The fact that the experiments are thought to localize large amounts of energy

in a mode that is almost certainly intimately involved in the reaction coordinate suggests that intramolecular relaxation out of the excited mode occurs quite rapidly and (in this case) into a number of modes. While a direct comparison cannot be made between the experimental results of Jasinski *et al.* for 2-methylcyclopentadiene and the classical trajectory result of Sumpter and Thompson on the dimethylnitramine molecule, it is worth noting that the latter workers report a possible mode-specific enhancement in the rate of HONO elimination resulting from selective excitation of the methyl C-H bonds. It seems unlikely that excitation of C-H bonds in dimethylnitramine would be as likely to induce mode-specific behavior as would excitation of the C-H bond corresponding to the migrating hydrogen atom in the 2-methylcyclopentadiene isomerization reaction. The preceding statement is made intuitively on the basis that the coupling of the C-H stretch in 2-methylcyclopentadiene to the reaction coordinate would seemingly be greater than the coupling of the C-H stretch in dimethylnitramine to the reaction coordinate for HONO elimination. Perhaps a resolution of this interesting result resides in the reported pooling of energy in the methyl modes of dimethylnitramine reported by Sumpter and Thompson.[320]

1-Cyclopropylcyclobutene. The final investigation in the experiments by Jasinski, Frisoll, and Moore dealt with the single-photon-induced isomerization of 1-cyclopropylcyclobutene to 2-cyclopropyl-1,3-butadiene.[75]

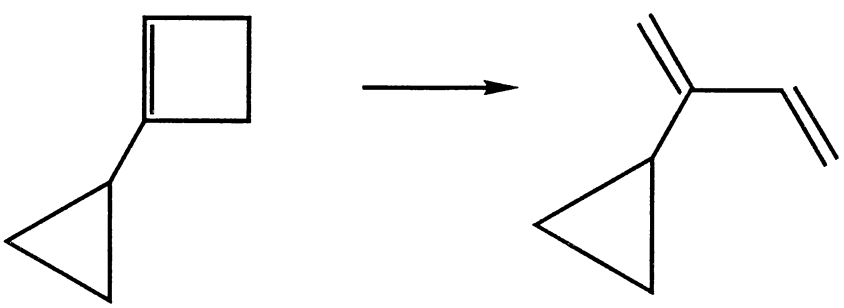

(R11)

The reactant molecule contains olefinic C-H bonds in the cyclobutene ring and methylenic C-H bonds in both the cyclobutene ring and the cyclopropenyl ring. The cyclopropenyl group should not be directly involved in the isomerization reaction and, thus, the cyclopropenyl group might be expected to act as a set of bath modes, capable of accommodating large quantities of energies initially localized in one of its C-H stretching modes. The experiment carried out on 1-cyclopropylcyclobutene investigated whether selective excitation of the methylenic C-H stretch in the cyclobutenyl ring to v = 6 would lead to a higher rate of isomerization than the corresponding excitation in the cyclopropenyl ring. The results indicated that there was no significant group-dependent effect on the rate of isomerization, suggesting that energy redistribution is complete within a few picoseconds.

1-methylcyclopropene. Baggot and Law[80] have studied the unimolecular isomerization of 1-methylcyclopropene following C-H overtone excitation.

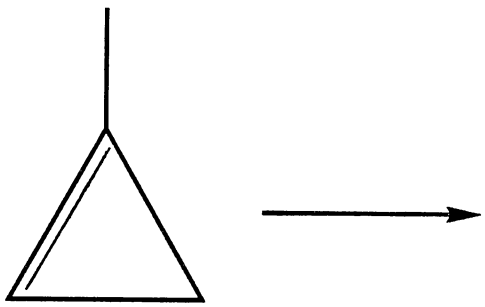

$H_3C\text{-}C{\equiv}C\text{-}CH_3$ (R12.a)

$H_2C{=}CH\text{-}CH{=}CH_2$ (R12.b)

$H_2C{=}C{=}CH\text{-}CH_3$ (R12.c)

They considered results from overtone pumping of two of the three kinds of C-H modes in the system, specifically, the methyl group C-H and the olefinic C-H modes. They measured the photoacoustic spectra in the appropriate regions of the spectrum and then accomplished photolysis by tuning a laser to the desired absorption feature. Products were determined by gas-chromatographic techniques. The excitation energies were 17090 cm^{-1} and 15619 cm-1 (excitation of the olefinic and methyl C-H mode to v=6,

respectively). The experimental measurements of the product yields were adequately reproduced (to within the accuracy of the model) by a RRKM treatment. Further, within the experimental uncertainty, there were no mode-specific effects due to excitation of C-H overtones corresponding to C-H modes in the two chemical environments considered.

Molecules Containing X-H Bonds (X = O or N)

Hydrogen Peroxide. The search for mode-specific chemical behavior has led to several studies of peroxides by experimentalists[4,93,95-96,305,315-318] and theorists[98,193,195-197,306,319]. All peroxides have an O-O-H group, and spectra resulting from overtone excitation of the O-H stretching modes in peroxides have been found to be well described by equations corresponding to one-dimensional anharmonic oscillators.[4,305] This empirical result has been exploited in experiments designed to probe systems containing this functional group to see whether they can be induced to exhibit mode specificity.

Hydrogen peroxide, H_2O_2, is the simplest peroxide. Its small size makes it attractive for theoretical studies and its small O-O bond dissociation energy makes it experimentally possible to induce photodissociation by absorption of a single photon of radiation. Moreover, the OH fragment created in the photodissociation process is readily detectable using laser induced fluorescence. Extensive studies of the photodissociation dynamics of hydrogen peroxide have been carried out by Crim and co-workers.[315-318] They have succeeded in measuring the rotational state distribution for the OH fragments generated from single-photon induced dissociation of H_2O_2. The decomposition of H_2O_2 was effected in these experiments by exciting the O-H local stretch to v = 5, 6, and 7 levels as well as by excitation of a combination band (v_{OH} +v_X). Their results were indicative of a small shift of the rotational distribution to

slightly higher energies than predicted from a statistical model. The lifetime for the decomposition of the molecule was inferred to be 5 - 50 ps.

Numerous theoretical studies of intramolecular vibrational relaxation in hydrogen peroxide have been carried out.[193,195-197,306,319] These studies have been performed using potential energy surfaces of varying complexity and a fairly complete picture of the IVR dynamics of H_2O_2 is beginning to emerge.

Calculations based on simple models of H_2O_2 have been performed by Sumpter and Thompson.[306,319] They found that energy flow out of an initially excited local O-H stretch was slow and irreversible over a wide range of energies ($v = 6$ up to $v = 14$). The time scale for relaxation of the initially excited bond was on the order of 10 ps. In a detailed calculation using a more complicated force field that included attenuation of O-O-H bending force constants Uzer, Hynes, and Reinhardt also studied the energy transfer and dissociation of hydrogen peroxide following excitation of a local-mode overtone to $v = 6$.[193] They observed complex dynamics in the intramolecular relaxation which they attributed to nonlinear resonances. The presence of the attenuation terms in the potential energy surface were found to be of considerable importance due to their effect on the frequency with which resonant effects could come into play. Namely, the introduction of the attenuation terms affected the instantaneous bending frequency as a function of the O-O bond length, thereby allowing facile energy transfer through stretch-bend coupling with a greater probability than in the absence of anharmonicity in the bending motion. The torsional mode does not appear to interact significantly with the other modes of vibration. They obtained an approximate lifetime for decomposition of H_2O_2 in the neighborhood of 6 ps.

Sumpter and Thompson have probed the effects of molecular rotation on the energy transfer and decomposition lifetime of H_2O_2 and found that the inclusion of a small amount of rotational energy results in a substantial increase in the rate of energy

flow as well as a decrease in the lifetime for dissociation.[196] The details of the partitioning of rotational energy have a notable effect on the details of the resulting IVR, with the simultaneous placement of energy in all three directions of rotation leading to the faster relaxation than when the same total energy is partitioned into only one of the rotational directions. Moreover, for the simultaneous distribution in all three degrees of rotational freedom, the rate of relaxation is observed to increase with increasing rotational energy (over the energy range studied).

A recent study by Uzer, MacDonald, Guan, and Thompson on hydrogen peroxide has yielded results indicating a strong dependence of the dissociation lifetime on the initial distribution of energy within the H_2O_2 molecule.[195] The study was carried out by including a small quantity of rotational energy , one or zero quanta of energy in the modes corresponding to the O-O stretch and O-O-H bends, and one or more quanta of excitation in the torsional mode. Additionally, an O-H local mode was excited to v = 5. The authors observe an order of magnitude difference in the observed lifetimes depending on the initial localization of energy within the molecule, with the inclusion of one quanta in the O-O stretch leading to a much shorter lifetime than the other combinations. Moreover, the inclusion of varying amounts of zero-point energy is observed to have a significant effect on the lifetimes obtained, with inclusion of increasing fractions of the zero-point energy leading to shorter lifetimes. The conclusions drawn from this set of calculations are that in small systems such as the one studied here the details of initial energy distribution can have profound influences on the subsequent dynamics, even in the presence of considerable potential energy coupling.

<u>*t*-Butyl Hydroperoxide.</u> *t*-Butyl hydroperoxide, $(CH_3)_3COOH$, contains C-H and O-H bonds on opposite ends of the molecule. The O-H bond is directly adjacent to the O-O bond reaction coordinate whereas the nine C-H bonds are separated from the reaction coordinate by an intervening C-C and C-O bond. Due to these structural

characteristics *t*-butyl hydroperoxide could, in principle, provide experimentalists with a means of selectively exciting two different X-H oscillators within a single chemical system and comparing the observed results with predictions of statistical theory. An interesting aspect of such an experiment relates to the spatial separation of the degrees of freedom of the molecule. Most of the the degrees of freedom are separated from the O-H bond due to the O-O linkage, which is also the reaction coordinate. In order for statistical behavior to result following selective excitation of the O-H bond a large fraction of the energy of excitation would be required to pass "through" the reaction coordinate without inducing chemical reaction. On the other hand, excitation of a C-H local mode to levels high enough to cause reaction would lead to an initial distribution of energy that would seemingly be more more likely to be statistically redistributed among the molecular degrees of freedom before reaction.

Zare and co-workers[95-96] and Crim and co-workers[93] have carried out experiments on the rate of dissociation of *t*-butyl hydroperoxide following selective excitation of the O-H local mode. Although the high overtones of the C-H stretch are accessible, the intensity of the spectra for these excitations are very weak and thus no direct experimental comparison of the sort mentioned above is presently possible; Crim and co-workers have reported that such experiments are being attempted.[93]

Chandler, Farneth, and Zare investigated the decomposition of *t*-butyl hydroperoxide following excitation of the O-H local mode to v = 5.[95] They measured the overtone spectra using an intracavity dye laser apparatus and photoacoustic detection device. The dissociation of t-butyl hydroperoxide following irradiation at the v = 5 overtone frequency was monitored as a function of the increase in the intensity of the absorption band corresponding to the v = 5 O-H overtone of *t*-butyl alcohol. They observed minor deviations from linearity in the Stern-Volmer analysis of their data in the high pressure region. This nonlinearity was postulated to arise from nonstatistical decay

of a small fraction (approximately 1%) of the excited molecules. Chandler *et al.* were able to successfully model this behavior using a mechanism that incorporated a small component of nonstatistical unimolecular decay. Chuang, Baggott, Chandler, Farneth, and Zare extended the work just mentioned to include the v = 6 O-H overtone excitation.[96] The techniques employed were similar, as were the results. There was once again a deviation from linearity in the Stern-Volmer analysis of the data. The authors were able to model the data in the same fashion as Chandler *et al.* but also mentioned the possibility of the nonstatistical component of the data resulting from a small fraction of the reactant species being promoted to a rapidly decaying excited electronic state. However, subsequent work in the same laboratory demonstrated that the electronic-state contribution cannot completely account for the nonstatistical contribution to the rate, suggesting the existence of a small mode-specific effect arising from pumping of the 0-5 O-H overtone.[97]

Very recently, Fleming and Rizzo[94] studied the $4\nu_{OH}$ level of *t*-butyl hydroperoxide using an optical-infrared double resonance method to collect predissociation spectra. The object of the experiment was to determine the degree of mixing of the initially prepared state with the background states. The pattern and extent of the mixing led the investigators to conclude that O-H overtone excitations in *t*-butyl hydroperoxide will yield results that are very similar to those obtained using thermal excitation.

Methyl Hydroperoxide. The large number of atoms in *t*-butyl hydroperoxide makes calculations of classical trajectories a large computational task. Recognizing that the methyl hydroperoxide molecule, CH_3OOH, contains the same fundamental linkages that make t-butyl hydroperoxide attractive for mode-specific studies, Gai, Thompson, and Fisk[98] have carried out a set of classical trajectory calculations on methyl hydroperoxide in which they investigate intramolecular relaxation and unimolecular

decomposition as a function of the initial distribution of energy. They employed a simple potential energy surface comprised of anharmonic stretches, harmonic bends, and a torsional potential represented by a truncated Fourier series. The attenuation of the O-O-H and C-O-O bending potentials as a function of the O-O bond length was accounted for through the use of switching functions.

Gai *et al.* computed ensembles of trajectories for initial conditions corresponding to excitation of either a C-H or O-H local stretch to overtone levels in the range $v_{XH} = 2 - 12$. The results for vibrational relaxation of an initially excited C-H stretch are in accord with the results of other work. Namely, relaxation of the initially excited bond is fast and irreversible on a time scale of approximately 0.2 ps. Relaxation initially occurs into the modes associated with the motion of the methyl group and only then does a significant amount of energy begin to transfer into the remaining vibrational degrees of freedom. There is a corresponding agreement between previously reported results obtained for relaxation of an excited O-H local mode.[193,306] Relaxation of the O-H local mode in methyl hydroperoxide is energy dependent but is much slower on the whole than for the case of C-H relaxation in the same molecule. There is essentially no energy transfer within 1.0 ps for an initial excitation of the O-H local mode to $v = 2$. For an intermediate excitation the rate of energy flow increases substantially but is primarily into the O-O-H bending motion (with considerable beating between these two modes). For high levels of excitation the relaxation occurs much faster and no O-H/O-O-H beating is observed.

Site-specific rate enhancements appear to be possible in methyl hydroperoxide on the basis of these classical dynamics calculations. Gai, Thompson, and Fisk[98] report an increase in the rate of decomposition of the molecule when the O-H local mode is excited rather than the C-H local mode. Under approximately isoenergetic conditions the first-order rate coefficient for O-O bond scission is roughly twice as large when the

O-H local-mode is excited. This result is not too surprising in light of the possible avenues for relaxation for the two different local modes excited in these numerical simulations. The O-H local mode is relatively isolated from the rest of the molecule and energy relaxation must initially occur through a smaller set of modes than in the case of a C-H overtone excitation, for which the large number of oscillators associated with the methyl group provide a large set of bath modes.

More recently, Chapman and Uzer[99] also computed classical trajectories for the overtone-induced fragmentation of methyl hydroperoxide. They considered seven different potential-energy surfaces that differed in the forms of the switching functions used or in the presence or absence of explicit potential-energy couplings in the force field. They considered short-time (2 ps) IVR dynamics and "long-time" (5 ps) fragmentation dynamics on the different surfaces by varying initial excitation schemes and energies. They found that, for nearly isoenergetic excitations of the C-H or O-H modes, the pathways of IVR were very different (fast initial relaxation of an initially excited C-H mode as opposed to slow relaxation of the O-H mode) but that the rates of dissociation were quite similar. The results of Chapman and Uzer are in fair agreement with those of Gai and Thompson.

It is of interest that in the experiments of Jasinski *et al.*[74-77] no evidence for mode-specific behavior was observed following selective excitation of C-H local modes in widely separated regions of molecules (some of which were considerably larger than methyl hydroperoxide) while in methyl hydroperoxide a large enhancement in the rate was observed (at least in one case)when one local mode was selectively excited over another. The fact that, for the positive result reported for methyl hydroperoxide, the local modes excited corresponded to hydrogen atoms linked to different heteroatoms may be of importance. In light of this possibility the selection of either cyclobutene or

2-methylcyclopentadiene would seem like propitious choices for further dynamics studies.

Dimethyl peroxide. Budenholzer and co-workers have investigated the unimolecular dissociation of dimethyl peroxide using classical trajectories.[322] They performed calculations on three different potential-energy surfaces to examine the influence of various factors such as anharmonicity in the stretches and explicit potential-energy coupling *via* non-diagonal force constants in the force field. The force fields were based on an experimental normal-mode analysis derived from spectroscopic information. In the case of harmonic stretches, only the dissociative O-H bond was treated anharmonically (as a Morse oscillator with D_e = 37 kcal/mol). There were some noticeable (and acknowledged) differences in the normal-mode frequencies resulting from the diagonal and non-diagonal force fields. Torsional motion was not explicitly included in any of the force fields. Initial conditions were obtained by partitioning zero-point energy along the normal modes and then exciting one of the C-H local modes to an overtone state corresponding to either a Morse or harmonic potential.

The primary emphasis of the work was to examine the effects of the various potential-energy surfaces on the IVR and dissociation rates. Budenholzer *et al.* were able to run only a limited number of trajectories for long periods of time (40 ps) and were therefore unable to accumulate quantitative lifetime data. However, they examined individual trajectories rather closely and observed that the anharmonic, diagonal force field gave the slowest rate of dissociation. The diagonal, harmonic force field appeared to give an intermediate result and the harmonic, non-diagonal force field gave noticeably faster rates of dissociation. They examined the mode energies of various (assumed) local modes as a function of time for individual trajectories and observed that the energy transfer leading to dissociation occurred "impulsively", i.e., there was not a substantial buildup of energy in the reaction coordinate until immediately before reaction occurred.

One of the more interesting results of the calculations was the observation that the introduction of anharmonicity into the stretches using Morse potentials led to *slower* relaxation of the initially prepared "state". This stands in sharp contrast to a rather large body of data which would suggest that anharmonicity in the stretches gives rise to more rapid IVR from an initially prepared state. Budenholzer[322] *et al.* attribute this result to the absence of any near 2:1 resonances for the anharmonic stretching potential at the excitation energies they considered. By contrast, the harmonic force fields gave rise to a nearly exact 2:1 resonance between the symmetric CH_3 stretch and the asymmetric deformation modes.

The work on dimethyl peroxide did not include calculations designed to probe mode-specific effects. The table of lifetimes did, however, suggest nonmonotonic behavior in the probability of reaction with respect to increasing excitation energy; but such assertions must be regarded with suspicion due to the small number of trajectories computed. Budenholzer *et al.* did, however, state in the conclusions section that work aimed towards making comparisons of the dynamics results with RRKM theory was currently under way in their laboratory.

HONO. HONO has been studied experimentally in a matrix environment and has been observed to exhibit mode-specific behavior in the rate of *cis-trans* isomerization reaction.[100-101] McDonald and Shirk[100] measured the rates of *cis-trans* interconversion in N_2 and Ar matrices and found that excitation of the O-H stretch is much more effective than excitation of the N=O stretch at inducing *trans* -> *cis* isomerization. They also noted that excitation of the O-H stretching frequency in *cis*-HONO leads to isomerization rates on the order of one hundred times faster than excitation of the analogous mode in the *trans* conformation. They attributed this effect to more efficient coupling of the O-H stretching motion in *cis*-HONO to the torsional vibration, which is the reaction coordinate in the isomerization process. Shirk and Shirk[101] compared the

rates of isomerization obtained by exciting the *cis* N=O stretch versus the *trans* O-H stretch and found that the *cis* N=O stretch led to higher rates of reaction even though the *trans* O-H excitation imparted more energy to the molecule. Based on these experiments there is significant evidence that HONO might be a prime example of a demonstrably mode-specific chemical system.

Thompson and co-workers have carried out calculations on the HONO molecule using two different potential energy surfaces.[102-103,323-324] Guan, Lynch, and Thompson[102] investigated the isomerization process using a simple potential energy surface which did not include any potential energy coupling terms or attenuation terms to account for changes in the potential energy surface and equilibrium geometrical parameters as the molecule underwent isomerization. Trajectories were run beginning in both the *cis* and *trans* conformations and for a number of different initial energy distributions. The rate of energy transfer out of an initially excited O-H local mode was found to be much slower in the *trans* conformer than in the *cis*. Additionally, the rate of *cis* -> *trans* isomerization was observed to be approximately 22 times faster than *trans* -> *cis* isomerization. However, in contrast to the experimental results,[100-101] Thompson and co-workers obtained results indicating that excitation of the N=O stretch was more efficient at inducing isomerization than was excitation of the O-H stretch. The largest computed rates of isomerization were achieved by exciting the mode corresponding to the H-O-N bend, leading the workers to surmise that this mode is most strongly coupled to the reaction coordinate. Based on the results of power spectra computed for the individual internal coordinates, Guan *et al.* concluded that the O-H stretching mode was effectively decoupled from the rest of the vibrational modes of the molecule except for very high levels of excitation.

Guan and Thompson[103] extended the calculations on the HONO molecule by formulating a more realistic potential energy surface that remedied some of the

deficiencies of their initial work. They incorporated switching functions into the potential energy surface so as to attenuate the potential energy and geometrical parameters as the molecule underwent isomerization. In some of the trajectories they added rotational energy to examine its influence on the isomerization and unimolecular decomposition processes. The results obtained using this more realistic potential energy surface were quite similar to those for the earlier work. In most cases the differences arising as a result of the changes in the potential energy surface were small, with a maximum variation of about a factor of two.

The effects of molecular rotation are found to be rather significant and strongly dependent upon the distribution of rotational energy in the molecule. For an approximately uniform initial distribution of vibrational energy the rate of isomerization is enhanced by almost a factor of seven when the rotational excitation is aligned with the axis of internal rotation. Distribution of the same total amount of energy evenly about the three axes of rotation results in a rate that is significantly larger than the case for no rotational energy, but is somewhat smaller than the case for alignment of rotational energy with the torsional motion. Assigning all of the rotational energy to the axis perpendicular to both the axis of internal rotation and the N=O bond results in a rate smaller than the rate obtained for the case of no molecular rotation at the same total energy.

Qin and Thompson[323] have incorporated a semiclassical tunneling model into the isomerization dynamics of HONO. The impetus for the work was the observations of Pimentel and co-workers in the 1960's.[325] Pimentel *et al.* reported a non-Arrhenius dependence on the rate of isomerization of matrix-isolated HONO. Specifically, they found that, below a certain temperature, the dependence of the isomerization rate became independent of temperature. Moreover, substitution of DONO for HONO at the cryogenic temperatures resulted in no isomerization. Substitution of $H^{18}ON^{18}O$ for

HONO led to a much reduced rate of isomerization. These non-Arrhenius and primary/secondary isotope effects strongly suggest the presence of tunneling effects in the isomerization process of cryogenically cooled HONO. The method Qin and Thompson used to study the role of tunneling in the *cis-trans* isomerization of HONO and, in particular, on the mode-specific effects is the "classical + tunneling model" of Waite and Miller.[144-145] The ansatz of this method is that the classical dynamics can be computed as normal but that, at appropriate times, semiclassical calculation of the tunneling probability is obtained using a simple semiclassical prescription. Accumulation of the tunneling probability as a function of time over an ensemble of trajectories leads to a rate of isomerization that can be ascribed to quantum mechanical penetration of the barrier. Using an accurate (and computationally efficient) method of treating the barrier penetration, Qin and Thompson found that the classical + tunneling results closely resembled the classical results in most (but not all) cases, i.e., the effect of tunneling was to increase the rates of isomerization, but to do so in such a way as to leave the relative rates of reaction resulting from various initial excitations largely unaffected. They rationalized the results by carefully examining the distributions of the factors that enter into the tunneling expressions (frequency of turning points along the reaction coordinate; and the energy in the reaction coordinate and effective mass terms at the turning points). They found that distributions which would seemingly facilitate tunneling correlated to initial excitations that did, in fact, give larger tunneling rates.

The results of the experimental and theoretical studies of nitrous acid lend very strong support for concluding that mode-specific behavior exists in this molecule.[100-103,324] Furthermore, the lack of sensitive dependence on the presence of coupling and attenuation terms in the potential energy surface allows a tentative statement concerning the necessity of inclusion of such factors in dynamics studies. In systems such as HONO, where the differences in the force field and geometry are relatively small for

"reactants" and "products", the attenuation terms are probably not crucial (in the absence of detailed knowledge concerning their behavior). However, the effect of such terms is demonstrably non-negligible in systems for which significant changes occur in these parameters as the system evolves from reactant to product. Finally, the qualitative agreement between the results of the work devoted to determining the influence of rotation on the dynamics of HONO and a similar study on H_2O_2[196] is pleasing. Significant effects are seen to arise as a consequence of rotational energization, but the results appear to be fairly consistent from system to system.

Hydrogen Isocyanide. Hydrogen isocyanide, HNC, is the prototype of all isocyanide molecules. However, it has never been isolated experimentally in the gas phase.[91] Nonetheless, due to the small size of the hypothetical molecule, hydrogen isocyanide has received considerable attention from theorists attempting to understand mode specificity.[163-166]

Uzer and Hynes performed calculations on a simple model of the HNC $\rightarrow$ HCN system in an effort to determine the importance of a 2:1 stretch bend resonance in directing the intramolecular dynamics of polyatomic systems.[163] The two-dimensional model used in this work consisted of a Morse potential for the H-N bond and a symmetric bending potential chosen so as to approximately yield the correct barrier height for isomerization. Thus, the C≡N bond was not explicitly included in this study.

The calculation was carried out in two parts. First, trajectories were computed for initial conditions corresponding to zero-point energy in the bend and excitation of the stretching mode to v = 7 - 13 and lifetime distributions for first crossing of the barrier were compiled as a function of the overtone level of the stretching mode. The results for this portion of the calculation yielded very interesting results that were readily explained by the authors. An identifiable 2:1 resonance between the stretching and bending degrees of freedom is present in this system for stretch excitations between v = 8 and

v = 9, suggesting that excitations in this neighborhood should result in rapid energy transfer. The trajectory calculations dramatically confirmed this prediction. Excitation of the stretch to v = 9 yielded many more reaction events than either higher or lower levels of excitation. Detuning of the resonance occurred as overtone excitations successively farther from the resonant level were considered, and the distribution of lifetimes reflected this fact, yielding many fewer reactive events in spite of the fact that the total system energy was increasing.

The second part of the calculation was performed by assigning zero-point energy to the stretching mode and exciting the bending mode to v = 19 - 21, yielding approximately the same energy as the v = 9 stretching excitation described above. The results for this set of calculations yield a monotonically increasing rate as a function of energy, a result in accordance with statistical prediction.

A considerably more detailed calculation was performed on the HNC system by Holme and Hutchinson.[164] These workers attempted to accurately model the HNC → HCN isomerization using an analytical fit to *ab initio* results. As a test of the simple model proposed by Uzer and Hynes,[163] Holme and Hutchinson first carried out calculations on a simplified version of the realistic potential. The C≡N motion was frozen and calculations were performed for excitation of the H-X bond up to v = 22. No detectable average energy flow occurred under any of these levels of excitation. The authors explained this in terms of the anharmonicity of the stretching potential. In order for resonant energy transfer to occur the required excitation of the stretching motion corresponds to a level for which the frequency is a rapidly varying function of energy. Thus, any transfer of energy induced by the resonance condition would almost immediately destroy the 2:1 resonance. While this result does not in any way detract from the work of Uzer and Hynes, it does demonstrate that a simple 2:1 stretch bend

resonance is not a pathway for rapid energy transfer leading to mode-specific behavior in HNC.

Using the full Hamiltonian, Holme and Hutchinson found that the maximum probability for reaction in HNC occurred for excitation of the local stretch to v = 9, with a decrease in probability with increasing energy, in clear contradiction to statistical predictions. They were able to demonstrate that the mechanism responsible for the nonstatistical behavior was a combination resonance effect involving a three-way coupling between the C≡N stretch, the bending motion, and the X-H stretching motions. Elimination of any one of the elements of the coupling mechanism resulted in a substantial decrease in overall reactivity.

Smith, Shirts, and Patterson[165] have carried out calculations based on the same *ab initio* potential energy surface as was used by Holme and Hutchinson. The C≡N bond length was held to a fixed value, reducing the problem to two dimensions. They used the method of adiabatic switching to select initial conditions for their trajectories and analyzed their results through the use of Poincare surfaces of section. They selected the levels of excitation of the stretching and bending motions independently using a zeroth-order separable Hamiltonian. Their results indicate that the rate of isomerization is more dependent upon the level of excitation in the bending degree of freedom than upon the total energy of the system. Isomerization was not observed for bending excitations of less than v = 6, regardless of the level of excitation of the stretching motion ($2 < v_{stretch} < 8$). For such initial conditions the trajectories were found to be quasiperiodic (as determined from the Poincare surface of section for the bending motion). For approximately the same total energy, excitation of the bending degree of freedom to v = 6 or greater leads to larger rates of isomerization. Reactive trajectories were observed to undergo a transition from quasiperiodic behavior to irregular behavior whereas trajectories that were nonreactive remained quasiperiodic. The transition was

only observed to occur for bending excitations to v = 6 or greater. Smith *et al.* suggest that this is due to a feature of the potential energy surface that correlates to an excitation of v = 6. Specifically, they propose that a sudden change in the curvature of the minimum energy path for isomerization may be responsible for the transition to chaos, and in turn, to isomerization.

The importance of the C≡N degree of freedom is once again demonstrated in a subsequent paper by Smith and Shirts.[166] In this work they included the C≡N degree of freedom that was held fixed in their earlier work. The effect of including the C≡N stretch results in a significant amount of coupling between the X-H stretch and the bending motion. They obtained results that are similar to those reported by Holme and Hutchinson[164] in that the maximum probability for prompt isomerization occurs for $v_{stretch} = 9$, with successively higher levels of stretching excitation yielding lower rates. They analyzed the dynamics using power spectra and deduced a mechanism that is in qualitative agreement with that of Holme and Hutchinson.

The hypothetical HNC system obviously exhibits mode-specific characteristics in its dynamical behavior. The rates of isomerization are not only nonmonotonically increasing with energy, but are highly sensitive to the initial distribution of energy within the molecule. The different results obtained for studies carried out on the HNC system underscore the sensitivity of the resulting dynamics to the details of the potential energy surface. The effect of coupling terms in HNC is undoubtedly magnified (compared to larger systems) as a result of the small number of degrees of freedom.

Summary

The search for mode-specific unimolecular reactions has met with only halting success. Although a few experimental results have been attributed to mode specificity, most of these results have also been explained without the necessity of invoking non-

statistical arguments. As the time resolution of experimental techniques improves it will probably become possible to make stronger statements concerning the nature of mode-specific behavior. At present, however, the general conclusion that must be drawn from the available experimental results is that mode specificity is a rather elusive phenomenon in unimolecular processes.

Theoretical investigations have been more successful at uncovering mode-specific behavior. Whether this is a result of the artificially simple potential energy functions usually employed in classical trajectory calculations is not clear. For example, the studies carried out for HNC using the best *ab initio* potential energy surface currently available have yielded results that exhibit distinct mode specificity. However, they also demonstrate the extreme sensitivity of the results to the detailed nature of the potential energy surface. These studies emphasize that the advantage gained due to the ability of theoretical calculations to probe unimolecular processes on a much finer level than experiments must always be tempered with suspicion due to the difficulties in successfully implementing the methodology.

A series of calculations on systems for which experiments have been performed seems to be in order. The negative results of the experiments of Jasinski *et al.* provide useful data that can be used for determining the utility of classical trajectory methods in simulations of the dynamics of large polyatomic systems. In particular, the experiments on 2-methylcyclopentadiene and cyclobutene should be seriously considered as starting points for classical trajectory simulations. Although formulating reasonable potential energy functions would be an extremely difficult task, the potential benefits are large. Also, perhaps somewhat surprisingly, no trajectory calculations have been performed for allyl isocyanide. The system that has stimulated so much interest in the possibility of inducing site-selective mode specificity has not yet been treated theoretically. Although there are many systems for which theoretical (classical trajectory) simulations are

warranted, these three systems should be seriously considered as important candidates for study.

CHAPTER IV

CLASSICAL TRAJECTORY STUDIES OF UNIMOLECULAR DISSOCIATION OF 2-CHLOROETHYL RADICAL

Introduction

The success of RRKM theory as a tool for predicting the rates of unimolecular reactions has been recognized for many years.[180,326] One of the fundamental assumptions of the theory is that the time required for energy randomization in an activated molecule is short compared to the reaction time of the activated species and, therefore, the rate of reaction of an energized molecule is independent of the means of excitation. The chemical-activation experiments of Rabinovitch and co-workers[63-70] were among the first to investigate the "rapid energy redistribution" assumption of statistical theories and shed light on the possible existence of mode-specific phenomena. It is now well known that energy which is selectively deposited into a particular vibrational mode of a molecule (e.g., by direct laser pumping of high-frequency X-H overtones[4,305]) will, in many cases, transfer out of that mode along well-defined pathways.[6,327-331] This fact, along with a few tantalizing experimental indications of mode specificity, has prompted continuing interest in the possibility of inducing mode-specific behavior in chemical systems.[332]

Relaxation of excited C-H stretching modes occurs quite rapidly in many molecules, often on a timescale of a few tenths of a picosecond. Furthermore, with some reported exceptions,[306,331] the decay appears to be irreversible. If this rapid,

irreversible loss of energy from the C-H bond occurs in such a way that the excess energy is quickly redistributed among most or all of the "bath modes" of the molecule then the chances of observing mode-specific behavior will be substantially decreased since it is usually necessary for a large fraction of the excitation energy to channel into the reaction coordinate. In spite of the speed with which energy decays from an excited C-H stretch, there is evidence that the relaxation usually involves fairly well-defined pathways.[89,171,175,299,320,333]

Since relaxation of C-H stretching modes occurs along specific pathways, why is mode specificity not more frequently observed for C-H overtone excitations? Part of the answer is that the upper limits to the energy that can be deposited in a molecule using single-photon C-H overtone excitations (*ca.* 50 kcal/mol) are usually just within the lower bounds of the energy required to surmount the barrier for bond-rupture reactions. Thus, if almost all of the excitation energy does not flow into the reaction-coordinate modes in the initial stages of energy redistribution, then the result is energy randomization rather than mode-selectively enhanced reaction. However, a recent study by Raff[171] indicates considerable mode specificity in the unimolecular reaction dynamics of 1,2-difluoroethane, in spite of the fact that coarse-grain energy redistribution is complete on timescales shorter than the reaction lifetimes. This evidently provides an example of how relatively long-term retention of energy in groups of modes in a polyatomic molecule can, in at least some cases, lead to mode specificity. In molecules with vibrations giving 2:1 nonlinear resonances, such as in benzene, the initial relaxation occurs preferentially into the bending modes but is then followed by efficient randomization among the active groups of normal modes. Unless the group of normal modes is closely coupled to the reaction coordinate it is improbable that the energy retained in those modes will migrate into the reaction-coordinate modes and effect chemical reaction at a rate greater than some other initial excitation. When excitation of a

methyl C-H overtone is used in an attempt to induce mode specificity in a bond-rupture reaction not directly involving the methyl group, the experiment is almost certain to meet with failure because of the initial trapping of energy within the methyl group and the relatively slow transfer of energy from the methyl modes to the rest of the molecule.

We[56] have investigated the influence of initial C-H stretch local-mode excitations on the decomposition of the 2-chloroethyl radical[304,334-344] . The study focuses on the simple bond-rupture reactions,

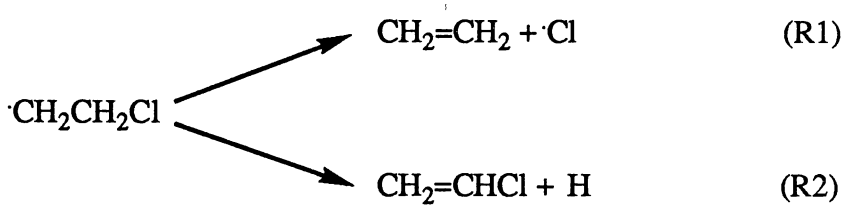

with initial excitation of a C-H stretch on the radical end of $\cdot CH_2CH_2Cl$. The reaction channels, (R1) and (R2), have dissociation energies of approximately 20 and 40 kcal/mol, respectively.[312,340,344] These low dissociation energies are such that single-photon overtone excitation of a C-H stretching mode on the radical end of the reactant is capable of depositing energy in excess of that required for fission of the C-Cl and C-H bonds of the chloromethyl group.[311] In order to determine the effect of initial localization of the excitation energy, we calculated first-order rate coefficients for a uniform distribution of energy and compared them with the results for mode-selected initial conditions designed to simulate localized C-H overtone excitations. We have used a local-mode approximation (Eq. II.33) to compute the average energy content of each of the four C-H bonds in order to monitor the flow of energy as a function of time. The dependence of the calculated rate coefficients on the initial energy distribution is rationalized in terms of the energy transfer results.

Details of the Calculations

We have treated the three-dimensional dynamics of all the atoms in the 2-chloroethyl radical in a study of the C-Cl and C-H bond-rupture reactions, (R1) and (R2). We have formulated an approximate, anharmonic potential-energy surface that is in agreement with the available theoretical spectroscopic, thermochemical, and kinetic information about the radical and reaction products. Initial conditions simulating uniform and mode-selected distributions of energy were studied for five total energies in the range $70 \leq E \leq 118$ kcal/mol. The trajectories were calculated using methods outlined in Chapter II. Thus, we give only a brief summary of the methods here.

Initial Conditions and Trajectory Calculations.

Ensembles of 200 trajectories were calculated for each set of initial conditions. Trajectories were calculated for total energies corresponding to zero-point energy plus excitation of a single C-H local mode to an overtone state (v=5, 6, 9, 12, or 14). The trajectories were numerically integrated by solving Hamilton's equations (Eqs. II.26 and II.27) in a lab-fixed Cartesian coordinate system using a fourth-order Runge-Kutta-Gill routine with a fixed stepsize of 1.22×10^{-16} s. The maximum duration of a given trajectory was 20 ps for energies corresponding to excitation of the C-H local mode to v=5, 10 ps for v=6, 9, and 12, and 1.71 ps for v=14.

We considered two qualitatively different types of initial conditions. In one case, all of the normal modes of the radical were assigned zero-point energies and a C-H local mode on the radical end of the system was excited to an overtone state. For the other type of initial conditions, a "uniform" distribution of energy was obtained by assigning each of the normal modes equal amounts of energy. The total angular momentum was zero in all of the calculations.

Analysis of the Trajectories.

Bond fission was considered to have occurred if the internuclear distance exceeded 2.25 Å or 3.42 Å for the C-H and C-Cl bonds, respectively. These criteria were chosen based on the Morse potentials, $V_M(r)$, that were used to represent the C-H and C-Cl stretches and are such that the ratio $V_M(r)/D_e = 0.95$, where D_e is the well-depth of the Morse potential. The time of dissociation was taken to be the time of the last inner turning point of the dissociating bond. Although all bond lengths were monitored throughout the trajectory calculations, only bonds of the chloromethyl moiety were observed to undergo dissociation.

First-order rate coefficients were calculated for the overall rate of decomposition for both types of initial conditions. The first-order rate coefficient, k, was obtained by fitting the trajectory lifetimes to Eq. II.28. Rate coefficients for the two dissociation channels, (R1) and (R2), were obtained by computing the ratio of the number of trajectories resulting in C-H bond fission, N_{C-H}, to the number of trajectories which ended in C-Cl bond rupture, N_{C-Cl}, and relating this ratio to the individual rates in a manner consistent with Eqs. II.29 to II.31.

Energy transfer within the 2-chloroethyl radical was monitored by computing the energy in the four C-H bonds using the local-mode approximation given in Eq. II.33. Averages of the C-H local-mode energies were computed for ensembles of trajectories corresponding to both types of initial conditions.

Potential Energy Surface

The first step in the formulation of the potential-energy surface was to adjust the parameters of diagonal force-field potentials to achieve good agreement with theoretical normal-mode frequencies for the 2-chloroethyl radical,[312] and the experimental normal-

mode frequencies for ethene[345] and chloroethene[346]. Having accomplished this, the next step was to develop reasonable switching functions that smoothly connect the potentials of the reactant and product species.

Form of the Potential-Energy Surface. The potential-energy surfaces for the reactant and products were written as a sum of potential terms for the bond stretching, angle bending, and torsional motions. There are six stretching terms, nine angle bending terms, four wag-angle bending terms, and six dihedral terms in the potential. No non-diagonal terms are included in the potential-energy surface.

Stretches were represented by Morse functions,

$$V_M=D_e\{[1-\exp(-\alpha(r-r_o))]\}^2, \qquad \text{(IV.1)}$$

where D_e is the dissociation energy, α is the curvature parameter, and r_o is the equilibrium bond length. (The form of this potential differs from the one given in Eq. II.2 by a constant value of D_e. The asymptotic value of Eq. II.2 is zero whereas Eq. IV.1 approaches $+D_e$ for large r.) The bends (valence and wag angles, θ and γ, respectively) were approximated as harmonic oscillators, Eq. II.4. The torsional potentials were represented by six-term cosine series, Eq. II.6, with the a_i adjusted to give the correct torsional frequency and barrier to internal rotation. As discussed below, the torsional potential was used only in the product molecules. There were no nondiagonal terms in the force field.

Geometry of Reactant and Products. The numerical designations of the atoms and the definitions of the bonds and bond angles are given in Fig. 1. Equilibrium geometrical parameters for 2-chloroethyl radical, ethene, and chloroethene are given in Table I. There have been several calculations of the equilibrium geometry of 2-chloroethyl radical.[312,338-339,342-343] The structure used here is that reported by Schlegel and Sosa.[312] The equilibrium structure of ethene is taken from Raff[275] and the

equilibrium geometry of chloroethene is based on the experimental structure reported by Kivelson and Wilson.[347] Experimentally, it has been determined that the geminal C-C-H bond angles of the chloroethene molecule have slightly different equilibrium values, as do the geminal C-H bonds.[347] Since these differences are small, we have taken the geminal C-C-H angles in chloroethene to be the same as in ethene and have used the average of the experimental values for the equilibrium geminal C-H bond length.

Development of the Force Fields. The force field for the 2-chloroethyl radical was obtained by adjusting the parameters to fit (unscaled) *ab initio* normal-mode frequencies.[312] Then, the bond-stretching parameters were scaled by 0.9 and angle-bending parameters by 0.8. These scale factors are comparable to those used by others[278-280], and were found to give a fairly uniform (by about 10%) reduction in the values of all the normal-mode frequencies. Since the barrier to rotation about the C-C bond in the 2-chloroethyl radical has been reported to be 2 to 4 kcal/mol,[312,336,339,341] the radical was treated as a free rotor.

Force-field parameters for the ethene and chloroethene molecules were adjusted such that the calculated normal-mode frequencies are in good agreement with experimental values.[345-346] The barrier to internal rotation in ethene is between 60 and 65 kcal/mol.[348-352] We used the same value (63 kcal/mol) as used by Hase *et al.*[270] in their studies of the ethyl radical. The Fourier coefficients for the torsional potential of ethene and chloroethene were fit to give this barrier height. We assumed that the barrier to internal rotation for chloroethene is the same as for ethene. Force-field parameters for the 2-chloroethyl radical, ethene, and chloroethene are given in Table II. *Ab initio*, unscaled, and scaled normal-mode frequencies for the 2-chloroethyl radical are given in the first three columns of Table III, followed by the calculated and experimental normal-mode frequencies for ethene and chloroethene.

Figure 1. (a) Definition of bonds and three atom bond angles in the 2-chloroethyl radical.(b) Numerical designation of atoms used to define wag angles and dihedral angles in the 2-chloroethyl radical.

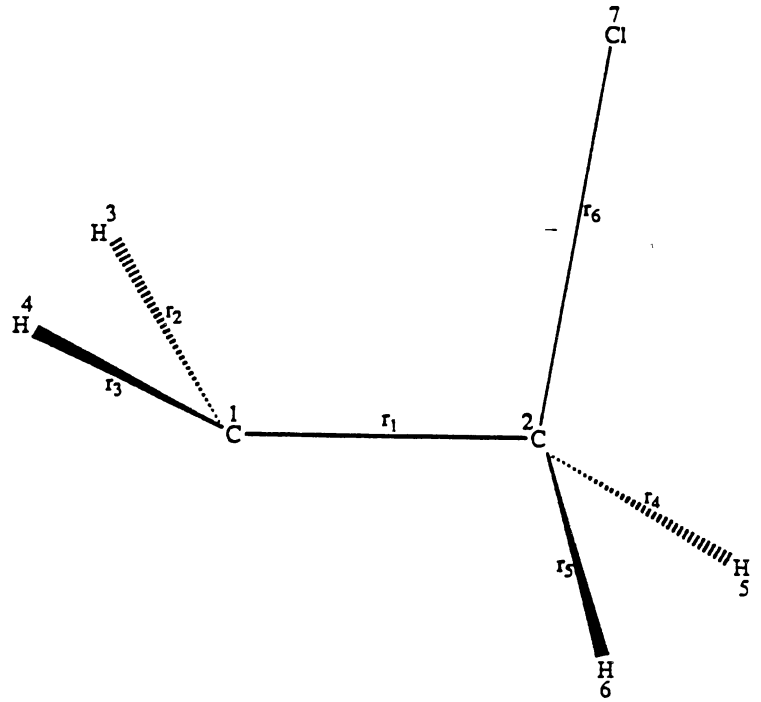
7
Cl
r6
3
H
r2
4
H
r3
1
C
r1
2
C
r4
H
5
r5
H
6

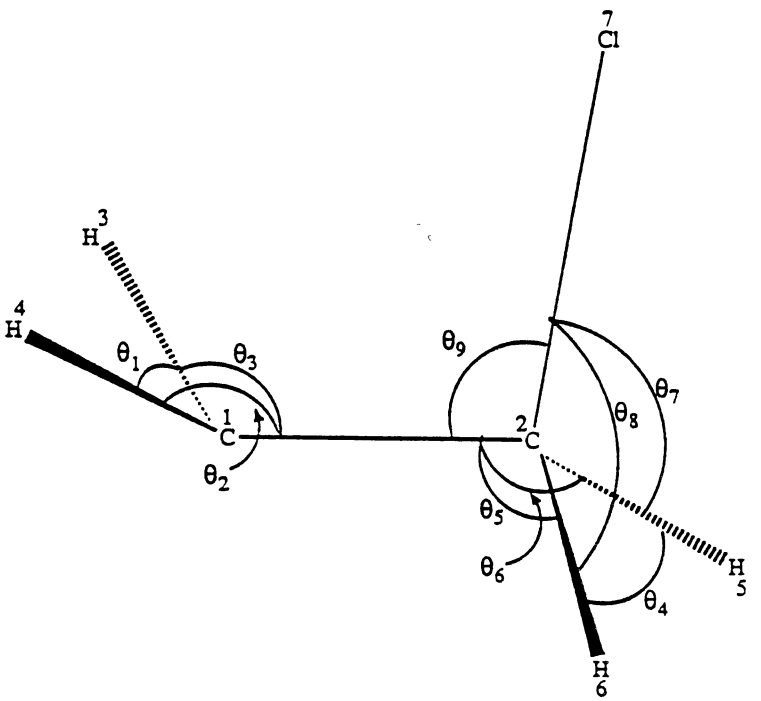
7
Cl
3
H
4
H
θ1
θ3
θ9
θ7
θ8
1
C
2
C
θ2
θ5
θ6
H
5
θ4
H
6

Table I. Equilibrium Geometrical Parameters for 2-chloroethyl Radical (PES-I).[a]

Coordinate		Molecule		
Bond Number[b]	Bond Type	2-Chloroethyl Radical[c]	Ethene[d]	Chloroethene[e]
1	C-C	1.4508	1.353	1.332
2	C-H	1.0708	1.071	1.084[f]
3	C-H	1.0708	1.071	1.084[f]
4	C-H	1.0723	1.071	1.079
5	C-H	1.0723	1.071	-------
6	C-Cl	1.9799	-------	1.728
Angle Number	Angle Type			
1	H-C-H	118.2606	120.04	120.04
2	H-C-C	120.3040	119.98	119.98
3	H-C-C	120.3040	119.98	119.98
4	H-C-H	112.1544	120.04	---------
5	C-C-H	115.3499	119.98	123.80
6	C-C-H	115.3499	119.98	---------
7	H-C-Cl	101.5368	--------	---------
8	H-C-Cl	101.5368	--------	113.90
9	C-C-Cl	108.8985	--------	122.30
Wag Number	X-Y-Z--W[g]			
1	3-1-4--2	10.4432	0.0	0.0
2	5-2-6--1	39.8985	0.0	----
3	7-2-5--1	53.2494	----	----
4	7-2-6--1	-53.2494	----	0.0
Dihedral Number	W-X-Y-Z--A-B[h]			
1	5-2-1-3--6-3	-29.5191	0.0	----
2	6-2-1-4--5-2	29.5191	0.0	0.0
3	6-2-1-3--5-3	-162.849	180.0	180.0
4	5-2-1-4--6-2	162.849	180.0	----
5	7-2-1-3--9-3	83.816	-------	0.0
6	7-2-1-4--9-2	-83.816	-------	180.0

[a] Distances are in Å and angles are in degrees.

[b] See Fig. 1.

[c] Theoretical results from Schlegel and Sosa, Ref. 312.

[d] Values given by Raff, Ref. 275.

[e] Experimental results from Kivelson and Wilson, Ref. 347.

[f] Experimentally, the two C-H bond lengths were found to differ by 0.012 Å. The value used is the average of the two experimental values.

[g] Atom W is the wagging atom and atom Y is the anchor atom.

[h] W, X, Y, and Z are the atoms required to define the dihedral angle. A and B are bond angles.

Table II. Force-field Parameters for 2-chloroethyl Radical (PES-I).

	2-Chloroethyl Radical		Ethene		Chloroethene	
Morse Parameters[a]						
Bond Type	D_e	α	D_e	α	D_e	α
C-C	90.514	1.9111	148.835	1.905	148.8350	1.8500
·C-H	111.670	1.8304	----------	-------	----------	--------
C-H	35.000[b]	3.2175	116.4137	1.777	116.4137	1.7895
C-Cl	20.000[b]	2.6325	----------	-------	84.0000[c]	1.7743
Harmonic Force Constants						
Angle	Force Constant (kcal mol^{-1} rad^{-2})					
H-·C-H	54.1222		--------		----------	
H-·C-C	66.2133		--------		----------	
H-C-·C	92.1229		--------		----------	
H-C-H	51.8191		39.22		28.7884	
H-C-C	----------		108.75		86.3652[d]	
					115.1536[e]	
H-C-Cl	93.2744		---------		48.9403	
·C-C-Cl	161.215		---------		----------	
C-C-Cl	--------		---------		142.5025	
Wag Angle						
1	4.6061		15.9056		15.0000	
2	0.0000		15.9056		----------	
3	0.0000		----------		----------	
4	0.0000		----------		11.2500	

Fourier Coefficients[f] (kcal/mol)

	a_0	a_2	a_4
Ethene	6.7344	-7.9375	1.2031
Chloroethene	6.8125	-7.9375	1.1250

[a] Unless otherwise indicated, all D_e values were taken from Raff, Ref. 275; units are kcal/mol and $Å^{-1}$.

[b] Values taken from Schlegel and Sosa, Ref. 312.

[c] R.T. Morrison and R.N.Boyd, *Organic Chemistry*, 4th ed. Allyn and Bacon, Inc., 1983.

[d] Angles involving ·H atoms on Carbon atom #1 (see Fig. 1).

[e] Angle involving ·H atom on Carbon atom #2 (see Fig. 1).

[f] The 2-chloroethyl radical was treated as a free rotor.

Table III. Theoretical, Experimental, and Calculated Normal-mode Frequencies for 2-chloroethyl Radical, Ethene, and Chloroethene.

Frequency (cm^{-1})

2-Chloroethyl Radical			Ethene		Chloroethene	
ab initio[a]	unscaled[b]	calculated[c]	experimental[d]	calculated	experimental[e]	calculated
309	----[f]	----[f]	826	824	395	397
316	321	287	943	881	620	493
415	459	412	949	1011	720	733
707	706	634	1073	1072	896	865
860	887	792	1220	1181	941	977
1113	1096	984	1342	1343	1030	1077
1124	1103	985	1444	1461	1279	1153
1323	1351	1208	1630	1656	1369	1376
1372	1368	1224	3021	2995	1608	1608
1602	1570	1403	3026	3015	3030	3018
1648	1682	1506	3103	3112	3086	3084
3319	3315	2992	3105	3129	3121	3136
3326	3328	3030				
3400	3421	3080				
3433	3440	3141				

[a] Schlegel and Sosa, Ref. 312.

[b] Best fit to the *ab initio* frequencies.

[c] The bending force constants were scaled by 0.8 and the Morse curvature parameters were scaled by 0.9.

[d] Duncan, McKean, and Mallison, Ref. 345.

[e] Gullikson and Nielsen, Ref. 346.

[f] The 2-chloroethyl radical was treated as a free rotor.

Attenuation of the Potential-energy Surface. Switching functions were employed to smoothly connect the potential-energy surface and geometrical parameters for the 2-chloroethyl radical to those for the ethene and chloroethene molecules. The switching function employed is of the form[284]

$$S(r)=1-A\tanh[B(r-r^R)(r-C)^n], \qquad \text{(IV.2)}$$

where r is the bond length governing a particular switching function, r^R is the equilibrium bond length of the bond in the reactant molecule, and A is a dimensionless constant that depends upon both the parameter being attenuated and the length of the bond on which the switching function depends. The parameters B, C, and n were adjusted to fix the rate at which S(r) changes between the asymptotic limits. The values of the constants B, C, and n are 3.0×10^{-5} $Å^{-17}$, -0.08 Å, and 16, respectively, for switching functions defined in terms of C-H bonds, and 1.06×10^{-6} $Å^{-13.6}$, -3.0×10^{-3} Å, and 12.6, respectively, for the switching functions governed by the C-Cl bond. The purpose of the parameter A is to regulate the asymptotic limit of the switching function as the magnitude of the coordinate r changes and to simplify the simultaneous treatment of the three reaction channels. The instantaneous value of a parameter x ($x = D_e$, α, r_o, f, γ_o, θ_o, and a_i) is given by

$$x=x^P-(x^P-x^R)S(r), \qquad \text{(IV.3)}$$

where the superscripts R and P denote reactant and product, respectively.

For small, and negative, $r-r^R$, the switching functions controlled by bond r approach unity. As $r-r^R$ becomes large, the switching functions approach the asymptotic limit appropriate to the product being formed. Plots of the switching functions $S(r_{C-Cl})$ and $S(r_{C-H})$ are given in Figs. 2 and 3, respectively. In both cases the coefficient A (see Eq. IV.2) is unity. Schlegel and Sosa[312] have reported calculations that indicate that

Figure 2. Plot of the switching function used to attenuate molecular parameters as a function of the C-Cl bond length. The constant A is set to unity.

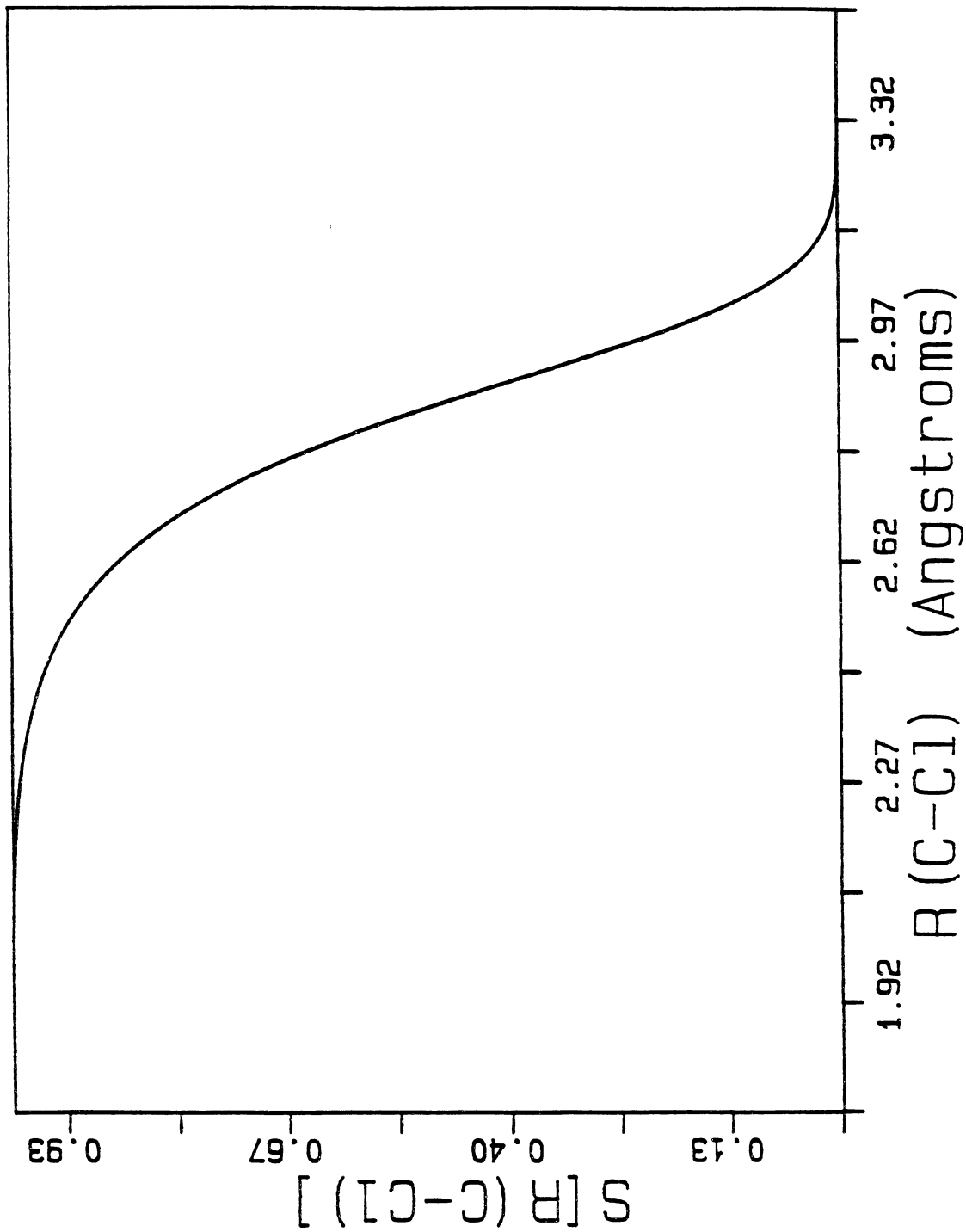
S [R (C-Cl)]
0.13
0.40
0.67
0.93
1.92
2.27
2.62
2.97
3.32
R (C-Cl) (Angstroms)

Figure 3. Plot of the switching function used to attenuate molecular parameters as function of the C-H bond length. The constant A is set to unity.

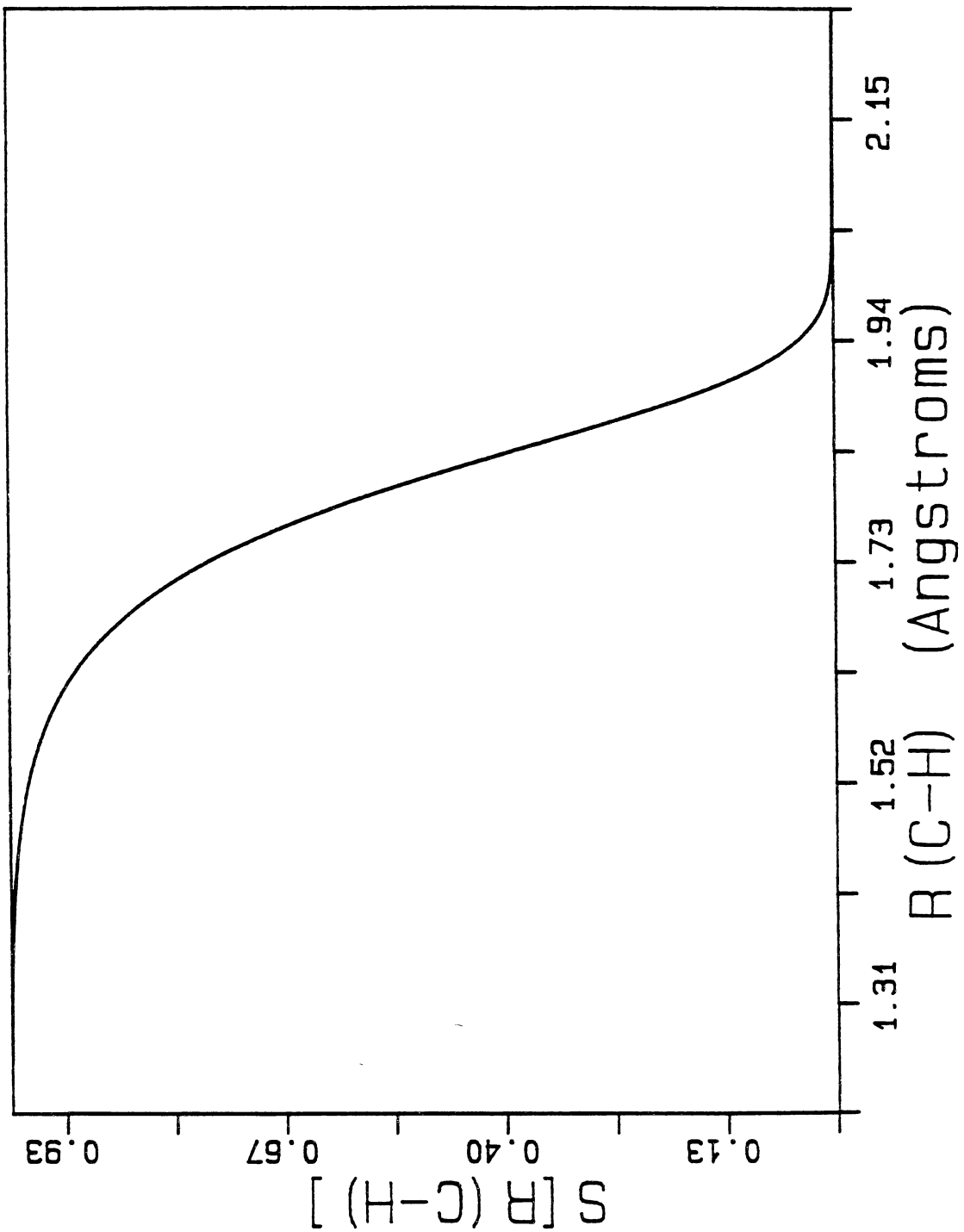
S [R (C-H)]
0.13
0.40
0.67
0.93
1.31
1.52
1.73
1.94
2.15
R (C-H) (Angstroms)

when the C-Cl internuclear distance is 2.6 Å the molecular geometry is nearly the same as in the ethene molecule. For C-H bond distances greater than 2.0 Å the geometry closely resembles that of chloroethene. The rate of attenuation in our potential is somewhat slower than is implied by Schlegel and Sosa for ·Cl elimination but is quite reasonable for C-H bond rupture. *Ab initio* molecular orbital calculations have been performed for the H_2CCH_2F --> H_2CCHF + ·H system by Kato and Morokuma.[353] They examined the variations of some of the molecular parameters with extension of the C-H bond and found that the domain over which the individual parameters changed is relatively invariant. Thus, due to the lack of detailed knowledge concerning how individual potential and geometrical parameters vary in the 2-chloroethyl radical as a C-H or C-Cl bond undergoes dissociation, all parameters were attenuated using values for the constants B, C, and n that depended only on the nature (i.e., C-H or C-Cl) of the dissociating bond.

The overall attenuation of the potential is accomplished by defining three independent sets of switching functions, $\{S(r_4)\}$, $\{S(r_5)\}$, and $\{S(r_6)\}$. The bonds (r_4, r_5, and r_6) are the two C-H bonds and the C-Cl bond, respectively (see Fig. 1). The instantaneous value of some molecular parameter x depends simultaneously on the values of r_4, r_5, and r_6:

$$x=x^P-(x^P-x^R)S(r_4)S(r_5)S(r_6). \qquad \text{(IV.4)}$$

When either of the three bonds that regulate switching functions undergo dissociation, the potential parameters (including those for the other two potentially reactive bonds) are attenuated to values appropriate for the product. If the differences between the reactant and product equilibrium bond lengths for the two remaining reaction-coordinate bonds are sufficiently small, then the attenuation of the potential are dominated by the set of switching functions defined in terms of the dissociating bond, with the two remaining

sets of switching functions having little effect (i.e., as reaction occurs only one of the factors in the product in Eq. IV.4 deviates substantially from unity). The differences between reactant and product equilibrium bond lengths for the relevant bonds are small enough that they can be neglected.

The values of the A parameters in Eq. IV.2 for each of the three dissociation channels were obtained in terms of the equilibrium geometries and force-field parameters of the 2-chloroethyl radical and the ethene molecule. Thus, the parameters x^R and x^P appearing in Eq. IV.4 were taken to be the equilibrium values for the 2-chloroethyl radical and ethene molecule, respectively. Hence, the constants A are unity for C-Cl dissociation (except in a small number of cases to be discussed below). The values of the constants A for the two C-H bond-rupture channels were obtained by solving for $S(r_{C\text{-}H})_\infty$ in the equation

$$z^P=x^P-(x^P-x^R)S(r_{C\text{-}H})_\infty. \qquad \text{(IV.5)}$$

Here, z^P is the value of a molecular parameter in chloroethene (corresponding to the parameters x^R and x^P in the 2-chloroethyl radical and ethene) and $S(r_{C\text{-}H})_\infty$ is the asymptotic limit of the switching function for the particular parameter under consideration. Using the explicit form of $S(r_{C\text{-}H})$ and Eq. IV.5 gives

$$1-A\tanh(B(r-r^R)(r-B)^n)=(z^P-x^P)/(x^R-x^P). \qquad \text{(IV.6)}$$

As $r_{C\text{-}H}$ becomes large, $\tanh(B(r-r^R)(r-b)^n)$ approaches unity. Thus, the desired value for A is

$$A=1-(z^P-x^P)/(x^R-x^P). \qquad \text{(IV.7)}$$

This is based on the requirement that the differences in the reactant and product equilibrium bond lengths be small for the bonds controlling the switching functions

since there is really a product of three switching functions in Eq. IV.5. If the difference is sufficiently small, then the two remaining switching functions can be suppressed (as in Eq. IV.5) since they will have values close to unity.

There is a complication in this formulation because the dissociating bond does not have an attenuating effect on itself and, as a consequence, some of the equilibrium parameters for the 2-chloroethyl radical and ethene are the same, rendering Eq. IV.5 inadequate. This difficulty was circumvented by "redefining" some of the x^p, which are the equilibrium parameters for the ethene molecule. The values of the affected A parameters for C-Cl dissociation are then determined in the same way as were those for C-H dissociation. The values of the A parameters for all three reaction channels are given in Table IV.

Figures 4 and 5 show the effect of C-Cl bond rupture on one of the torsional potentials and on the potential of one of the chloromethyl C-H bonds, respectively. The horizontal axis in Fig. 4 is the dihedral angle, the axis projected into the page is the C-Cl bond length, and the vertical axis is the torsional potential. The dihedral angle is a free rotor in the reactant (region A). As the C-Cl bond length increases the torsional potential varies with the value of the dihedral angle (region B). As the C-Cl bond length becomes sufficiently large the torsional potential assumes the form for $H_2C{=}CH_2 + \cdot Cl$ (region C).

Figure 5 is a contour plot demonstrating the attenuation of the potential of one of the chloromethyl C-H bonds as a function of the C-Cl bond length. The horizontal and vertical axes are the C-H and C-Cl bond lengths, respectively. The contours represent the potential energy of the C-H bond as as a function of its extension and that of the C-Cl bond. Variation of the C-Cl bond length results in an attenuation of r_o, D_e, and α for the C-H bond. The figure illustrates that the equilibrium bond length changes by only a small amount (region A). However, the well depth and curvature of the C-H stretching

Table IV. Switching Function Parameters for 2-chloroethyl Radical (PES-I).

Constants appearing in argument of tanh function (Eq. IV.2)

$B_{C\text{-}H} = 3.0 \times 10^{-5}$ Å^{-17}	$C_{C\text{-}H} = -0.08$ Å	$n_{C\text{-}H} = 16.0$
$B_{C\text{-}Cl} = 1.06 \times 10^{-6}$ Å$^{-13.6}$	$C_{C\text{-}Cl} = -0.003$ Å	$n_{C\text{-}Cl} = 12.6$

Reaction-channel- and parameter-dependent constants, A (Eq. IV.2)

	Reaction Channel		
Attenuated Parameter	Bond Four (C-H)	Bond Five (C-H)	Bond Six (C-Cl)
Eq. Bond Length			
r_1^o	1.214723926	1.214723926	1.0
r_2^o	66.0	66.0	1.0
r_3^o	66.0	66.0	1.0
r_4^o	0.0	-5.153846154	1.0
r_5^o	-5.153846154	0.0	1.0
r_6^o	0.257067048	0.257067048	0.0[a]
Angle Number			
θ_1^o	1.0	1.0	1.0
θ_2^o	1.0	1.0	1.0
θ_3^o	1.0	1.0	1.0
θ_4^o	-2.8094655	-2.8094755	1.0
θ_5^o	1.825036176	-5.475022138	1.0
θ_6^o	-5.475022138	1.825036176	1.0
θ_7^o	1.0	-1.071631648	1.0
θ_8^o	-1.071631648	1.0	1.0
θ_9^o	-0.709130354	-0.709130354	1.0
Wag Number			
γ_1^o	1.0	1.0	1.0
γ_2^o	-0.408570727	-0.408570727	1.0
γ_3^o	0.657343556	-7.864758523	1.0
γ_4^o	-7.864758523	0.657343556	1.0

Table IV continued,

Dissociation Energy			
$D_{e,1}$	1.0	1.0	1.0
$D_{e,2}$	1.0	1.0	1.0
$D_{e,3}$	1.0	1.0	1.0
$D_{e,4}$	0.0	1.0	1.0
$D_{e,5}$	1.0	0.0	1.0
$D_{e,6}$	2.1333333333	2.1333333333	0.0[b]
Morse Parameter			
α_1	10.01639344	10.01639344	1.0
α_2	0.840650894	0.840650894	1.0
α_3	0.840650894	0.840650894	1.0
α_4	0.0	0.991294828	1.0
α_5	0.991294828	0.0	1.0
α_6	1.356895652	1.356895652	0.0[c]
Force Constant f_θ			
$f_{\theta,1}$	1.700004026	1.700004026	1.0
$f_{\theta,2}$	0.473753253	0.473753253	1.0
$f_{\theta,3}$	0.473753253	0.473753253	1.0
$f_{\theta,4}$	4.112920764	4.112920764	1.0
$f_{\theta,5}$	1.397543769	-5.540527212	1.0
$f_{\theta,6}$	-5.540527212	1.397543769	1.0
$f_{\theta,7}$	1.0	0.475308552	1.0
$f_{\theta,8}$	0.475308552	1.0	1.0
$f_{\theta,9}$	0.116071706	0.116071706	1.0
Force Constant f_γ			
$f_{\gamma,1}$	0.919854861	0.919854861	1.0
$f_{\gamma,2}$	0.0	0.0	1.0
$f_{\gamma,3}$	0.0	11.25	0.0[d]
$f_{\gamma,4}$	11.25	0.0	0.0[d]
Dihedral Angle			
τ_1			
a_0	0.0	1.011597173	1.0
a_2	0.0	1.0	1.0
a_4	0.0	0.93508436	1.0
τ_2			
a_0	1.011597173	0.0	1.0
a_2	1.0	0.0	1.0
a_4	0.935084365	0.0	1.0

Table IV continued,

τ_3				
	a_0	1.011597173	0.0	1.0
	a_2	1.0	0.0	1.0
	a_4	0.935084365	0.0	1.0
τ_4				
	a_0	0.0	1.011597173	1.0
	a_2	0.0	1.0	1.0
	a_4	0.0	0.935084365	1.0
τ_5				
	a_0	1.0	1.0	0.0[e]
	a_2	1.0	1.0	0.0[f]
	a_4	1.0	1.0	0.0[g]
τ_6				
	a_0	1.0	1.0	0.0[e]
	a_2	1.0	1.0	0.0[f]
	a_4	1.0	1.0	0.0[g]

[a] r_6^P is set to 1.0Å and the switching function coefficients are adjusted so as to yield the correct equilibrium C-Cl bond lengths in all products.

[b] $D_{e_6}^P$ is set to 50.0 kcal/mol and the switching function coefficients are adjusted to yield the correct dissociation energies for all reaction products.

[c] α_6^P is set to 2.0 $Å^{-1}$ and the switching function coefficients are adjusted to yield the correct curvature parameter for all reaction products.

[d] $f_{\gamma,6}^P$ is set to 1.0 kcal mol^{-1} rad^{-2} and the switching function coefficients are adjusted to yield the correct wag angle harmonic force constants for γ_3 and γ_4 for all reaction products.

[e] a_0^P is set to 6.8125 kcal/mol and the switching function coefficients are adjusted to yield the correct Fourier coefficients for all reaction products.

[f] a_2^P is set to -7.9375 kcal/mol and the switching function coefficients are adjusted to yield the correct Fourier coefficients for all reaction products.

[g] a_4^P is set to 1.125 kcal/mol and the switching function coefficients are adjusted to yield the correct Fourier coefficients for all reaction products.

Figure 4. Torsional potential (kcal/mol) for one of the dihedral angles as a function of the C-Cl bond length.(Å). All variables other than the dihedral angle and C-Cl bond length are frozen at their equilibrium values. Region A corresponds to the 2-chloroethyl radical. Region B corresponds to a C-Cl bond length substantially larger than its equilibrium value. Region C corresponds to C_2H_4 + ·Cl.

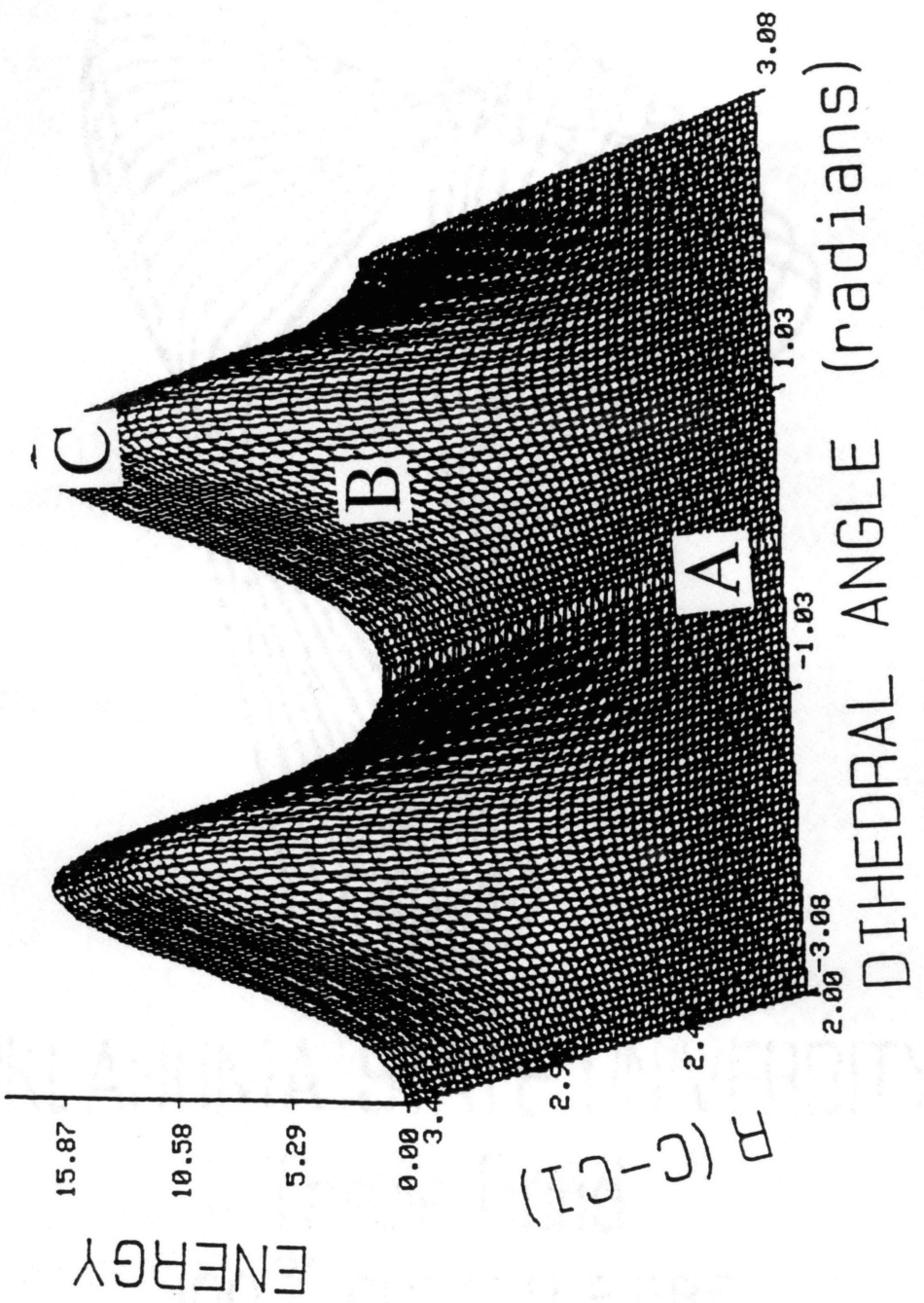
ENERGY
15.87
10.58
5.29
0.00
3.4
2.9
2.4
2.00
C
B
A
-3.08
-1.03
1.03
3.08
DIHEDRAL ANGLE (radians)
D (C-C1)

Figure 5. Contour plot illustrating the effect of ·Cl elimination on the potential-energy function for one of the reactive C-H bonds. The contour denoted by "A" shows the location of the minimum potential energy in the C-H bond as the molecule decomposes through the C-Cl channel. Region B corresponds to the energy required to rupture a C-H bond in the reactant molecule. Region C shows the potential in transition from that of the reactant species to that of ethene. Region D corresponds to the C-H stretching potential for loss of ·Cl. Distances are in Å and energies are in kcal/mol.

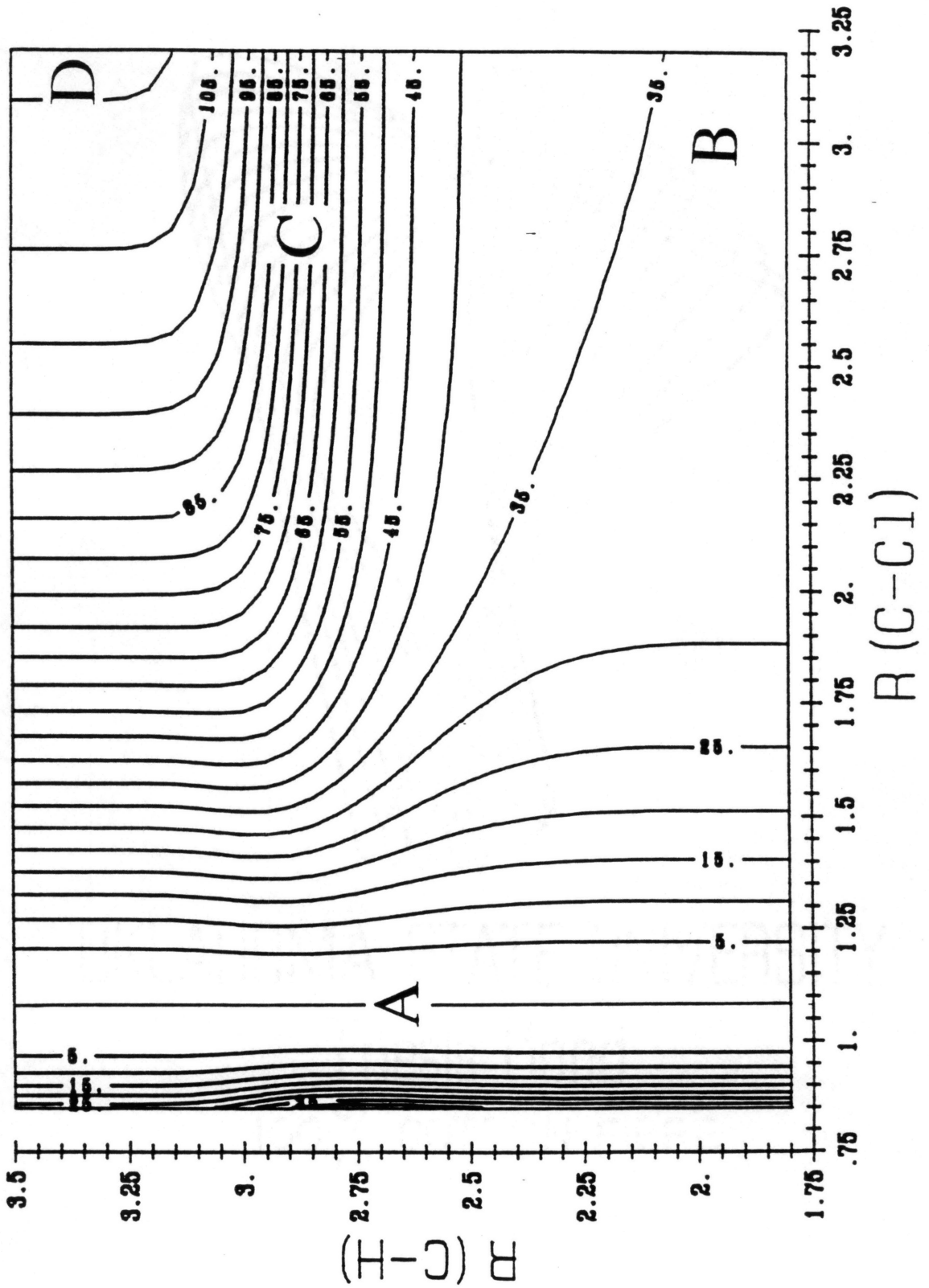
D
C
B
A
105.
95.
85.
75.
65.
55.
45.
35.
25.
15.
5.
R (C-Cl)
D (C-H)
.75
1.
1.25
1.5
1.75
2.
2.25
2.5
2.75
3.
3.25
1.75
2.
2.25
2.5
2.75
3.
3.25
3.5

Figure 6. Plot showing the behavior of the dissociation energy for the C-C bond as a simultaneous function of the C-Cl and C-H bond length in the 2-chloroethyl radical. The actual energies are ten times those shown in the Figure. Region A corresponds to the equilibrium well depth of the C-C bond in the reactant. Regions B and C correspond to the equilibrium well depths in the ethene and chloroethene molecules, respectively. Region D shows the behavior in the (energetically disallowed) event that the C-Cl and C-H bonds undergo simultaneous dissociation. Distances are in Å and energies are in kcal/mol.

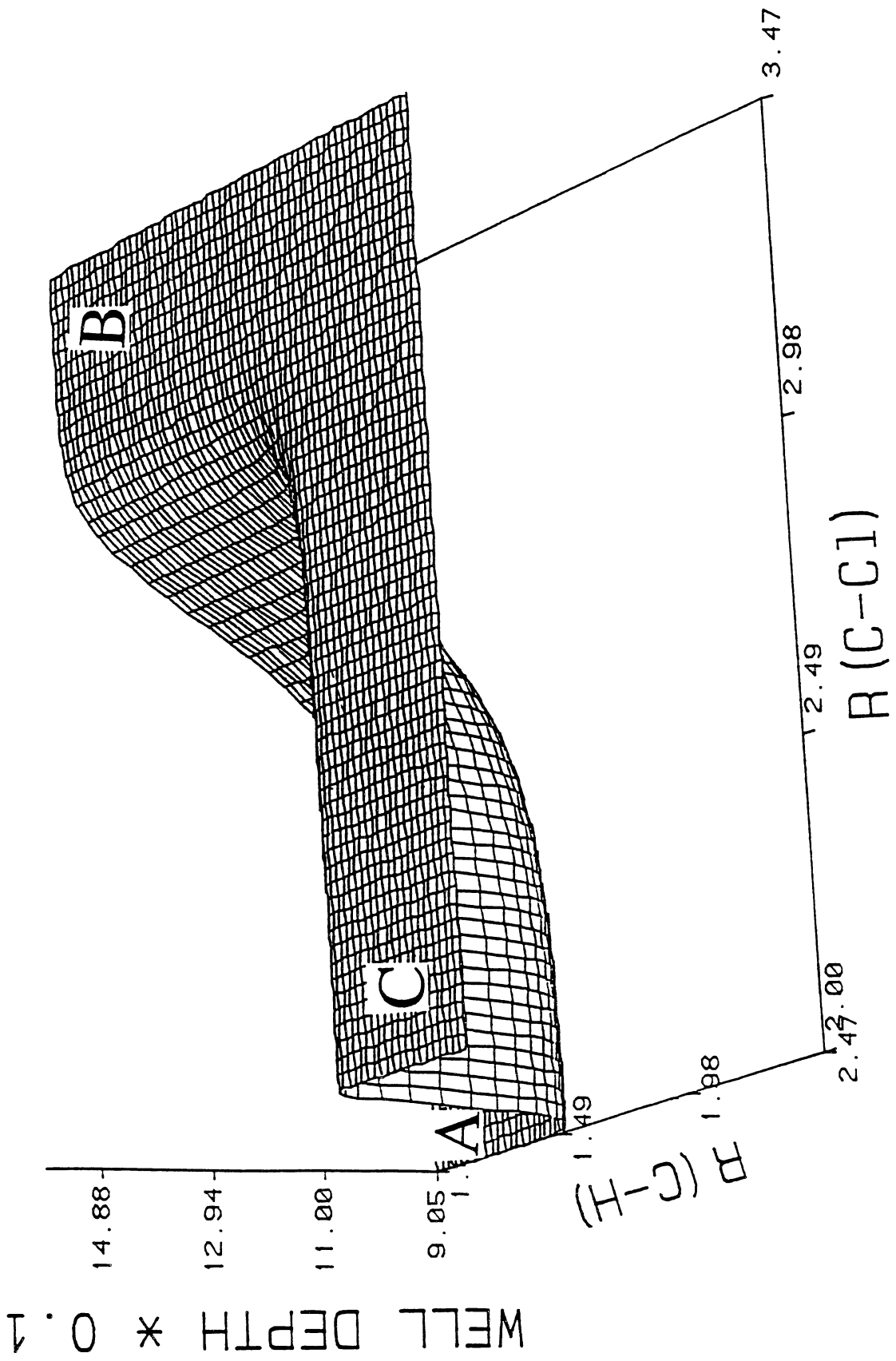
WELL DEPTH * 0.1
14.88
12.94
11.00
9.05
A
B
C
R (C-H)
1.49
1.98
2.47
3.00
R (C-C1)
2.49
2.98
3.47

Figure 7. Plot showing the behavior of the Morse curvature parameter for the C-C bond as a simultaneous function of the C-Cl and C-H bond length in the 2-chloroethyl radical. Region A corresponds to the curvature parameter for the C-C bond in the reactant. Regions B and C correspond to the curvature parameter in the ethene and chloroethene molecules, respectively. Region D shows the behavior in the (energetically disallowed) event that the C-Cl and C-H bonds undergo simultaneous dissociation. Distances are in Å and the curvature parameter is in $Å^{-1}$.

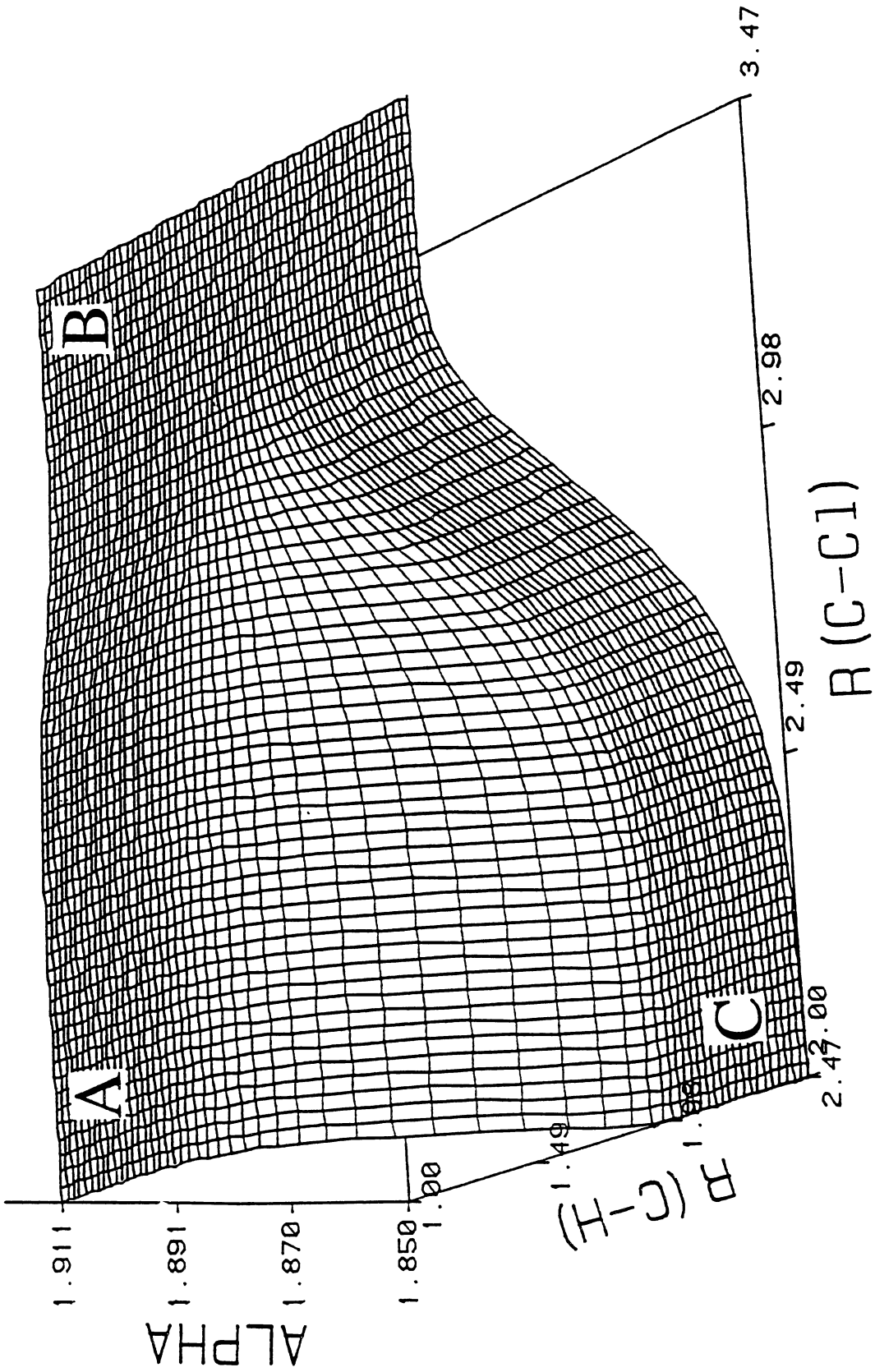
ALPHA
1.911
1.891
1.870
1.850
A
B
C
R (C-H)
1.00
1.49
2.00
2.47
R (C-Cl)
2.49
2.98
3.47

Figure 8. Plot showing the behavior of the equilibrium C-C bond length as a simultaneous function of the C-Cl and C-H bond length in the 2-chloroethyl radical. Region A corresponds to the equilibrium length of the C-C bond in the reactant. Regions B and C correspond to the equilibrium C-C bond length in the ethene and chloroethene molecules, respectively. Region D shows the behavior in the (energetically disallowed) event that the C-Cl and C-H bonds undergo simultaneous dissociation. Distances are in Å.

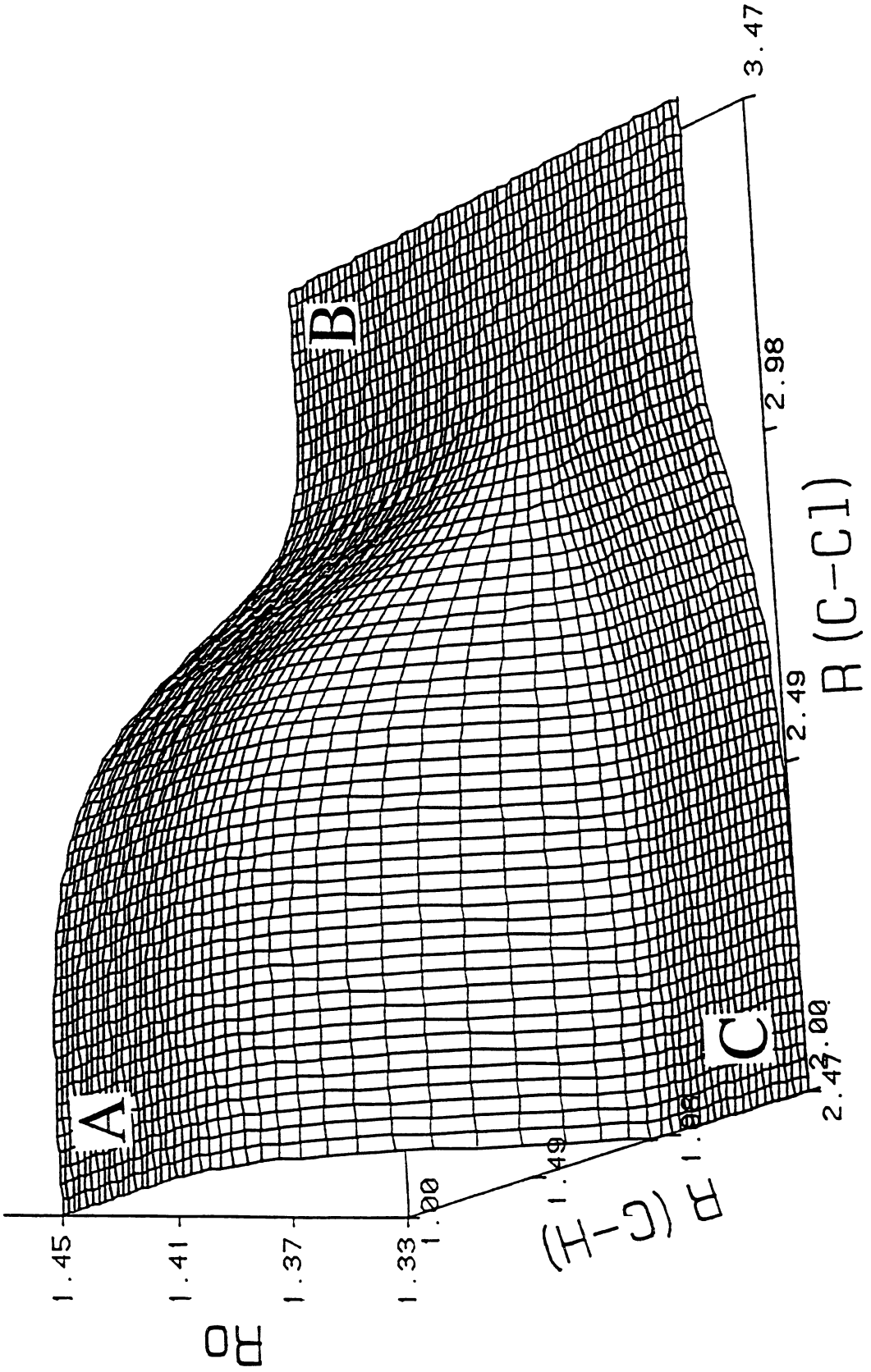
A
B
C
1.45
1.41
1.37
1.33
1.00
1.49
1.66
2.49
2.98
3.47
2.47
2.00
R (C-H)
R (C-C1)

potential show a marked dependence on $r_{C\text{-}Cl}$. For small $r_{C\text{-}Cl}$ the well depth is 35 kcal/mol, which is the contour extending out along the bottom right corner of the plot (region B). In the region where the switching functions are rapidly changing there is a corresponding change in the radial dependence of the C-H stretching potential (region C). The behavior for large $r_{C\text{-}H}$ clearly illustrates the attenuation of the C-H bond-stretching potential as the C-Cl bond length is increased. Finally, for large $r_{C\text{-}Cl}$ the Morse potential has become that for the ethene molecule (region D).

Graphical representations of the attenuation of individual molecular parameters as simultaneous functions of all three internal coordinates that govern attenuation of the potential- energy surface is not possible, but it is possible to illustrate the behavior of some of the parameters as two of the three coordinates are simultaneously varied. This is done in Figs. 6-8 for $D_{e_{C\text{-}C}}$, $\alpha_{C\text{-}C}$, and $r_{o_{C\text{-}C}}$, as simultaneous functions of the C-Cl bond length and one of the C-H bond lengths. Regions A, B, and C in Figs. 6-8 correspond to the 2-chloroethyl radical, ethene, and chloroethene, respectively. Comparison of Figs. 6-8 with the values given in Tables I and II for the C-C bond-stretching parameters shows that the limiting behavior in the regions A, B, and C yield the correct asymptotic values for the parameters depicted. It is also clear from the figures that the domains over which the parameters are varying do not depend on the type of parameter being attenuated, but rather only on the type of bond dominating the attenuation of the potential. Finally, it was stated earlier that the entire switching formalism was defined in terms of the product obtained by the loss of a chlorine atom. This is evident in Figs. 6-8 which show that, in the unlikely event that the C-Cl bond and one (or more) of the two C-H bonds simultaneously undergo dissociation, the resulting value of a given parameter will take on the value appropriate to ethene. This does not pose a problem for the energies we considered.

Figure 9. Plot of the potential energy of the 2-chloroethyl radical system as the C-Cl bond length is incrementally increased and the remaining internal coordinates are relaxed. A constant value of 20 kcal/mol has been subtracted uniformly from the potential computed using the actual potential-energy surface.

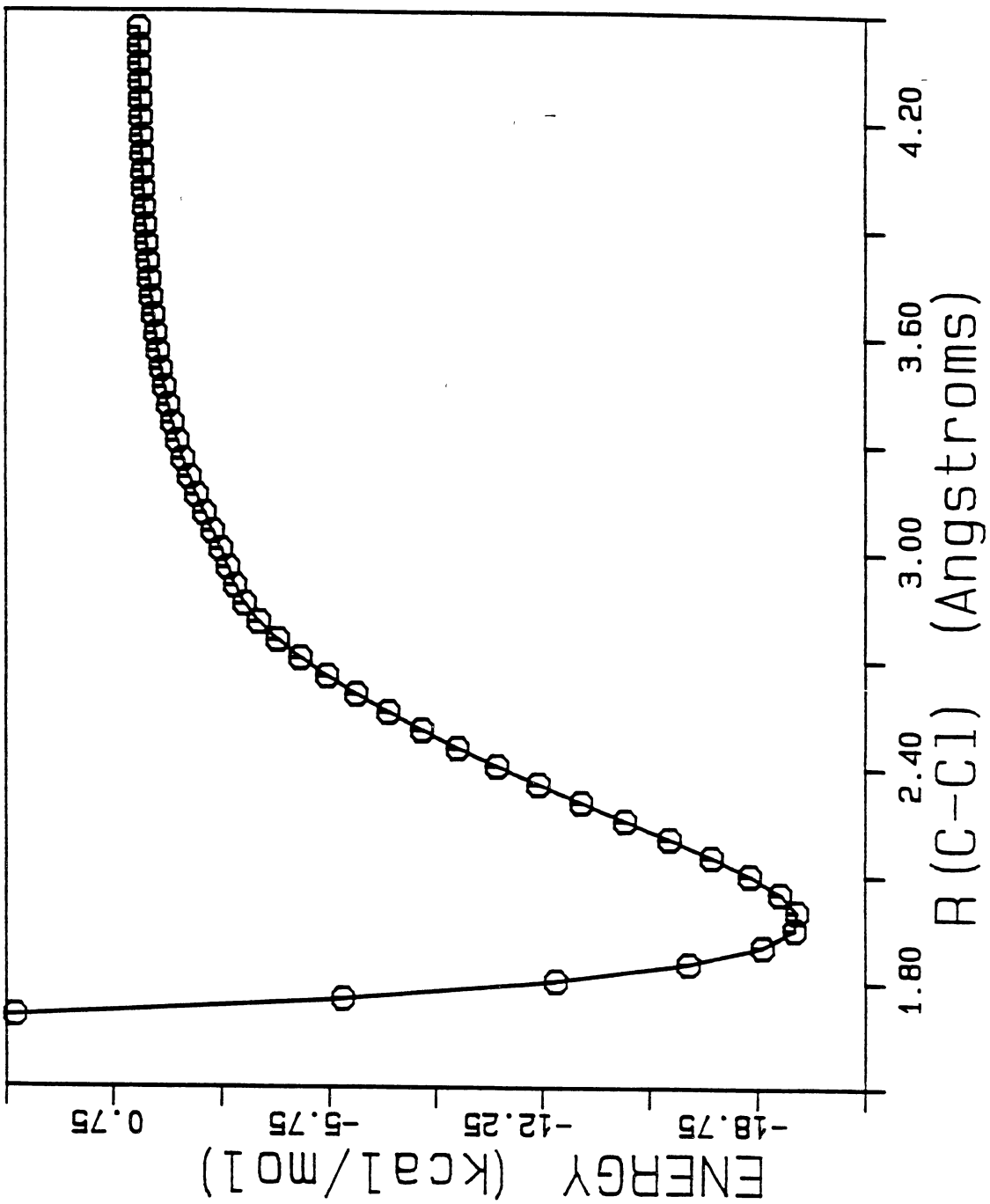
ENERGY (kcal/mol)
-18.75
-12.25
-5.75
0.75
1.80
2.40
3.00
3.60
4.20
R(C-Cl) (Angstroms)

Minimum Energy Profile for C-Cl Fission. Figure 9 is a plot of the minimum potential energy of the 2-chloroethyl radical system for the elimination of a ·Cl atom. The curve was generated by numerically searching the configuration space of the 2-chloroethyl radical and recording the minimum potential energy obtained for a given C-Cl extension. Circles in Fig. 9 indicate the fixed C-Cl bond lengths for which a search was performed. The circles are connected by straight lines. The relative energy difference between the reactant and the C_2H_4 + ·Cl product is 20 kcal/mol, as dictated by theoretical calculations.[312] Examination of the minimum-energy molecular configurations generated in the searches did not indicate any discontinuities in the internal coordinates along the minimum-energy profile.

Results of the Calculations

We have used classical trajectory methods to calculate first-order rate coefficients for the two bond-rupture reactions (R1) and (R2) of the 2-chloroethyl radical for two different types of initial conditions, one corresponding to local excitation of a C-H bond and the other to a uniform distribution of energy among the normal modes of the reactant. The impetus for the study was to investigate the possibility of mode-specific reaction.

First-order Rate Coefficients

The computed first-order rate coefficients are summarized in Table V, according to both the type of excitation scheme used and the total system energy. The quantum number v in the first column of Table V indicates the level of excitation of the C-H bond for initial conditions in which all of the energy in excess of the zero-point level is initially localized in a single C-H local mode. The energy in the next-to-last column of Table V is the total energy of the 2-chloroethyl radical (including the zero-point energy).

Table V. Rate Coefficients for 2-chloroethyl Radical Dissociation (PES-I)[a]

	Local-Mode Excitation					Uniform Excitation						
v[b]	k	$k_{C\text{-}H}$	$(N_{C\text{-}H})$	$k_{C\text{-}Cl}$	$(N_{C\text{-}Cl})$	k	$k_{C\text{-}H}$	$(N_{C\text{-}H})$	$k_{C\text{-}Cl}$	$(N_{C\text{-}Cl})$	Energy[c]	t_{max}[d]
5	0.041	0.004	(10)	0.037	(100)	0.040	0.004	(12)	0.036	(98)	69.8	20.0
6	0.058	0.006	(8)	0.053	(77)	0.073	0.007	(9)	0.066	(84)	76.5	10.0
9	0.193	0.057	(49)	0.138	(117)	0.219	0.070	(54)	0.150	(116)	94.6	10.0
12	0.379	0.159	(82)	0.221	(114)	0.372	0.156	(82)	0.216	(114)	109.0	10.0
14	0.486	0.203	(40)	0.284	(56)	0.526	0.240	(52)	0.286	(62)	117.8	1.7

[a] Rate coefficient units are ps^{-1}.
[b] C-H local-mode quantum number.
[c] Total energy in kcal/mol.
[d] Maximum trajectory integration time in ps.

The maximum duration of a trajectory t_{max}, at a given energy, is given in the last column of Table V. The overall first-order rate coefficients k are calculated from Eq. II.28. The rate coefficients for ·H and ·Cl elimination, $k_{C\text{-}H}$ and $k_{C\text{-}Cl}$, respectively, are calculated using the overall rate coefficient, k, and Eqs. II.29 to II.31. The numbers of trajectories leading to elimination of ·H and ·Cl in a given ensemble of trajectories are given by $N_{C\text{-}H}$ and $N_{C\text{-}Cl}$, respectively. Thus, the total number of reactive trajectories in any particular ensemble is $N_{C\text{-}H} + N_{C\text{-}Cl}$. A total of 200 trajectories were computed for each set of initial conditions.

We computed ensembles of trajectories for energies corresponding to a C-H local-mode excitation to the v=5 level (total energy of 69.8 kcal/mol). This energy approaches those attainable in the laboratory. Trajectories at this energy were integrated for up to 20 ps. Fifty-five percent of the trajectories underwent reaction within this time cutoff for both types of initial conditions. For the local-mode excitation, 10 trajectories led to ·H elimination and 100 led to loss of ·Cl. Rupture of C-H and C-Cl bonds occurred 12 and 98 times, respectively, for the uniform excitation. The calculated rate coefficients at this energy do not indicate a significant dependence on the type of excitation. Local-mode excitation led to an overall rate coefficient of 0.041 ps^{-1} while uniform excitation resulted in a rate coefficient of 0.040 ps^{-1}. The branching ratios for the two excitation schemes are similarly in close agreement. The rate coefficient for C-Cl bond rupture is 0.037 ps^{-1} for local-mode excitation and 0.036 ps^{-1} for uniform excitation. The rate coefficient for C-H bond rupture is 0.004 ps^{-1} for both excitation schemes. The first-order decay curves for energies corresponding to v=5 local-mode excitation (69.8 kcal/mol) are given in Fig. 10. Asterisks and open circles in Fig. 10 represent calculated lifetimes for uniform and local-mode excitations, respectively. The solid lines are least-squares fits to the data. There is a period of about 0.75 ps during which the only observed lifetimes arise from the initially uniform distribution of energy.

Figure 10. First-order decay curve for the overall decomposition of the 2-chloroethyl radical at an energy corresponding to zero-point energy plus excitation of a single C-H local mode to the v=5 state. (*) denotes initial conditions corresponding to uniform distribution of energy over the normal modes of the molecule. (o) denotes initial conditions corresponding to excitation of a single C-H stretch. The straight lines are least squares fits to the data.

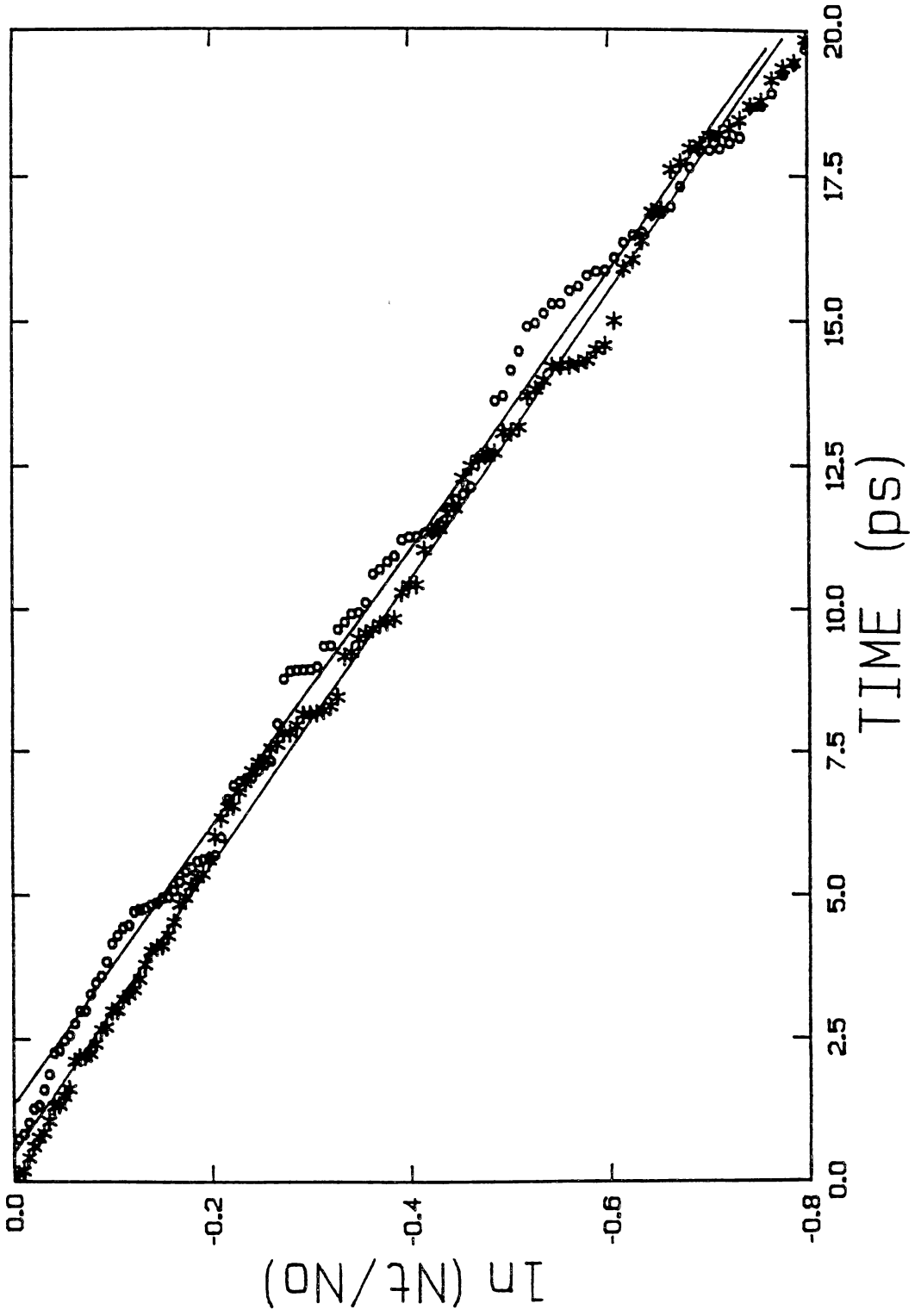
ln (Nt/No)
0.0
-0.2
-0.4
-0.6
-0.8
0.0
2.5
5.0
7.5
10.0
12.5
15.0
17.5
20.0
TIME (ps)

Figure 11. First-order decay curve for the overall decomposition of the 2-chloroethyl radical at an energy corresponding to zero-point energy plus excitation of a single C-H local mode to the v=6 state. (*) denotes initial conditions corresponding to uniform distribution of energy over the normal modes of the molecule. (o) denotes initial conditions corresponding to excitation of a single C-H stretch. The straight lines are least squares fits to the data.

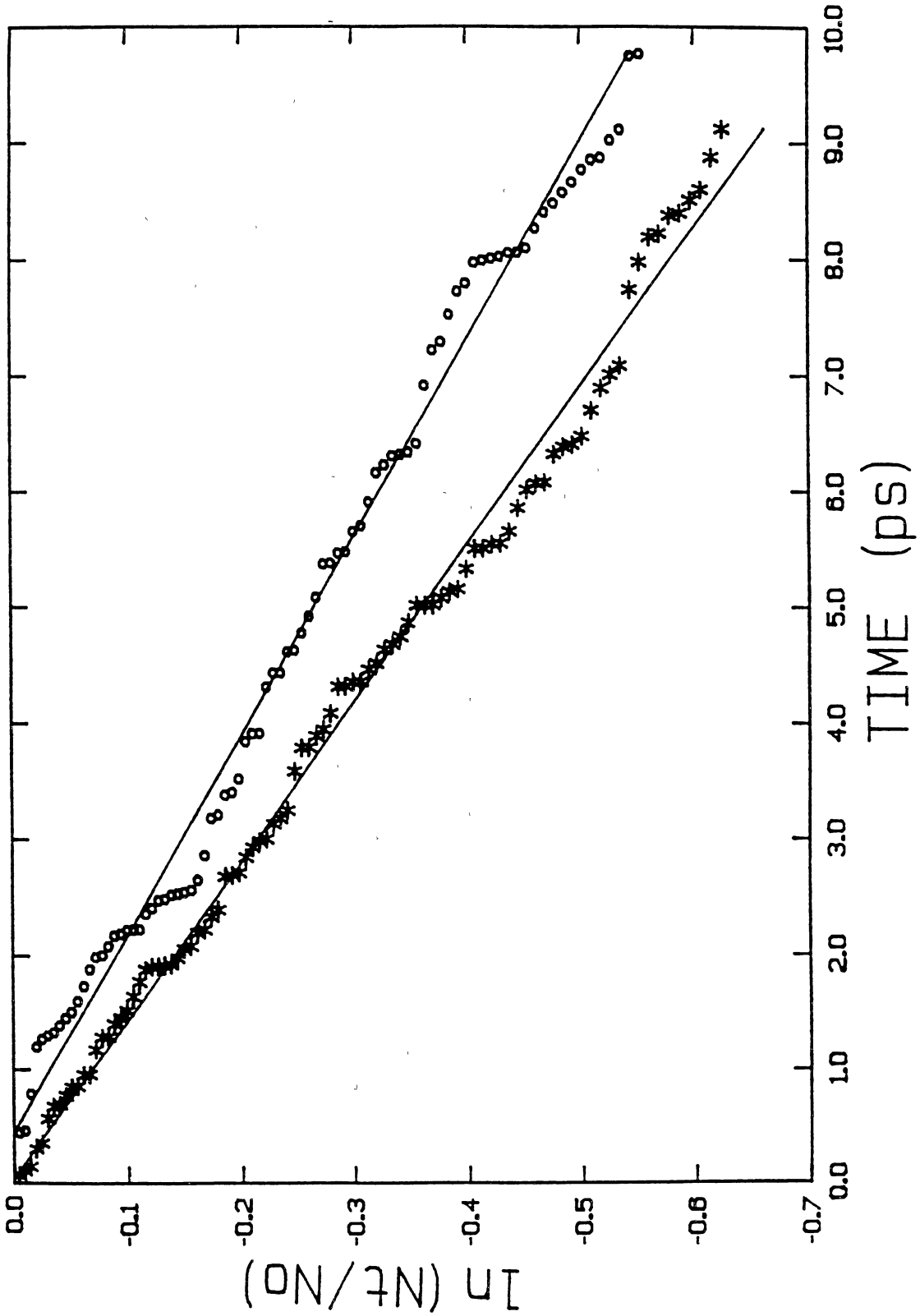
0.0
-0.1
-0.2
-0.3
-0.4
-0.5
-0.6
-0.7
ln (Nt/No)
0.0
1.0
2.0
3.0
4.0
5.0
6.0
7.0
8.0
9.0
10.0
TIME (ps)

This is because of the time required (following local-mode excitation of a C-H bond on the $\cdot CH_2$ group) for energy to transfer from the excited C-H bond of the $\cdot CH_2$ group to the chloromethyl group. For initial conditions in which the energy is evenly distributed over the normal modes more energy is located in the chloromethyl moiety than in the $\cdot CH_2$ group and the reactant can dissociate almost immediately. The time lag decreases as the energy in the 2-chloroethyl radical is increased.

The first-order rate coefficients for energies corresponding to zero-point energy plus local-mode excitation of a C-H bond to the v=6 level (total energy of 76.5 kcal/mol) follow the behavior of those for v=5 (Table V). The time cutoff for trajectories computed at this energy was 10 ps. For the local-mode excitation at this energy a total of 85 trajectories underwent reaction within 10 ps. Eight of these led to C-H rupture with the remaining 77 resulting in fission of the C-Cl bond. Uniform excitation at the same energy led to 93 reactive events, 9 of which were C-H dissociations. There were 84 C-Cl bond ruptures. Thus, the major difference between the two ensembles at this energy is the increase in the number of C-Cl dissociations for an initially uniform distribution of the energy, a result we tentatively attribute to the small number of trajectories calculated. The overall first-order rate coefficient for C-H local-mode excitation to v=6 is 0.058 ps^{-1}. Uniform excitation led to a computed rate coefficient 1.26 times as large, with a value of 0.073 ps^{-1}. The major difference in the rate coefficients appears in the C-Cl channel. The factor of 1.26 in the rates obtained for the two excitation schemes is the largest obtained in our study. Local-mode excitation led to a rate coefficient for C-Cl bond rupture of 0.053 ps^{-1} while the uniform distribution of energy led to a rate coefficient of 0.066 ps^{-1}. The first-order rates for C-H fission at this energy are nearly equal, with the local-mode and uniform excitation leading to rate coefficients of 0.006 ps^{-1} and 0.007 ps^{-1}, respectively. The decay curves for trajectories calculated at this energy are given in Fig. 11. Once again there is a time lag

between the first lifetime for uniform and local-mode excitations, although in this case the delay (0.44 ps) is somewhat smaller than before (0.75 ps in Fig. 10). The difference between the slopes in Fig. 11 is small and, we think, is a consequence of the small number of reactive trajectories. There are gaps in the decay curve for the local-mode excitation, results that are probably a consequence of the small ensemble size. Based on the relatively small discrepancy between the computed values of the rate coefficients and the large uncertainty in the rate coefficients obtained from so few lifetimes, we do not believe that mode-specific effects are important at this energy.

The behavior of the first-order rate coefficients computed for higher energies is qualitatively similar to that for lower energies. The zero-point energy plus that due to excitation of a C-H local mode to v=9 gives a total energy of 94.6 kcal/mol. At this energy 166 of 200 trajectories reacted within 10 ps following local-mode excitation. Of these, 49 were C-H dissociations and 117 were C-Cl ruptures. Uniform distribution of the same total energy resulted in 170 reactive events, with 54 and 116 C-H and C-Cl fissions, respectively. In contrast to the previous case for which the main difference in reactivity appeared to be an increase in the number of C-Cl bond ruptures for the uniform distribution of the energy, here the reverse is true with local-mode excitation giving rise to one more C-Cl bond fission than uniform distribution of energy, but with the latter leading to five more C-H ruptures. The overall first-order rate for local-mode excitation at this energy is 0.193 ps^{-1} and that for uniform distribution of the energy is 0.219 ps^{-1}, the latter being larger by a factor of 1.13. The rate coefficients for C-H bond-rupture are 0.057 ps^{-1} and 0.070 ps^{-1} for local-mode and uniform excitation, respectively. Rate coefficients for C-Cl bond fission are 0.138 ps^{-1} and 0.150 ps^{-1} for local-mode and uniform excitation, respectively. Once again, the differences in the computed rate coefficients are small and are probably attributable to statistical error due to the small ensemble sizes.

Zero-point energy plus excitation of the C-H local mode to v=12 results in a total energy of 109.6 kcal/mol. Of the 200 trajectories calculated for local-mode excitations at this energy, 196 underwent reaction within the 10 ps time cutoff. The same number reacted following uniform distribution of the same total energy. Moreover, the number of C-H and C-Cl bond ruptures were identical in both ensembles, with 82 C-H and 114 C-Cl dissociations, respectively, in both ensembles. The overall first-order rate coefficients are almost identical, with values of 0.379 ps^{-1} and 0.372 ps^{-1} for local-mode and uniform excitation, respectively. The rate coefficients for ·H and ·Cl elimination are 0.159 ps^{-1} and 0.221 ps^{-1}, respectively, following local-mode excitation and 0.156 ps^{-1} and 0.216 ps^{-1}, respectively, following uniform distribution of the energy among the normal modes of the reactant.

The largest energy for which we calculated trajectories is 117.8 kcal/mol, which corresponds to zero-point energy plus excitation of the C-H local mode to v=14. The maximum duration of trajectories at this energy was 1.7 ps. During this time 96 of 200 trajectories resulted in reaction following local-mode excitation, with 40 and 56 trajectories leading to C-H and C-Cl bond rupture, respectively. For a uniform distribution of the same total energy 114 trajectories reacted, with 52 and 62 trajectories reacting through the C-H and C-Cl channels, respectively. The overall first-order rate obtained for uniform distribution of the energy is 1.08 times that for local-mode excitation, the prior having a value of 0.526 ps^{-1} and the latter a value of 0.486 ps^{-1}. The greatest difference in the rate coefficients is in the C-H channel, with local-mode excitation giving a value of 0.203 ps^{-1} and uniform distribution of the energy a value of 0.240 ps^{-1}. The computed rate coefficients for the C-Cl channel are in near agreement, with values of 0.284 ps^{-1} and 0.286 ps^{-1} for the local-mode and uniform excitations, respectively.

RRK Fits to the Data.

The overall first-order rate coefficients increase exponentially with the total energy, and the rate coefficients are well described using the RRK formula,[354]

$$k(E) = A(1 - E_0/E)^{s-1}, \qquad \text{(IV.8)}$$

where k(E) is the overall first-order rate coefficient at a given energy E, A is the frequency factor, E_0 is the minimum energy required for reaction, and s is the number of degrees of freedom in the system. For a collection of classical oscillators that is well described statistically, a plot of lnk(E) vs ln(1-E_0/E) yields a straight line having an intercept of ln(A) and a slope of s-1. The normal implementation of Eq. IV.8 is to use the rate coefficients k(E) and the critical energy E_0 to obtain an estimate of the number "effective degrees of freedom" in the molecule, s.

Application of Eq. IV.8 to the data in Table V yields good least-squares fits (R^2=0.98 or better). The results of this fitting procedure for the 2-chloroethyl radical are given in Table VI. Results for both the overall first-order rate coefficients and the C-H/C-Cl branching ratios and for both types of excitation schemes are given. The value of the critical energy E_0 used to fit the overall rate coefficients is the weighted average of the C-H and C-Cl dissociation energies. Since there are two C-H bond-rupture channels and only one for C-Cl bond rupture, the value of E_0 is $(2D_{e,C\text{-}H} + D_{e,C\text{-}Cl})/3.0$ = 30.0 kcal/mol. The dissociation energies of the C-H and C-Cl bonds (35.0 and 20.0 kcal/mol, respectively) were used for the calculations involving the branching ratios. Comparison of the results presented in Table VI for the two excitation schemes suggests that the initial distribution of energy in the 2-chloroethyl radical does not play an important role in the reaction dynamics.

Table VI. Calculated RRK s Parameter for 2-chloroethyl Radical (PES-I).

Local-Mode Excitation			Uniform Excitation		
k_{tot}	k_{C-H}	k_{C-Cl}	k_{tot}	k_{C-H}	k_{C-Cl}
10.5	13.6	14.5	10.5	3.3	14.2

The value of s for the overall rate-coefficient data is calculated to be 10.5 for both the localized and uniform distributions of energy. The results obtained for the branching ratios are similarly in good agreement. The calculated values of s for the C-H channel are 13.6 and 13.3 for the local-mode and uniform excitation schemes, respectively. The C-Cl channel s values are 14.5 and 14.2 for the local-mode and uniform excitations, respectively. The theoretical value is s = 3N - 6 for a molecule consisting of N atoms. However, for many polyatomic molecules the effective number of degrees of freedom calculated by fitting Eq. IV.8 to experimental data is considerably less than the theoretical value. In the case of the 2-chloroethyl radical, the effective number of degrees of freedom for reactions (R1) and (R2) is close to the theoretical value (within about 3% - 11% of the theoretical prediction), a result that may be a consequence of the extensive potential-energy coupling due to the switching functions. While the close agreement between the RRK fits for the local-mode and uniform excitations does not prove that mode-specific effects are unimportant in the 2-chloroethyl radical, they do lend further support to the conclusions presented above in the discussion of the individual rate coefficients. Moreover, the quality of the fit of the results in Table V to Eq. IV.8 suggests that the energy dependence of the first-order rate coefficients for the 2-chloroethyl radical is described by RRK theory, which is based on statistical assumptions.

Other Dynamics Calculations on 2-chloroethyl.

Reinhardt and Duneczky[304] have reported the results of calculations performed on a model of the 2-chloroethyl radical. They compared lifetime distributions for C-Cl fission during the first picosecond following excitation of C-H bonds on different ends of the reactant. C-H fission was not considered in their study since they treated the four C-H bonds as being "almost isoenergetic". They found that, for excitations of one of

the C-H bonds to v=5 or v=6, there is a propensity for "prompt" reaction to occur when one of the chloromethyl group C-H bonds was excited, suggesting that short-time localization of energy does occur. The effect becomes more pronounced with increasing energy, with the v=6 excitation giving about twice as many "prompt" reactions as the v=5 excitation. This is in accord with the results of a number of calculations dealing with IVR following methyl C-H excitation, in which energy appears to be temporarily trapped in the methyl-group modes, leaking "slowly" to the remainder of the molecule.[13a,15,18,27,,29] Also, their observations are in accord with those reported here insofar as we see "prompt" dissociation following uniform initial distributions of energy (relative to highly localized excitations of the $\cdot CH_2$ group). There are more degrees of freedom associated with the chloromethyl moiety than with the $\cdot CH_2$ group and, thus, uniformly distributing energy over the normal modes of the 2-chloroethyl radical places more energy in the chloromethyl group than in the $\cdot CH_2$ group, as pointed out above.

Energy Transfer Results

The results for the computed first-order rate coefficients indicate that the initial distribution of energy has little or no effect on the rate of reaction in the 2-chloroethyl radical. One explanation for this observation is that the timescale for energy randomization is significantly shorter than that for chemical reaction. We have monitored the energy redistribution in the 2-chloroethyl radical as a function of time by using a local-mode approximation (Eq. II.33) to compute the energies of the four C-H bonds. Ensembles of 25 trajectories were followed for 1.0 ps and the average energies in the C-H local-modes were obtained for zero-point energy plus a C-H overtone excitations to v=3, 6, 8, 10, or 12. An ensemble of 100 trajectories was computed for both types of initial conditions and the C-H local-mode energies were averaged for an energy corresponding to zero-point energy plus a v=14 overtone excitation. In all cases

Figure 12. Average energy of C-H local modes as a function of time for an ensemble of 25 trajectories corresponding to local-mode excitation of a C-H stretch to the v=3 state. The top curve is the average energy in the initially excited stretch. The second curve is the energy in the initially unexcited C-H stretch on the same end of the molecule as the initially excited bond. The bottom two curves are for the initially unexcited C-H stretches on the "reactive" end of the molecule.

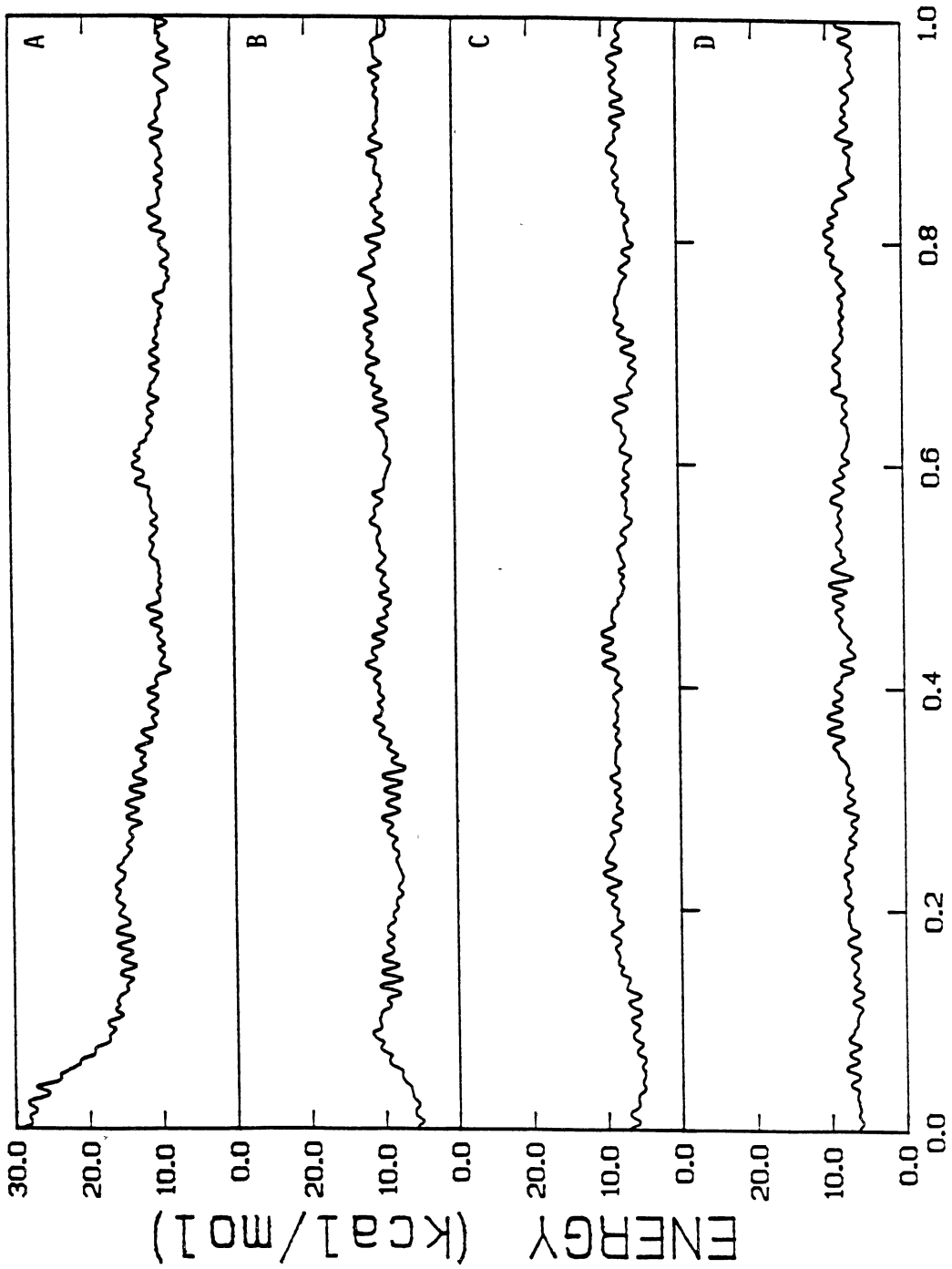
A
B
C
D
30.0
20.0
10.0
0.0
20.0
10.0
0.0
20.0
10.0
0.0
20.0
10.0
0.0
0.0
0.2
0.4
0.6
0.8
1.0
ENERGY (kcal/mol)
TIME (ps)

Figure 13. Average energy of C-H local modes as a function of time for an ensemble of 25 trajectories corresponding to local-mode excitation of a C-H stretch to the v=6 state. The top curve is the average energy in the initially excited stretch. The second curve is the energy in the initially unexcited C-H stretch on the same end of the molecule as the initially excited bond. The bottom two curves are for the initially unexcited C-H stretches on the "reactive" end of the molecule.

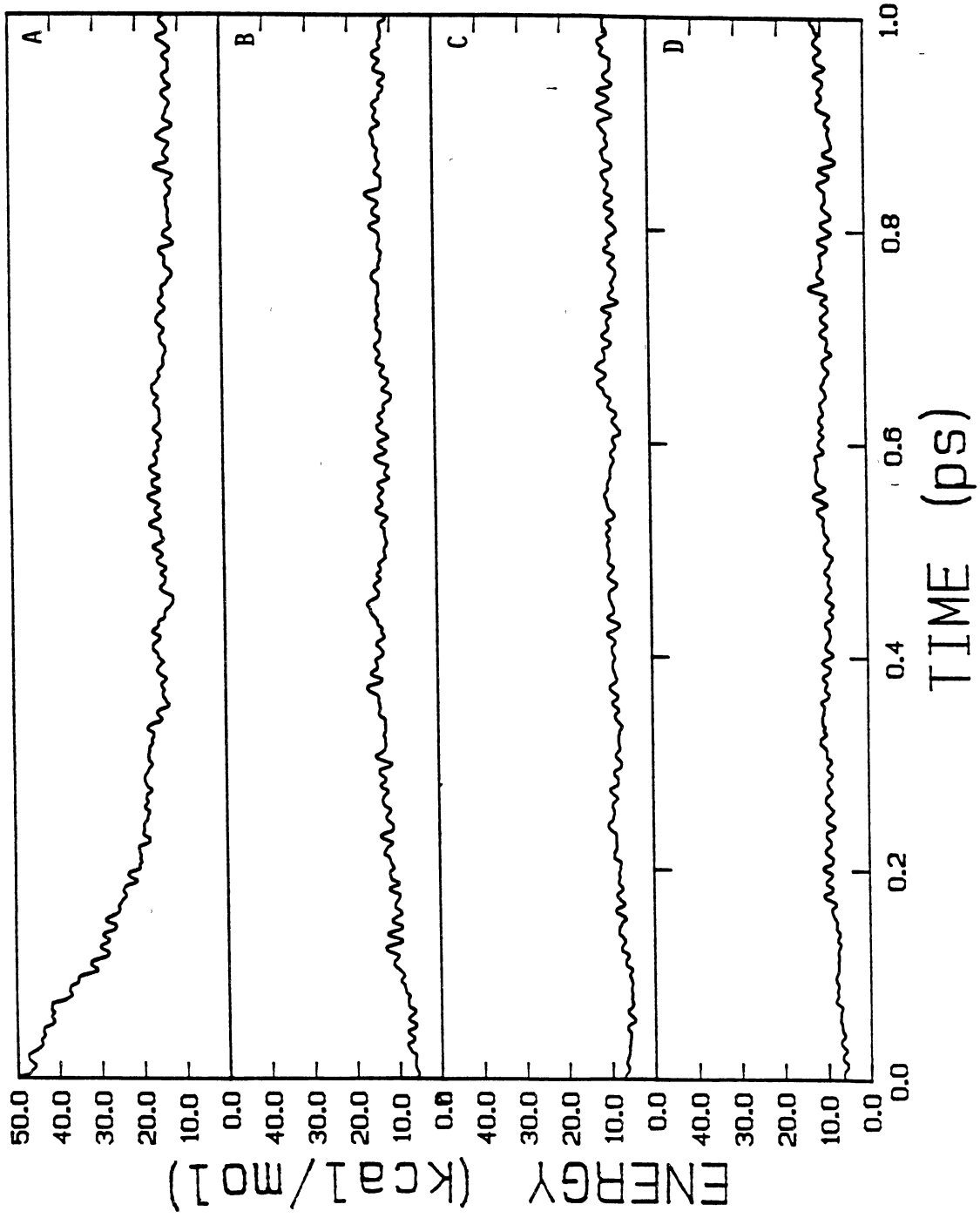
A
B
C
D
50.0
40.0
30.0
20.0
10.0
0.0
0.2
0.4
0.6
0.8
1.0
ENERGY (kcal/mol)
TIME (ps)

Figure 14. Average energy of C-H local modes as a function of time for an ensemble of 25 trajectories corresponding to local-mode excitation of a C-H stretch to the v=8 state. The top curve is the average energy in the initially excited stretch. The second curve is the energy in the initially unexcited C-H stretch on the same end of the molecule as the initially excited bond. The bottom two curves are for the initially unexcited C-H stretches on the "reactive" end of the molecule.

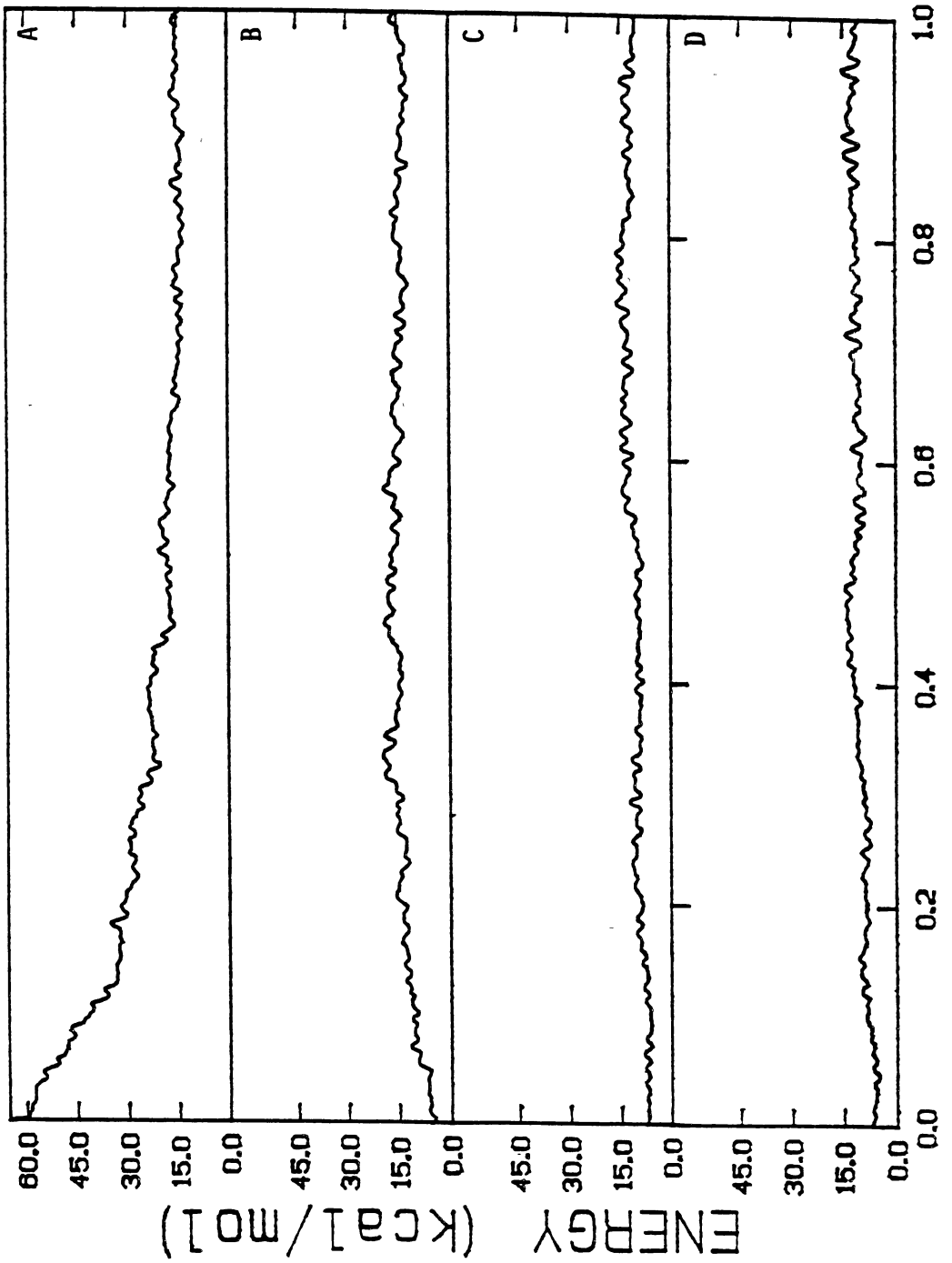
A
B
C
D
60.0
45.0
30.0
15.0
0.0
ENERGY (kcal/mol)
0.0
0.2
0.4
0.6
0.8
1.0
TIME (ps)

Figure 15. Average energy of C-H local modes as a function of time for an ensemble of 25 trajectories corresponding to local-mode excitation of a C-H stretch to the v=10 state. The top curve is the average energy in the initially excited stretch. The second curve is the energy in the initially unexcited C-H stretch on the same end of the molecule as the initially excited bond. The bottom two curves are for the initially unexcited C-H stretches on the "reactive" end of the molecule.

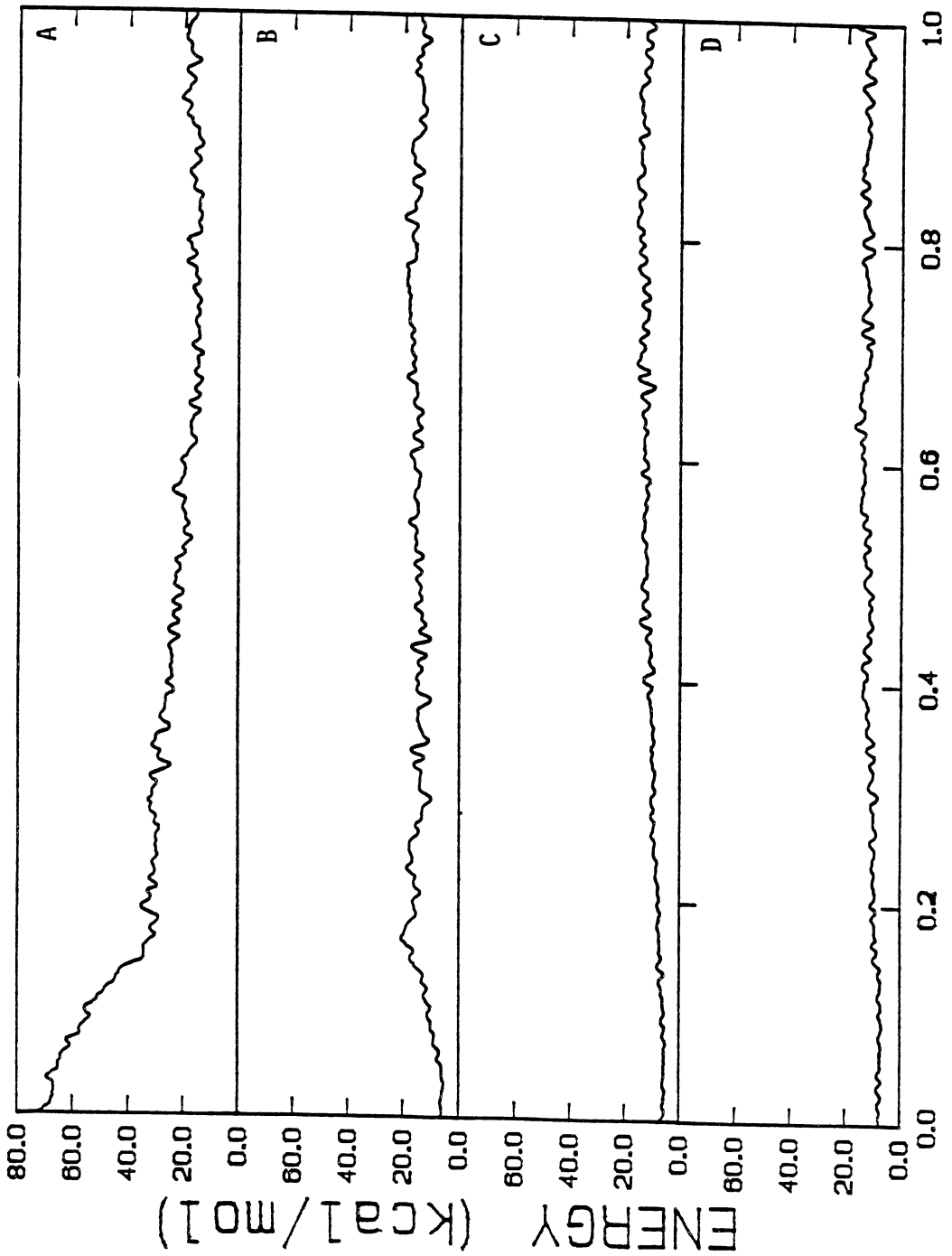
A
B
C
D
80.0
60.0
40.0
20.0
0.0
ENERGY (kcal/mol)
0.0
0.2
0.4
0.6
0.8
1.0
TIME (ps)

Figure 16. Average energy of C-H local modes as a function of time for an ensemble of 25 trajectories corresponding to local-mode excitation of a C-H stretch to the v=12 state. The top curve is the average energy in the initially excited stretch. The second curve is the energy in the initially unexcited C-H stretch on the same end of the molecule as the initially excited bond. The bottom two curves are for the initially unexcited C-H stretches on the "reactive" end of the molecule.

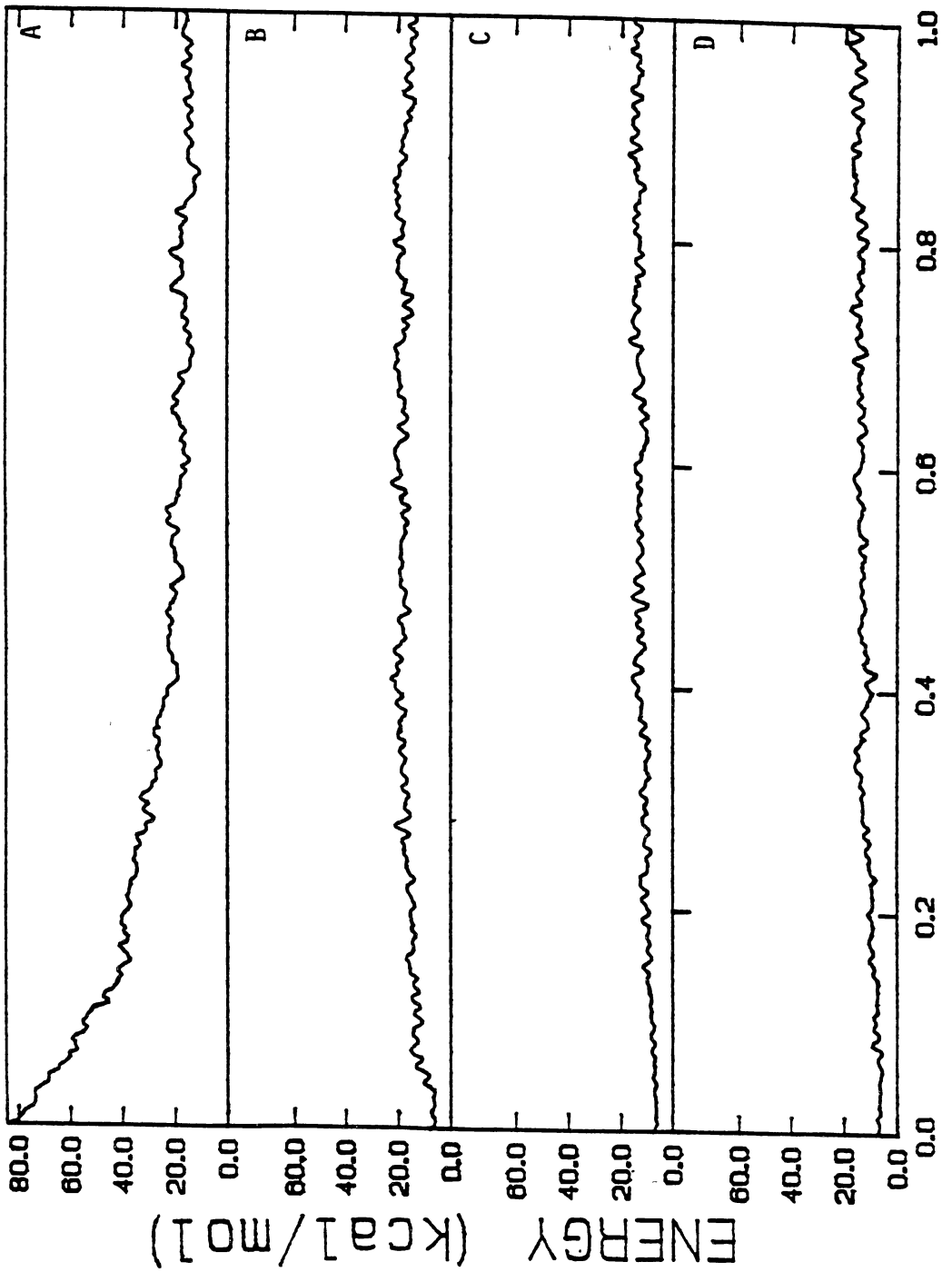
A
B
C
D
80.0
60.0
40.0
20.0
0.0
0.0
0.2
0.4
0.6
0.8
1.0
ENERGY (kcal/mol)
TIME (ps)

Figure 17. Average energy of C-H local modes as a function of time for an ensemble of 100 trajectories corresponding to local-mode excitation of a C-H stretch to the v=14 state. The top curve is the average energy in the initially excited stretch. The second curve is the energy in the initially unexcited C-H stretch on the same end of the molecule as the initially excited bond. The bottom two curves are for the initially unexcited C-H stretches on the "reactive" end of the molecule.

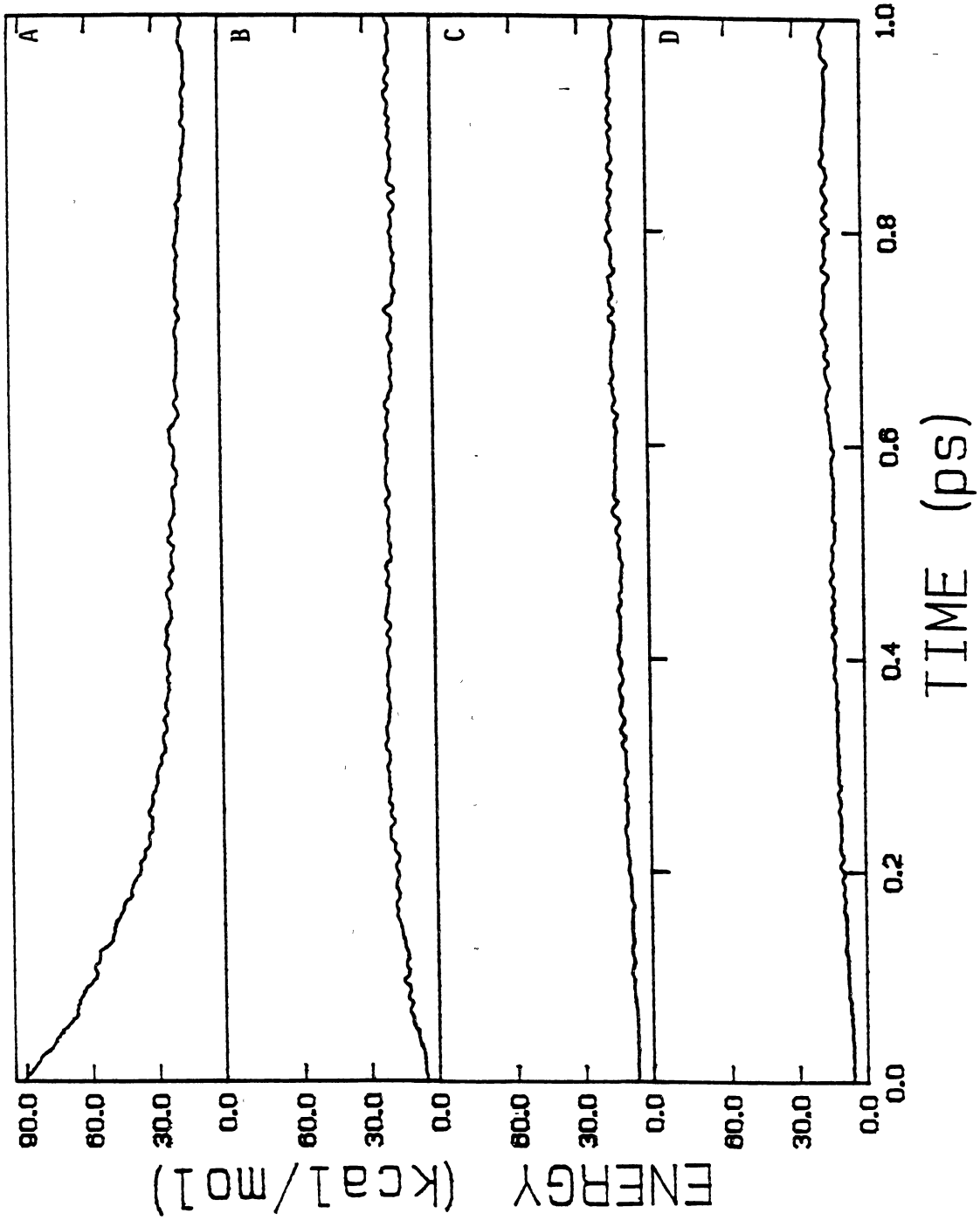
A
B
C
D
90.0
60.0
30.0
0.0
0.0
0.2
0.4
0.6
0.8
1.0
ENERGY (kcal/mol)
TIME (ps)

Figure 18. Average energy of C-H local modes as a function of time for an ensemble of 100 trajectories corresponding to uniform distribution of 117.8 kcal/mol of energy over the normal modes. The top curve is the average energy in the initially excited stretch. The second curve is the energy in the initially unexcited C-H stretch on the same end of the molecule as the initially excited bond. The bottom two curves are for the initially unexcited C-H stretches on the "reactive" end of the molecule.

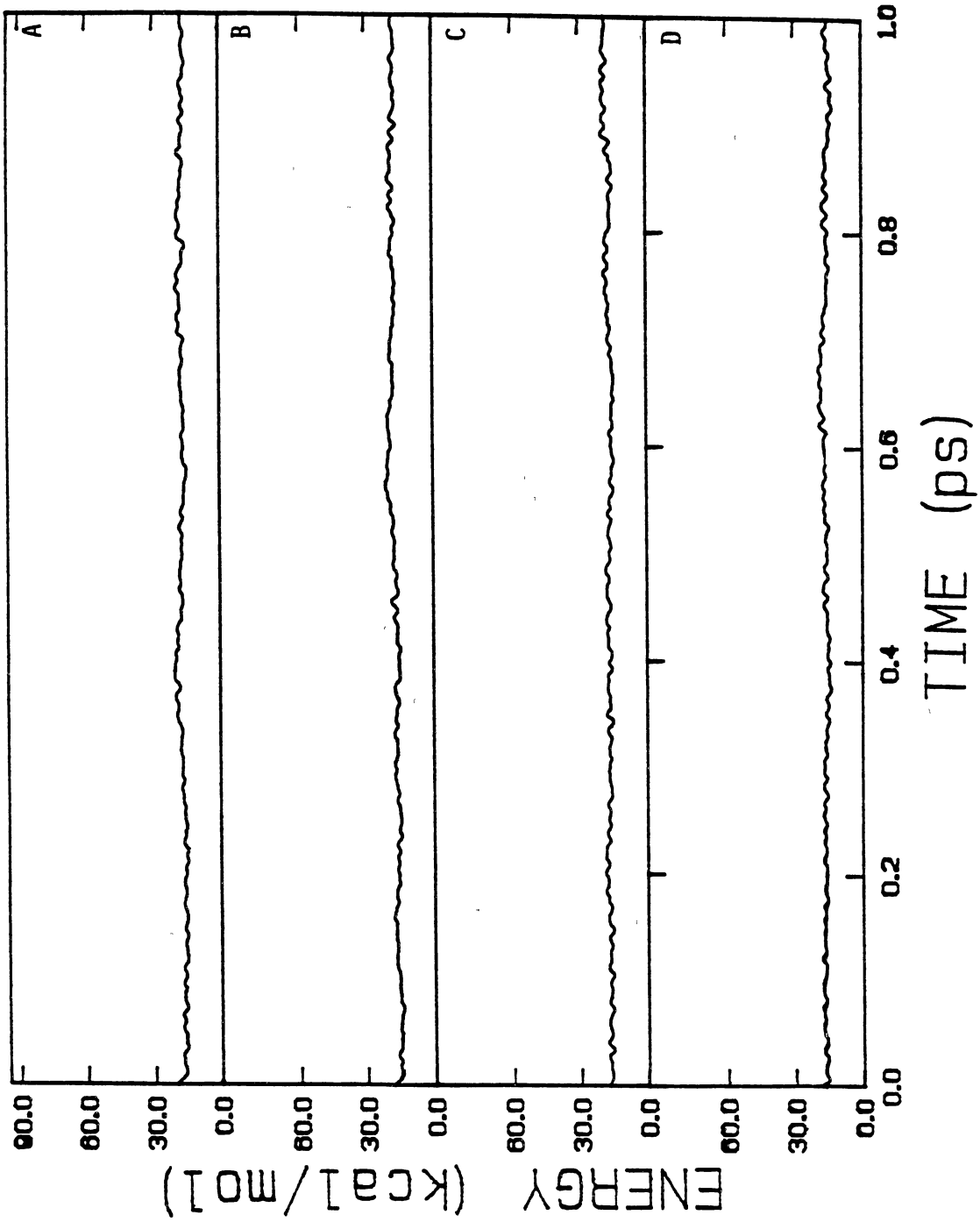
A
B
C
D
90.0
60.0
30.0
0.0
60.0
30.0
0.0
60.0
30.0
0.0
60.0
30.0
0.0
0.0
0.2
0.4
0.6
0.8
1.0
ENERGY (kcal/mol)
TIME (ps)

the averaging was appropriately weighted if a trajectory underwent dissociation before the time cutoff. The results of these calculations for local-mode excitations are given in Figs. 12-17 (for v=3, 6, 8, 10, 12, and 14, respectively), and for a uniform distribution of energy corresponding to a v=14 C-H overtone excitation in Fig. 18. In Figs. 12-17 the top curve (A) is the C-H local-mode energy in the initially excited bond. The second curve (B) is the C-H energy in the initially unexcited C-H bond of the $\cdot CH_2$ group, and the bottom two plots (C and D) are for the C-H local-mode energies of the chloromethyl group. The correspondence between the C-H bonds and the energy transfer curves A-D in Fig. 18 is the same as in Fig. 12-17.

For this wide range of energies the relaxation of the initially excited C-H local mode is fast and irreversible. There is a rapid, short-time transfer of energy lasting ~0.15 to 0.20 ps followed by a slower relaxation. The energy in the initially unexcited C-H bond of the $\cdot CH_2$ group increases more rapidly than do the energies of the chloromethyl C-H bonds, both of which increase in energy at approximately the same rate. Roughly 50% of the energy in the excited C-H bond (curve A in Figs. 12-17) has been lost within about 0.15 ps. The sum of the C-H local-mode energies comprises roughly one-half to three-quarters of the total energy in the 2-chloroethyl radical after equilibration of energy among the C-H local modes. In all cases the energy has become evenly distributed among the C-H local modes within about 0.6 ps. Figure 18 is a plot of the C-H local-mode energies for the uniform initial distribution of energy at a total energy corresponding to the v=14 overtone excitation. The immediately obvious, and expected, result is that when the trajectories are begun with a uniform distribution of energy, the energy to remains evenly distributed.

The mean lifetime (k^{-1}) of the set of initial conditions yielding the largest rate coefficient (uniform distribution of 117.8 kcal/mol of energy among the normal modes) is calculated to be 1.9 ps. Thus, based on the energy transfer results for the C-H local

modes, the time required for the "average" trajectory to react under these conditions is roughly 3.3 times larger than that needed for energy randomization. The mean lifetimes for the v=5 excitations are much larger, having values of about 24 ps. In this case the ratio of the "average" time required for reaction to the time needed for energy randomization increases from 3.3 to 40. Energy redistribution is complete long before most trajectories react and, as a consequence, the calculated first-order rate coefficients obtained for initial conditions in which all of the energy in excess of the zero-point level is localized in a single C-H bond are essentially the same as those obtained for initial conditions in which the same total energy is distributed uniformly over the normal modes of the reactant. Mode-specific effects due to C-H local-mode excitation do not appear to be important in the unimolecular decomposition of the 2-chloroethyl radical.

Summary

We have performed classical trajectory calculations to investigate the possibility of mode-specific unimolecular dissociation in the 2-chloroethyl radical. Ensembles of trajectories were computed for five different total energies and two different types of initial conditions. Rate coefficients for initial conditions corresponding to C-H local-mode excitations were compared to rate coefficients for the same total energy uniformly distributed over the reactant. These results indicate little or no difference in the overall rate coefficients for the two types of initial conditions, and the branching ratios for the ·Cl and ·H elimination reactions are approximately the same for both types of initial conditions. These results suggest that there is no mode specificity for C-H local-mode excitations.

The observed lack of mode-specific behavior is seemingly reconcilable with the rates of intramolecular energy transfer obtained using a local-mode approximation. The time required for relaxation of an initially excited C-H bond is roughly 32% of that

required for the average dissociative trajectory to react under conditions yielding the shortest average lifetime. Assuming that C-H local mode energies are a valid measure of energy content within the radical, redistribution of energy is complete before most trajectories undergo dissociation. This result is in accord with most of the theoretical and experimental evidence to date for various systems.

Both types of excitation schemes employed in this study lead to linear RRK plots, suggesting that the 2-chloroethyl radical behaves statistically with respect to the energy dependence of the rate coefficients. Calculated values of the RRK s parameter do not depend strongly on the initial distribution of energy.

CHAPTER V

STATISTICAL BEHAVIOR IN UNIMOLECULAR DISSOCIATIONS OF 2-CHLOROETHYL RADICAL

Introduction

It is clear that mode-specific chemistry will be observed whenever the reaction rate is fast relative to the intramolecular energy transfer rate. However, it is now known that the inverse of this statement is not always true. That is, the existence of a very fast intramolecular energy transfer rate out of a given set of modes is not a sufficient condition to ensure the absence of mode-specific dynamical effects. It is possible to have a molecular system in which the IVR rate out of a given set of modes is fast relative to the unimolecular reaction rate but is such that the energy tends to remain confined within a small subset of modes rather than become completely randomized over all internal degrees of freedom. Under such conditions, pronounced mode-specific and other dynamical effects will often be observed.

The number of systems that have been found to exhibit such non-RRKM dynamics has increased significantly since 1985. Borchardt and Bauer[109] found that the unimolecular inversion of aziridine, which occurs with an activation energy of 15.8 ± 0.4 kcal/mol, does not exhibit the expected RRKM falloff at lower pressures. In order to fit the observed kinetics, Borchardt and Bauer had to employ a restricted phase-space model which assumes that the internal energy is not rapidly randomized throughout the entire molecule. A reexamination by these investigators[109] of the kinetic data for the unimolecular decomposition of methyl nitrite[111,355], cyclohexane[356],

tetrahydropyran[357], and sulfur tetrafluoride[358] revealed that these systems also exhibit similar non-RRKM behavior.

Newman-Evans *et al.*[106] have found that 1- and 2-phenylbicyclo[2.1.1]hex-2-ene-5-d exhibit pronounced dynamical effects in thermal decomposition reactions that cannot be explained using statistical theories. These molecules undergo unimolecular cleavage of either the 4-5 or the 4-6 bond to form products that differ only in the position of the isotopic label. Both reaction pathways have almost identical activation energies of 35.7 kcal/mol. When the 4-5 bond breaks, two energetically equivalent stereoisomeric products are formed.

Since such reactions will be much slower than the expected energy transfer rates in the molecule, we would expect statistical transition-state theories to hold. This would lead to a1:1 ratio of the two stereoisomers. In sharp contrast, the observed result is a 9:1 product ratio. The Authors have suggested that the mechanism for these reactions is dynamically controlled and that statistical theories such as RRKM, variational phase-space theory, etc. lead to incorrect predictions due to a nonstatistical partitioning of the molecular internal energy[106].

Newman-Evans *et al.*[106] have also reported data on the decomposition of trans-2-methyl-1-(trans-2-phenylethenyl) cyclopropane. This reaction proceeds with an activation energy of 39.7 ± 3.8 kcal/mol to form three products, a diene, two optical isomers of *trans* cyclopentene, and two optical isomers of *cis* cyclopentene. The observed 5.9:1 product ratio for the *trans* cyclopentenes is inconsistent with the predictions of all statistical rate theories. Most recently, these investigators have found that the decomposition of 2,3-diazabicyclo[2.2.1]hept-2-ene-exo,exo-5,6-d_2 may also exhibit similar nonstatistical dynamics[359].

Several additional examples of nonstatistical behavior have recently been found in theoretical investigations of these effects[171-173,211,360-361]. For example, Raff,

Thompson, and co-workers[172,361] have shown that unimolecular bond cleavage in disilane and 1,2-difluoroethane are nonstatistical processes in spite of the fact that these reactions are much slower than the intramolecular energy transfer rate out of Si-H, C-F, or C-H vibrational modes. This determination is made from the results of a detailed comparison of microcanonical rate coefficients for the bond fission reactions obtained from a statistical transition state theory (EMS-TST) and those computed from trajectory calculations on the same potential-energy surface[171,211]. The microcanonical rate coefficient, k(E), is obtained from an average over the microcanonical ensemble[178,183,363,364,365]

$$k(E) = \frac{1}{2} \frac{\int d\Gamma\ \delta[H(\Gamma)-E]\ \delta[q_{RC} - q_C]\ |\dot{q}_{RC}|}{\int d\Gamma\ \delta[H(\Gamma)-E]}, \qquad (V.1)$$

where Γ is the complete set of position and momentum coordinates [**q**,**p**], H(Γ) is the Hamiltonian of the system excluding the center-of-mass motion, $q_{RC} = q_{RC}(\mathbf{q})$ is the reaction coordinate, which may be a function of some or all of the coordinates, **q**, and q_C is the critical value required for reaction. The integrals in Eq. V.1 are understood to be over the reactant part of phase space. If the critical surfaces employed in the EMS-TST calculations completely separate the reactant and product configuration space, it is impossible for reaction to occur without traversing the critical surface. Consequently, due to trajectories that recross the critical surface, the numerator of Eq.V.1 will always tend to yield an upper bound to the corresponding trajectory rate provided both calculations are done on the same potential-energy surface. Therefore, the only way the inequality $[k(E)]_{EMS\text{-}TST} < [k(E)]_{trajectory}$ can be observed is for the denominator of Eq.(V.1), which sums the total phase space available to the reactant system, to be larger than that which is actually accessed in the trajectory calculations. Such a result would mean that the trajectories are not sampling the entire phase space that is energetically

accessible. Under such conditions, statistical transition state theories would be expected to fail.

When the above analysis was applied to bond fission reactions in Si_2H_6 and 1,2-difluoroethane, it was found that trajectory rate coefficients are considerably larger than the corresponding EMS-TST predictions computed on the same potential-energy surface[171-173,211,360]. Numerous mode-specific effects are present in both systems; the trajectory rates were found to be very sensitive to the nature of the initial energy partitioning. Investigations of the intramolecular energy transfer rates and pathways in these systems[173,299] show that the total IVR rate out of a given mode is generally much faster than the total dissociation rate. However, many of the individual mode-to-mode rate coefficients are significantly smaller than this rate. Consequently, IVR is not globally rapid on the timescale of the reactions. These data are consistent with the principle that a *total* intramolecular energy transfer rate from a given vibrational mode that is fast relative to the unimolecular reaction rate is not a sufficient condition to ensure statistical behavior and an absence of mode-specific chemistry.

In the preceding chapter we described trajectory studies of the dissociation dynamics of the 2-chloroethyl radical. The results of these calculations show that the microcanonical rate coefficients are insensitive to the initial partitioning of the internal energy. No mode-specific effects were observed. However, the results of classical trajectory calculations alone do not allow for an unequivocal statement as to whether 2-chloroethyl radical is, in fact, behaving statistically. In order to answer that question, the results of classical dynamics calculations must be compared to the results of a classical statistical calculation performed on the same potential-energy surface.

In this chapter, the unimolecular dissociation dynamics of the 2-chloroethyl radical system are reexamined and compared in detail with those for 1,2-difluoroethane. The statistical nature of the 2-chloroethyl dissociation reactions is verified by

comparison of the trajectory results with those obtained from variational EMS-TST calculations and from a J-conserving EMS-TST method denoted by EJS-TST. The nature of the potential coupling terms that lead to intermode energy transfer in 2-chloroethyl and 1,2-difluoroethane are compared and suggestions are advanced to explain the reasons for the significantly different dynamics observed for the two systems.

Potentials, Initial Conditions, and Trajectory Integration

Potential-energy Surface

The potential employed in the present study is very similar to that used for the calculations on 2-chloroethyl radical described in Chapter IV (which we shall denote as PES-I; the potential used in the present calculation shall be denoted as PES-II) . The functional forms of the potential-energy terms are identical to those used of PES-I, except that the Morse potentials used to represent the bond stretches are now replaced with the form given in Eq. II.2. Potential-energy surface PES-II incorporates the torsional barrier for rotation about the 2-chloroethyl C-C bond (which was approximated as a free rotor in PES-I) and yields thermodynamic properties in better agreement with the *ab initio* transition-state energies and back-reaction barriers[312,321].

In the interim between the calculations on PES-I and those described here, configuration interaction calculations on 2-chloroethyl radical were published by Peyerimoff and co-workers.[321] They assumed that the equilibrium wag angle for the radical $\cdot CH_2$ group was zero degrees and reported different values for the C-C and C-Cl bond lengths. We used their values in order to simplify the addition of the torsional potential in the reactant. Also, the reaction endothermicities were revised in light of the more recent calculations. Finally, the bond-stretching terms in the potential-energy

surface were significantly reparamaterized so as to employ more realistic values for the bond dissociation energies. The values of D_e were adjusted both in 2-chloroethyl radical and the two product molecules.

The geometry of 2-chloroethyl radical used in this calculation is given in Table VII. The revised potential for the bond stretches of the reactant and products and the torsional potential of 2-chloroethyl radical is presented in Table VIII (the product torsional potentials were not affected). The resulting normal-mode frequencies for 2-chloroethyl radical are given in Table IX. By construction, the normal-mode frequencies for ethene and chloroethene are unaffected by the changes in the potential-energy surface.

The attenuation of the potential-energy surface was accomplished as described in Chapter IV. However, a somewhat different form was used for the switching functions. The form chosen is

$$S(r) = 1 - A \tanh[B(r - r_o)^2] \qquad (r \geq r_o)$$

$$S(r) = 1.0 \qquad \text{(otherwise)} \qquad \text{(V.2)}$$

The switching function parameters for PES-II are listed in Table X in the same fashion as was done in Table IV.

The thermochemistry predicted by the new potential is given in Fig. 19. The curves represent the minimum-energy paths for C-H and C-Cl bond fission. The reaction profiles were obtained using the STEPIT[366] subroutine to minimize the potential energy as a function of incremental changes in the C-Cl or C-H bond lengths. The global minimum corresponds to 2-chloroethyl radical. The asymptote extending to the left corresponds to C_2H_4 + ·Cl. The one extending to the right is for C_2H_3Cl + ·H. Values shown in parentheses are energies (relative to 2-chloroethyl radical) derived from

Table VII. Equilibrium Geometrical Parameters for 2-chloroethyl Radical (PES-II).

Bond Number[b]	Bond Type	Equilibrium Value[c]
1	C-C	1.4800
2	C-H	1.0708
3	C-H	1.0708
4	C-H	1.0723
5	C-H	1.0723
6	C-Cl	1.8600
Angle Number	**Angle Type**	**Equilibrium Value**
1	H-C-H	118.0000
2	H-C-C	121.0000
3	H-C-C	121.0000
4	H-C-H	112.1544
5	C-C-H	115.3499
6	C-C-H	115.3499
7	H-C-Cl	101.5368
8	H-C-Cl	101.5368
9	C-C-Cl	108.8985
Wag Number	**X-Y-Z--W[d]**	**Equilibrium Value**
1	3-1-4--2	0.00000
2	5-2-6--1	39.8985
3	7-2-5--1	53.2494
4	7-2-6--1	-53.2494
Dihedral Number	**W-X-Y-Z--A-B[e]**	**Equilibrium Value**
1	5-2-1-3--6-3	-23.3351
2	6-2-1-4--5-2	23.3351
3	6-2-1-3--5-3	-156.6640
4	5-2-1-4--6-2	156.6640
5	7-2-1-3--9-3	90.0000
6	7-2-1-4--9-2	-90.0000

[a] Distances are in Å and angles are in degrees.

[b] See Fig. 1.

[c] *ab initio* results, Refs. 312 and 321.

[d] Atom W is the wagging atom and atom Y is the anchor atom.

[e] W, X, Y, and Z are the atoms required to define the dihedral angle. A and B are bond angles.

Table VIII. Force-field Parameters for PES-II.

	2-Chloroethyl Radical		Ethene		Chloroethene	
Bond Type	D_e (kcal/mol)	α (A^{-1})	D_e (kcal/mol)	α (A^{-1})	D_e (kcal/mol)	α (A^{-1})
C-C	130.98	1.588689	173.69	1.763438	180.44	1.680188
·C-H	112.38	1.824551	---	---	---	---
C-H	102.38	1.881244	112.38	1.808610	112.38	1.821332
C-Cl	82.42	1.296782	---	---	85.05	1.763314

Fourier Coefficients for 2-chloroethyl radical (PES-II)[a,b]

a_0=1.0450 a_2=1.0450

[a] kcal/mol

[b] Refers to the two dihedral angles involving the Cl atom.

Table IX. Theoretical and Calculated Normal-mode Frequencies for the 2-chloroethyl Radical (PES-II).

Frequency (cm^{-1})	
ab initio[a,b]	calculated
278	248
284	308
374	451
636	639
774	795
1002	985
1012	986
1191	1206
1235	1224
1442	1407
1483	1508
2987	2992
2993	3031
3060	3080
3090	3140

[a] Schlegel and Sosa, Ref. 312.

[b] The *ab initio* frequencies were uniformly scaled by 0.9 for presentation.

Table X. Switching Function Parameters for 2-chloroethyl Radical (PES-II).

Constants appearing in argument of tanh function (Eq. V.2)[a]

$b_{C-H} = 0.550$ Å^{-2} $b_{C-Cl} = 0.225$ Å^{-2} $b'_{C-Cl} = 0.700$ Å^{-2}

Reaction-channel- and parameter-dependent constants, A (Eq. V.2)[b]

	Reaction Channel	
Attenuated Parameter	Bond Four (C-H)	Bond Five (C-H)
Eq. Bond Length		
r_1^o	1.165354331	1.165354331
r_2^o, r_3^o	66.0	66.0
r_4^o	0.0	-5.153846154
r_5^o	-5.153846154	0.0
r_6^{oc}	2.0	2.0
Angle Number		
θ_4^o	-2.8094655	-2.8094755
θ_5^o	1.825036176	-5.475022138
θ_6^o	-5.475022138	1.825036176
θ_7^o	1.0	-1.071631648
θ_8^o	-1.071631648	1.0
θ_9^o	-0.709130354	-0.709130354
Wag Number		
γ_2^o	-0.408570727	-0.408570727
γ_3^o	0.657343556	-7.864758523
γ_4^o	-7.864758523	0.657343556
Dissociation Energy		
$D_{e,1}$	1.158042613	1.158042613
$D_{e,4}$	0.0	1.0
$D_{e,5}$	1.0	0.0
$D_{e,6}$[d]	2.0	2.0

Table X continued,

Morse Parameter		
α_1	0.523602420	0.523602420
α_2, α_3	0.201932125	0.201932125
α_4	0.0	0.824847867
α_5	0.824847867	0.0
α_6[e]	2.0	2.0
Force Constant f_θ		
$f_{\theta,1}$	1.700004026	1.700004026
$f_{\theta,2}$, $f_{\theta,3}$	0.473753253	0.473753253
$f_{\theta,4}$	4.112920764	4.112920764
$f_{\theta,5}$	1.397543769	-5.540527212
$f_{\theta,6}$	-5.540527212	1.397543769
$f_{\theta,7}$	1.0	0.475308552
$f_{\theta,8}$	0.475308552	1.0
$f_{\theta,9}$	0.116071706	0.116071706
Force Constant f_g		
$f_{\gamma,1}$	0.919854861	0.919854861
$f_{\gamma,2}$	0.0	0.0
$f_{\gamma,3}$[f]	0.0	2.0
$f_{\gamma,4}$[f]	2.0	0.0
Dihedral Angle		
τ_1, τ_4		
a_0	0.0	1.011597173
a_2	0.0	1.0
a_4	0.0	0.93508436
τ_2, τ_3		
a_0	1.011597173	0.0
a_2	1.0	0.0
a_4	0.935084365	0.0
τ_5, τ_6[g,h,i]		
a_0	-5.519138756	-5.519138756
a_2	8.59569378	8.59569378
a_4	1.0	1.0

Table X continued,

[a] $b_{C\text{-}H}$ appears in switching functions governed by C-H bonds. $b_{C\text{-}Cl}$ appears in switching functions governed by C-Cl bonds for all potential parameters except those corresponding to C-H bonds. $b'_{C\text{-}Cl}$ appears in switching functions governed by C-Cl bonds for potential parameters corresponding to C-H bonds.

[b] Any coefficient not explicitly shown is unity. In the case of footnotes c-h (below), $A_{C\text{-}Cl} = 0.0$.

[c] r_6^P is set to 1.794 Å and the switching function coefficients are adjusted so as to yield the correct equilibrium C-Cl bond lengths in all products.

[d] D_{e6}^P is set to 83.735 kcal/mol and the switching function coefficients are adjusted to yield the correct dissociation energies for all reaction products.

[e] α_6^P is set to 1.530048 $Å^{-1}$ and the switching function coefficients are adjusted to yield the correct curvature parameter for all reaction products.

[f] $f_{\gamma,6}^P$ is set to 5.625 kcal/mol and the switching function coefficients are adjusted to yield the correct wag angle harmonic force constants for γ_3 and γ_4 for all reaction products.

[g] a_0^P is set to 0.0 kcal/mol and the switching function coefficients are adjusted to yield the correct Fourier coefficients for all reaction products.

[h] a_2^P is set to 0.0 kcal/mol and the switching function coefficients are adjusted to yield the correct Fourier coefficients for all reaction products.

[i] a_4^P is set to 1.125 kcal/mol and the switching function coefficients are adjusted to yield the correct Fourier coefficients for all reaction products.

Figure 19. Thermochemistry and reaction profiles for the C-H and C-Cl bond fission channels of 2-chloroethyl radical. Energy values are given in kcal/mol relative to equilibrium 2-chloroethyl. Values given in parentheses are the *ab initio* results reported by Schlegel and Sosa in Ref. 312 and Engels *et al.* Ref. 321.

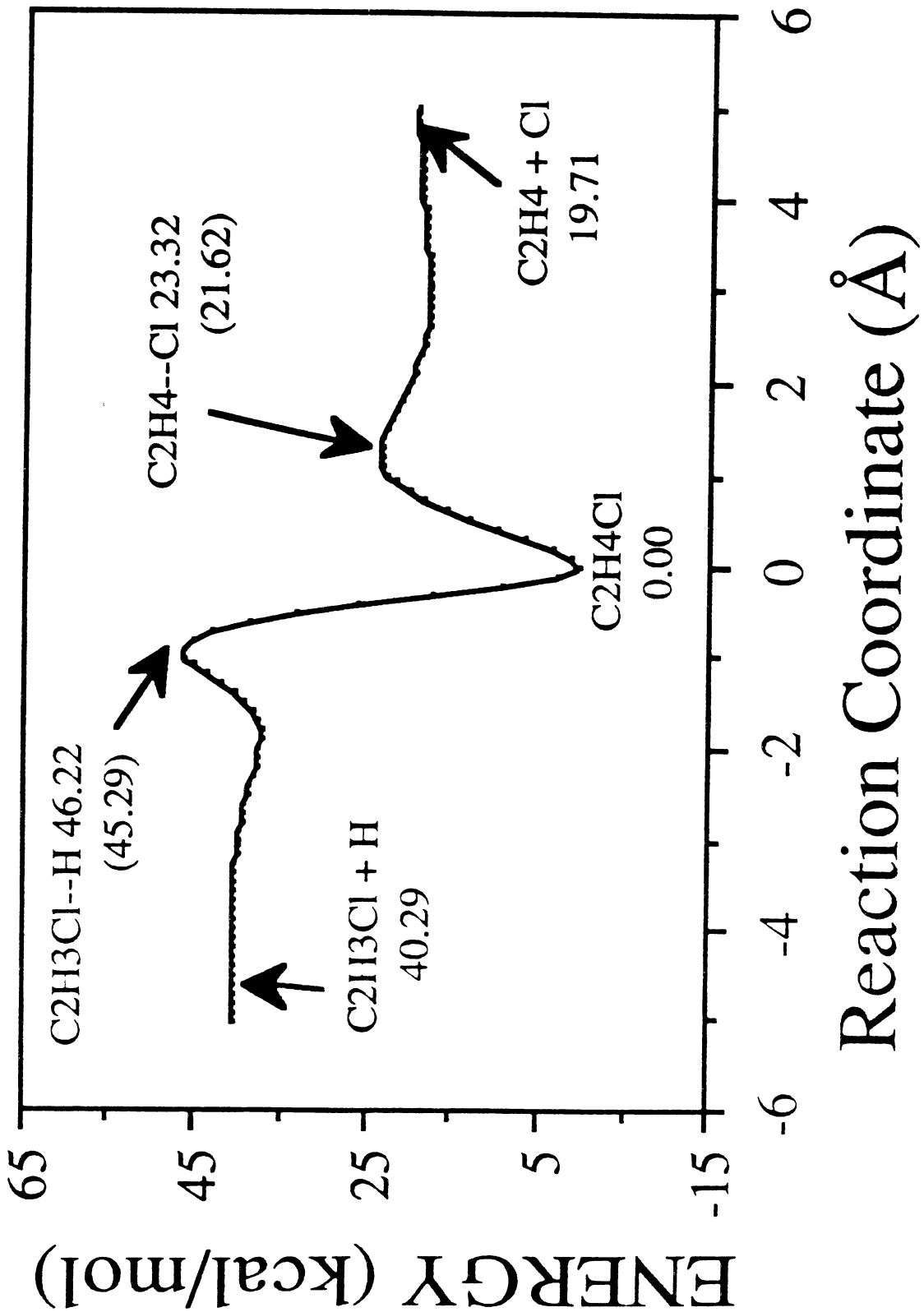
ENERGY (kcal/mol)
65
45
25
5
-15
-6
-4
-2
0
2
4
6
Reaction Coordinate (Å)
C2H3Cl--H 46.22
(45.29)
C2H3Cl + H
40.29
C2H4--Cl 23.32
(21.62)
C2H4Cl
0.00
C2H4 + Cl
19.71

the *ab initio* results[312,321]. The "reaction coordinate" corresponds to the displacement of the extended bond from the equilibrium value. Displacement of the C-H bond is plotted as a negative number for visual clarity.

Initial Conditions and Trajectory Integration

Calculations were performed using the same kinds of initial conditions as in the preceding chapter. However, in the current work, random microcanonical sampling was also used to select initial conditions for trajectories. This was done using Eqs. II.22 and II.23 as the weight function for the random walks for the cases of unrestricted angular momentum and $\mathbf{L} = 0$, respectively. Ensembles of 200-300 trajectories were computed for all four kinds of initial conditions for total energies corresponding to zero-point energy plus C-H local-mode excitation to $v = 6$, 8, 10, 12, 14, 16, or 18. The maximum integration time for individual trajectories was set at 25 and 50 ps for $v \geq 10$ and $v \leq 8$, respectively. A fixed stepsize of 4.89×10^{-17} s was used for all calculations.

Computational Results

Statistical Calculations[367]

The dissociation dynamics of 2-chloroethyl radical have been investigated using two variational transition-state theory methods and trajectory calculations. The transition-state methods are the EMS-TST procedure[172,361] that was briefly described in the Introduction and a J-conserving variant of that method that we denote as EJS-TST. This latter method introduces constraining equations in the Efficient Microcanonical Sampling (EMS) procedure that restrict the sampling to phase-space points associated with a constant value of the system angular momentum. For the specific case J=0, the method is denoted by EJZ-TST. Except for the sampling algorithm employed, these

procedures are identical to the variational MCTST methods previously described by Raff, Thompson and co-workers.[368,369]

In a manner analogous to the EMS-TST method[172], the angular momentum resolved (J=0) microcanonical rate coefficient, k(E,0), may be written in the form

$$k(E,0) = \frac{1}{2} \frac{\int dq\ W_{E0}(q)\ \delta(q_{RC}-q_c)\ \langle|\dot{q}_{RC}|\rangle_{E0}}{\int dq\ W_{E0}(q)} . \qquad (V.3)$$

The average absolute velocity through the critical surface is given by

$$\langle|\dot{q}_{RC}|\rangle_{E0} = \frac{\int dp\ \delta(T(p)-K)\ \delta(L(p,q)-J)\ |\dot{q}_{RC}|}{\int dp\ \delta(T(p)-K)\ \delta(L(p,q)-J)} \qquad (V.4)$$

where T(**p**) is the kinetic energy, L(**p**,**q**) is the magnitude of the total angular momentum, and

$$K = E - V(q) . \qquad (V.5)$$

As in the EMS-TST method[172], a Markov walk is used to evaluate k(E,0) but with the weight function $W_{E0}(q)$. The average absolute velocity through the critical surface $\langle|q_{RC}|\rangle$ is evaluated by standard Monte Carlo sampling techniques. The importance sampling techniques employed to evaluate Eq.V.3 are identical to those previously used in the EMS-TST calculations[172]. For comparison with trajectory calculations which were generated from initial states with zero total angular momentum, we have restricted the present study to ensembles with J=0. Such results are identified as EJZ-TST.

The critical surfaces used in the phase-space calculations are defined in terms of a reaction coordinate $q_{RC}(q)$ which may be a function of some or all of the coordinates **q**. For the case of simple bond fission considered here, a suitable reaction coordinate

will generally focus upon the motion of the separating atoms or the separating fragments. Schranz, Raff, and Thompson have previously considered three definitions of the reaction coordinate[172]:

RC1: $q_{RC}(\mathbf{q})$ is a bond-length reaction coordinate using the reduced mass corresponding to the two separating atoms,

RC2: a bond-length coordinate with a reduced mass corresponding to the separating fragments, and

RC3: $q_{RC}(\mathbf{q})$ is identified with the center-of-mass separation of the dissociating fragments using a reduced mass corresponding to the fragments.

Previous studies on bond fission in Si_2H_6 have shown that the rate coefficients obtained with these definitions differ by 4% or less.[172] The variational transition-state calculations reported here employ the RC1 definition, and the rate coefficients are variationally minimized with respect to the critical value q_C for this reaction coordinate by computation of the flux across a series of critical surfaces of width 0.1 Å located at $\{r_e + (i-1)0.5$ Å; i=1,2,...,10$\}$, where r_e is the equilibrium value of the bond undergoing fission[12].

For the case of simple bond fission in EMS-TST calculations, an exact analytical result for the average absolute velocity through the critical surface $\langle|\dot{q}_{RC}|\rangle$ can be derived. Schranz, Raff, and Thompson[361] have shown that

$$\langle|\dot{q}_{RC}|\rangle = [2K/\pi\mu]^{1/2}\,[(3N-5)/2]!\,/\,[(3N-4)/2]!\,, \qquad (V.6)$$

where m is the reduced mass described above, and N is the number of atoms in the molecule. The use of Eq.V.6 permits the integrals over the momentum coordinates in Eq.V.1 and V.3 to be done analytically thereby significantly reducing the computational

requirements of the calculations. Table XI gives the parameter values employed in the EMS-TST calculations.

Variationally minimized, microcanonical rate coefficients, k(E), have been computed at 7 internal energies in the range $77 \leq E \leq 131$ kcal/mol using EMS-TST methods. At four of these energies, we have used the J-conserving EJS-TST method to compute k(E,0) for J=0. At most of the energies considered (all but the lowest), the convergence of the configuration integrals in Eq.V.1 is essentially complete after 10^7 Markov states have been computed. In the case of C-H fission at the lowest energy, equivalent convergence requires about 2.5×10^7 states. The rate of convergence for the lowest and highest energies considered is shown in Figs. 20 and 21, respectively, for both k(E) and k(E,J=0) for reactions R1 and R2. Note that the vertical scales on these figures are substantially different and that, except for C-H fission at the lowest energy, convergence to a result with a similar relative error (10-20%) is obtained. The minimization procedure used here is identical to that employed in our previous study of bond fission reactions of disilane[172]. Typical results are shown in Fig. 22 for E = 131 kcal/mol. At this energy, k(E) and k(E,J=0) for C-H bond fission attain minimum values at $q_C = 2.1 \pm 0.3$ Å. For C-Cl bond fission, k(E) and k(E,J=0) reach a minimum at $q_C = 3.0 \pm 0.3$ and 3.5 ± 0.3 Å, respectively.

The variationally minimized EMS-TST and EJZ-TST microcanonical rate coefficients obtained in the calculations are given in Table XII. Statistical errors are given for 95% confidence limits and are calculated using the "bootstrap" method [298] As can be seen, the J-conserving constraint with J=0 results in a significant increase in the C-H bond fission rates. The ratio k(E,J=0)/k(E) is 4.2 at E=77 kcal/mol. This ratio decreases as the total internal energy increases. Over the range $118.5 \leq E \leq 131$ kcal/mol, the ratio becomes relatively constant around the value 2.0. These results are in accord with previous calculations reported by Viswanathan *et al.*[184] on C-H bond

Table XI. Values of Parameters Used in the EMS-TST Calculations.

Parameter	Value
Number of incubation Markov steps	10^5
Number of Markov states, M	2.5×10^7
Number of atoms moved/step	4
Markov Cartesian step size, Δq/Å	0.2
Importance weight exponent, α (see Ref. 12)	7
Critical surface positions, q_C/Å	$\{r_e + 0.5(i-1), i=1,10\}$
Critical surface width, Δ_C/Å	0.1
Upper limit on bond lengths, R_{max}/Å	$r_e + 4.5$

Figure 20. Convergence of the microcanonical rate coefficient k(E) for bond fission reactions of the 2-chloroethyl radical as a function of number of Markov states sampled at an energy E=77.0 kcal/mol. Filled squares: (■), C-Cl fission, EMS-TST, q_C=3.0 Å; Open squares: (□), C-Cl fission, EJZ-TST, q_C=3.0 Å; Filled circles: (●), C-H fission, EMS-TST, q_C=2.1 Å; Open circles: (O), C-H fission, EJZ-TST, q_C=2.1 Å.

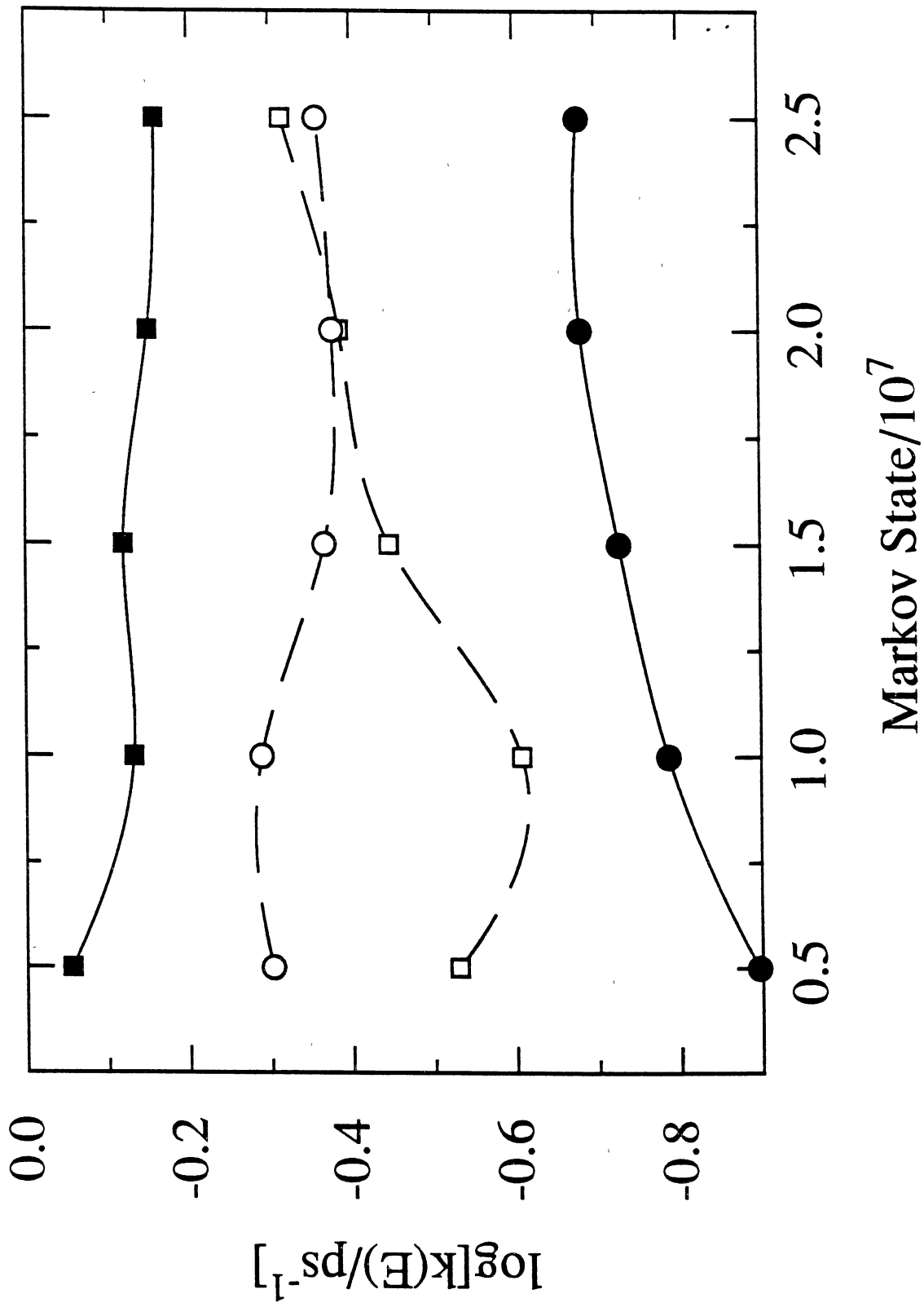
0.0
-0.2
-0.4
-0.6
-0.8
log[k(E)/ps^{-1}]
0.5
1.0
1.5
2.0
2.5
Markov State/10^7

Figure 21. Convergence of the microcanonical rate coefficient k(E) for bond fission reactions of the 2-chloroethyl radical as a function of number of Markov states sampled at an energy E=131.0 kcal/mol. Filled squares: (■), C-Cl fission, EMS-TST, q_C=3.0 Å; Open squares: (□), C-Cl fission, EJZ-TST, q_C=3.5 Å; Filled circles: (●), C-H fission, EMS-TST, q_C=2.1 Å; Open circles: (O), C-H fission, EJZ-TST, q_C=2.1 Å.

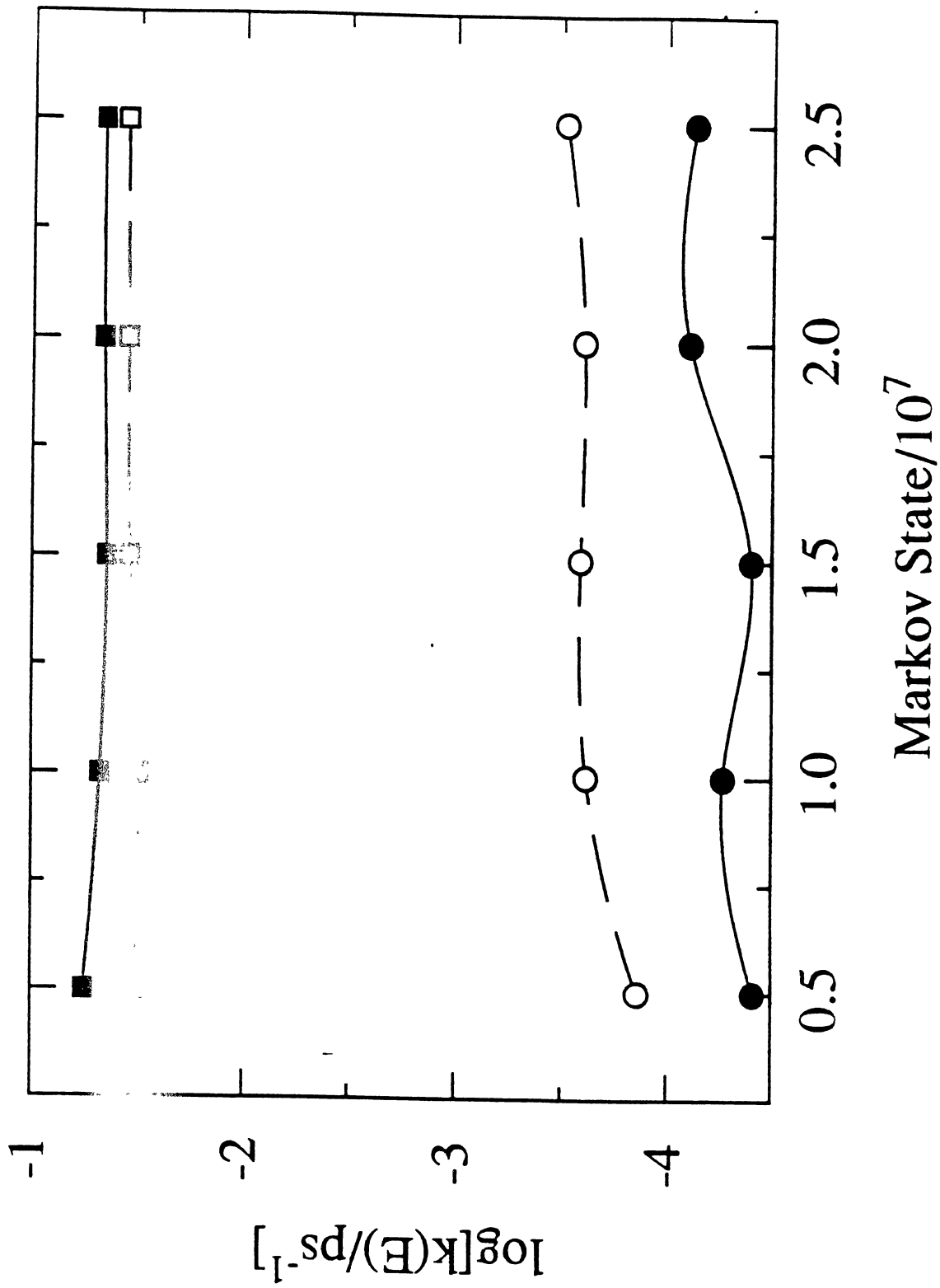
-1
-2
-3
-4
log[k(E)/ps^{-1}]
0.5
1.0
1.5
2.0
2.5
Markov State/10^7

Figure 22. Microcanonical rate coefficient k(E) for the bond fission reactions of the 2-chloroethyl radical as a function of the placement of the critical surface along the bond length reaction coordinate, q_C, at an energy E=131.0 kcal/mol. Filled squares: (■), C-Cl fission, EMS-TST; Open squares: (□), C-Cl fission, EJZ-TST; Filled circles: (●), C-H fission, EMS-TST; Open circles: (O), C-H fission, EJZ-TST. The C-Cl curves have been shifted upwards by 1.5 log units for clarity.

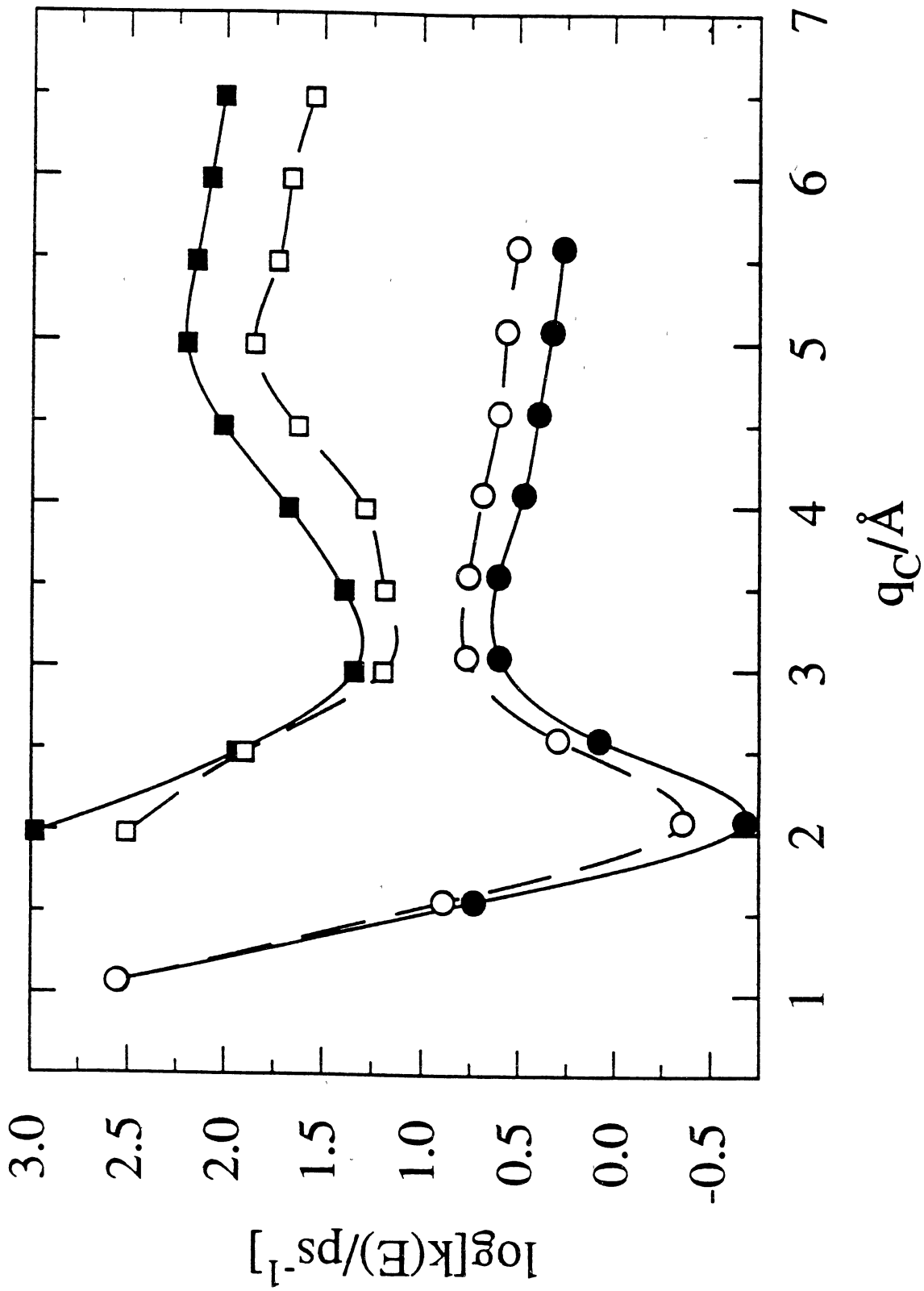
log[k(E)/ps^{-1}]
3.0
2.5
2.0
1.5
1.0
0.5
0.0
-0.5
1
2
3
4
5
6
7
q_C/Å

Table XII. Variationally Minimized EMS-TST and EJZ-TST Microcanonical Rate Coefficients for Total Fissions, C-Cl Fissions, and C-H Fissions in the 2-chloroethyl Radical. Error Limits are 95% Confidence Limits.

Energy	k(E)/ps^{-1}	
	EMS-TST	EJZ-TST
77.0	0.046±0.007	0.036±0.005
	0.046±0.007	0.036±0.005
	(7.4±8.0)x10^{-5}	(3.1±1.2)x10^{-4}
89.5	0.131±0.028	____
	0.129±0.029	____
	(1.5±0.2)x10-3	____
100.5	0.215±0.033	0.155±0.031
	0.204±0.031	0.129±0.027
	0.011±0.002	0.026±0.004
110.2	0.360±0.063	____
	0.325±0.058	____
	0.035±0.005	____
118.5	0.580±0.069	0.448±0.262
	0.500±0.050	0.287±0.227
	0.080±0.019	0.161±0.035
125.4	0.804±0.068	____
	0.651±0.051	____
	0.153±0.017	____
131.0	0.904±0.156	0.924±0.291
	0.694±0.115	0.485±0.201
	0.210±0.041	0.439±0.090

cleavage in CH_4. These investigators employed a J-conserving MCTST method and found that angular momentum acts to reduce the microcanonical rate coefficient k(E,0) by an amount in excess of the centrifugal barrier effect. They also found that the magnitude of the decrease due to angular momentum decreases as the ratio of the rotational energy to the total energy above threshold decreases. Similar results have also been reported by Brown and Miller[189].

In contrast, the data in Table XII show that the k(E,J=0)/k(E) ratio for C-Cl bond fission is generally less than unity. This ratio is relatively constant over the energy range investigated. Its average value is 0.67. This result can be rationalized by consideration of the partitioning of the internal vibrational energy. The dual constraints of energy and momentum conservation always result in partitioning most of the vibrational energy into motion of the light atoms. As the molecular angular momentum increases at a constant internal energy E, vibrational energy is converted into rotational motion. Because of the vibrational energy partitioning, most of this energy comes from light-atom motion. As a result, the centrifugal effects produced by the increased angular momentum are not sufficient to compensate for the loss of light-atom vibrational energy and k(E,0) decreases with increasing J for light-atom bond fissions. Since very little of the converted vibrational energy comes from heavy-atom motion, such as chlorine in a C-Cl bond, the centrifugal effects more than compensate and k(E,0) increases with increasing J for heavy-atom bond fissions.

Trajectory Calculations

The decay plots obtained from the trajectory results, in general, exhibit a high degree of linearity, as expected for a first-order process in a statistical system. In addition, the slopes of the decay curves are found to be insensitive to the method employed to select the initial states. Typical examples are shown in Figs. 23a-d and

Table XIII. Microcanonical Rate Coefficients for Total Fissions, C-Cl Fissions, and C-H Fissions in the 2-chloroethyl Radical for Trajectories Initiated Using EMS, EJZ, Uniform, and Local Excitations. Error Limits are 95% Confidence Limits.

Energy	k(E)/ps^{-1}			
	EMS	EJZ	Local	Uniform
77.0	0.032 ±0.003	0.032 ±0.003	0.030±0.004	0.030 ±0.004
	0.032 ±0.003	0.031 ±0.003	0.030±0.004	0.029 ±0.004
	----------	0.0007 ±.0005	----------	0.0003±0.0004
89.5	0.082 ±0.009	0.068 ±0.020	0.07 ±0.01	0.07 ±0.01
	0.081 ±0.009	0.066 ±0.007	0.066±0.007	0.063 ±0.009
	0.0006±0.0006	0.002 ±0.001	0.005±0.002	0.003 ±0.002
100.5	0.130 ±0.01	0.14 ±0.01	0.15 ±0.02	0.15 ±0.02
	0.120 ±0.01	0.11 ±0.01	0.13 ±0.02	0.12 ±0.02
	0.008 ±0.003	0.021 ±0.005	0.023±0.007	0.026 ±0.008
110.2	0.21 ±0.02	0.17 ±0.02	0.24 ±0.03	0.24 ±0.03
	0.18 ±0.02	0.13 ±0.02	0.20 ±0.03	0.18 ±0.02
	0.021 ±0.006	0.039 ±0.008	0.04 ±0.01	0.07 ±0.02
118.5	0.28 ±0.03	0.31 ±0.03	0.29 ±0.04	0.28 ±0.04
	0.24 ±0.03	0.20 ±0.02	0.22 ±0.03	0.21 ±0.03
	0.042 ±0.009	0.11 ±0.02	0.07 ±0.02	0.08 ±0.02
125.4	0.36 ±0.04	0.40 ±0.05	0.46 ±0.07	0.4 ±0.1
	0.30 ±0.03	0.25 ±0.03	0.28 ±0.05	0.25 ±0.04
	0.06 ±0.01	0.15 ±0.02	0.18 ±0.04	0.12 ±0.04
131.0	0.47 ±0.06	0.39 ±0.04	0.48 ±0.08	0.51 ±0.07
	0.40 ±0.05	0.25 ±0.03	0.32 ±0.06	0.31 ±0.05
	0.07 ±0.02	0.14 ±0.02	0.16 ±0.04	0.20 ±0.04

Figure 23. Decay plots at E=77 kcal/mol for (a) local mode excitation; (b) uniform excitation; (c) EJZ sampling; and (d) EMS sampling. In each case, the line is a linear least-squares fit to the calculated points. The rate coefficients computed from the slope of the least-squares fit is given in the Figure along with the correlation coefficient for the fitting.

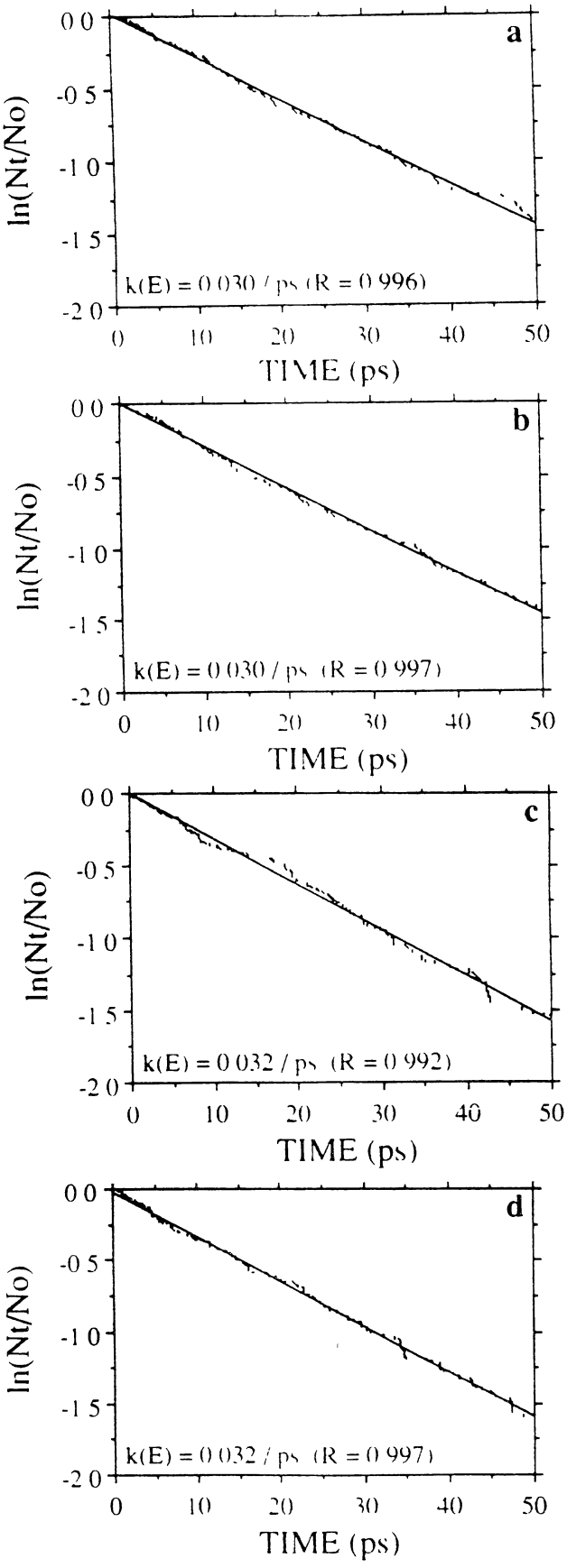
a
ln(Nt/No)
0.0
-0.5
-1.0
-1.5
-2.0
k(E) = 0.030 / ps (R = 0.996)
0
10
20
30
40
50
TIME (ps)
b
ln(Nt/No)
k(E) = 0.030 / ps (R = 0.997)
TIME (ps)
c
ln(Nt/No)
k(E) = 0.032 / ps (R = 0.992)
TIME (ps)
d
ln(Nt/No)
k(E) = 0.032 / ps (R = 0.997)
TIME (ps)

Figure 24. Decay plots at E=131.0 kcal/mol for (a) local mode excitation; (b) uniform excitation; (c) EJZ sampling; and (d) EMS sampling. In each case, the line is a linear least-squares fit to the calculated points. The rate coefficients computed from the slope of the least-squares fit is given in the Figure along with the correlation coefficient for the fitting.

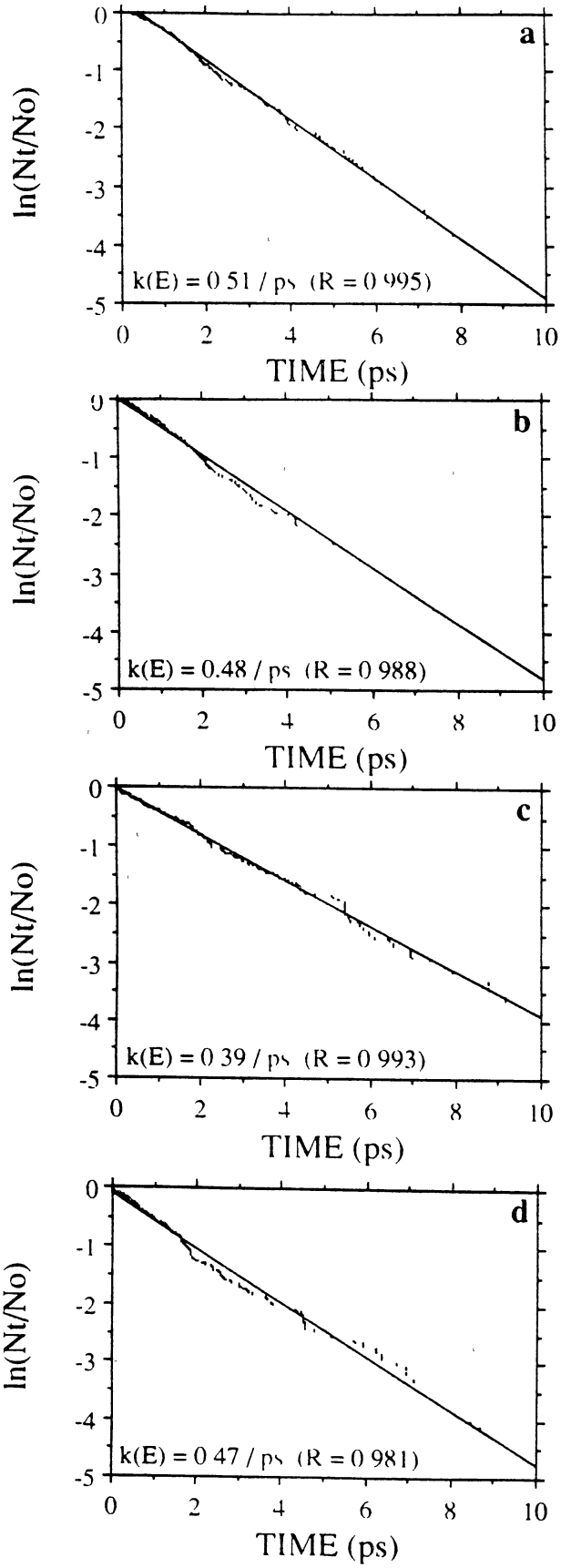
a
ln(Nt/No)
k(E) = 0 51 / ps (R = 0 995)
TIME (ps)
b
ln(Nt/No)
k(E) = 0.48 / ps (R = 0 988)
TIME (ps)
c
ln(Nt/No)
k(E) = 0 39 / ps (R = 0 993)
TIME (ps)
d
ln(Nt/No)
k(E) = 0 47 / ps (R = 0 981)
TIME (ps)

Table XIV. RRK Parameters (E_0, ν, s) and Correlation Coefficient, r, for RRK Fits to Rate Coefficients in Tables XII and XIII for the Simple Bond Fission of the 2-chloroethyl Radical.

Reaction	Calculation	E_0(kcal/mol)	ν/ps^{-1}	s	r
C_2H_4Cl ---> CH_2=CH_2 + Cl					
	EMS-TST	23.3	18.4	17.7	0.997
	EJZ-TST		8.88	16.5	0.994
	EMS		6.21	15.7	0.996
	EJZ[a]		3.31	14.0	0.995
	uniform		5.64	15.5	0.997
	local[a]		5.02	15.3	0.997
C_2H_4Cl ---> CH_2-CHCl + H					
	EMS-TST	46.3	305.	17.6	1.000
	EJZ-TST		277.	15.9	1.000
	EMS[a]		105.	17.1	0.983
	EMS[b]		71.6	16.3	0.993
	EJZ[a]		31.9	13.1	0.978
	uniform[a]		34.8	13.1	0.989
	uniform[b]		253.	16.9	0.984
	local[a]		73.0	14.4	0.993

(a) RRK fit to rate coefficients at energies ranging from 89.5 to 131.0 kcal/mol.

(b) RRK fit to rate coefficients at energies ranging from 89.5 to 131.0 kcal/mol and an estimated upper bound rate coefficient at E=77.0 kcal/mol assuming that one trajectory in a batch of 500 would react via the C-H fission channel. In actual fact, there were no such reactions in a batch size of 250.

24a-d which give the results for each initial-state selection procedure for E = 77 and 131.0 kcal/mol, respectively. The near linearity of these plots is obvious. The rate coefficients obtained from the slopes of the least-squares fits are given in Table XIII. For C-H bond fission, the maximum percent variations in k(E) for the four initial-state selection methods are 15%, 20%, and 38% at E=100.5, 118.5, and 131.0 kcal/mol, respectively. Such variations are close to the statistical accuracy of the method.

The data for each of the calculations given in Table XII and XIII have been fitted to the RRK equation[354]

$$k(E) = \nu [(E - E_0)/E]^{s-1} , \qquad (V.7)$$

where E_0 is taken to be the barrier height for bond fission for a given channel. The results of this fitting are given in Table XIV for each of the 12 calculations.

Discussion

Comparison of Statistical[367] and Dynamical Results

The data presented above indicate that the 2-chloroethyl radical behaves statistically at internal energies above 77 kcal/mol. This is demonstrated by the relative insensitivity of the decomposition dynamics and the computed microcanonical rate coefficients to the initial energy partitioning. There is no evidence for mode-specific effects. The fitted values of s in Eq. V.6 are close to the full classical limiting value of 3N-6, which may suggest statistical dynamics. In addition, the EMS-TST calculations are found to be upper bounds for the corresponding EMS trajectory calculations and the EJZ-TST results are likewise upper bounds for the trajectory rates with EJZ initial-state sampling. Figures 25 and 26 compare the EMS-TST and EJZ-TST results with the corresponding trajectory data for C-Cl and C-H bond cleavage, respectively. In each

Figure 25. Comparison of microcanonical rate coefficients for the C-Cl bond fission of the 2-chloroethyl radical evaluated by variational EMS-TST and EJZ-TST calculations with various trajectory calculations. Curves are the corresponding RRK fits. Statistical calculations: EMS-TST, filled squares: (■); EJZ-TST, open squares (□). Trajectory calculations: EMS, filled circles (●); EJZ, open circles (O); uniform, crosses (x); local, plus signs (+).

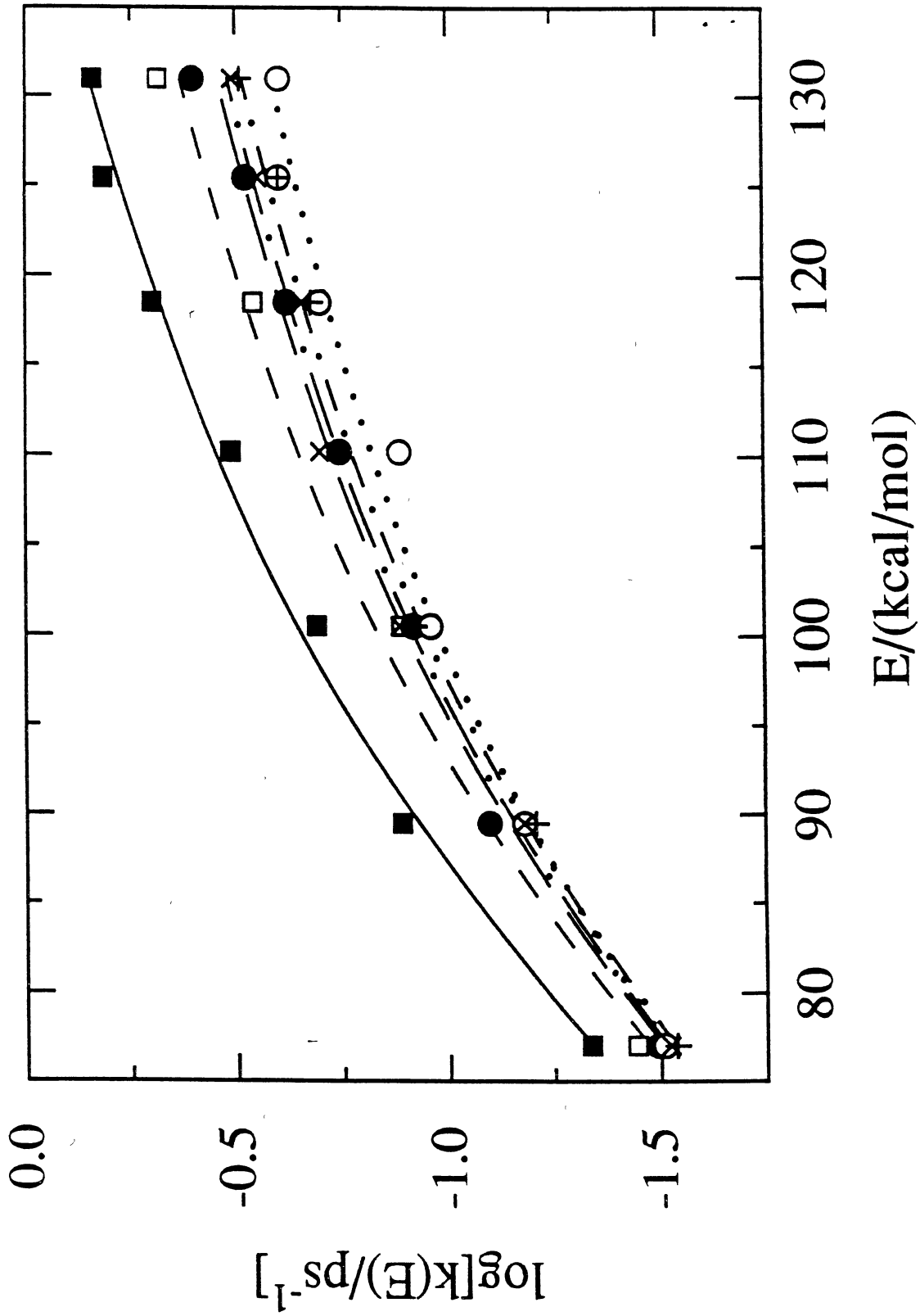
0.0
-0.5
-1.0
-1.5
log[k(E)/ps^{-1}]
80
90
100
110
120
130
E/(kcal/mol)

Figure 26. Comparison of microcanonical rate coefficients for the C-H bond fission of the 2-chloroethyl radical evaluated by variational EMS-TST and EJZ-TST calculations with various trajectory calculations. Curves are the corresponding RRK fits. Statistical calculations: EMS-TST, filled squares: (■); EJZ-TST, open squares (□). Trajectory calculations: EMS, filled circles (●); EJZ, open circles (O); uniform, crosses (x); local, plus signs (+).

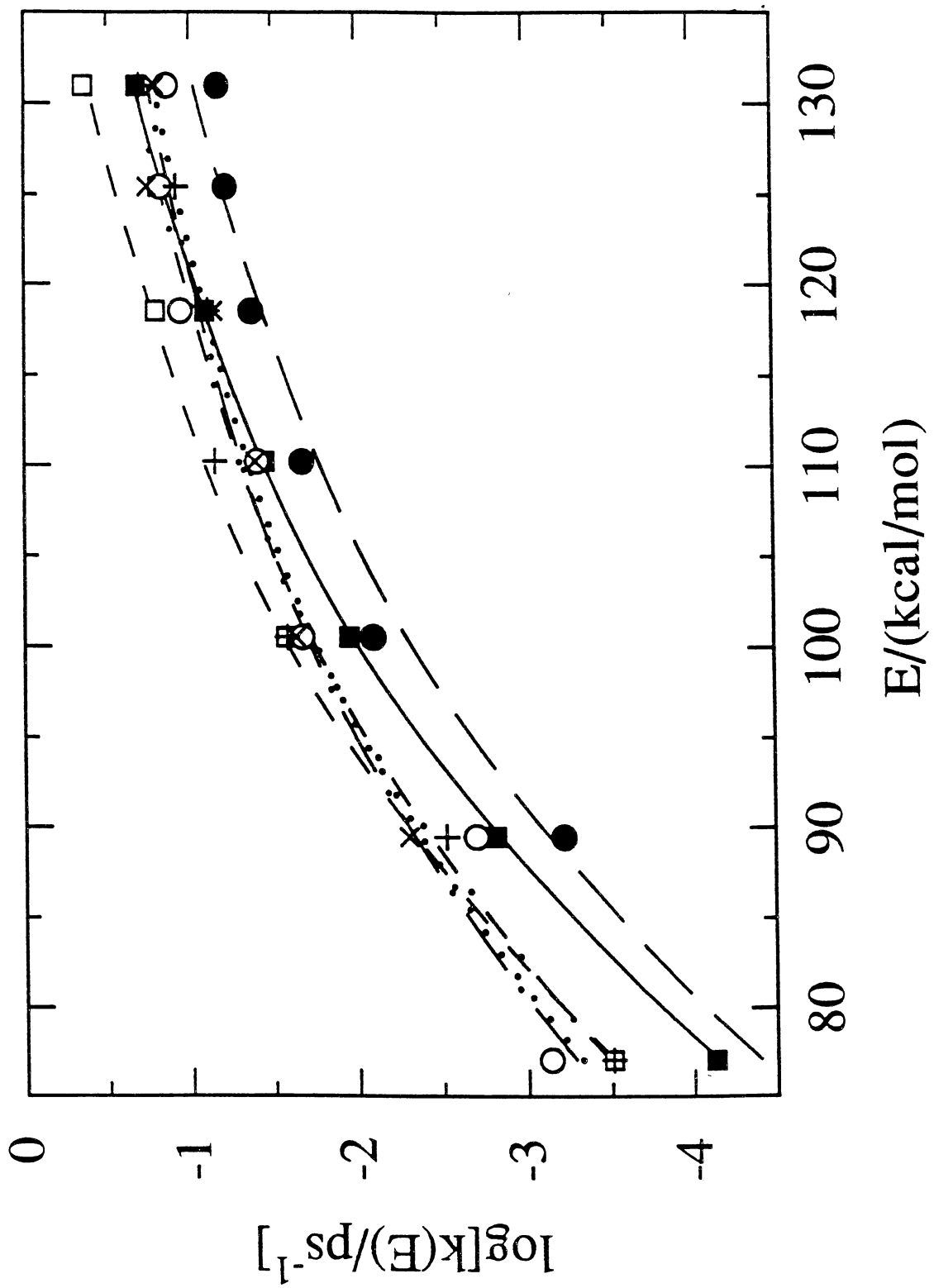
0
-1
-2
-3
-4
log[k(E)/ps^{-1}]
80
90
100
110
120
130
E/(kcal/mol)

case, the curves are the RRK fits to the data obtained from Eq.V.6. For C-Cl fission, both statistical calculations provide clear upper bounds to all of the trajectory calculated rate coefficients. In the case of C-H bond rupture, there is some evidence for a crossover at energies below 90 kcal/mol, but above this energy, the transition-state theory results provide the expected upper limits. As noted in the Introduction, the existence of such upper bounds is a requirement for statistical behavior in any system. In this respect, the present results are in qualitative accord with those for PES-I.

The statistical behavior of the 2-chloroethyl radical stands in sharp contrast to the dissociation dynamics previously reported for unimolecular decomposition of disilane[172-173,211] and 1,2-difluoroethane[360,171]. In both of these systems, the dissociation dynamics are strongly dependent upon the initial-state energy partitioning and, most importantly, EMS-TST calculations fail to yield upper bounds to the trajectory-computed rate coefficients. In some cases, we find that the $[k(E)]_{traj}/[k(E)]_{EMS\text{-}TST}$ ratio is on the order of 10^2. Such differences in dynamical behavior seem strange and are certainly unexpected. This is particularly true for the 2-chloroethyl and 1,2-difluoroethane systems that would appear to be, in many respects, similar molecules. If the origin of such differences can be determined, the information may provide important clues that permit nonstatistical behavior to be anticipated in other systems.

Possible Explanations for the Observed Behavior

Internal Energies? Let us first consider the effect of the magnitude of the internal energy upon the degree of statistical behavior in the 2-chloroethyl radical, Si_2H_6, and 1,2-difluoroethane. In all cases, the $[k(E)]_{traj}/[k(E)]_{EMS\text{-}TST}$ ratio decreases as the total internal energy increases[172-173,360]. Since we must have $[k(E)]_{traj}/[k(E)]_{EMS\text{-}TST} \leq 1$ for any system that exhibits statistical behavior, this result suggests that the dissociation

dynamics of 1,2-difluoroethane, 2-chloroethyl radical, and disilane all become more ergodic at higher internal energies. Such behavior is in accord with generalizations that may be drawn from many previously reported studies. However, it is important to note that *the lowest energies at which statistical behavior is observed are frequently far above the dissociation threshold.* For example, we find that Si-H bond fission reactions in disilane are nonstatistical at internal energies below 7.2 eV, which is over 5 eV in excess of the dissociation threshold[172-173]. There is also evidence that C-H bond fissions in 1,2-difluoroethane are nonstatistical at energies below 7 eV.[360]

The energy ranges over which the statistical behavior of these three systems were examined are 77-131.0 kcal/mol [CH_2-CH_2Cl], 138.4-207.5 kcal/mol [CH_2F-CH_2F], and 122.4-214.7 kcal/mol [H_3Si-SiH_3]. Consequently, a simple examination of these energies ranges alone would suggest that the 2-chloroethyl radical would be the most nonstatistical of the three. In reality, just the opposite is true. If we consider only the internal energy above threshold, the qualitative picture is essentially unchanged. For the C-H and Si-H bond fissions, the energy ranges above threshold are 30.7-84.7 kcal/mol [CH_2-CH_2Cl], 27.1-96.3 kcal/mol [CH_2F-CH_2F], and 33.9-126.1 kcal/mol for [H_3Si-SiH_3]. 1,2-difluoroethane and disilane both exhibit nonstatistical behavior for hydrogen-bond fission at internal energies less than 80 kcal/mol in excess of threshold. In contrast, C-H bond fission in the 2-chloroethyl radical is statistical even at energies of 30.7 kcal/mol in excess of threshold. Si-Si bond fission in disilane and C-C fission in 1,2-difluoroethane are both nonstatistical at internal energies over 200 kcal/mol in excess of threshold whereas C-Cl bond fission in the chloroethyl radical is found to behave statistically at internal energies only 53.7 kcal/mol in excess of threshold. Thus, while we may be confident that the behavior of a given system will become more ergodic as the internal energy increases, it is clearly not possible to predict the onset of statistical

behavior from energy considerations alone. Many polyatomic molecules exhibit ergodic dynamics only at energies much greater than the dissociation threshold.

Relative Reaction Rates? Since it is known that a prerequisite for statistical behavior is an IVR rate that is globally fast relative to the unimolecular reaction rate, it might be expected that non-statistical dynamics would tend to occur in those systems whose unimolecular reaction rates are relatively large. For the three systems examined, this consideration would suggest that the 2-chloroethyl radical should be the most nonstatistical. The bond fission energy barriers for C-H and C-Cl in this molecule are 46.3 and 23.3 kcal/mol, respectively, compared to 75.9 and 88.6 kcal/mol for Si-Si and Si-H bond fission in disilane, and 90.5 and 110.7 kcal/mol for C-C and C-H cleavage in 1,2-difluoroethane[172-173,360]. We therefore expect and observe unimolecular decomposition to be more rapid for the 2-chloroethyl radical than for either 1,2-difluoroethane or disilane[172-173,360]. Yet, it is the 2-chloroethyl radical that exhibits statistical dynamics.

These considerations show clearly that it is not just the magnitude of the unimolecular reaction rate that is important but rather the relative value of that rate compared to that required for global intramolecular energy randomization. Since the IVR rate is critically dependent upon the extent of intermode coupling present in the potential-energy surface, the differences in the three systems might be presumed to lie in such potential coupling terms.

Form of the Potential-energy Surfaces? A qualitative examination of the potential surfaces for 2-chloroethyl and 1,2-difluoroethane[275] suggests that the intermode coupling should be very similar. In both systems, all bond stretching interactions are represented by the Morse-type functions given in Eq.II.2. All three-atom bending potentials have the quadratic form given by Eq.II.4. In both surfaces, the parameters in the bending and stretching interactions are varied continuously along the

dissociation coordinate using switching functions that have hyperbolic tangent form. However, the arguments of the switching functions are different. For 2-chloroethyl, the argument depends quadratically upon the displacement from equilibrium whereas for 1,2-difluoroethane, this dependence is exponential in form. There are also differences in the form of the switching functions used for the bending force constants. In addition, the potential surface for 2-chloroethyl contains quadratic wagging interactions and a small dihedral angle dependence whereas these interactions are not present in the empirical 1,2-difluoroethane potential.

A Promising Explanation for The Observed Behavior

Coupling Coefficient. To obtain a more quantitative evaluation of the intermode coupling present in 2-chloroethyl and 1,2-difluoroethane, we have numerically evaluated the force constant matrix in Cartesian coordinates for both systems at several points along the dissociation paths for C-H and C-X (X=Cl or F) bond fission and at equilibrium. In this coordinate system, the kinetic energy matrix is diagonal and all intermode coupling is present as potential coupling. To facilitate comparison of the two systems, we define a total average atom-atom coupling constant, C_{ij} ,

$$C_{ij} = \frac{1}{9}\sqrt{\sum_{\alpha=1}^{3}\sum_{\beta=1}^{3}\left\{\frac{\partial^2 V}{\partial q_{\alpha i}\partial q_{\beta j}}\right\}^2} \qquad \text{(V.8)}$$

where α and β run over the three Cartesian (x,y,z) coordinates of atoms i and j. As defined, C_{ij} is invariant under translation of or rotation about the molecular center-of-mass. It sums the magnitude of the coupling terms between all coordinates of atom i and all those of atom j. It therefore gives a direct measure of the extent of potential coupling in the molecule. The results for the equilibrium configurations of

Table XV. Total Atom-atom Potential Coupling Constants, C_{ij}, Calculated From Eq.(V.8) for the 2-chloroethyl Radical and 1,2-difluoroethane in Their Equilibrium Configurations. The Atom Designations are as Given in the Inset to Figs. 27 and 28. All Constants are Given in Units of eV/Å^2.

i	j	Atoms	2-chloroethyl radical C_{ij}	i	j	1,2-difluroethane C_{ij}
			Bonded Interactions			
1	2	C1-C2	3.409	1	2	2.775
1	3	C1-H	3.677	1	5	3.476
1	4	C1-H	3.677	1	6	3.476
2	5	C2-H	3.534	2	7	3.476
2	6	C2-H	3.534	2	8	3.476
2	7	C2-Cl(F)	1.323	2	4	5.221
				1	3	5.221
			Non-bonded, Bending Interactions			
1	5	C1 H	0.280	1	7	0.228
1	6	C1 H	0.280	1	8	0.228
2	3	C2 H	0.203	2	5	0.228
2	4	C2 H	0.203	2	6	0.228
1	7	C1 Cl(F)	0.282	1	4	0.369
		C2 F		2	3	0.369
3	4	H H	0.228	5	6	0.334
5	6	H H	0.217	7	8	0.334
		HF		5	3	0.343
		H F		6	3	0.343
5	7	H Cl(F)	0.225	7	4	0.343
6	7	H Cl(F)	0.225	8	4	0.343
			Dihedral Interactions			
3	5	H H	7.4×10^{-6}	5	7	5.6×10^{-4}
3	6	H H	7.4×10^{-6}	5	8	5.6×10^{-4}
4	5	H H	7.4×10^{-6}	6	7	5.6×10^{-4}
4	6	H H	7.4×10^{-6}	6	8	5.6×10^{-4}
3	7	H Cl(F)	1.25×10^{-2}	5	4	4.8×10^{-4}

Figure 27. Calculated coupling constants C_{ij} as defined by Eq.V.8 for bonded atoms for 2-chloroethyl and 1,2-difluoroethane as a function of position along the dissociation coordinates for C-H and C-X (X=Cl or F) bond fissions as measured by V/E_o, where V is the potential relative to the reactant and E_o is the barrier height for bond cleavage. Positive values of V/E_o denote motion along the C-X (X=Cl or F) dissociation path; negative values motion along the C-H dissociation path. For the C-H bond fissions, hydrogen atom #5 is the one undergoing dissociation. The atom numbering is as given in the Figure insets. The solid lines have no significance other than to increase visual clarity. (A) 1,2-difluoroethane: (*) C-C coupling, C_{12}; (#) C-F coupling, C_{24}; (O) C-H coupling, C_{15}. (B) 2-chloroethyl: (*) C-C coupling, C_{12}; (#) C-Cl coupling, C_{27}; (O) C-H coupling, C_{25}.

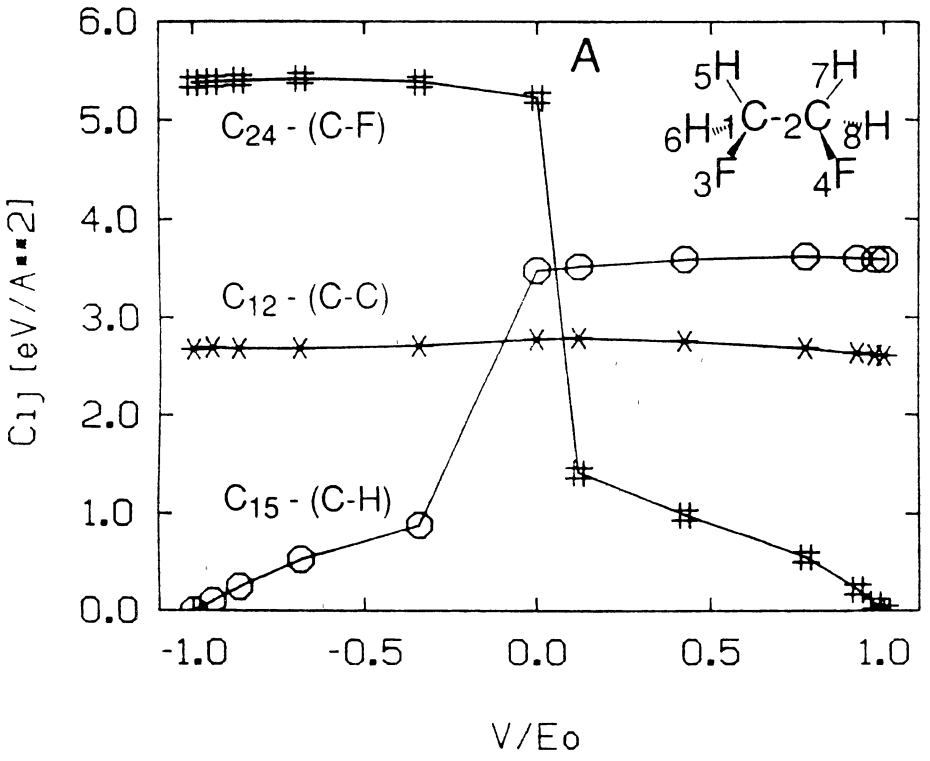
A
C_{24} - (C-F)
C_{12} - (C-C)
C_{15} - (C-H)
C_{1J} [eV/A**2]
V/Eo
6.0
5.0
4.0
3.0
2.0
1.0
0.0
-1.0
-0.5
0.0
0.5
1.0
5H
7H
6H
1C-2C
8H
3F
4F

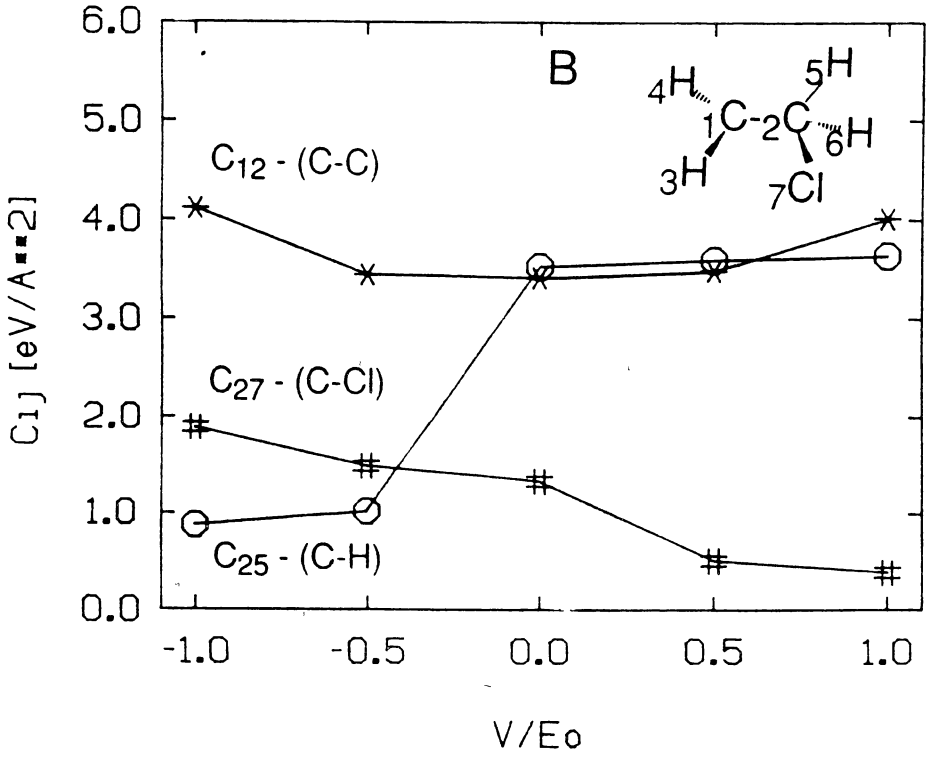
B
C_{12} - (C-C)
C_{27} - (C-Cl)
C_{25} - (C-H)
C_{1J} [eV/A**2]
V/Eo
6.0
5.0
4.0
3.0
2.0
1.0
0.0
-1.0
-0.5
0.0
0.5
1.0
4H
5H
1C-2C
6H
3H
7Cl

Figure 28. Calculated coupling constants C_{ij} as defined by Eq.V.8 for nonbonded atoms for 2-chloroethyl and 1,2-difluoroethane as a function of position along the dissociation coordinates for C-H and C-X (X=Cl or F) bond fissions as measured by V/E_0, where V is the potential relative to the reactant and E_0 is the barrier height for bond cleavage. Positive values of V/E_0 denote motion along the C-X (X=Cl or F) dissociation path; negative values motion along the C-H dissociation path. For the C-H bond fissions, hydrogen atom #5 is the one undergoing dissociation. The atom numbering is as given in the insets in Figures. 27A and 27B. The solid lines have no significance other than to increase visual clarity. (#) 2-chloroethyl, C-H coupling, C_{15}; (O) 2-chloroethyl, C-Cl coupling, C_{17}; (*) 1,2-difluoroethane, C-F coupling; C_{23}; (+) 1,2-difluoroethane, C-H coupling, C_{25}.

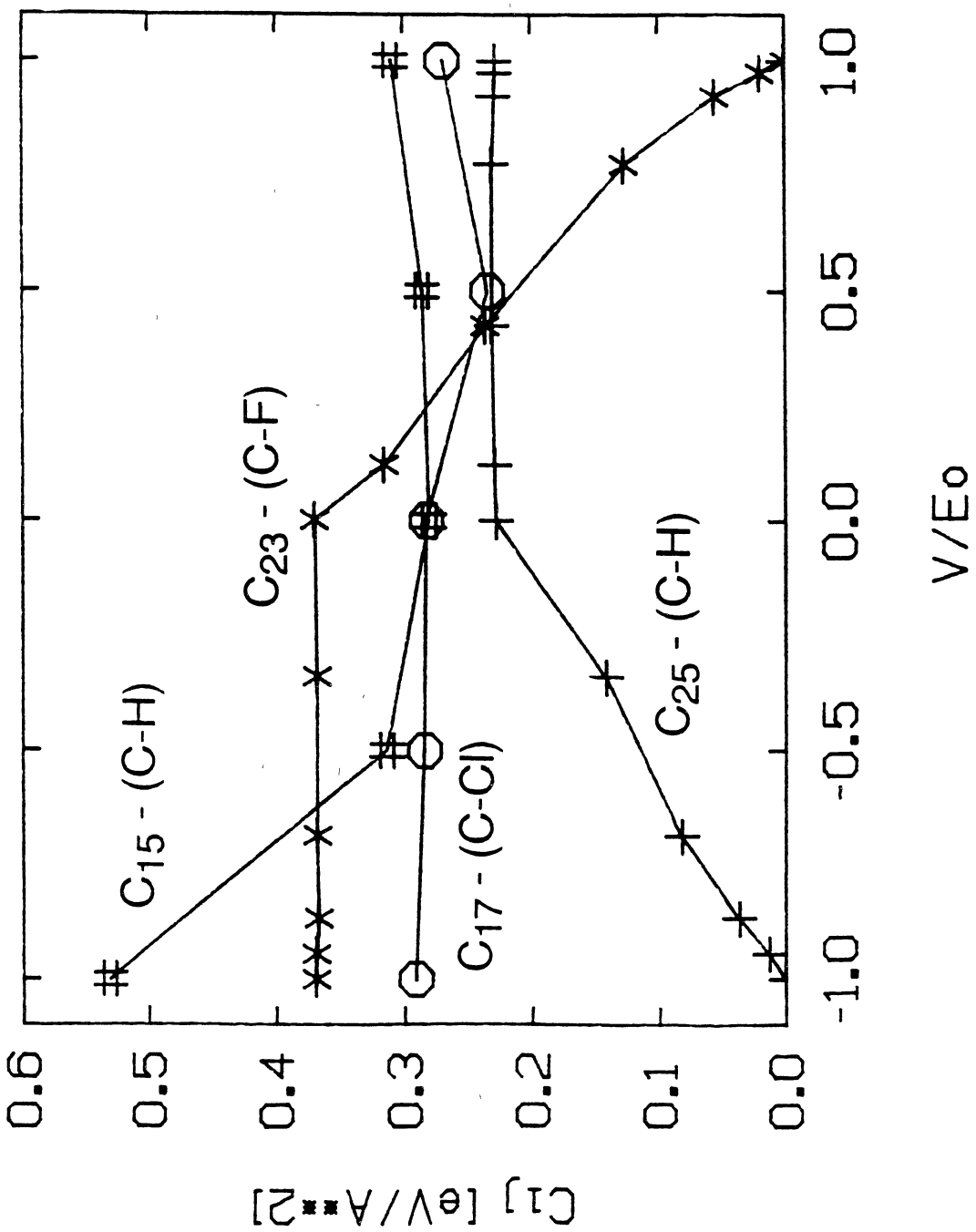
C15 - (C-H)
C23 - (C-F)
C17 - (C-Cl)
C25 - (C-H)
0.6
0.5
0.4
0.3
0.2
0.1
0.0
-1.0
-0.5
0.0
0.5
1.0
V/Eo
[eV/A**2]

2-chloroethyl and 1,2-difluoroethane are given in Table XV. In general, the coupling forces in the two molecules are very similar in magnitude. Except for the C-X bonds, the couplings due to direct bonding interactions are slightly larger in 2-chloroethyl, but this is counterbalanced by larger coupling in 1,2-difluoroethane resulting from the non-bonded, bending interactions. In both molecules, the coupling between dihedral atoms is very small. It seems unlikely that the differences in potential coupling at equilibrium are sufficiently large to account for the pronounced variations observed in the statistical behavior and IVR rates between the two molecules.

Figures 27 and 28 show the variations of selected couplings at different points along the C-H and C-X (X=Cl or F) dissociation coordinates represented by the ratio of the potential at the point in question to the dissociation barrier height, E_0. The point $V/E_0=1.0$ corresponds to the transition state for C-X (X=F,Cl) dissociation; $V/E_0=0.0$ is the equilibrium configuration, and $V/E_0=-1.0$ represents the transition state for C-H bond fission. Figures 27A and 27B show the variation of potential coupling between bonded atoms. The coupling between nonbonded atoms connected by bending potential terms is shown in Fig. 28. The C-C coupling, C_{12}, is nearly constant along both dissociation paths although this coupling in 2-chloroethyl does increase slightly as the C-H bond breaks and the C=C double bond forms. As noted in Table XV, the C-C coupling in 2-chloroethyl is about 25% larger than the corresponding interaction in 1,2-difluoroethane. The potential coupling between bonded C-H atoms (C_{15} for 1,2-difluoroethane and C_{25} for 2-chloroethyl) is very nearly identical along both reaction paths. In each case, this coupling is nearly equal and essentially constant as the C-X bond breaks. Along the C-H dissociation pathway, the coupling attenuates rapidly. Since a back-reaction barrier exists for C-H bond fission in 2-chloroethyl (see Fig. 19) but not for 1,2-difluoroethane, the transition state in the former is more reactant-like than in the latter. Consequently, the C-H coupling approaches zero more rapidly upon C-H

bond fission in 1,2-difluoroethane. The only major difference between the two systems for bonded atoms involves the C-X bonds. Because of the much stronger C-F interaction, the carbon/fluorine coupling (C_{24}) is much larger than the carbon/chlorine coupling (C_{27}) in 2-chloroethyl. However, this is in the wrong direction to explain the larger IVR rates and increased degree of statistical behavior in 2-chloroethyl radicals.

It appears that variations in the potential coupling constants between the dissociating atom and their next-nearest neighbors are primarily responsible for the differences in statistical behavior found for disilane,[172-173,211] 1,2-difluoroethane,[171,360] and 2-chloroethyl radical. The calculated coupling constants involving only non-dissociating atoms are very similar for both systems. For example, the β-carbon/hydrogen coupling for nondissociating hydrogen atoms is very similar for 2-chloroethyl and 1,2-difluoroethane at all points along both dissociation pathways. However, there exist significant differences in the nonbonded coupling involving the dissociating atoms (H or X). Figure 28 shows that the β-carbon/fluorine interaction, C_{23}, rapidly approaches zero as the a-C-F bond breaks. In contrast, the corresponding β-carbon/chlorine coupling, C_{17}, increases slightly upon C-Cl bond rupture. This interaction eventually attenuates to zero, but much later along the reaction coordinate. As a result, the $[C_{17}]/[C_{23}]$ ratio becomes extremely large as the reacting systems approach their respective transition states. A similar trend is seen in Fig. 28 for the β-carbon/hydrogen interaction upon a-C-H bond cleavage. This interaction, C_{25}, drops to zero at $V/E_0=1.0$ in 1,2-difluoroethane, but it increases significantly for the corresponding reaction in 2-chloroethyl radicals.

Since there is considerable energy present in the atom undergoing dissociation, the large increase in coupling to the beta-carbon in 2-chloroethyl can be expected to significantly enhance energy transfer out of the potentially dissociative C-H or C-Cl stretching motion and thereby simultaneously slow the unimolecular bond fission while

increasing the IVR rate. Calculations on IVR in disilane[173] have shown that it is primarily the heavy-atom Si-Si stretching mode that prevents IVR from being globally rapid and is hence responsible for the observed nonstatistical behavior. The existence of an enhanced coupling between the dissociating atom and the beta-carbon in 2-chloroethyl radical will therefore serve to eliminate this IVR bottleneck and cause the dissociation dynamics of to be well-described by statistical theories. In this regard, Newman-Evans *et al.*[106] have suggested that relatively weak coupling between the reaction coordinate(s) and the other internal motions of the molecule is a prerequisite for the observation of nonstatistical dynamics. The present results support this suggestion.

The origin of these effects lies in the bonding changes that occur in the molecule as the unimolecular reaction takes place. The α-C-H and α-C-Cl bond cleavages in 2-chloroethyl cause the formation of a C=C double bond which is significantly stronger than the corresponding single bond. Consequently, the coupling between the reaction coordinate and the C=C stretching motion will increase as the dissociation occurs. This increase is reflected by the increasing values of the H/β-carbon and Cl/β-carbon coupling constants upon C-H and C-Cl bond rupture, respectively. Since there are only small differences between the bond strengths in 1,2-difluoroethane and 2-fluoroethyl, we would not expect to observe any significantly enhanced coupling between the dissociating atom and the beta-carbon. This expectation is confirmed by the results shown in Fig. 28. The hydrogen/β-carbon and fluorine/β-carbon couplings, C_{25} and C_{23}, respectively, are seen to attenuate to zero monotonically as the dissociations proceed.

Model Demonstration of the Proposed Explanation. The coupling effects produced by bond energy changes resulting from the unimolecular dissociation may be qualitatively illustrated by consideration of a simple, three-atom linear model. Consider three atoms constrained to be collinear with coordinates (x_1, x_2, x_3), respectively. Let

the system potential be described by two Morse-type functions operating between the adjacent bonds such that the strength of the 1-2 bond is altered by cleavage of the 2-3 bond. Such a potential is given by

$$V = [D^o_1 + (D'_1 - D^o_1)\tanh\{a(x_3-x_2-x_o)^2\}][\exp\{-2\alpha(x_2-x_1-x_o)\}- 2\exp\{-\alpha(x_2-x_1-x_o)\}] + D_2[\exp\{-2\alpha(x_3-x_2-x_o)\}-2\exp\{-\alpha(x_3-x_2-x_o)\}] \quad , \quad (V.9)$$

where D^o_1, D'_1, α, a, and x_o are constants. The form of this potential represents a case in which the well-depth associated with the 1-2 bond changes from D^o_1 to D'_1 as $x_3 \rightarrow \infty$, that is, as the 2-3 bond dissociates. The 1-3 coupling defined by Eq.V.9 is given by

$$C_{13} = 4\alpha a(D'_1-D^o_1)(x_3-x_2-x_o)[\exp\{-2\alpha(x_2-x_1-x_o)\} - \exp\{-\alpha(x_2-x_1-x_o)\}] \quad x \quad \mathrm{sech}^2[a(x_3-x_2-x_o)^2]. \quad (V.10)$$

This coupling approaches zero whenever $x_3 \rightarrow \infty$, $x_2-x_1 \rightarrow x_o$, $x_3-x_2 \rightarrow x_o$, or $D'_1 \rightarrow D^o_1$. That is, there will be no coupling enhancement upon cleavage of the 2-3 bond unless there is a change in the 1-2 bond energy. If, on the other hand, $D'_1 \neq D^o_1$, C_{13} will rise to a maximum whenever

$$\tanh[a(x_3-x_2-x_o)^2] = \frac{1}{[4a(x_3-x_2-x_o)^2]} \quad (V.11)$$

which occurs at $(x_3-x_2-x_o) \approx [0.52181/a]^{1/2}$. We would therefore expect to see C_{13} increase as the system approaches its transition state for dissociation.

Our calculations suggest that these observations may be generalized. If unimolecular reaction produces large energetic changes in one or more bonds in the remainder of the molecule, then large increases in some coupling constants will occur as the reaction proceeds. As a result, the IVR rate will increase, unimolecular reaction will

be impeded, and the system will tend obey the assumptions of statistical theories. In addition to the present results, our previous studies of the unimolecular reaction dynamics of disilane,[172-173,211] disilene,[188,370] and 1,2-difluoroethane[171,360] lend support to this generalization. For example, trajectory investigations[171] of the reactions

$$H_2FC\text{-}CH_2F \rightarrow 2 \cdot CH_2F \,, \qquad \text{(R13)}$$

$$H_2FC\text{-}CH_2F \rightarrow H_2FC\text{-}CHF + H \,, \qquad \text{(R14)}$$

$$H_2FC\text{-}CH_2F \rightarrow HFC{=}CH_2 + HF \qquad \text{(R15)}$$

have shown that reactions (R13) and (R14) exhibit significant nonstatistical behavior. The calculated rate coefficients for C-C bond rupture vary by at least a factor of 25 at a total internal energy of 7.5 eV depending upon the initial partitioning of the energy. The actual variation may be much larger since for some initial distributions of the energy, no C-C reactions are observed, which implies a near-zero rate coefficient. Relatively large variations are also computed for the rate coefficients for reaction (R14) although the statistical accuracy of these results is much less due to the low rate for this process. In contrast, the computed rate coefficients for the four-center HF elimination reaction, (R15), are nearly statistical. The rate coefficient for (R15) for an initially random distribution of the internal energy is $k_R = 7.58 \times 10^{11}\ s^{-1}$. Calculation of this rate for initial distributions in which all of the energy in excess of zero-point energy is partitioned into one of the 18 normal modes shows that all of the 18 computed rate coefficients fall in the range $0.85\ k_R \leq k \leq 1.25\ k_R$. These results are in accord with the above generalization. Reactions (R13) and (R14) involve simple bond ruptures which produce little or no change in the energetics of the remaining bonds. The four-center HF elimination reaction, however, converts the C-C single bond into a much stronger C=C double bond. Consequently, we expect a large increase in the atom-atom coupling constants as this process proceeds. Near statistical behavior is the result.

Figure 29. Calculated coupling constants, C_{ij}, as defined by Eq.V.8 for hydrogen/β-carbon coupling, C_{16}, and fluorine/β-carbon coupling, C_{13}, in the 2-fluoroethyl radical as a function of position along the dissociation coordinates for C-H and C-F bond fissions as measured by V/E_0, where V is the potential relative to the reactant and E_0 is the barrier height for bond cleavage. Positive values of V/E_0 denote motion along the C-F dissociation path; negative values motion along the C-H dissociation path. For the C-H bond fissions, hydrogen atom #6 is the one undergoing dissociation. The atom numbering for the 2-fluoroethyl radical is as given in the Figure inset. The solid lines have no significance other than to increase visual clarity.

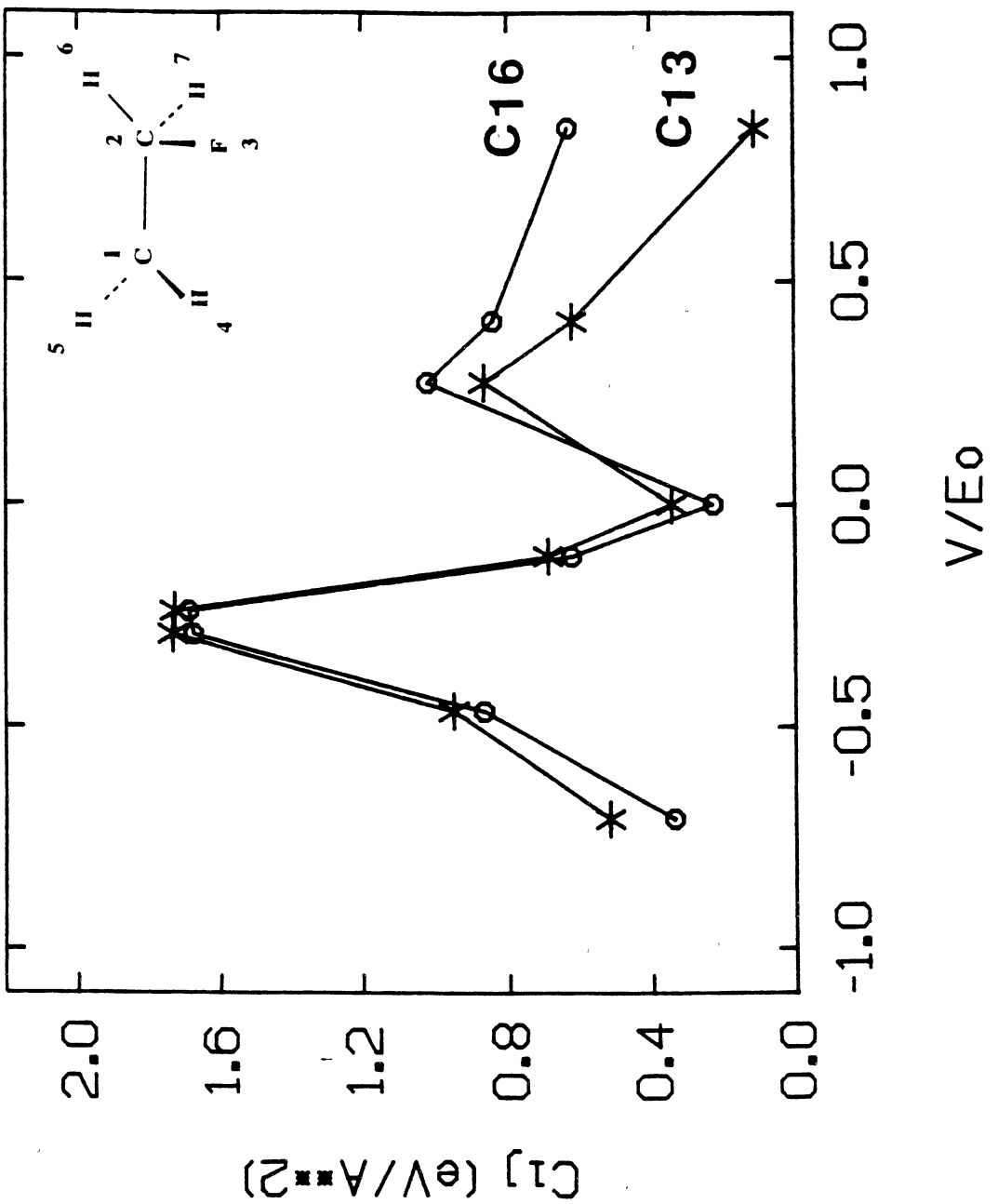
C16
C13
C1 (eV/A**2)
V/Eo
2.0
1.6
1.2
0.8
0.4
0.0
-1.0
-0.5
0.0
0.5
1.0
H
C
F
1
2
3
4
5
6
7

We may use the 1,2-difluoroethane potential[299] to provide an additional example in support of the above generalization. The potential-energy surface for a model 2-fluoroethyl radical (FE) is given by

$$V_{FE} = \lim_{F \to \infty}[V_{DFE}] \ , \qquad \text{(V.12)}$$

where V_{DFE} is the potential surface for 1,2-difluoroethane. C-H and C-F bond cleavage in 2-fluoroethyl yield

$$\cdot CH_2\text{-}CH_2F \text{ ----> } H_2C{=}CH_2 + \cdot F \qquad \text{(R16)}$$

or

$$\cdot CH_2\text{-}CH_2F \text{ ----> } H_2C{=}CHF + \cdot H \ . \qquad \text{(R17)}$$

In either case, there will be a large change in the energetics of the carbon-carbon bond. Consequently, the above generalization predicts that the fluorine/β-carbon coupling in reaction (R16) and the hydrogen/β-carbon coupling in reaction (R17) will increase significantly as we move along the reaction coordinate toward the transition state. These couplings have been computed using Eqs.V.8 and V.12 for the model 2-fluoroethyl system. The results are shown in Fig. 29. The predicted increases in coupling are clearly present as are the maxima predicted by the simple, collinear model discussed above.

Other Examples From the Literature

Many previously reported experimental results and theoretical calculations are in accord with the generalization we have drawn. Some relevant examples are considered below:

Si_2H_4. Raff, Thompson and co-workers have previously examined the reactions

$$H_2Si{=}SiH_2 \text{ ----> } SiH_2 + SiH_2 \text{ ,} \qquad \text{(R18)}$$

$$H_2Si{=}SiH_2 \text{ ----> } H_2Si{=}Si + H_2 \text{ , and} \qquad \text{(R19)}$$

$$H_2Si{=}SiH_2 \text{ ----> } HSi{\equiv}SiH + H_2 \qquad \text{(R20)}$$

under conditions corresponding to an initial random distribution of the internal energy over the available disilene phase space[188] and for disilene formed by the recombination of two silylene molecules, the reverse of reaction (R18)[370]. Since reaction (R18) produces only minor energetic changes in the Si-H bonds (on the potential surface employed in the calculations[370], Si-Si bond cleavage produces no change in the Si-H bonds), we would not expect any enhanced coupling between the leaving SiH_2 group and the other silylene. In addition, the disilene formation coordinate in the reverse of reaction (R18) is strongly coupled to the Si-Si dissociation coordinate. Under these conditions, Newman-Evans *et al.*[106] have suggested that the dynamics will likely be nonstatistical. Thus, both of these considerations suggest that the rate coefficients for Si-Si bond fission subsequent to formation by silylene recombination will not be in accord with statistical predictions. In contrast, reactions (R19) and (R20) produce significant energetic changes in the Si-Si and Si-H bonds. We might therefore expect to see enhanced coupling between the departing hydrogen atoms and the Si_2H_2 moiety with statistical dynamics being the result. Comparison of the trajectory results obtained for a random partitioning of the internal disilene energy[188] with those computed subsequent to formation via silylene recombination[370] supports these qualitative predictions. Statistical dynamics are observed for reactions (R19) and (R20) but not for reaction (R18).

F + C_2H_4. Hase and Bhalla[371] have examined the dynamics for hydrogen-atom dissociation from fluoroethyl radical formed by the recombination of ethylene and fluorine, i.e.,

$$F + C_2H_4 \text{ ----> } H_2C\text{-}CH_2F \qquad \text{(R21)}$$

followed by

$$H_2C\text{-}CH_2F \text{ ----> } H + H_2C{=}CHF \ . \qquad \text{(R22)}$$

Although the fluoroethyl potential used in these calculations differs from that obtained from Eq. V.12, we would nevertheless expected similar enhanced coupling to occur upon C-H dissociation in reaction (R22) which would, in turn, lead to statistical dynamics. Hase and Bhalla[371] find that the calculated relative translational energy distributions at the saddle point for reaction (R22) are in excellent agreement with the predictions of harmonic classical RRKM theory. The number of fluoroethyl dissociations observed within one ps (106) is in favorable agreement with the harmonic RRKM prediction of 131. Since the inclusion of anharmonicity in the RRKM calculations is expected to lower the predicted number of dissociations, the extent of agreement with anharmonic RRKM theory could be even greater. The statistical fluctuations present in the trajectory data prevented the authors from determining whether or not the fluoroethyl lifetime distribution is statistical. Hase and Bhalla[371] have pointed out the statistical distribution of relative translational energy at the exit-channel saddle point does not require that the molecular lifetime distribution also be statistical. Nevertheless, no indications of nonstatistical behavior were found for this system.

Ethyl Radical. Very similar results on ethyl radical decomposition have been reported by Hase, Wolf, and Sloane.[168] These authors investigated the unimolecular dissociation dynamics of

$$H_2C\text{-}CH_3 \text{ ----> } H_2C{=}CH_2 + H \qquad \text{(R23)}$$

using classical trajectory methods and RRKM theory. At an internal energy of 150 kcal/mol, the rate coefficient for (R23) obtained from the trajectory results was in the range 6.3×10^{11} - 1.1×10^{12} s^{-1} depending upon the sampling method used. The corresponding RRKM result obtained using a minimum state density criterion to select the location of the critical surface is 5.22×10^{12} s^{-1}. At an internal energy of 100 kcal/mol, both methods gave a rate coefficient of 1.7×10^{11} s^{-1}. Consequently, at internal energies $E \geq 100$ kcal/mol, statistical rate theory yields a rate coefficient equal to or greater than the corresponding trajectory calculation, as required for a statistical system. In this sense, reaction (R23) in this energy range may be said to be statistical. It should be noted that at E=100 kcal/mol, Hase *et al.*[168] reported evidence for nonrandom lifetimes in the trajectory results. This is not surprising since at this energy we are very close to obtaining $k_{traj} > k_{RRKM}$. This system therefore provides an additional example of the principle stated earlier that the ergodic threshold for a polyatomic molecule is frequently at an energy much greater than the dissociation energy. Since there is a significant alteration of the C-C bond upon H-atom dissociation in reaction (R23), the calculated statistical behavior is in accord with the principles discussed above. The presence of strong coupling between the departing hydrogen atom and the C_2H_4 moiety was noted and discussed by Hase *et al.*.[168]

SiH_4. Viswanathan *et al.*[191,368] compared statistical theory[368] and trajectory[191] results for the unimolecular dissociation of silane. The principal modes of decomposition are

$$SiH_4 \text{ ----> } SiH_3 + H \qquad \text{(R24)}$$

and

$$SiH_4 \text{ ----> } SiH_2 + H_2 \ . \qquad \text{(R25)}$$

The results of this comparison indicated the presence of essentially statistical behavior. Experimentally and on the potential-energy surface employed in the calculations, the Si-H bond energy undergoes a significant change upon Si-H bond cleavage. For example, the Si-H bond energy in SiH_4 is 3.92 eV whereas in SiH_3, it is only 2.75 eV.[191] Therefore, Si-H bond fission produces large alterations in the remaining Si-H bonds which would lead us to expect statistical dynamics.

1-methylcyclopropene. In chapter II we reviewed studies by Baggott and Law[80] dealing with the isomerization of 1-methylcyclopropene induced by C-H stretch overtone excitation in an effort to search for mode-specific effects. This process proceeds *via* three major channels:

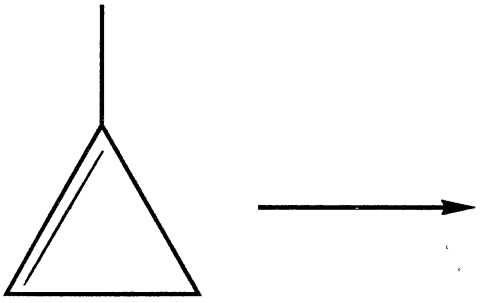

$$H_3C\text{-}C{\equiv}C\text{-}CH_3 \qquad \text{(R12.a)}$$

$$H_2C{=}CH\text{-}CH{=}CH_2 \qquad \text{(R12.b)}$$

$$H_2C{=}C{=}CH\text{-}CH_3 \qquad \text{(R12.c)}$$

Reactions (R12.a)-(R12.c) are clearly associated with significant changes in the bonding energetics throughout the molecule. Based on our hypothesis, we would therefore predict these reactions to exhibit statistical dynamics. Baggott and Law[80] report that the measured quantum yields together with the ratios of the yields of the major isomerization products are adequately represented by RRKM theory.

Cyclobutene, 2-methylcyclopentadiene, and 1-cyclopropylcyclobutene. Jasinski, Frisoli, and Moore[74-76] have examined the unimolecular reactions of

2-methylcyclopentadiene[74], cyclobutene[76], and 1-cyclopropylcyclobutene[75] upon laser excitation of high C-H stretching overtones.

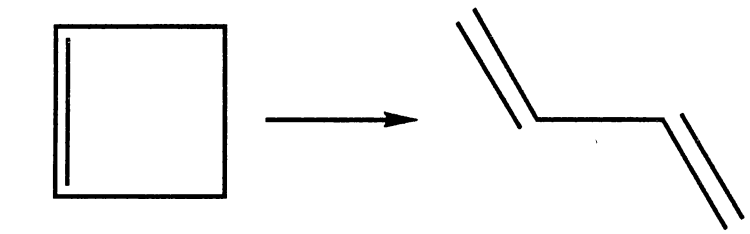

(R9)

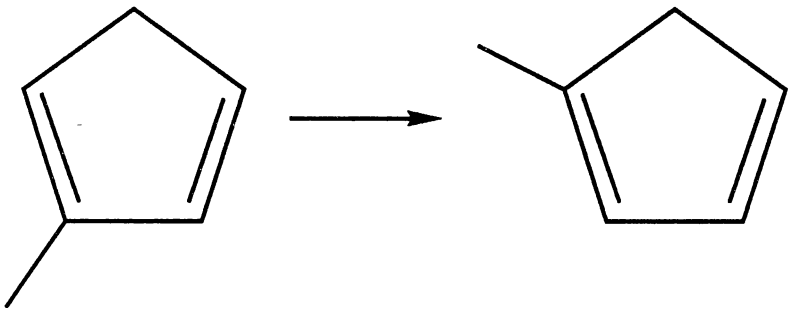

(R10)

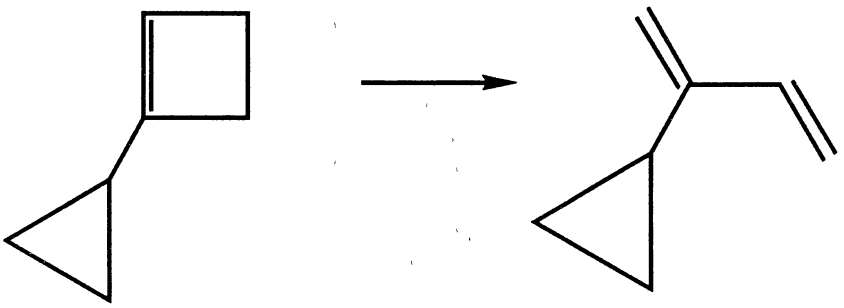

(R11)

In each case, they report that there is no evidence of any mode-specific rate enhancement. All of the data are compatible with the conclusion that the energy introduced by overtone excitation is randomized over the molecule prior to reaction. In each case, the kinetics are in quantitative accord with the predictions of RRKM theory. In all of these reactions, large bonding changes occur throughout the molecule as the reaction proceeds which would lead us to expect the statistical behavior that is observed.

Conditions Likely to Result in Nonstatistical Behavior

The two generalizations drawn above, coupled with the point made by Newman-Evans *et al.*[106] concerning coupling between the formation and reaction coordinates, provide a reasonably clear picture of statistical/nonstatistical behavior. The results of the present study indicate that the factors favoring nonstatistical dynamics are:

1. *Low Internal Energy Close to the Dissociation Threshold.* Several theoretical studies have indicated that the ergodic threshold in larger polyatomic molecules is frequently significantly above the dissociation limit[12-14,33]. Therefore, multiphoton dissociation (MPD) experiments with very low levels of excitation or thermal experiments are more likely to exhibit nonstatistical dynamics.

2. *A reaction coordinate that does not produce large energetic changes in one or more bonds in the remainder of the molecule.* When such energetic changes occur, there will frequently be an enhanced coupling between the dissociation coordinate and the remainder of the molecule that leads to increased IVR rates and decreased reaction rates, both of which will tend to eliminate nonstatistical effects.

The experimental studies reported by Newman-Evans et al.[106] indicate that a third factor favoring nonstatistical dynamics may be added:

3. *A formation coordinate for the activated reactant that is strongly coupled to the dissociation coordinate but only weakly coupled to the other internal coordinates of the molecule[10] favors nonstatistical dynamics.* The dynamics of reactions (R18)-(R20) are a case in point as discussed previously. This principle suggests that processes involving activation via overtone excitation of a C-H bond that require a relatively slow IVR to some other reaction coordinate, such as a low-frequency bending or torsional

mode, are unlikely to exhibit nonstatistical dynamics. Reactions (R12.a) - (R12.c) reported by Baggott and Law[80] are examples. These processes do not satisfy any of the three conditions. The internal energies present in the MPD experiments are probably significantly greater than the dissociation threshold. As noted previously, all of these reactions produce major energetic changes throughout the molecule which probably lead to enhanced coupling between the dissociation coordinate and other internal modes. Finally, the excitation coordinate is a C-H stretching mode which is probably only weakly coupled to the much lower frequency torsional modes that are likely to be involved in the opening of the cyclopropane ring. Consequently, the observed nonstatistical dynamics is predictable.

When all factors point in the same direction, it is likely that the nature of the dynamics may be anticipated. Reactions (R12.a) - (R12.c) are examples. The ring opening reactions studied by Jasinski *et al.*[74-76] also fall into this category for the same reasons discussed above for the cyclopropane reactions[80]. The 2-chloroethyl radical is another example. The energy ranges over which the calculations were done is 30.7 to 84.7 kcal/mol in excess of the dissociation threshold. Without additional data, it is not possible to determine whether this level of excitation is sufficient to place the radical in the ergodic regime. However, the energy is certainly not near threshold where the first principle listed above would lead us to expect nonstatistical dynamics. The C-H and C-Cl dissociation coordinates are highly coupled to the remainder of the molecule because of the energetic changes in the C-C bond that occur as the reaction proceeds. Point #2 would therefore favor statistical dynamics. Finally, in the EMS, EJS, and uniform sampling calculations, there is no formation coordinate that could be highly coupled the C-H or C-Cl dissociation coordinates. The third principle therefore points to statistical dynamics. The present results confirm that this is indeed the result.

Whenever the above three factors are opposed, *a priori* prediction is much more difficult. Two cases in point are the thermal rearrangements of 1- and 2-phenylbicyclo[2.1.1]hex-2-enes-5-d and of trans-2-methyl-1-(trans-2-phenylethenyl) cyclopropane reported by Newman-Evans *et al.*.[106] The major products of these reactions are

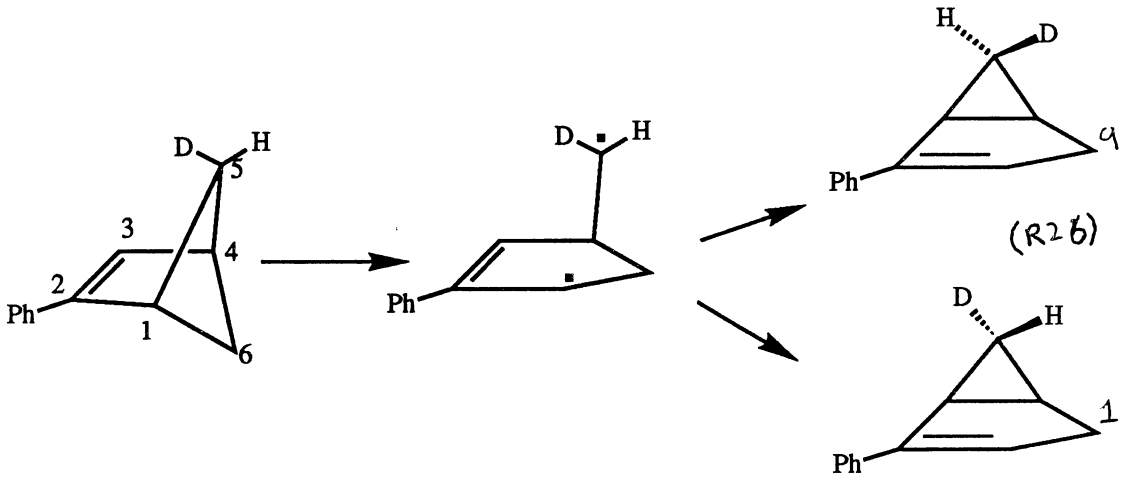

and

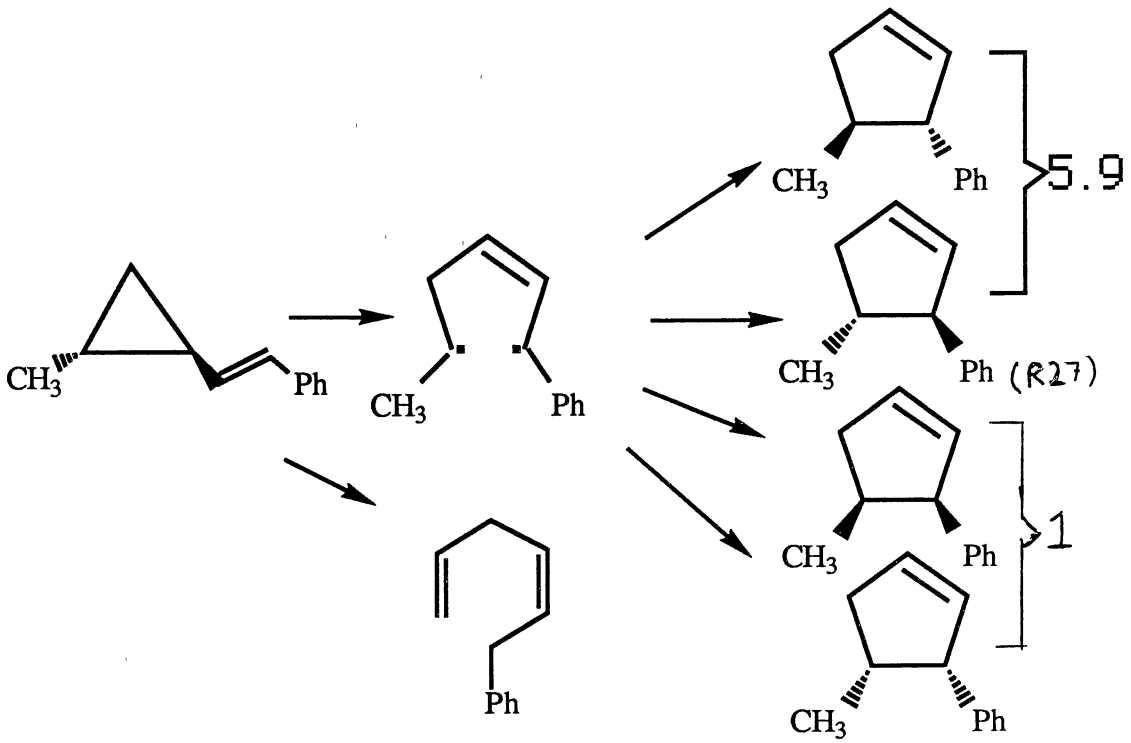

In reaction (R26), a statistical partitioning of the internal energy coupled with the nearly free rotation of the ·CHD group in the biradical intermediate would be expected to yield a 1:1 ratio of the two product stereoisomers instead of the 9:1 ratio actually observed.[106] In reaction (R27), similar arguments would lead to an expected 1:1 ratio of the two optical isomers of the *trans* cyclopentenes. In contrast, a 5.9:1 ratio is found.[106]

For reactions (R26) and (R27), factors #1 and #3 favor nonstatistical dynamics while factor #2 suggests that the dynamics will be statistical. The reported experiments[106] are carried out thermally at temperatures in the range 408 to 533 K. Under these conditions, the activated reactants will probably have an internal energy only a few kcal/mol in excess of the reaction threshold. Factor #1 therefore suggests nonstatistical dynamics. There are clearly numerous energetic changes produced throughout the molecule as the reaction proceeds. We would therefore expect to see enhanced coupling between the reaction coordinate and other vibrational modes. This suggests that the dynamics will be statistical. Finally, the activation mechanism involves molecular collisions at thermal energies. It is unlikely that such collisions would be very effective in excitation of the high-frequency stretching modes of the reactants. The low-frequency torsional modes are much more likely to be the activation coordinate. Reactions (R26) and (R27) involve the opening of four- and three-membered rings, respectively. The mechanism by which these ring openings occur probably involves either disrotatory or conrotatory torsional motions about the C-C bonds of the ring.[359] In the case of reaction (R27), such a disrotatory torsional motion, if continued throughout the reaction, leads to the formation of one of the optically active *trans* pentenes that are observed to be formed in a 5.9:1 ratio.[106] If both the activation and reaction coordinates involve torsional motion, we would expect strong coupling between them. Factor #3 therefore suggests nonstatistical dynamics. As the experiments show, this is the result.

Conclusions

We have investigated the unimolecular dissociation reactions of the 2-chloroethyl radical using classical trajectories and two variational transition-state theory methods on the same potential-energy surface. The results demonstrate that the unimolecular dissociation reactions of 2-chloroethyl radical are well described by statistical theories that assume an equal weight for all energetically accessible phase-space points. The statistical theory yields upper bounds to the trajectory-computed rate coefficients, as expected for a statistical system. We find no evidence of any mode-specific dynamics. Comparison of the present results with previously reported theoretical results for disilane[172-173,211] and 1,2-difluoroethane[171,360], both of which exhibit pronounced nonstatistical dynamics, indicates that larger polyatomic systems can remain in the quasiperiodic regime even at internal energies significantly greater than the dissociation threshold. It is found that the statistical behavior observed for 2-chloroethyl is due, in large part, to an increase in the potential coupling between the dissociating atom and the β-carbon that occurs as the bond breaks. This coupling is shown to be associated with the conversion of the C-C single bond to a C=C double bond upon C-Cl or C-H bond fission.

The results of this study provide a clear picture of some of the factors that can be expected to promote the observation of nonstatistical dynamics in larger polyatomic molecules. These factors are:

(1) *low internal energy close to the dissociation threshold*

and

(2) *a reaction coordinate that does not produce large energetic changes in one or more bonds in the remainder of the molecule.*

If we combine the above results with the coupling arguments advanced by Carpenter and co-workers[106,359], we may add a third factor favoring nonstatistical dynamics:

(3) *a formation coordinate for the activated reactant that is strongly coupled to the dissociation coordinate but only weakly coupled to the other internal coordinates of the molecule*[106] *favors nonstatistical dynamics.*

CHAPTER VI

CLASSICAL DYNAMICS STUDY OF UNIMOLECULAR DISSOCIATION OF RDX

Review of Gas-phase Decomposition of RDX

Considerable effort has been expended over the course of several decades in an attempt to gain an understanding of the combustion of the high-explosive solid propellant molecules hexahydro-1,3,5-trinitro-1,3,5-triazine (RDX) and octahydro-1,3,5,7-tetranitro-1,3,5,7-tetrazine (HMX).[372-376] Various experimental techniques including thermally-induced reaction,[377-388] shock waves,[389-390] differential scanning calorimetry,[391] laser-induced reaction in the vapor,[392] molecular-beam technology[222,393] and others have been used and a rather large number of potentially important reaction pathways have been posited. Nonetheless, the mechanistic details are still not understood.

Most of the experiments have dealt with bulk-phase materials, due to both the very low vapor pressure[391,394-395] of the materials and their inherent instability. There are, however, a number of reported studies of the gas-phase decomposition dynamics of the RDX/HMX family of explosives,[377-378,380-381,222,391-393] including a few carried out in molecular beams.[222,393]

The references just given provide an ample (though not exhaustive) sampling of the literature Since our interest in RDX is directed towards gaining an understanding of the gas-phase decomposition, most of the studies on bulk RDX are of relatively little

interest. Of the gas-phase experiments, molecular-beam experiments are particularly useful in that investigations can be performed on "thermally hot" molecules under essentially collision-free conditions, thereby eliminating in large measure the difficulties associated with discriminating between primary and secondary reactions. These experiments are of paramount importance for the work we have performed.

Due to the absence of RDX molecules in the product gases of most of the early experiments, it was often conjectured that decomposition of RDX occurs only in the solid and liquid phases when heated to temperatures near the melting point. To our knowledge, the earliest report of a gas-phase decomposition was reported in 1968 by Cosgrove and Owen.[377] In a very short communication, Cosgrove and Owen described experiments in which they placed 0.02-0.2 g of RDX in reaction vessels having capacities of 11 to 150 ml. The flasks were either evacuated or filled to a known pressure with nitrogen prior to sealing. After immersion for one hour in a bath thermostated to 195 ^{o}C, the flasks were cooled to room temperature and the products were determined. (This temperature is several degrees below the melting point.) The results indicated that the rate of decomposition is i) directly proportional to the volume of the container, ii) insensitive to the total amount of solid RDX (for a constant volume) and iii) inhibited by the presence of inert gas. Based on their measurements, Cosgrove and Owen argued that RDX does not undergo significant reaction in the solid phase, and that the dominant reaction is a gas-phase decomposition.

The following year, Rauch and Fanelli[378] described more detailed experiments in which they obtained concentration-versus-time profiles for the small molecules generated by decomposition of RDX heated to temperatures in excess of the melting point. The experimental apparatus was similar in most respects to that used by Cosgrove and Owen.[377] However, whereas Cosgrove and Owen only determined the *loss* of RDX following one hour in a thermostated bath, Rauch and Fanelli determined

the concentrations of the various reaction products as a function of time. They started with six to eight reaction vessels in the bath and successively removed and quenched them over a period of time spanning approximately twenty-five minutes. Using combinations of gas chromatography, infrared and ultraviolet spectroscopy, and mass spectrometry, they determined the time dependence of the concentrations of N_2O, CO_2, HCN, H_2O, CH_2O, NO_2, and unreacted RDX. The results indicated concurrent gas- and liquid-phase decomposition: The time dependencies of the concentration of N_2O and CO_2 (and, according to the authors, all of the other products excepting NO_2) were found to be more-or-less independent of both the volume of the reactor and the mass of RDX initially present. By contrast, the rate of (initial) buildup of NO_2 was found to be independent of the initial mass of RDX but proportional to increasing reactor volume. Following an initial increase,the NO_2 concentration decreased, indicating secondary reaction processes in the complicated reaction mixture resulting from RDX decomposition. These results are consistent with a scenario in which liquid-phase decomposition is the dominant avenue for reaction but with the reaction(s) leading to NO_2 taking place in the gas phase. The absolute magnitude of the concentration of NO_2 was much smaller than that of the other products, indicating that the reaction leading to NO_2 is a rather minor channel and, in fact, repression of the gas-phase reaction by addition of 400 torr of an inert gas had essentially no effect on the initial rate of disappearance of RDX. Rauch and Fanelli hypothesized that the origin of NO_2 formation in their experiments was homolytic cleavage of the N-N bonds in RDX.[378]

Farber and Srivastava[382] used a mass spectrometer coupled to a thermostated effusion chamber to study the short-time thermal dissociation of RDX at temperatures in the neighborhood of the melting point. They estimated that the time required for species to travel from the liquid/solid surface of the heated RDX to the ionization chamber of the mass spectrometer was on the order of 10 μs. They observed numerous low molecular

weight fragments at the detector, as well as a sizeable quantity of fragments having masses of 148 and 74 amu (the molecular weight of RDX is 222 amu). The latter mass combination corresponds to what would be obtained if a RDX molecule (which can be regarded as a cyclic trimer of methylenenitramine, $CH_2N_2O_2$) were to split into two large fragments: one $CH_2N_2O_2$ monomer and one "dimer". These products are unstable and were predicted to undergo spontaneous dissociation to low-weight fragments. Other fragmentation patters indicated the stripping of two or more NO_2 groups from the ring (in conjunction with H or H_2 elimination). Interestingly (and contrary to the results reported by Cosgrove and Owen[377]; and Rauch and Fanelli[378]), Farber and Srivastava[382] were not able to detect unreacted RDX in their experiment, leading them to conclude that no RDX molecules were present in the vapor at the temperatures they were considering.

Zuckermann, Greenblatt, and Haas[393] were the first to report a molecular beam study of the infrared multiphoton dissociation (IRMPD) of RDX and HMX. Following an IRMP excitation pulse, they used a pump-probe technique to detect fluorescence following excitation of the $A^2\Sigma(v=1) \leftarrow X^2\Pi(v=1)$ transition of nascent OH radicals. The estimated mean time between collisions in the beam was about 100 times greater than the temporal separation of the IR-pump pulse and the UV probe. They were not able to ascertain whether the OH fragments were produced in a primary reaction or as a result of secondary dissociations of vibrationally excited HONO molecules (both possibilities are thought to occur through the formation of an intermediate five-membered ring). They determined that low OH rotational states were preferentially populated and argued that this observation was consistent with the formation of a five-member intermediate leading to primary formation of OH since the torque on the exiting fragment would be relatively small. However, the observation of a sizeable quantity of

rotationally hot OH radicals indicated the possibility of multiple processes leading to OH formation.

Capellos, Papagiannakopoulos, and Liang[392] studied the photodissociation of gas-phase RDX following irradiation at 248 nm. They detected electronically excited $NO_2(^2B_2)$ and $OH(A\ ^2\Sigma)$ fragments and concluded that the NO_2 was formed by N-N bond scission in a prompt photodissociation process requiring the absorption of one photon; OH formation required the absorption of two photons but the exact mechanism for dissociation was not clear. They could not determine with certainty whether the OH was a primary photodissociation product (resulting from a five-membered intermediate) or a secondary reaction product due to spontaneous dissociation of hot HONO molecules. Their analysis considered four possible mechanisms and, based on a number of arguments, they tentatively concluded that the most likely route for formation of OH is initial formation of vibrationally hot HONO which dissociates to give the observed OH fragment. Capellos *et al.*[392] found that the NO_2 fragments were formed in high rovibrational states and suggested that N-N bond cleavage occurs faster than relaxation of the initial excitation (which is localized in the NO_2 moiety)

Zhao, Hintsa, and Lee[222] studied the IRMPD of RDX in a molecular beam using a time-of-flight mass spectrometric detection system in an effort to determine the mechanism for thermal decomposition of gas-phase RDX. A molecular beam was generated by heating RDX to 130 ^oC in an oven, passing He over the sample material, and allowing the mixture of RDX molecules and He to pass through a nozzle. Infrared multiphoton excitation was accomplished by crossing the molecular beam with the beam of a CO_2 laser tuned to 942.3 cm^{-1}.. A time-of-flight mass spectrometer was used to detect the products. By rotating the oven containing the RDX, time-of-flight spectra could be obtained at a number of laboratory angles. It should be pointed out that, whereas Farber and Srivastava were unable to detect RDX in their study of the thermal

decomposition of RDX, Zhao *et al.* found that, for temperatures below 200 °C, the molecular beam consisted primarily of RDX molecules (if the laser was turned off).

Zhao *et al.*[222] were able to use the time-of-flight data to model the translational energy distributions that would result from various possible decomposition mechanisms. The inability of the model to adequately describe the experimental data was taken as evidence for the absence of a particular reaction and, based on these fits to the data, several previously suggested reactions were eliminated as possibilities. They concluded that the dominant primary dissociation steps are simple N-N bond fission (R3) and a concerted reaction involving simultaneous cleavage of three C-N ring bonds to yield three $CH_2N_2O_2$ molecules (R4):

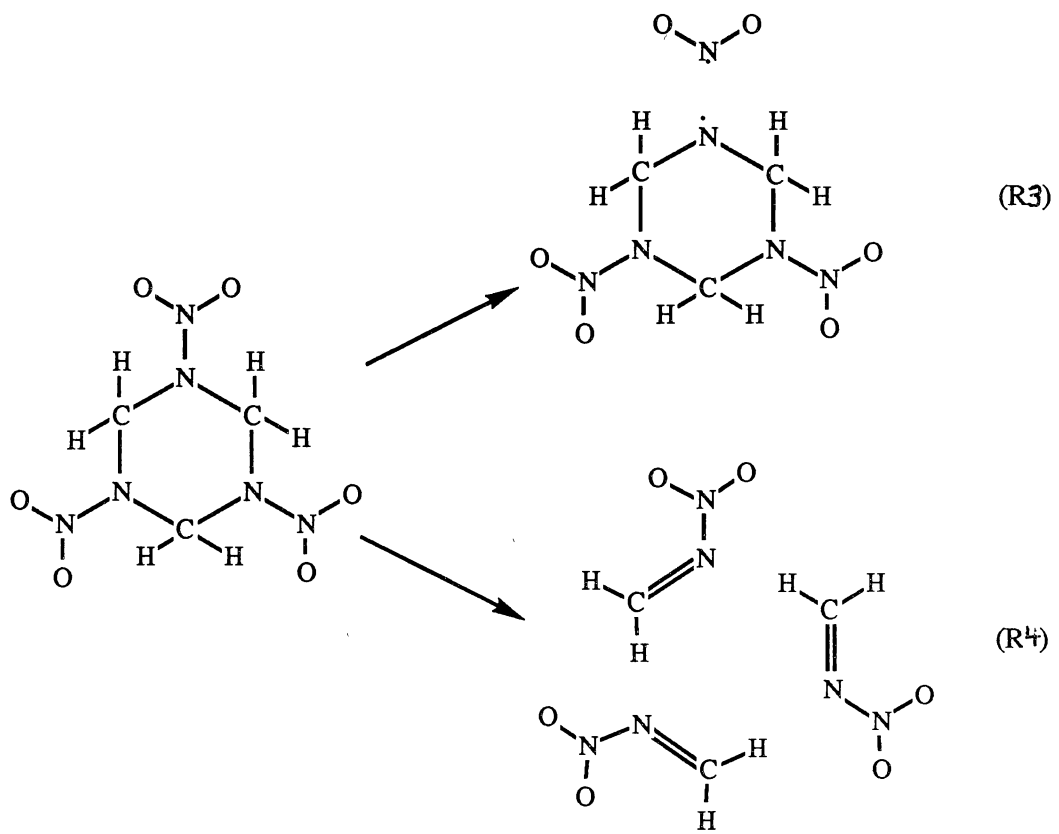

(R3)

(R4)

They reported a branching ratio of approximately 2:1 for ring dissociations to N-N bond fissions. They concluded that the ring dissociation is a concerted process due to the absence of fragments indicative of primary elimination of a $CH_2N_2O_2$ molecule followed by secondary dissociation of $C_2H_4N_4O_4$ to produce either $2CH_2N_2O_2$ or $C_2H_4N_3O_2 + NO_2$. They were unable to reconcile five-center elimination of HONO with their experimental results (a result which has direct bearing on the interpretation of the source of OH in Ref. 393).

Zhao *et al.*[222] also considered numerous secondary reaction schemes and concluded that, subsequent to ring fission, the principal fate of the $CH_2N_2O_2$ molecules is unimolecular rearrangement and dissociation to yield HCN + HONO (or HNO_2). Formation of $N_2O + H_2CO$ was also observed but was determined to be relatively unimportant. Simple bond fission of the N-N bond in $CH_2N_2O_2$ to yield $CH_2N + NO_2$ was not discussed, although the bond-dissociation energy (*ca.* 30.6 kcal/mol[218]) is comparable to the barrier to HONO formation (*ca.* 31 kcal/mol[219]). The large amino radical resulting from simple N-N rupture was found to decompose primarily through elimination of HONO. Another proposed secondary reaction following loss of NO_2 is formation of $CH_2N + 2CH_2N_2O_2$.[72-376,218] Calculations have shown that loss of NO_2 results in a considerable weakening of the second-neighbor C-N bond to the amino radical center, possibly leading to an "unzipping" of the ring structure.[218] Zhao *et al.*[222] considered three possible mechanisms for this process and ultimately argued (on the basis of energetics and time-of-flight spectra) that the proposed mechanism plays little or no role in the gas-phase unimolecular reaction dynamics.

We have performed a classical trajectory investigation of the primary unimolecular decomposition reactions (R3) and (R4) in gas-phase RDX. The main purposes of the study were to investigate the ring-dissociation mechanism suggested by Zhao *et al.*[222] and to compute the branching ratio between reactions (R3) and (R4).

Another motivation was to demonstrate that classical dynamics is a viable tool for studies of reaction dynamics of large polyatomic systems

Computational Details

The three-dimensional motion of all twenty-one atoms in the RDX molecule was considered in this study of the competition between the simple N-N bond fission reactions (R3) and the ring-fission processes (R4). We have formulated an approximate, anharmonic potential-energy surface that is in reasonable agreement with the available experimental[212-217] and theoretical[218-219,217-221] data for the reactant and products. Random initial conditions in the reactant phase space were generated using an efficient microcanonical Monte Carlo sampling procedure.[255] Individual trajectories were computed using methods described in Chapter II.

The conditions under which we are carrying out calculations are ideal for classical studies of the dynamics of molecular systems. We are considering reaction processes in a large (twenty-one atom) system at elevated energies, and none of the reactions considered directly involves light atoms. These conditions help minimize effects due to tunneling and contribution of zero-point energy to the reaction rate.

Initial Conditions

Microcanonical ensembles of 200 to 400 trajectories were computed at eight total energies in the range 250 to 350 kcal/mol. Initial conditions selection was accomplished using an efficient microcanonical sampling procedure.[255] The random walk was initiated by placing the RDX molecule in its equilibrium geometry after which a warm-up walk of 1,000,000 steps was performed to relax the molecule away from the initial configuration. All twenty-one atoms were moved at each step of the chain. The maximum allowable stepsize for each atom was chosen such that an acceptance

Table XVI. Parameters Used in Selection of Initial Conditions for RDX.

Energy (kcal/mol)	Maximum Stepsize (Å)	Acceptance Probability
250.0	0.0275	0.450
275.0	0.0275	0.490
287.5	0.0275	0.500
300.0	0.0300	0.471
312.5	0.0300	0.480
325.0	0.0300	0.489
337.5	0.0300	0.496
350.0	0.0300	0.504

Maximum Bond Extensions (Å): $r_{CN} \leq 2.0$; $r_{NN} \leq 2.5$; $r_{NO} \leq 2.8$; $r_{CH} \leq 3.0$

Figure 30. Numerical designation of the atoms in the RDX molecule.

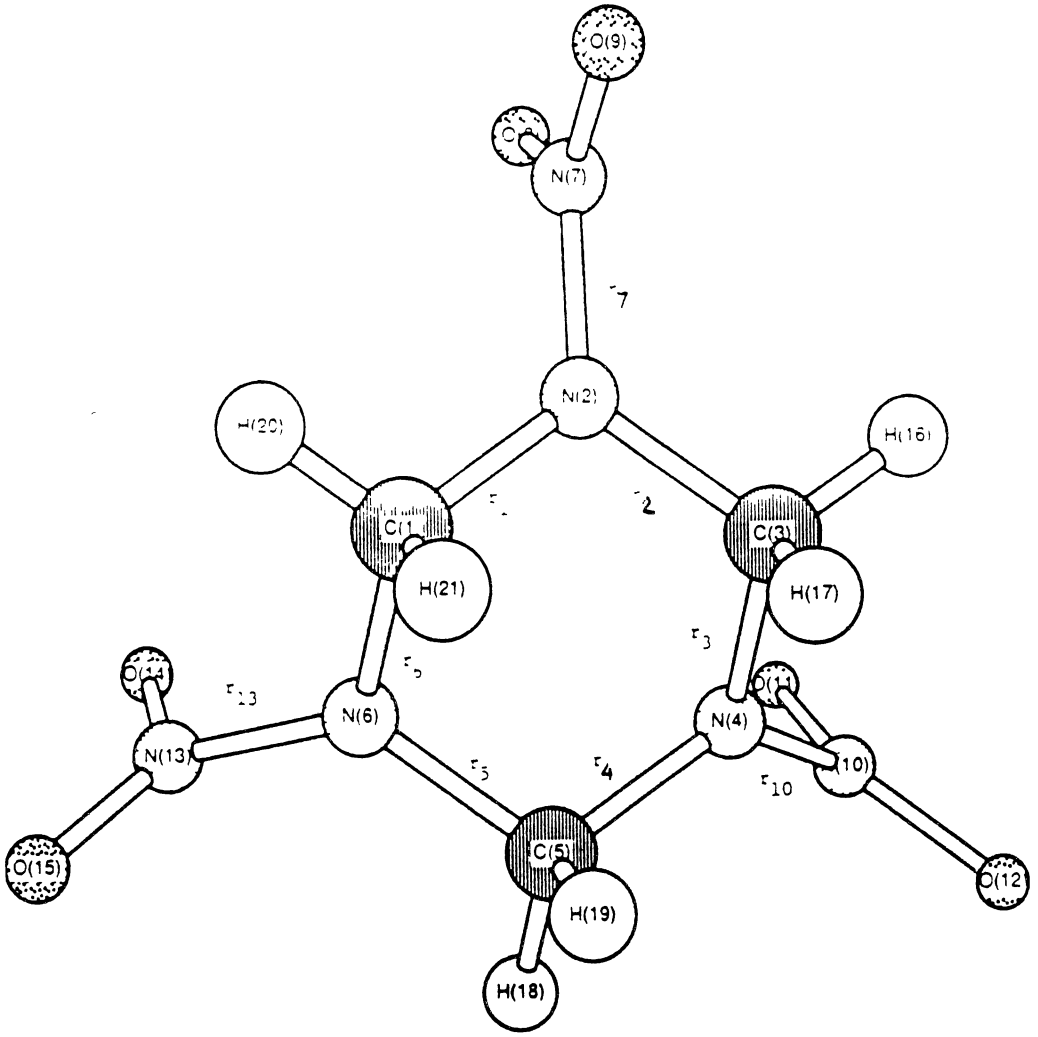
O(9)
N(7)
N(2)
H(20)
H(16)
C(1)
C(3)
H(21)
H(17)
N(6)
N(4)
N(13)
O(15)
C(5)
H(19)
H(18)
O(12)

probability of 0.45 to 0.50 was achieved at each energy. Maximum extensions of individual bonds were imposed in order to restrict the Markov chain to reactant configurations. The length of the initial walk was chosen so as to ensure convergence of average quantities (potential energy and internal coordinates). Values of the momenta were then selected and the trajectory computed. After the first trajectory, the original Markov chain was continued, with every 100,000th subsequent configuration being used as the initial geometry for a trajectory. Each trajectory and its outcome (i.e., dissociation or nondissociation, reaction time, product state distributions, etc.) was counted m times, where m is the number of times the initial configuration of the trajectory was repeated in the Markov chain.[254] This procedure was repeated until the desired number of trajectories had been computed. Parameters pertaining to the selection of initial conditions and the acceptance probability are summarized in Table XVI.

Trajectory Integration

Trajectories were integrated in a lab-fixed Cartesian coordinate system, using a fourth-order Runge-Kutta-Gill routine with a fixed stepsize of 1.22×10^{-16} s. The maximum time for which individual trajectories were propagated was 50 ps. The accuracy of the integration was monitored by energy conservation (typically to six significant figures) and back integrability over short (<0.5 ps) periods of time. Due to the size and nonlinearity of the force field, full back integration is not achievable. However, it has been demonstrated[203] that, in systems exhibiting chaotic behavior, accurate back integrability of individual trajectories is not a prerequisite for calculation of lifetime distributions, branching ratios, or product energy partitioning, which are the quantities of primary interest in this work.

Endtests

The internuclear distances for the twenty-one bonds in RDX were monitored during the course of the trajectory integrations. If any of the N-N bonds (r_7, r_{10}, r_{13}, see Fig. 30), C-H, or N-O bonds exceeded 4.5 Å, then reaction was considered to have occurred. The time of reaction was taken to be the time up to the last inner turning point in the dissociating bond. No N-O or C-H bond fission was observed in any of the calculations. In the case of the ring-fission channels, reaction was assumed to have occurred if either r_1, r_3, and r_5 or r_2, r_4, and r_6 all exceeded 4.5 Å. In such cases, the time of reaction was taken to be the average of the times of the last inner turning points of the three bonds involved in the particular dissociation event. The bond-distance criteria chosen to define the dividing surfaces for the various reactions were based on the ranges of the bond potentials in the reactant. A small number of trajectories in the high-energy ensembles underwent dissociation as defined by the above criteria without experiencing inner turning points. The time of dissociation of these trajectories was taken to be zero.

First-order Rate Coefficients and Branching Ratios

Values of the branching ratio between simple N-N bond fission and ring dissociation were computed for each microcanonical ensemble. First-order rate coefficients for the overall reaction process were computed by fitting the lifetimes to Eq. II.28. The branching ratio for the two chemically distinct reactions (R3) and (R4) was computed using Eqs. II.29 to II.31.

We employed the "bootstrap method"[298] in an effort to determine the degree of variability in the rate coefficients, based on the set of computed lifetimes for a given ensemble of trajectories. Ten-thousand sample data sets were generated by selecting at random from the pool of computed trajectory outcomes, i.e., either a lifetime

corresponding to bond fission or ring dissociation, or a trajectory that did not lead to dissociation within the imposed time cutoff.

Product-state Analysis

The center of mass of the system is fixed at the origin of the coordinate system. The center-of-mass translational energy of each reaction product i (i = NO_2, $CH_2N_2O_2$) relative to this space-fixed origin is given by

$$T_{cm,i} = \frac{1}{2M_i}\mathbf{P'}_i \cdot \mathbf{P'}_i \qquad \text{(VI.1)}$$

where

$$\mathbf{P'}_i = (\sum P_{lx})\mathbf{i} + (\sum P_{ly})\mathbf{j} + (\sum P_{lz})\mathbf{k}; \qquad \text{(VI.2)}$$

P_{lx}, P_{ly}, and P_{lz} are the Cartesian components of the momenta of the atoms of the product molecule, the index l runs over all the atoms of fragment i, and M_i is the total mass of the fragment.

We obtain the kinetic energy of internal motion (vibration and rotation) $T_{int,i}$ of fragment i using

$$T_{int,i} = T_{tot,i} - T_{cm,i}, \qquad \text{(VI.3)}$$

where $T_{cm,i}$ is defined in Eq. VI.1 and $T_{tot,i}$ is given by

$$T_{tot,i} = \frac{1}{2}\sum m_j \mathbf{v_j} \cdot \mathbf{v_j} \qquad \text{(VI.4)}$$

Here, $\mathbf{v_j}$ is velocity vector of the jth particle and the summation runs over the constituent atoms of the fragment.

We compute the rotational energy $E_{rot,i}$ using

$$E_{rot,i} = \frac{\omega \cdot \mathbf{I} \cdot \omega}{2} \qquad \text{(VI.5)}$$

where ω is the angular momentum vector (calculated relative to the center of mass of fragment i) and $\mathbf{I}$ is the moment-of-inertia tensor, also calculated relative to the center of mass of the fragment. The kinetic energy of vibration is then given by

$$T_{vib,i} = T_{int,i} - E_{rot,i}. \qquad \text{(VI.6)}$$

The total vibrational energy is the sum

$$E_{vib,i} = T_{vib,i} + V_i, \qquad \text{(VI.7)}$$

where V_i is the potential energy of fragment i.

In order to assure that the bond-distance criteria used to define reaction are sufficiently large, the quantity

$$E_{tot} = \sum (T_{tot,i} + E_{vib,i}) \qquad \text{(VI.8)}$$

was divided by the total system energy and compared to unity. The ratio was greater than 0.995 for all trajectories and for all energies considered, with most being 0.998 or larger.

The rotational and vibrational energies as defined above are not in fact separable as we have tacitly assumed; they are actually time-dependent quantities whose sum must be constant (since the translational energy of the products is a constant of the motion). However, monitoring product rotational energies (as defined in Eq. VI.5) for a representative set of trajectories revealed that the time dependence is more-or-less oscillatory in nature. The period of the oscillation is rather long. By continuing each trajectory for, say, 2 ps after reaction has occurred, we could compute time averaged vibrational and rotational energies of the products and use these average quantities in the

construction of product-energy distributions. While this would certainly be more accurate than simply taking the instantaneous values at the end of each reactive trajectory, we think that the net effect on the distributions would be minimal, especially when it is realized that in order to do so for each reactive trajectory would have required an additional 4646 ps of trajectory integration.

Equilibrium Geometry of Gas-phase RDX

At the time that these calculations were performed, the equilibrium structure of the gas-phase RDX molecule was not known, but was thought to possess C_{3v} symmetry.[216-217,220] Since then, the gas-phase structure has been reported by Shishkov and co-workers [Struct. Chem. **2**, 57 (1991)]. The measured geometry is generally in good agreement with the assumed structure described below.

Several studies of the crystal-phase structure have been reported.[212-214] We assumed that the geometry of the ring is tetrahedral, and that the three C_2N-N wag angles are at equilibrium at $\gamma=0^0$, based on theoretical studies.[217,220] The three methylene groups are assumed to be tetrahedral. Equilibrium bond lengths, N-N-O angles, and O-N-O angles are taken to be the averages of the crystal-phase structure values reported by Choi and Prince.[212] This information is sufficient to uniquely define the geometry of RDX. The resulting structure possesses C_{3v} symmetry and should be a reasonable model for the present purpose. The numerical designations of the atoms are given in Fig. 30 and values for all equilibrium geometric parameters are given in Table XVII. The Cartesian coordinates for the assumed equilibrium structure of RDX are given in Table XVIII.

Potential-Energy Surface

RDX. The potential-energy surface used in this calculation is written as a sum of twenty-one bond stretching terms, thirty-six angle-bending terms, three wag angle-bending terms, and nine nonbonded interactions. The valence bond-stretching terms are represented by the Morse potential, Eq. II.2. Reasonable values for the dissociation energies were obtained from various sources.[222,218-219,221,320] All bending terms for bond and wag angles are approximated by harmonic oscillator functions, Eq. II.4. The Lennard-Jones potential, Eq. II.7, is used to represent nonbonded interactions.

All force-field parameters, with the exception of those appearing in the Lennard-Jones functions, are either taken directly from or, as in the case of the Morse parameters, derived from a harmonic force field developed by Wallis and Thompson.[396] The values of the potential parameters are given in Table XIX.

The calculated normal-mode frequencies are compared with experimental values in Table XX. The normal-mode frequencies were obtained using analytical second derivatives of the potential-energy surface and are in good agreement with experiment; a majority of the frequencies are within 30 cm^{-1} of the experimental values.[215] Power spectra of the internal coordinates were computed for a low-energy trajectory. The frequencies of the power spectra and the normal-mode frequencies are in agreement with one another to within a few cm^{-1}. Differences greater than 1 cm^{-1} arise due to the fact that some of the switching functions used in this work have nonzero second derivatives at the equilibrium geometry of RDX and switching functions were ignored in the calculation of analytical second derivatives of the potential-energy surface. Power spectra of individual internal coordinates indicate that the majority of the normal-mode vibrations are complicated combinations of internal-coordinate displacements (as expected), making it difficult to assign most of the normal-mode frequencies to particular motions.

Table XVII. Equilibrium Valence Coordinates for RDX[a].

Bond	Value (Å)	Angle	Value (deg)
r_{CN}	1.454	θ_{CNC}	109.500
r_{CH}	1.081	θ_{NCN}	109.500
r_{NN}	1.380	θ_{CNN}	125.250
r_{NO}	1.210	θ_{NNO}	117.202
		θ_{ONO}	125.596
		θ_{NCH}	109.500
		θ_{HCH}	109.328
		γ_{CNC-N}	000.000

[a]Based on crystal-phase structure, Choi and Prince, Ref. 212.

Table XVIII. Equilibrium Geometry for RDX

Atom Number[b]	Cartesian Coordinates[a]		
	x	y	z
C_1	-1.187396821	0.685543876	-0.241988832
N_2	0.000000000	1.371087755	0.241988832
C_3	1.187396821	0.685543876	-0.241988832
N_4	1.187396821	-0.685543876	0.241988832
C_5	0.000000000	-1.371087755	-0.241988832
N_6	-1.187396821	-0.685543876	0.241988832
N_7	0.000000000	2.498453557	1.037882258
O_8	0.000000000	2.329652968	2.236050177
O_9	0.000000000	3.570986611	0.477727952
N_{10}	2.163724251	-1.249226779	1.037882258
O_{11}	2.017538653	-1.164826484	2.236050177
O_{12}	3.092565122	-1.785493306	0.477727952
N_{13}	-2.163724251	-1.249226779	1.037882258
O_{14}	-2.017538653	-1.164826484	2.236050177
O_{15}	-3.092565122	-1.785493306	0.477727952
H_{16}	2.070183456	1.195220975	0.117841716
H_{17}	1.189279827	0.686631029	-1.322986645
H_{18}	0.000000000	-2.390441951	0.117841716
H_{19}	0.000000000	-1.373262057	-1.322986645
H_{20}	-2.070183456	1.195220975	0.117841716
H_{21}	-1.189279827	0.686631029	-1.322986645

[a]Coordinates are in Å.

[b]See Fig. 30.

Table XIX. Potential Parameters for RDX.

Morse Parameters:

	RDX		$CH_2N_2O_2$	
Coordinate	D_e (kcal/mol)	α (Å^{-1})	D_e (kcal/mol)	α (Å^{-1})
r_{CN}	85.0[a]	2.01600	153.07c	1.57694
r_{NN}	47.8[a]	3.05535	030.60a	3.72678
r_{NO}	98.0[b]	2.33907	098.00d	2.33907
r_{CH}	95.0[a]	1.94432	108.00	1.82355

Harmonic Force Constants:

	RDX	$CH_2N_2O_2$
Coordinate:	k (mdyn Å rad^{-2})	k (mdyn Å rad^{-2})
θ_{CNC}	0.4898[e]	---------[f]
θ_{NCN}	0.4030	---------[f]
θ_{CNN}	0.5713	0.5713
θ_{NNO}	0.7008	0.7008
θ_{ONO}	0.4033	0.4033
θ_{NCH}	0.4570	0.4570
θ_{HCH}	0.3874	0.3874
γ_{C2N-N}	0.6600	0.0

Lennard-Jones Parameters:

Coordinate	ε (kcal/mol)	r^o (Å)
r_{CN} (cross ring)	0.04308	2.86
r_{CN} (NO_2 N atom)	0.04308	3.86
r_{NN} (ring-exocyclic)	0.06155	3.64

[a]Melius and Binkley, Ref. 218.

[b]Sumpter and Thompson (dimethylnitramine), Ref. 320.

[c]Estimated (see text).

[d]Assumed to be the same as in the reactant.

[e]Wallis and Thompson, Ref. 396.

[f]Coordinate does not exist in $CH_2N_2O_2$.

Table XX. Comparison of Calculated and Experimental Normal-Mode Frequencies of RDX.

This work (cm^{-1})	Experimental (cm^{-1})[a]
50	----[b]
55 (2)[c]	----[b]
219 (2)	----[b]
255 (2)	----[b]
258	----[b]
302	----[b]
355 (2)	----[b]
416	----[b]
421 (2)	----[b]
436	----[b]
602	595
628 (2)	610
720 (2)	740
759	750
760 (2)	794
847	885
945 (2)	910
966	935
1039 (2)	1015
1043	-----[b]
1046	1045
1123 (2)	-----[b]
1270	1230
1272 (2)	1270
1347 (2)	1320
1413	1392
1496	1435
1543 (2)	1460
1554	1550
1556 (2)	1585
2986 (3)	2980
3061 (2)	-----[b]
3062	3080

[a]Liquid-phase RDX, Iqbal *et al.*, Ref. 215.

[b]Unavailable.

[c]Indicates degenerate frequencies.

Reaction Products. The three product species $C_3H_6N_5O_4$, NO_2 , and $CH_2N_2O_2$ were treated in an approximate manner. We limited the attenuation of the potential-energy surface along the reaction coordinates for the N-N bond fission reactions to "switching off" the appropriate bending force constants as the N-N internuclear separation becomes large. Thus, the potential-energy surfaces for the "isolated" $C_3H_6N_5O_4$ and NO_2 fragments differ from that of the reactant only in the absence of four angle-restoring forces and one wag-angle-restoring force (for each broken N-N bond). The values of the well-depths, equilibrium geometrical parameters, etc. are unchanged as reaction occurs. Attenuation of these parameters requires information, which is unavailable, of either normal-mode frequencies or bond strengths in the $C_3H_6N_5O_4$ fragment.

Ab initio calculations of the equilibrium structure and normal-mode frequencies of $CH_2N_2O_2$ have been reported by Mowry, Page, Adams, and Lengsfield.[219] In the work reported here, we neglected small differences in some of the geometric parameters obtained by Mowry *et al.*, e.g., minor differences between the two equilibrium H-C-N angles. Additionally, certain sacrifices in the quality of the force field for the isolated $CH_2N_2O_2$ molecule were made to simplify of the overall potential-energy surface. Most notably, the out-of-plane degrees of freedom in the $CH_2N_2O_2$ molecule were neglected. Finally, the values of most of the force constants and Morse parameters for the $CH_2N_2O_2$ product were taken to be the same as those in RDX. In cases where sizeable differences are known to exist between RDX and $CH_2N_2O_2$ parameters, e.g., the N-N and C-N well depths, they were taken into account by using switching functions. The equilibrium geometry and normal-mode frequencies calculated by Mowry *et al.*[219] are compared with those used in this work in Table XXI. Morse Parameters and harmonic force constants are given in Table XIX. We emphasize that while the agreement with

Table XXI. Geometry and Normal-Mode Frequencies of $CH_2N_2O_2$.

	Geometry[a]		Frequencies (cm^{-1})	
	ab initio[b]	This Work	*ab initio*[b,c]	This Work
r_{CN}	1.274	1.274	70	214
r_{NN}	1.514	1.514	358	386
r_{NO}	1.212	1.210	499	448
$r_{NO'}$	1.242	------[d]	546	----[e]
r_{CH}	1.071	1.072	576	----[e]
$r_{CH'}$	1.073	------[d]	760	----[e]
θ_{CNN}	113.3	113.3	828	810
θ_{NNO}	113.7	117.202	1139 (2)[f]	996
$\theta_{NNO'}$	119.4	------[d]	1223	1102
θ_{ONO}	126.9	125.596	1410	1412
θ_{NCH}	124.3	120.0	1487	1488
$\theta_{NCH'}$	115.7	------[d]	1634	1542
θ_{HCH}	120.0	120.0	3029	2967
			3137	3080

[a]Bond lengths in Å, bond angles in degrees.

[b]Mowrey *et al.*, Ref. 219.

[c]The *ab initio* frequencies were scaled by 10%.

[d]Indicates neglect of differences between similar coordinates.

[e]The force field neglects out-of-plane modes.

[f]Indicates degenerate frequencies.

the *ab initio* results could be improved, to do so would require a significant increase in the complexity of the potential-energy surface.

Attenuation of the Potential-energy Surface. Attenuation of the potential-energy surface between the reactant and product molecules as a function of the coordinates for the five reaction channels was accomplished through the use of a set of self-consistent switching functions. Two general functional forms for the switching functions were employed, namely,

$$S_I(r) = 1+a(r;q^R,q^P)\tanh[b(r-r^R)^n] \qquad (r > r^R)$$
$$= 1.0, \qquad \text{(otherwise)} \qquad \text{(VI.9)}$$

which we will refer to as S_I-type switching functions, and

$$S_{II}(r) = \exp[-\beta(r-r^R)^n] \qquad (r > r^R)$$
$$= 1.0, \qquad \text{(otherwise)} \qquad \text{(VI.10)}$$

which we refer to as S_{II}-type switching functions.

In Eqs. VI.9 and VI.10, r represents either a C-N or N-N bond, r^R is the equilibrium value of that particular bond in the reactant molecule and b, β, and n are parameters that control where (and at what rate) the switching functions change between the asymptotic limits. For S_I-type switching functions the constant b has a value of 3.5 $Å^{-2}$ and n has a value of 2.0. For S_{II}-type switching functions the value of β is 1.0 $Å^{-2}$ and 5.5 $Å^{-4}$ for switching functions depending on N-N and C-N bonds, respectively. The value of n for S_{II}-type switching functions is 2.0 and 4.0 for switching functions depending on N-N and C-N bonds, respectively. The equilibrium value of r_{NN} in $CH_2N_2O_2$ is considerably larger than in RDX. For this reason, the

parameter r^R appearing in switching functions governed by N-N bonds was taken to be 1.514 Å, the equilibrium N-N bond length in $CH_2N_2O_2$. The constant $a(r;q^R,q^P)$ in Eq. VI.9 is defined either as

$$a(r;q^R,q^P) = [q^P/q^R]^{1/2}-1 \qquad \text{(VI.11)}$$

for a given coordinate q (geometrical parameter, well depth, force constant, etc.) that depends on two S_I-type switching functions, or

$$a(r;q^R,q^P) = [q^P/q^R] -1 \qquad \text{(VI.12)}$$

for a given parameter q that depends on only one S_I-type switching function. The quantities q^R and q^P are the asymptotic values of the parameter q in the reactant and product wells, respectively. Thus, the instantaneous value of some parameter q that depends, for example, on two switching functions of the S_I type is,

$$q=q^R S_I(r_i)S_I(r_j), \qquad \text{(VI.13)}$$

where q^R is the value of q in the equilibrium configuration of the reactant. For the case of large values of both r_i and r_j, q must take on the value appropriate to the product. Thus, we write

$$q^P=q^R\{1+a(r_i,q^R,q^P)\tanh[b(r_i-r_i^R)^n]\}\{1+a(r_j,q^R,q^P)\tanh[b(r_j-r_j^R)^n]\}$$
$$\text{-----> } q^R[1+a(r;q^R,q^P))]^2 \qquad \text{(VI.14)}$$

which, upon rearranging, gives Eq. VI.11. The result of Eq. VI.12 is obtained in the same way, except that only one switching function of type S_I is involved in the product.

In all subsequent references to S_I-type switching functions we will write S_I' and S_I'' for cases corresponding to the a's of Eqs. VI.12 and VI.11, respectively. We note that (1) the notation just defined is completely independent of S_{II}-type switching

functions and (2) that it is possible for combinations of S_I' and S_I'' dependencies to affect the instantaneous value of a given parameter q. As an example, consider the overall attenuation of one of the C-N bond well depths, D_{CN}^i. The well depth varies between the asymptotic limits of 85.0 and 153.07 kcal/mol in the reactant and product ($CH_2N_2O_2$), respectively. The C-N well depths are not attenuated in the case of N-N bond rupture. However, there are two distinct ring-fission channels. Thus, a particular C-N bond may in one trajectory become the C=N bond in a $CH_2N_2O_2$ molecule while in another trajectory it may become one of the three C-N bonds broken in a ring dissociation. Both possibilities are accounted for by writing $D_{C\text{-}N}^i$ as

$$D_{CN}^i(r_{CN}^{i-2},r_{CN}^{i-1},r_{CN}^{i+1},r_{CN}^{i+2}) = D_{CN}^R S_I''(r_{CN}^{i-1})S_I''(r_{C\text{-}N}^{i+1})S_{II}(r_{CN}^{i-2})S_{II}(r_{CN}^{i+2}), \quad \text{(VI.15)}$$

where the labels i±1 and i±2 refer to the two C-N bonds adjacent to C-N bond i and the two C-N bonds separated from bond i by one intervening C-N bond, respectively. The two S_I''-type switching functions serve to adjust the well depth of the C-N bond between asymptotic limits. In order to achieve the limit corresponding to the $CH_2N_2O_2$ molecule, it is necessary for both C-N bonds i and j to become "large". For any intermediate configuration, e.g., bond i-1 large and bond i+1 small, the value of D_{CN}^i will be intermediate between its asymptotic limits (assuming reasonably small displacements of C-N bonds i±2). The purpose of the S_{II}-type switching functions is to destabilize the ring appropriately as one or more of the C-N bonds become large. The S_I''- and S_{II}-type switching functions engage the triazine ring in a "competitive feedback loop" wherein extension of bond i destabilizes C-N bonds i±2 while making bonds i±1 more stable. Of course, as bond i extends, weakening bonds i±2, they too will tend to undergo larger amplitude vibrations, thereby destabilizing bond i (hence the term "feedback loop"). However, extension of C-N bond i+1 destabilizes C-N bonds i-1 and i+3 while

Table XXII. Summary of Potential-Energy Surface Attenuation for RDX.[a]

Coordinate	Required Switching Functions
C-N Bond[b]	$D_{e,CN}^{i} = D_{e,CN}{}^{R}S_{I}''(r_{CN}^{i-1})S_{I}''(r_{CN}^{i+1})S_{II}(r_{CN}^{i-2})S_{II}(r_{CN}^{i+2})$ $\alpha_{CN}^{i} = \alpha_{CN}{}^{R}S_{I}''(r_{CN}^{i-1})S_{I}''(r_{CN}^{i+1})$ $r^{o}{}_{CN}^{i} = r_{CN}{}^{R}S_{I}''(r_{CN}^{i-1})S_{I}''(r_{CN}^{i+1})$
N-N Bond[c]	$D_{e,NN} = D_{e,NN}{}^{R}S_{I}'(r_{CN}^{i})S_{I}'(r_{CN}^{i+1})$ $\alpha_{NN} = \alpha_{NN}{}^{R}S_{I}'(r_{CN}^{i})S_{I}'(r_{CN}^{i+1})$ $r^{o}{}_{NN} = r_{NN}{}^{R}S_{I}'(r_{CN}^{i})S_{I}'(r_{CN}^{i+1})$
C-H Bond[c]	$D_{e,CH} = D_{e,CH}{}^{R}S_{I}'(r_{CN}^{i})S_{I}'(r_{CN}^{i+1})$ $\alpha_{CH} = \alpha_{CH}{}^{R}S_{I}'(r_{CN}^{i})S_{I}'(r_{CN}^{i+1})$
Intraring Angle[b,d]	$k_{\theta}^{i} = k_{\theta}{}^{R}S_{II}(r_{CN}^{i})S_{II}(r_{CN}^{i+1})$
C-N-N Angle[c]	$k_{\theta,CNN}^{i} = k_{\theta,CNN}{}^{R}S_{II}(r_{CN}^{i})S_{II}(r_{NN})$ $\theta^{o}{}_{CNN}^{i} = \theta^{o}{}_{CNN}{}^{R}S_{I}'(r_{CN}^{i+1})$
N-N-O Angle[c]	$k_{\theta,NNO}^{i} = k_{\theta,NNO}{}^{R}S_{II}(r_{NN})$
N-C-H Angle[e]	$k_{\theta,NCH}^{i} = k_{\theta,NCH}{}^{R}\,S_{II}(r_{CN}^{i})$ $\theta^{o}{}_{NCH}^{i} = \theta^{o}{}_{NCH}{}^{R}S_{I}'(r_{CN}^{i+1})$ $k_{\theta,NCH}^{j} = k_{\theta,NCH}{}^{R}\,S_{II}(r_{CN}^{i})$ $\theta^{o}{}_{NCH}^{j} = \theta^{o}{}_{NCH}{}^{R}S_{I}'(r_{CN}^{i+1})$
H-C-H Angle[e]	$\theta^{o}{}_{HCH} = \theta^{o}{}_{HCH}S_{I}'(r_{CN}^{i})S_{I}'(r_{CN}^{i+1})$
C_2N-N Wag Angle	$k_{\gamma}^{i} = k_{\gamma}{}^{o}S_{II}(r_{NN}^{i})$

[a]Geometric or potential parameters not explicitly included in the table were not attenuated.

[b]Refer to Fig. 31, panel a.

[c]Refer to Fig. 31, panel b.

[d]Includes C-N-C and N-C-N angles.

[e]Refer to Fig. 31, panel c.

Figure 31. Coordinates used in definition of potential-energy surface attenuation (see Table VII).

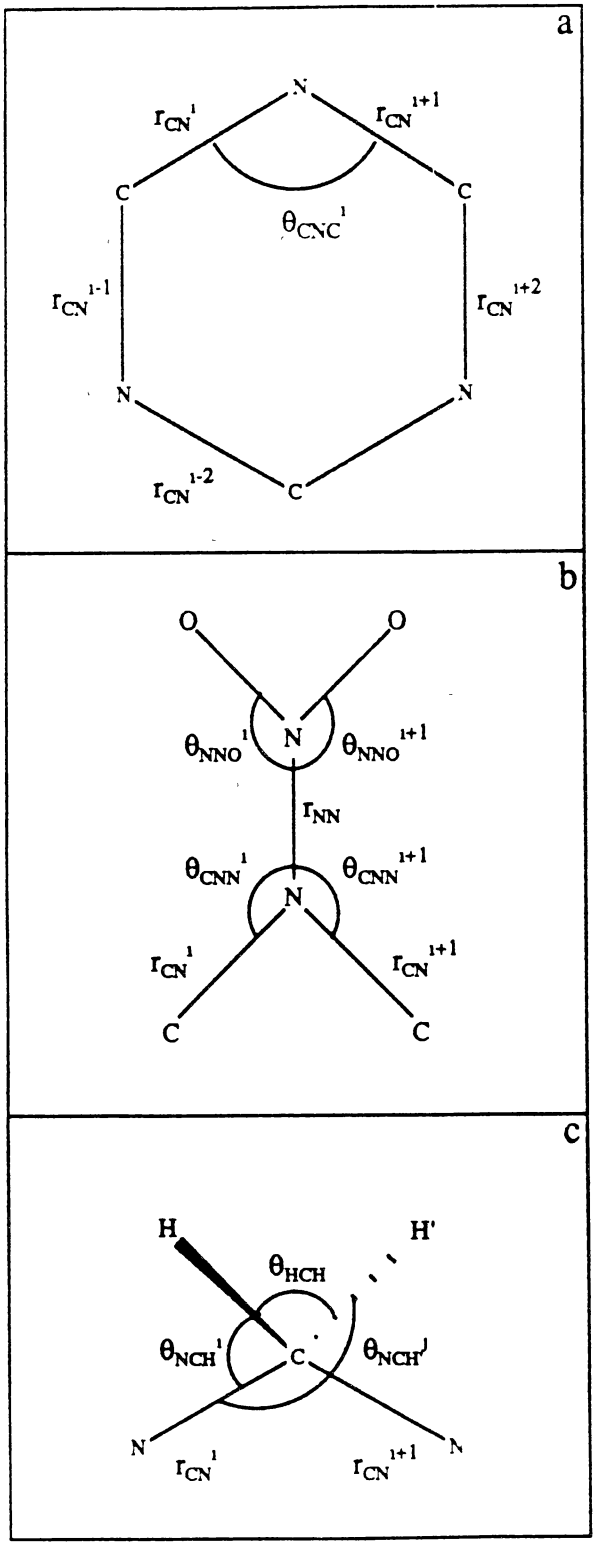
a
N
r_{CN}^{1}
r_{CN}^{1+1}
C
C
θ_{CNC}^{1}
r_{CN}^{1-1}
r_{CN}^{1+2}
N
N
r_{CN}^{1-2}
C
b
O
O
θ_{NNO}^{1}
N
θ_{NNO}^{1+1}
r_{NN}
θ_{CNN}^{1}
θ_{CNN}^{1+1}
N
r_{CN}^{1}
r_{CN}^{1+1}
C
C
c
H
H'
θ_{HCH}
θ_{NCH}^{1}
C
$\theta_{NCH'}^{1}$
N
N
r_{CN}^{1}
r_{CN}^{1+1}

stabilizing bonds i and i+2 (and so on, simultaneously, around the ring). Thus, there is an interplay between these competing processes.

The preceding example serves to demonstrate the approach we have taken in consistently incorporating the five reaction channels into a single functional form for the potential-energy surface. We summarize the attenuation of the potential-energy surface in Table XXII and Fig. 31. The information presented in Table XXII, when interpreted with the help of Fig. 31, completely describes the attenuation employed in the potential-energy surface.

Thermochemistry

The well-depth for the N-N bond in the RDX molecule is taken to be 47.8 kcal/mol.[218] Since most simple bond-rupture reactions usually have little or no barrier to back reaction (indeed, the translational-energy distribution for the NO_2 fragment is peaked at zero in the IRMPD molecular-beam data of Zhao *et al.*[222]), we have taken the barrier to reaction (R3) to be 47.8 kcal/mol. As stated in the preceding section, we have assumed that the entire change in molecular energy associated with N-N bond fission is due to cleaving the N-N bond; therefore, the thermodynamic stabilities of the remaining bonds are unattenuated as a function of the N-N bond extension.

The thermodynamic description of the ring-fission channel (R4) requires more careful consideration due to its complexity. Whereas in many unimolecular dissociations it is *perhaps* appropriate to equate the reaction endothermicity with potential energy localized in a breaking bond [as we have assumed for reaction (R3)], such a zeroth-order description is not correct for a ring-breaking process such as (R4). For example, C-N single bonds evolve into double bonds as the reaction proceeds, resulting in large changes in the hybridization of the carbon centers and hence in bond strengths in the reactants and products. It is therefore necessary to either use the heat of

reaction as a means of calibrating changes in well depths as reaction occurs or to use known values of the well depths for the reactants and products as a means of predicting the heat of reaction. In this work, we have taken the former approach because information required to do the latter is unavailable.

The gas-phase RDX molecules used in the experiments of Zhao *et al.*[222] were generated by heating solid RDX in an evacuated oven heated to 130°C. The resulting vapor was passed through a nozzle maintained at 154°C, yielding an "intense supersonic beam" of RDX molecules. After conditioning, the molecular beam was crossed with a pulsed CO_2 laser beam, effecting infra-red multiphoton dissociation of the reactant molecules. Since the sublimation of RDX in the experiments occurred *prior* to laser irradiation, we assume in the following that the value of 80 kcal/mol quoted by Zhao *et al.*[222] refers to the endothermicity of the *gas-phase* triple dissociation (Reaction IV in Ref. 222). Based on a calculated value of 33.6 kcal/mol for $\Delta H_f^\circ{}_{CH_2N_2O_2}(g,300K)$ reported by Melius and Binkley[218], Zhao *et al.*[222] estimated an endothermicity of 80 kcal/mol for the concerted ring fission (R4). We were unable to reproduce this value using the available thermochemical data.

Using a Hess' Law analysis and published values for $\Delta H_f^\circ{}_{RDX}(s,300K)$, $\Delta H_f^\circ{}_{CH_2N_2O_2}(g,300K)$, and $\Delta H_{sub,RDX}$,[218,391,394-395,221,397-400] we can readily obtain a value for the heat of reaction for the ring-dissociation. The reported experimental values of the heat of formation of solid RDX at 300K range from 12.9 kcal/mol to 16.9 kcal/mol.[397-398] The value considered by Pedley, Naylor, and Kirby to be the "best" is $\Delta H_f^\circ{}_{RDX}(s,300K) = 15.9 \pm 0.5$ kcal/mol.[397] The heat of sublimation of RDX has been measured by different techniques at least three times.[391,394-395] Using a method based on scanning differential calorimetry, Rogers and Daub[391] arrived at a value of $\Delta H_{sub,RDX} = 29$ kcal/mol for RDX in the temperature range 505 to 520 K. Edwards[394] reported a value of 26.8 kcal/mol in 1953, for the temperature range 384 to

411 K. Rosen and Dickinson[395] obtained a value of 31.1 kcal/mol for RDX over the temperature range 329 to 371 K. Thus, the variation of the $\Delta H_{sub,RDX}$ is not strongly sensitive to temperature. We have arbitrarily used the value reported by Rosen and Dickinson,[395] $\Delta H_{sub,RDX}$ = 31.1 kcal/mol, and have made no attempt to correct for the temperature dependence of the heat of sublimation.

Using $\Delta H_f^\circ{}_{RDX}(s,300K)$ = 15.9 kcal/mol[397] and $\Delta H_{sub,RDX}$ = 31.1 kcal/mol[395], we obtain a value of $\Delta H_{f,RDX}(g)$ = 47.0 kcal/mol. This value agrees with other reported values, 40.6, 45.8 and 47.7 kcal/mol, obtained using MOPAC[399], molecular mechanics[400], and Hess' Law analyses (with different choices in constituent data)[400], respectively.

The value of the heat of formation of $CH_2N_2O_2$ used by Zhao, Hintsa, and Lee[222] to obtain their estimate of the ring-dissociation endothermicity is that reported by Melius and Binkley[218], $\Delta H_f^\circ{}_{CH_2N_2O_2}(g,300K)$ = 33.6 kcal/mol. However, Zhao *et al.*[222]noted that "... the endoergicity derived from the heat of formation of CH_2NNO_2 given by Melius and Binkley seems unreasonably high." Employing experimentally derived data, Shaw and Walker[221] estimate a value of $\Delta H_f^\circ{}_{CH_2N_2O_2}(g,300K)$ = 23.8 kcal/mol. MOPAC calculations yield $\Delta H_f^\circ{}_{CH_2N_2O_2}(g,300K)$ = 26.8 kcal/mol.[399]

Uncertainty in $\Delta H_f^\circ{}_{CH_2N_2O_2}(g,300K)$ is exacerbated here because the value must be multiplied by three (since RDX dissociates to yield three $CH_2N_2O_2$ molecules). The MOPAC value for the endothermicity of the triple dissociation is 3(26.8 kcal/mol) - 40.6 kcal/mol = 39.8 kcal/mol.[399] Using $\Delta H_{f,RDX}(g)$ = 47.0 kcal/mol, we obtain reaction endothermicities of 24.4 kcal/mol and 53.8 kcal/mol, using $\Delta H_f^\circ{}_{CH_2N_2O_2}(g,300K)$ = 23.8 kcal/mol[395] and 33.6 kcal/mol[218], respectively.

Insight as to which of the above values is most accurate may be gained *via* qualitative consideration of the energetics of the secondary reactions following triple dissociation. Specifically, the difference between the vibrational zero-point energy of

three $CH_2N_2O_2$ molecules and that of RDX should be on the order of only several kcal/mol (and may therefore be neglected to within a first approximation). Zhao *et al.*[222] state that the average internal energy of RDX following IRMPE is near 80 kcal/mol (presumably referring to energy in excess of the zero-point). If the reaction endothermicity for gas-phase ring dissociation is 80 kcal/mol then, on average, essentially all of the excitation energy will be consumed in cleaving the ring, with no residual energy remaining for vibrational or translational excitation of the products. Experimentally,[222] the nascent products have considerable translational and vibrational energy, a significant fraction of them containing sufficient internal energy to undergo unimolecular dissociations and/or rearrangements having barriers of *ca.* 30-35 kcal/mol.[218-219] Moreover, the fact that the products are created with a fairly large translational energy suggests a non-negligible barrier to the back reaction, further increasing the energetic requirements such that only activated molecules on the high-energy tail of the IRMPE energy distribution would be able to react under collisionless conditions. A qualitatively similar conclusion is reached for an endothermicity of 53.8 kcal/mol.

The situation seems more reasonable for an endothermicity of 24.4 kcal/mol. Here, the total excess energy would be roughly 55-65 kcal/mol, allowing for a 10 kcal/mol difference in the ZPE of the reactant and products; and the excess energy will be sufficient to allow for unimolecular dissociation of some of the products as well as product translational-energy distributions peaked away from zero. Based on these considerations, we have chosen to use a reaction endothermicity of 24.4 kcal/mol for the triple dissociation reaction channel (R4).

Having obtained an estimate for the heat of reaction for ring fission, we can proceed to assign values to the well-depths in $CH_2N_2O_2$. Melius and Binkley[218] estimate the C-H bond energy in RDX to be 95 kcal/mol and the N-N bond energy in

$CH_2N_2O_2$ to be 30.6 kcal/mol. The value of 95 kcal/mol for the C-H bond energy is typical of sp^3 C-H bonds.[401] The hybridization of the C-H bonds in $CH_2N_2O_2$ is nominally sp^2, suggesting a C-H bond energy of roughly 108 kcal/mol.[401] Assuming that the N-O bond dissociation energies do not change appreciably as the ring breaks, we obtain by subtraction a bond dissociation energy of 153.07 kcal/mol for the C=N bond in $CH_2N_2O_2$ (typical of C=N bonds[401]). Thus, the relative stabilities of the RDX molecule and the three $CH_2N_2O_2$ molecules obtained *via* ring fission are correct based on an endothermicity of 24.4 kcal/mol.

Minimum-Energy Profile for Concerted Ring Dissociation

We have obtained a minimum-energy profile assuming symmetric, concerted ring dissociation using the technique of adiabatic mapping.[52] Briefly, the method consists of assuming a reasonable reaction coordinate, constraining the coordinates of the atoms that define the reaction coordinate to change incrementally in the direction leading to products, and allowing the remaining coordinates to relax to the local minimum corresponding to that particular value of the reaction coordinate. Starting at the equilibrium geometry of RDX, we systematically expand the ring such that, say, bonds one, three, and five (see Fig. 30) are uniformly extended while bonds two, four, and six are relaxed to their equilibrium values (dictated by the values of bonds one, three, and five). This procedure imposes C_{3v} symmetry in the ring as the molecule is stepped along the reaction coordinate for ring fission (see Fig. 32). At each ring configuration, the STEPIT[366] program was used to minimize the potential energy with respect to the fifteen exocyclic atoms, starting with the lowest-energy configuration from the previous step.

The minimum-energy profile obtained for the concerted ring dissociation in RDX using this procedure is shown in Fig. 33. The abscissa corresponds to the length for the

Figure 32. Illustration of the expansion of triazine ring along the reaction coordinate for ring fission.

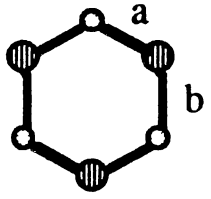

a = 1.454 Å
b = 1.454 Å

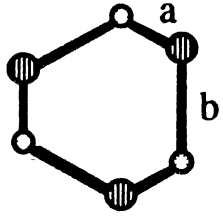

a = 1.311 Å
b = 2.006 Å

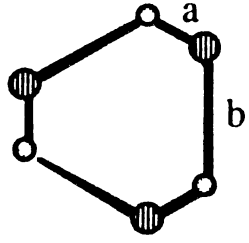

a = 1.274 Å
b = 2.445 Å

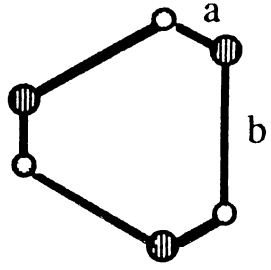

a = 1.274 Å
b = 2.873 Å

Figure 33. Minimum-energy path for ring dissociation along reaction coordinate for ring fission.

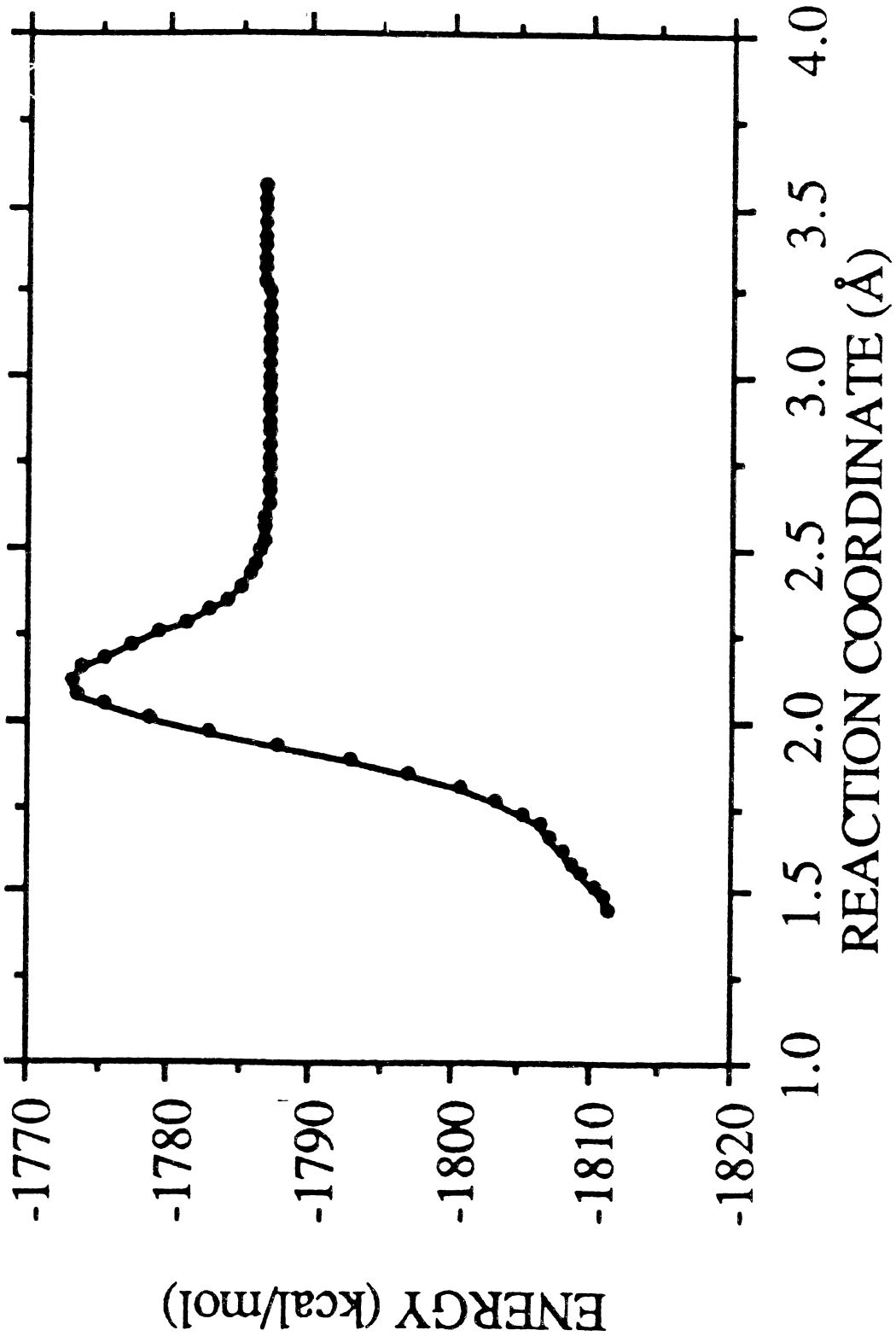
ENERGY (kcal/mol)
-1770
-1780
-1790
-1800
-1810
-1820
1.0
1.5
2.0
2.5
3.0
3.5
4.0
REACTION COORDINATE (Å)

three C-N bonds that are broken in the projection along the symmetric reaction coordinate and the ordinate is the minimum potential energy as a function of the abscissa values. Solid points in Fig. 33 denote values of the abscissa for which the minimum potential energy was computed. Individual points are connected by straight lines for clarity. The overall minimum occurs at 1.454 Å, which is the equilibrium value of the six C-N bond lengths in the RDX molecule. The barrier to reaction, 38.3 kcal/mol, occurs at 2.12 Å. For values of the abscissa greater than about 2.5 Å, the minimum potential energy is 24.6 kcal/mol, measured relative to RDX at equilibrium. Thus, there is a back barrier of about 13.6 kcal/mol in this potential-energy surface. For convenience, the six intra-ring angles were not minimized in the energy minimization. However, the error in the minimum potential energy due to deformation of the ring angles was computed as a function of the reaction coordinate and was found to never exceed 0.5 kcal/mol. The numerical value increased and then decreased rapidly with the diminution of the ring-angle-bending force constants.

Zhao *et al.*[222] found that the $CH_2N_2O_2$ molecules resulting from IRMPD of RDX are created with excess translational energy, with a distribution that peaks at about 12 kcal/mol. The presence of a back barrier in our potential-energy surface will lead to kinetic-energy release in the products and, although we cannot be certain what the value of the barrier to back reaction is in the real system, comparison of calculated and experimentally determined translational-energy distributions provides us with another check of the quality of the potential-energy surface we have constructed.

Results and Discussion

Rate Coefficients and Branching Ratios

First-order rate coefficients and branching ratios, Eqs. II.28 to II.31, were calculated over the energy range 250 to 350 kcal/mol. The results are summarized in Table XXIII, where the values of the first-order rate coefficients for the two individual reaction channels, k_{rng} and k_{NN}, represent the mean of the 10,000 sets of sample rate coefficients generated using the bootstrap algorithm. The first and second columns of Table XXIII are the first-order rate coefficients for ring dissociation and N-N bond fission, respectively. Branching ratios are given in the third column and the total energy in the fourth column. The total numbers of trajectories computed at each energy (including recounting) are given in the last column of Table XXIII. All trajectories were reactive within the time cutoff of 50 ps.

The rate coefficients are monotonically increasing functions of the total energy. Fits of the rate-coefficient data in Table XXIII to the RRK expression,[180]

$$\ln[k(E)] = \ln(A) + (s-1)\ln(1-E_0/E), \qquad \text{(VI.16)}$$

are shown in Fig. 34. Panels a and b in Fig. 34 correspond to the N-N bond fission and ring dissociation rate coefficients, respectively. The solid lines are linear least-squares fits to the data. The critical energy, E_0, is taken to be the well depth of the N-N bond (47.8 kcal/mol) for the case of N-N fission (R3), and the barrier height (38.3 kcal/mol) obtained *via* the adiabatic mapping of the minimum-energy profile for the ring-dissociation channel (R4) (see Fig. 33). The parameters A and s were adjusted to fit the rate coefficient values. It is clear from the plots in Fig. 34 that the energy dependence of the computed rate coefficients is fairly well described by this simple statistical theory. The calculated values of the frequency factor, A, are 9673 cm^{-1} and 1433 cm^{-1} for

Table XXIII. Rate Coefficients (ps^{-1}) and Branching Ratios for RDX.[a]

k_{ring}	k_{NN}	k_{ring}/k_{NN}	Energy[b]	Number of Trajectories[c]
0.67 ±0.06	0.66 ±0.05	1.0±0.1	350.0	563
0.44 ±0.03	0.43 ±0.03	1.0±0.1	337.5	395
0.31 ±0.02	0.30 ±0.02	1.0±0.1	325.0	429
0.28 ±0.02	0.20 ±0.01	1.4±0.1	312.5	554
0.34 ±0.02	0.20 ±0.01	1.7±0.1	300.0	854
0.21 ±0.01	0.13 ±0.01	1.6±0.2	287.5	428
0.156±0.008	0.097±0.006	1.6±0.1	275.0	386
0.082±0.003	0.034±0.002	2.4±0.2	250.0	868

[a]The uncertainties for both the rate coefficients and branching ratios are for one standard deviation about the mean as obtained using bootstrap sampling. We reemphasize that the error bars reflect the uncertainty in the rate coefficients based on single ensembles and do not address possible variation in the computed rates for, say, n independent ensembles.

[b]Units are kcal/mol.

[c]Reflects recounting.

Figure 34. RRK plots of computed first-order rate coefficients for reactions (R3) and (R4) (panels a and b, respectively).

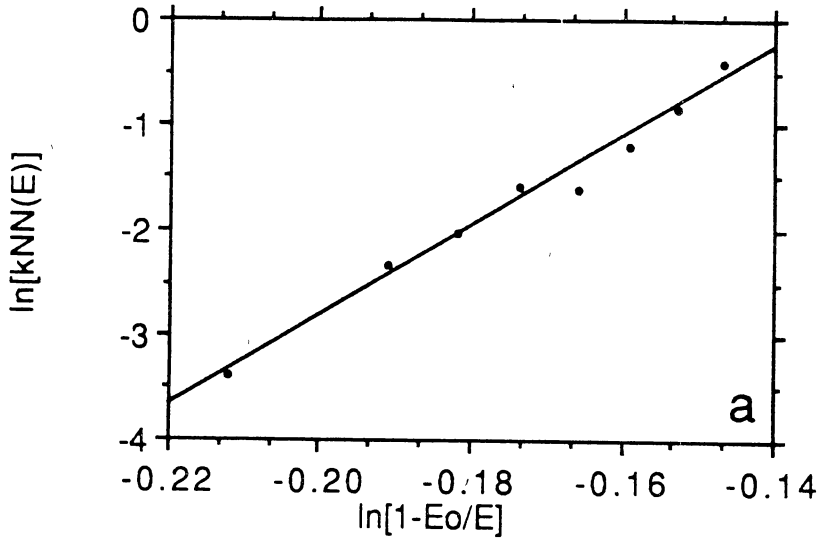
0
-1
-2
-3
-4
ln[kNN(E)]
a
-0.22
-0.20
-0.18
-0.16
-0.14
ln[1-Eo/E]

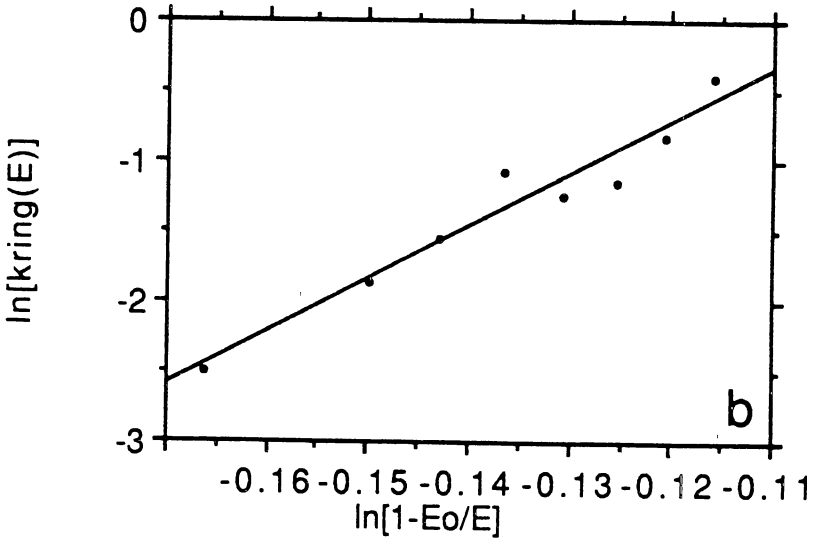
0
-1
-2
-3
ln[kring(E)]
b
-0.16
-0.15
-0.14
-0.13
-0.12
-0.11
ln[1-Eo/E]

Figure 35. Calculated first-order rate coefficients as a function of the barrier to ring dissociation and ensemble energy. (a) Overall first-order rate coefficient, k(E); (b) same as panel a except for $k_{ring}(E)$; (c) same as panel a except for $k_{NN}(E)$. Ring-dissociation barriers are: solid diamonds: 35.7 kcal/mol; open circles: 38.3 kcal/mol; solid squares: 41.0 kcal/mol. The barrier to N-N bond rupture is 47.8 kcal/mol for all three.

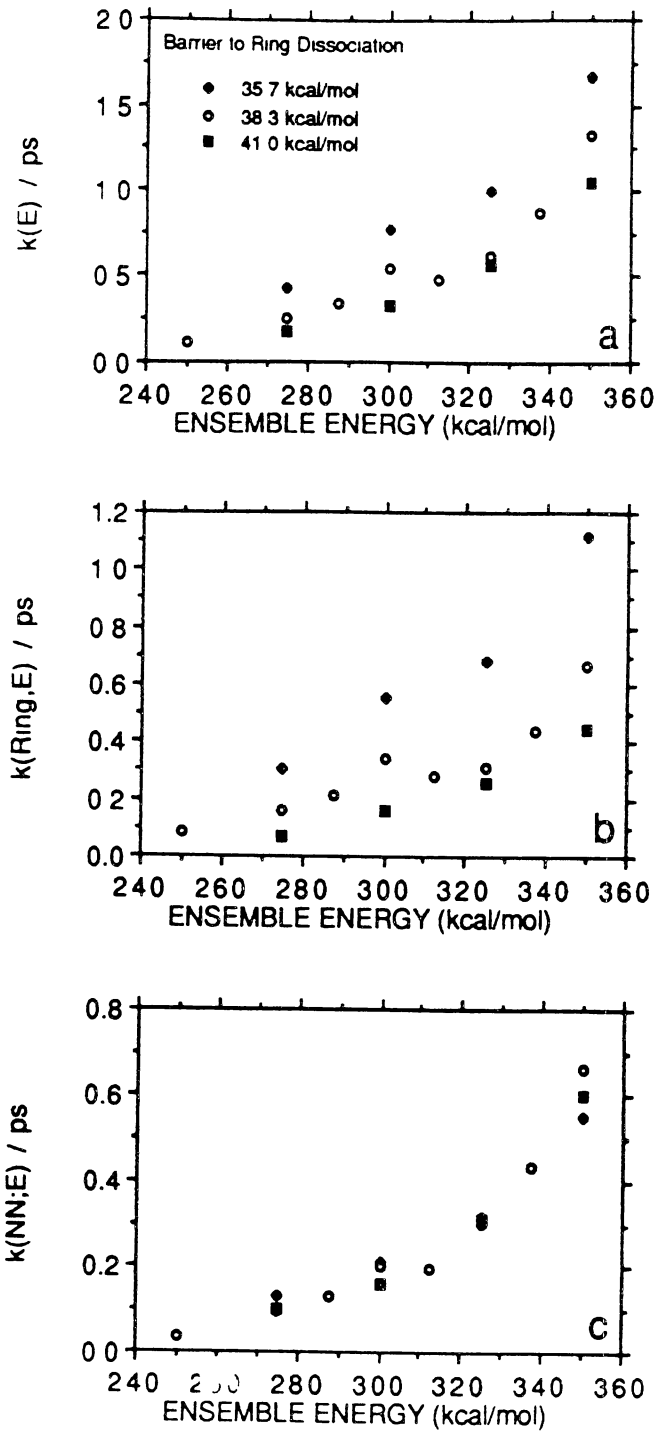
Barrier to Ring Dissociation
35 7 kcal/mol
38 3 kcal/mol
41 0 kcal/mol
k(E) / ps
2 0
1 5
1 0
0 5
0 0
240 260 280 300 320 340 360
ENSEMBLE ENERGY (kcal/mol)
a
k(Ring,E) / ps
1.2
1 0
0 8
0.6
0.4
0 2
0.0
240 260 280 300 320 340 360
ENSEMBLE ENERGY (kcal/mol)
b
k(NN;E) / ps
0.8
0.6
0.4
0.2
0 0
280 300 320 340 360
ENSEMBLE ENERGY (kcal/mol)
c

Figure 36. Branching ratio (k_{ring}/k_{NN}) as a function of barrier to ring dissociation and total energy. Ring-dissociation barriers are: solid diamonds: 35.7 kcal/mol; open circles: 38.3 kcal/mol; solid squares: 41.0 kcal/mol. The experimental value is plotted as an asterisk at 160 kcal/mol.

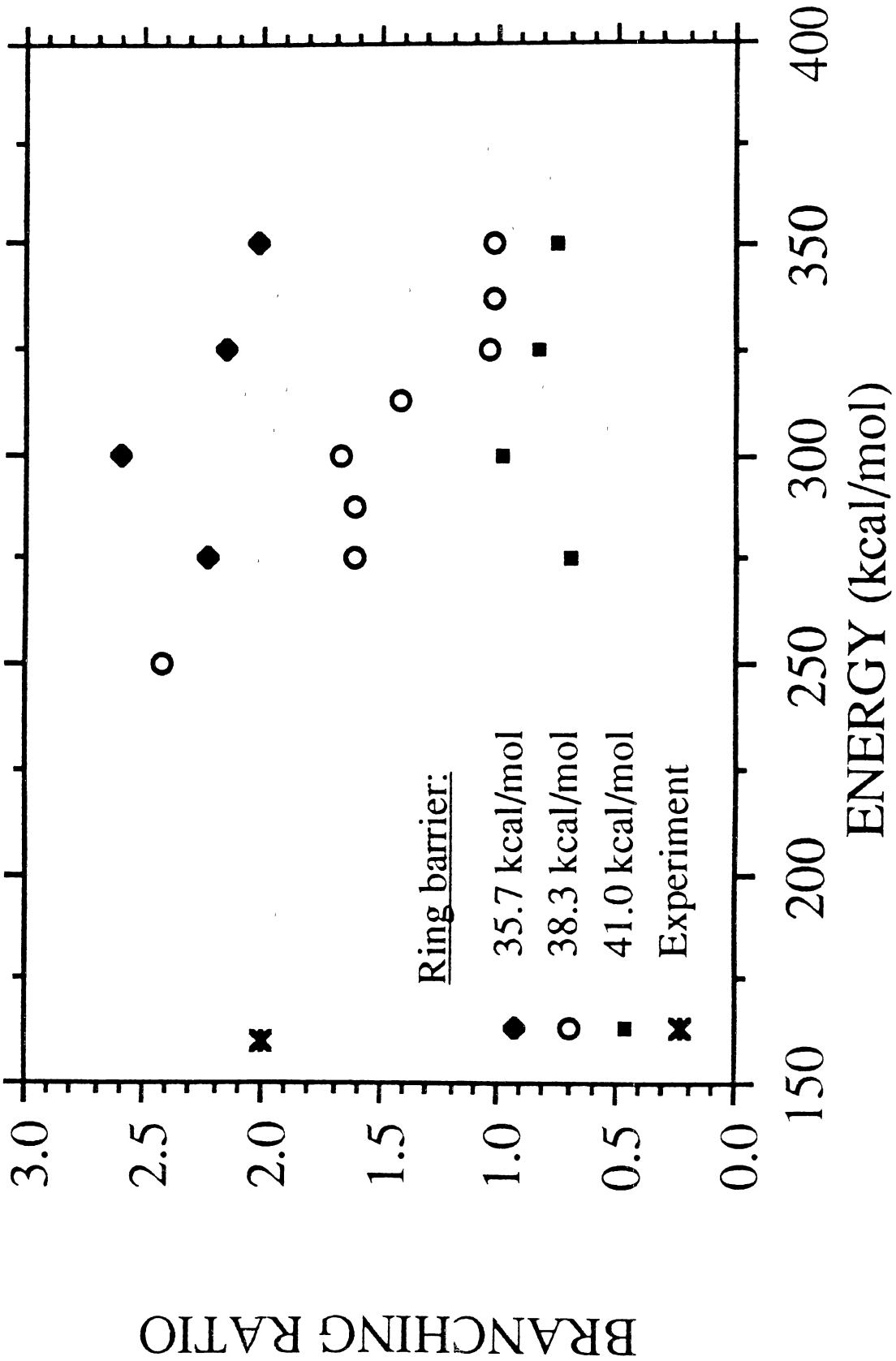
BRANCHING RATIO
3.0
2.5
2.0
1.5
1.0
0.5
0.0
150
200
250
300
350
400
ENERGY (kcal/mol)
Ring barrier:
35.7 kcal/mol
38.3 kcal/mol
41.0 kcal/mol
Experiment

reactions (R3) and (R4), respectively. While the frequency factor for the ring-fission reaction is on the order of molecular vibrational frequencies, the frequency factor for N-N fission is more than three times that of a typical C-H frequency of 3000 cm^{-1}. The values of the "effective" number of degrees of freedom, s, are 43.4 and 38.4 for reactions (R3) and (R4), respectively. The theoretical prediction for RDX is $s = 3N - 6 = 57$. Agreement between the RRK s value and the theoretical prediction of 3N - 6 tends to be good for molecules containing only a few atoms,[187,402] however, as the number of atoms in a molecule increases, the level of agreement tends to decrease.[56,209,211]

Some preliminary calculations were performed on potential-energy surfaces with barriers to ring dissociation of 35.7 and 41.0 kcal/mol, at energies over the range 275 to 350 kcal/mol. The barrier to N-N bond fission was 47.8 kcal/mol. The ensemble sizes used in these calculations were 100 to 200 trajectories. The rate coefficients were computed as above and, not surprisingly, the overall values of k(E) decrease monotonically as the barrier to ring fission is increased. This is illustrated in Fig. 35a, where the overall first-order rate coefficients k(E) are plotted as a function of total energy and for the three values of the barrier to ring dissociation (35.7, 38.3, and 41.0 kcal/mol). The decrease in k(E) as the ring-dissociation barrier increases is due almost wholly to the decrease in the rate of ring fission (panel b) since the rate of N-N dissociation is essentially unaffected (panel c).

Figure 36 presents the branching ratio as a function of ensemble energy and ring-dissociation barrier for all three potential-energy surfaces. Over the range of energies considered, the branching ratio varies from approximately 0.8 to 2.6. Generally, increasing the barrier to ring dissociation decreases the branching ratio. For a given barrier to ring dissociation, there is an overall increase in the branching ratio as the energy decreases. This is the energy dependence that one would expect. However,

the statistical error in the trajectory results plotted in Fig. 36 makes it difficult to extrapolate them to estimate the barrier height that would give the desired (experimental) branching ratio.

The zero-point vibrational energy of RDX is about 80 kcal/mol. Zhao *et al.*[222] deposited roughly 80 kcal/mol of internal energy into the parent RDX molecule in their molecular beam experiment. Given the uncertainty in determining the excitation energy in infrared multiphoton experiments,[4] we therefore estimate 150 to 170 kcal/mol as the energy range for the experimental results. The experimentally determined branching ratio (2.0) is plotted in Fig. 36 as an asterisk at the midpoint of this energy range (160 kcal/mol). From Fig. 36 it is seen that all computed branching ratios corresponding to the potential-energy surface having a ring-dissociation barrier of 35.7 kcal/mol (denoted by diamonds) are greater than this value. The trend in the branching ratio for the potential-energy surface having a ring-dissociation barrier of 38.3 kcal/mol (open circles) suggests that a reasonable extrapolation to the experimental range would lead to a ratio much greater than two. Finally, the results for the potential-energy surface having a ring-dissociation barrier of 41.0 kcal/mol are all less than the experimental value (solid squares). Unfortunately, the statistical error in our results is such that we cannot determine the energy dependence of the branching ratio so that we can reliably extrapolate to the region of the experimental measurements. Nevertheless, the results in Fig. 36 indicate that the potential-energy surface is qualitatively correct. The validity of the surface is further supported by the agreement of the computed product energy distributions with the experimental results; these are discussed below.

Translational-Energy Distributions

Zhao *et al.*[222] measured translational-energy distributions for the products of reactions (R3) and (R4). They found that the translational-energy distribution for the NO_2 fragments in (R3) is peaked at zero, as expected for simple bond-rupture processes. They report that translational-energy distributions for the concerted ring dissociation (R4) peak at about 12 kcal/mol and tail off to considerably larger energies. We have computed the analogous distribution based on the results of our classical trajectory studies, using Eqs. VI.1 and VI.2.

$CH_2N_2O_2$. Figure 37 consists of a normalized distribution of the total kinetic energy released in the ring-dissociation reaction (R4) at total energies 250 , 300, and 350 kcal/mol (panels a, b, and c, respectively). The binwidth for each histogram was determined using the method of Gislason and Goldfield,[403] thus, they vary with the total energy.

The general appearance of the translational-energy distributions in Fig. 37 is consistent with what is expected for dissociations with a barrier to the back reaction.[404] The fragments exit with nonzero kinetic energies and the distributions taper off more rapidly to the left of the maximum than they do to the right. Over this range of energies, the translational energy released in the ring dissociation increases slowly with increasing total energy. The average translational energy released for trajectories computed at 250 kcal/mol is 24 kcal/mol. Increasing the total energy to 300 kcal/mol results in an average kinetic-energy release of 31 kcal/mol, while at 350 kcal/mol an average of 33 kcal/mol is channeled into translational energy of the fragments. Linear extrapolation of the results (R4=0.90) predicts an average translational energy release of 17 kcal/mol at a total energy of 160 kcal/mol. This can be compared to the results of Zhao *et al.*[222]. Based on visual inspection of their translational-energy distribution for reaction (R4), the

Figure 37. Normalized distribution of the total translational energy release in reaction (R4). Total energies are (a): 250 kcal/mol; (b): 300 kcal/mol; (c): 350 kcal/mol.

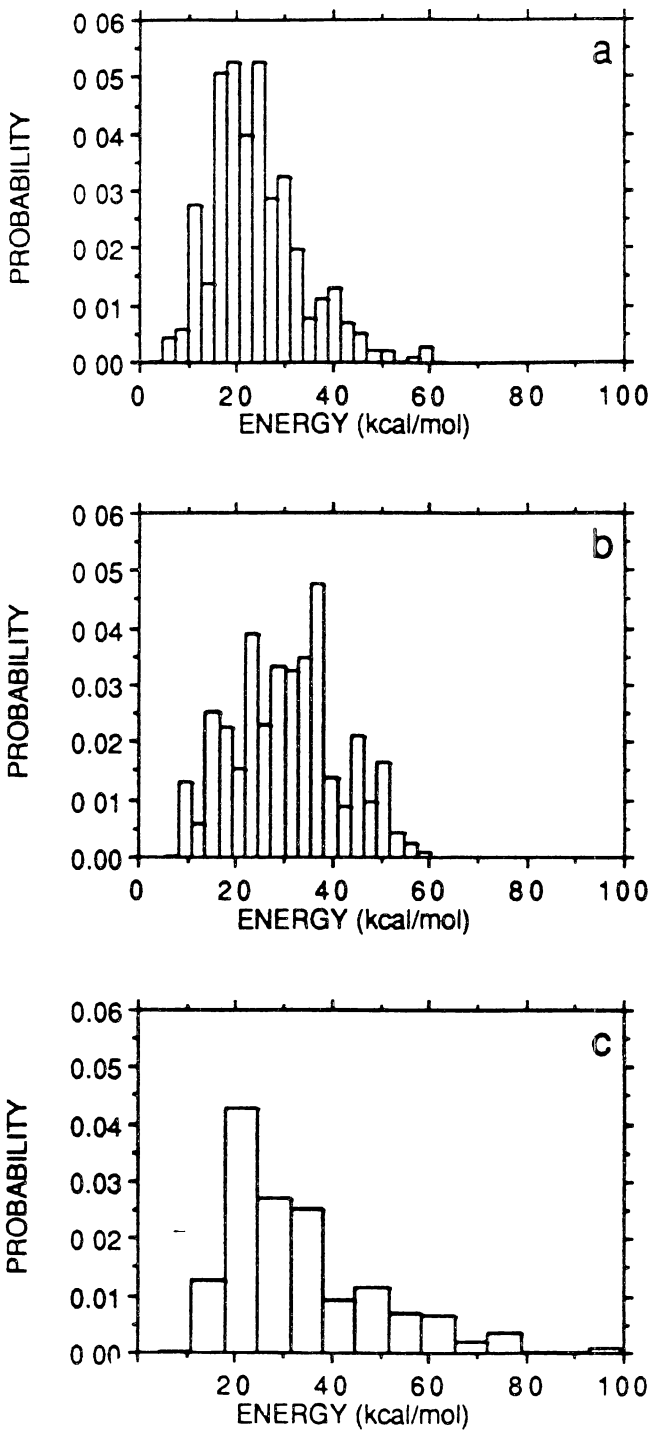
a
PROBABILITY
0 06
0 05
0 04
0 03
0 02
0 01
0 00
0
20
40
60
80
100
ENERGY (kcal/mol)
b
PROBABILITY
0 06
0 05
0 04
0.03
0.02
0 01
0.00
0
20
40
60
80
100
ENERGY (kcal/mol)
c
PROBABILITY
0.06
0.05
0.04
0.03
0 02
0.01
0 00
20
40
60
80
100
ENERGY (kcal/mol)

Figure 38. Normalized distribution of the translational energy of the NO_2 molecules formed *via* the N-N bond fission reaction (R3). Total energies are (a): 250 kcal/mol; (b): 300 kcal/mol; (c): 350 kcal/mol.

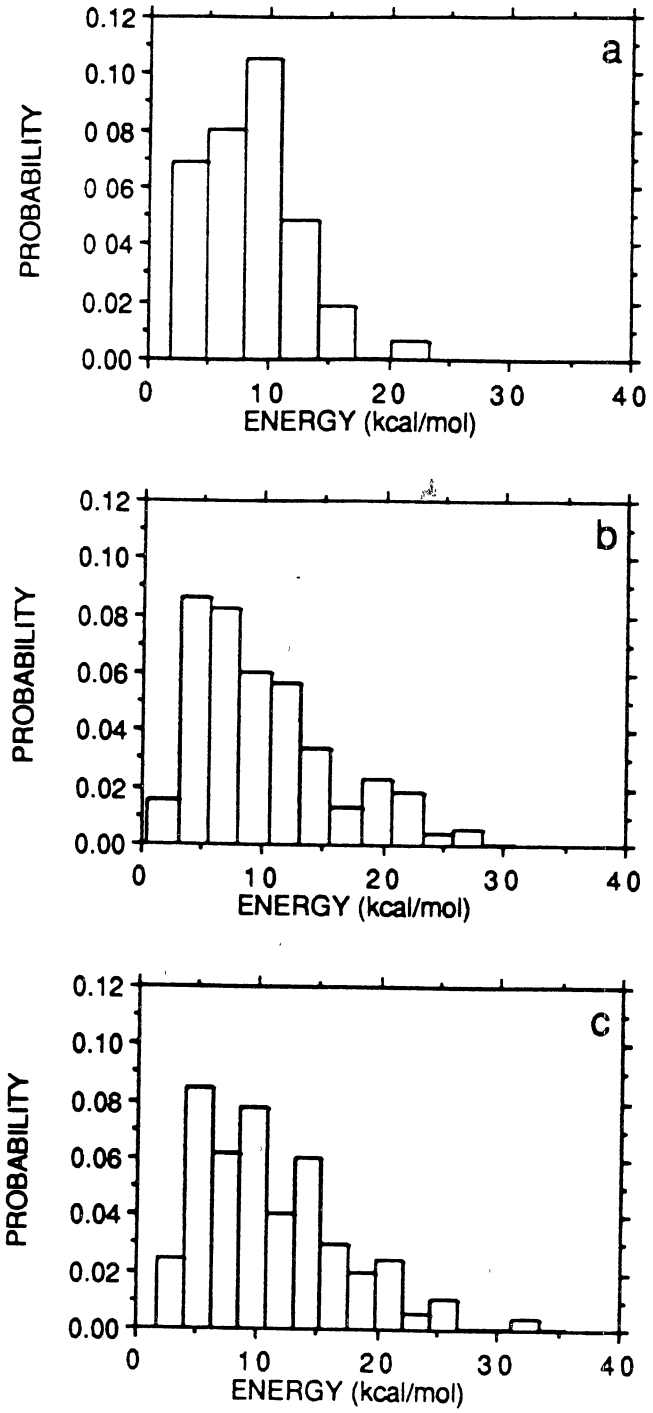
a
b
c
PROBABILITY
ENERGY (kcal/mol)
0.12
0.10
0 08
0 06
0 04
0.02
0.00
0
10
20
30
40

trajectory result appears to be about 3 to 7 kcal/mol higher than the experimentally determined value.

NO_2. Zhao *et al.*[222] found that the NO_2 molecules produced in the molecular beam experiments carried off little excess translational energy. They reported a translational-energy distribution peaked at zero and tailing off rapidly at larger energies. In Fig. 38 we present the normalized translational-energy distribution of the NO_2 molecules produced as a consequence of the N-N bond fission, reaction (R3). Panels a, b, and c refer to ensemble energies of 250, 300, and 350 kcal/mol, respectively. The results indicate that NO_2 is produced with a small but nonzero quantity of translational energy. An average of 8.6 kcal/mol is released as translational energy of NO_2 for the ensemble of trajectories computed at 250 kcal/mol. Increasing the total energy to 350 kcal/mol yields an average translational energy of 11.3 kcal/mol. Linear extrapolation suggests an average translational energy of 6.0 kcal/mol at a total energy of 160 kcal/mol.

Internal Energy Distributions

$CH_2N_2O_2$ Vibrational Energy. We have calculated internal-energy distributions of products resulting from the ring-fission and N-N dissociation reactions using Eqs. VI.2 to VI.7. Figure 39 shows the product vibrational-energy distribution for the ring-fission reaction (R4), for trajectories computed at 250, 300, and 350 kcal/mol (panels a, b, and c, respectively). At 250 kcal/mol, the average vibrational energy of the $CH_2N_2O_2$ molecules is 45 kcal/mol, which is approximately twice the zero-point energy of $CH_2N_2O_2$. A small fraction of the product molecules were formed with (slightly) less than zero-point energy at 250 kcal/mol, but not at the higher total energies. As is evident from Fig. 39, the overall shapes of the distributions are relatively invariant with changing total energy, except for a shift towards higher vibrational energies as the level

Figure 39. Normalized distribution of the vibrational energy of the $CH_2N_2O_2$ molecules formed as a result of ring dissociation (R4). Total energies are (a): 250 kcal/mol; (b): 300 kcal/mol; (c): 350 kcal/mol.

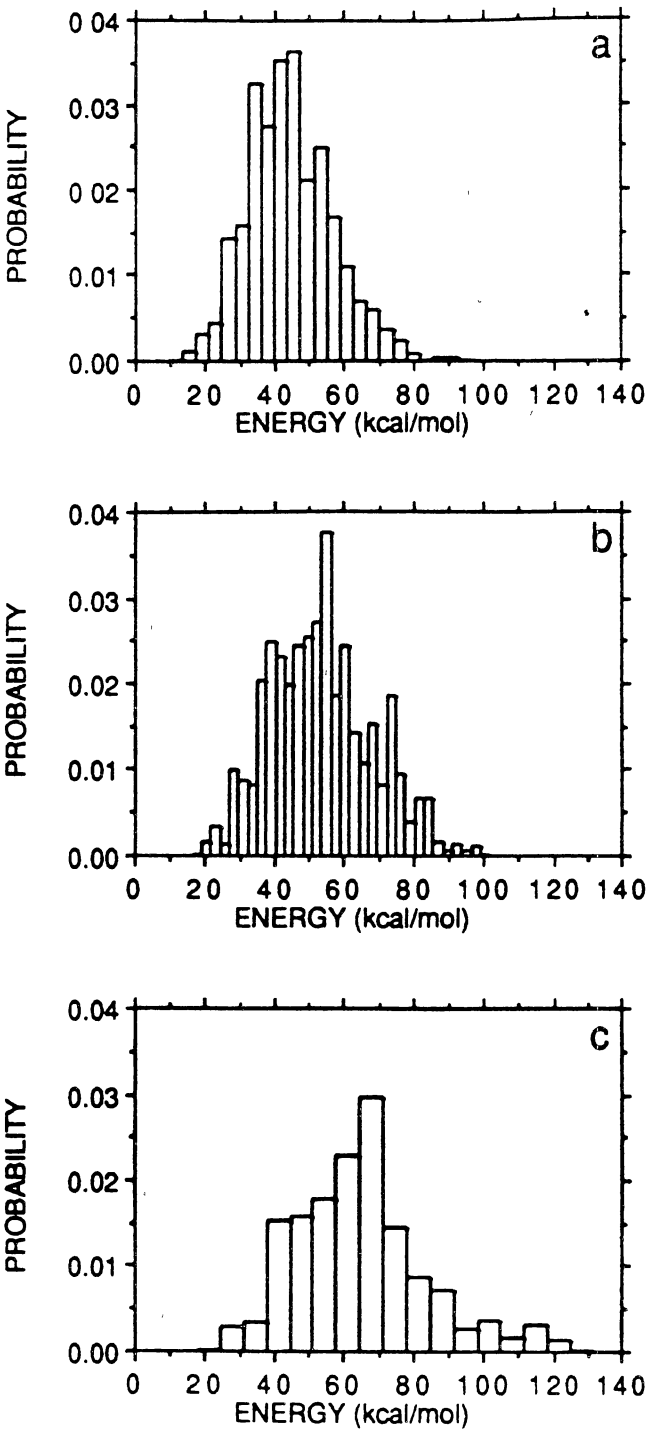
a
b
c
PROBABILITY
ENERGY (kcal/mol)
0.00
0.01
0.02
0.03
0.04
0
20
40
60
80
100
120
140

Figure 40. Normalized distribution of the rotational energy of the $CH_2N_2O_2$ molecules formed as a result of ring dissociation (R4). Total energies are (a): 250 kcal/mol; (b): 300 kcal/mol; (c): 350 kcal/mol.

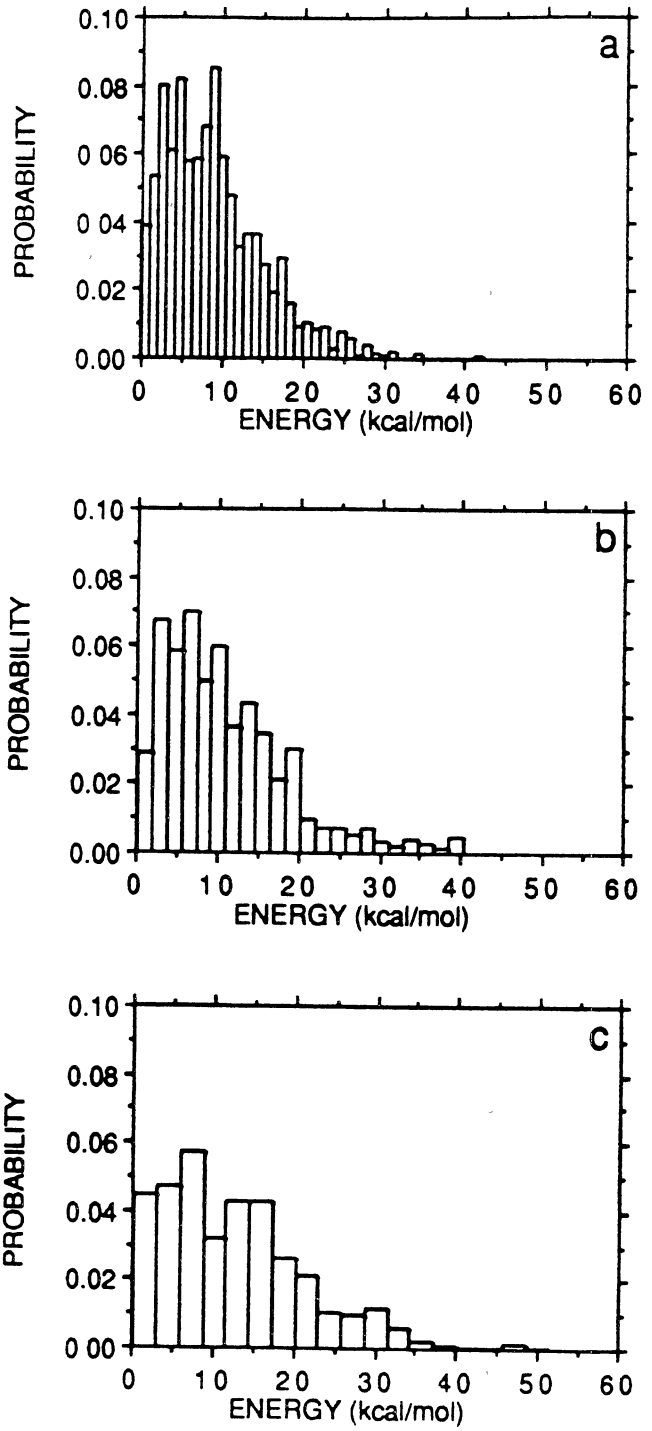
a
PROBABILITY
0.10
0.08
0 06
0 04
0.02
0.00
0 10 20 30 40 50 60
ENERGY (kcal/mol)
b
PROBABILITY
0.10
0.08
0.06
0.04
0.02
0.00
0 10 20 30 40 50 60
ENERGY (kcal/mol)
c
PROBABILITY
0.10
0.08
0.06
0.04
0.02
0 00
0 10 20 30 40 50 60
ENERGY (kcal/mol)

Figure 41. Normalized distribution of the vibrational energy of the NO_2 molecules formed *via* the N-N bond fission reaction (R3). Total energies are (a): 250 kcal/mol; (b): 300 kcal/mol; (c): 350 kcal/mol.

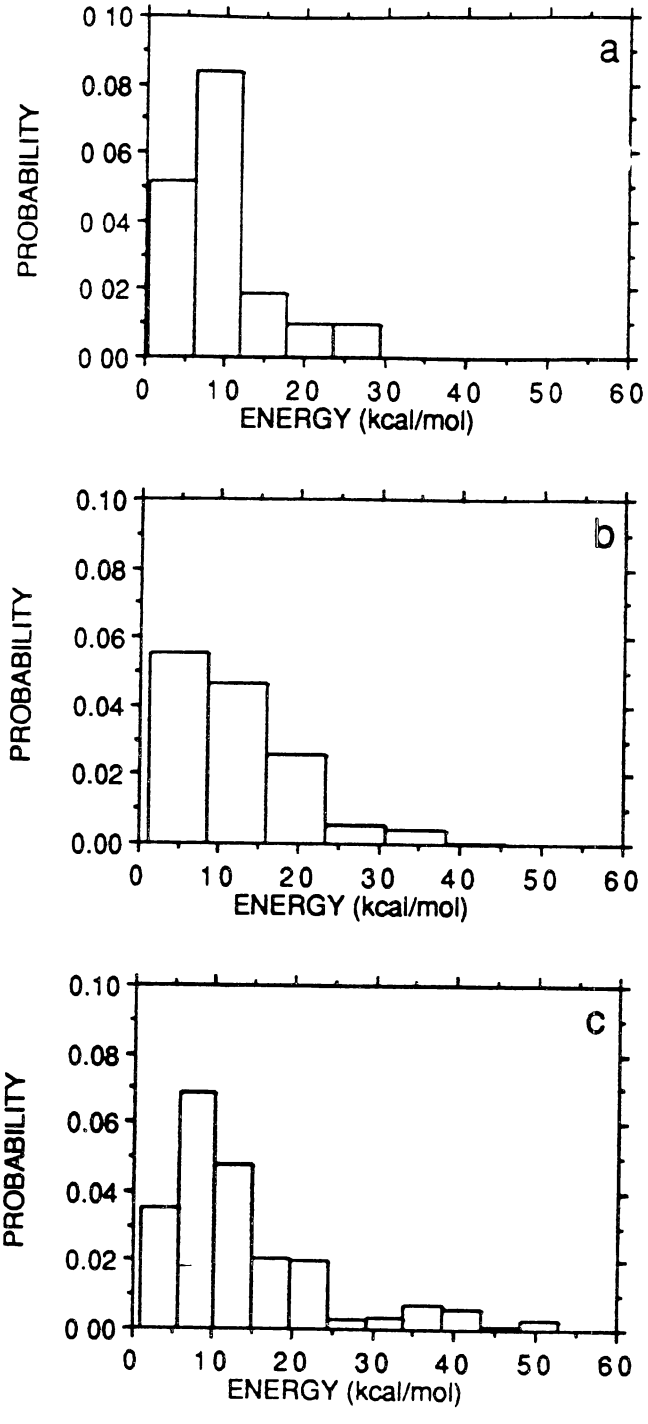
a
PROBABILITY
0 10
0.08
0 06
0 04
0 02
0 00
0 10 20 30 40 50 60
ENERGY (kcal/mol)
b
PROBABILITY
0.10
0.08
0.06
0.04
0.02
0.00
0 10 20 30 40 50 60
ENERGY (kcal/mol)
c
PROBABILITY
0.10
0.08
0.06
0.04
0.02
0 00
0 10 20 30 40 50 60
ENERGY (kcal/mol)

Figure 42. Normalized distribution of the rotational energy of the NO_2 molecules formed *via* the N-N bond fission reaction (R3). Total energies are (a): 250 kcal/mol; (b): 300 kcal/mol; (c): 350 kcal/mol.

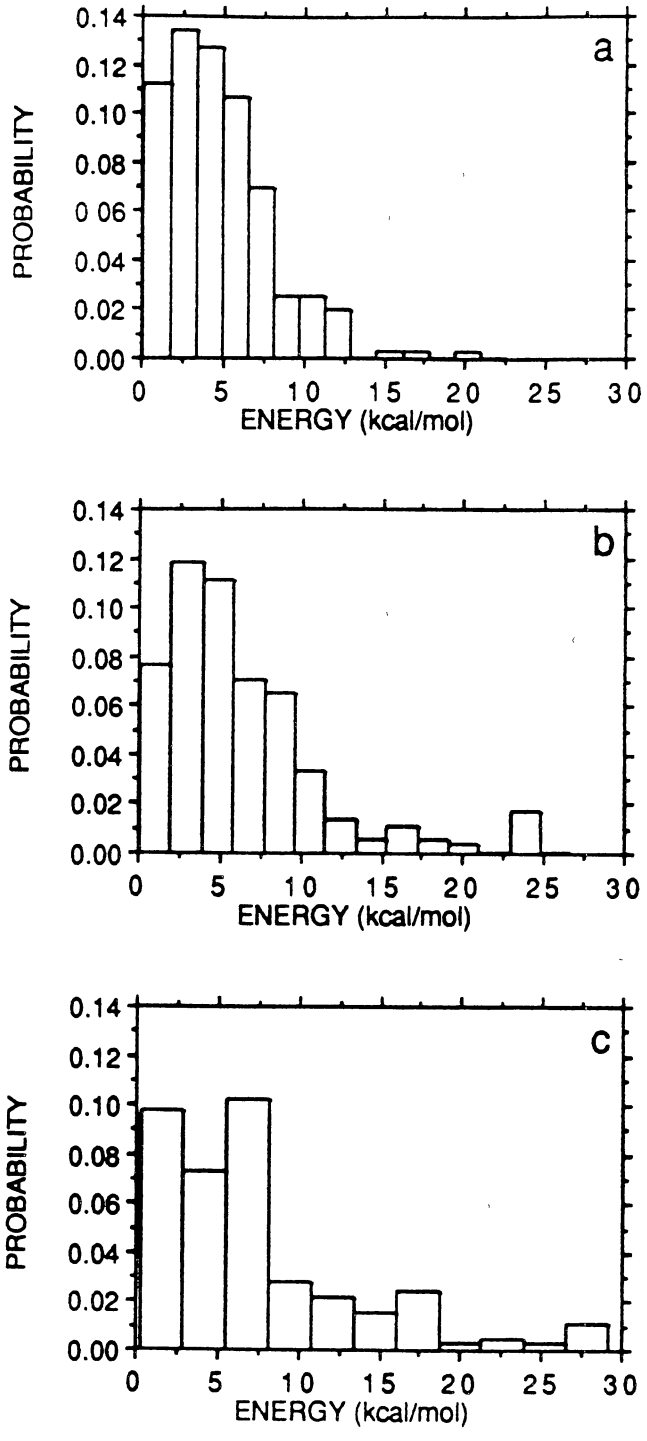
a
b
c
PROBABILITY
ENERGY (kcal/mol)
0.14
0.12
0.10
0.08
0 06
0.04
0.02
0.00
0
5
10
15
20
25
30

of excitation in the reactant molecule is increased. The average vibrational energy increases linearly with total energy over the range 250 to 350 kcal/mol. Based on a least-squares fit of the average vibrational energy to a straight line (R4 = 0.99), we estimate an average vibrational energy of about 25 kcal/mol for a total energy of 160 kcal/mol in the parent RDX molecule. Thus, it is likely that a sizeable fraction of the $CH_2N_2O_2$ molecules produced by ring fission at lower energies are vibrationally hot, some sufficiently energized to be capable of undergoing subsequent unimolecular dissociation or rearrangement, in agreement with experiment.[222]

$CH_2N_2O_2$ Rotational Energy. Normalized rotational-energy distributions for the $CH_2N_2O_2$ molecules formed in the ring-fission process (R4) are presented in Fig. 40. Panels a, b, and c correspond to total energies of 250, 300, and 350 kcal/mol, respectively. The product rotational distributions are peaked at or near zero and fall off rather quickly with increasing energy. The average rotational energy only increases from 9 kcal/mol to 12.6 kcal/mol as the total system energy is increased from 250 to 350 kcal/mol. If ring fission occurs through a concerted process involving a symmetric intermediate then one would expect little rotational excitation in the products, due to the absence of strong net torques in the exit channel. On the other hand, if the reaction is a sequential depolymerization of the ring, then it would be possible for the products to be produced with considerable rotational energy. Some products are formed with relatively high rotational energies (*ca.* 20-40 kcal/mol), indicating that sequential breakup of the ring occurs in some cases.

NO_2 Vibrational Energy. Internal energy distributions of the NO_2 molecules resulting from N-N bond fission are shown in Figs. 41 and 42. Vibrational-energy distributions of NO_2 are presented in Fig. 41, with panels a, b, and c corresponding to ensemble energies of 250, 300, and 350 kcal/mol, respectively. Corresponding rotational-energy distributions are shown in panels a, b, and c of Fig. 42. Qualitatively,

the distributions are unremarkable; the average energy partitioned into both vibration and rotation increases rather slowly with increasing total energy. The average vibrational energy at 250 kcal/mol, 9.8 kcal/mol, is about twice the zero-point energy (*ca.* 5 kcal/mol). However, the standard deviation about the mean is rather large, 6 kcal/mol, and a considerable amount of NO_2 is therefore created with less than zero-point vibrational energy; this "aphysical" result persists up to the highest ensemble energies we considered.

NO_2 Rotational Energy. The rotational-energy distributions shown in Fig. 42 are peaked within a few kcal/mol of zero. This is expected since there is no inherent asymmetry along the minimum-energy profile for N-N bond fission. The force constants for wagging and C-N-N bending diminish to zero as NO_2 elimination proceeds and, since the C-N-N force constants are unattenuated as ring fission occurs (see Table XXII), they do so independently of the ring geometry.

Mechanistic Details

The qualitative features of the translational- and internal-energy distributions are largely in accord with the usual behavior expected for these types of processes. The extrapolated translational-energy release in the concerted ring-fission reaction agrees with the experimental result to within a few kcal/mol. Based on these results the potential-energy surface used in this study is useful for qualitative studies of the unimolecular dissociation of RDX and can be used to elucidate some of the details of the ring-fission process. We have examined the details of the partitioning of the available energy among the three $CH_2N_2O_2$ molecules and, by extension, the "degree of concertedness" of the reaction dynamics of reaction (R4).

Proximity-in-time Correlations. We begin by examining the temporal spread in the times of the last inner turning points of the three chemical bonds that sever in the ring

Figure 43. Temporal spread of the last inner turning points in the three bonds broken in the ring-fission reaction (R4). Total energies are (a): 250 kcal/mol; (b): 300 kcal/mol; (c): 350 kcal/mol.

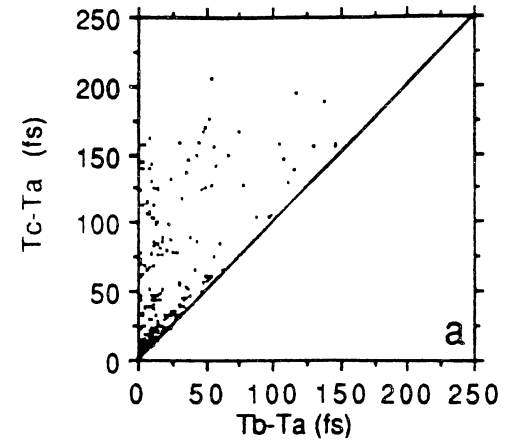
250
200
150
100
50
0
Tc-Ta (fs)
a
0 50 100 150 200 250
Tb-Ta (fs)

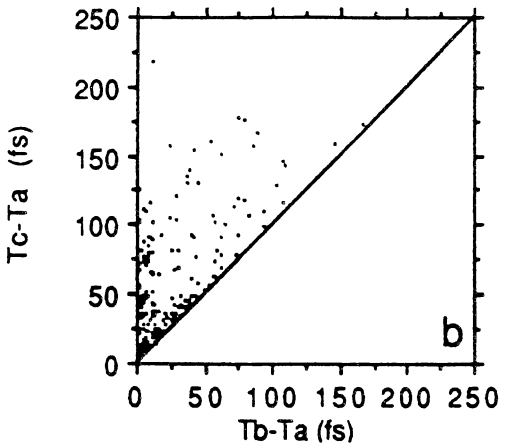
250
200
150
100
50
0
Tc-Ta (fs)
b
0 50 100 150 200 250
Tb-Ta (fs)

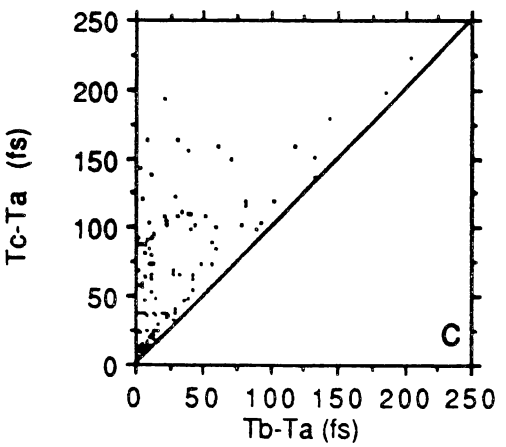
250
200
150
100
50
0
Tc-Ta (fs)
c
0 50 100 150 200 250
Tb-Ta (fs)

dissociation. We define the times of the last inner turning points of the breaking bonds as t_a, t_b, and t_c such that $t_a \leq t_b \leq t_c$. We have plotted t_c-t_a versus t_b-t_a in Fig. 43 for ring dissociations occurring at total energies 250, 300, and 350 kcal/mol (panels a, b, and c, respectively). The units of the axes are femtoseconds (for reference, the period of vibration of the C-N bond in the ground vibrational state is about 27 fs).

A hypothetical trajectory for which all three breaking bonds are vibrating in phase with one another such that they experience their last inner turning points simultaneously would result in a point at the origin. Points lying close to the origin in Fig. 43 correspond roughly to symmetric dissociation. The closer a point is to the diagonal line the shorter the time separation between breaking of the second and third bonds. Moving up along the ordinate (for small values of the abscissa) corresponds to nearly simultaneous fission of the first and second C-N bond, i.e., "elimination" of one $CH_2N_2O_2$ molecule, with increasing values of the ordinate correlating to longer separations in time between the elimination of the first $CH_2N_2O_2$ and the subsequent fission to yield the two remaining $CH_2N_2O_2$ molecules. A fairly large fraction of the dissociations occur near the origin (see Fig. 43), corresponding to rapid decomposition of the ring on a timescale of no more than a few vibrational periods of the C-N bond (about 100 fs).

Energy Partitioning Into Ring Dissociation Products

Vibrational Energy. Further insight into the dissociation process can be gained by examining the energy partitioning of the nascent product molecules as a function of center-of-mass distance from the origin of the lab-fixed coordinate system. Figure 44 shows the partitioning of vibrational energy for all trajectories that resulted in ring dissociation at a total energy of 250 kcal/mol. Panel a is the normalized cumulative distribution which includes all $CH_2N_2O_2$ molecules produced at that energy. Panels b,

Figure 44. Vibrational-energy distribution as a function of the final center-of-mass distance of the ring-fission fragments from the stationary origin of the Cartesian coordinate system. (a) is the cumulative distribution, and panels (b), (c), and (d) are the distributions for the fragments having the largest, intermediate, and smallest center-of-mass distances, respectively. The total energy is 250 kcal/mol.

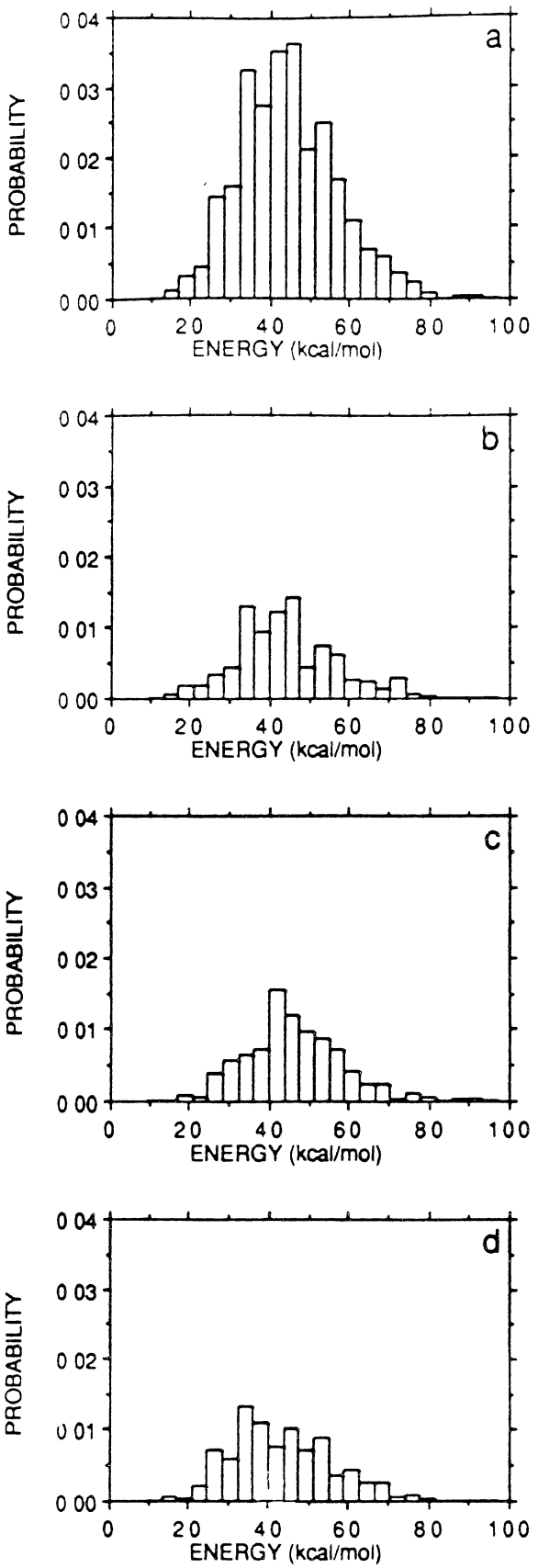
a
b
c
d
PROBABILITY
0 04
0 03
0 02
0 01
0 00
0
20
40
60
80
100
ENERGY (kcal/mol)

Figure 45. Rotational-energy distribution as a function of the final center-of-mass distance of the ring-fission fragments from the stationary origin of the Cartesian coordinate system. (a) is the cumulative distribution, and panels (b), (c), and (d) are the distributions for the fragments having the largest, intermediate, and smallest center-of-mass distances, respectively. The total energy is 250 kcal/mol.

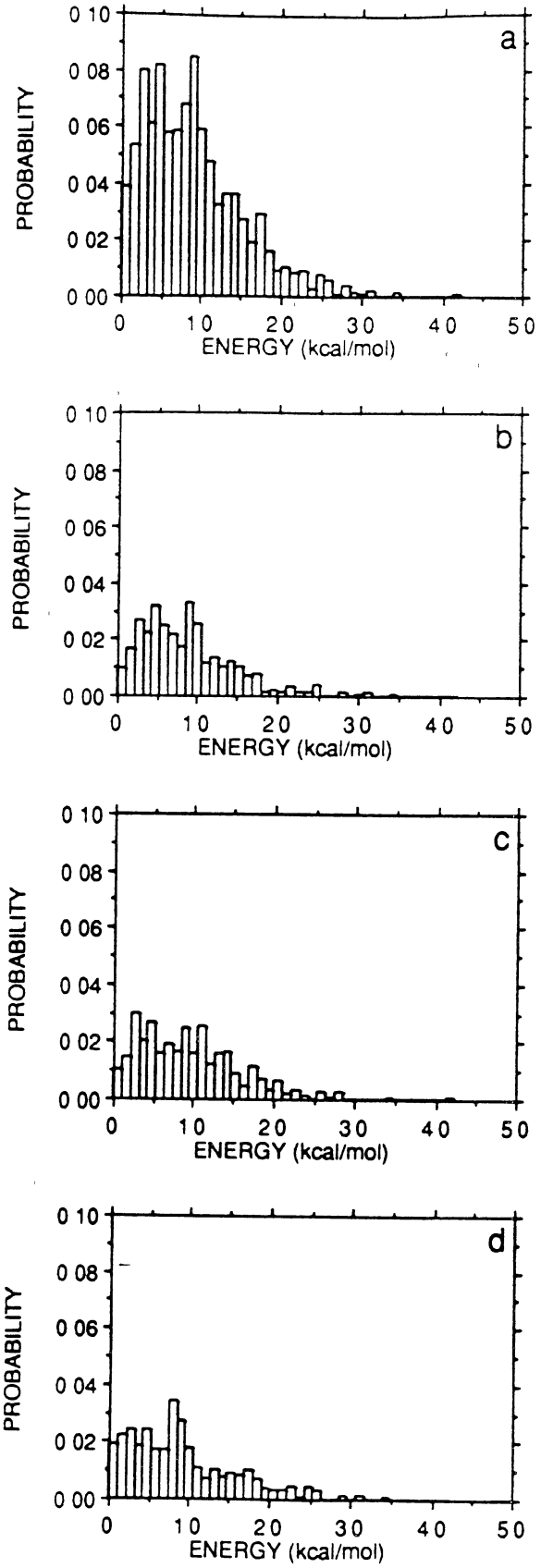
a
b
c
d
PROBABILITY
ENERGY (kcal/mol)
0 10
0 08
0 06
0 04
0 02
0 00
0
10
20
30
40
50

Figure 46. Translational-energy distribution as a function of the final center-of-mass distance of the ring-fission fragments from the stationary origin of the Cartesian coordinate system. (a) is the cumulative distribution, and panels (b), (c), and (d) are the distributions for the fragments having the largest, intermediate, and smallest center-of-mass distances, respectively. The total energy is 250 kcal/mol.

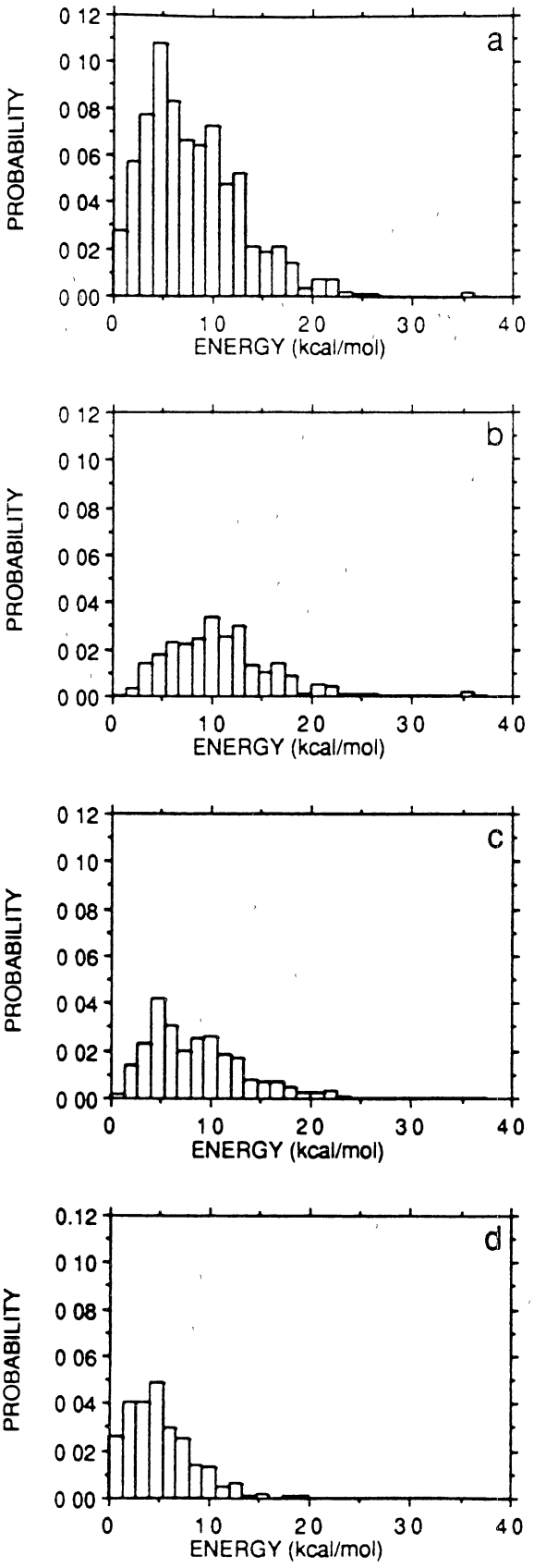
a
b
c
d
PROBABILITY
ENERGY (kcal/mol)
0 12
0 10
0 08
0 06
0 04
0 02
0 00
0.12
0
10
20
30
40

c, and d correspond to fragments having the largest, intermediate, and smallest center-of-mass distances, respectively, measured relative to the stationary center of mass of the system (Recall that the center of mass of the reactant molecule and the lab-fixed Cartesian coordinate system are coincident.). The sum of the areas of panels b, c, and d in Fig. 44 add to unity. There is fairly uniform partitioning of the vibrational energy among the three fragments. No clear correlation is seen between the center-of-mass ordering of the products and the average vibrational energy. In fact, for all calculated ensembles, the average vibrational energies of the "sorted" $CH_2N_2O_2$ molecules were always within a range of about ±3 kcal/mol of the mean of the overall distribution (panel a), and are independent of the relative center-of-mass ranking.

Rotational Energy. The rotational-energy distributions for the same ensemble of trajectories are presented in Fig. 45. Panel a is the cumulative distribution. Panels b, c, and d correspond to fragments having the largest, intermediate, and smallest center-of-mass distances, respectively. The overall distribution of rotational energies indicates rotationally cold products whose distributions are peaked near zero. Once again, the relative magnitude of the distance of the product molecule from the center of mass does not appear to correlate with the average distribution of rotational energy.

Translational Energy. The calculated translational-energy distributions are decomposed according to center-of-mass distance in Fig. 46. The distribution of translational energy among the products is clearly nonuniform, with the $CH_2N_2O_2$ molecule having the largest center-of-mass distance also having the largest translational energy (panel b). The intermediate fragment (panel c) has a distribution of translational energy comparable to the first (panel b), but shifted to lower energies by a few kcal/mol. There is a noticeable difference between the results in panels b and c and those in panel d, which correspond to the fragment having the smallest center-of-mass distance at the end of each trajectory. The distribution shown in panel d is peaked near zero and falls

off rapidly with increasing energy. The results corresponding to other total energies are qualitatively similar to the 250 kcal/mol results shown in Fig. 46. Without exception the product $CH_2N_2O_2$ molecules having the largest center-of-mass distance also have the largest average translational energy while the products having the smallest center-of-mass distance have the lowest average translational energy. The total difference ranges between 5 and 8 kcal/mol. In the case of a completely symmetric, concerted reaction the partitioning of translational energy among the fragments would be expected to be the same for all three fragments. The observed trend in the translational-energy distributions does not agree well with what is expected for a concerted dissociation occurring along such a reaction coordinate. However, given the spread in the results in Figs. 43 and 46, the observed distribution of translational energies among the ring-dissociation products is probably not unreasonable.

Concluding Remarks

We have investigated the simple N-N bond fission and symmetric, concerted triple C-N fission in RDX using classical trajectories computed on model potential-energy surfaces. The potential-energy surfaces are based on the available experimental and theoretical data. The endothermicity of the ring-dissociation reaction was taken to be 24.4 kcal/mol and that of the simple N-N bond fission to be 47.8 kcal/mol. The barrier to N-N fission was set equal to the reaction endothermicity, 47.8 kcal/mol. Most of the calculations are for a potential-energy surface with a barrier of 38.3 kcal/mol to the ring-fission reaction; some calculations were done for barriers of 35.7 and 41.0 kcal/mol. The two reactions we considered are those identified as the principal primary reactions in the gas-phase decomposition of RDX in IRMPD molecular-beam experiments performed by Zhao *et al.*[222]

The branching ratio (defined as the quotient of the number of ring fissions to N-N bond fissions) has been determined by Zhao *et al.*[222] The reported value, 2.0, probably corresponds to total energies in the range 150 to 170 kcal/mol. The branching ratios computed over the energy range 250 to 350 kcal/mol are between 1.0 and 2.4. Unfortunately, the statistical error in the trajectory results is such that we cannot accurately determine the energy dependence of the branching ratios, and then extrapolate our results to the experimental energy range. Nevertheless, our results show that the potential-energy surface is qualitatively correct.

Distributions of the energy released into translation of the ring-fission products have been calculated. The calculated distributions gradually shift towards higher translational energies as the excitation energy of the reactant is increased, with the average value of the translational energy increasing linearly as a function of the total energy. Extrapolating the average translational energy to experimentally attainable conditions leads to a value that is within a few kcal/mol of the experimentally measured value.[21] The overall shapes of the calculated distributions are in good agreement with the experimental results.

The ring-dissociation products are created vibrationally hot and rotationally cold. The majority of the excess energy appears in vibrations of the nascent molecules. The average rotational energy increases by only 3.5 kcal/mol as the excitation energy (in excess of the zero-point energy) is raised from 170 to 270 kcal/mol. A significant number of the $CH_2N_2O_2$ molecules produced *via* ring fission contain sufficient internal energy to undergo subsequent unimolecular reaction or rearrangement, as observed experimentally.[222]

Typically, the product translational-energy distribution for a simple bond-fission reaction in the absence of a back barrier is peaked at or near zero.[404] Our computed translational-energy distributions for NO_2 produced *via* N-N bond fission were found to

be peaked at small but nonzero values, in reasonable agreement with the expected outcome, especially given the level of excitation of the reactant. Vibrational-energy distributions for NO_2 indicate low levels of vibrational excitation, with many molecules having less than the vibrational zero-point energy. The rotational-energy distributions are peaked near zero, which is the anticipated result since strong torques in the exit channel would not be expected, given the functional form of the potential-energy surface and the molecular symmetry.

The mechanism by which decomposition of the triazine ring occurs to yield three $CH_2N_2O_2$ molecules has been studied by examining the final partitioning of the energy among translation, rotation, and vibration in the nascent reaction products. Additionally, "proximity-in-time" correlations were computed. Most of the ring fissions are complete within a few vibrational periods of the ground-state C-N bond, measured relative to the time of the last inner turning point of the first C-N bond to exceed the critical distance for bond dissociation. Based on the outcome of these various quantities, decomposition of the ring appears to occur through a mixture of concerted dissociations and sequential depolymerizations.

The results presented here are encouraging and further work employing a more realistic potential-energy surface is probably warranted. The flexibility of the potential-energy surface we have constructed allows for simple adjustment of the ring-dissociation barrier over a fairly wide range and a reasonably accurate value for the barrier can probably be obtained (for instance by low-energy statistical calculations of the rate coefficients and branching ratio in which the barrier to ring dissociation is treated as a parameter). In addition to examining more closely the effect of variation of the barrier to ring fission, subsequent attempts at modelling the detailed gas-phase reaction dynamics of RDX should perhaps incorporate more detailed attenuation of the potential-energy surface along the various reaction coordinates describing the system, as

well as the dominant secondary reactions. Alternatively, it may be of interest to employ the final energy distributions of the fragments computed here in studies addressing the classical reaction dynamics of the $CH_2N_2O_2$ system.

We make a final comment concerning the applicability of the classical trajectory method to full-dimensional studies of the intramolecular reaction dynamics in large polyatomic systems. Using a relatively simple form for the potential-energy surface that incorporates attenuation of the intramolecular forces in a straightforward (if somewhat cumbersome) manner, we have been able to reproduce the available experimental data with reasonably good accuracy. This is in spite of almost complete lack of knowledge of the details of the potential-energy surface in regions other than those corresponding to the reactants and products. This suggests that it may be possible to extend the scope of these kinds of studies to other large chemical systems.

CHAPTER VII

NONCHAOTIC DYNAMICS IN HIGHLY EXCITED POLYATOMIC MOLECULES

Introduction

Numerous studies have shown that the dynamics of few-mode models and molecules are chaotic at "high energies" [144,165-166,223-239] It is not as clear to what extent chaos is a factor in unimolecular reactions involving large molecules.[171-174,203] Chaos obviously leads to statistical behavior in chemical reactions. Schlag and Levine[132] have pointed out that, at the energies required for dissociation of a many-mode molecule, the energy per mode is sufficiently small that it is unlikely that the dynamics are chaotic. The validity of statistical theories (such as RRKM[180]) and the possibility of observing mode-selective chemistry depend on the nature of the dynamics at energies at and just above reaction thresholds. While a large body of literature deals with the phase-space structure of small (mostly three atom), highly excited molecules,[130,134,156,163-166,225,227-231,233-238] relatively little has been reported for the dynamics of large molecules.[132] This is primarily due to difficulties in extending the theoretical techniques used to study small molecules to large-molecule dynamics.

Among the more common ways of "detecting" chaos are techniques such as monitoring the separation in phase space of "initially adjacent" trajectories[224,228-229,306] or examination of the Poincaire surface of section[156,165,225,229,231,242,405-406] for a dynamical system. Focusing on the first of these two possibilities, Brumer and Duff[224] have shown that the rate of divergence of initially adjacent trajectories can be used as a

tool for diagnosing chaotic dynamics. Specifically, if the Euclidean distance in phase space between two trajectories increases linearly, then the dynamics are regarded as regular. If, however, the distance increases exponentially, then the dynamics are considered to be chaotic. Carter and Brumer[227] and Davis and Wagner[228-229] published a number of papers using this method to study chaotic vibrational motion in a three degree-of-freedom model of OCS.

The surface-of-section method is another simple way to study the dynamics of small systems.[156,165,225,229,231,242,405-406] The method is usually restricted to two degree-of-freedom systems although generalizations to three-dimensional systems have been developed.[405-406] Surfaces of section are constructed by recording the value of the phase-space coordinates for one of the degrees of freedom at such time as the position coordinate for the other other degree of freedom passes through some predetermined value (and usually with a predetermined sign of the conjugate momentum). The surface of section for a regular (quasiperiodic) system will consist of sharply defined closed (invariant) curves corresponding to individual trajectories.[242] Chaotic motion leads to a random scatter of points on the surface of section. The transition from regular to irregular motion is evidenced by a mixture of both kinds of behavior in the surface of section.[242]

Another simple, though not totally satisfactory, way of studying the dynamics of large systems is by calculating power spectra from classical trajectories.[166,173,227,230-231,260,407-414] Power spectra can provide information about the structure of the phase space. For instance, purely periodic motion gives a "stick" spectrum. By contrast, chaotic motion gives a broadband spectrum having a characteristic pattern that, strictly speaking, only emerges in the long-time limit.[407,414] From a more pragmatic point of view, a"grassy" spectrum is usually associated with chaos in the (relatively) short-time dynamics of small systems. For most conditions of interest the spectra will likely be

intermediate between these two extremes, and will be such that precise conclusions cannot be drawn. Nevertheless, power spectra are useful for obtaining information about the *qualitative* behavior of the dynamics.

Among the earliest publications in the chemical dynamics literature concerning power spectral analysis of the vibrational dynamics of "chemical" systems is a paper by Noid, Kozykowski, and Marcus.[414] In this work they demonstrated that the coordinates of two and three degree-of-freedom model Hamiltonians could be used to obtain the vibrational spectrum and semiclassical eigenvalues of the system. Since then, there have been numerous studies that used power spectra as a qualitative means of classifying the classical dynamics as being either regular or chaotic.[227,230-231,407-413]

Smith and Shirts[166] concluded on the basis of power spectra that the dynamics of HNC isomerization become chaotic at a fairly well defined energy. They reported "grassy" structure and broadening in the power spectra. Averaging the spectra over a small ensemble of trajectories tended to smooth out the grassiness but the broad features remained prominent in the spectra. Their analysis allowed them to identify two pathways for energy transfer leading to isomerization.

Sumpter and Thompson[196-319] have used power spectra to qualitatively examine the effects of rotational motion on the vibrational dynamics of hydrogen peroxide. They reported that spectra obtained from individual trajectories for rotating and nonrotating H_2O_2 were qualitatively different. The presence of angular momentum results in a substantial broadening in the peaks relative to the nonrotating case and, additionally, introduces new peaks into the spectrum. This is due to enhanced energy transfer resulting from rotational-vibrational coupling.[196] Interestingly, Sumpter and Thompson found that the direction of the angular momentum, i.e., either random orientation of the angular momentum vector or alignment along one of the principal axes, yielded qualitatively different results, presumably due to the degree of interaction between

various internal coordinates and rotational motion. (Guan and Thompson[103] corroborated this finding concerning the role of alignment of angular momentum in similar calculations on the isomerization and predissociation of HONO.)

Qin and Thompson[323] have used power spectra in conjunction with dynamical constraints[34] in an effort to map out the energy transfer pathways in HONO. They found that by "freezing out" selected vibrational modes (internal coordinates) they could significantly influence the IVR pathways. They determined this by examination of spectra for individual trajectories (and small ensembles) in the presence of different constraints. Spectra for constrained trajectories differed from those obtained in the absence of constraints. First, there (obviously) is no spectral intensity arising from the constrained coordinate. More interestingly, depending upon which internal coordinates are removed from the dynamics, the behavior of a given mode can be either completely quasiperiodic or somewhat irregular. When the HON bend is removed from the dynamics, no relaxation occurs within several picoseconds. The power spectrum in such a case consists entirely of very narrow peaks, with essentially no broadening. One other interesting observation that can be made concerning the constrained dynamics calculations in HONO addresses the statements made in earlier chapters concerning the "resolution" of the normal- and/or local-mode excitation scheme. When the "normal- and/or local-mode excitation followed by scaling" procedure is used, individual trajectories have slightly different internal distributions of energy. In their calculations, Qin and Thompson[323] found that , when the HON bend was frozen, there was considerable variation in the location of the peaks for the OH stretching and torsional modes from one trajectory to another. This finding is a direct result of the inexactness of the normal-mode excitation.

We have employed power spectra[258-260] to attempt to ascertain whether the dynamics of several polyatomic molecules are primarily chaotic or nonchaotic. The

molecules we have chosen to study are: SiF_4, C_2H_4, CH_3ONO, $\cdot CH_2CH_2Cl$, and RDX. The results indicate the existence of well resolved (and assignable) bands in the vibrational spectrum of SiF_4, CH_3ONO, and (to a lesser extent) $\cdot CH_2CH_2Cl$ and RDX for energies up to and above the threshold for unimolecular dissociation. These bands are found to be present at low energies (i.e., the zero-point energy) and remain relatively unchanged over a wide range of internal energies. By contrast, the vibrational spectrum of C_2H_4 indicates a transition to chaotic motion at energies below the reaction threshold. The implication of this finding is that, contrary to conclusions often drawn for "small" molecular systems, the dissociation of large polyatomic molecules is likely *not* to be governed by chaotic dynamics; and this in turn suggests that, under appropriate conditions,[57] nonstatistical processes may be present in the chemical dynamics.

Computational Details

Potential-energy Surfaces

Methyl Nitrite. The potential-energy surface for methyl nitrite is taken from Preiskorn and Thompson.[114] Specifically, it corresponds to "PES-III" (for the *trans* conformer) used by Preiskorn and Thompson in their calculation of the rate of *trans-cis* isomerization in CH_3ONO. The potential is diagonal and consists of Morse stretches for the bonds, harmonic functions for the angles, and a six-term cosine series for the dihedrals (see Chapter II). This force field is a simplification of an experimentally derived potential-energy surface published by Ghosh and Günthard.[415] See Ref. 114 for details of the potential-energy surface.

2-chloroethyl Radical. The potential-energy surface for 2-chloroethyl radical is described accurately in Chapter V. It corresponds to the parameterization denoted as

PES-II. Full attenuation (as described in Chapters IV and V) was included in the potential.

RDX. The potential-energy surface for RDX radical is described accurately in Chapter VI. Full attenuation (as described in Chapters VI) was included in the potential.

Ethene. The potential-energy surface for ethene is the same as used in our study of the unimolecular dissociation of 2-chloroethyl radical, for which C_2H_4 is one of the reaction products. The surface chosen corresponds to PES-I and is described in Chapter IV.

The correspondence between the experimental and calculated normal-mode assignments for C_2H_4 is given in Table XXIV. Note that some of the normal modes are switched relative to the those given in Herzberg.[276] The agreement between the calculated and experimental out-of-plane frequencies is not very good; however, the out-of-plane modes do correspond to the three lowest frequencies in both cases. According to Herzberg, the symmetry of out-of-plane modes ν_7 and ν_8 are reversed. The in-plane modes are in better agreement, except that modes ν_3 and ν_6 are reversed. The correspondence between the results obtained using this empirical force field and the experimental data could be improved (e.g., by including nondiagonal terms in the force field and/or using a least-squares optimization to give closer agreement with the experimental frequencies).

The original purpose of the potential-energy surface was to describe one of the reaction products of 2-chloroethyl radical decomposition, and inclusion of the nondiagonal terms would have likely resulted in undesirable behavior. Thus, the approximate force field was deemed acceptable for its role in the reaction dynamics study. We think that it should be suitable for the work we describe here as well, since

Table XXIV. Comparison of Experimental and Calculated Normal-mode Frequencies of C_2H_4.

Symmetry[a]	Experimental Frequency[b]	Calculated Frequency
ν_4 (A_u)	826	824
ν_7 (B_{1u})	949	881
ν_8 (B_{2g})	943	1011
ν_{10} (B_{2u})	1073	1072
ν_3 (A_g)	1342	1181
ν_6 (B_{1g})	1220	1343
ν_{12} (B_{3u})	1444	1461
ν_2 (A_g)	1630	1656
ν_{11} (B_{3u})	3021	2995
ν_1 (A_g)	3026	3015
ν_9 (B_{2u})	3103	3112
ν_5 (B_{1g})	3105	3129

a. Experimental normal-mode assignments are taken from Herzberg, Ref. 275.

b. J. L. Duncan, D. C. McKean, and P. D. Mallison, Ref. 345

we are only trying to answer a qualitative question concerning the vibrational dynamics in "large" molecules.

SiF_4. The force field for SiF_4 is based on unpublished results[416] of a calculation performed using the GAMESS molecular orbital package.[417] Starting with an *ab initio* structure and Hessian matrix,[416] a 3N-6 X 3N-6 force field was obtained in terms of a set of nonredundant internal coordinates (four bonds and five angles). (This is a standard option in GAMESS.) However, since the resulting force field only includes five of the six valence angles in SiF_4 it is unsuitable for dynamics calculations at high energies -- for example, the F-Si-F angles do not all experience the same restoring forces for large displacements from equilibrium. Also, many of the off-diagonal interaction force constants are quite large. This can lead to aphysical behavior in dynamics calculations. The *ab initio* structure[416] and frequencies[416] are given in Table XXV and the nonredundant force field is given in Table XXVI.

For the present purpose, all of the bond-angle and some of the angle-angle interactions were removed and the remaining force constants were then adjusted to give agreement with the *ab initio* results using a least-squares optimization. This procedure leads to a nearly exact match between the *ab initio* and empirical frequencies but introduces some error into the empirical Hessian. However, the magnitude of the deviation between *ab initio* and empirical Hessian matrix elements was found to be rather small. This is demonstrated in Table XXVII, where we compare representative *ab initio* Hessian matrix elements[416] to the corresponding ones based on the empirical force field. We also show the percent error in the Hessian elements (assuming the *ab initio* values to be "correct") and the magnitude of the individual elements, relative to the largest element in the matrix. The largest errors occur in the elements having the smallest magnitude. Although some of the elements are in error by as much as 178%,

Table XXV. Ab initio[a] Structure and Frequencies for SiF_4.

Geometric Parameters			Frequency (cm^{-1})	
r_{Si-F}	=	1.56150 Å	E	271.6 (2)
θ_{F-Si-F}	=	109.47122 °	F_2	403.0 (3)
			A_1	842.4
			F2	1099.5 (3)

a. Ref. 416.

Table XXVI. Nonredundant Force Field for SiF_4.[a]

Atom	No.	Atomic Mass (amu)
Si	1	27.97693
F	2	18.99840
F	3	18.99840
F	4	18.99840
F	5	18.99840

Definition of Internal Coordinates

Bond No.	Atoms Involved
1	1 2
2	1 3
3	1 4
4	1 5

Angle No.	Atoms Involved
1	2 1 3
2	2 1 4
3	2 1 5
4	3 1 4
5	3 1 5

Diagonal Force Constants (kcal $mol^{-1}Å^{-2}$ or kcal $mol^{-1}rad^{-2}$)

$k_{r_1r_1}$ = 1055.179 $k_{\theta_1\theta_1}$ = 331.911
$k_{r_2r_2}$ = 1055.179 $k_{\theta_2\theta_2}$ = 262.591
$k_{r_3r_3}$ = 1055.179 $k_{\theta_3\theta_3}$ = 262.591
$k_{r_4r_4}$ = 1055.179 $k_{\theta_4\theta_4}$ = 262.591
$k_{\theta_5\theta_5}$ = 262.591

Bond-Bond Interaction Force Constants (kcal mol^{-1} $Å^{-2}$)

$k_{r_1r_2}$ = 29.373
$k_{r_1r_3}$ = 29.373
$k_{r_1r_4}$ = 29.373
$k_{r_2r_3}$ = 29.373
$k_{r_2r_4}$ = 29.373
$k_{r_3r_4}$ = 29.373

Angle-Angle Interaction Force Constants (kcal $mol^{-1}rad^{-2}$)

$k_{\theta_1\theta_2}$ = 165.956 $k_{\theta_2\theta_3}$ = 131.295
$k_{\theta_1\theta_3}$ = 165.956 $k_{\theta_2\theta_4}$ = 131.295
$k_{\theta_1\theta_4}$ = 165.956 $k_{\theta_3\theta_5}$ = 131.295
$k_{\theta_1\theta_5}$ = 165.956 $k_{\theta_4\theta_5}$ = 131.295
$k_{\theta_2\theta_5}$ = 96.635
$k_{\theta_3\theta_4}$ = 96.635

Bond-Angle Interaction Force Constants (kcal mol^{-1} $Å^{-1}$ rad^{-1})

$k_{r_1\theta_1}$ = 38.937 $k_{r_3\theta_1}$ = -38.937
$k_{r_1\theta_2}$ = 38.937 $k_{r_3\theta_3}$ = -38.937

Table XXVI, continued

$k_{r_1\theta_3} = 38.937$	$k_{r_3\theta_5} = -38.937$
$k_{r_2\theta_1} = 38.937$	$k_{r_4\theta_1} = -38.937$
$k_{r_2\theta_4} = 38.937$	$k_{r_4\theta_2} = -38.937$
$k_{r_2\theta_5} = 38.937$	$k_{r_4\theta_4} = -38.937$

a. Ref. 416.

Table XXVII. Comparison of Ab Initio and Empirical Hessian Matrix Elements for SiF4.

i j	$\mathcal{H}_{ij}$ (*ab initio*)[a]	$\mathcal{H}_{ij}$ (empirical)[b]	%Error	Rel. Magnitude
1 1	0.688406	0.735766	-6.879676	1.000000
1 4	-0.172099	-0.183942	-6.881269	-0.249996
1 5	0.127091	0.118935	6.417844	0.184616
4 4	0.180987	0.173076	4.371316	0.262908
4 5	-0.144939	-0.135411	6.573863	-0.210543
4 7	-0.008334	-0.005386	35.377580	-0.012107
4 8	0.017845	0.016477	7.669272	0.025922
4 9	0.005204	-0.000225	104.319659	0.007559
4 13	0.007778	0.021638	-178.197711	0.011298

a. Ref. 416
b. Redundant force field.

Table XXVIII. Redundant Force Field for SiF_4 (Used in Dynamics Calculations).

Atom	No.	Atomic Mass (amu)
Si	1	27.97693
F	2	18.99840
F	3	18.99840
F	4	18.99840
F	5	18.99840

Definition of Internal Coordinates

Bond No.	Atoms Involved
1	1 2
2	1 3
3	1 4
4	1 5

Angle No.	Atoms Involved
1	2 1 3
2	2 1 4
3	2 1 5
4	3 1 4
5	3 1 5
6	4 1 5

Diagonal Force Constants (kcal $mol^{-1}Å^{-2}$ or kcal $mol^{-1}rad^{-2}$)

$k_{r_1r_1} = 994.747$	$k_{\theta_1\theta_1} = 177.600$
$k_{r_2r_2} = 994.747$	$k_{\theta_2\theta_2} = 177.600$
$k_{r_3r_3} = 994.747$	$k_{\theta_3\theta_3} = 177.600$
$k_{r_4r_4} = 994.747$	$k_{\theta_4\theta_4} = 177.600$
	$k_{\theta_5\theta_5} = 177.600$
	$k_{\theta_6\theta_6} = 177.600$

Bond-Bond Interaction Force Constants (kcal mol^{-1} $Å^{-2}$)

$k_{r_1r_2} = 49.496$
$k_{r_1r_3} = 49.496$
$k_{r_1r_4} = 49.496$
$k_{r_2r_3} = 49.496$
$k_{r_2r_4} = 49.496$
$k_{r_3r_4} = 49.496$

Angle-Angle Interaction Force Constants (kcal $mol^{-1}rad^{-2}$)

$k_{\theta_1\theta_2} = 40.4$	$k_{\theta_2\theta_3} = 40.4$
$k_{\theta_1\theta_3} = 40.4$	$k_{\theta_2\theta_4} = 40.4$
$k_{\theta_1\theta_4} = 40.4$	$k_{\theta_3\theta_5} = 40.4$
$k_{\theta_1\theta_5} = 40.4$	$k_{\theta_4\theta_5} = 40.4$
$k_{\theta_2\theta_6} = 40.4$	$k_{\theta_4\theta_6} = 40.4$
$k_{\theta_3\theta_6} = 40.4$	$k_{\theta_5\theta_6} = 40.4$

the relative size of such terms is quite small. The larger terms tend to have an error of roughly ± 6%.

Anharmonicity was included in the bond stretching terms by replacing the harmonic oscillator terms used to fit the force field with Morse oscillators. A typical value of 135 kcal/mol[418] was used for the well depth of the Si-F bonds and the range parameter, α, was obtained using Eq. II.3. The force field used in the dynamics calculations reported here is given in Table XXVIII.

The potential-energy surfaces for CH_3ONO and C_2H_4 completely neglect attenuation of the force-field parameters as reaction occurs (through dissociation and, in the case of CH_3ONO, isomerization). The force field for SiF_4 is attenuated as a function of the four Si-F bond lengths. Attenuation of the geometrical parameters has been neglected.

The appropriate diagonal angle-bending force constants and off-diagonal bond-bond, angle-angle, and bond-angle interaction constants are attenuated to zero as one (or more) of the Si-F bond lengths becomes highly extended. The attenuation is accomplished by writing a given force constant as

$$k_{q_i,q_j}(\mathbf{r}) = k^{o}_{q_i,q_j} \prod S(r_k), \qquad \text{(VII.1)}$$

where q_i and q_j are the internal coordinates explicitly involved in a given potential-energy term (diagonal bond-stretching terms are never attenuated) and $S(r_k)$ is a switching function dependent on the length of bond k. The switching function used is

$$S(r) = e^{-(r-r^{o})^4}. \qquad \text{(VII.2)}$$

Figure 47. Minimum-energy profile for scission of one of the Si-F bonds in SiF_4. The endothermicity is 135 kcal/mol.

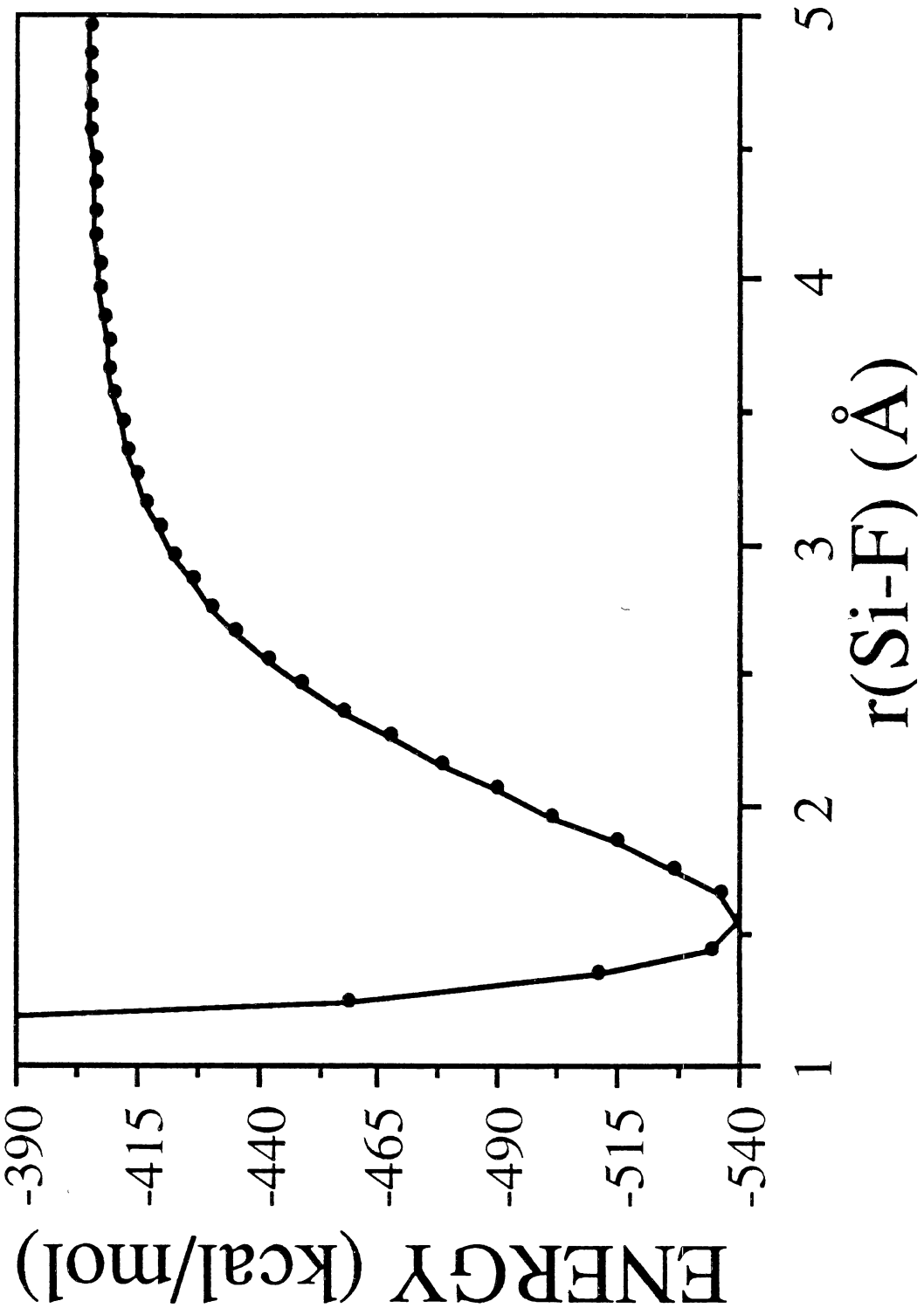
ENERGY (kcal/mol)
-390
-415
-440
-465
-490
-515
-540
1
2
3
4
5
r(Si-F) (Å)

The product of switching functions appearing in Eq. (VII.2) includes factors for all Si-F bonds involving F atoms that are involved in the definition of the internal coordinates q_i and q_j. Thus, while the attenuation of the potential-energy surface does not account for changes in the equilibrium geometry or force constants in the product radical, SiF_3, forces that are present in SiF_4 but absent in SiF_3 + F diminish to zero as one of the Si-F bonds dissociates.

The minimum-energy profile for removal of one of the F atoms is shown in Fig. 47. The Figure was generated by incrementally extending one of the Si-F bonds and minimizing the potential energy using the STEPIT[366] subroutine. Identical results were obtained for each of the four possible bond-fission channels. The results do not indicate the presence of any spurious minima along the reaction coordinate due to the nondiagonal terms in the force field. Further tests were performed to search for minima away from the minimum-energy path: A random walk was performed in order to search for deep wells in the potential-energy surface. Also, individual trajectories were computed and plots of the internal coordinates versus time were examined. Neither of these procedures gave evidence for anomalous behavior.

Trajectory Integration

Classical trajectories were computed in a space-fixed Cartesian coordinate system using a fourth-order Runge-Kutta-Gill integrator with a fixed step size of 1.5×10^{-16} s (except for C_2H_4 calculations at E = 155 kcal/mol, for which a stepsize of 7.5×10^{-17} s was used; and for RDX, for which the stepsize was 9.78×10^{-17} s). In most cases, ensembles of twenty trajectories (each of ten picosecond duration) were computed for a given distribution of energy. The internal coordinates were recorded after every 3.0 fs of trajectory time. An exception to this rule is the RDX calculations, for which fewer trajectories were computed for each set of initial conditions, the

duration of individual (nondissociative) trajectories was 16.7 ps, and the coordinates were written every 4.9 fs.

Calculation of Power Spectra

In this work we have chosen to transform the time histories of the internal coordinates. It is equally valid to transform, say, the Cartesian momenta or the normal coordinates. The reason for selecting the internal coordinates is that they are provide a relatively "intuitive" description of the molecular motions (displacements of bond lengths, bond angles, etc) and are independent of any space-fixed reference frame. By contrast, the Cartesian momenta are not readily associated with particular vibrational modes. The normal coordinates do not provide a convenient alternative since we are, in some cases, examining the influence of angular momentum on the power spectra and, in order to use them, we would have to set up a rotating frame with respect to which the normal modes could be calculated.

Ensemble averaged autocorrelation functions of the internal coordinates were computed for each ensemble of trajectories by first computing single-trajectory autocorrelation functions (Eq. II.39) and then averaging over the ensemble. Power spectra were obtained as the Fourier transform of the ensemble-averaged autocorrelation functions. The cumulative vibrational spectrum was then calculated by direct superposition of the spectra for the individual coordinates.

Results

Reference Spectra

A single low-energy trajectory was computed for each of the five molecules considered in order to provide a "reference" spectrum to be used for comparison with

results obtained for higher energies. Initial conditions for these trajectories were obtained by assigning $0.001h\nu_i$ of energy to each normal mode (i.e., a "quantum number" of v_i =-0.499) The resulting cumulative spectra are shown in panel Figs. 48 to 52 for SiF_4, C_2H_4, CH_3ONO, $\cdot CH_2CH_2Cl$, and RDX, respectively. The reference spectrum for a given molecule consists of very narrow peaks at the normal-mode frequencies. The positions of the peaks for SiF_4, C_2H_4, and CH_3ONO (Figs. 48 to 50, respectively) agree with the analytical normal-mode analysis to within the resolution of the power spectrum (1.67 cm^{-1}). A few of the peaks in the power spectra for 2-chloroethyl radical and RDX (Figs. 51 and 52) are shifted by several wavenumbers from the predictions of the normal-mode analysis. This is due to the fact that the second derivative terms for the switching functions were neglected in the normal-mode analysis. However, the shifts are not very large and we do not think that they pose a problem. .

<u>SiF_4</u>

The zero-point energy of SiF4 is eight kcal/mol. Ensemble-averaged spectra are shown for SiF4 at this energy in Figs. 53 to 58 . Initial conditions were obtained using a random walk as described in chapter II. Figures 53 to 55 are for the case of zero angular momentum . The cumulative spectrum is shown in Fig.53; Figs. 54 and 55 are for the bonds and angles, respectively. Figs. 56 - 58 are similar to Figs. 53 - 55 except that no angular momentum constraints were imposed. It is clear that, for nonrotating SiF_4, the zero-point energy dynamics are quasiperiodic (Fig. 55). Based on the results in Figs. 54 and 55, the two low-frequency modes are principally associated with bending modes and the two high-frequency modes appear to be primarily stretching motions. The mode at 272 cm^{-1} is a pure bending mode while the one at 842 is a pure stretching mode .

Figure 48. Reference power spectrum for SiF_4.

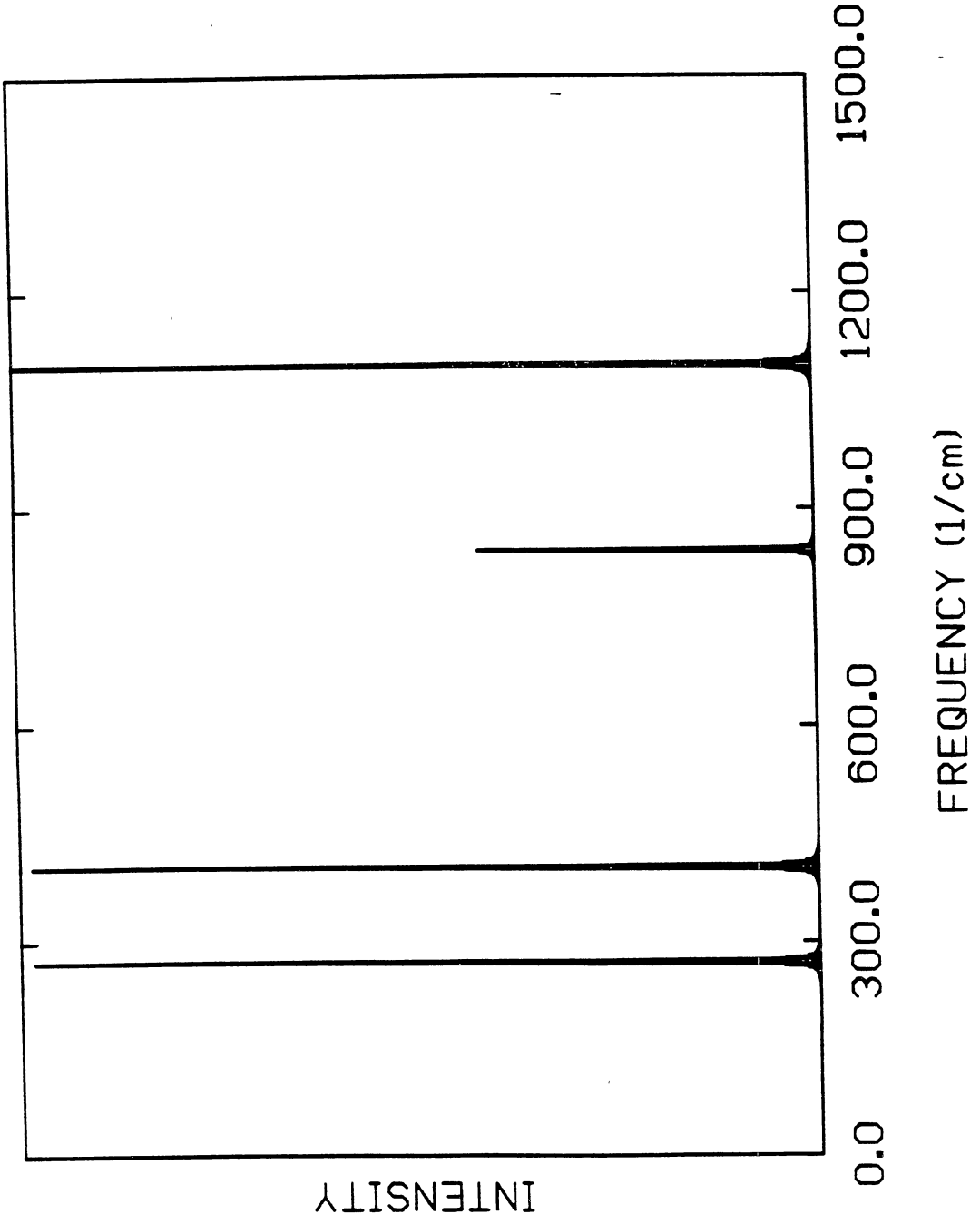
INTENSITY
0.0
300.0
600.0
900.0
1200.0
1500.0
FREQUENCY (1/cm)

Figure 49. Reference power spectrum for C_2H_4.

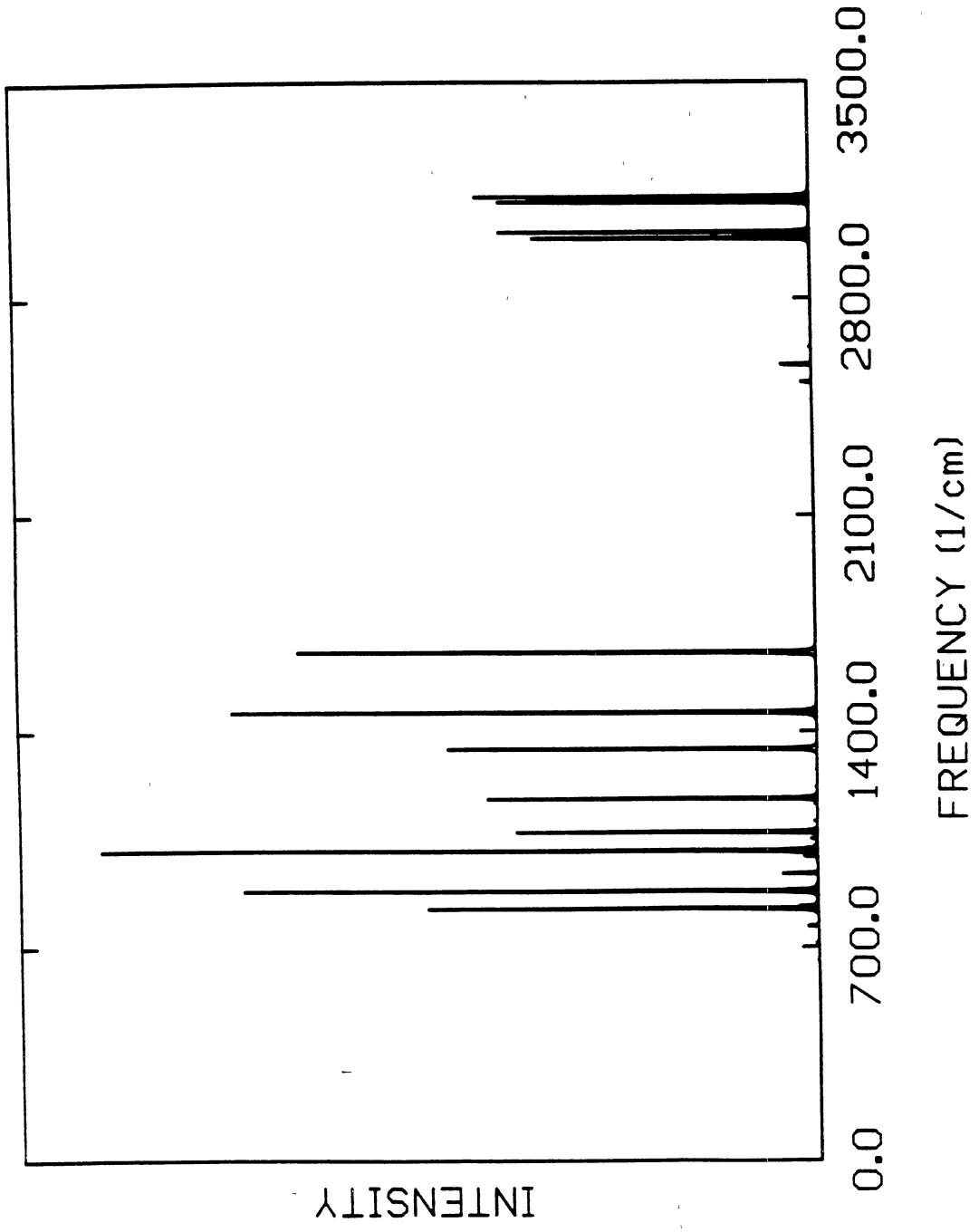
INTENSITY
0.0
700.0
1400.0
2100.0
2800.0
3500.0
FREQUENCY (1/cm)

Figure 50. Reference power spectrum for CH_3ONO.

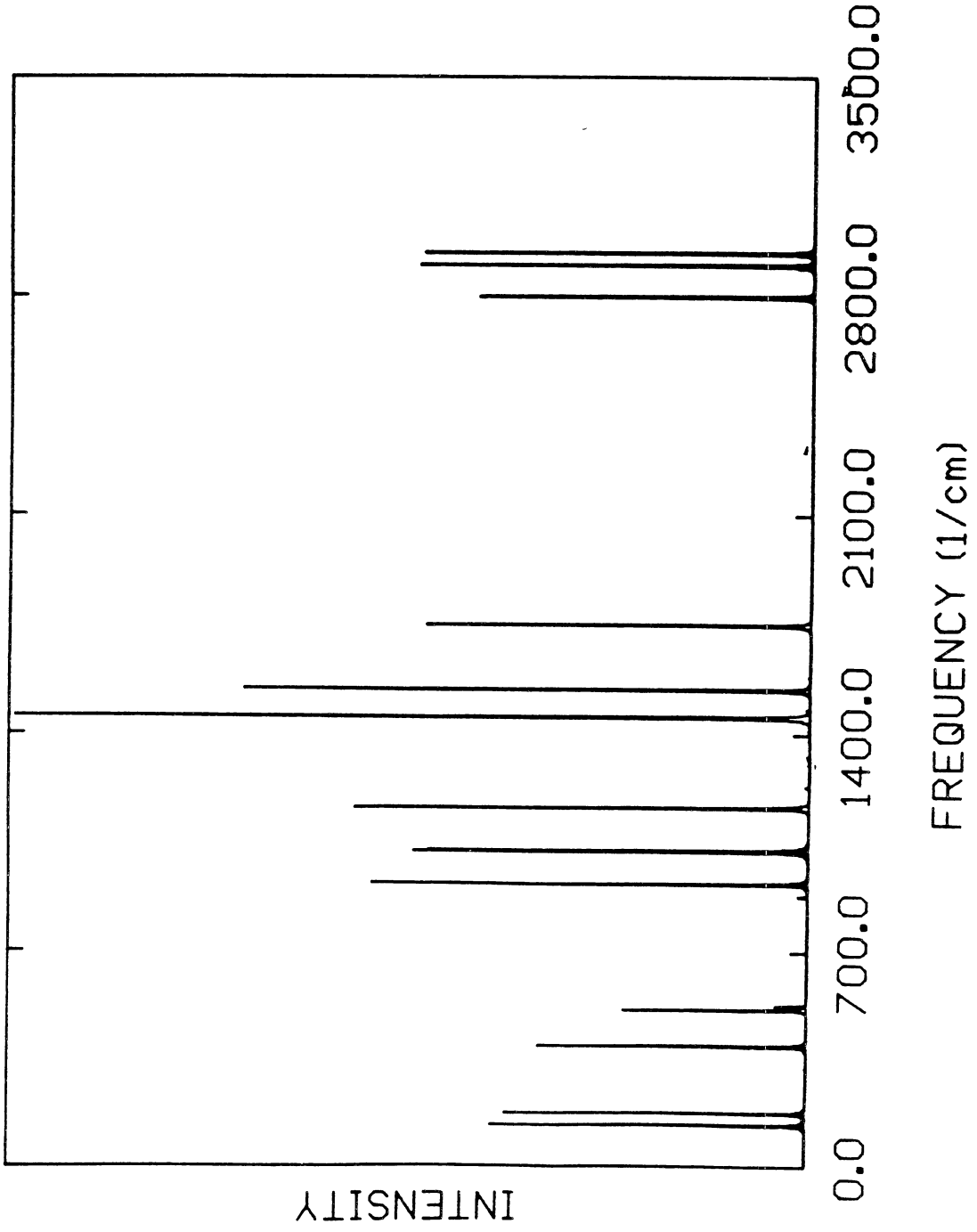
INTENSITY
0.0
700.0
1400.0
2100.0
2800.0
3500.0
FREQUENCY (1/cm)

Figure 51. Reference power spectrum for 2-chloroethyl radical.

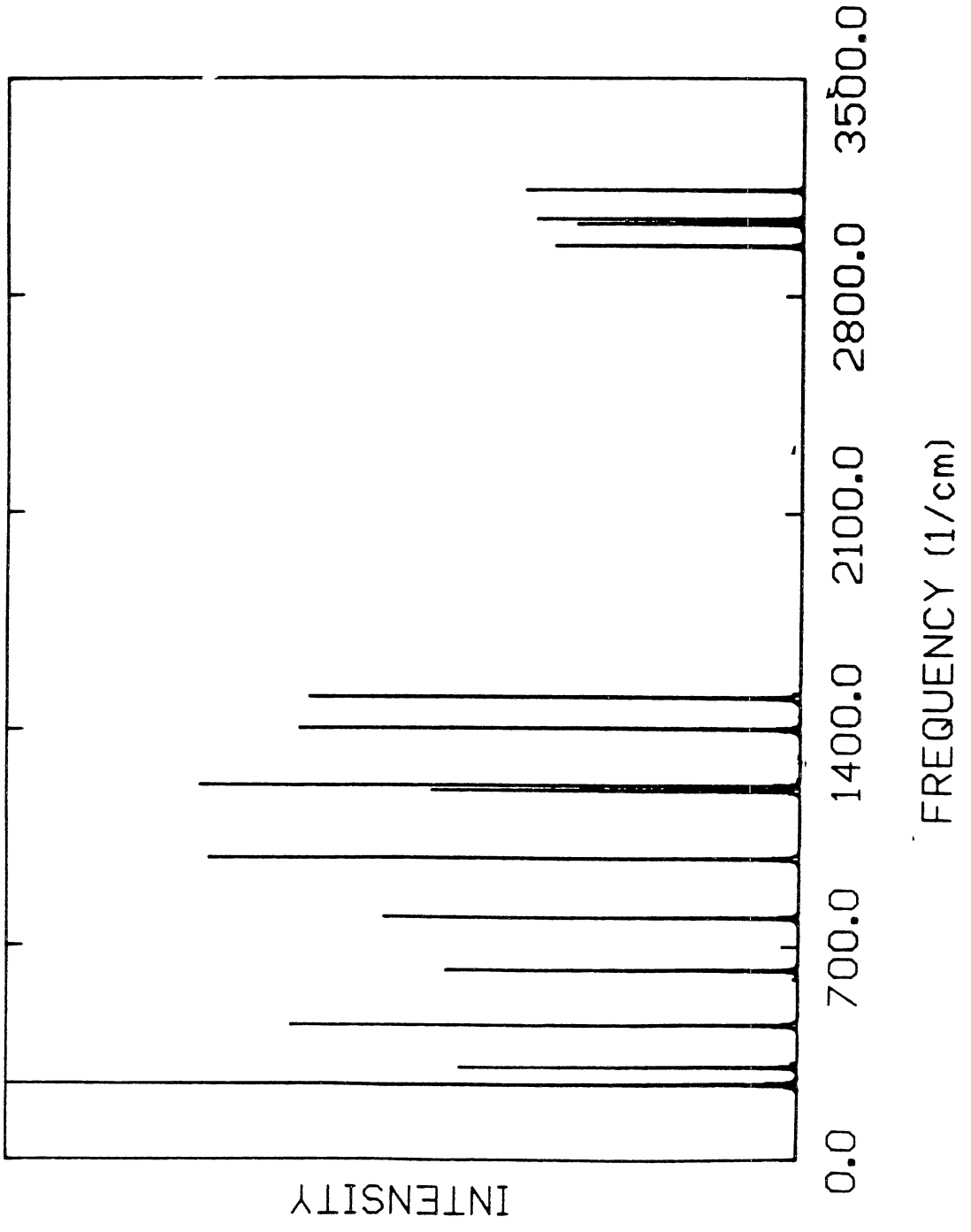
INTENSITY
0.0
700.0
1400.0
2100.0
2800.0
3500.0
FREQUENCY (1/cm)

Figure 52. Reference power spectrum for RDX.

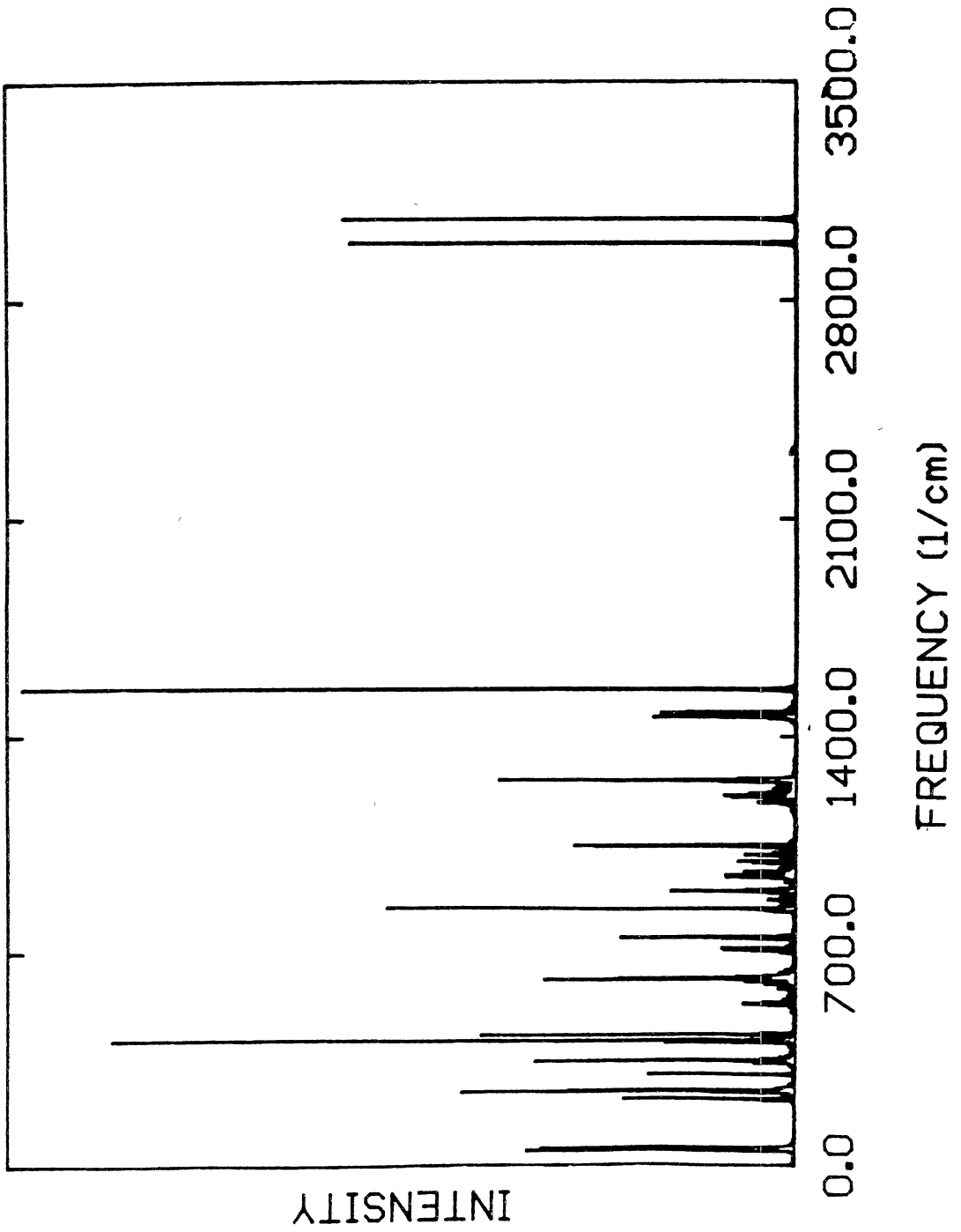
INTENSITY
0.0
700.0
1400.0
2100.0
2800.0
3500.0
FREQUENCY (1/cm)

Figure 53. Cumulative power spectrum for nonrotating SiF_4 vibrating with zero-point energy. The spectrum was obtained as a superposition of the Fourier transforms of ensemble-averaged sample autocorrelation functions of the internal coordinates.

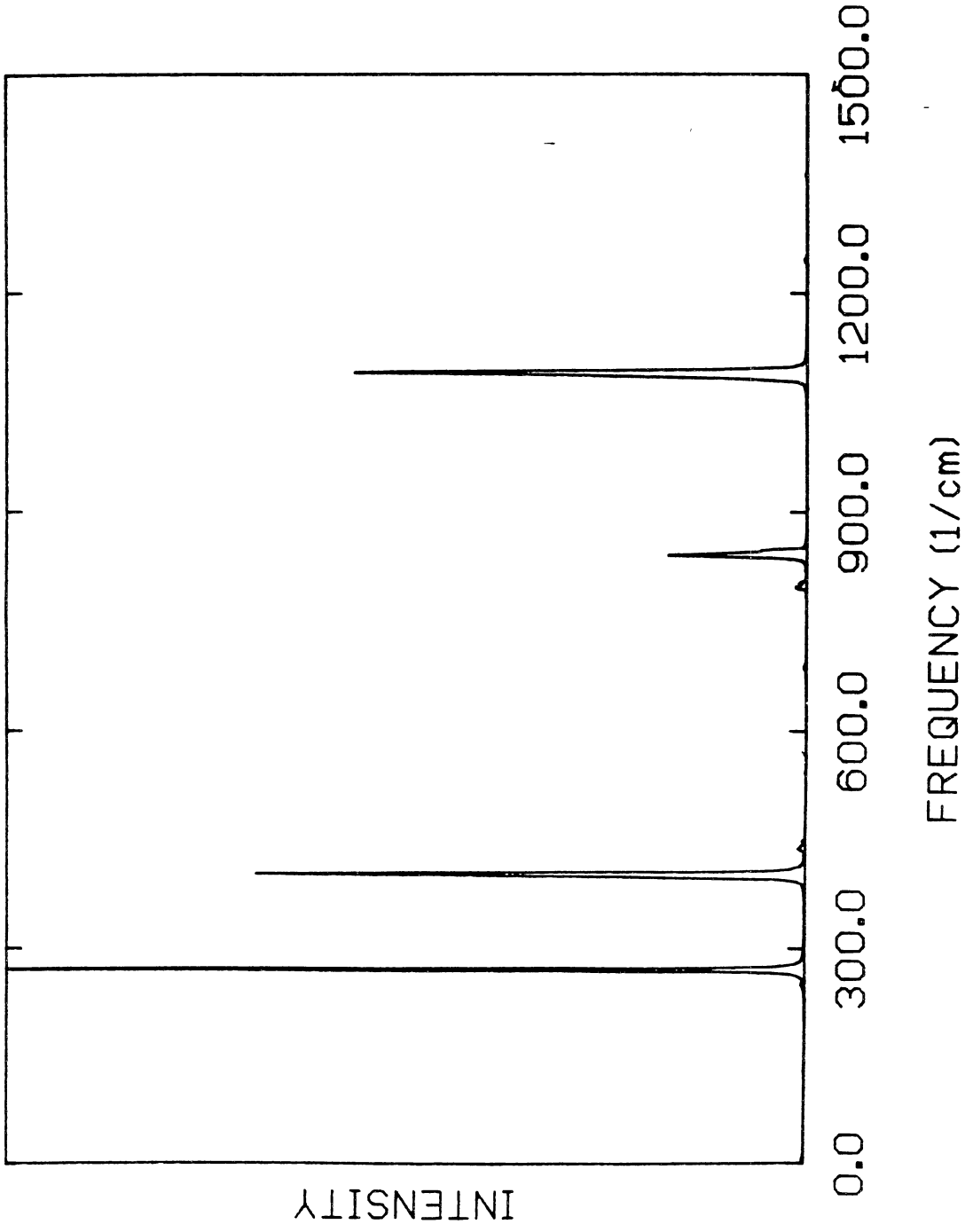
INTENSITY
0.0
300.0
600.0
900.0
1200.0
1500.0
FREQUENCY (1/cm)

Figure 54. Power spectrum for the bonds of nonrotating SiF_4 vibrating with zero-point energy.

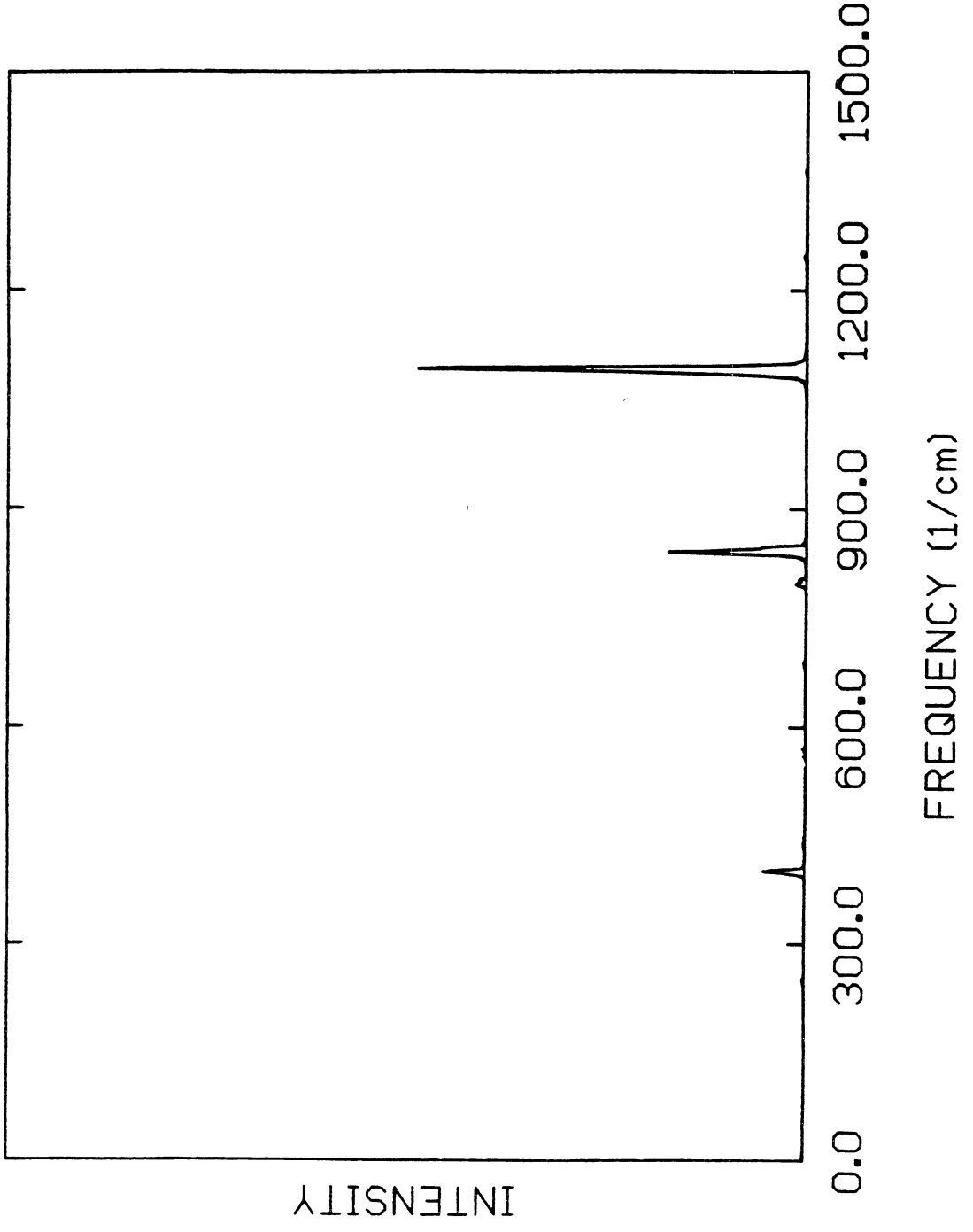
INTENSITY
0.0
300.0
600.0
900.0
1200.0
1500.0
FREQUENCY (1/cm)

Figure 55. Power spectrum for the angles of nonrotating SiF_4 vibrating with zero-point energy.

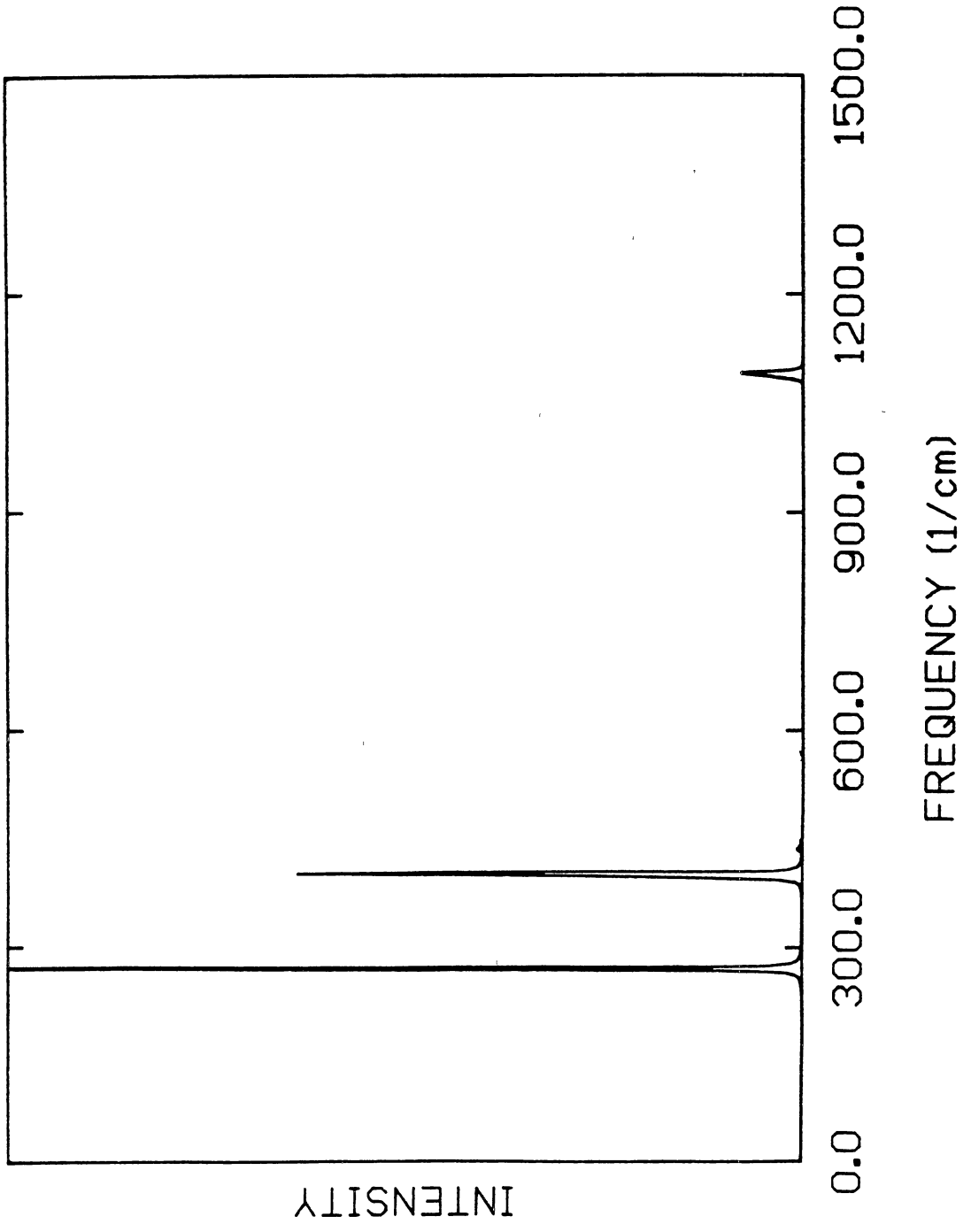
INTENSITY
0.0
300.0
600.0
900.0
1200.0
1500.0
FREQUENCY (1/cm)

Figure 56. Cumulative power spectrum for SiF_4 vibrating and rotating with zero-point energy. The spectrum was obtained as a superposition of the Fourier transforms of ensemble-averaged sample autocorrelation functions of the internal coordinates.

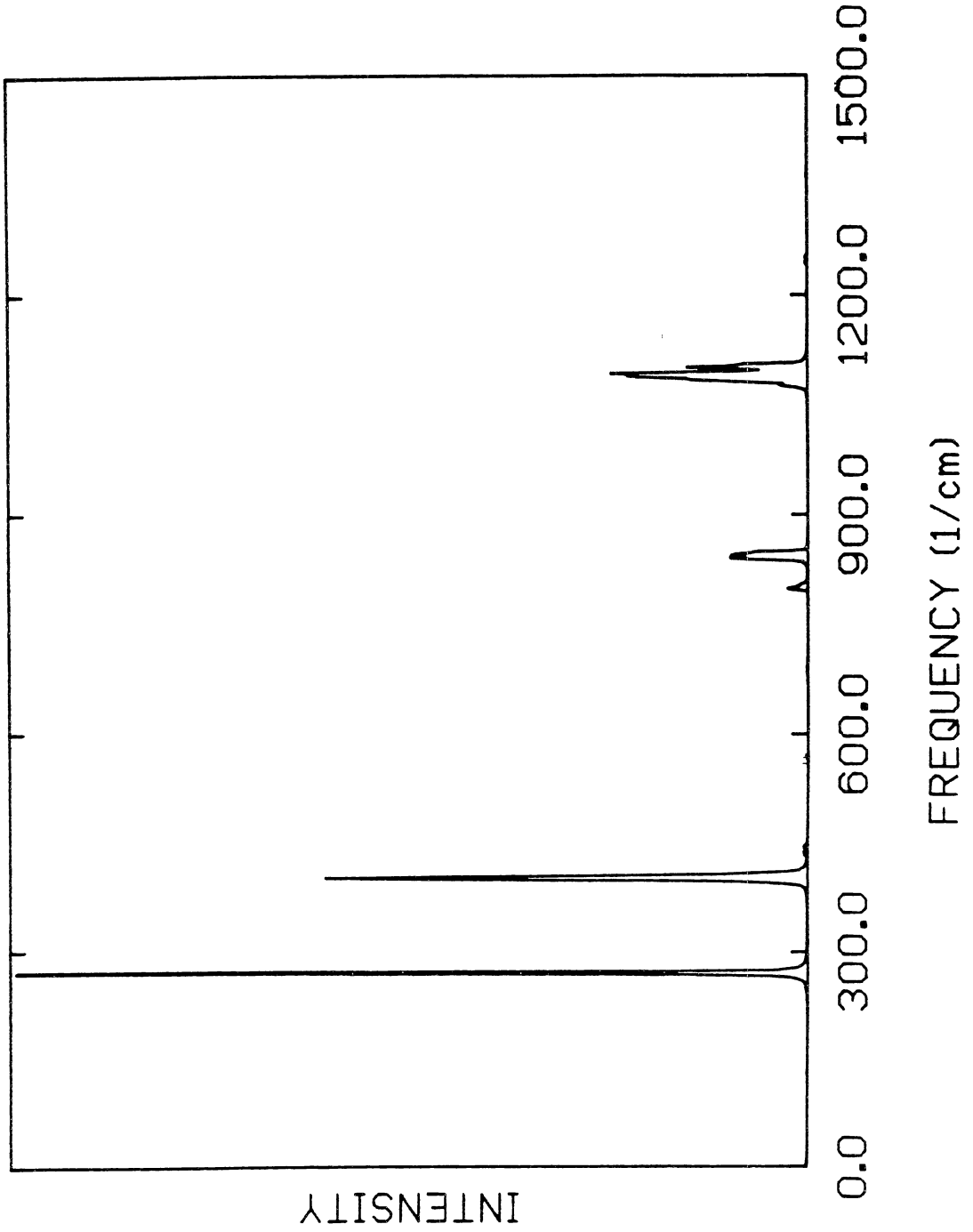
INTENSITY
0.0
300.0
600.0
900.0
1200.0
1500.0
FREQUENCY (1/cm)

Figure 57. Power spectrum for the bonds of SiF_4 vibrating and rotating with zero-point energy.

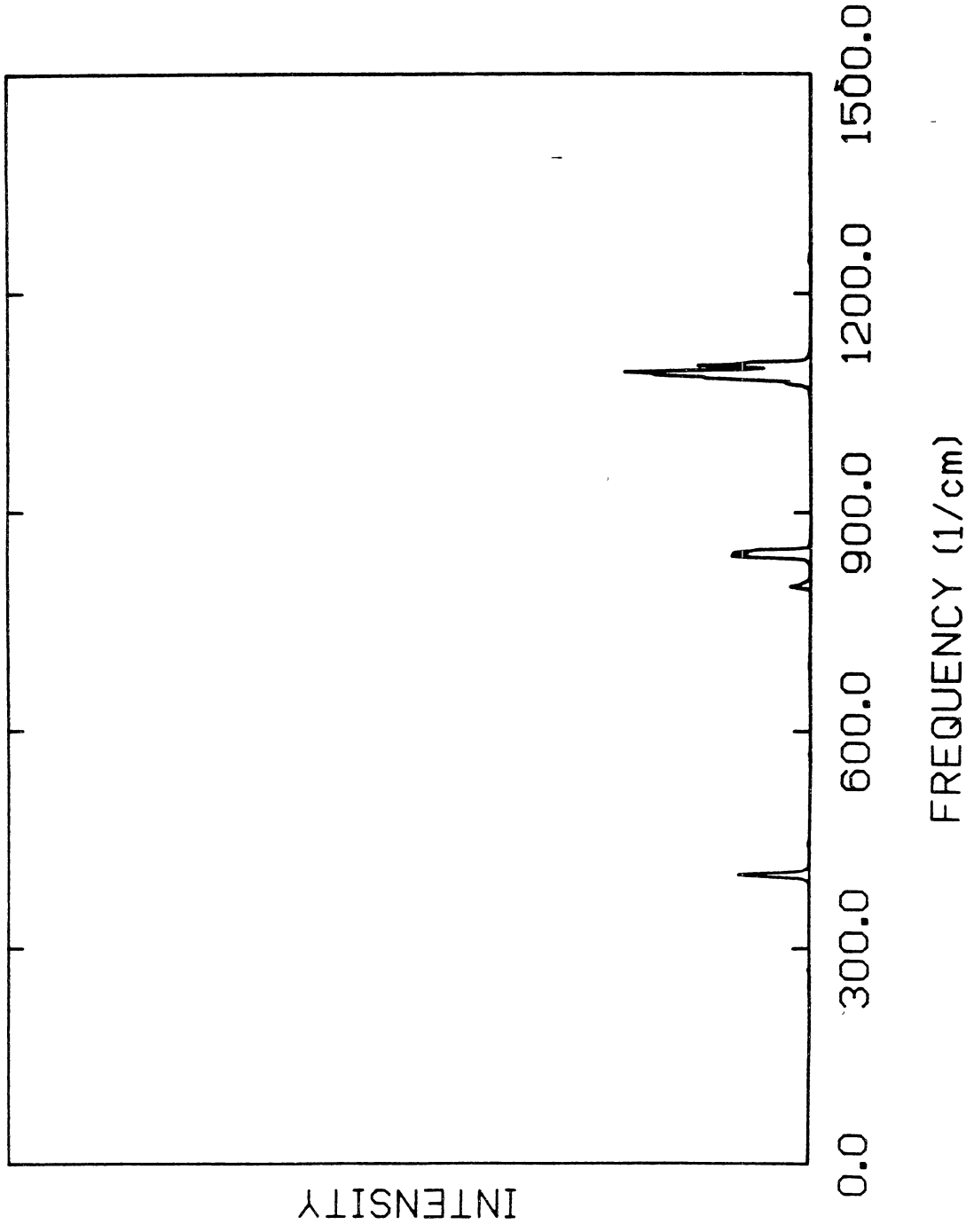
INTENSITY
0.0
300.0
600.0
900.0
1200.0
1500.0
FREQUENCY (1/cm)

Figure 58. Power spectrum for the angles of rotating SiF_4 vibrating and rotating with zero-point energy.

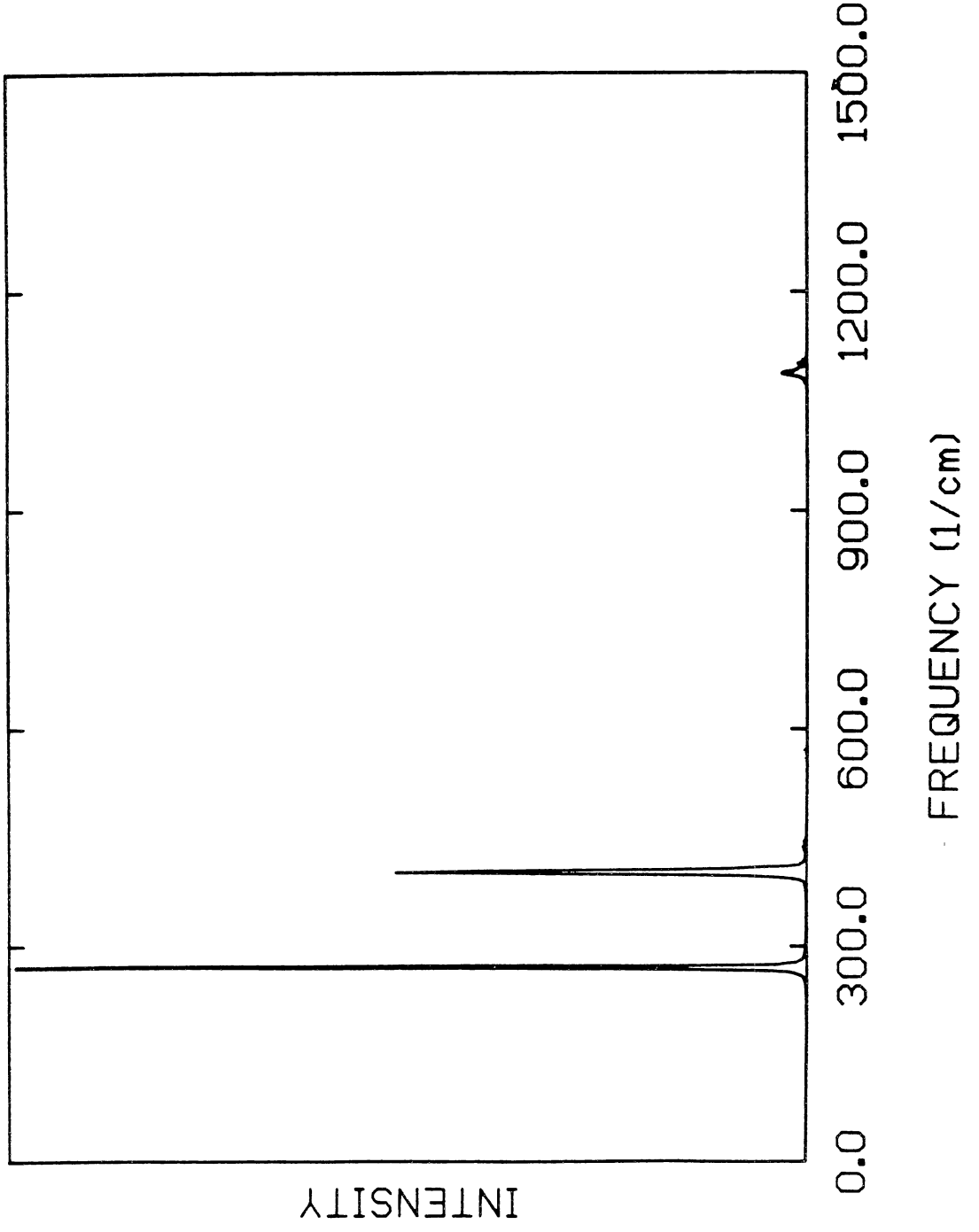
INTENSITY
0.0
300.0
600.0
900.0
1200.0
1500.0
FREQUENCY (1/cm)

Figure 59. Cumulative power spectrum for nonrotating SiF4 vibrating with 42 kcal/mol of energy. The spectrum was obtained as a superposition of the Fourier transforms of ensemble-averaged sample autocorrelation functions of the internal coordinates.

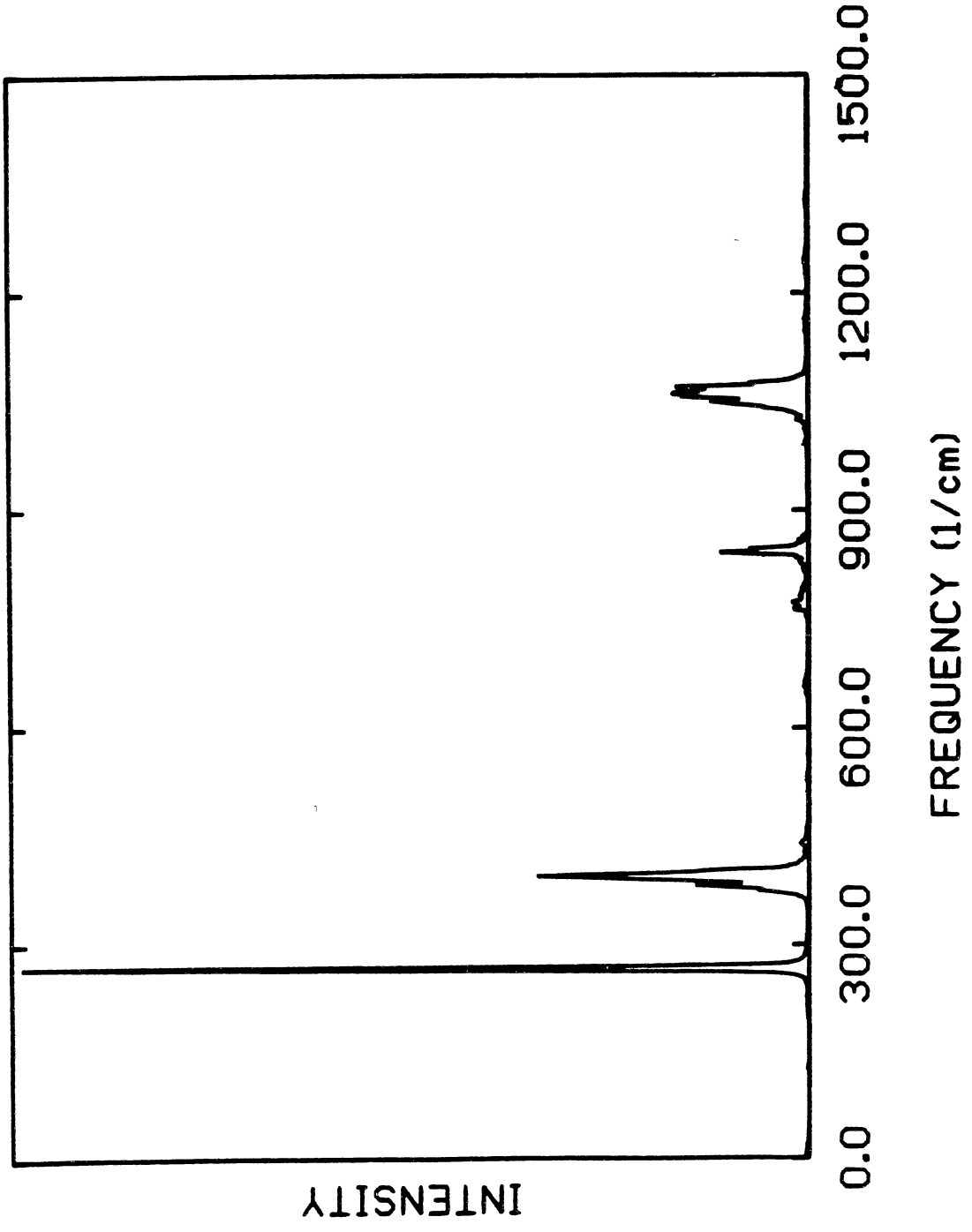
INTENSITY
0.0
300.0
600.0
900.0
1200.0
1500.0
FREQUENCY (1/cm)

Figure 60. Cumulative power spectrum for SiF4 vibrating and rotating with a total energy of 42 kcal/mol. The spectrum was obtained as a superposition of the Fourier transforms of ensemble-averaged sample autocorrelation functions of the internal coordinates.

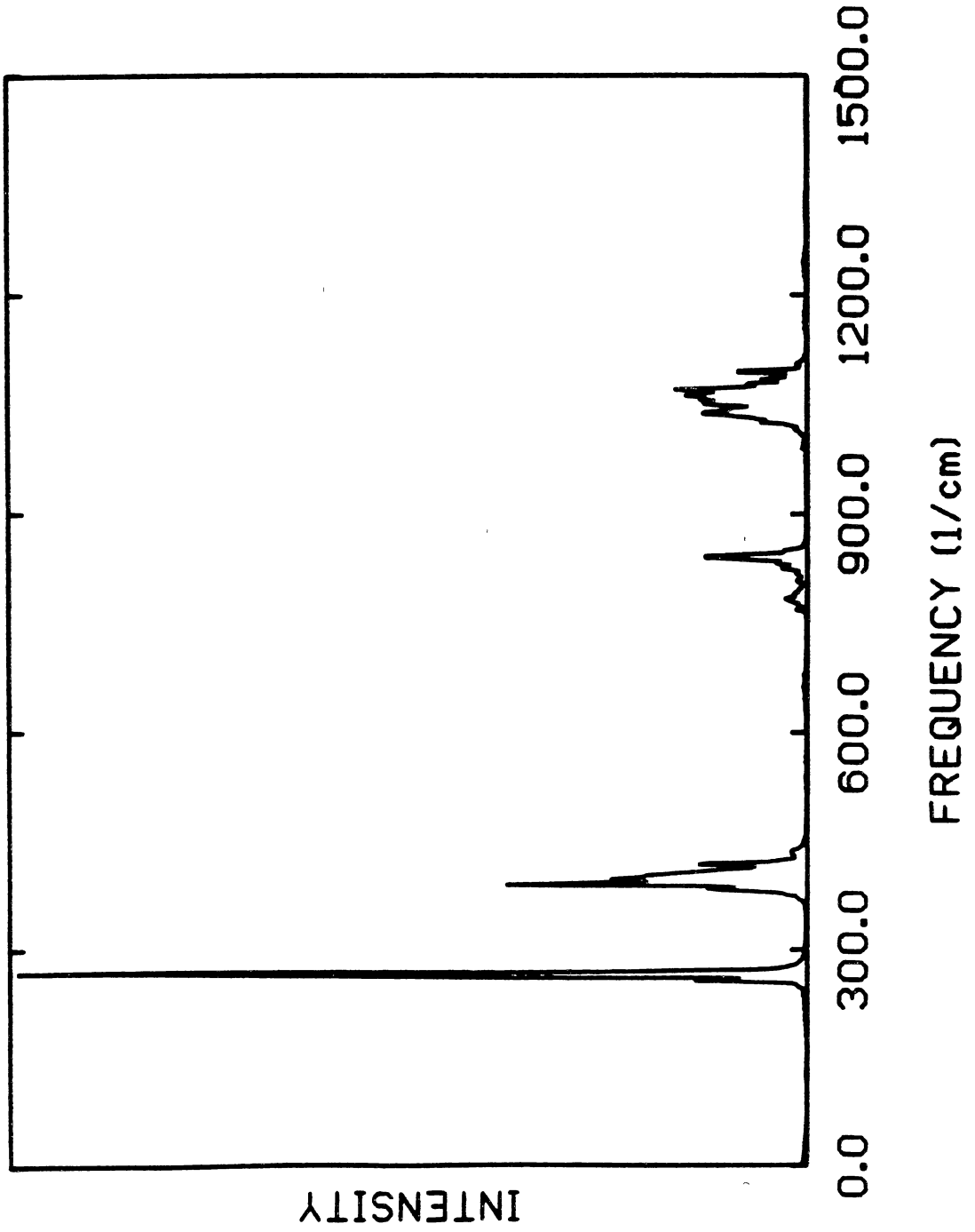
INTENSITY
0.0
300.0
600.0
900.0
1200.0
1500.0
FREQUENCY (1/cm)

Inclusion of angular momentum at the zero-point energy results in noticeable broadening of the two high-frequency modes (Figs. 56 to 58). The modes strongly associated with angle bending appear to be unaffected. Thus, it seems that (for low energies) the interaction between rotation and vibration occurs mainly through the stretches. This conclusion is apparently valid for higher energies as well. Figures 59 and 60 are power spectra for nonrotating and rotating SiF_4, respectively, at a total energy of 42 kcal/mol. Once again the highest-frequency mode is the most affected by rotation. The lowest-frequency (pure bending) mode is perturbed very little by angular momentum. The two central peaks are affected somewhat, but not as significantly as the high-frequency one.

Spectra for SiF_4 vibrating at 143 kcal/mol are shown in Figs. 61 and 62, for zero and nonzero angular momentum, respectively. This energy is approximately equal to the zero-point level plus the dissociation energy of one of the Si-F bonds. Comparison of Fig. 61 with Fig. 62 leads to the conclusion that angular momentum does not play a large role in the dynamics at such high energies. The peak at 403 cm^{-1} is redshifted in nonrotating SiF_4 (relative to the rotating case). Also, the width of the peak at 403 cm-1 is a little broader for rotating SiF_4. However, the other peaks are very similar for both cases. The stretching modes are highly diffuse due to the anharmonicity in the stretching modes. The spectrum for the bonds (not shown) indicate that the stretching modes give rise to most of the low intensity noise seen in Figs. 61 and 62. By contrast, the peaks associated with angle bending are still easily identifiable. In particular, the pure-bending peak has undergone minimal broadening, even though the total energy is nearly eighteen times the zero-point energy. Apparently, the coupling between stretching and bending modes in SiF_4 is weak.

Although the dynamics of SiF_4 are not quasiperiodic at E = 143 kcal/mol, the prominence of the well-defined bending bands in the spectra indicate that the motion has

Figure 61. Cumulative power spectrum for nonrotating SiF_4 vibrating with 143 kcal/mol of 143 energy. The spectrum was obtained as a superposition of the Fourier transforms of ensemble-averaged sample autocorrelation functions of the internal coordinates.

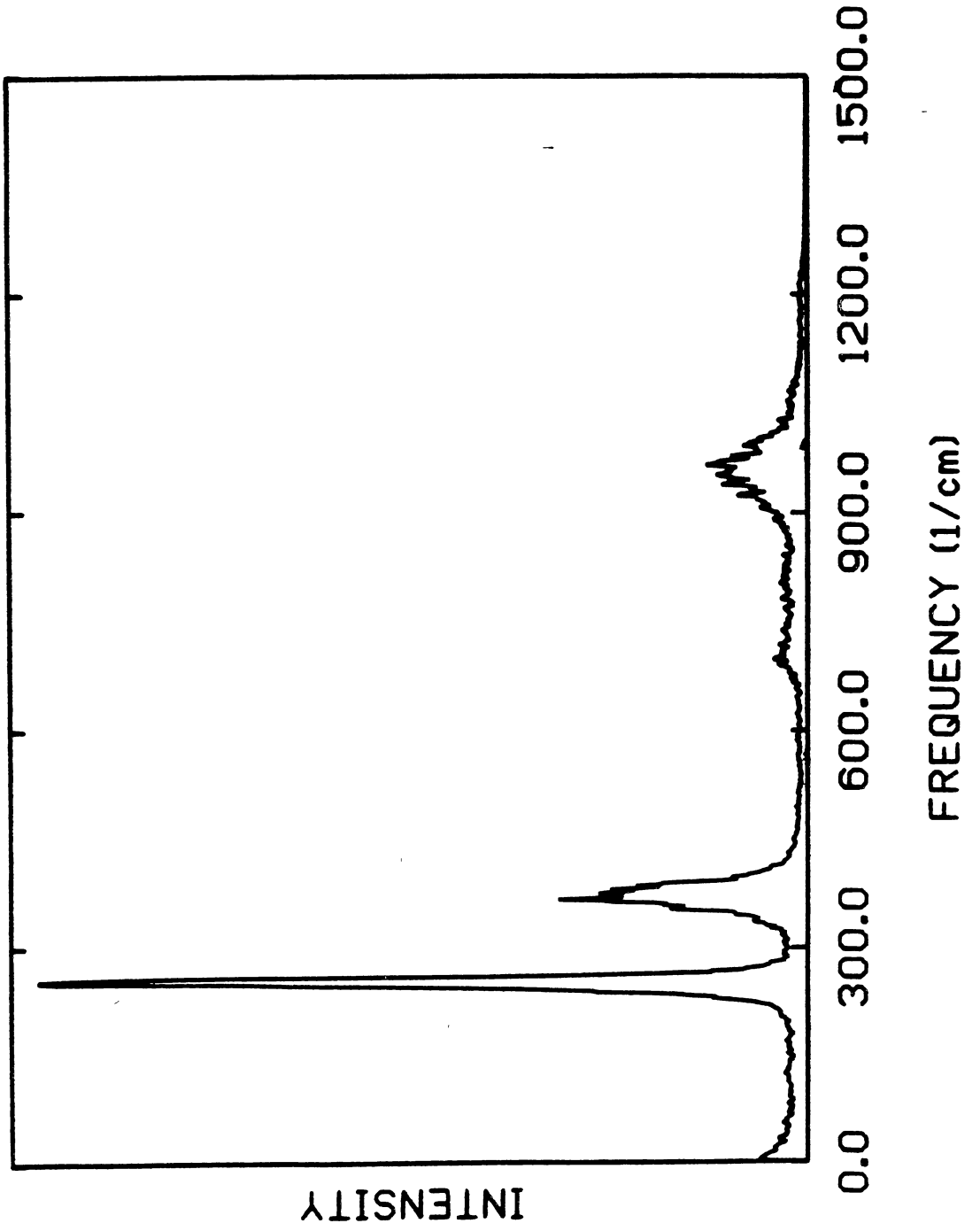
INTENSITY
0.0
300.0
600.0
900.0
1200.0
1500.0
FREQUENCY (1/cm)

Figure 62. Cumulative power spectrum for SiF_4 vibrating and rotating with a total energy of 143 kcal/mol. The spectrum was obtained as a superposition of the Fourier transforms of ensemble-averaged sample autocorrelation functions of the internal coordinates.

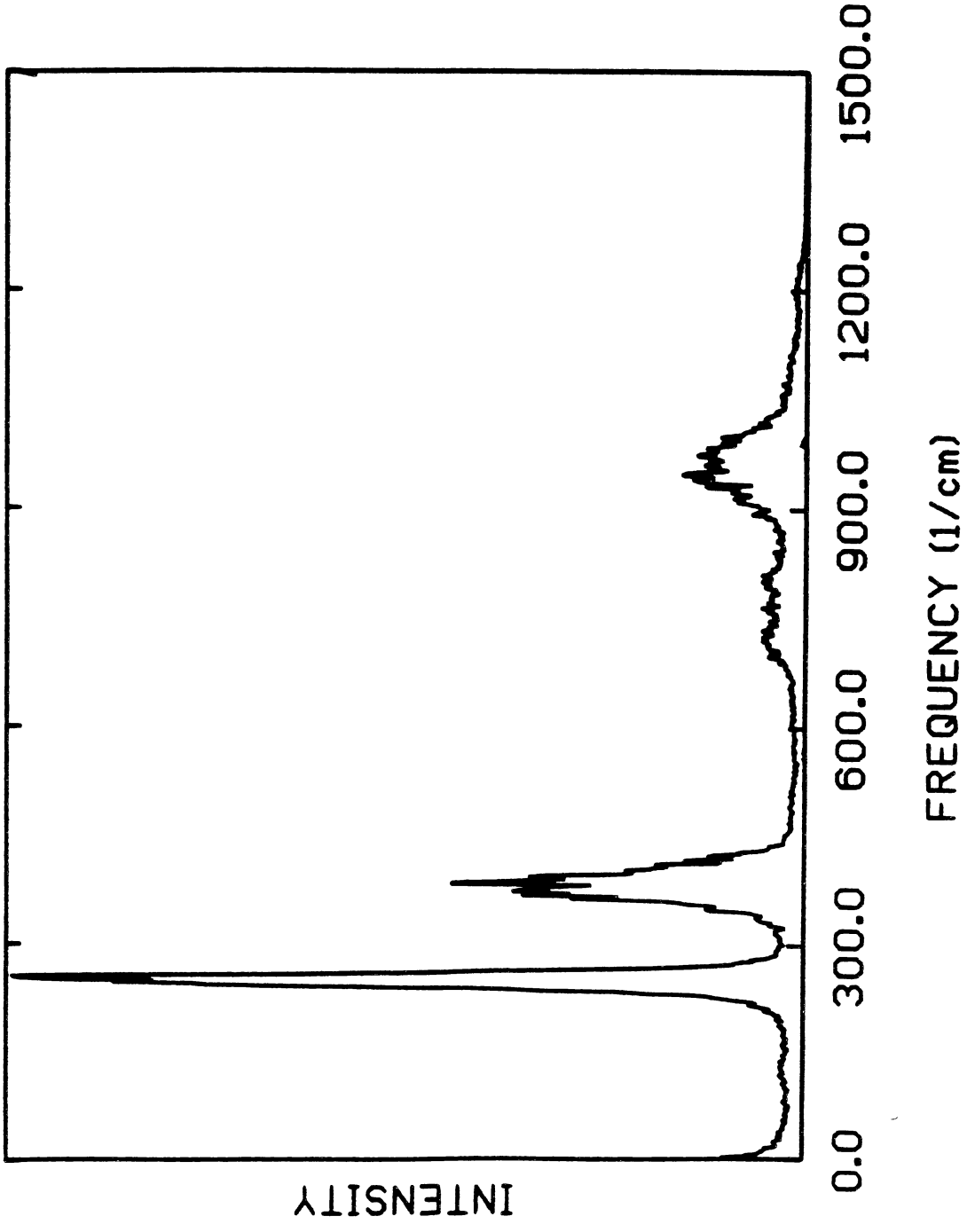
INTENSITY
0.0
300.0
600.0
900.0
1200.0
1500.0
FREQUENCY (1/cm)

Figure 63. Semi-logarithmic plot of the ensemble-averaged sample autocorrelation function for one of the bonds in nonrotating SiF_4. The molecule is vibrating with zero-point energy.

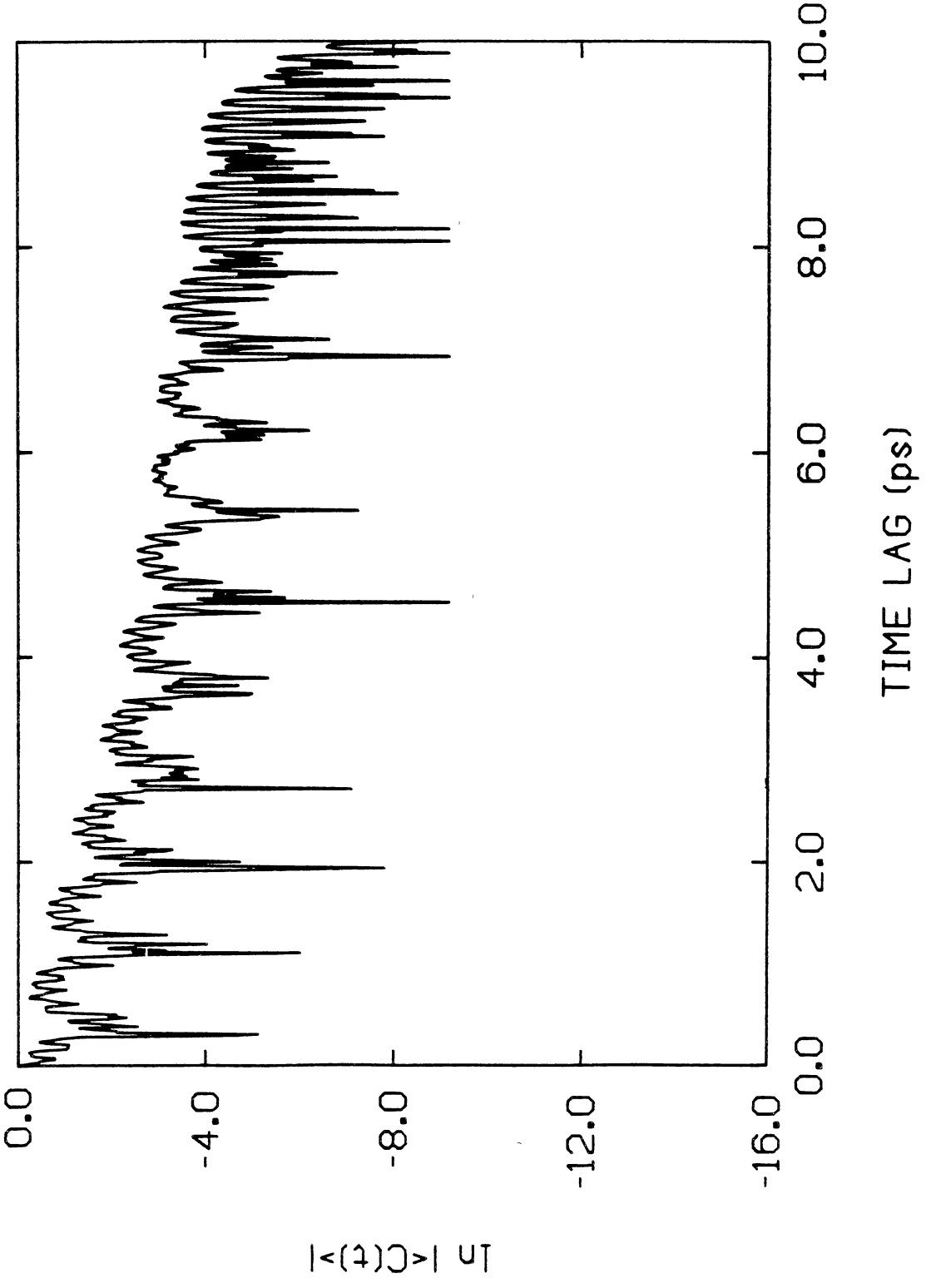
0.0
-4.0
-8.0
-12.0
-16.0
ln |<C(t)>|
0.0
2.0
4.0
6.0
8.0
10.0
TIME LAG (ps)

Figure 64. Semi-logarithmic plot of the ensemble-averaged sample autocorrelation function for one of the bonds in nonrotating SiF_4. The molecule is vibrating with 143 kcal/mol of energy.

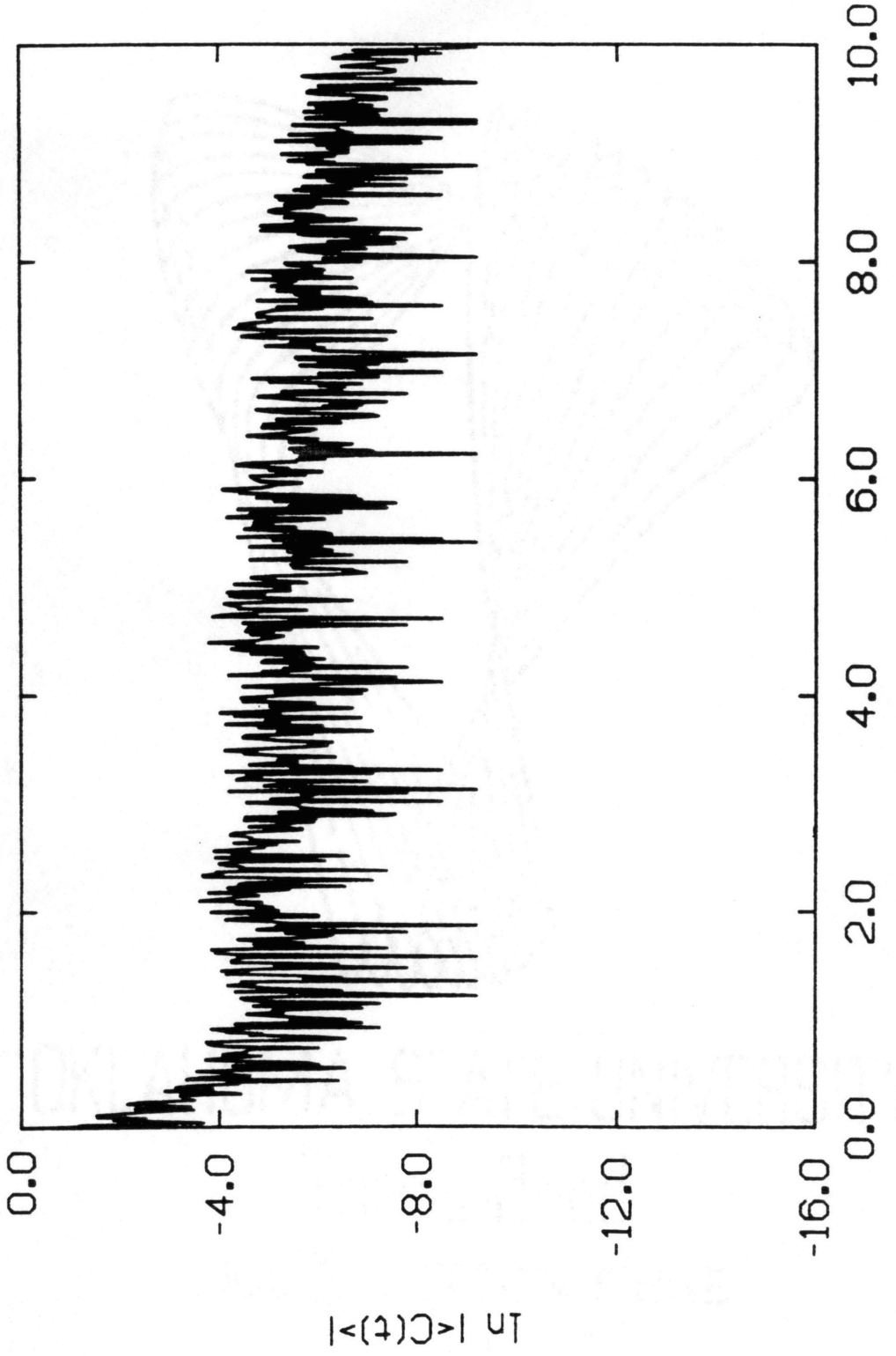
0.0
-4.0
-8.0
-12.0
-16.0
ln |<C(t)>|
0.0
2.0
4.0
6.0
8.0
10.0
TIME LAG (ps)

Figure 65. Semi-logarithmic plot of the ensemble-averaged sample autocorrelation function for one of the angles in nonrotating SiF_4. The molecule is vibrating with zero-point energy.

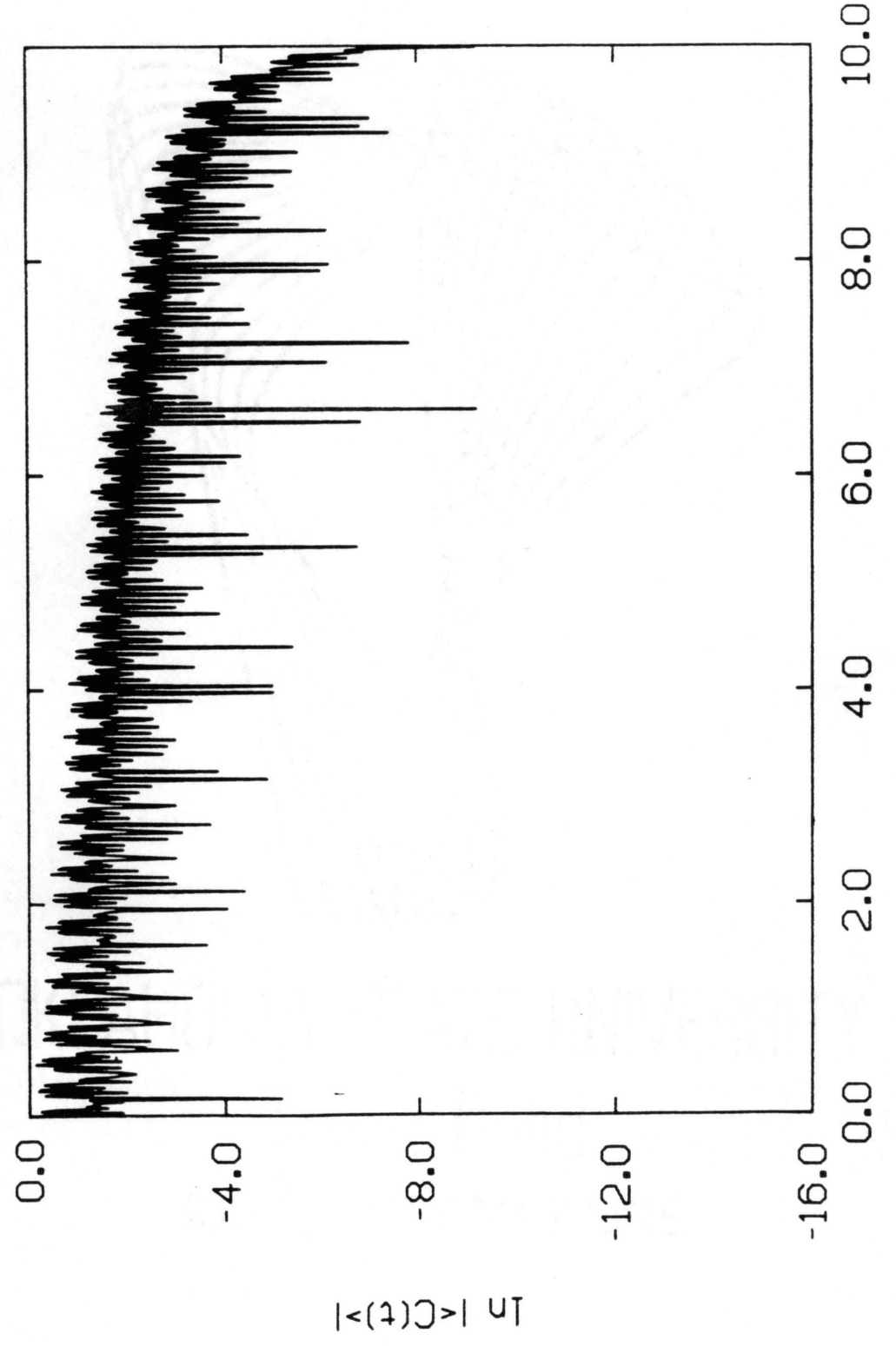
0.0
-4.0
-8.0
-12.0
-16.0
ln |<C(t)>|
0.0
2.0
4.0
6.0
8.0
10.0
TIME LAG (ps)

Figure 66. Semi-logarithmic plot of the ensemble-averaged sample autocorrelation function for one of the angles in nonrotating SiF_4. The molecule is vibrating with 143 kcal/mol of energy.

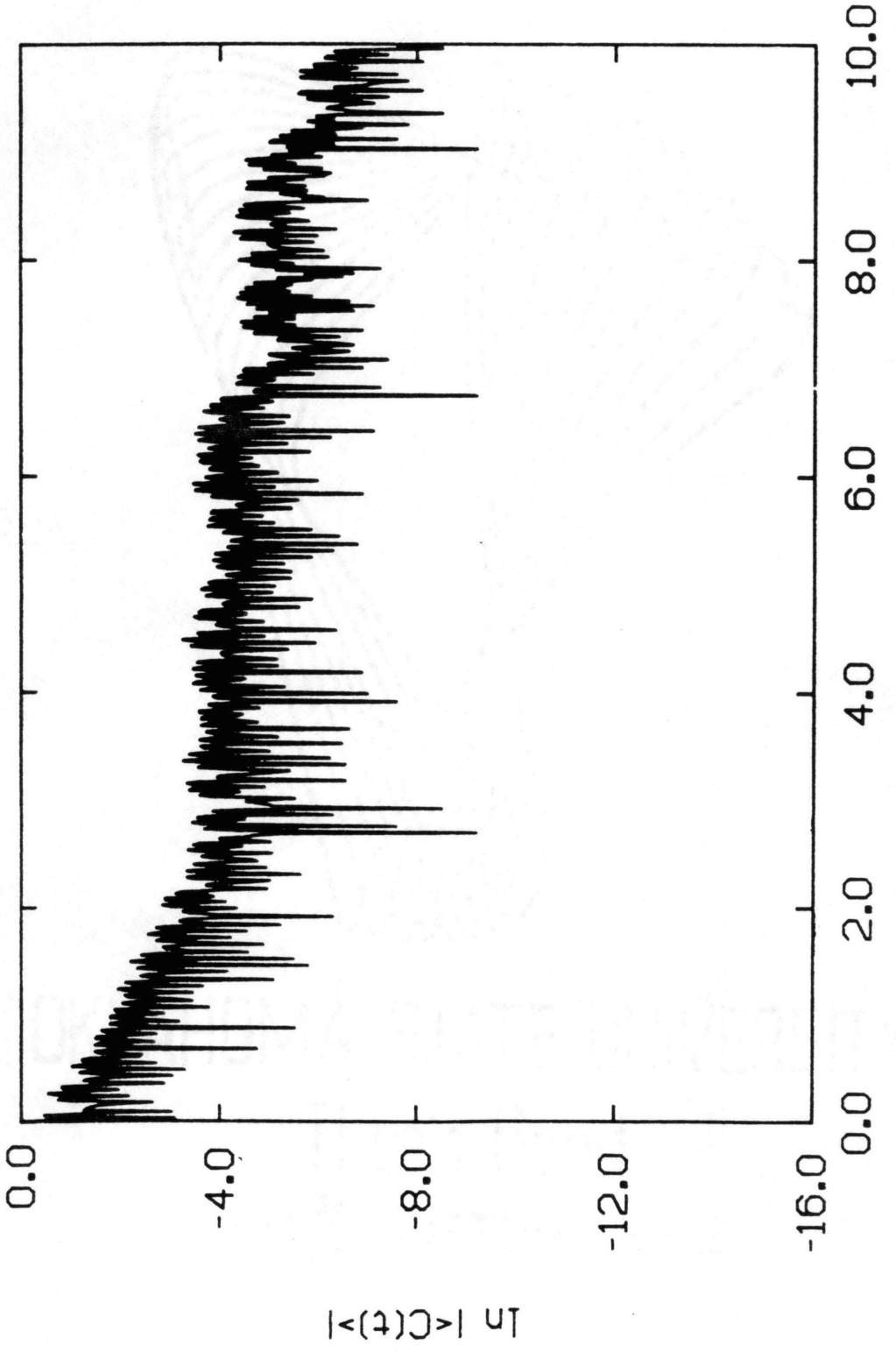
0.0
-4.0
-8.0
-12.0
-16.0
0.0
2.0
4.0
6.0
8.0
10.0
TIME LAG (ps)
ln |<C(t)>|

not become globally chaotic. Another way of viewing this is to look at the decay of the autocorrelation function.[258,408,411] For a periodic function the autocorrelation function will oscillate forever between ±1 with the same frequency as the input.[258] The sample autocorrelation function, Eq. II.39, will oscillate with the frequency of the input but the amplitude of the envelope of the function will *linearly* decrease such that the amplitude for τ=T (see Eq. II.35) will be zero. For a "totally random" input, the autocorrelation function will be a delta function at $\tau = 0$.[258] Figures 63 and 64 show the autocorrelation functions for the bonds for nonrotating SiF_4 at the zero-point energy and 143 kcal/mol, respectively. The results are plotted as ln | <C(τ)> | versus time lag, τ. The zero-point energy autocorrelation function for the bonds varies fairly regularly and the envelope undergoes a slow decay that is uniform in time (Fig. 63). By contrast, the corresponding autocorrelation function for 143 kcal/mol behaves irregularly and, more importantly,[411] the envelope decays sharply for short times (roughly one ps) then flattens out for the remaining time (Fig. 64). The difference is dramatic, particularly when one notes that the natural logarithm of the decay is being plotted!

Plots of the autocorrelation functions for the angles are shown in Figs. 65 and 66 for the same ensembles of trajectories as in Figs. 63 and 64, respectively. The zero-point energy autocorrelation function for the angles (Fig. 65) decays more slowly than that for the bonds (Fig. 63). When the energy is increased to 143 kcal/mol (Fig. 66), the function decays more rapidly than for the zero-point energy case, but still the decay is slow relative to the corresponding plot for the bonds.

The conclusions based on the autocorrelation functions are entirely consistent with those that can be drawn from the power spectra. At low energies, the motion is , loosely speaking, quasiperiodic. At high energy, the bond modes are behaving irregularly while the bending modes are much more regular. This apparent separability between the modes is interesting and would be worthy of further study. SiF_4 is a

particularly simple case since there are four identical bonds and six identical angles. The results for more complex systems are not so readily interpreted, as will be seen.

The fact that the stretching and bending modes are nearly separable even for high energies raises the question of how specific are the IVR pathways in SiF_4; and if they are, what signature (if any) is left in the power spectrum? We briefly investigated this question. Ensembles of twenty five trajectories were computed for the two following excitations : zero-point energy in all modes except i) mode 15 excited to v=6; and ii) mode 7 excited to v=24. The total energy is 27 kcal/mol (to within 0.27 kcal/mol) in both cases. Cases i) and ii) correspond to selective excitation of nearly pure stretching and bending modes, respectively. Averaged normal-mode energies and power spectra were computed for both sets of initial conditions. The results for the IVR are shown in Figs. 67 and 68. The results in Fig. 67 indicate that, when the high-frequency stretching mode is initially excited, there is a rapid loss of energy from that mode, however, there is substantial "beating" between this mode and the other degenerate modes of the same symmetry. Eventually, the mode at 842.4 cm^{-1} (a stretching mode) begins to increase significantly in energy. Note, however, that the low-frequency bending modes gain very little energy within the ten ps for which the mode energies are presented. (The normal-mode approximation begins to break down after a while, however, and as a result, the calculated normal-mode energies for some of the modes become aphysically large.) By contrast, when the bending mode ν_7 is initially excited, the IVR is slower and follows a completely different pathway (Fig. 68). The only modes that exchange appreciable amounts of energy with mode ν_7 are the other low-frequency bending modes. The energy transfer is more gradual, however, and there is much less energy beating. The stretching modes are not active in the relaxation of mode ν_7 and are therefore essentially unaffected by the process.

Figure 67. Plot of the ensemble-averaged normal-mode energies in nonrotating SiF_4. The initial conditions correspond to zero-point energy in all normal modes except ν_{15}, which is in the v=6 state. The excited mode corresponds to a nearly pure stretching motion. The total energy is 27 kcal/mol.

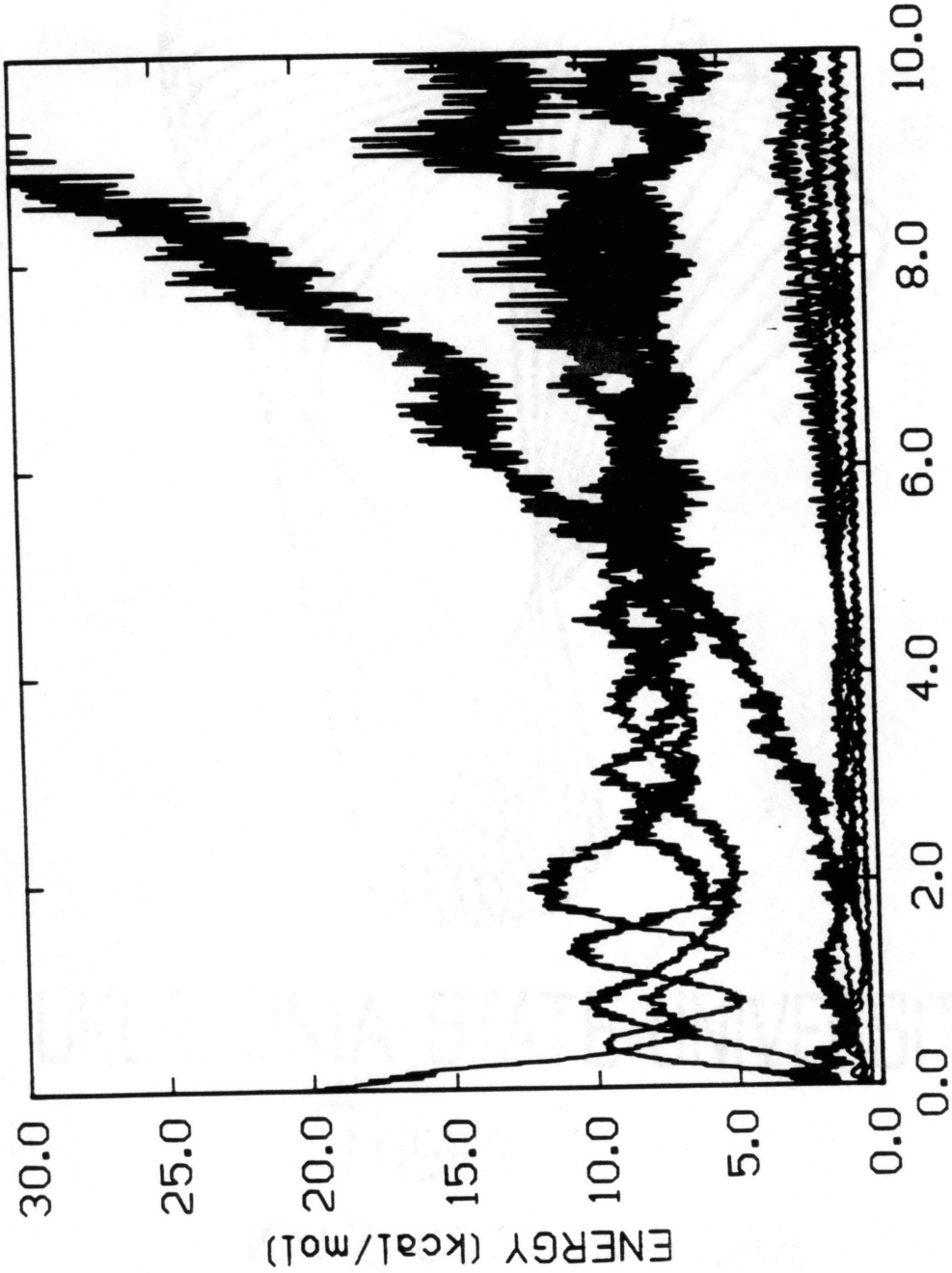
30.0
25.0
20.0
15.0
10.0
5.0
0.0
ENERGY (kcal/mol)
0.0
2.0
4.0
6.0
8.0
10.0
TIME (ps)

Figure 68. Plot of the ensemble-averaged normal-mode energies in nonrotating SiF_4. The initial conditions correspond to zero-point energy in all normal modes except ν_7, which is in the v=24 state. The excited mode corresponds to a nearly pure bending motion. The total energy is 27 kcal/mol.

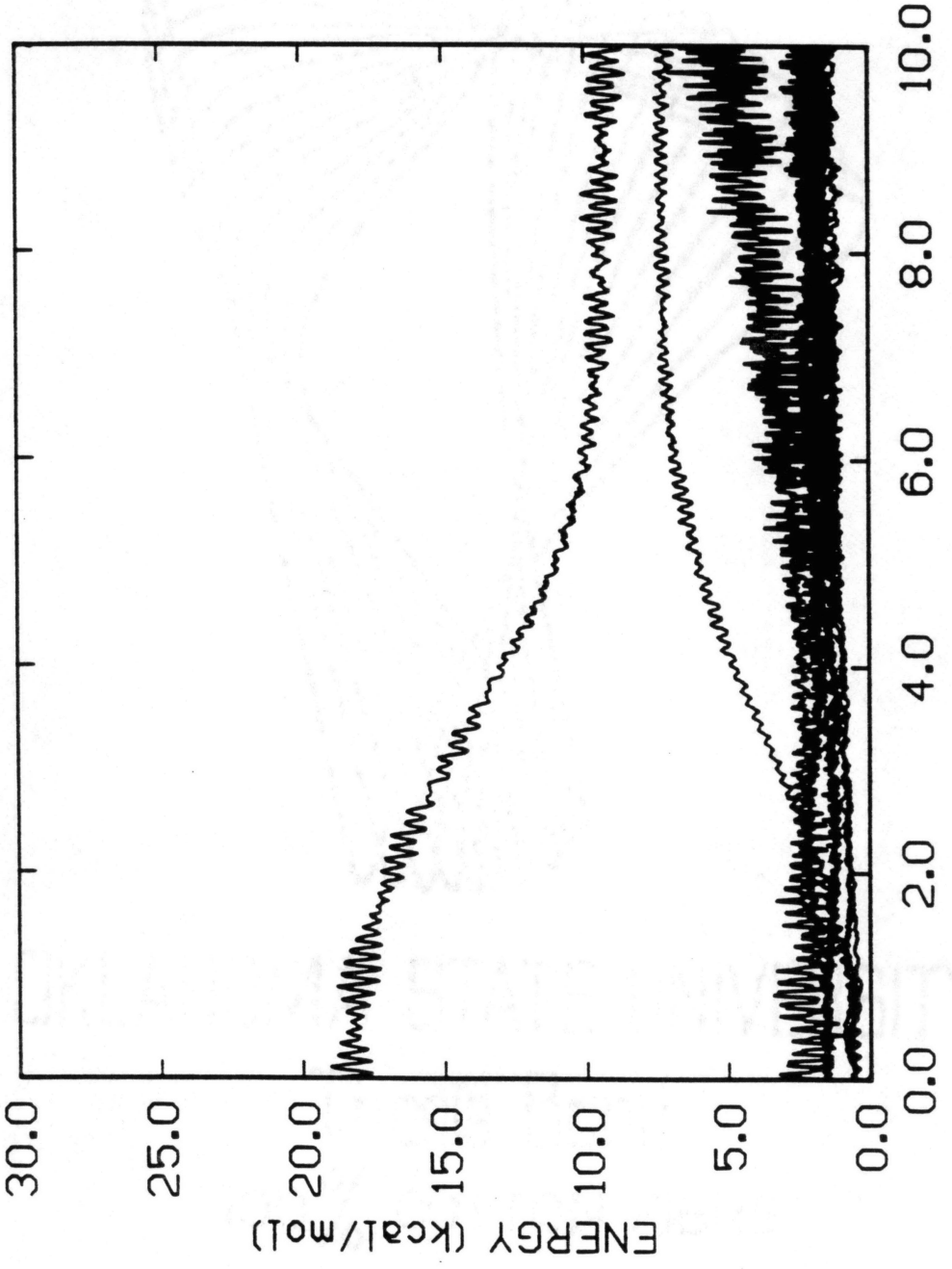
30.0
25.0
20.0
15.0
10.0
5.0
0.0
ENERGY (kcal/mol)
0.0
2.0
4.0
6.0
8.0
10.0
TIME (ps)

Figure 69. Cumulative power spectrum for SiF_4 for the same conditions as in Fig. 67.

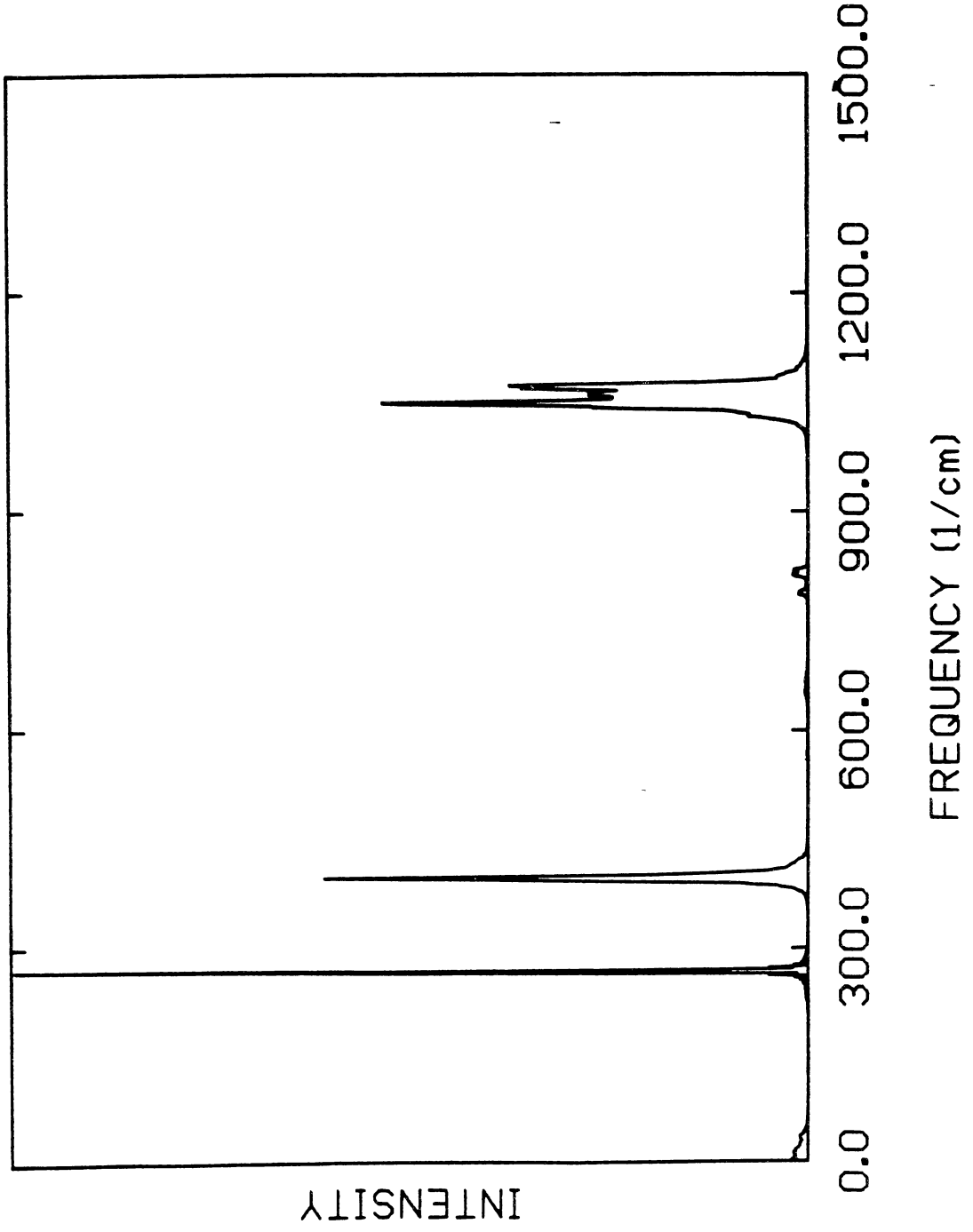
INTENSITY
0.0
300.0
600.0
900.0
1200.0
1500.0
FREQUENCY (1/cm)

Figure 70. Cumulative power spectrum for SiF_4 for the same conditions as in Fig. 68.

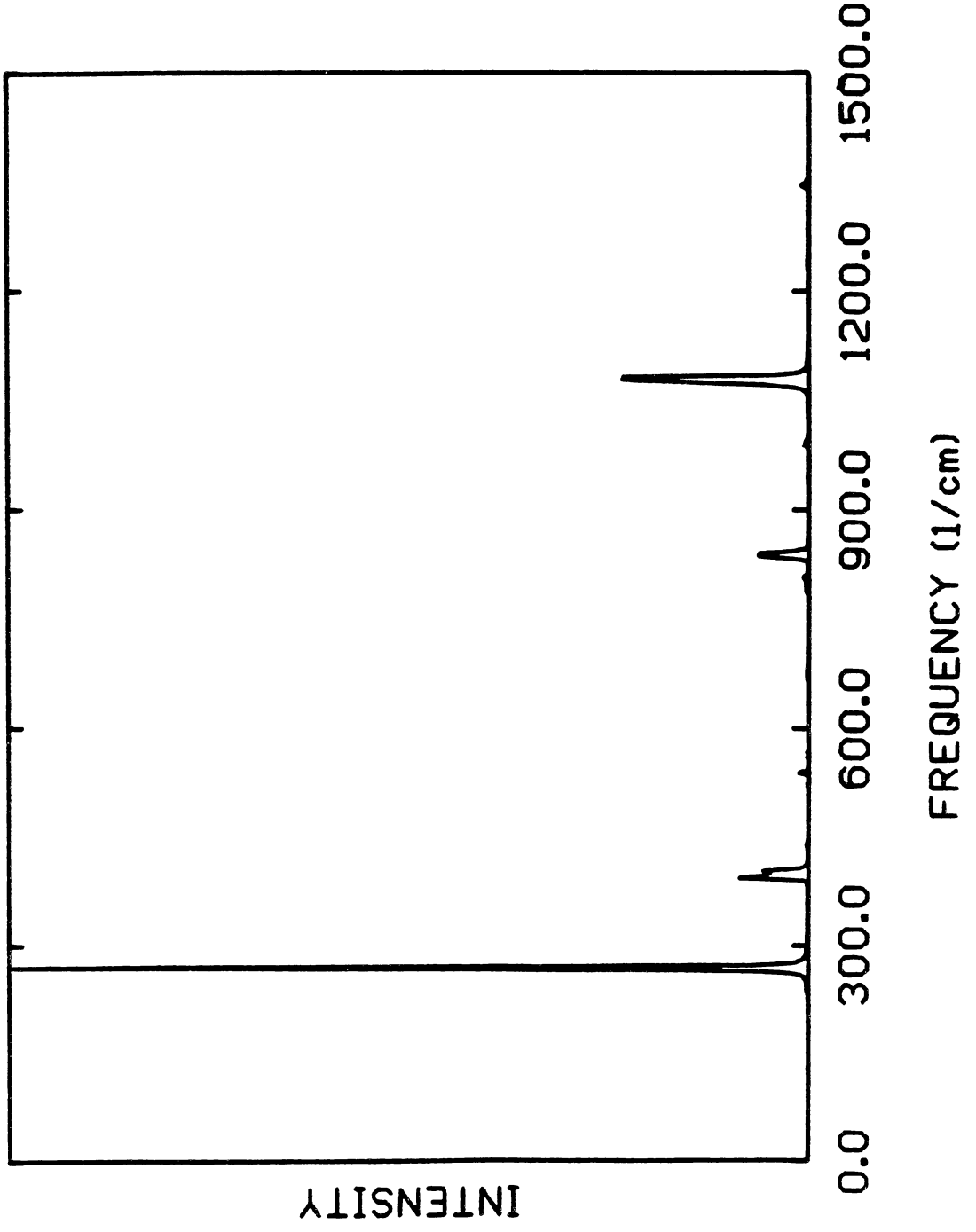
INTENSITY
0.0
300.0
600.0
900.0
1200.0
1500.0
FREQUENCY (1/cm)

The fact that the IVR pathways are different is also evident from the power spectra shown in Figs. 69 and 70, respectively. Initial excitation of the stretching mode results in substantial broadening and splitting of the peak associated with the modes vibrating at 1100 cm^{-1} (Fig. 69). The other peaks remain narrow. Also, there is a low-frequency "clump" of intensity that implies near-transient behavior. By contrast, the spectrum resulting from excitation of the angle-bending mode consists of narrow peaks at all of the fundamental frequencies (Fig. 70). That one of the modes is highly excited is not evident from the spectrum, except possibly through the relative intensities of the peaks.

SiF_4 represents an extreme case in that the spectrum is sparse and the various modes of the system are both highly degenerate and far from resonance with other modes. It is therefore perhaps not too surprising that the modes behave so independently of one another. The SiF_4 molecule might provide a useful basis for a study of the effects of varying the stretch-stretch, bend-bend, and stretch-bend coupling on the IVR. It would be of interest to test the limits of the (apparently) quite stable separation between the stretching and bending modes. Further studies should also attempt to answer the question of whether the bending modes are, in fact, actually quasiperiodic while the stretching modes seem to vibrate chaotically.

$\underline{C_2H_4}$

Power spectra for C_2H_4 were obtained for ensembles of trajectories initialized using random microcanonical sampling with zero angular momentum. Three energies were considered: 31 kcal/mol, 77 kcal/mol, and 155 kcal/mol. The lowest energy is the zero-point level; the upper energy is just greater than the C=C bond dissociation energy (149 kcal/mol) and is substantially greater than the C-H bond dissociation energy (116 kcal/mol). (These dissociation energies are probably not quantitative but should be

accurate to within a few kcal/mol.) The cumulative zero-point energy spectrum is shown in Fig.71. At this energy most of the peaks are fairly sharp. There is a noticeable redshift of many of the peaks in the zero-point energy spectrum relative to the reference spectrum in Fig. 49. This is not surprising given the large zero-point energy of the molecule. The broad C-H stretching band is well separated from the remained of the modes. Close inspection of the spectra for the C=C bond and C-C-H angles (not shown) indicate a barely perceptible contribution to this band. The other modes of the system appear to be more closely coupled to one another. None of the individual coordinates in C_2H_4 contribute appreciable intensity to only one frequency. Nor do any of the peaks in the cumulative spectrum derive all of their intensity from a single internal-coordinate vibration. Thus, the normal modes are made up of complicated combinations of the internal coordinates. There are no good "local modes" other than the C-H bonds, although, at this energy the spectra for the out -of-plane coordinates (the two lowest-frequency bands) do not overlap appreciably with those for the in-plane coordinates. Of the low-frequency, in-plane modes, the power spectrum for the C=C bond-stretching coordinate is the most localized. This behavior is observed at the zero-point energy and persists up to 155 kcal/mol.

The cumulative spectrum obtained from an ensemble of trajectories computed at 77 kcal/mol is shown in Fig. 72. The increased energy has resulted in further shifting and broadening of several peaks. The most noticeable shifts occur in the peaks strongly associated with bond-stretching or torsional vibrations. This is not surprising since these modes are represented by anharmonic potential-energy functions whereas the angle-bending coordinates are represented by harmonic oscillators. The spectrum resulting from C=C bond stretching appears to be the least affected of the anharmonic coordinates. This is probably due to the relative stiffness of the C=C bond. A much more dramatic change occurs when the total energy is increased to 155 kcal/mol. The

Figure 71. Cumulative power spectrum for nonrotating C_2H_4 vibrating with zero-point energy. The spectrum was obtained as a superposition of the Fourier transforms of ensemble-averaged sample autocorrelation functions of the internal coordinates.

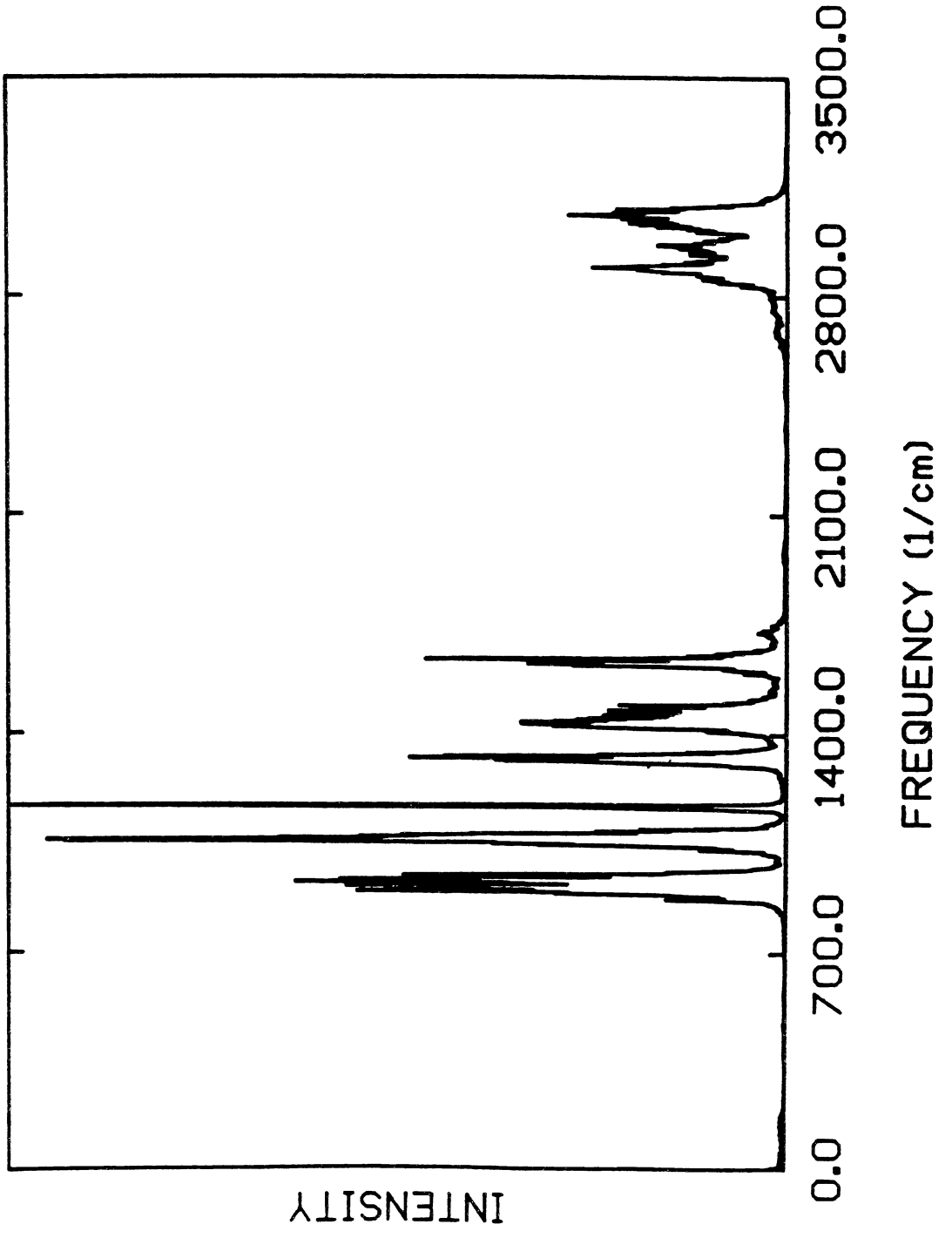
INTENSITY
0.0
700.0
1400.0
2100.0
2800.0
3500.0
FREQUENCY (1/cm)

Figure 72. Cumulative power spectrum for nonrotating C_2H_4 vibrating with 77 kcal/mol of energy. The spectrum was obtained as a superposition of the Fourier transforms of ensemble-averaged sample autocorrelation functions of the internal coordinates.

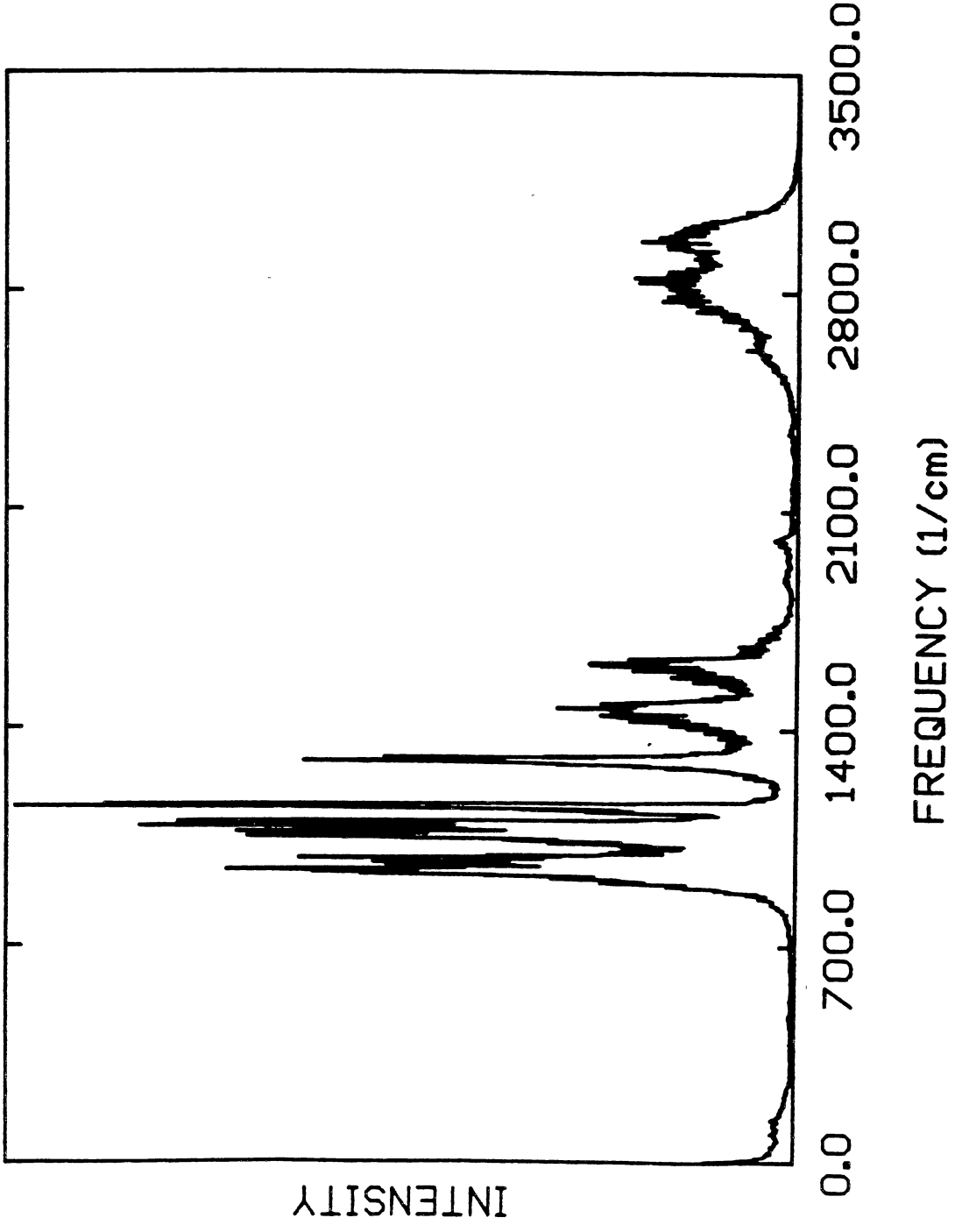
INTENSITY
0.0
700.0
1400.0
2100.0
2800.0
3500.0
FREQUENCY (1/cm)

Figure 73. Cumulative power spectrum for nonrotating C_2H_4 vibrating with 155 kcal/mol of energy. The spectrum was obtained as a superposition of the Fourier transforms of ensemble-averaged sample autocorrelation functions of the internal coordinates.

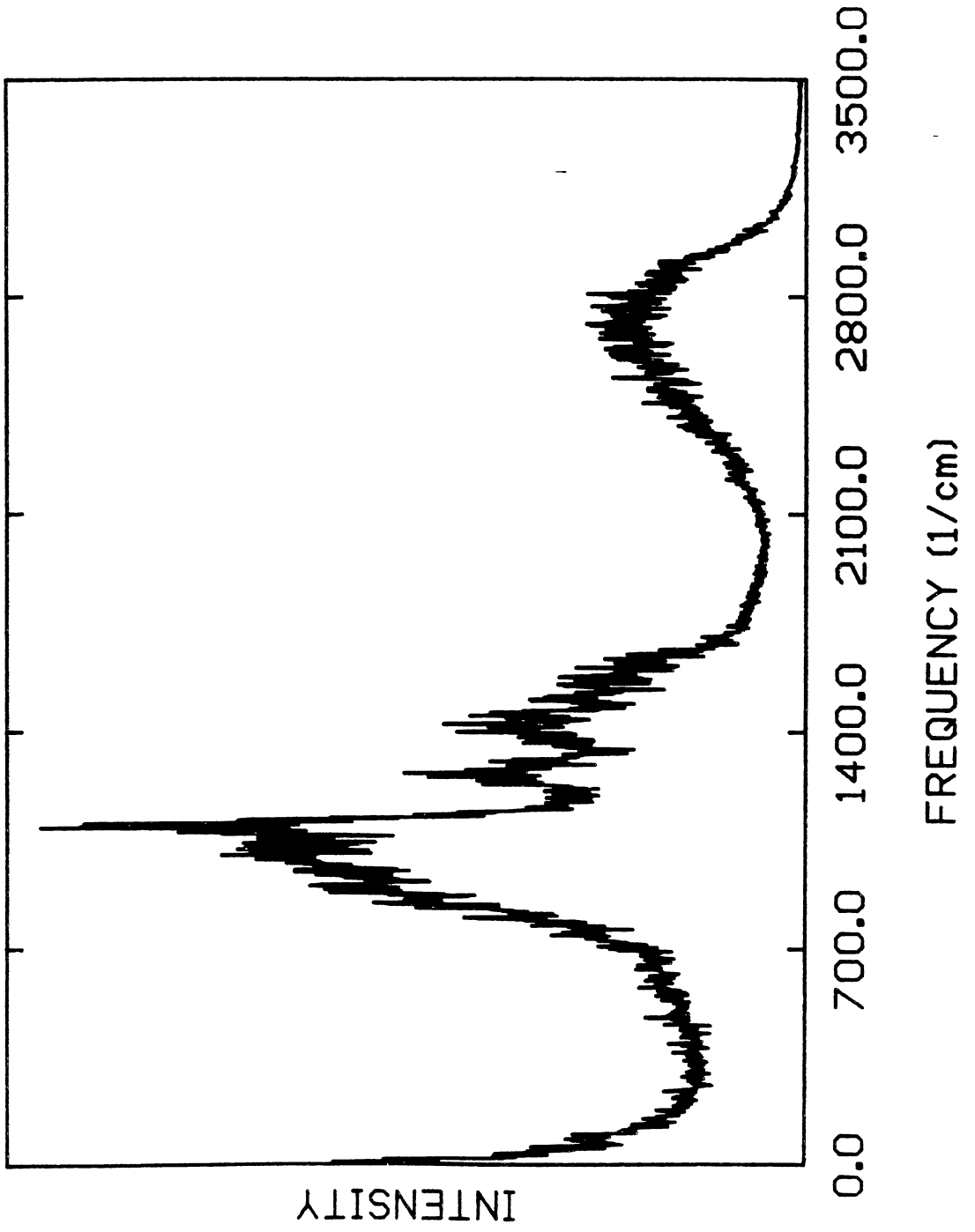
INTENSITY
0.0
700.0
1400.0
2100.0
2800.0
3500.0
FREQUENCY (1/cm)

Figure 74. Power spectrum for the one of the C-C-H angles in nonrotating C_2H_4 vibrating with zero-point energy.

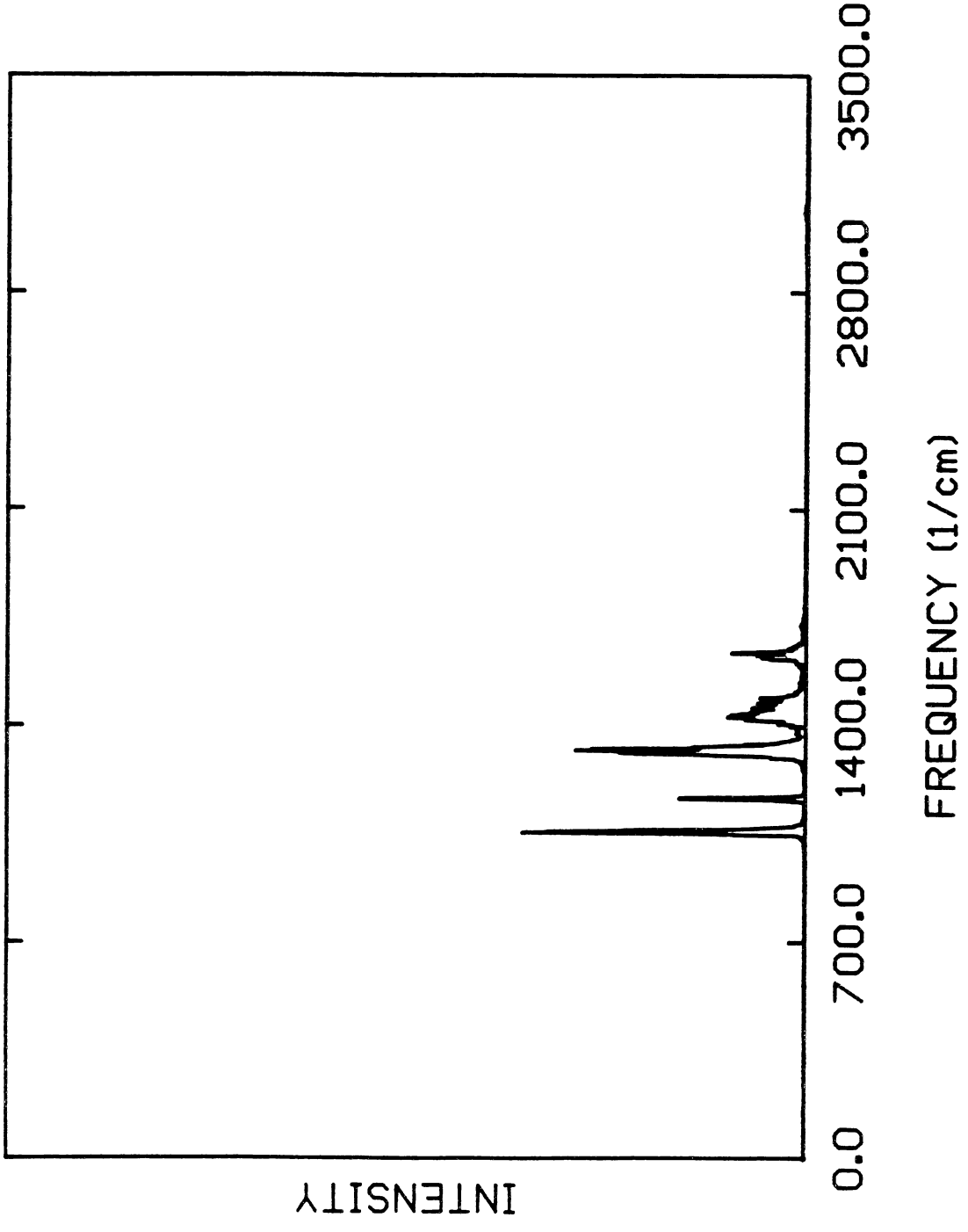
INTENSITY
0.0
700.0
1400.0
2100.0
2800.0
3500.0
FREQUENCY (1/cm)

Figure 75. Power spectrum for the one of the C-C-H angles in nonrotating C_2H_4 vibrating with 155 kcal/mol of energy.

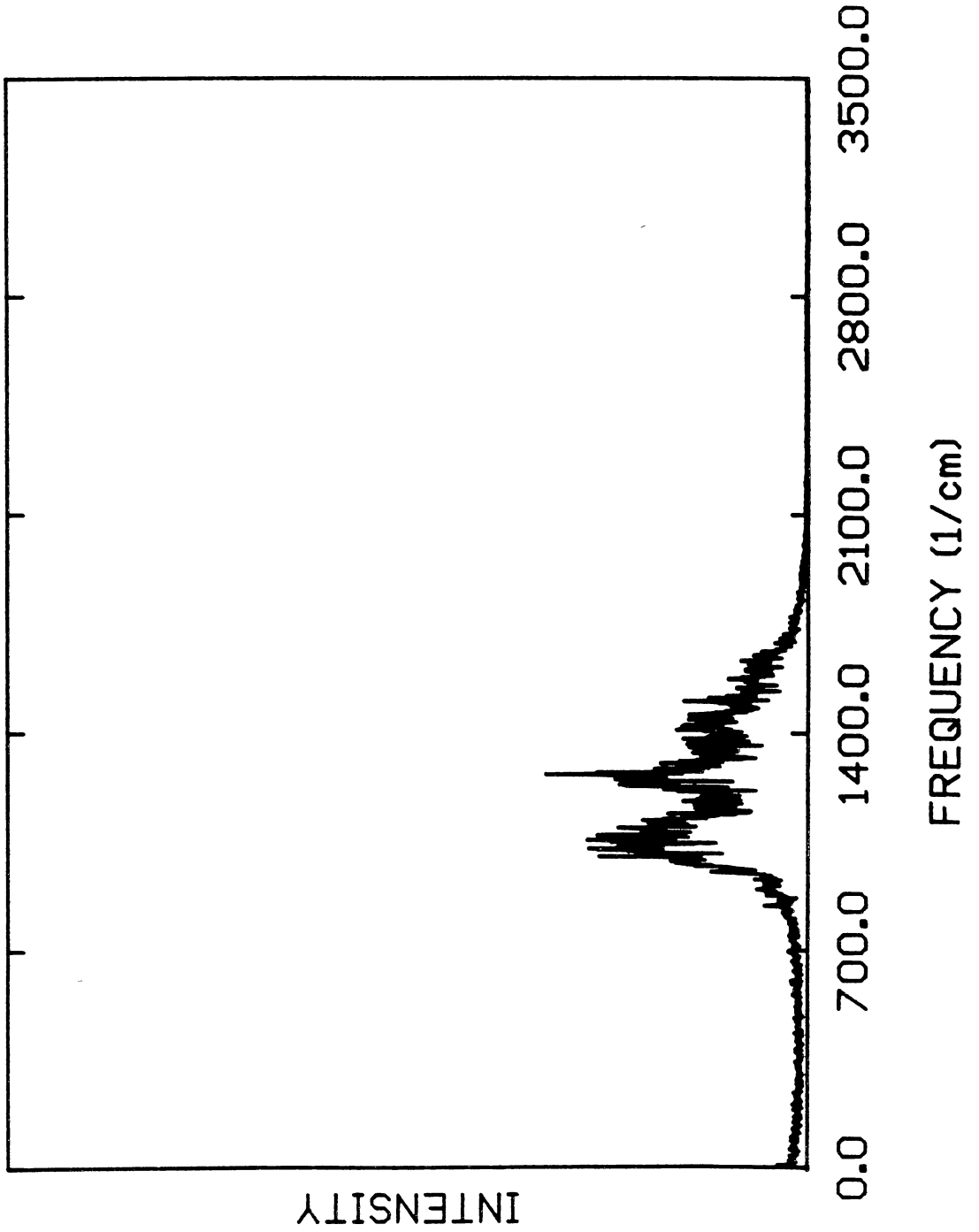
INTENSITY
0.0
700.0
1400.0
2100.0
2800.0
3500.0
FREQUENCY (1/cm)

Figure 76. Power spectrum for the one of the wag angles in nonrotating C_2H_4 vibrating with zero-point energy.

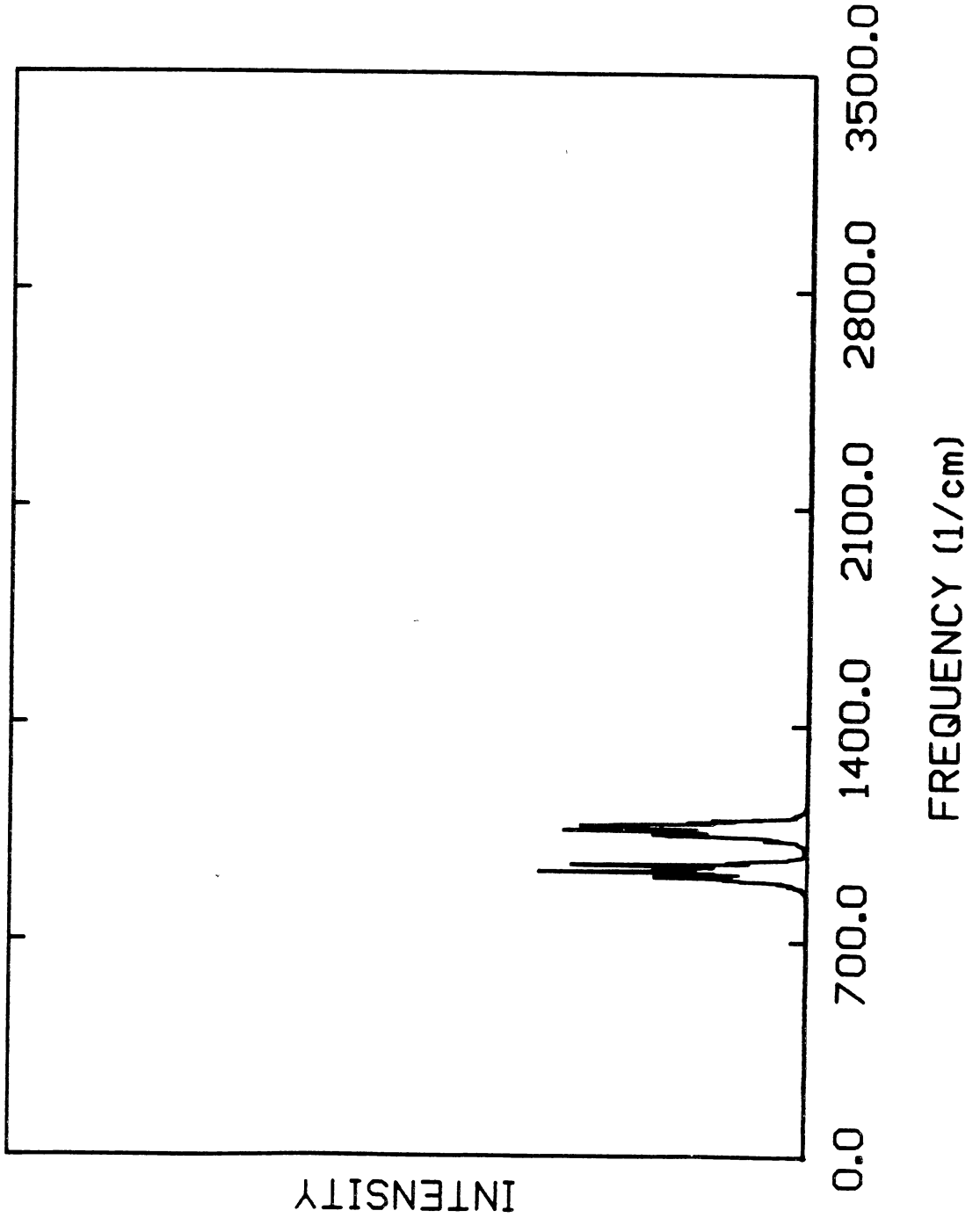
INTENSITY
0.0
700.0
1400.0
2100.0
2800.0
3500.0
FREQUENCY (1/cm)

Figure 77. Power spectrum for the one of the wag angles in nonrotating C_2H_4 vibrating with 155 kcal/mol of energy.

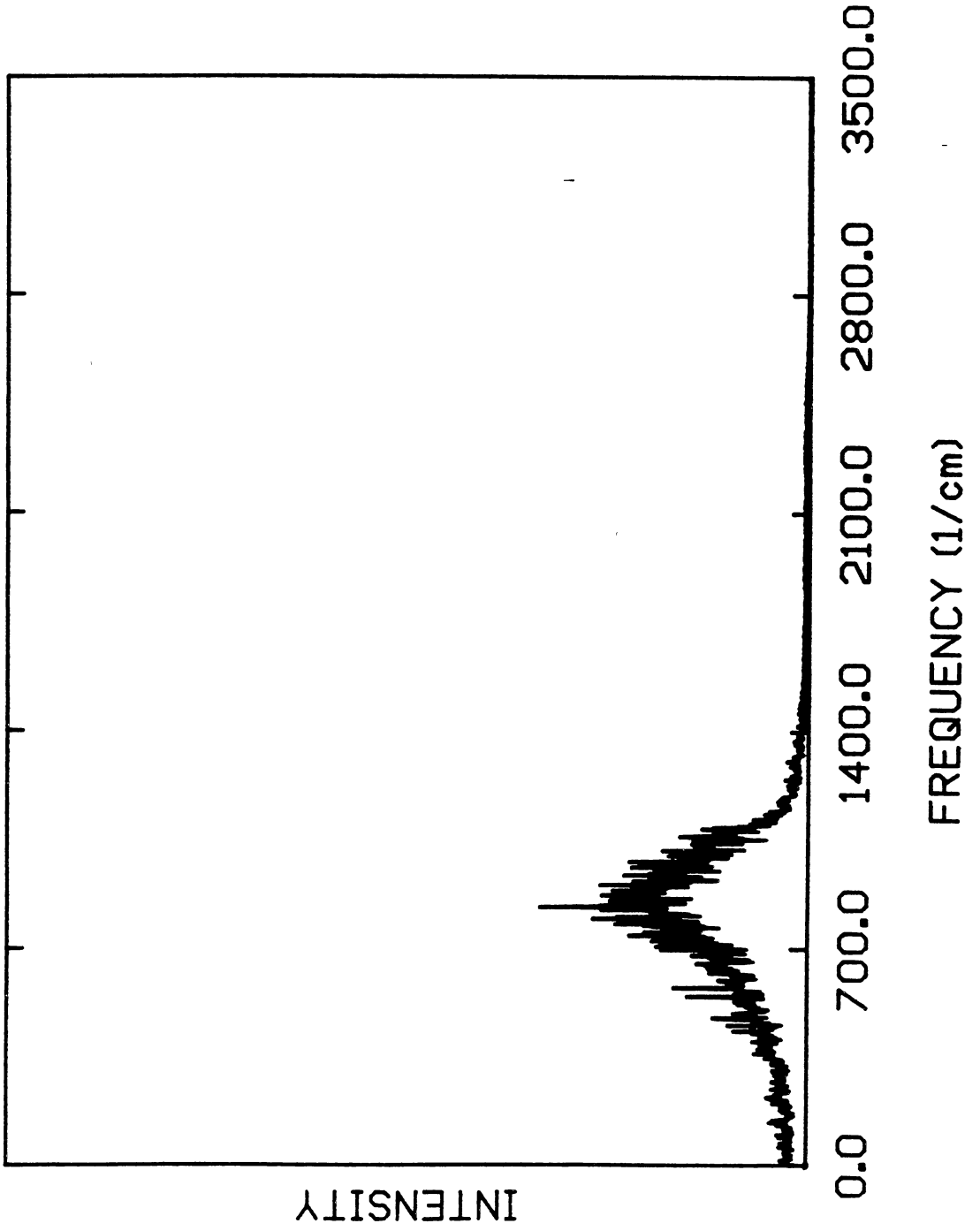
INTENSITY
0.0
700.0
1400.0
2100.0
2800.0
3500.0
FREQUENCY (1/cm)

cumulative power spectrum for trajectories computed this energy is shown in Fig. 73. Based on the results shown in Fig. 73, one would probably conclude that C_2H_4 vibrates chaotically at 155 kcal/mol. The spectrum is quite diffuse and exhibits significant intensity over the entire range for which the spectrum was generated. Most of the peaks that were well defined at the two lower energies are now nearly completely obscured. The large peak at zero frequency is a further indicator of significant chaotic motion, particularly since there are no low-frequency normal modes in the molecule.

In order to demonstrate the transition from nonchaotic motion to chaotic motion more clearly, we present the spectrum of one of the C-C-H angles and one of the out-of-plane wag angles at the the zero-point energy and at 155 kcal/mol. Spectra for the C-C-H angle are shown in Figs. 74 and 75. Those for the wag angle are shown in Figs. 76 and 77. The C-C-H angle contributes intensity to five modes; the peaks are clearly distinguishable at the zero-point energy and most are quite narrow. When the system is chaotic, the five peaks become nearly indistinguishable and form a broad band spanning over 1000 cm^{-1} (Fig. 75). The situation is similar for the wag-angle. The two sharply defined peaks in Fig. 76 are completely obscured by a broad band of intensity in Fig. 77. The low-frequency noise referred to earlier is clearly present in both Figs. 75 and 77. We have not identified the chaotic threshold for C_2H_4. However, the spectra computed for an energy of 77 kcal/mol rather closely resemble the zero-point energy results, allowing us to conclude that it occurs at an energy between 77 and 155 kcal/mol.

Although they are not presented here, the autocorrelation functions for some of the coordinates in highly excited C_2H_4 were examined and were found to decay much more rapidly and completely than those shown earlier for SiF_4. The autocorrelation functions for C_2H_4 excited to 155 kcal/mol were found to "level out" at around 10^{-6} whereas the ones shown for energized SiF_4 level out at around 10^{-4}.

CH_3ONO

The *cis-trans* isomerization of CH_3ONO has been shown to be moderately mode specific.[114] This makes it an interesting candidate for study using power spectra. Since the molecule is mode specific the IVR must be nonstatistical, which suggests (but does not guarantee) that the power spectra will exhibit structure. However, it turns out that this is the case. Power spectra for ensembles of trajectories computed at energies of 29, 71, and 144 kcal/mol are shown in Figs. 78 to 80. Random microcanonical sampling was used to initiate the trajectories.[255] The total angular momentum was zero in all cases. The lowest energy corresponds to the zero-point level. For reference, the barrier to rotation about the N-O bond is roughly ten kcal/mol; the dissociation energy of the N-O bond is 41.1 kcal/mol.[114]

The comments made concerning the shifting and broadening of the peaks in the other molecules are true here as well. The amount of broadening is intermediate between the SiF_4 and C_2H_4 cases. There are several coordinates that have appreciable spectral intensity at only one peak (at the zero-point energy). Among these are the N=O bond, the C-O-N angle, and the C-O-N-O dihedral angle. Spectra for the N=O bond and C-O-N angle are not greatly broadened by increasing the energy from the zero-point to 71 kcal/mol. However, excitation to 144 kcal/mol results in substantial broadening. The spectra for the N=O bond are presented in Figs. 81 to 83 (29, 71, and 144 kcal/mol, respectively).

The barrier for internal rotation of the methyl group in *trans*-CH_3ONO is quite small, less than one kcal/mol (the barrier to methyl rotation in *cis*-CH3ONO is also small, about one kcal/mol). Thus, it acts as a weakly hindered rotor. Not surprisingly, then, the power spectrum for this coordinate (not shown) is "chaotic", even at the zero-point energy. The peak is diffuse and, in the cumulative spectrum, appears as "noise" over the low-frequency end of the spectrum.

Figure 78. Cumulative power spectrum for nonrotating CH_3ONO vibrating with zero-point energy. The spectrum was obtained as a superposition of the Fourier transforms of ensemble-averaged sample autocorrelation functions of the internal coordinates.

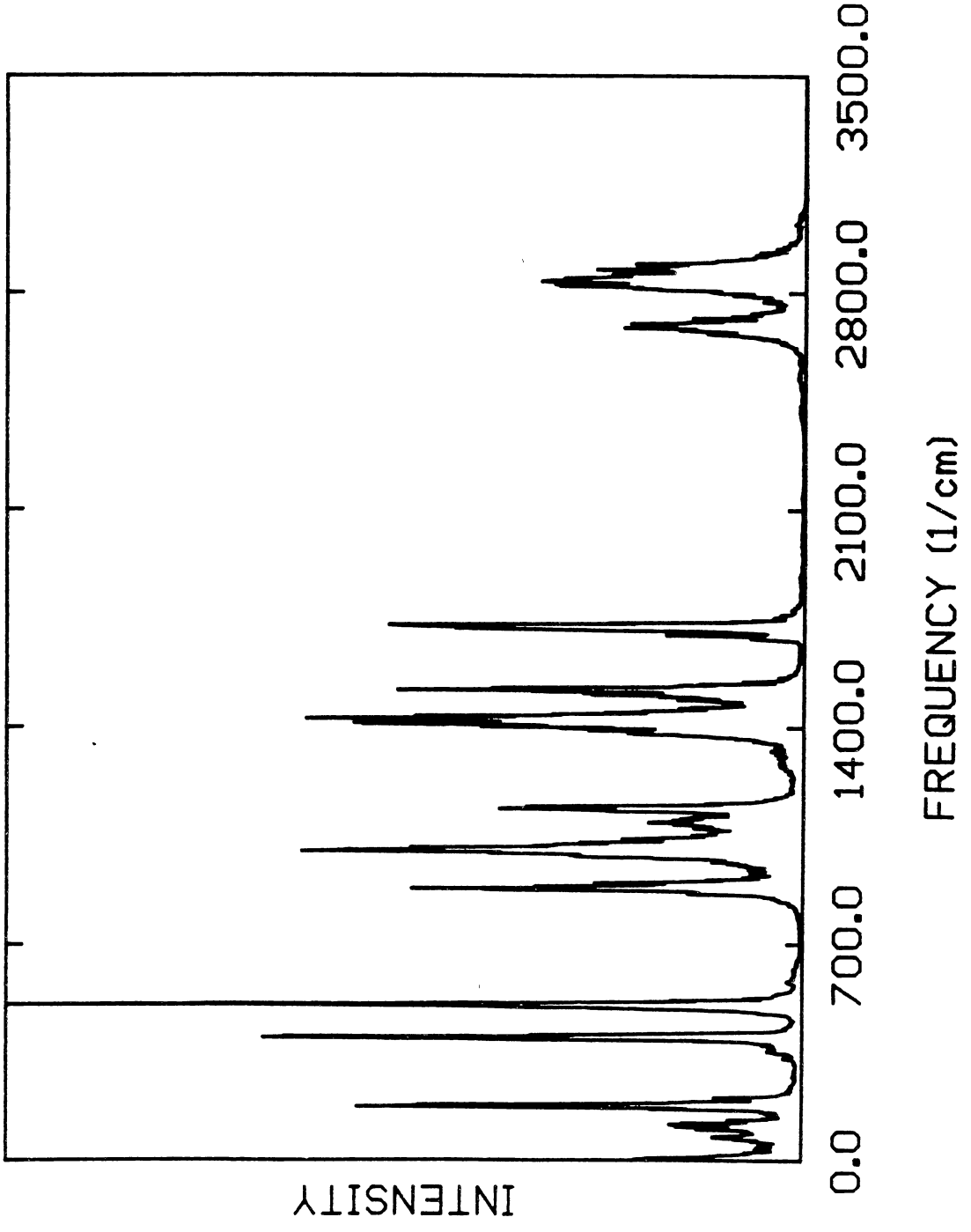
INTENSITY
0.0
700.0
1400.0
2100.0
2800.0
3500.0
FREQUENCY (1/cm)

Figure 79. Cumulative power spectrum for nonrotating CH_3ONO vibrating with 71 kcal/mol of energy. The spectrum was obtained as a superposition of the Fourier transforms of ensemble-averaged sample autocorrelation functions of the internal coordinates.

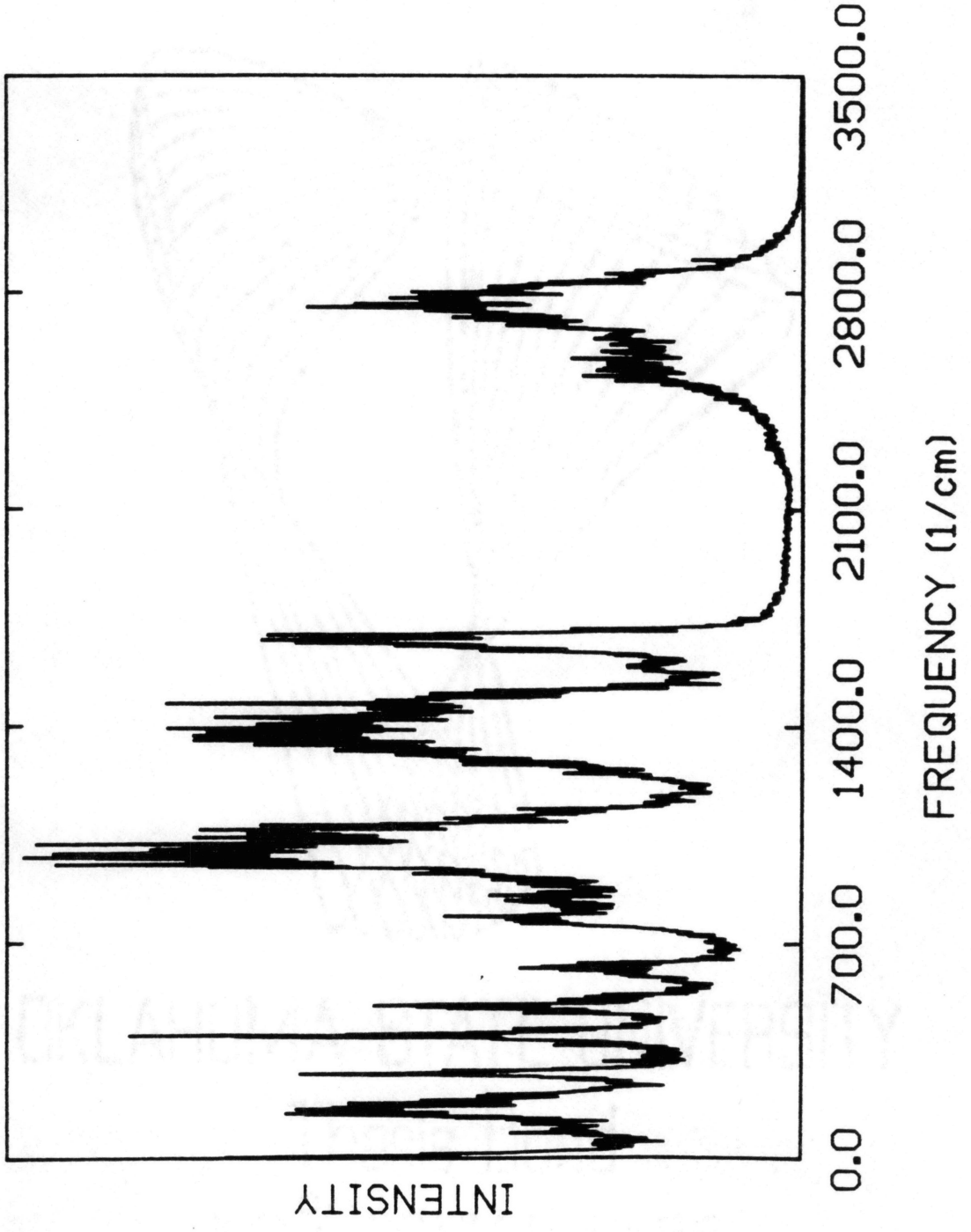
INTENSITY
0.0
700.0
1400.0
2100.0
2800.0
3500.0
FREQUENCY (1/cm)

Figure 80. Cumulative power spectrum for nonrotating CH_3ONO vibrating with 144 kcal/mol of energy. The spectrum was obtained as a superposition of the Fourier transforms of ensemble-averaged sample autocorrelation functions of the internal coordinates.

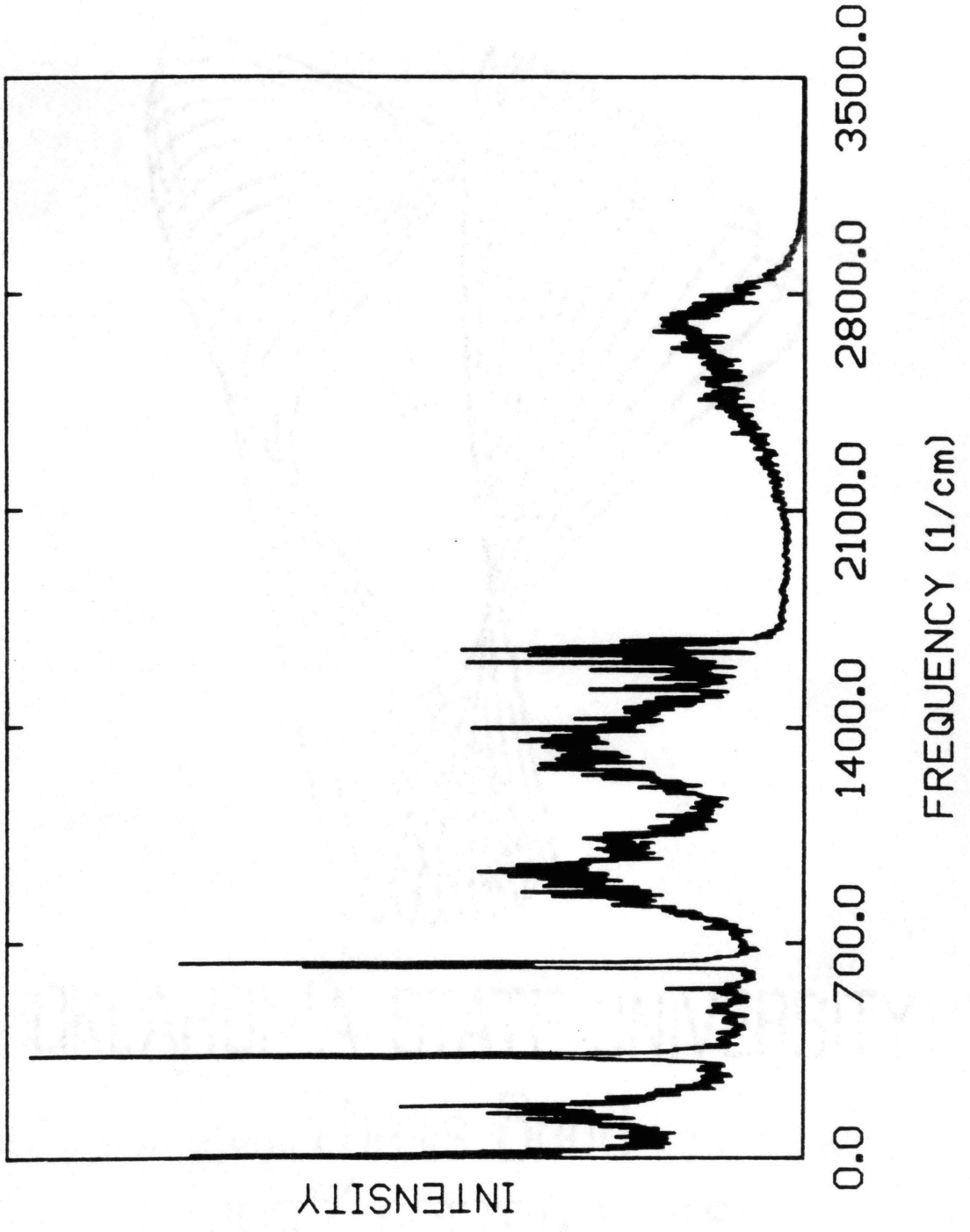
INTENSITY
0.0
700.0
1400.0
2100.0
2800.0
3500.0
FREQUENCY (1/cm)

Figure 81. Power spectrum for the N=O bond in nonrotating CH_3ONO vibrating with zero-point energy.

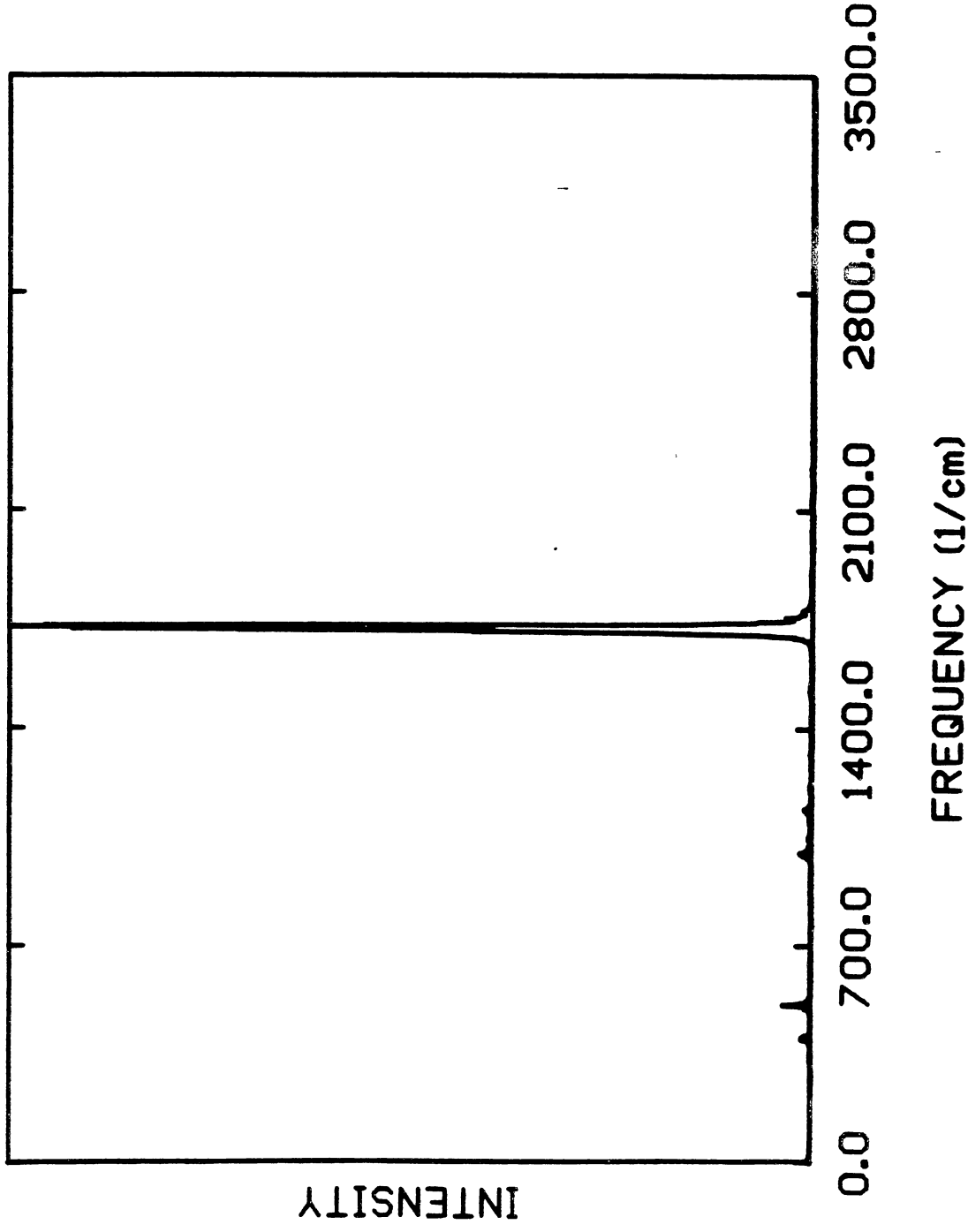
INTENSITY
0.0
700.0
1400.0
2100.0
2800.0
3500.0
FREQUENCY (1/cm)

Figure 82. Power spectrum for the N=O bond in nonrotating CH_3ONO vibrating with 71 kcal/mol of energy.

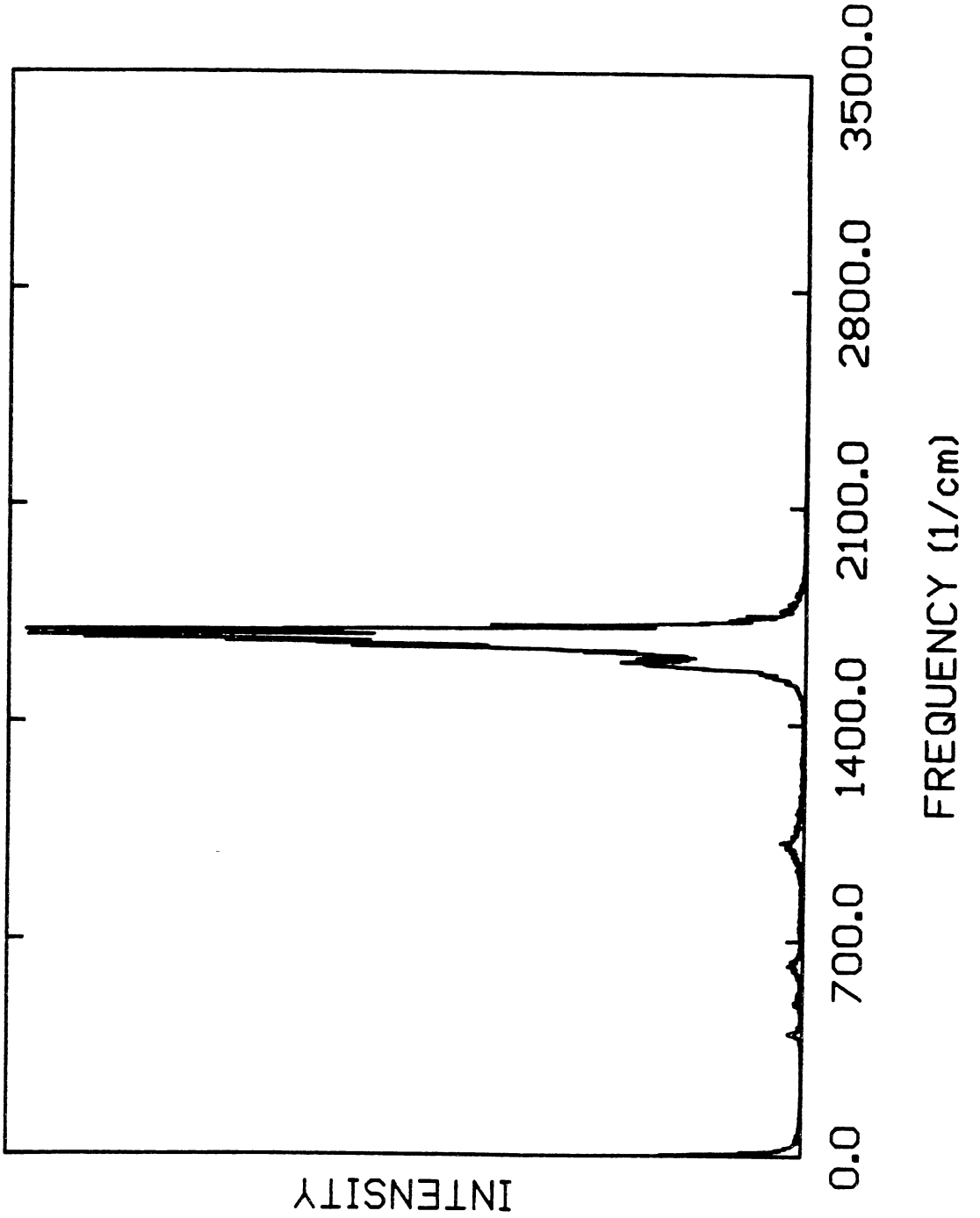
INTENSITY
0.0
700.0
1400.0
2100.0
2800.0
3500.0
FREQUENCY (1/cm)

Figure 83. Power spectrum for the N=O bond in nonrotating CH_3ONO vibrating with 144 kcal/mol of energy.

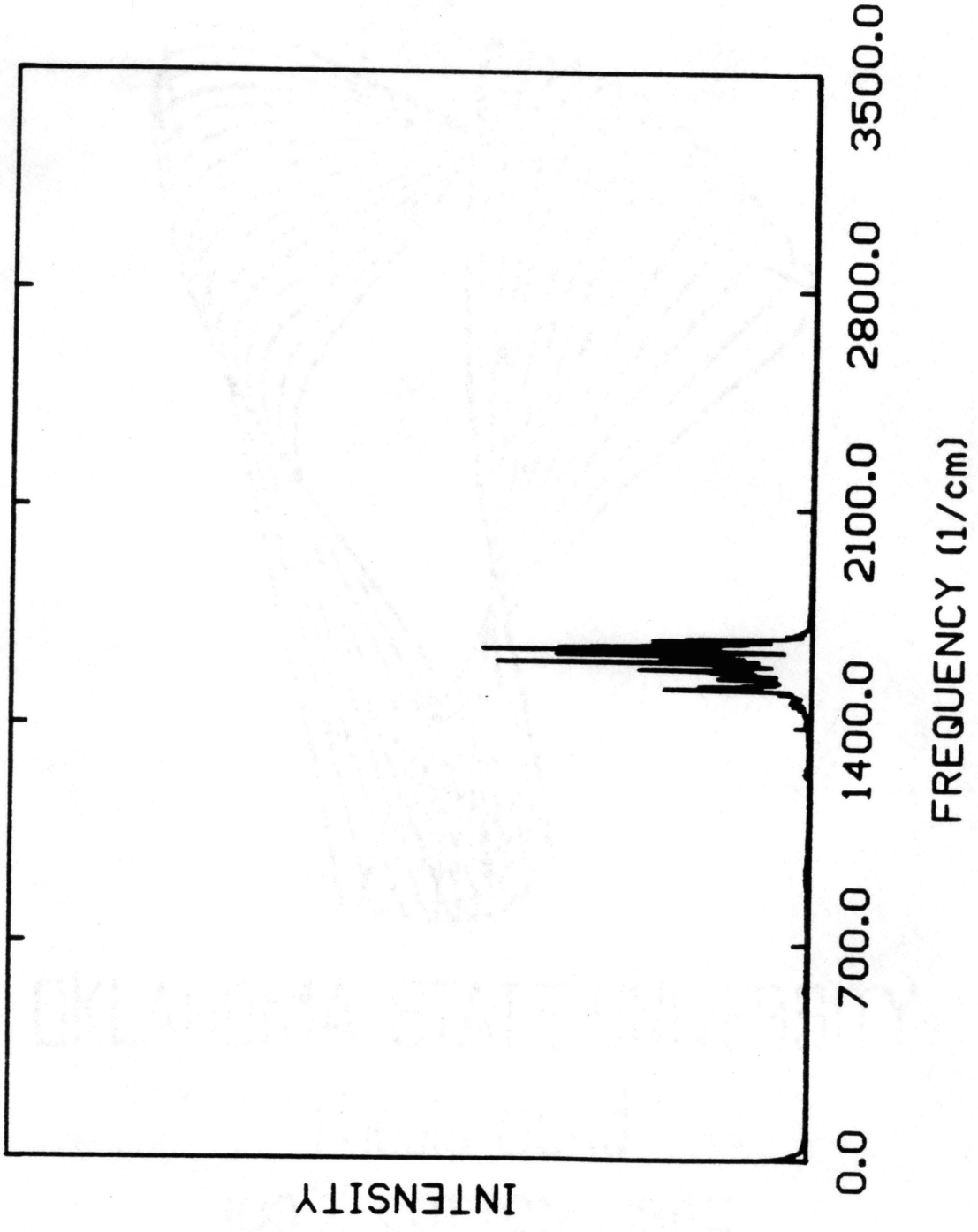
INTENSITY
0.0
700.0
1400.0
2100.0
2800.0
3500.0
FREQUENCY (1/cm)

The behaviors of the spectra for the C-O-N and O-N-O angles are interesting. Inspection of the low-frequency range of the spectra shown in Figs. 78 to 80 reveals an increase in the complexity of the spectrum as the energy is increased from zero-point to 71 kcal/mol (Figs. 78 and 79, respectively). New peaks appear in the spectrum. However, as the energy is increased from 71 to 144 kcal/mol (Fig. 80), the spectrum becomes much less congested and two intense, sharp peaks are seen that did not exist in the zero-point energy results. The peaks that evolve with increasing energy are associated with the C-O-N and O-N-O angles.

Although the details of the origin of these peaks are not clear, it seems likely that they arise from a combination of factors associated with i) a deficiency in the potential-energy surface that becomes apparent for high energies and ii) the way the trajectories were computed. The potential-energy surface does not attenuate the force-field parameters as bond dissociation occurs (The Preiskorn and Thompson study was restricted to energies unlikely to result in bond fission.[114]). All of the trajectories computed at 144 kcal/mol dissociated (*via* N-O bond fission) within the ten ps that they were followed. In some cases, the N-O bond lengths at the end of the trajectories were over 100 Å. (Trajectories computed at lower energies did not dissociate within the allotted time.) The fact that the trajectories were not terminated upon scission of the N-O bond means that data was collected for CH_3O + NO, rather than CH_3ONO.

The power spectra computed at the zero-point energy shed light on another shortcoming of the potential-energy surface. Specifically, attenuation of the potential due to either methyl-group rotation or rotation about the N-O bond was neglected. The equilibrium structures of both *cis*- and *trans*-CH_3ONO are such that there are five atoms in a plane (H-C-O-N-O) and two hydrogen atoms out of the plane. Preiskorn and Thompson treated the force-field parameters involving the in-plane

Figure 84. Power spectrum for the "in-plane" H-C-O angle in nonrotating CH_3ONO vibrating with zero-point energy.

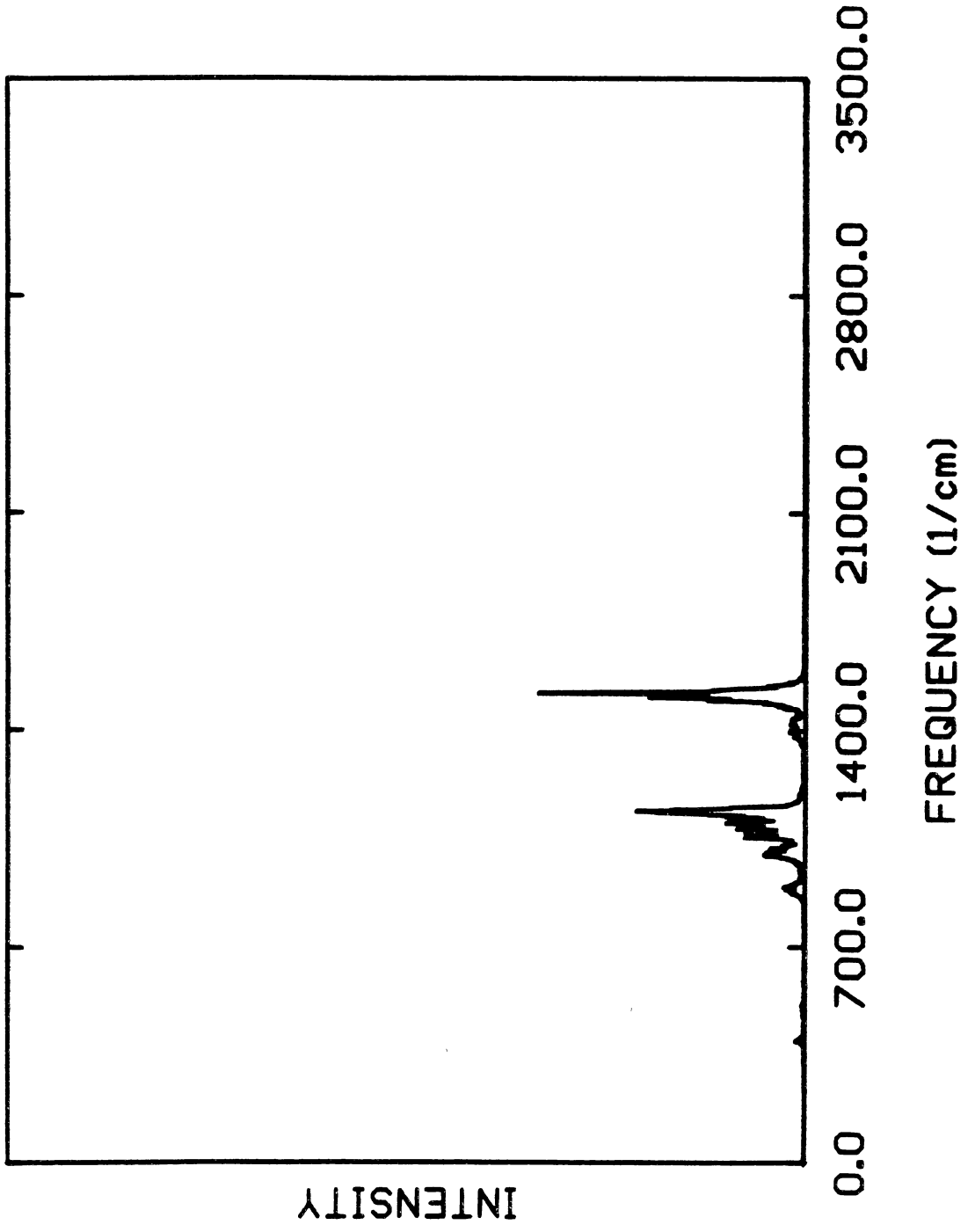
INTENSITY
0.0
700.0
1400.0
2100.0
2800.0
3500.0
FREQUENCY (1/cm)

Figure 85. Power spectrum for the one of the "out-of-plane" H-C-O angles in nonrotating CH_3ONO vibrating with zero-point energy.

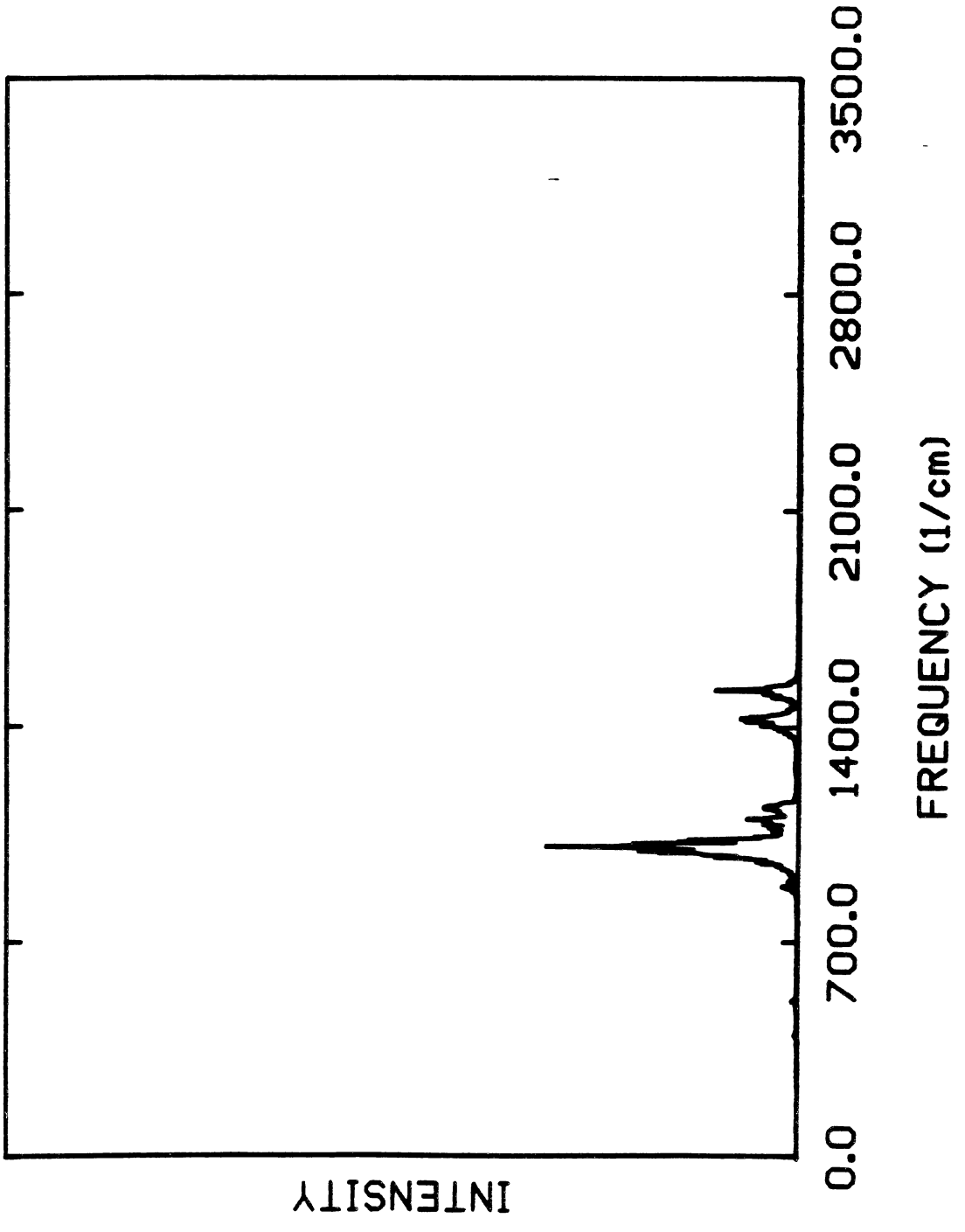
INTENSITY
0.0
700.0
1400.0
2100.0
2800.0
3500.0
FREQUENCY (1/cm)

and out-of-plane H atoms differently (for both conformers) but did not attenuate them with respect to methyl-group rotation. The Morse curvature parameter for the "in-plane" C-H bond is (slightly) different than that for the "out-of-plane" C-H bonds. Similar bias was applied to the three H-C-O angle-bending force constants. Finally, the H-C-H angle-bending force constants involving the "in-plane" H atom differ from the force constant for the H-C-H angle defined in terms of the two "out-of-plane" H atoms. The energies we considered are such that methyl-group rotation is practically unhindered. Thus, the spectra for these coordinates should all be the same. However, for all energies considered, the spectra for all of the above mentioned coordinates (except the C-H bond stretch) are readily distinguishable. As an example, we show the zero-point energy results for the "in-plane" and "out-of-plane" H-C-O angles in Figs. 84 and 85, respectively. (The spectrum for only one of the "out-of-plane" H-C-O angles is shown. The second one is entirely similar in peak widths, positions, and intensities.) Although the corresponding spectra computed at higher energies are somewhat different from the zero-point energy results, the "in-plane" spectra remain clearly distinguishable from the "out-of-plane" ones.

2-chloroethyl Radical

We have argued that 2-chloroethyl radical is i) non-mode specific (Chapter IV) and ii) statistical (Chapter V) with respect to the simple bond-fission reactions (R1) and (R2). It is therefore interesting to determine whether power spectra indicate chaotic motion. We have carried out limited calculations of power spectra for 2-chloroethyl radical for four total energies: a very-low energy trajectory (Fig. 51), 32, 77 kcal/mol, and 110 kcal/mol. Random microcanonical sampling with zero angular momentum was used.[255] Ensembles of twenty trajectories were computed, however, for the larger

Figure 86. Cumulative power spectrum for nonrotating 2-chloroethyl radical vibrating with zero-point energy. The spectrum was obtained as a superposition of the Fourier transforms of ensemble-averaged sample autocorrelation functions of the internal coordinates.

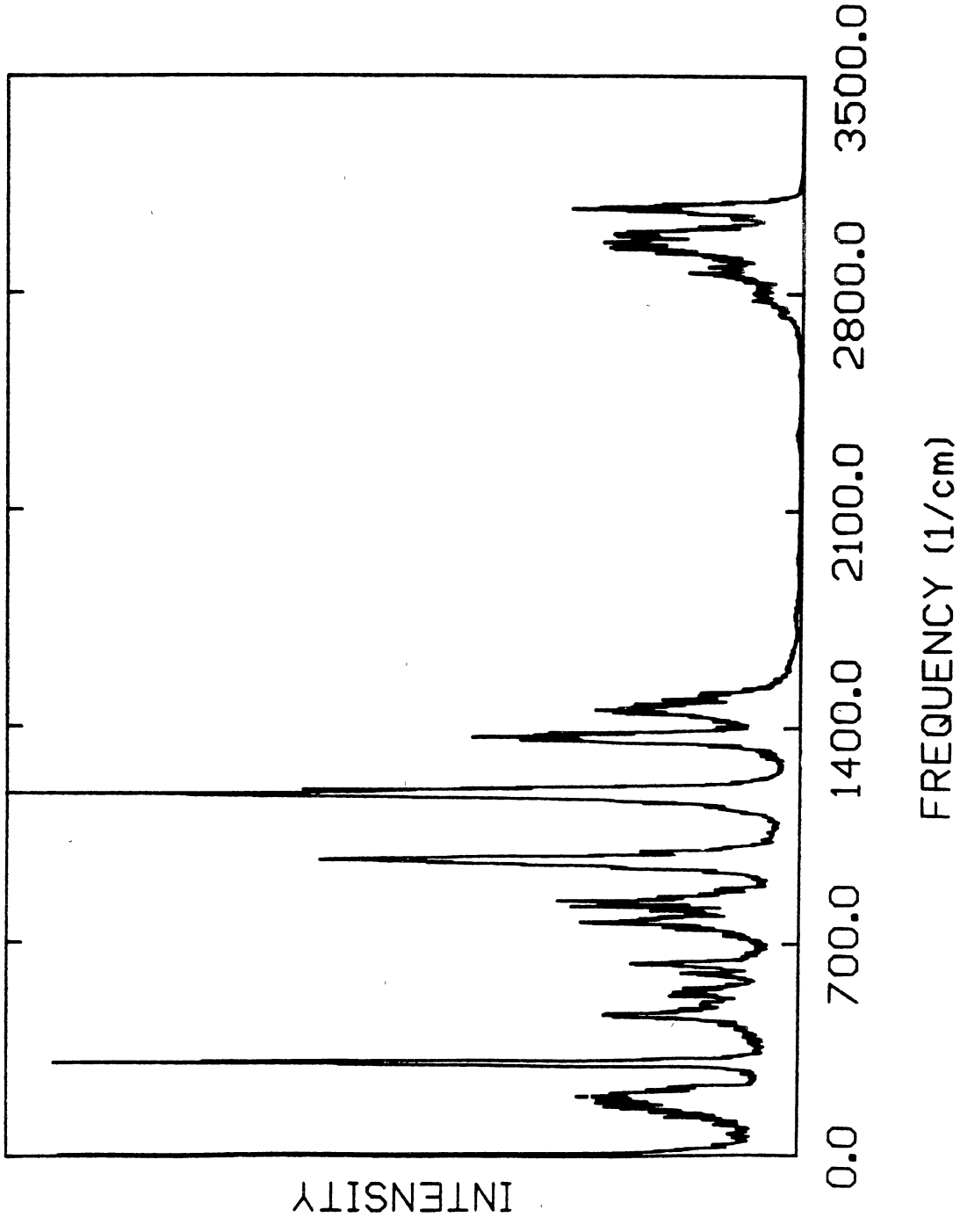
INTENSITY
0.0
700.0
1400.0
2100.0
2800.0
3500.0
FREQUENCY (1/cm)

Figure 87. Cumulative power spectrum for nonrotating 2-chloroethyl radical vibrating with 77 kcal/mol of energy. The spectrum was obtained as a superposition of the Fourier transforms of ensemble-averaged sample autocorrelation functions of the internal coordinates.

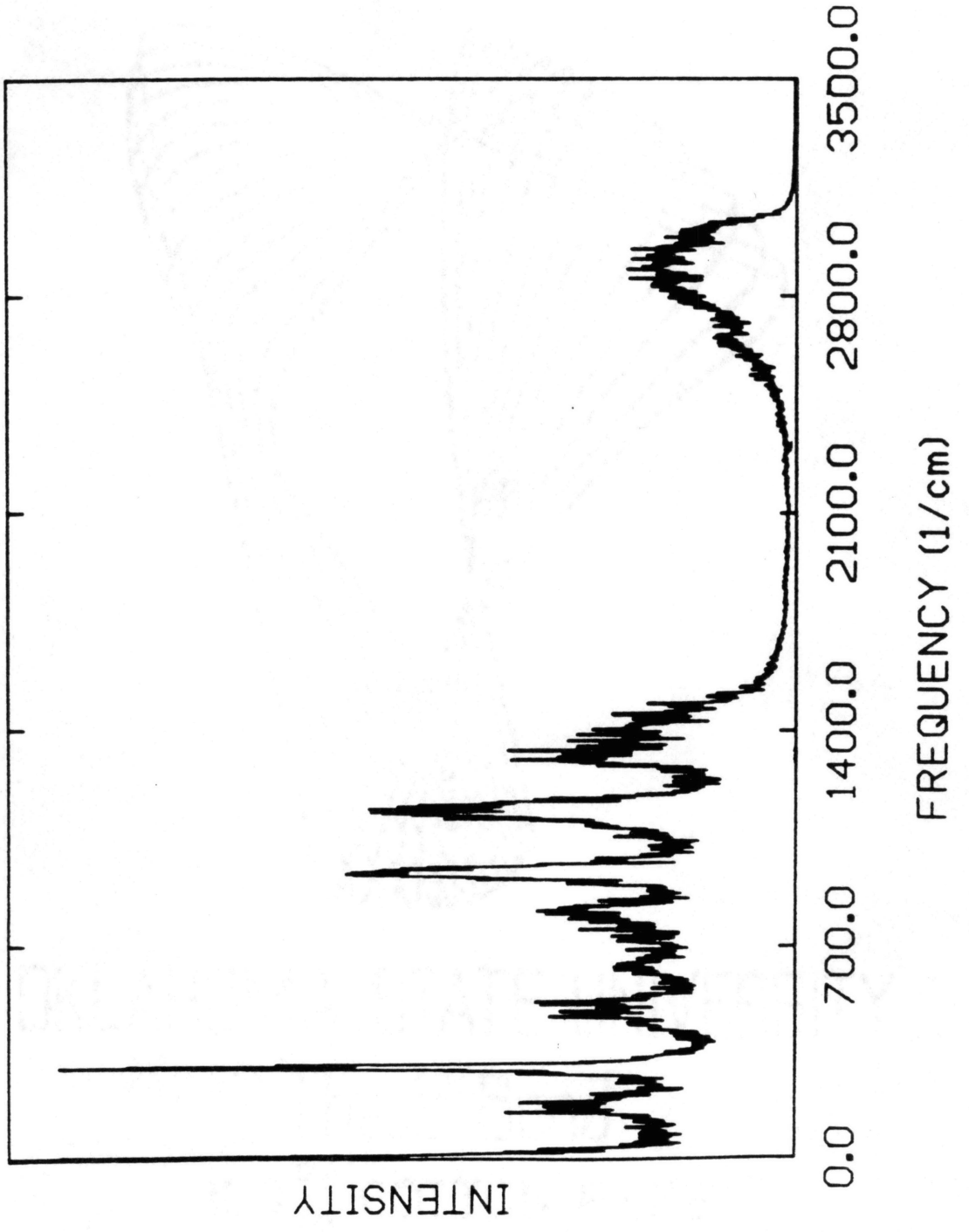
INTENSITY
0.0
700.0
1400.0
2100.0
2800.0
3500.0
FREQUENCY (1/cm)

Figure 88. Cumulative power spectrum for nonrotating 2-chloroethyl radical vibrating with 110 kcal/mol of energy. The spectrum was obtained as a superposition of the Fourier transforms of ensemble-averaged sample autocorrelation functions of the internal coordinates.

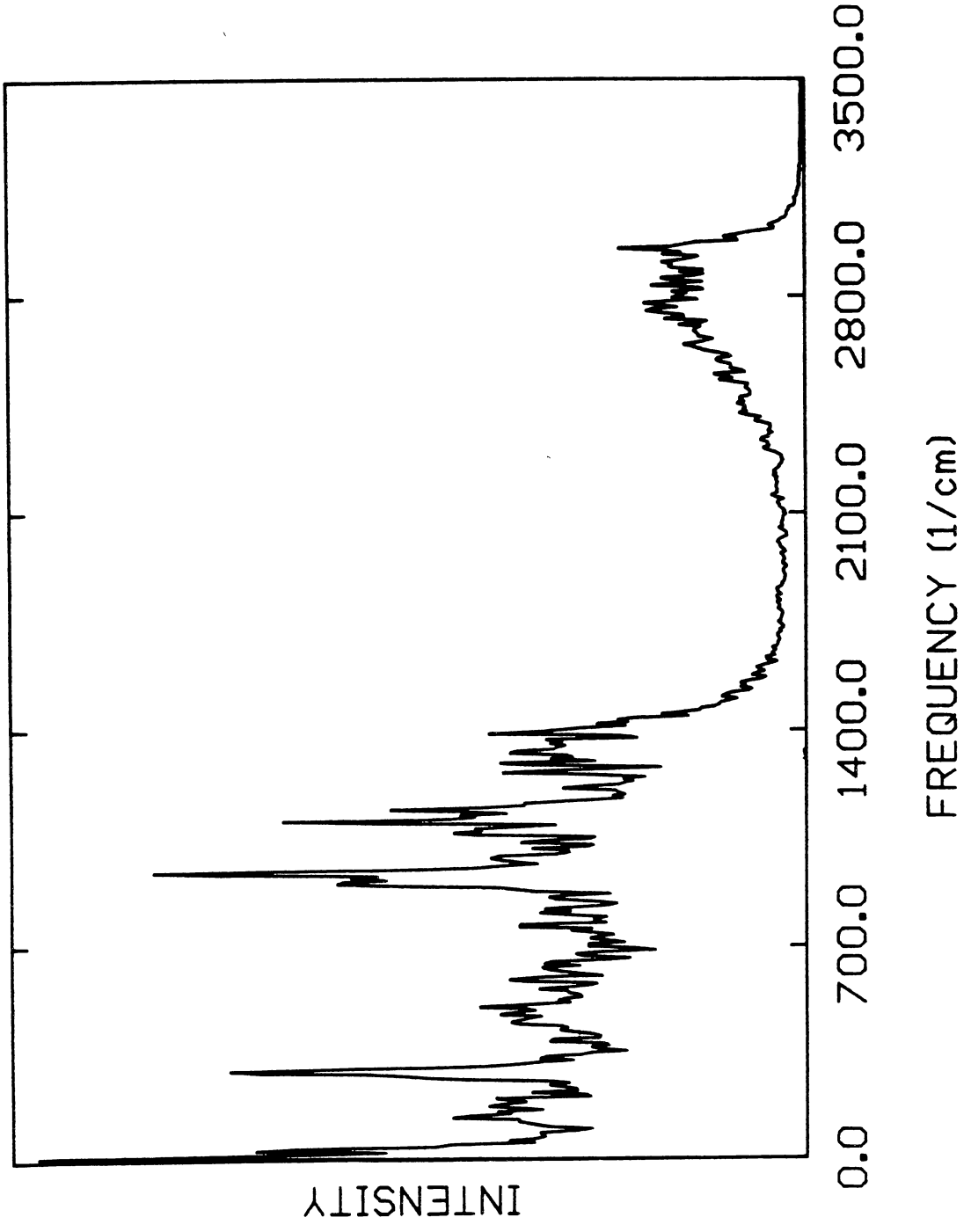
INTENSITY
0.0
700.0
1400.0
2100.0
2800.0
3500.0
FREQUENCY (1/cm)

energies some of the trajectories dissociated. Rather than neglecting ignoring dissociation (as was done for CH_3ONO above), we have retained only the trajectories that survive for at least some prescribed time. This time cutoff is less than 10 ps; therefore, the resolution for the two high-energy ensembles is somewhat lower than for the zero-point energy.

Figures 86 to 88 are the cumulative spectra for 2-chloroethyl radical at the zero-point energy (32 kcal/mol), 77 kcal/mol, and 110 kcal/mol, respectively. As in the earlier cases, the zero-point energy spectrum is well resolved (Fig. 86). The spectrum corresponding to a total energy of 77 kcal/mol is also relatively regular (Fig. 87). This energy is not too much higher than those accessed in overtone-induced dissociation experiments on 2-chloroethyl radical.[311] Finally, the spectrum corresponding to a total energy of 110 kcal/mol is shown in Fig. 88. There is still some structure in the spectrum, but it is significantly more diffuse than the spectra computed for lower energies, suggesting that 155 kcal/mol is probably near the chaotic threshold. This energy is roughly 30-40 kcal/mol less than the highest energies we considered for SiF_4, C_2H_4, and CH_3ONO. It seems likely that, like C_2H_4, the dynamics of 2-chloroethyl radical at energies in excess of 150 kcal/mol will be highly chaotic which, in turn, implies statistical behavior.

RDX

RDX is an interesting molecule to study in the present context due to its large size and dense spectrum (see Fig. 52). The large number and close spacing of the vibrational modes would seemingly promote efficient IVR. Also, the potential-energy surface we have constructed is highly coupled through the extensive use of switching functions. On the other hand, due to the the large size of the molecule, the average energy per mode will be relatively small, even when the system is excited to energies

above the decomposition threshold. The first two points would tend to argue in favor of statistical IVR; the latter supports normal-mode-like behavior.

We have computed power spectra for four energies: 78 , 160, 250, and 350 kcal/mol. The lowest energy is the zero-point level. The second lowest is approximately the same as the energy of the RDX molecules following multiphoton excitation in the molecular beam experiments of Zhao et al..[222] Finally, the two higher bracket the range that we considered in the reaction dynamics study described in Chapter VI.

Initial conditions for the trajectories were obtained using two methods designed to give mode-selective distributions of the energy: Zero-point energy was partitioned into all of the normal modes, followed by excitation of selected normal modes (see Chapter II). In one case, all of the energy in excess of the zero-point level was projected onto normal modes primarily involving displacements of the three NO_2 moieties. In the other case, the excess energy was assigned to normal modes principally associated with ring modes. In order to distinguish the NO_2 modes from the ring modes, the cumulative reference spectrum shown in Fig. 52 was compared with the spectra for individual internal coordinates (not shown) and the contributions of various individual coordinates to particular frequencies was estimated. The assignment is not precise, of course, but allows for a qualitative description of the vibrations in some cases.

The power spectrum of a single trajectory propagated for 16.7 ps at a total energy of 0.15 kcal/mol is shown in Fig. 52. This energy results from excitation of the entire set of vibrational normal mode "quantum numbers" to v = -0.499. At this low energy, the individual peaks in the power spectrum are well defined. Thirty of the more intense peaks are tabulated in Table XXIX. The agreement of the frequencies to those computed using analytical second derivatives of the potential-energy surface (*sans* switching functions) is good (compare with Table XX. There are a large number of

Table XXIX. Vibrational Frequencies of RDX.

Frequency (cm^{-1})
49
56
220
245
249
301
347
405
412
431
615
710
715
747
752
844
901
946
952
1045
1048
1210
1260
1265
1463
1476
1479
1553
2983
3061

symmetry-based degeneracies in the analytical normal-mode frequencies which are, of course, indistinguishable in the reference spectrum.

There are several noteworthy features in the spectrum shown in Fig. 52. First is the (expected) separation of the two C-H stretch frequencies (*ca.* 3060 cm^{-1}) from the remaining frequencies. Also, several of the individual internal coordinate spectra contribute intensity to only one or a very few of the peaks in the composite power spectrum; and there are a number of frequencies for which the intensity can largely be attributed single internal coordinates. Of particular interest in this regard are the spectra of the NO_2-NO_2 Lennard-Jones interactions (*ca.* 50 cm^{-1}), the ONO angle bend (*ca.* 412 cm^{-1}), the HCH angle bend (*ca.* 1260 cm^{-1}) the NN bond stretch (*ca.*1470 cm^{-1}), and the NO bond stretch (*ca.* 1553 cm^{-1}). By contrast, some of the spectra of the individual coordinates display a large number of low-intensity peaks, as exemplified by the spectra of the CN bond stretch and NCH angle bend. As seen below, some of the localized bands are prominent in the spectra for higher energies.

Three trajectories were computed at the zero-point energy of RDX (78 kcal/mol). The resulting spectra were observed to be similar to one another with respect to peak locations and intensities. Therefore, we present the arithmetic average of the three spectra in Fig. 89. Although the zero-point energy spectrum exhibits obvious broadening compared to the reference spectrum of Fig. 52, there are ten clearly distinguishable bands present. Many of the peaks are redshifted by several cm^{-1} relative to those in the reference spectrum. We point out that the total energy of the trajectories for the spectrum in Fig. 89 is over *500 times* that for the reference spectrum in Fig. 52. Thus, given the substantial anharmonicity of the potential-energy surface, the shifting of the bands is not unexpected.

In spite of the band shifting and broadening at the higher energy, many of the regions of appreciable intensity in the zero-point energy spectrum shown in Fig. 89 can

Figure 89. Cumulative power spectrum for nonrotating RDX vibrating with zero-point energy. The spectrum was obtained as the arithmetic mean of the spectra for three independent trajectories.

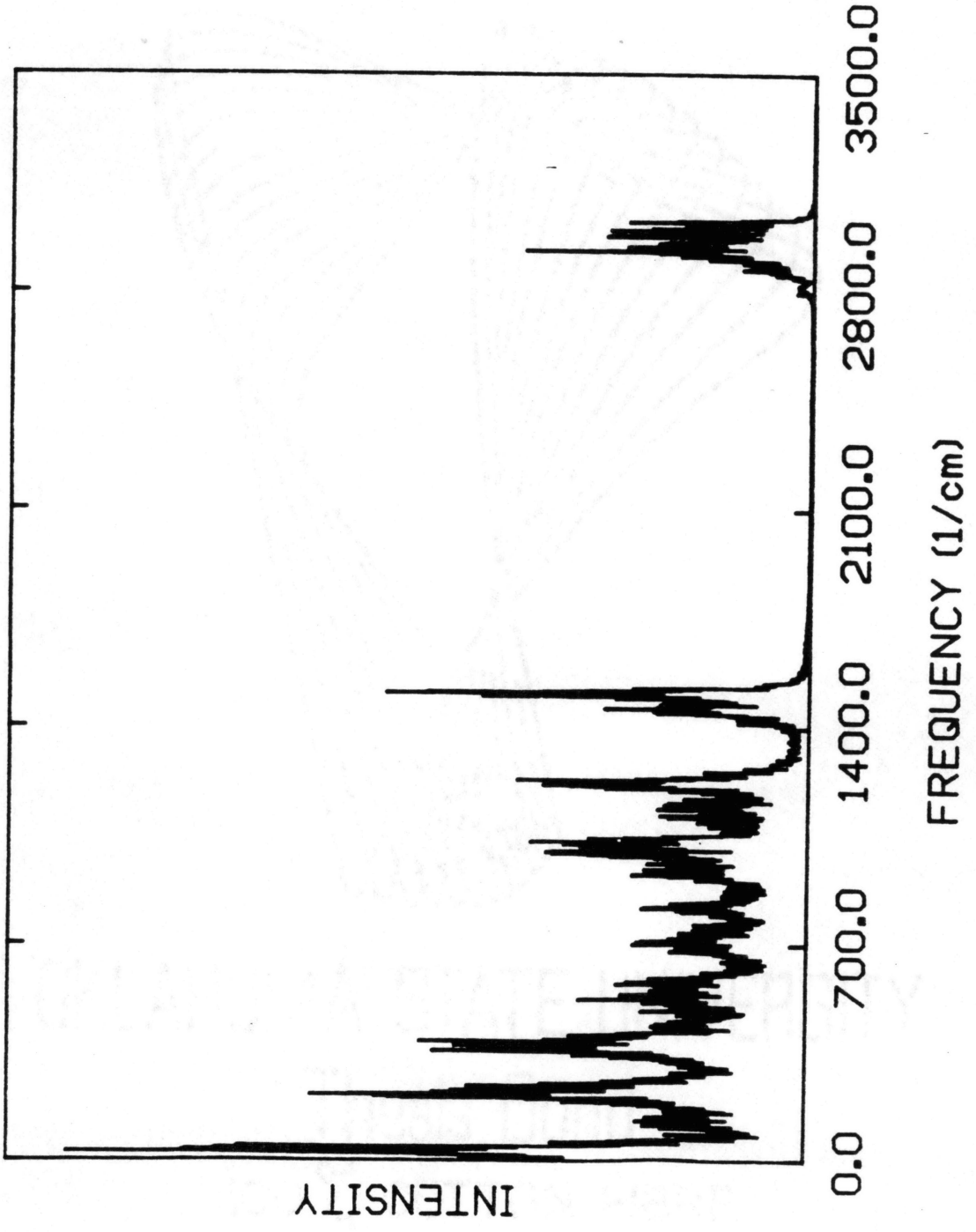
INTENSITY
0.0
700.0
1400.0
2100.0
2800.0
3500.0
FREQUENCY (1/cm)

Figure 90. Cumulative power spectrum for nonrotating RDX vibrating with 160 kcal/mol of energy. The spectrum was obtained as the arithmetic mean of the spectra for five independent trajectories. Initial conditions were designed to preferentially excite the ring modes.

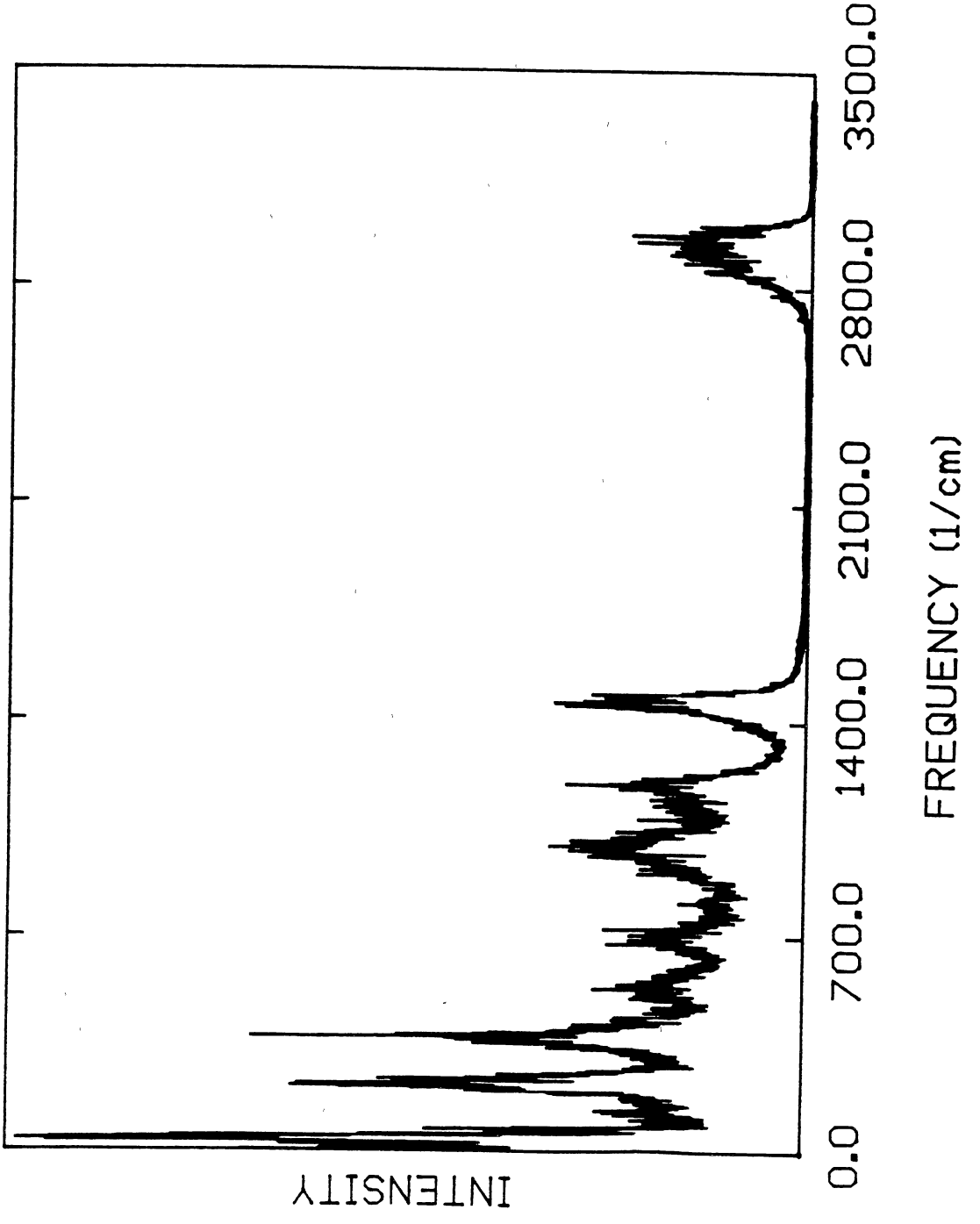
INTENSITY
0.0
700.0
1400.0
2100.0
2800.0
3500.0
FREQUENCY (1/cm)

Figure 91. Cumulative power spectrum for nonrotating RDX vibrating with 160 kcal/mol of energy. The spectrum was obtained as the arithmetic mean of the spectra for five independent trajectories. Initial conditions were designed to preferentially excite the NO_2 modes.

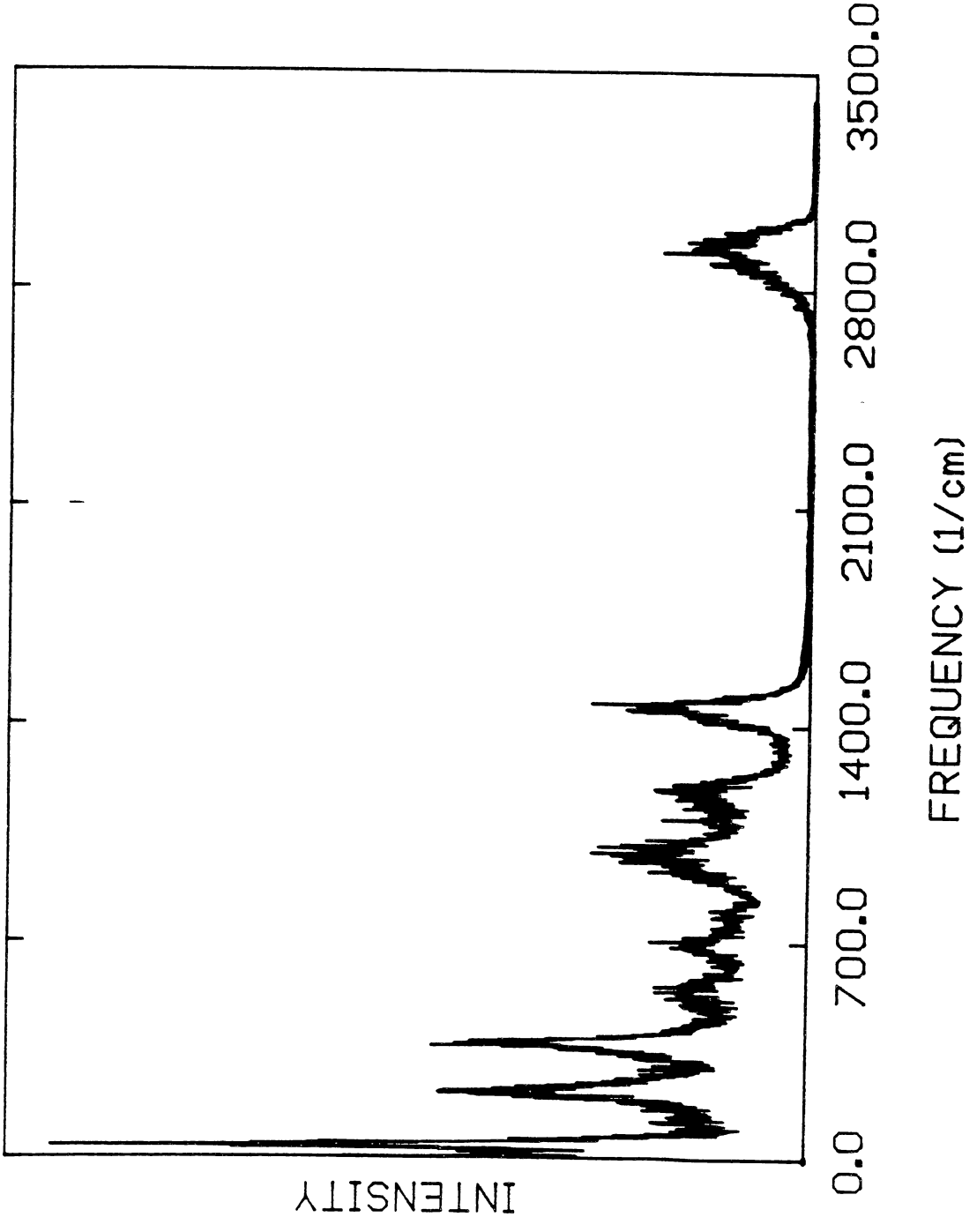
INTENSITY
0.0
700.0
1400.0
2100.0
2800.0
3500.0
FREQUENCY (1/cm)

Figure 92. Cumulative power spectrum for nonrotating RDX vibrating with 250 kcal/mol of energy. The spectrum corresponds to a single trajectory. Initial conditions were designed to preferentially excite the ring modes.

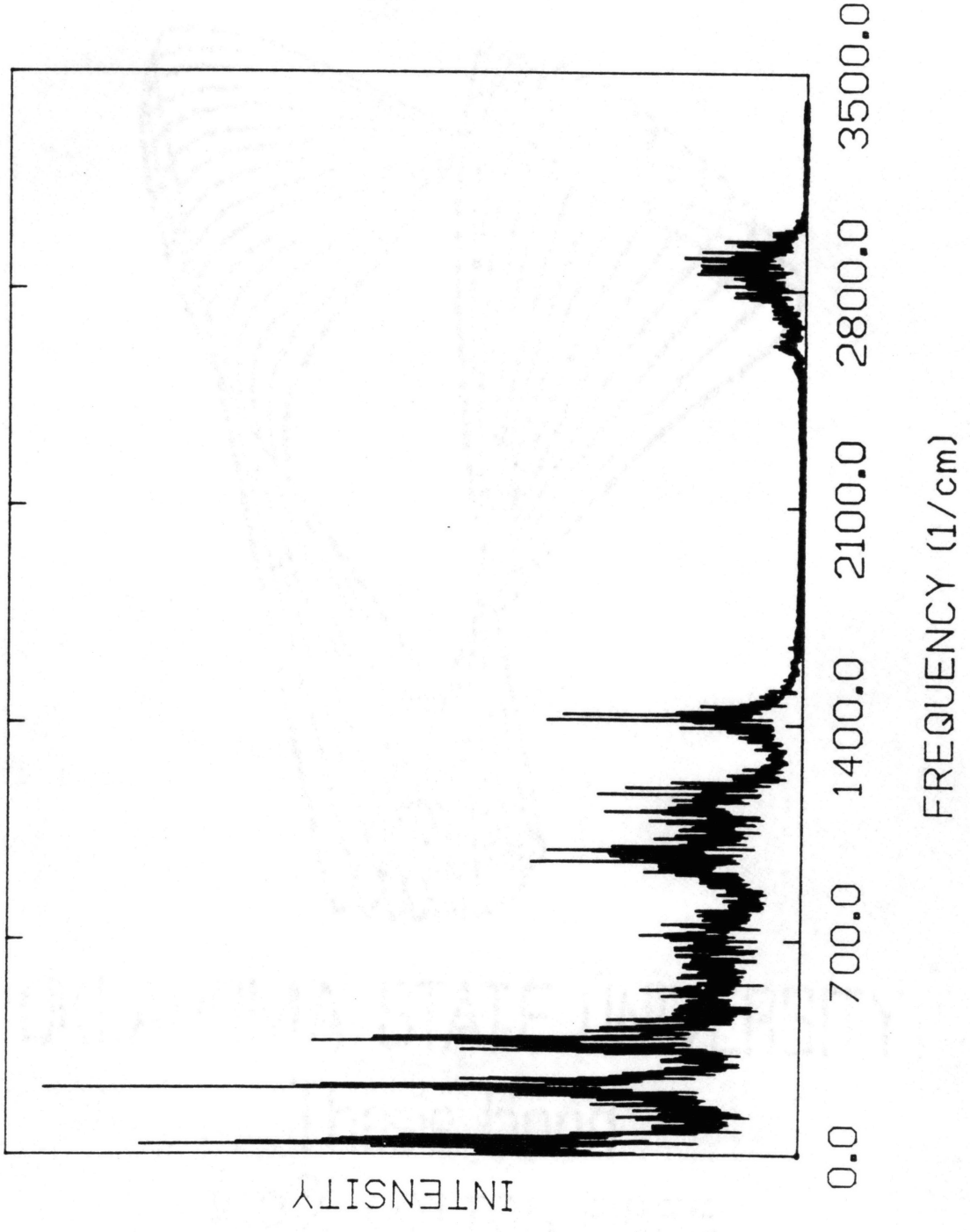
INTENSITY
0.0
700.0
1400.0
2100.0
2800.0
3500.0
FREQUENCY (1/cm)

Figure 93. Cumulative power spectrum for nonrotating RDX vibrating with 250 kcal/mol of energy. The spectrum corresponds to a single trajectory. Initial conditions were designed to preferentially excite the NO_2 modes.

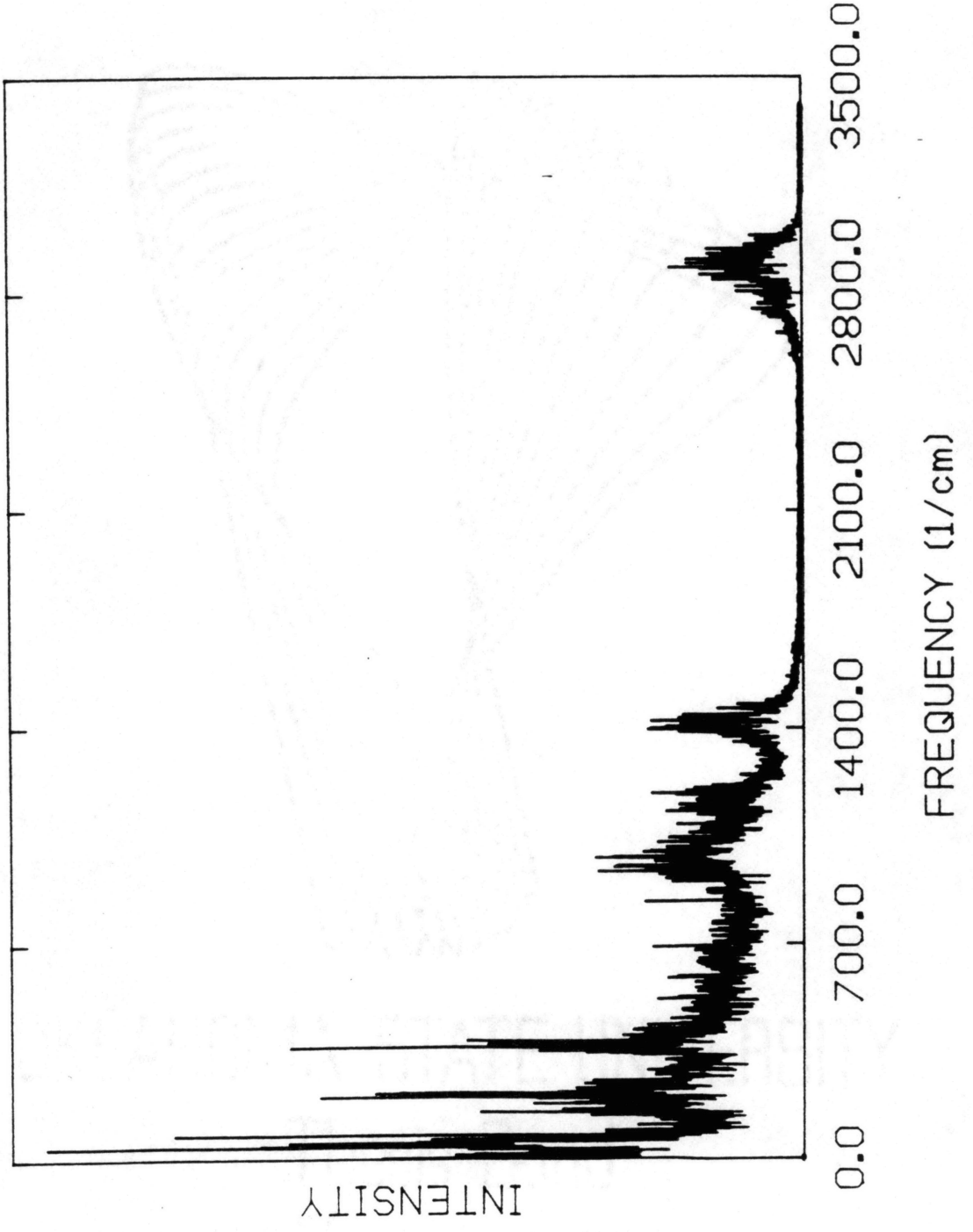
INTENSITY
0.0
700.0
1400.0
2100.0
2800.0
3500.0
FREQUENCY (1/cm)

Figure 94. Cumulative power spectrum for nonrotating RDX vibrating with 350 kcal/mol of energy. The spectrum corresponds to a single trajectory. Initial conditions were designed to preferentially excite the ring modes.

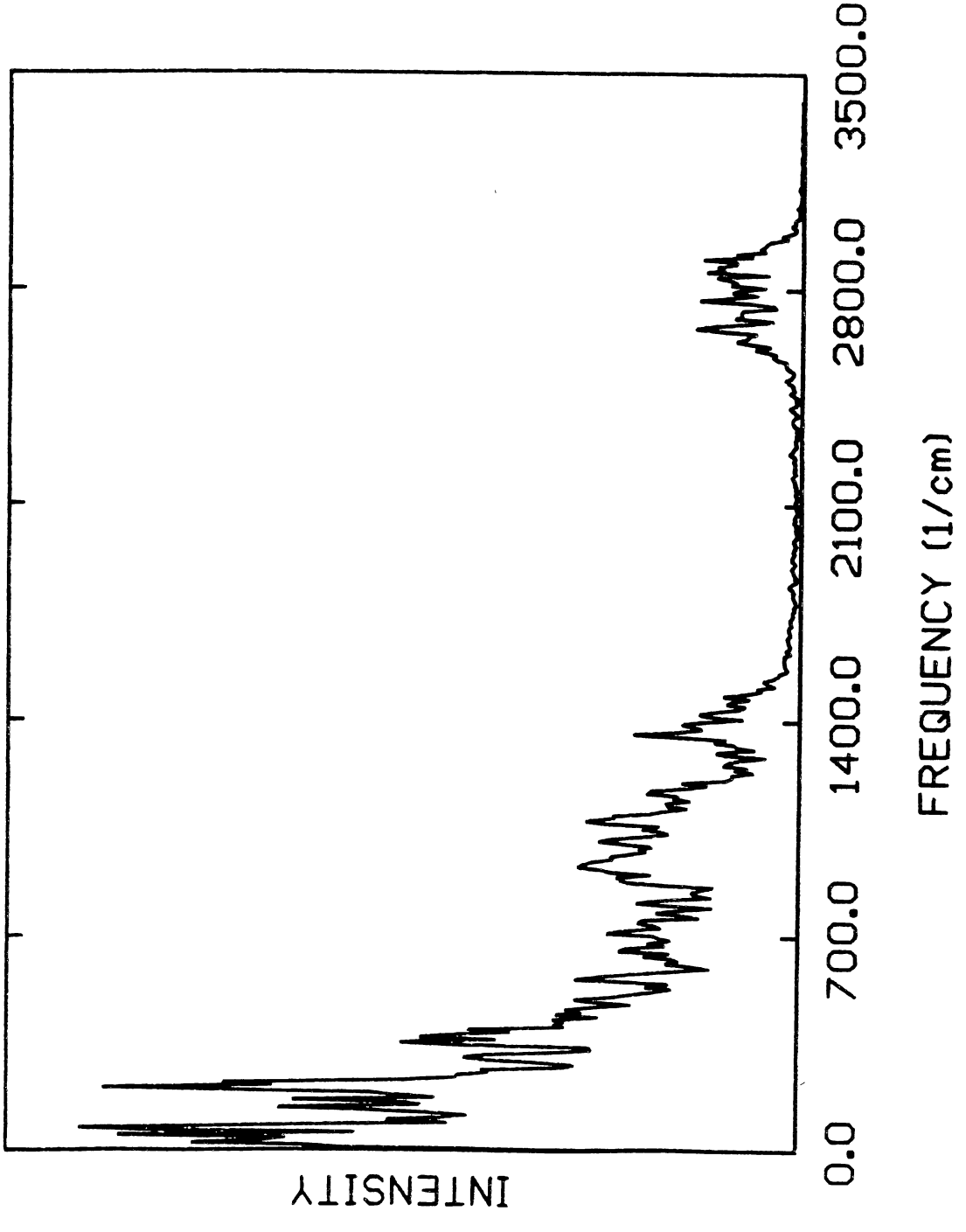
INTENSITY
0.0
700.0
1400.0
2100.0
2800.0
3500.0
FREQUENCY (1/cm)

Figure 95. Cumulative power spectrum for nonrotating RDX vibrating with 350 kcal/mol of energy. The spectrum corresponds to a single trajectory. Initial conditions were designed to preferentially excite the NO_2 modes.

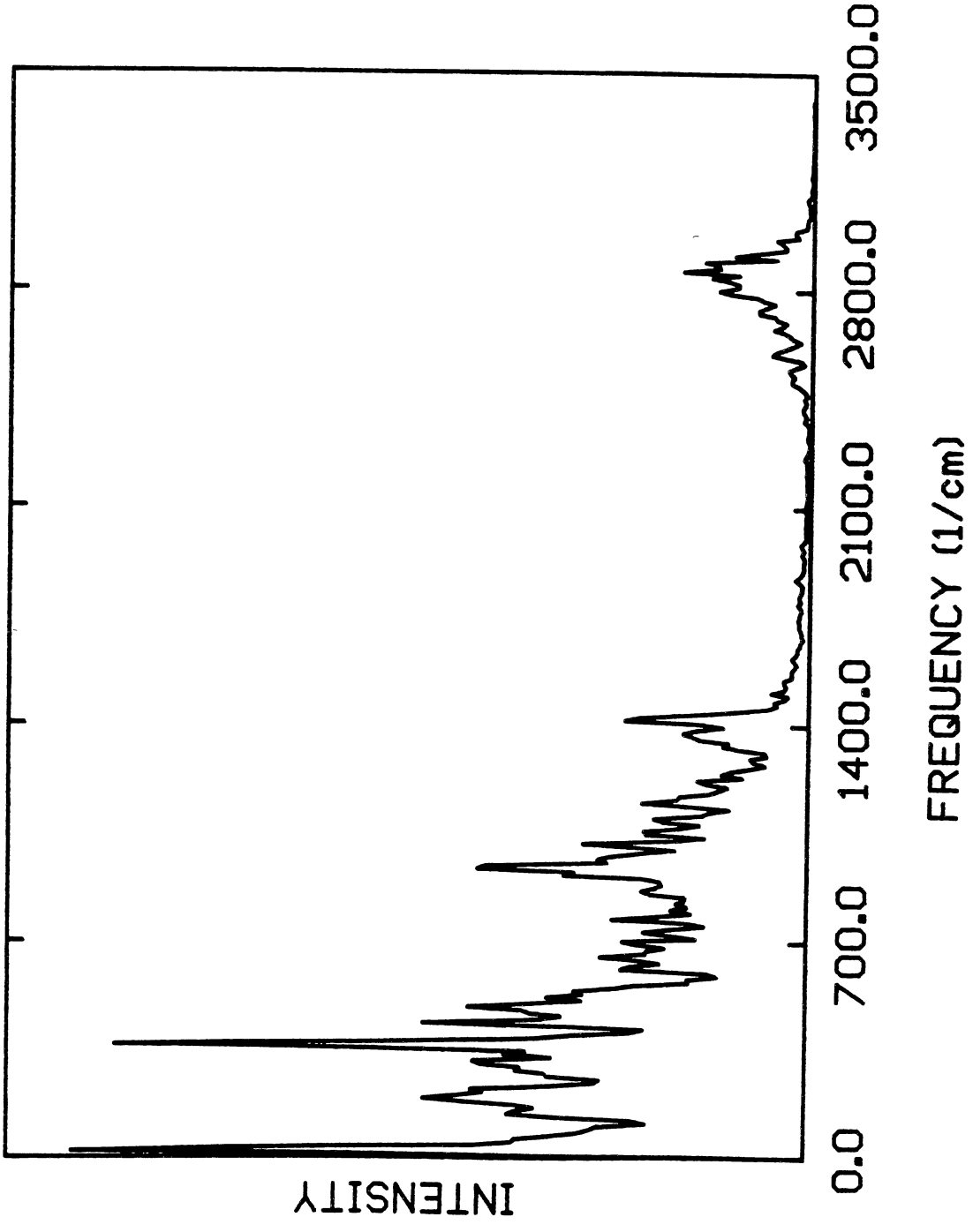
INTENSITY
0.0
700.0
1400.0
2100.0
2800.0
3500.0
FREQUENCY (1/cm)

still be assigned to essentially single (or a few) internal coordinate displacements. A number of the spectra for individual coordinates in the reference spectrum that were characterized as being localized behave similarly in the case of the zero-point energy spectrum shown in Fig. 89. For example, the spectra of the NO_2-NO_2 Lennard-Jones interaction and the HCH bend are both highly localized. The spectra for the NO and NN bond stretching coordinates are also sharply peaked; however, they display relatively intense bands at frequencies other than those present at the lower energy, particularly in the case of the NN bond stretching coordinate. This is a result of potential and kinetic coupling.

Zhao, Hintsa, and Lee[222] estimated that an average of 80 kcal/mol of excitation energy was deposited into the RDX molecules in their IRMPD experiments. Since the zero-point energy is about 78 kcal/mol, this results in an average of nearly 160 kcal/mol of internal energy in the dissociating molecule. The power spectra in Figs. 90-91 are averages over the cumulative spectra of five individual trajectories computed at 160 kcal/mol. The initial conditions for the trajectories are for selective excitation of the ring modes (Fig. 90) and the NO_2 modes (Fig. 91). The two spectra exhibit comparable band structures, peak locations, and band widths, even though the initial conditions for the spectra in Fig. 90 differ dramatically from those of Fig. 91. This is probably due to the long length of the time histories from which the spectra were computed: The coarse-grain IVR is almost certainly complete within the 16.7 ps for which the individual trajectories were propagated. The bands in Figs. 90 and 91 are noticeably redshifted relative to those in Fig. 89, however, the spectra in Figs. 90 and 91 are quite similar to the zero-point energy spectrum; the differences are of a quantitative nature. *Spectra computed at the energy of the experimental IRMPD studies possess the same qualitative features as do spectra computed at the vibrational zero-point energy. This suggests that,*

if the dynamics of RDX are regular at the zero-point energy, then they are probably regular at the experimental energies.

Power spectra were also computed for trajectories having total energies of 250 and 350 kcal/mol. At these high energies most trajectories dissociate within the maximum allowed time of 16.7 ps. Therefore, we present in Figs. 92-95 the power spectra resulting from individual trajectories computed at an energies of 250 (Figs. 92 and 93) and 350 (Figs. 94 and 95) kcal/mol, for trajectories initiated with ring mode (Figs. 92 and 94) and NO_2 mode selective excitations (Figs. 93 and 95). As is the case at lower energies (Figs. 90 and 91), the spectra resulting from selective excitation of NO_2 normal modes are qualitatively similar to those corresponding to ring-mode excitation.

Some of the bands which are well resolved at the lower energies become increasingly obscured at the high energies (see Figs. 92-95). The spectra are particularly diffuse in the range 500 to 900 cm^{-1}. The loss of the band structure is due to a number of factors: The results shown in Figs. 92-95 are for individual trajectories which results in more "noise"; and the resolution is somewhat less than in the earlier figures due to dissociation. And, as the energy increases, the degree of irregular motion probably increases, resulting in considerable broadening of the spectral features. Finally, unimolecular dissociation results in substantial changes in most of the potential-energy surface parameters (the geometric and force-field parameters in the reactant are much different than those of the products), giving rise to shifts of many of the fundamental vibrational frequencies.

Interestingly, the single-band character of some of the internal coordinate spectra for lower energies are present at 350 kcal/mol, indicating relatively invariant behavior over this wide energy range. Examples are shown for the HCH bending angle (Figs. 96-100) and the NO bond stretch (Figs. 101-105). Figures 96-100 and 101-105

Figure 96. Power spectrum for one of the H-C-H angles in nonrotating RDX vibrating with 0.15 kcal/mol of energy. The spectrum corresponds to a single trajectory.

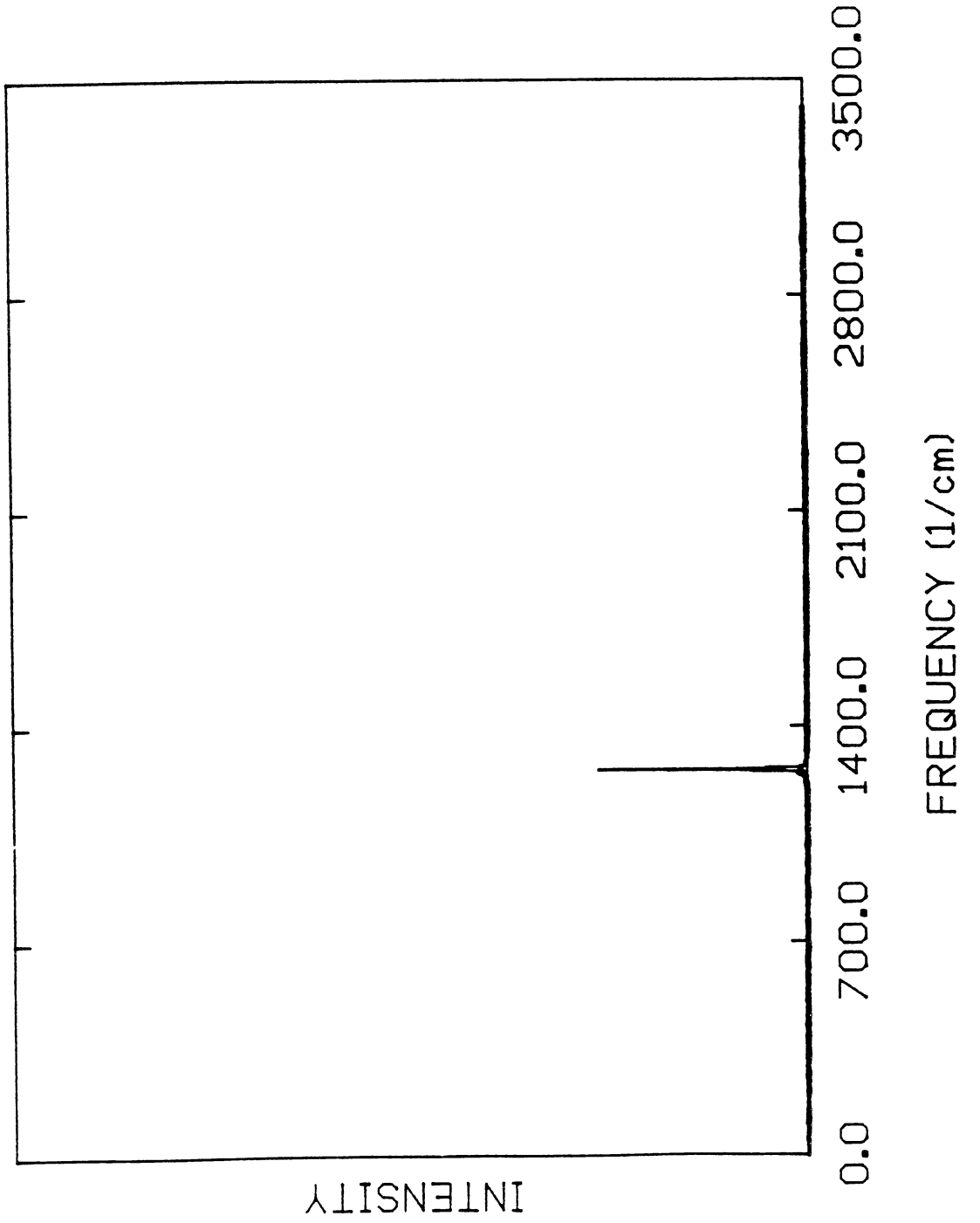
INTENSITY
0.0
700.0
1400.0
2100.0
2800.0
3500.0
FREQUENCY (1/cm)

Figure 97. Power spectrum for one of the H-C-H angles in nonrotating RDX vibrating with zero-point energy. The spectrum was obtained as the arithmetic mean of the spectra for three independent trajectories.

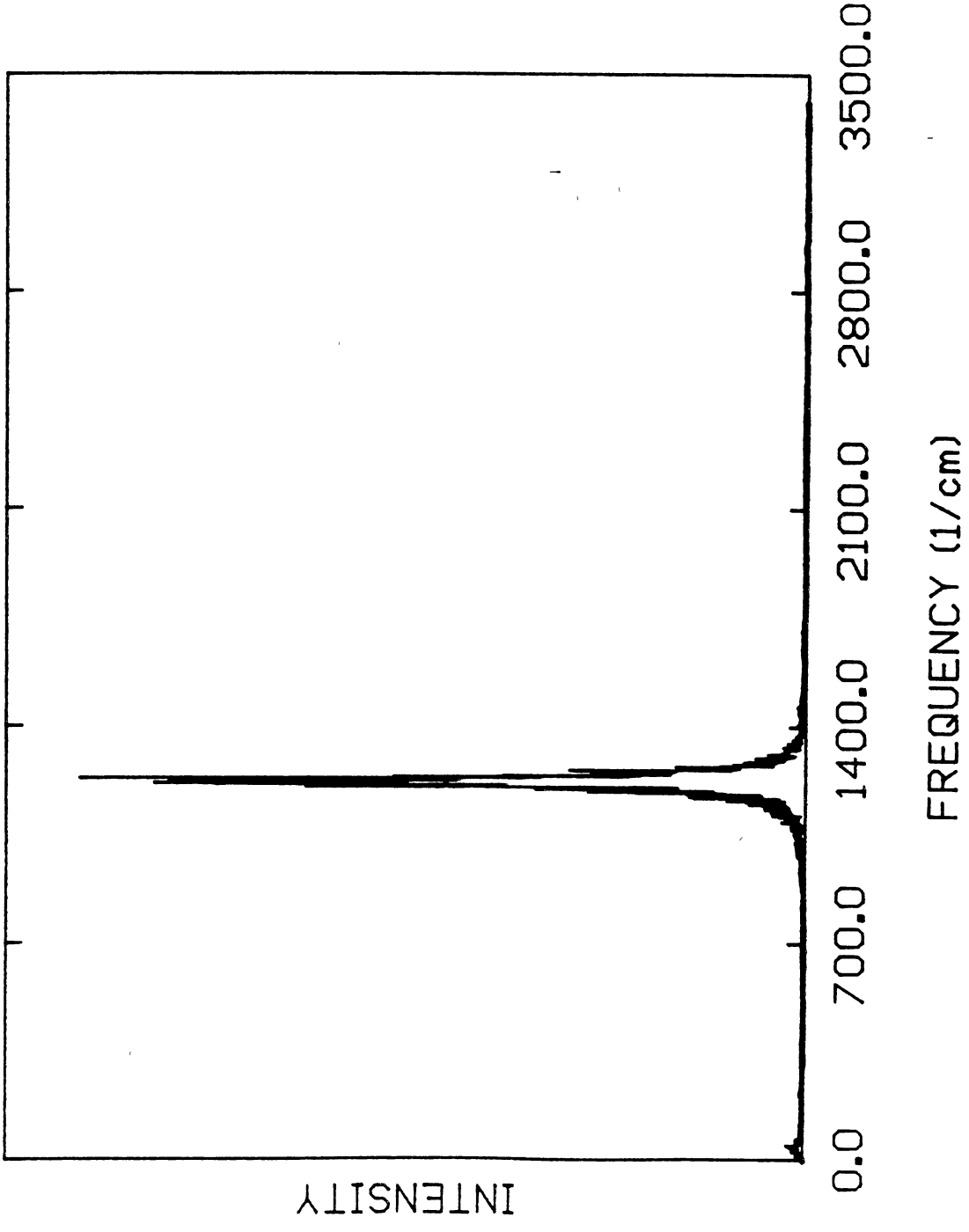
INTENSITY
0.0
700.0
1400.0
2100.0
2800.0
3500.0
FREQUENCY (1/cm)

Figure 98. Power spectrum for one of the H-C-H angles in nonrotating RDX vibrating with 160 kcal/mol of energy. The spectrum was obtained as the arithmetic mean of the spectra for five independent trajectories.

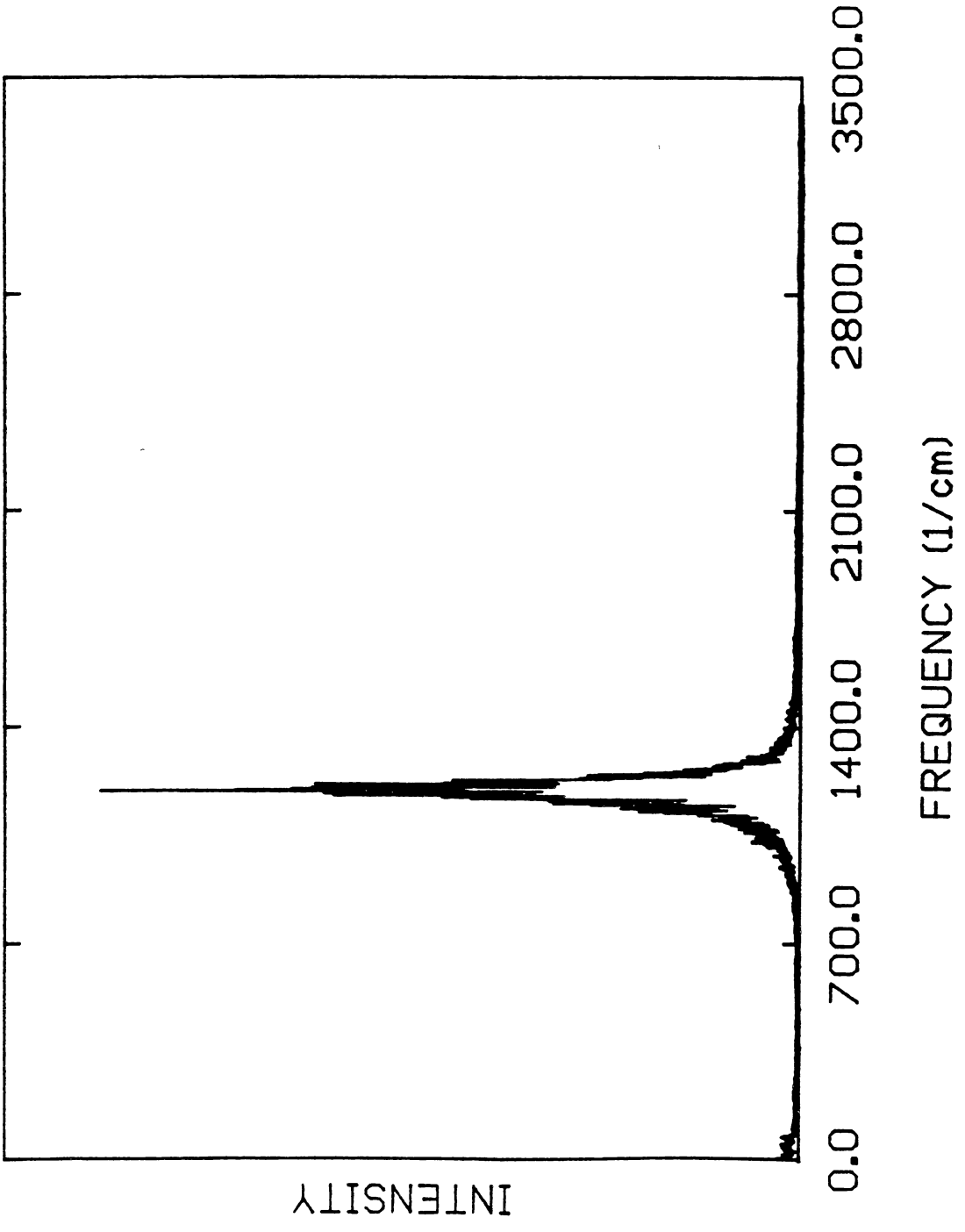
INTENSITY
0.0
700.0
1400.0
2100.0
2800.0
3500.0
FREQUENCY (1/cm)

Figure 99. Power spectrum for one of the H-C-H angles in nonrotating RDX vibrating with 250 kcal/mol of energy. The spectrum corresponds to a single trajectory.

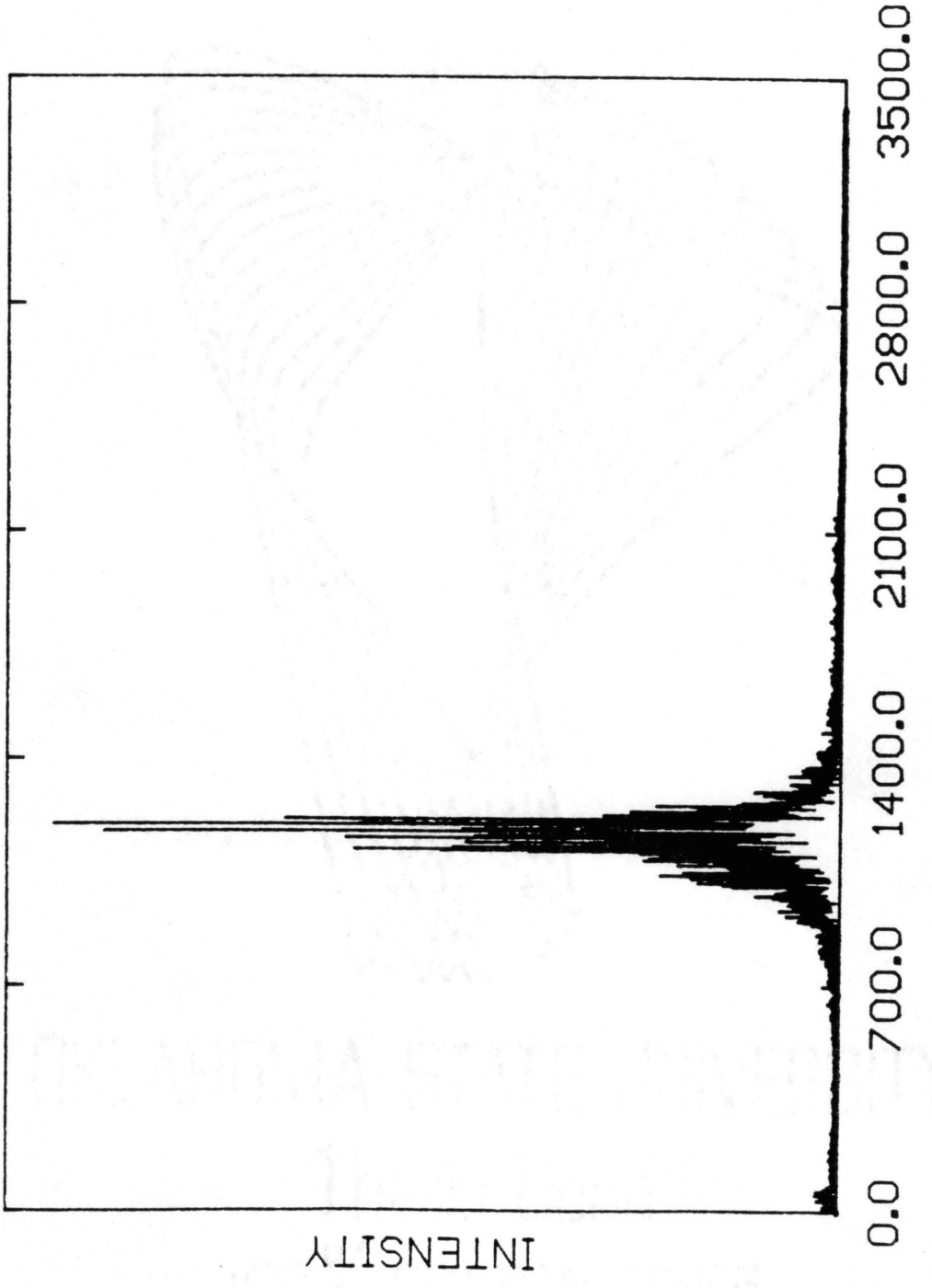
INTENSITY
0.0
700.0
1400.0
2100.0
2800.0
3500.0
FREQUENCY (1/cm)

Figure 100. Power spectrum for one of the H-C-H angles in nonrotating RDX vibrating with 350 kcal/mol of energy. The spectrum corresponds to a single trajectory.

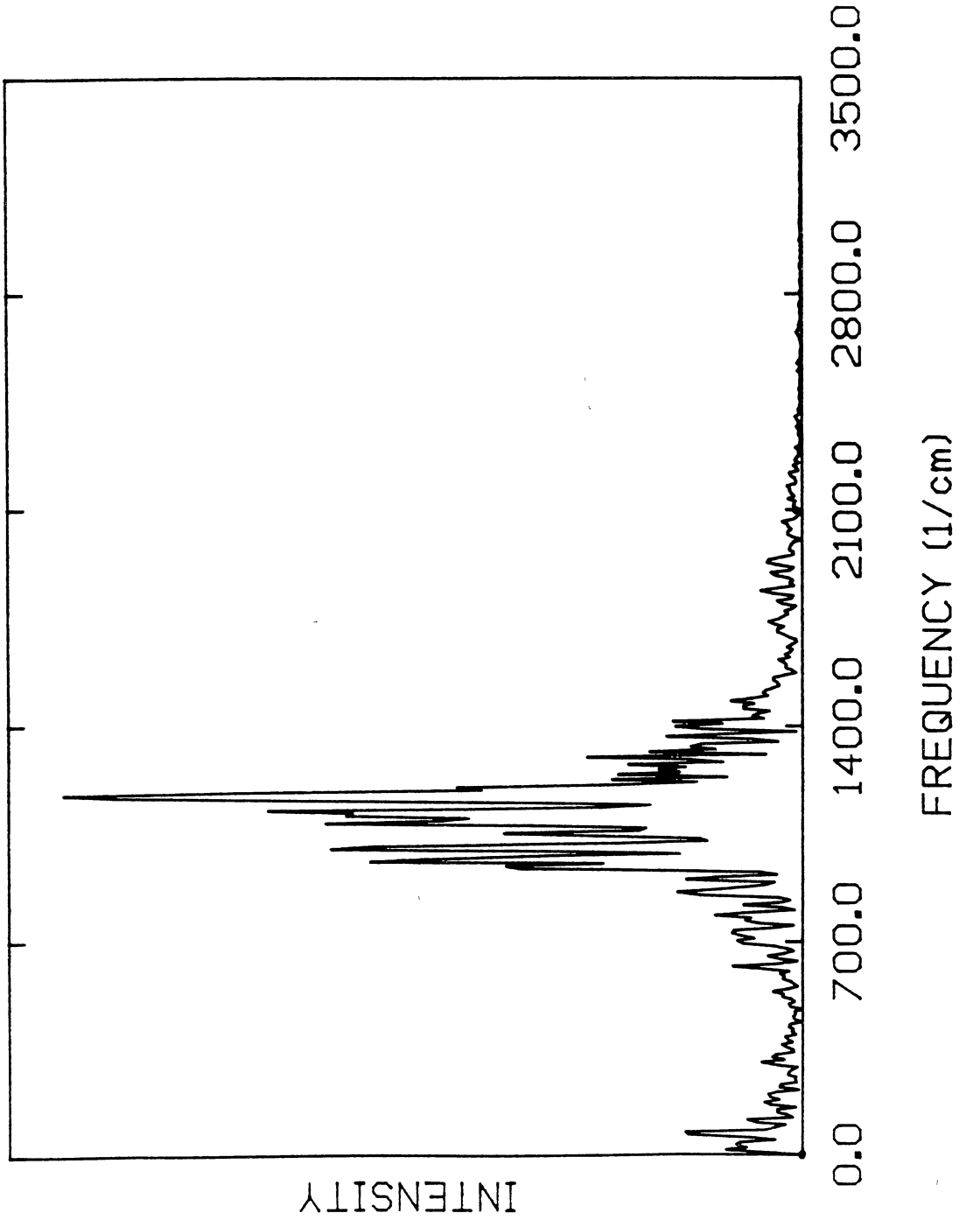
INTENSITY
0.0
700.0
1400.0
2100.0
2800.0
3500.0
FREQUENCY (1/cm)

Figure 101. Power spectrum for one of the N-O bonds in nonrotating RDX vibrating with 0.15 kcal/mol of energy. The spectrum corresponds to a single trajectory.

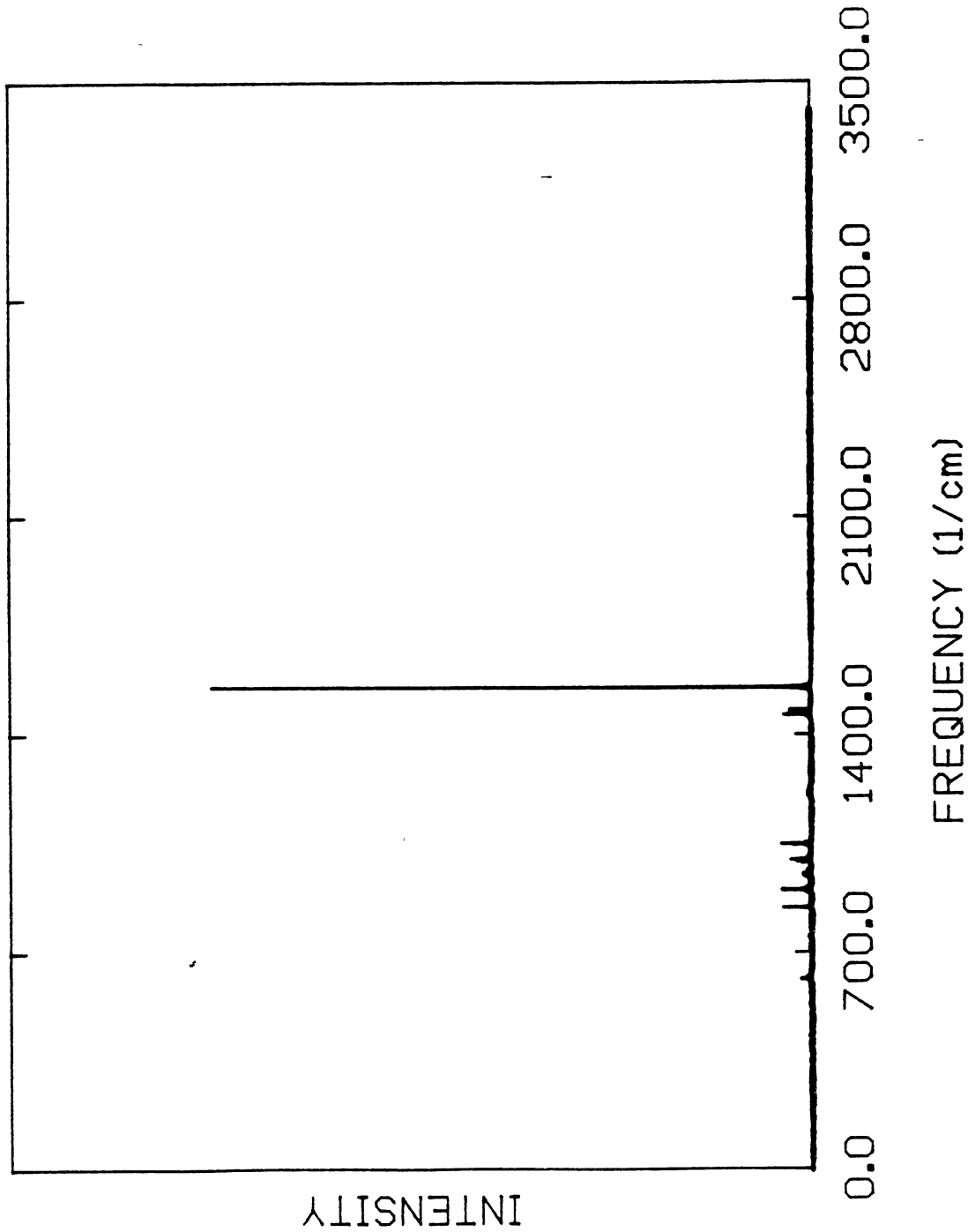
INTENSITY
0.0
700.0
1400.0
2100.0
2800.0
3500.0
FREQUENCY (1/cm)

Figure 102. Power spectrum for one of the N-O bonds in nonrotating RDX vibrating with zero-point energy. The spectrum was obtained as the arithmetic mean of the spectra for three independent trajectories.

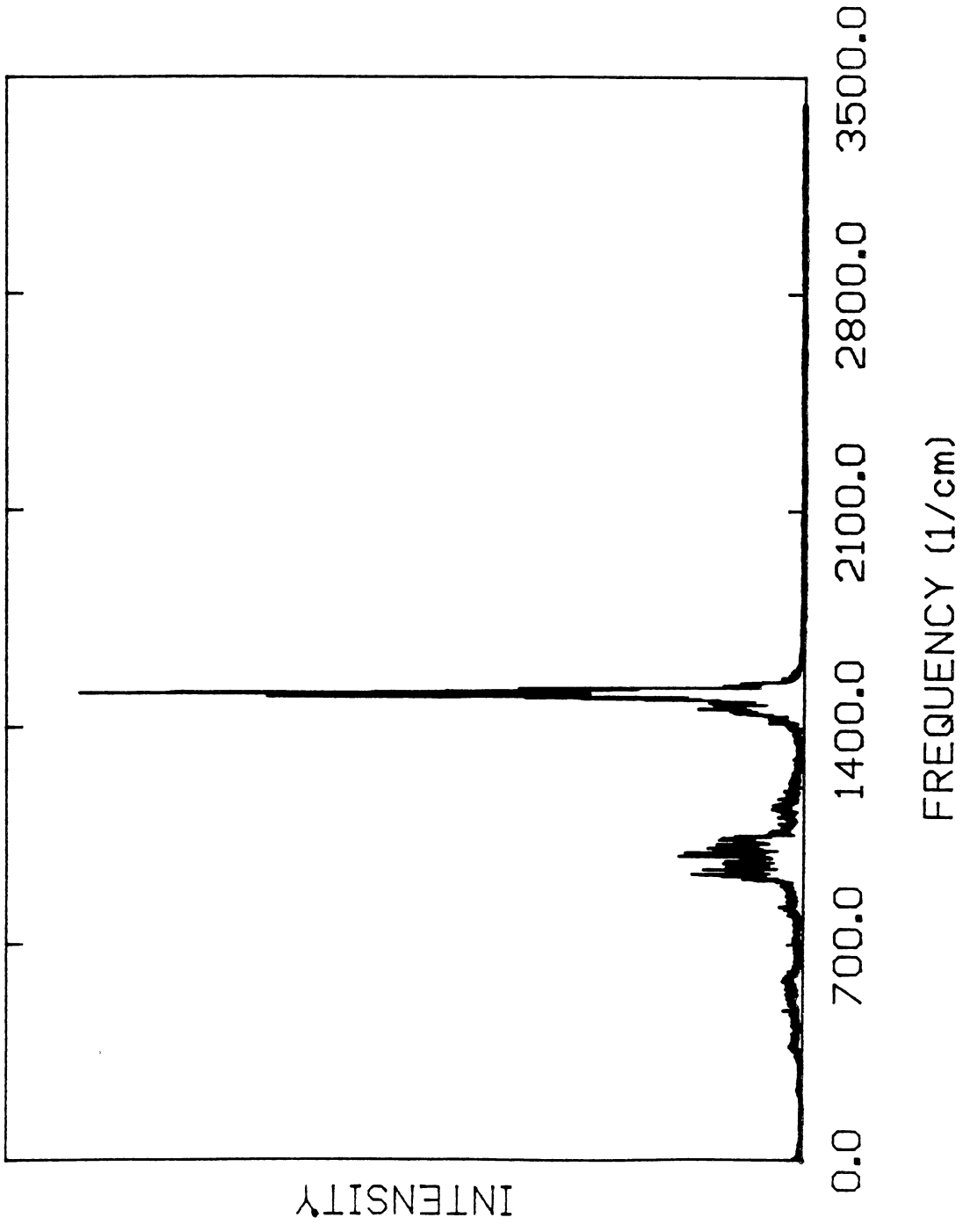
INTENSITY
0.0
700.0
1400.0
2100.0
2800.0
3500.0
FREQUENCY (1/cm)

Figure 103. Power spectrum for one of the N-O bonds in nonrotating RDX vibrating with 160 kcal/mol of energy. The spectrum was obtained as the arithmetic mean of the spectra for five independent trajectories.

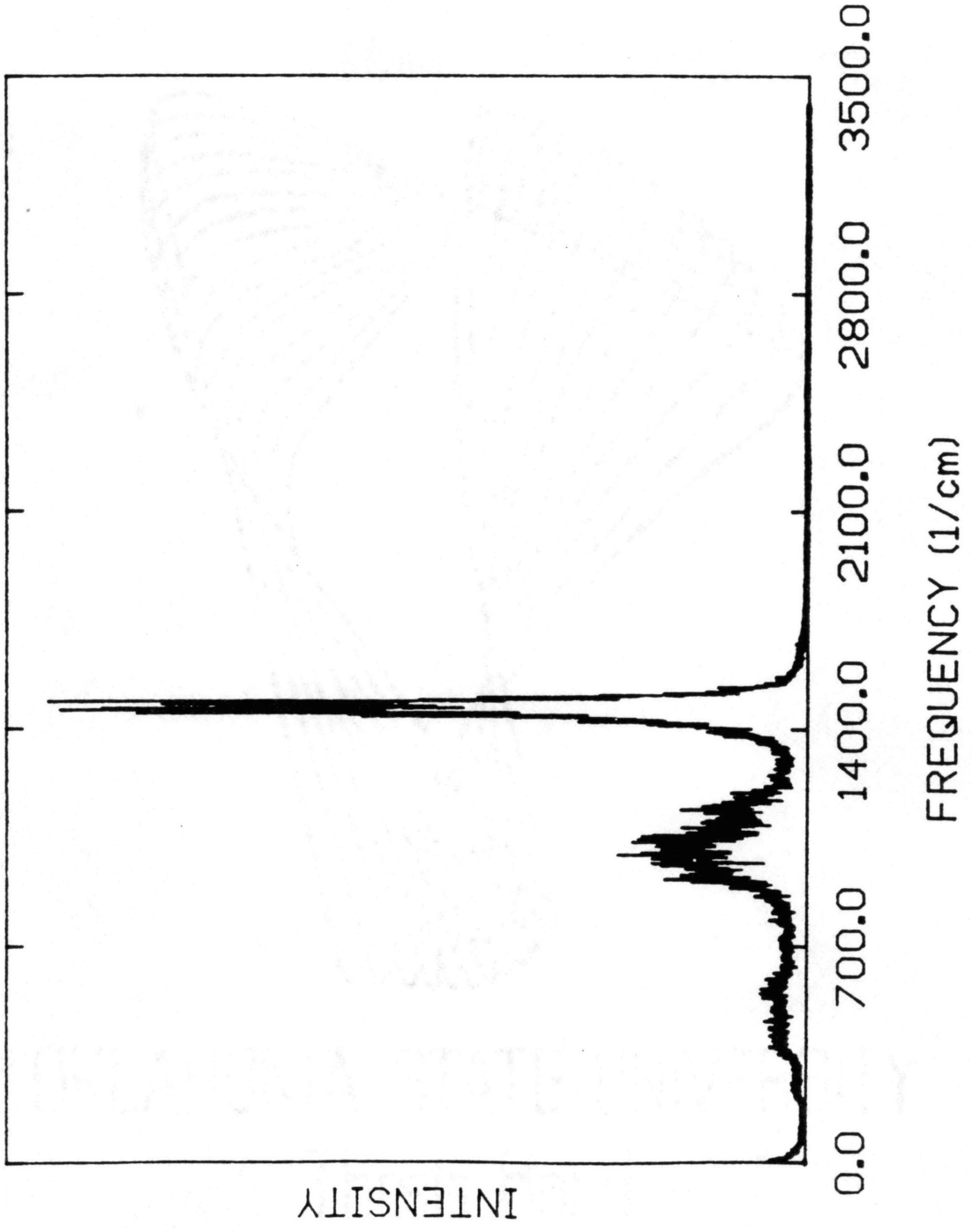
INTENSITY
0.0
700.0
1400.0
2100.0
2800.0
3500.0
FREQUENCY (1/cm)

Figure 104. Power spectrum for one of the N-O bonds in nonrotating RDX vibrating with 250 kcal/mol of energy. The spectrum corresponds to a single trajectory.

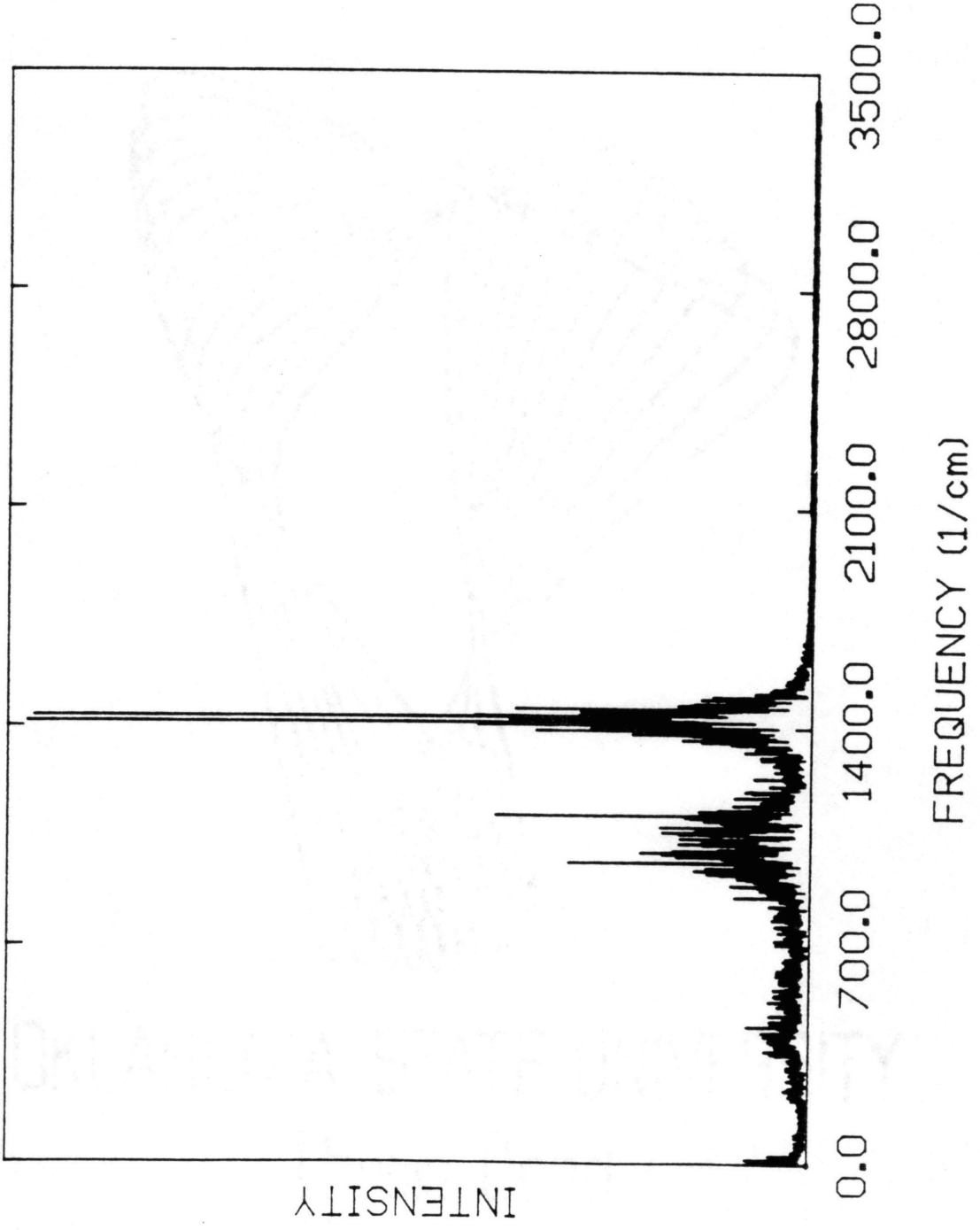
INTENSITY
0.0
700.0
1400.0
2100.0
2800.0
3500.0
FREQUENCY (1/cm)

Figure 105. Power spectrum for one of the N-O bonds in nonrotating RDX vibrating with 350 kcal/mol of energy. The spectrum corresponds to a single trajectory.

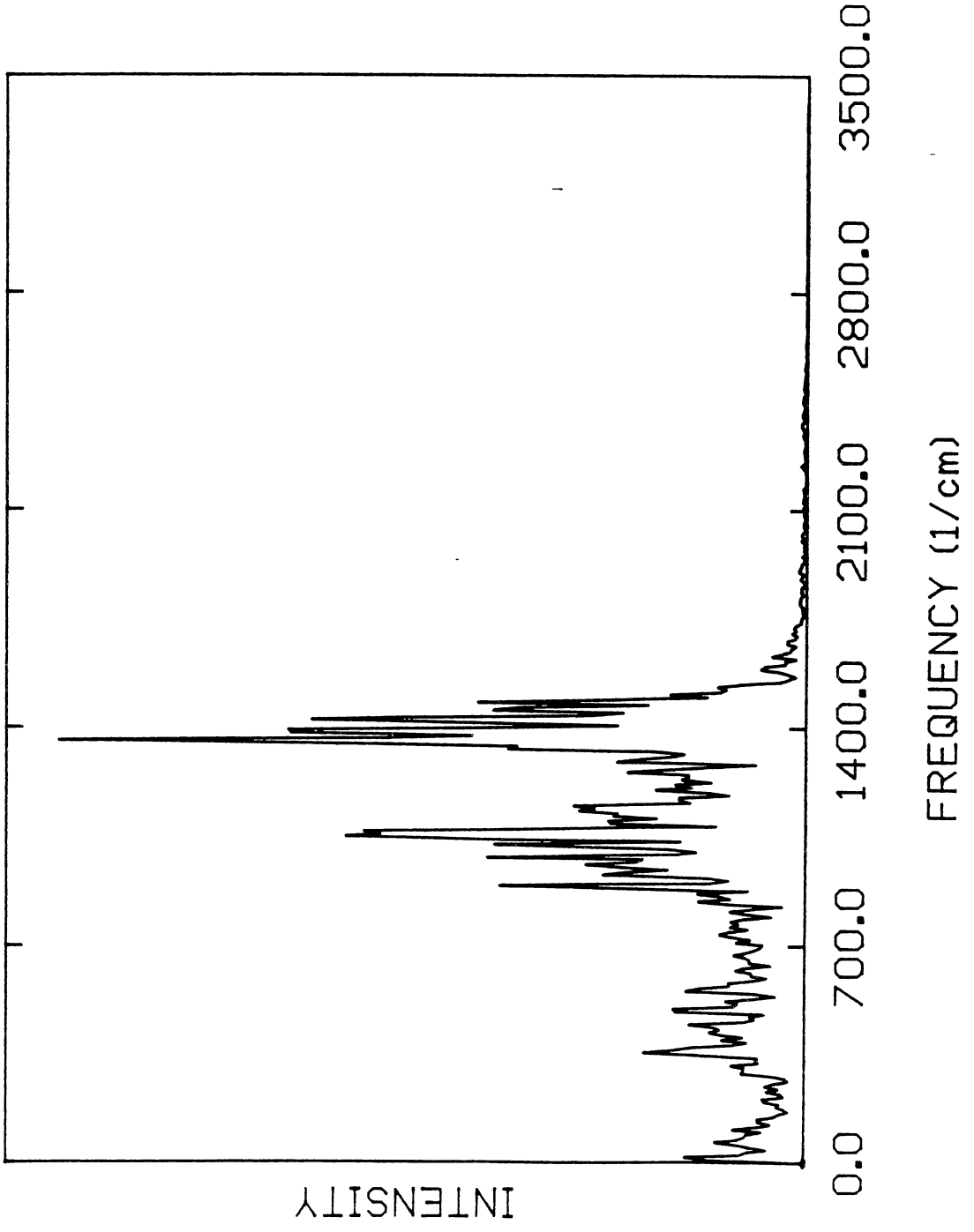
INTENSITY
0.0
700.0
1400.0
2100.0
2800.0
3500.0
FREQUENCY (1/cm)

correspond to total energies of 0.15, 78, 160, 250, and 350 kcal/mol, respectively. It is apparent that the clean structure in the spectra computed at 0.15, 78, and 160 kcal/mol becomes more and more congested as the energy approaches and exceeds 250 kcal/mol. Although the bands are still primarily localized about single maxima, the widths of the bands are becoming quite large (for example, the HCH band in Fig. 100 spans some 500 cm^{-1}). The spectrum of the NO bond stretching coordinate contains a second band (centered about 1000 cm^{-1}); the intensity increases relative to the fundamental band as the energy increases. Other individual internal coordinate spectra such as the NO_2-NO_2 Lennard-Jones interaction and the C-H modes (not shown) behave qualitatively the same as the HCH spectra. A number of the internal coordinate spectra are similar to the NO bond stretch in that, while they do begin to undergo significant broadening and new peaks of appreciable intensity evolve as the energy increases, they still exhibit distinct behavior over the wide range of energies considered.

In general, the greatest change in the qualitative features takes place upon increasing the energy from 250 to 350 kcal/mol. *The IRMPD experiments correspond to energies near 160 kcal/mol, where the spectra are well resolved and quite similar to the spectra for zero-point energy trajectories.*

Discussion

A few comments are in order concerning how to interpret the spectra. The power spectra computed for individual trajectories (at the lower energies where the dynamics are nonchaotic) do not differ significantly from one trajectory to another. They are similar in band locations, widths and, to a large extent, relative intensities within the spectrum. Thus, the features found in the averaged spectra are all present in those for individual trajectories (not shown). The major consequence of averaging over small ensembles is to decrease "noise" in the spectra. Dumont and Brumer[407] have

shown that it is not possible to make an unequivocal statement as to whether a given system is regular or chaotic based on power spectra of individual trajectories of finite duration. They proved this point analytically and additionally supplied numerical demonstrations. As an example, they computed two long trajectories and corresponding power spectra for the Hénon-Heiles Hamiltonian[242] in the chaotic regime, starting from initially adjacent points in phase space. The resulting spectra differ significantly. Thus, although the similarities we find between individual finite length trajectories do not *prove* that the underlying dynamics are nonchaotic, they do seem to argue that they are, especially given the complexity of the RDX molecule.

Taylor, Llorente, Pollak and co-workers[233-238,408-409] have developed methods for extracting useful information from apparently chaotic spectra. The main focus on their work has been directed towards gaining a theoretical understanding of experimental studies of the spectroscopy of highly excited molecules (such as are produced in stimulated emission pumping (SEP) experiments). They have been able to identify structure embedded within seemingly "chaotic" systems (e.g., H_3^+,[234-326] Na_3,[238] HCN,[409] and C_2H_2[233]) and have coined the term "reduced dimensional tori" in their explanation of the phenomena. The qualitative point that we are trying to make here is partially substantiated by the results of their very detailed investigations in that they are able to identify regular dynamics even when the power spectra are very "grassy".

It is not really surprising that the spectra tend to be so "regular" at "high" energies, given the fact that the seemingly large excitation energies are distributed over 9 to 57 degrees of freedom. For example, since there are 57 vibrational modes in RDX, this leads to less than 1.4 kcal/mol per degree of freedom for the zero-point energy level. The corresponding number at 160 kcal/mol is 2.8 kcal/mol. Thus, excitation of the RDX molecule to the energies attainable in IRMPD experiments only increases the average energy per mode by a factor of two. By contrast, the addition of 80 kcal/mol of

similar quantity to a three atom molecule can increase the average energy per mode by as much as an order of magnitude. This would be expected to exert a large influence on the dynamics (which makes the behavior of SiF_4 particularly interesting). Of course, there is not a uniform partitioning of energy among the vibrational modes (The high frequency modes involving significant hydrogen motion tend to retain more energy than do the low frequency, heavy-atom modes.). However, this fact bolsters our argument concerning the low energy per mode since the CH modes will tend to serve as "energy reservoirs" and effectively decrease the energy content of the low energy modes (which are usually more intimately involved with the reaction coordinate).

If the dynamics of large, highly excited polyatomic molecules will behave nonchaotically then, under favorable conditions, it may be possible to effect nonstatistical behavior in chemical reactions. Briefly, if one can somehow associate a band in the spectrum with a mode (the "activation coordinate") that couples strongly with some other mode (the "reaction coordinate") but not with other modes (for instance by overlap of two "localized" bands in an otherwise sparse region of the spectrum) then it may be possible to enhance the rate of reaction. Alternatively, if one can excite modes that must transfer energy "through" the reaction coordinate in order to relax (as in the methyl hydroperoxide[98-99]), then it may be possible to enhance the rate of reaction. Presumably, the coordinates needed to describe such "modes" will require considerably more work than just choosing the internal coordinates based on casual examination of power spectra, but the kernel of the idea should remain more or less intact upon taking a more sophisticated approach to selecting which modes to excite.

We have generated some tentative results for RDX that suggest that this may be true. In Table XXX we compare the results for three different excitations at a total energy of 350 kcal/mol. The excitations correspond to random microcanonical sampling

Table XXX. Rate Coefficients[a] for RDX Dissociation at 350 kcal/mol

Excitation	k_{ring}	k_{NN}	Ensemble Size
Microcanonical[b]	0.67	0.66	563
"Ring"[c]	0.62	0.59	600 (3 x 200)
"NO_2"[c]	0.50	0.82	600 (3 x 200)

a. Rates are in ps^{-1}.
b. Taken from Chapter VI.
c. See Table XXXI.

Table XXXI. Normal-mode Excitations Used in Trajectory Calculations.[a]

Ring Mode Excitation		NO_2 Mode Excitation	
Frequency (cm^{-1})	Quantum Number	Frequency (cm^{-1})	Quantum Number
50	35	355	10
55	35	355	10
55	35	416	10
219	30	421	10
219	30	421	10
720	15	436	10
720	15	1496	6
759	10	1543	8
760	10	1543	8
760	10	1554	8
1039	4	1556	8
1039	4	1556	8
1043	4		
1046	4		
1270	4		
1272	4		
1272	4		

a. The partitioning for other energies was accomplished by dividing the energy (in excess of the zero point) in the same proportions as was done for the case above.

(see Chapters II and VI) and the mode-selective excitations given in Table XXXI. Five hundred trajectories were computed starting from random initial conditions. Six hundred trajectories were computed for both the "ring" and "NO_2" excitations. Our hope was that the latter excitation would lead to an enhanced rate of dissociation of the N-N bond. The calculated results indicate that there may be a small mode-specific effect due to selective excitation of the NO_2 modes. The overall dissociation rates are 1.33, 1.21, and 1.31 ps^{-1} for microcanonical, "ring", and "NO_2" excitation, respectively. Thus, the total rate of dissociation is not significantly affected by the various excitation schemes considered. However, the branching ratios (k_{ring}/k_{NN}) do appear to be somewhat sensitive to the means of excitation. The branching ratio for microcanonical excitation is 1.02. That for "ring" excitation is 1.05. They are obviously in close agreement. The branching ratio resulting from "NO_2" excitation is 0.61. There is a factor of about 1.7 in the branching ratios resulting from microcanonical (and "ring") excitation to the value obtained for "NO_2" excitation. While this is certainly not a "dramatic" demonstration of mode-specific reaction, it does suggest that there may be a small nonstatistical effect in the rates.

Conclusions

We have used power spectra to demonstrate that the vibrational dynamics of several polyatomic molecules are largely nonchaotic. Several distinct bands are identified in the vibrational spectra of the molecules, and a number of these can be attributed to simple combinations of internal coordinate displacements. The bands are found to be relatively robust over a wide range of energies. An extreme example is provided by SiF_4,where the spectra for the bending modes remain highly defined even for energies in excess of the dissociation energy. An opposite extreme is observed in the case of C_2H_4 where the dynamics are apparently chaotic at 155 kcal/mol. The

qualitative differences in these two limiting cases are clearly manifested in the power spectra and also in the autocorrelation functions of the individual coordinates.

In the case of RDX, spectra computed for energies (160 kcal/mol) comparable to those probed in recent gas-phase IRMPD experiments are very similar to those at the vibrational zero-point energy. In contrast to reported results for small molecular systems, the dynamics of unimolecular dissociations of large molecules are likely to be nonchaotic.

CHAPTER VIII

ON SOME PROBLEMS OF CORRECTING THE ZERO-POINT ENERGY PROBLEM IN CLASSICAL TRAJECTORIES

Introduction

Classical trajectories have been, and continue to be, crucial in the evolution of our understanding of chemical dynamics. Classical simulations are feasible for many problems where quantum treatments are not and, fortunately, many chemical processes occur under conditions where the classical approximation is valid. However, we are still faced with the fact that real systems are quantum mechanical and there are many situations where classical trajectories fail. A serious problem is the failure to conserve zero-point energies. Various approaches have been tried to correct this problem.[43-47,195,420] We raise the question of whether it is possible to "fix" the zero-point energy problem without altering the dynamics such that more or equally serious aphysical behavior is introduced.

Some studies have been done to determine the contribution of the zero-point energy to reaction rates in classical studies by including only a fraction of the zero-point energy of the molecule.[43,45,195] Guan *et al.*[45,195] used this approach in studies of the near-threshold overtone-excitation induced photodissociation of H_2O_2. In their calculations, zero-point energy combined with excitation of an OH local mode to $v_{OH} = 5$ resulted in a total energy in excess of the barrier to O-O bond fission. However, excitation of $v_{OH} = 5$ alone provides insufficient energy to traverse the barrier

(*thermally-assisted*, single-photon overtone-induced photodissociation experiments pumping $v_{OH} = 5$ have been performed by Crim and co-workers[317,318]). Guan *et al.* found that there was a significant dependence of the classically calculated dissociation rates on the amount of zero-point energy. However, they found that mode-specific effects are qualitatively the same for various amount of zero-point energy: That is, various internal distributions of energy in excess of the "zero-point level" yield qualitatively similar behavior as the fraction of the zero-point energy is varied.

Lu and Hase[43] studied the effect of zero-point energy in calculations of the linewidth of C-H overtones following excitation of a C-H local mode in benzene. They considered cases in which they added a fraction of the zero-point energy ($0 \le f_{zpe} \le 1$) to the modes of the system and in which they excluded zero-point energy from selected normal modes. The calculated linewidth was less than 1.0 cm^{-1} for $f_{zpe} = 0$, regardless of which overtone state was sampled. Using $f_{zpe} = 0.04$ gave results in good agreement with experiments for the n=3 state. Larger values of f_{zpe} yielded linewidths an order of magnitude larger than experimental values. They found that excluding zero-point energy from seven normal modes having strong CCH bend character (with zero-point energy in the 14 remaining modes) had a significant effect on the linewidth, decreasing the value by a factor of 3 to 5 (relative to results obtained with all the zero-point energy present), depending on which overtone was excited. By contrast, excluding zero-point energy from the other 14 normal modes but adding it to the seven CCH modes gave results in near agreement with the full-ZPE case, except for higher overtone excitations. Lu and Hase suggest that one promising way to assign "zero-point energy" is to use the Wigner distribution as a means of selecting initial energies for unexcited modes since it is theoretically based and leads to a most probable classical "zero-point energy" of zero.

Lu and Hase[420] also considered the effects of decreasing the number of degrees of freedom in the system in an effort to reduce the effects of aphysical classical energy

flow. In particular, they extracted portions of the force field for the planar benzene molecule (C_6H_6) to yield force fields for two fragments (C_3H and C_3H_3) and compared linewidths for the two fragments with experimental measurements. The effect of doing so was to decrease the total energy content of the system and change the intramolecular couplings. They found that the overtone linewidths in the fragments were in considerably better agreement with the experimental measurements for benzene excited to the corresponding state.

Another possible route to understanding the effects of zero-point energy flow in classical trajectory calculations is illustrated by the work of Nyman and Davidsson[44] on the exchange reaction $O(^3P) + OH(^2\Pi)$ ----> $O_2(^3\Sigma^-_g) + H(^2S)$. They started with "all-or-none" of the vibrational zero-point energy in the $OH(^2\Pi)$ vibration , and then selectively "threw out" trajectories which did not satisfy predefined criteria regarding zero-point energy in the reaction products [$O_2(^3\Sigma^-_g)$ or, in the case of unreactive scattering, $OH(^2\Pi)$]. These criteria span a hierarchy of degrees to which zero-point energy flow is tolerated. They range from retaining all trajectories regardless of the final vibrational energy to retaining only those trajectories that had at least the zero-point energy. The results showed a strong dependence on which scheme of categorizing the trajectories is employed. The treatment that yields the best agreement between the calculated and experimental results depends upon what properties are being compared.

These examples serve to exemplify "passive" methods for dealing with the zero-point energy problem and also illustrate the effects of zero-point energy flow. They are based on the idea of allowing the trajectories to evolve according to the classical equations of motion. By contrast, an "active" method for controlling the flow of zero-point energy during the course of individual trajectories has been proposed simultaneously by Bowman, Gazdy, and Sun[46] and Miller, Hase, and Darling[47]. The approach by Bowman *et al.* is encompassed in that of Miller *et al.* The gist of the both

methods is that, so long as none of the (assumed separable) mode energies in a system fall below the zero-point level, it should be allowed to evolve according to the classical equations of motion. However, if one of the mode energies falls below the zero-point, an external, instantaneous force is applied so as to exactly reverse the velocity in that mode. If the kinetic energy is diagonal, then the total energy will be conserved.

Bowman *et al.*[46] used the Hénon-Heiles Hamiltonian to show that regions of phase space corresponding to individual mode energies having less than zero-point energy are, in fact, unavailable to trajectories in which the momentum reversal constraint is applied. Miller *et al.*[47] considered a general treatment more germane to "real" systems. They proposed that, for sufficiently small energies, one can use the equilibrium normal modes as a basis for determining whether a particular mode is in a state consistent with the zero-point energy requirement. That is, a trajectory can be computed in Cartesian phase space and the vibrational normal-mode energies (based on the equilibrium geometry of the molecule) monitored until the energy of a mode falls below the corresponding zero-point level and then the velocity of that normal mode is reversed. A new set of Cartesian momenta are obtained by back transformation and the trajectory is continued. They applied this method to a collinear HC_4 "molecule".

Miller *et al.*[47] further generalized their method to deal with zero-point energy in highly excited (e.g., reactive) systems. The more general version is quite similar to the simple approach except that, rather than computing the normal-mode energies using the equilibrium Cartesian coordinates as a basis, the instantaneous normal modes at configuration $\mathbf{q}(t)$ are computed at each step of the trajectory and used as a basis for determining the instantaneous zero-point energy.

The point we address here is whether or not it is feasible to employ "active" constraints to deal with the zero-point energy problem. Thus, we have examined the effects of the approach of Miller *et al.* on the fundamental behavior of the dynamics.

And, we have considered a new approach that constrains the energy to be a constant in one or more harmonic modes (individually or collectively) by introducing nonholonomic constraints. Whereas the methods of Bowman *et al.*[46] and Miller *et al.*[47] effect an instantaneous reversal of the velocity in one of the zeroth-order modes (when the energy in that mode falls below the zero-point), our approach acts continuously on the system. We apply the method to the Hénon-Heiles Hamiltonian and make comparisons between the dynamics resulting from the unconstrained case and the constraining procedure of Bowman *et al.* and Miller *et al.*

Nonholonomic Constraints

We have used nonholonomic constraints to conserve harmonic mode energies in the Hénon-Heiles system. The method is similar to that used by Haile and Gupta[419] to constrain the kinetic energy of a system of particles to have a constant value (i.e., constant temperature).

We begin by writing the Hamiltonian of the system in the form:

$$H(p_1,p_2,\ldots,p_n,q_1,q_2,\ldots,q_n) = \sum_{i=1}^{n} H_i(p_i,q_i) + H'(q_1,q_2,\ldots,q_n), \qquad \text{(VIII.1)}$$

where

$$H_i(p_i,q_i) = \frac{1}{2}(p_i^2+\omega_i^2 q_i^2), \qquad i = 1, 2, \ldots, n \qquad \text{(VIII.2)}$$

are the uncoupled harmonic terms and $H'(q_1, q_2, \ldots, q_n)$ represents potential-energy couplings.

We wish to constrain the value of one (or more) of the uncoupled quantities, H_j, to some fixed value, α_j. We require that

$$\alpha_j = \frac{1}{2}\left[\left(\frac{dq_j}{dt}\right)^2 + \omega_j^2 q_j^2\right] \qquad \text{(VIII.3)}$$

and

$$\frac{d\alpha_j}{dt} = 0. \qquad \text{(VIII.4)}$$

Equations (VIII.3) and (VIII.4) are a nonholonomic constraint involving the coordinate q_j and its time derivative dq_j/dt.

For an isolated system of n particles interacting under the influence of a potential, $U(q_1,q_2,...,q_n)$, Lagrange's equations are

$$\frac{\partial L}{\partial q_i} - \frac{d}{dt}\left\{\frac{\partial L}{\partial\left(\frac{dq_i}{dt}\right)}\right\} = 0, \qquad i = 1, 2,..., n; \qquad \text{(VIII.5)}$$

where

$$L = \frac{1}{2}\sum_{i=1}^{n}\left(\frac{dq_i}{dt}\right)^2 - U(q_1, q_2, ..., q_n). \qquad \text{(VIII.6)}$$

A set of equations of motion that satisfy the constraint Eqs. (VIII.4) and (VIII.5) is obtained by introducing an external, generalized force into Eq. (VIII.5):

$$\frac{\partial L}{\partial q_i} - \frac{d}{dt}\left\{\frac{\partial L}{\partial\left(\frac{dq_i}{dt}\right)}\right\} = - F\left(q_i, \frac{dq_i}{dt}\right). \qquad \text{(VIII.7)}$$

A generalized potential $V=V\left(\mathbf{q}, \frac{d\mathbf{q}}{dt}\right)$ that satisfies

$$F(q_i,\frac{dq_i}{dt}) = -\frac{\partial V}{\partial q_i} + \frac{d}{dt}\left\{\frac{\partial V}{\partial\left(\frac{dq_i}{dt}\right)}\right\} \qquad \text{(VIII.8)}$$

allows us to define a new Lagrangian, L', as[277]

$$L' = L - V \qquad \text{(VIII.9)}$$

subject to

$$\frac{\partial L'}{\partial q_i} - \frac{d}{dt}\left\{\frac{\partial L'}{\partial\left(\frac{dq_i}{dt}\right)}\right\} = 0, \qquad i = 1, 2, ..., n. \qquad \text{(VIII.10)}$$

The boldface arguments are introduced as a convenience and represent the complete set of generalized coordinates and velocities $q_1, q_2, ..., q_n, \frac{dq_1}{dt}, \frac{dq_2}{dt}, ..., \frac{dq_n}{dt}$.

We write $V(\mathbf{q},\frac{d\mathbf{q}}{dt})$ as a product of a function $\eta(\mathbf{q},\frac{d\mathbf{q}}{dt})$ and parameter $\xi(\mathbf{q},\frac{d\mathbf{q}}{dt})$:

$$V(\mathbf{q},\frac{d\mathbf{q}}{dt}) = \eta(\mathbf{q},\frac{d\mathbf{q}}{dt})\,\xi(\mathbf{q},\frac{d\mathbf{q}}{dt}). \qquad \text{(VIII.11)}$$

By defining the generalized momenta, p_i, as

$$p_i = \frac{\partial L'}{\partial(dq_i/dt)} = \frac{\partial L}{\partial(dq_i/dt)} - \frac{\partial V}{\partial(dq_i/dt)}, \qquad i = 1, 2, ..., n \qquad \text{(VIII.12)}$$

and evaluating Eq. (VIII.10) we can obtain

$$\frac{dp_i}{dt} = -\frac{\partial U(\mathbf{q})}{\partial q_i} - \eta(\mathbf{q},\frac{d\mathbf{q}}{dt})\frac{\partial\xi(\mathbf{q},d\mathbf{q}/\partial t)}{dq_i} - \xi(\mathbf{q},d\mathbf{q}/dt)\frac{\partial\eta(\mathbf{q},d\mathbf{q}/dt)}{\partial q_i}. \qquad \text{(VIII.13)}$$

Direct evaluation of Eq. (VIII.12) gives

$$\frac{dq_i}{dt} = p_i + \eta(\mathbf{q},d\mathbf{q}/dt)\frac{\partial\xi(\mathbf{q},d\mathbf{q}/\partial t)}{\partial(dq_i/dt)} + \xi(\mathbf{q},d\mathbf{q}/dt)\frac{\partial\eta(\mathbf{q},d\mathbf{q}/\partial t)}{\partial(dq_i/dt)}. \quad \text{(VIII.14)}$$

Equations (VIII.4), (VIII.13), and (VIII.14) are the constrained equations of motion.

To this point we have not specified the form of $\eta(\mathbf{q},d\mathbf{q}/dt)$. Formally, we can let it be zero; for example,

$$\eta(\mathbf{q},d\mathbf{q}/dt) = \alpha_i - \frac{1}{2}\left[\left(\frac{dq_i}{dt}\right)^2 + \omega_i^2 q_i^2\right] = 0, \quad \text{(VIII.15)}$$

which is just the constraint Eq. (VIII.4). This results in a considerable simplification of the equations of motion:

$$\frac{dp_i}{dt} = -\frac{\partial U(\mathbf{q})}{\partial q_i} - \xi(\mathbf{q},d\mathbf{q}/dt)\frac{\partial\eta(\mathbf{q},d\mathbf{q}/dt)}{\partial q_i} \qquad \{\eta(\mathbf{q},d\mathbf{q}/dt) = 0\} \quad \text{(VIII.16)}$$

and

$$\frac{dq_i}{dt} = p_i + \xi(\mathbf{q},d\mathbf{q}/dt)\frac{\partial\eta(\mathbf{q},d\mathbf{q}/dt)}{\partial(dq_i/dt)} \qquad \{\eta(\mathbf{q},d\mathbf{q}/dt) = 0\}. \quad \text{(VIII.17)}$$

Choosing Eq. (VIII.15) as the form for $\eta(\mathbf{q},d\mathbf{q}/dt)$ allows direct evaluation of the derivatives

$$\frac{\partial\eta(\mathbf{q},d\mathbf{q}/dt)}{\partial(dq_i/dt)} \text{ and } \frac{\partial\eta(\mathbf{q},d\mathbf{q}/dt)}{\partial q_i}.$$

Substitution of the two derivatives into Eqs. VIII.16 and VIII.17 leads to

$$\frac{dq_i}{dt} = \frac{p_i}{1+\xi(\mathbf{q},d\mathbf{q}/dt)} \quad \text{(VIII.18)}$$

and

$$\frac{dp_i}{dt} = -\frac{\partial U(q)}{\partial q_i} + \xi(q,dq/dt)\omega_i^2 q_i. \qquad \text{(VIII.19)}$$

Finally, making use of Eq. (VIII.4) yields the final equations of motion:

$$\frac{dq_i}{dt} = \frac{p_i}{|p_i|}\sqrt{2\alpha_i - w_i^2 q_i^2} \qquad \text{(VIII.20)}$$

and

$$\frac{dp_i}{dt} = -\frac{\partial U(q)}{\partial q_i} + \omega_i^2 q_i \left\{ \frac{|p_i|}{\sqrt{2\alpha_i - w_i^2 q_i^2}} - 1 \right\} \qquad \text{(VIII.21)}$$

These equations are for *independent* constraints on individual harmonic mode energies. Thus, they are applied to each mode for which a constraint is desired. The method can be extended to constraining the total energy of k modes to be constant by replacing Eq. (VIII.4) with

$$\alpha = \frac{1}{2}\sum_{j=1}^{k} \left(\frac{dq_j}{dt}\right)^2 + w_j^2 q_j^2 \qquad \text{(VIII.22)}$$

and proceeding in a fashion analogous to that outlined above.

The Model

We have applied the constraints, those described above as well as the method proposed by Bowman *et al.*[46] and Miller *et al.*[47], to the Hénon-Heiles Hamiltonian,[242]

$$V(x,y) = \frac{1}{2}(p_x^2 + p_y^2 + \omega_x^2 x^2 + \omega_y^2 y^2) + x^2 y - \frac{1}{3} y^3, \qquad \text{(VIII.23)}$$

Figure 106. Contour map of the Hénon-Heiles potential-energy surface for the case $\omega_x = \omega_y = 1$. The limits on the axes are $-1.25 \leq x \leq 1.25$ and $-1.25 \leq y \leq 1.25$. The barriers occur at $E = 1/6$.

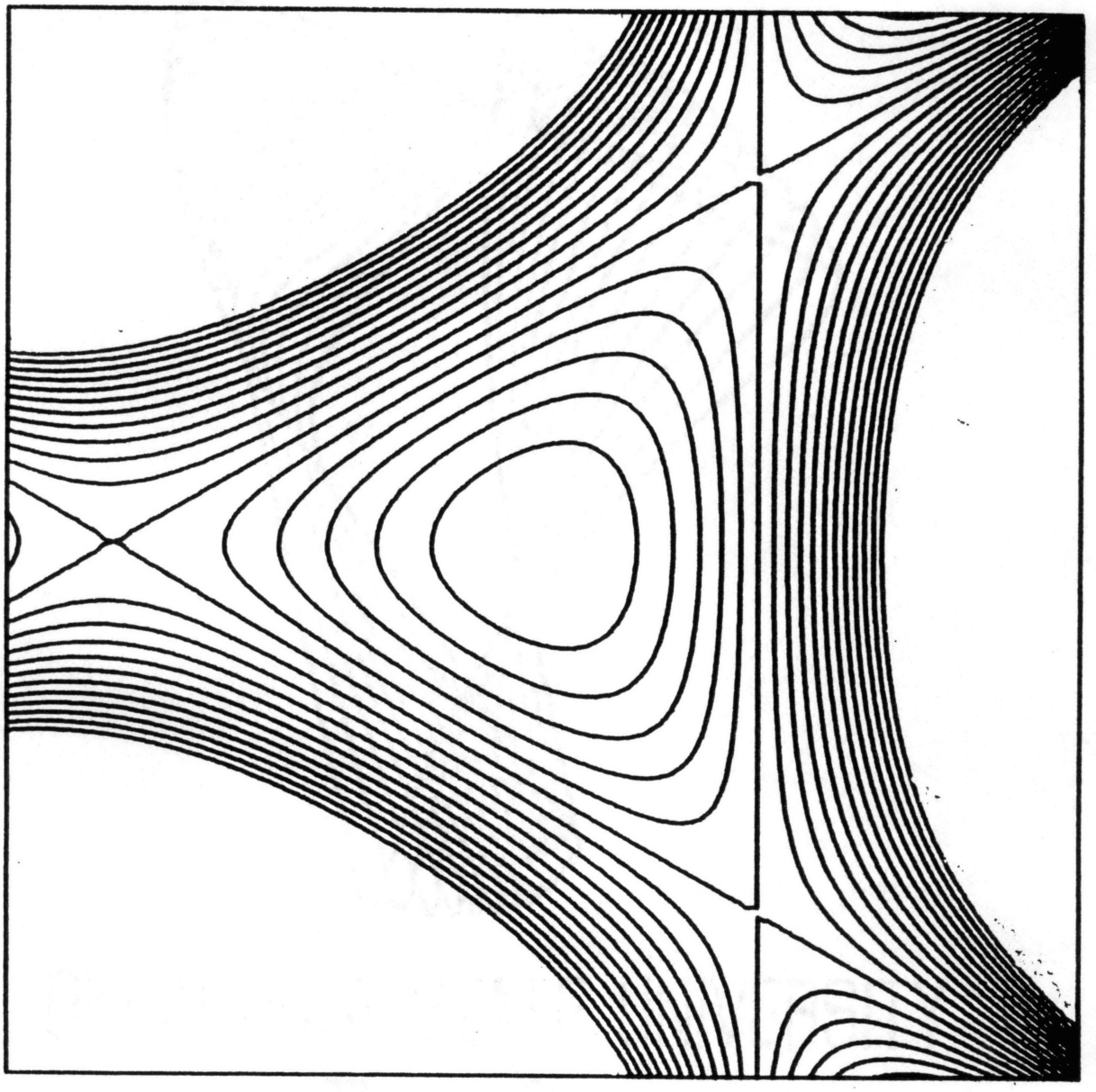

Figure 107. Contour map of the Hénon-Heiles potential-energy surface for the case $\omega_x = 2$, $\omega_y = 1$. The limits on the axes are $-1.25 \leq x \leq 1.25$ and $-1.25 \leq y \leq 1.25$. The barrier along the y axis occurs at $E = 1/6$.

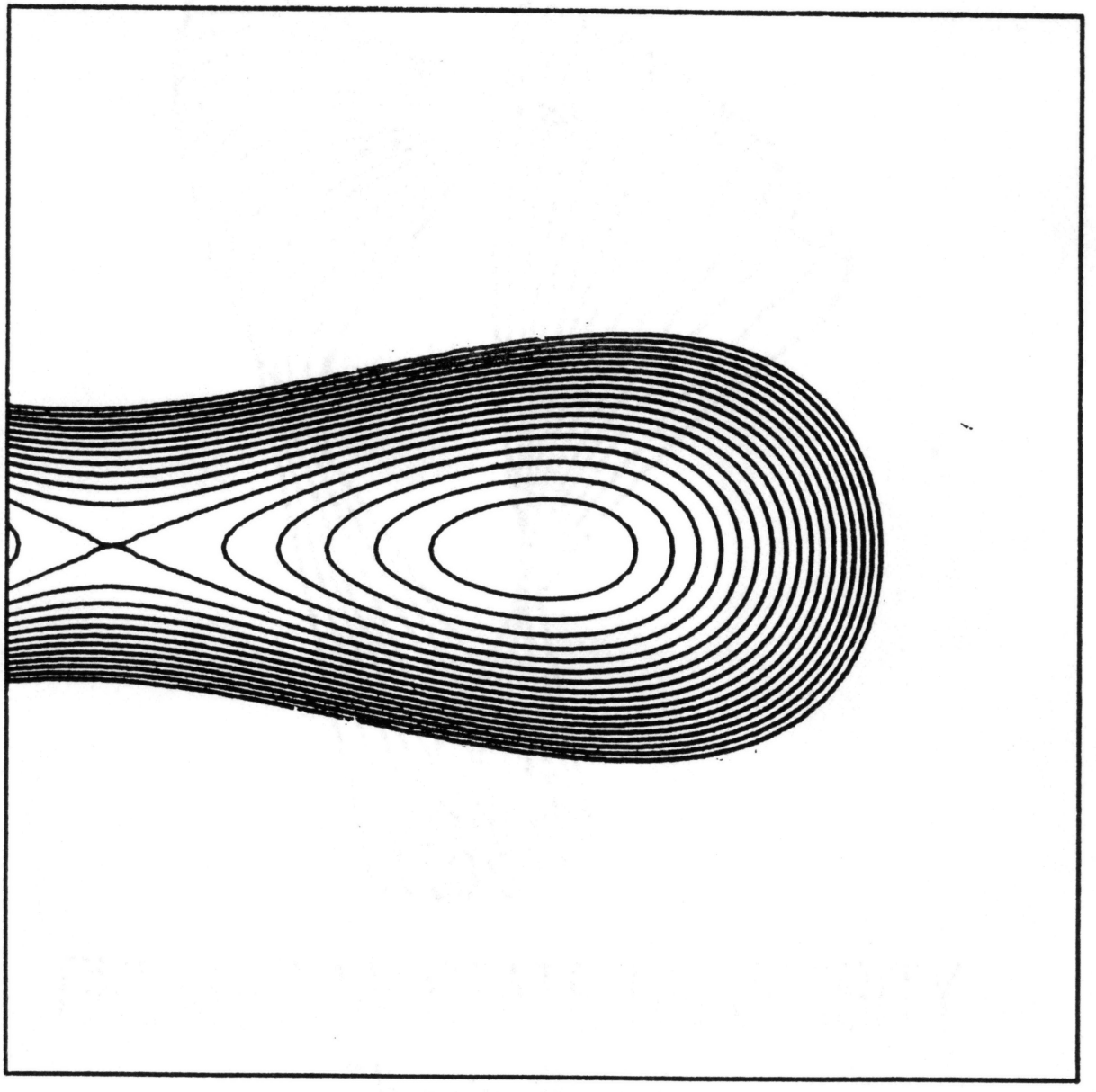

for cases with $\omega_x = \omega_y = 1$ and $\omega_x = 2$, $\omega_y = 1$. Contour plots of these two potentials are shown in Figs. 106 and 107, respectively. The potentials behave harmonically for low energies but become increasingly anharmonic for higher energies.

In order to partially assess the effects of the methods on the dynamics, the results of trajectories computed in the absence of any constraints are compared with those obtained using the nonholonomic constraint and with those resulting from the algorithm of Bowman *et al.*[46] Specifically, configuration-space plots, time histories of harmonic mode energies, and power spectra for trajectories started with identical initial conditions are compared.

Computational Details

Trajectory Integration

Trajectories were computed by numerically solving Hamilton's equation of motion for the case of unconstrained dynamics or the procedure of Bowman *et al.*[46] and Miller *et al.*[7] (Henceforth, we shall refer to the latter as "velocity-reversal".) or , in the case of the nonholonomic constraints, by solving Eqs. (VIII.20) and (VIII.21). In all cases the equations were solved using a fixed-stepsize fourth-order Runge-Kutta-Gill integrator. The time increment was $\Delta t = 0.005$ and 40,000 steps were computed per trajectory.

Initial Conditions

Initial conditions were selected by defining zero-point energies according to

$$E_{o,i} = \frac{1}{2}\hbar\omega_i, \qquad (i = x \text{ or } y) \qquad \text{(VIII.24)}$$

and then randomly selecting position coordinates and calculating velocities in accordance with Eq. (VIII.24) and the harmonic mode energies:

$$E_i = \frac{1}{2}p_i^2 + \frac{1}{2}\omega_i^2 i^2; \qquad (i = x \text{ or } y). \tag{VIII.25}$$

The value of $\hbar$ was treated as a variable parameter. (We note that Bowman *et al.*[46] included the separable cubic term appearing in Eq. (VIII.23) in their definition of E_y.) Identical initial conditions were used to compute trajectories for each of the three cases of interest, i.e., unconstrained, velocity-reversal constraints, and nonholonomic constraints..

Mode Energies

In the case of trajectories constrained using the velocity-reversal procedure, the harmonic mode energies were computed and compared with the zero-point energies after every twenty-fifth integration step. If either of the modes had an energy less than the zero-point then the velocity in that mode was reversed and the trajectory was continued. After the next twenty-five integration steps, the mode energies were computed again. If the mode energy that had fallen below the zero point was still less than the zero point, it was compared to the previous value. If $E_i(t) > E_i(t_{k-25})$ then no action was taken. If, on the other hand, $E_i(t_{k-25}) > E_i(t)$ then the velocity of that mode was once again reversed.

Results and Discussion

Configuration-space plots of trajectories computed at E = 0.095 for the case $\omega_x = 2$ and $\omega_y = 1$ are shown in Fig. 108; corresponding harmonic mode energies and power spectra are shown in Figs 109 and 110, respectively. The unconstrained

Figure 108. Configuration-space plots for trajectories having identical initial conditions but with different constraints on the energy flow. The results shown are for the case $\omega_x = 2$, $\omega_y = 1$ and a total energy of $E = 0.095$. Constraints are only applied to the x mode of the system. a) unconstrained trajectory; b) nonholonomic constraint, which forces the harmonic x mode to have a constant energy; c) velocity-reversal constraint, which prevents the x mode energy from falling below the zero-point level.

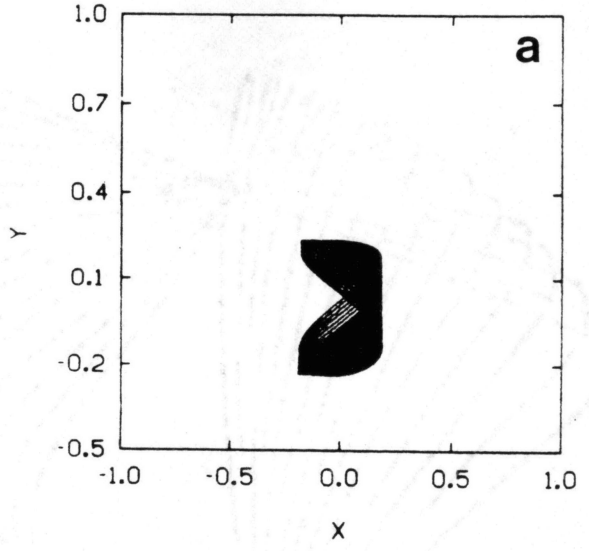
a
1.0
0.7
0.4
0.1
-0.2
-0.5
Y
-1.0
-0.5
0.0
0.5
1.0
X

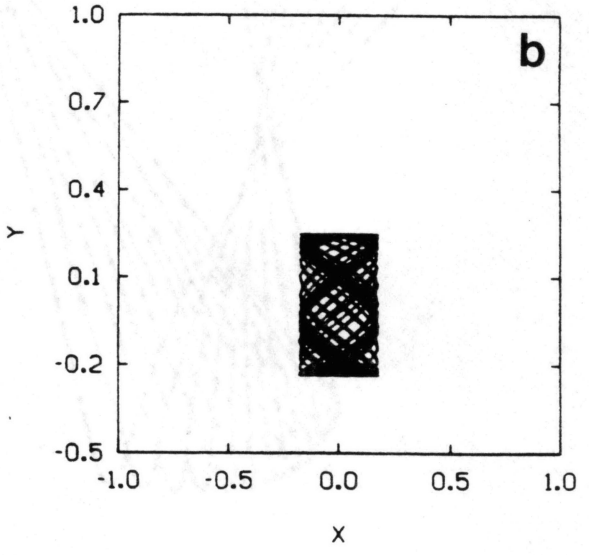
b
1.0
0.7
0.4
0.1
-0.2
-0.5
Y
-1.0
-0.5
0.0
0.5
1.0
X

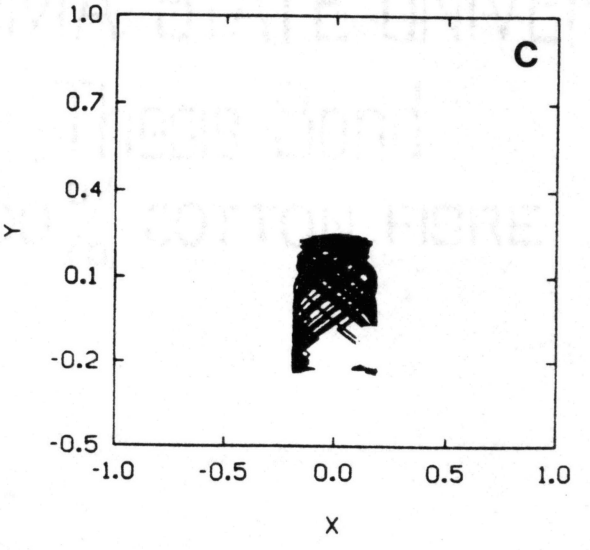
c
1.0
0.7
0.4
0.1
-0.2
-0.5
Y
-1.0
-0.5
0.0
0.5
1.0
X

Figure 109. Time histories of the harmonic mode energies for trajectories having identical initial conditions but with different constraints on the energy flow. The results shown are for the case $\omega_x = 2$, $\omega_y = 1$ and a total energy of $E = 0.095$. Constraints are only applied to the x mode of the system. a) unconstrained trajectory; b) nonholonomic constraint, which forces the harmonic x mode to have a constant energy; c) velocity-reversal constraint, which prevents the x mode energy from falling below the zero-point level.

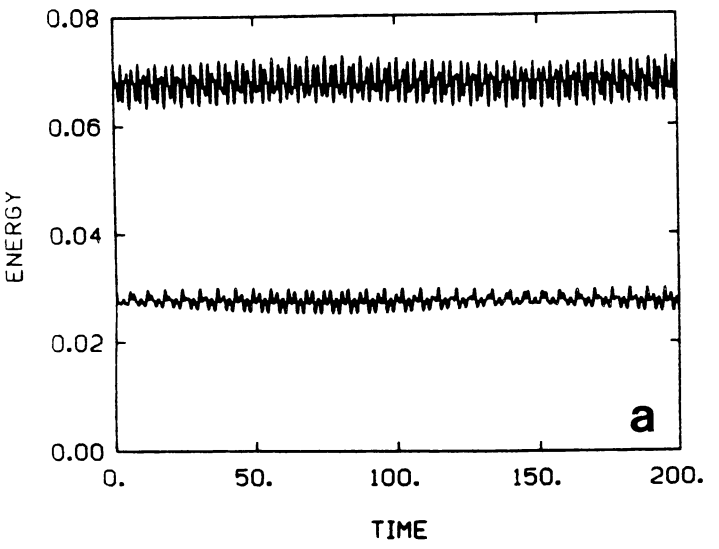
0.08
0.06
0.04
0.02
0.00
ENERGY
a
0.
50.
100.
150.
200.
TIME

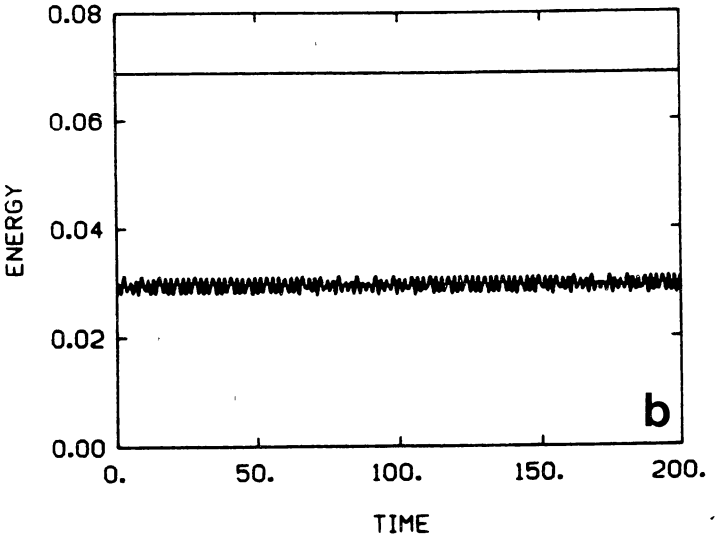
0.08
0.06
0.04
0.02
0.00
ENERGY
b
0.
50.
100.
150.
200.
TIME

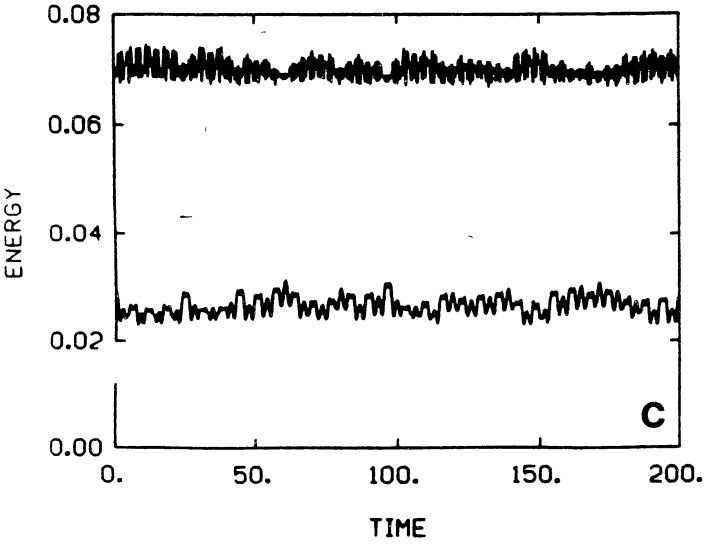
0.08
0.06
0.04
0.02
0.00
ENERGY
c
0.
50.
100.
150.
200.
TIME

Figure 110. Power spectra for trajectories having identical initial conditions but with different constraints on the energy flow. The results shown are for the case $\omega_x = 2$, $\omega_y = 1$ and a total energy of $E = 0.095$. Constraints are only applied to the x mode of the system. a) unconstrained trajectory; b) nonholonomic constraint, which forces the harmonic x mode to have a constant energy; c) velocity-reversal constraint, which prevents the x mode energy from falling below the zero-point level.

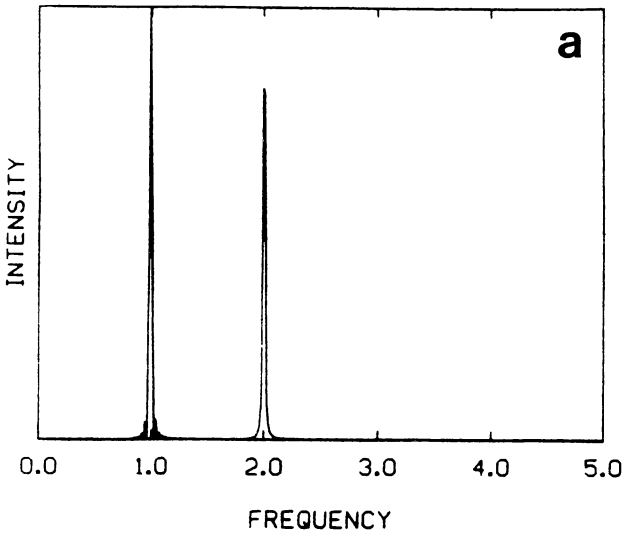
a
INTENSITY
0.0
1.0
2.0
3.0
4.0
5.0
FREQUENCY

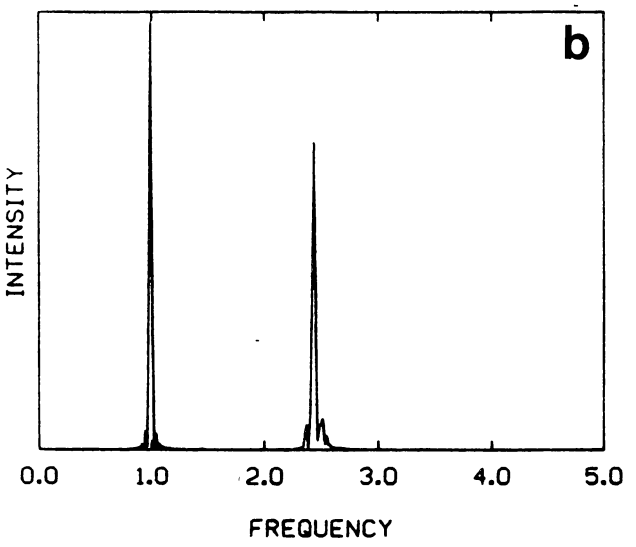
b
INTENSITY
0.0
1.0
2.0
3.0
4.0
5.0
FREQUENCY

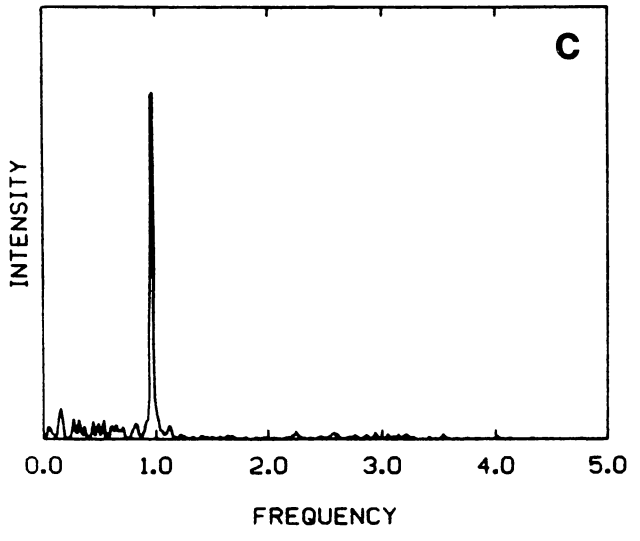
c
INTENSITY
0.0
1.0
2.0
3.0
4.0
5.0
FREQUENCY

trajectory results are shown in panel a of Figs. 108-110. Constrained results obtained by starting from identical initial conditions are shown in panels b for the case of the nonholonomic constraint; and in panels c and for the case of the velocity-reversal constraint. Only the x mode was constrained for the trajectories in frames b and c of Figs. 108 to 110. Recall that in the nonholonomic method the harmonic mode energy is required to be exactly constant, whereas in the velocity-reversal method the energy in the x mode will only be prevented from falling below the "zero-point" value. The unconstrained trajectory is quite regular in appearance (Fig. 108a). The trajectory constrained using the nonholonomic method also appears to behave in a relatively regular fashion (Fig. 108b), although it differs significantly from the unconstrained case. The corresponding result for the velocity-reversal constraint is shown in Fig. 108c. It is not as regular in appearance as the other two and there appears to be "chattering" (rapid vibrations) in the x mode.

The corresponding harmonic mode energies are shown in Fig. 109 for the unconstrained, nonholonomic-constrained, and velocity-reversal-constrained results, respectively. The particular trajectory in Figs. 108-110 does not exchange large quantities of energy (even when unconstrained). However, the exchange that does take place seems to have a fairly well-defined pattern (Fig. 109a). Application of the nonholonomic constraint to the x mode dictates that that mode have an exactly constant value (upper trace, Fig. 109b). The y mode varies somewhat, with the amplitude of the variation in the y mode being rather similar to that of the unconstrained case. When the velocity-reversal constraint is applied to the x mode, the energy transfer appears to become less regular compared to the other two (Fig. 109c).

An interesting consequence of the constraints is demonstrated in Fig. 110 where the power spectra for the trajectories are shown. The unconstrained Hamiltonian has zeroth-order frequencies of $\omega_x = 2$ and $\omega_y = 1$. These frequencies are clearly present in

the power spectrum shown if Fig. 110a. The trajectory (Fig. 108a) is quasiperiodic; the peaks are narrow and well resolved. A strange result of imposing the nonholonomic constraint on the system is that, while the "unconstrained" y mode still yields $\omega = 1$, the frequency of the constrained x mode shifts from $\omega = 2$ to $\omega \approx 2.4$ (Fig. 110b). Finally, the velocity-reversal constraint leads to the power spectrum shown in Fig. 110c. The peak at $\omega = 1$ corresponds to the unconstrained y mode. The power spectrum of the x mode is low-intensity noise over most frequencies, i.e., the velocity-reversal constraint induces what appears to be chaotic vibrations in the x degree of freedom.

The results for a set of trajectories where both the x and y modes are constrained are compared to the unconstrained result in Figs. 111 to 113. The frequencies and total energy are the same as in Fig. 108 to 110; however, the initial conditions are different. The plots are arranged in the same order as in Figs. 108-110. Once again, the unconstrained trajectory behaves quasiperiodically (panel a of Figs. 111 to 113). The trajectory sweeps out a slowly varying but predictable path in configuration space (Fig. 111a), the harmonic mode energies exchange energy in a regular fashion (Fig. 112a), and the spectrum is sharp and only shows appreciable intensity at the fundamentals (Fig. 113a). Application of the nonholonomic constraint alters the trajectory rather severely relative to the unconstrained case (panel b in Figs. 111 to 113). Although the configuration-space projection indicates that the trajectory is evolving in a fairly regular manner, it is quite different from the unconstrained trajectory (Fig. 111b). By construction, the harmonic mode energies shown in Fig. 112b are exactly constant. The effect of the nonholonomic constraint on the power spectrum is once again to shift the frequencies (both of them, in this case, since both modes are being constrained). Also, the peaks are somewhat broadened (Fig. 113b). Application of the velocity-reversal constraint to the x and y modes leads to an unacceptable result (panel c in Figs. 111 to 113). The configuration-space projection of the trajectory in no way resembles the

Figure 111. Configuration-space plots for trajectories having identical initial conditions but with different constraints on the energy flow. The results shown are for the case $\omega_x = 2$, $\omega_y = 1$ and a total energy of $E = 0.095$. Constraints are applied to both modes of the system. a) unconstrained trajectory; b) nonholonomic constraint, which forces the both harmonic modes to have a constant energy; c) velocity-reversal constraint, which prevents the both mode energies from falling below the level.

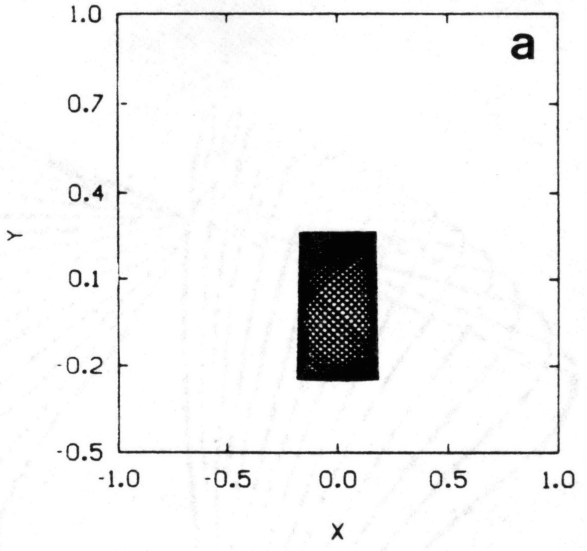
a
1.0
0.7
0.4
0.1
-0.2
-0.5
Y
-1.0
-0.5
0.0
0.5
1.0
X

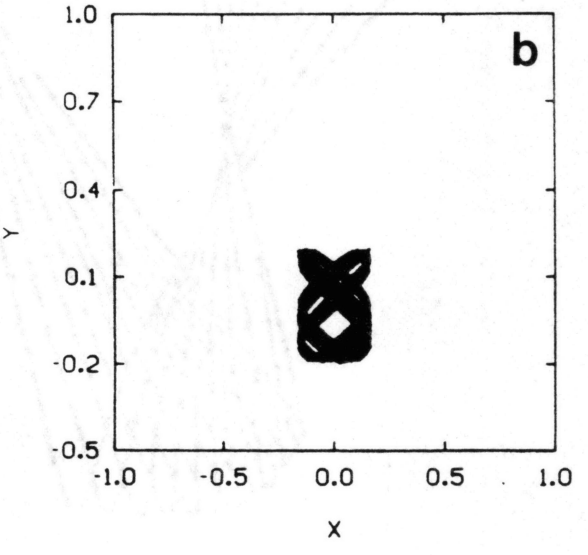
b
1.0
0.7
0.4
0.1
-0.2
-0.5
Y
-1.0
-0.5
0.0
0.5
1.0
X

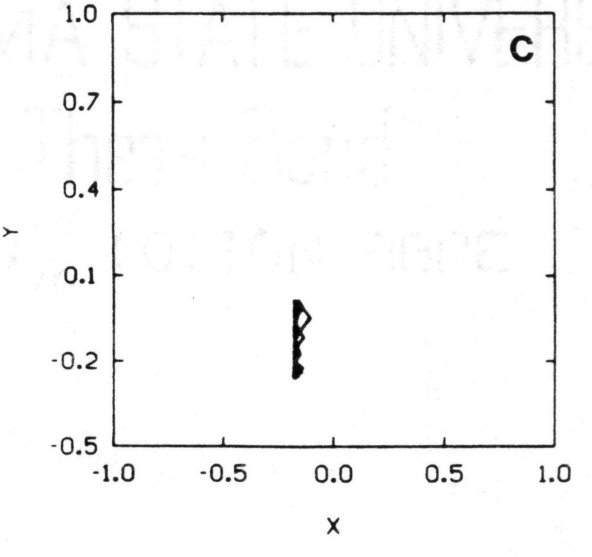
c
1.0
0.7
0.4
0.1
-0.2
-0.5
Y
-1.0
-0.5
0.0
0.5
1.0
X

Figure 112. Time histories of the harmonic mode energies for trajectories having identical initial conditions but with different constraints on the energy flow. The results shown are for the case $\omega_x = 2$, $\omega_y = 1$ and a total energy of $E = 0.095$. Constraints are applied to both modes of the system. a) unconstrained trajectory; b) nonholonomic constraint, which forces both harmonic modes to have a constant energy; c) velocity-reversal constraint, which prevents both mode energies from falling below the zero-point level.

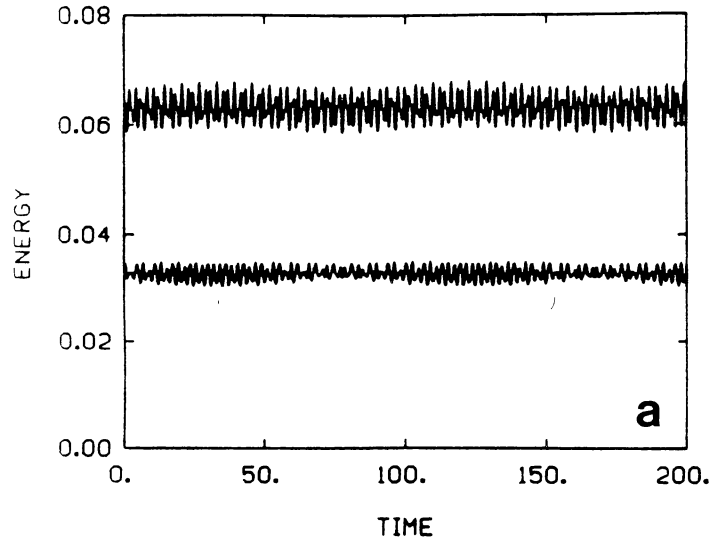
0.08
0.06
0.04
0.02
0.00
ENERGY
a
0.
50.
100.
150.
200.
TIME

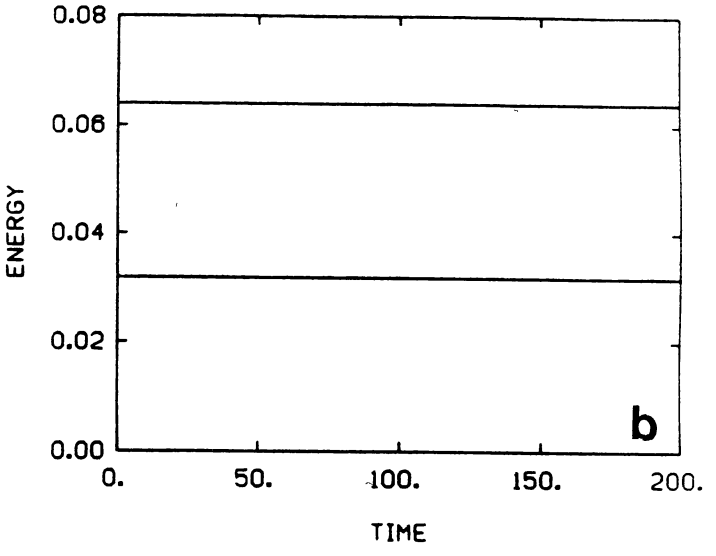
0.08
0.06
0.04
0.02
0.00
ENERGY
b
0.
50.
100.
150.
200.
TIME

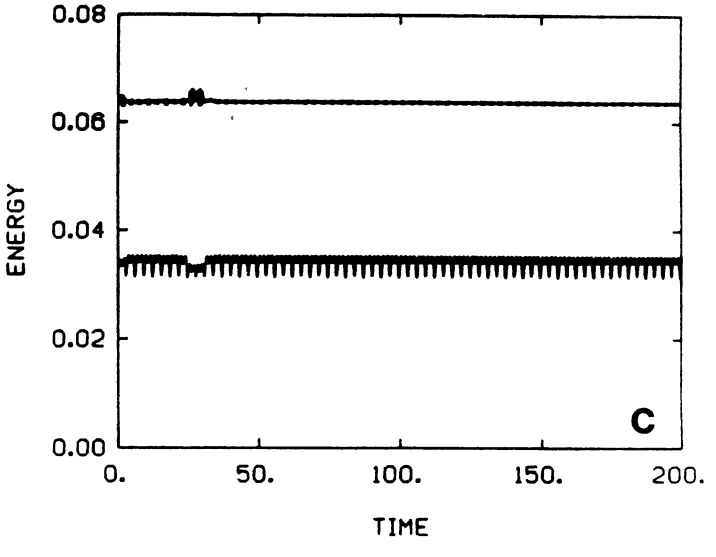
0.08
0.06
0.04
0.02
0.00
ENERGY
c
0.
50.
100.
150.
200.
TIME

Figure 113. Power spectra for trajectories having identical initial conditions but with different constraints on the energy flow. The results shown are for the case $\omega_x = 2$, $\omega_y = 1$ and a total energy of $E = 0.095$. Constraints are applied to both modes of the system. a) unconstrained trajectory; b) nonholonomic constraint, which forces both harmonic modes to have a constant energy; c) velocity-reversal constraint, which prevents both mode energies from falling below the zero-point level.

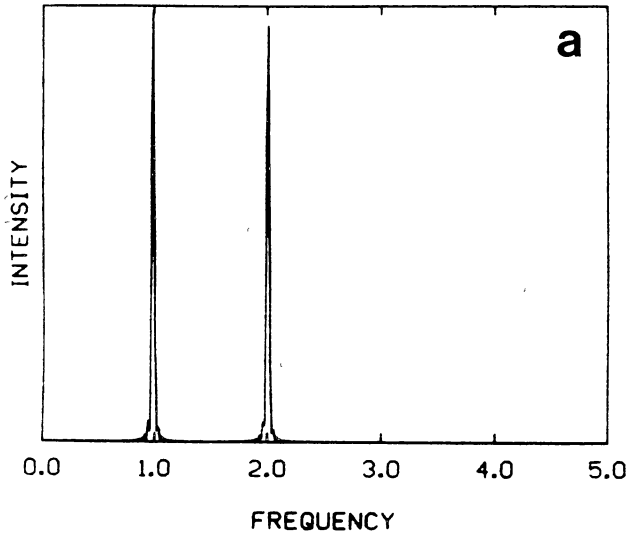
a
INTENSITY
0.0
1.0
2.0
3.0
4.0
5.0
FREQUENCY

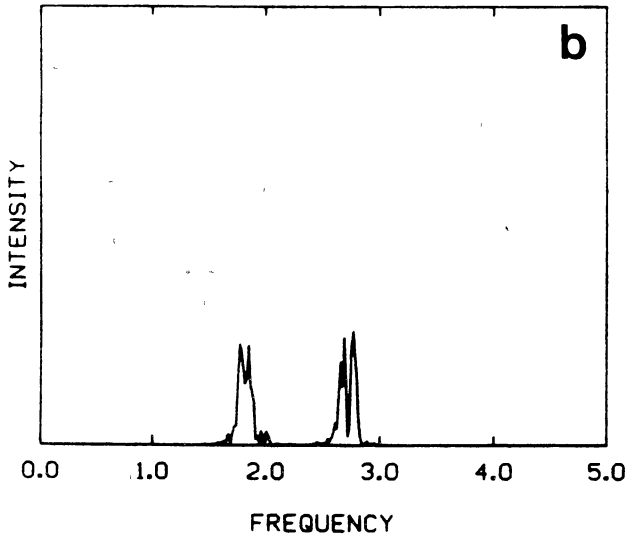
b
INTENSITY
0.0
1.0
2.0
3.0
4.0
5.0
FREQUENCY

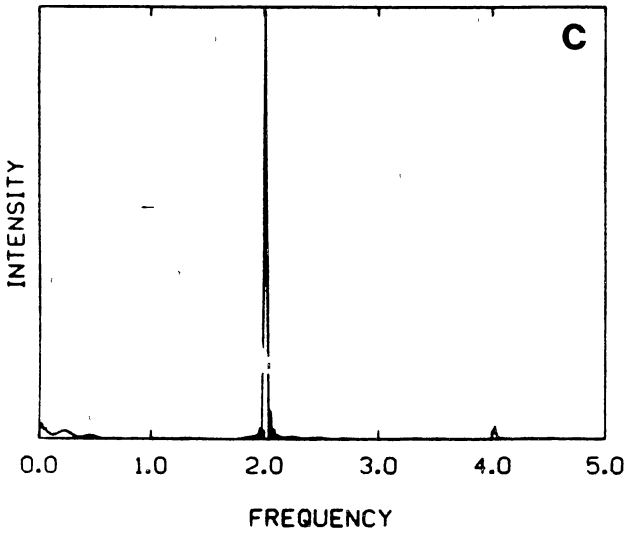
c
INTENSITY
0.0
1.0
2.0
3.0
4.0
5.0
FREQUENCY

unconstrained result (Fig. 111c). The trajectory is very restricted in its motion, exploring only a small fraction of the configuration space. Notice that the trajectory never passes through x = 0. This means that the trajectory is "vibrating" on the wall of the potential. However, the method does satisfy the requirement that the harmonic mode energies do not fall below the prescribed level (Fig. 112c) and does so rather well. In practice, twenty-five integration steps were taken between calculations of the mode energies (and potential applications of the constraint). Thus, the mode energies were allowed to fall slightly below the zero-point level; but this was due to the implementation of the method (checking the mode energies after every twenty-fifth step) and not the method itself. Monitoring the mode energies after each step did not result in substantial changes in the results.

We make one last comparison between the methods in Figs. 114 and 115. These results correspond to a set of initial conditions for $\omega_x = \omega_y = 1$. The total energy is E = 0.159. Constraints are applied to both the x and y modes. Panels a, b, and c in Fig. 114 correspond to configuration-space projections of the trajectories for the case of no constraint, nonholonomic constraint, and velocity-reversal constraints, respectively. Figure. 115 is organized in the same fashion as Fig. 114 but is for the power spectra corresponding to the trajectories shown in Fig. 114. Without belaboring the point, it is apparent that neither of the constraints work well in this case. Although the nonholonomic-constrained result does "look" like a trajectory (Fig. 114b), it in no way resembles the unconstrained result of Fig. 114a. Also, as was the case for many of the nonholonomic-constrained trajectories we examined, the trajectory covers a wide range of configurations during the first part of the trajectory but then approaches a sort of asymptotic "limit-cycle" like behavior. However, it is not at all regular, as is evidenced by the power spectrum shown in Fig. 115b. Once again, the velocity-reversal constraint

Figure 114. Configuration-space plots for trajectories having identical initial conditions but with different constraints on the energy flow. The results shown are for the case $\omega_x = \omega_y = 1$ and a total energy of $E = 0.159$. Constraints are applied to both modes of the system. a) unconstrained trajectory; b) nonholonomic constraint, which forces the both harmonic modes to have a constant energy; c) velocity-reversal constraint, which prevents the both mode energies from falling below the zero-point level.

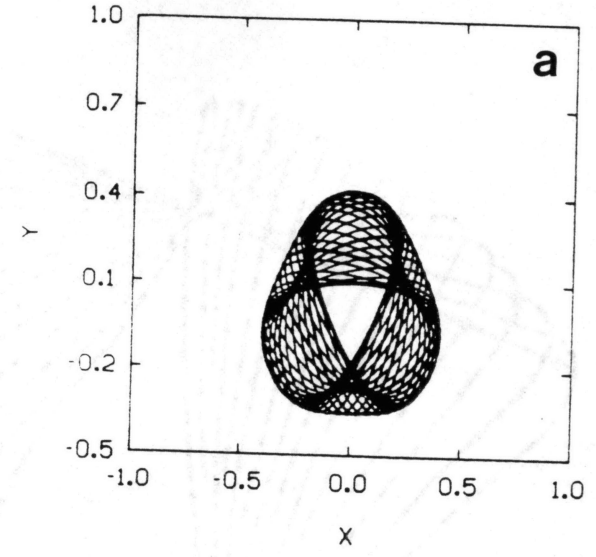
a
1.0
0.7
0.4
0.1
-0.2
-0.5
Y
-1.0
-0.5
0.0
0.5
1.0
X

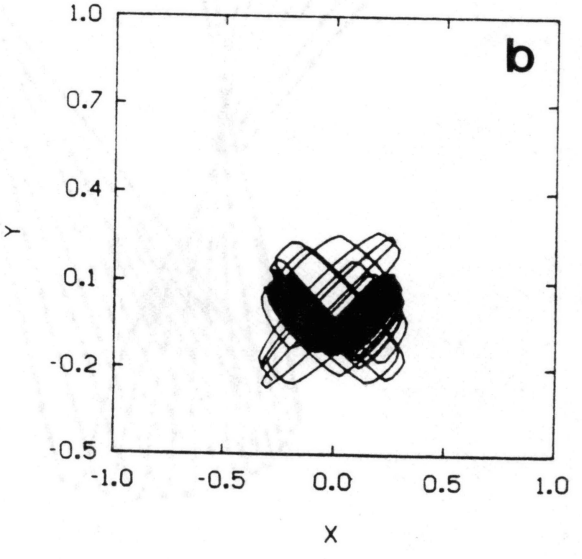
b
1.0
0.7
0.4
0.1
-0.2
-0.5
Y
-1.0
-0.5
0.0
0.5
1.0
X

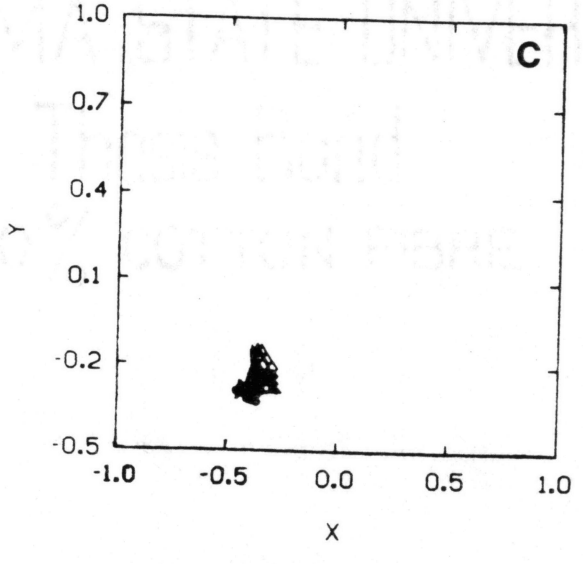
c
1.0
0.7
0.4
0.1
-0.2
-0.5
Y
-1.0
-0.5
0.0
0.5
1.0
X

Figure 115. Power spectra for trajectories having identical initial conditions but with different constraints on the energy flow. The results shown are for the case $\omega_x = \omega_y = 1$ and a total energy of $E = 0.159$. Constraints are applied to both modes of the system. a) unconstrained trajectory; b) nonholonomic constraint, which forces both harmonic modes to have a constant energy; c) velocity-reversal constraint, which prevents both mode energies from falling below the zero-point level.

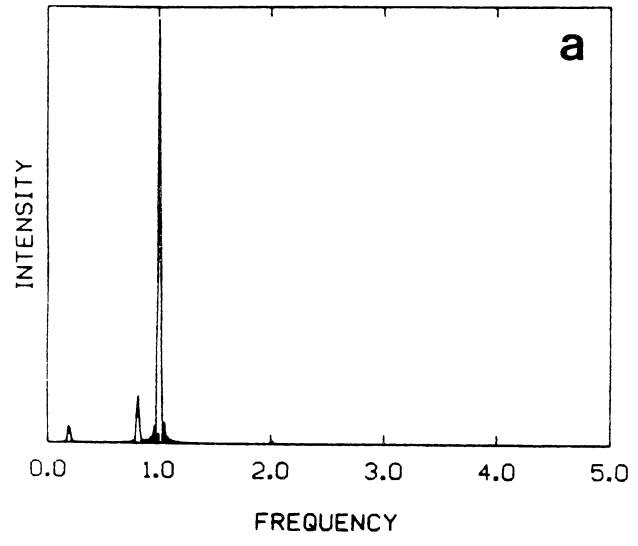
a
INTENSITY
0.0
1.0
2.0
3.0
4.0
5.0
FREQUENCY

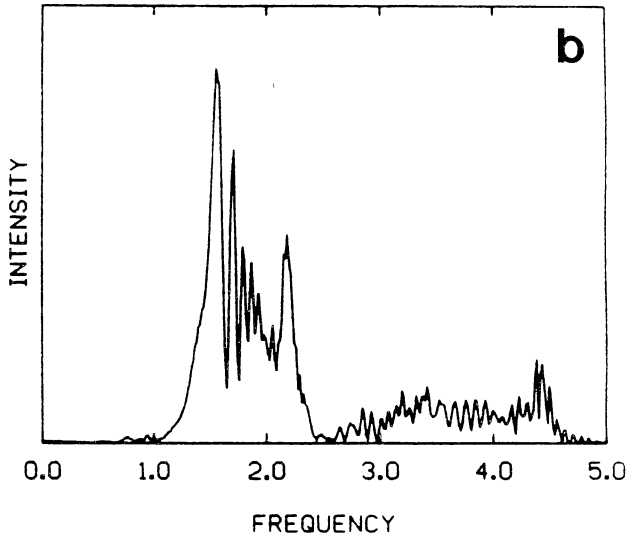
b
INTENSITY
0.0
1.0
2.0
3.0
4.0
5.0
FREQUENCY

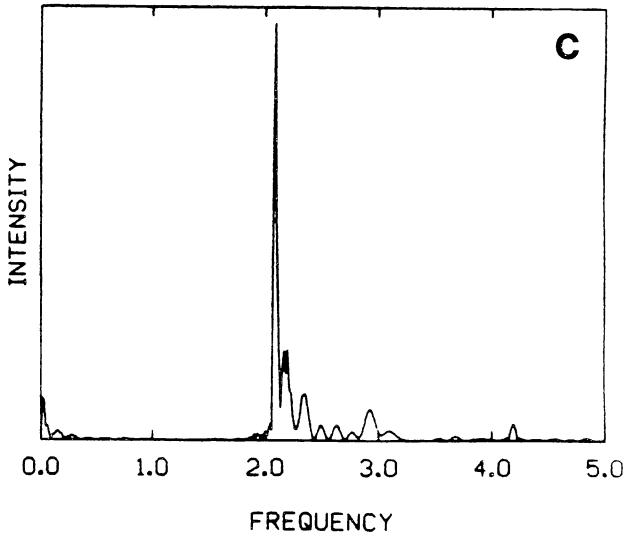
c
INTENSITY
0.0
1.0
2.0
3.0
4.0
5.0
FREQUENCY

fails to give a suitable result, even though the constraints are satisfied (panel c in Figs. 114 and 115).

It is apparent that both the methods of constraining zero-point energy in one or more of the modes lead to fundamental changes in the dynamics: The configuration-space projections of the trajectories are significantly altered and the associated power spectra exhibit large shifts in peak locations and considerably broadened. Classical resonances that are present in the unconstrained dynamics are destroyed when either of the constraints is applied.

One difficulty with the velocity-reversal method is that it seems to "work best when it is needed least". That is, while the method does prevent the energy in the zeroth-order modes from dropping below the zero-point (while conserving the total energy), the result for systems having only zero-point (or close to zero-point) energy is rather severe aphysical behavior, that is, it causes the system to vibrate far from equilibrium. This "chattering" is due to the constraint repeatedly reversing the momenta and originates from the fact that virtually any classical integration step will result in the trajectory moving off of the "zero-point energy surface". On the other hand, when the energies are large relative to the zero-point energies of the modes, the velocity-reversal method seems to work relatively well. This was demonstrated by Bowman *et al.*[46] in their paper and is reinforced by Figs. 116 to 118.

The results presented in Figs. 116 to 118 correspond to the case $\omega_x = \omega_y = 1$ and a total energy of 0.162, which is near the dissociation limit of the potential-energy surface ($E = 1/6$). We have arbitrarily defined the "zero-point" energy in each of the modes to be $E_0 = 0.0162$. Thus, the total energy is well in excess of the zero-point level. Figures 116a and 116b present the configuration-space projection of an unconstrained trajectory and the corresponding result using the velocity-reversal constraint, respectively (The nonholonomic constraint is not applicable since it is

Figure 116. Configuration-space plots for trajectories starting from identical initial conditions but with different constraints on the energy flow. The results shown are for the case $\omega_x = \omega_y = 1$ and a total energy of E = 0.162. Constraints are are applied independently to both the x and y modes. The "zero-point energy" has arbitrarily been defined as $E_0 = 0.0162$ for both the x and y modes. a) unconstrained trajectory; b) velocity-reversal constraint, which prevents the x and y mode energies from falling below E = 0.0162.

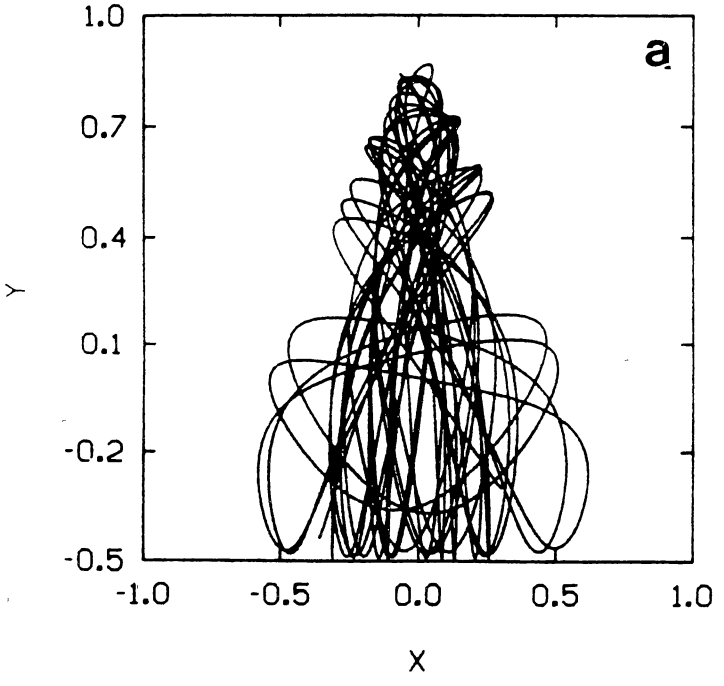
a
1.0
0.7
0.4
0.1
-0.2
-0.5
Y
-1.0
-0.5
0.0
0.5
1.0
X

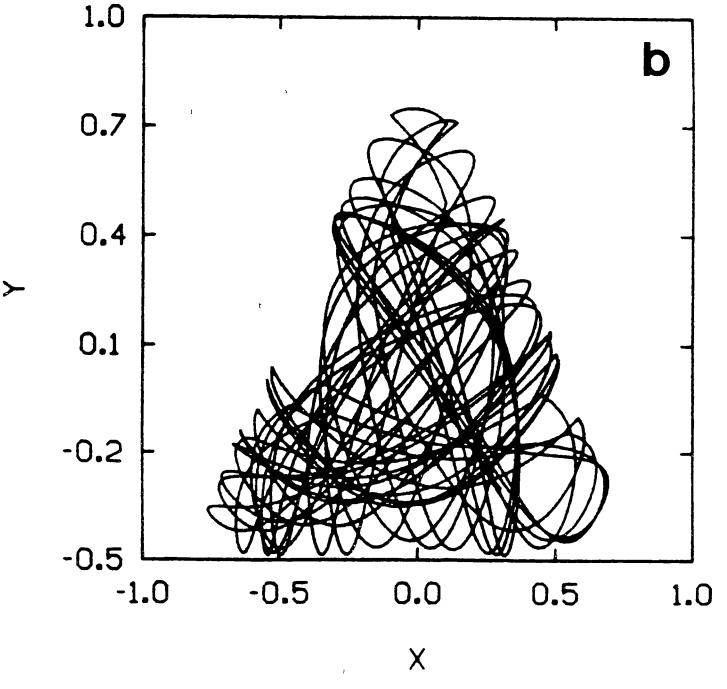
b
1.0
0.7
0.4
0.1
-0.2
-0.5
Y
-1.0
-0.5
0.0
0.5
1.0
X

Figure 117. Time histories of the harmonic mode energies for trajectories starting from identical initial conditions but with different constraints on the energy flow. The results shown are for the case $\omega_x = \omega_y = 1$ and a total energy of E = 0.162. Constraints are are applied independently to both the x and y modes. The "zero-point energy" has arbitrarily been defined as $E_0 = 0.0162$ for both the x and y modes. a) unconstrained trajectory; b) velocity-reversal constraint, which prevents the x and y mode energies from falling below E = 0.0162.

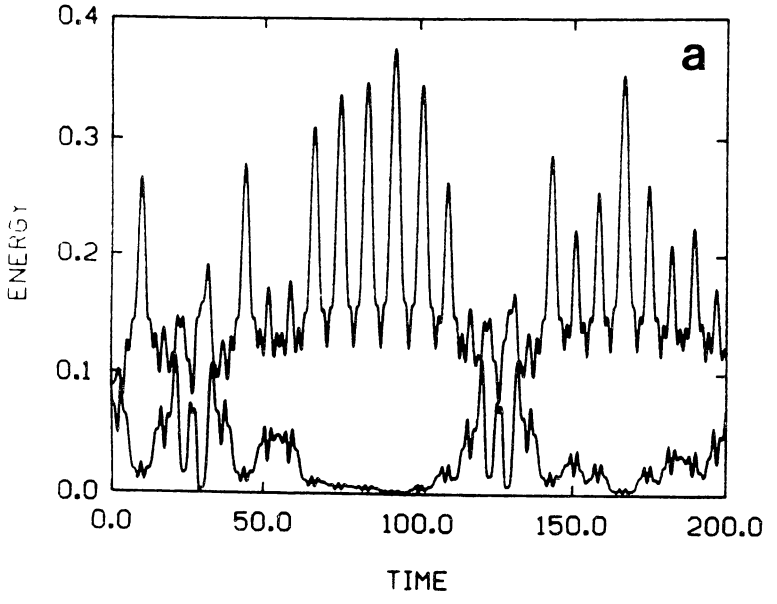
a
0.4
0.3
0.2
0.1
0.0
ENERGY
0.0
50.0
100.0
150.0
200.0
TIME

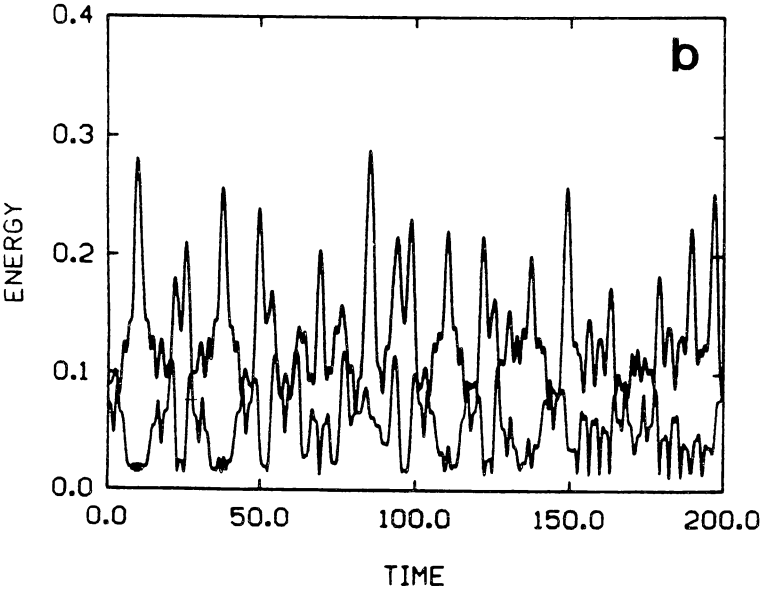
b
0.4
0.3
0.2
0.1
0.0
ENERGY
0.0
50.0
100.0
150.0
200.0
TIME

Figure 118. Power spectra for trajectories starting from identical initial conditions but with different constraints on the energy flow. The results shown are for the case $\omega_x = \omega_y = 1$ and a total energy of $E = 0.162$. Constraints are are applied independently to both the x and y modes. The "zero-point energy" has arbitrarily been defined as $E_0 = 0.0162$ for both the x and y modes. a) unconstrained trajectory; b) velocity-reversal constraint, which prevents the x and y mode energies from falling below $E = 0.0162$.

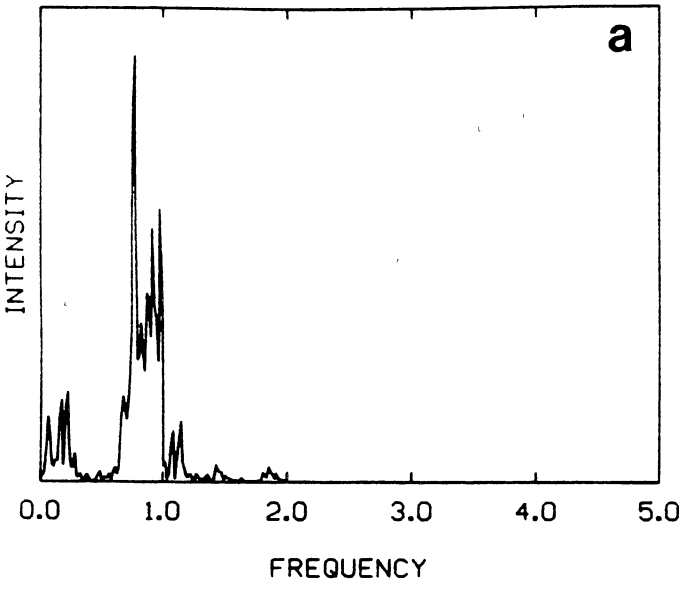
a
INTENSITY
0.0
1.0
2.0
3.0
4.0
5.0
FREQUENCY

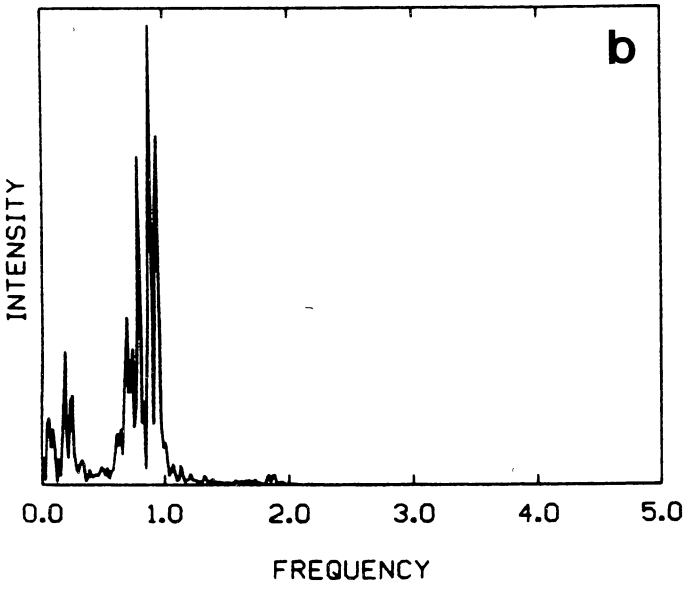
b
INTENSITY
0.0
1.0
2.0
3.0
4.0
5.0
FREQUENCY

restricted to maintaining constant mode energies.). The two trajectories, while quantitatively different, are both recognizable as evolving on the Hénon-Heiles potential-energy surface in the chaotic regime. It should be noted that, strictly speaking, in the velocity-reversal case a new trajectory is actually being generated each time the constraint results in a reversal of one of the momenta.

The important thing to note is that at the high energies (relative to the zero-point) the velocity-reversal constraint may provide a useful means of controlling the zero-point energy. Figure 117 presents the zeroth-order mode energies corresponding to the trajectories shown in Fig. 116. They are identical up until about 10 time units (the time of the first momentum reversal) and then differ, as expected, for the duration of the trajectories. The unconstrained trajectory evolves such that the x mode has less than zero-point energy (zero energy, essentially) for a rather large portion of the trajectory Fig. 117a). The similarities between the power spectra in shown in Fig. 118 imply that the dynamics between velocity reversals are not too different, which is not surprising since, at this energy, most trajectories are chaotic. If the energies are sufficiently elevated relative to the zero-point level, the velocity-reversal method of constraining the zero-point energy works fairly well, however, it does not work well at or just above the zero-point level for the reasons discussed above.

The use of nonholonomic constraints also causes significant changes in the nature of the dynamics. This approach is restricted, as presently formulated, to constraining mode energies to fixed values. It should be noted that, unlike velocity reversal, the nonholonomic constraints result in the system Hamiltonian not being conserved. Figure 119 shows the variation of the Hamiltonian Eq. (VIII.23) for the trajectory shown in Fig. 108b in which the x mode is constrained to have a constant harmonic mode energy. A more pathological defect in the method that we have devised is that it is numerically unstable. Equation (VIII.21) is singular whenever the potential

Figure 119. Demonstration of the nonconstancy of Eq. VIII.23 when the nonholonomic constraint is employed. The trace corresponds to the trajectory shown in Fig. 108b.

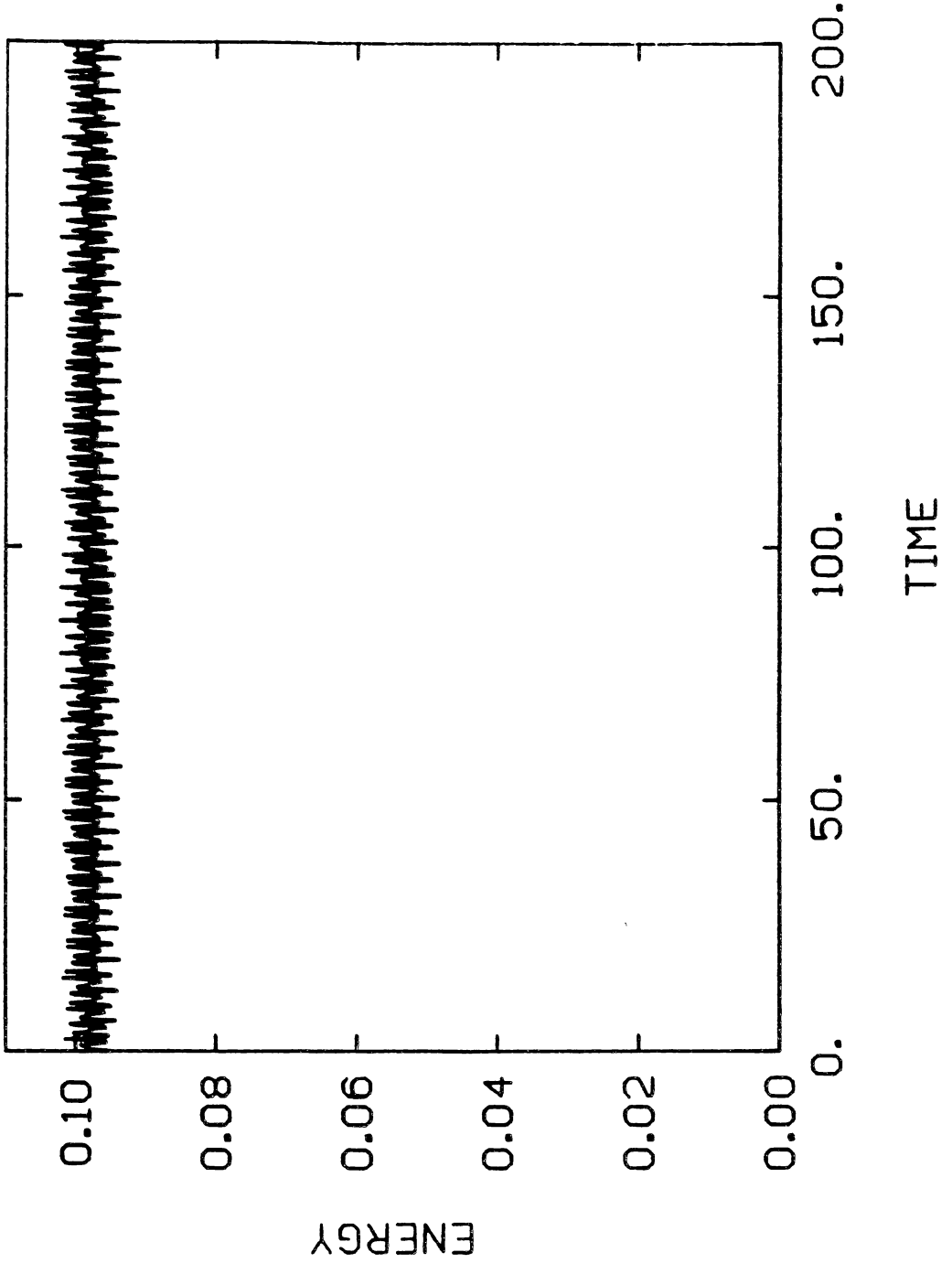
ENERGY
0.10
0.08
0.06
0.04
0.02
0.00
0.
50.
100.
150.
200.
TIME

energy of mode i is equal to the constant mode energy α_i. This leads to difficulty in propagating a large fraction of the trajectories and seriously inhibits the usefulness of the method. We note that the degree of difficulty encountered for this reason is somewhat reduced if, rather than constraining individual modes to have constant energies, sums of two or more mode energies are required to be invariant in time. Finally, the equations of motion, Eqs. (VIII.20) and (VIII.21), do not reduce back to Hamilton's equations if the coupling terms $H'(q_1, q_2, ...,q_n)$ are set to zero.

We attempted calculations in which we applied the velocity reversal procedure to polyatomic molecules (H_2O_2, HONO, C_2H_4) vibrating in three dimensions. We were interested in low-energy dynamics and therefore followed the "simple" prescription for the velocity-reversal method. The total energy was conserved, as was the linear momentum. However, each time the constraint condition led to a reversal of one of the normal-mode velocities, the angular momentum was changed (but was conserved between kicks). This behavior does not occur for collinear models. However, the fact it does occur for 2- or 3-D systems means that, in order to "successfully" implement the simple model, it would be necessary to apply a rigid rotation of the reference frame with respect to which the normal modes are calculated so as to provide a consistent basis for calculation of the normal modes.

Note: At the time of this writing, more extensive results have been generated. Specifically, we have applied the more "general version" of the velocity reversal method[47] to the Hénon-Heiles Hamiltonian. Also, we have entered into a collaboration with Dan Gezelter and Professor W. H. Miller of the University of California, Berkeley. They are performing quantum calculations for a number of different initial values of ω_x, ω_y, and Planck's constant while we perform the corresponding classical calculations. It is our hope that comparison of the classical and quantum results will give some sense of direction to subsequent studies of the zero-point energy problem.

Final Remarks

We have examined the effects on the dynamics of two methods for constraining zero-point energy flow in the Hénon-Heiles system. One method is due to Bowman *et al.*[46] and Miller *et al.*[47] The other is introduced here. Both methods introduce fundamental changes in the qualitative nature of the dynamics, including substantial shifts and broadening in the vibrational frequencies relative to the unconstrained dynamics. This results in the destruction of classical resonances, and in cases where classical resonances have quantum analogs, the methods are not expected to be useful. It seems likely that the aphysical behavior associated with these methods may be as undesirable as that resulting from zero-point energy flow. Therefore, the question of how best to handle the problem of zero-point energy in classical dynamics is still very much an open question.

CHAPTER IX

SEMICLASSICAL DEMONSTRATION OF MODE SPECIFICITY IN THE TUNNELING SPLITTING OF AN IDEALIZED MALONALDEHYDE MOLECULE

Introduction

The question of whether mode-specific effects can be induced in chemical reactions has received a lot of attention in recent years (See Chapter III for a timely review).[332] Although the majority of the demonstrations of mode specificity have been associated with computer "experiments", there are experimental indications that, under favorable circumstances, it may be possible to affect the rate of a specific chemical process as a function of the means of excitation or to influence the yield of one reaction product relative to another.

Another interesting phenomenon that has been a topic of considerable study is the tunneling splitting in "symmetric, double-well molecules".[20,22,30,243-249,421-427] In symmetric, double-well quantum mechanical systems, there is a splitting of the eigenvalues due to resonant tunneling between the two wells.[38] There are numerous experimental confirmations of this effect.[38,243-244,246,248,425-427] The symmetric hydrogen-transfer process in the malonaldehyde molecule has been particularly heavily studied in this regard.[243-246,248,425-427]

Wilson and co-workers[243,246,428] and Seliskar and Hoffmann[244] have performed experiments on malonaldehyde (and its isotopic relatives) and determined the splitting to be approximately 21 cm^{-1} for the ground-state parent species. They also

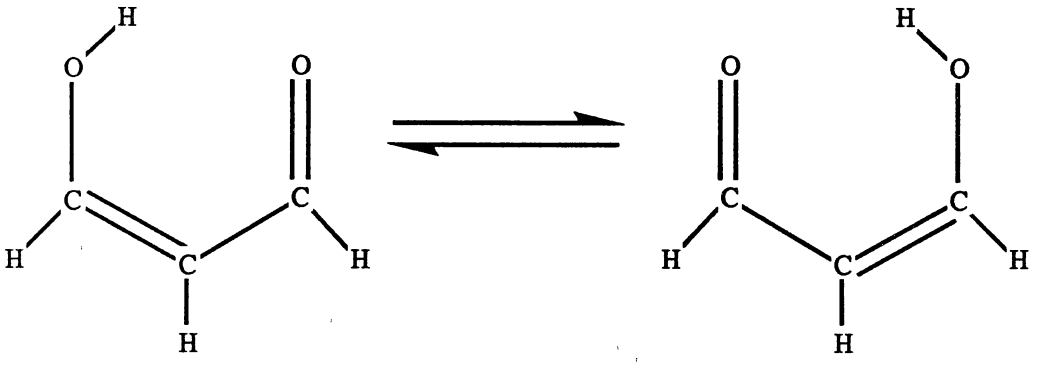

(R5)

reported the structure[243] and a harmonic force field[428], although there was some ambiguity in some of the force-field assignments. Recently, Leopold and co-workers[248] reported a very accurate microwave study of malonaldehyde. They obtained a ground-state tunneling splitting of 21.58476(17) cm^{-1}.

Malonaldehyde has been studied extensively by theoreticians.[20,22,30,245,247,249,429-430] The most reliable calculations of the barrier height yield a value in the range 5-10 kcal/mol. However, the tunneling splitting is apparently quite sensitive to the details of the model employed, as the range of calculated splittings spans some two orders of magnitude.[20,22,30,245-247]

Hutchinson[249] authored the only published study of the classical dynamics calculation of the hydrogen transfer in malonaldehyde. He employed a two degree-of-freedom potential-energy surface consisting of a constrained three-body LEPS potential and harmonic angle-bending terms. The model only treated the motion of the hydrogen atom; the skeletal C and O atoms were held fixed. Tunneling was not considered in the calculation. The study revealed the motion to be surprisingly regular even at energies considerably in excess of the barrier to hydrogen transfer (although as the energy

increased so did the degree of irregularity of the trajectories). Moreover, the phase space of the model gave rise to qualitatively distinct kinds of trajectories. Some of the trajectories corresponded to stable "bending" motion whereas other corresponded to nearly pure stretching motion along the equilibrium O-H bond axis.

We have used classical trajectories in conjunction with a semiclassical overlay[30,144,145] in order to calculate the splitting of a prototypical malonaldehyde molecule. The impetus for this study was not to attempt a quantitatively correct calculation but rather to attempt to extract in a qualitative manner the answer to the question of whether mode-specific effects are likely to be manifested in the tunneling splittings. The simple, reduced-dimensional potential-energy surface due to Hutchinson[249] was used. Tunneling was incorporated using a combination of the "classical plus tunneling" model of Waite and Miller[144-145] and a newer variant recently published by Makri and Miller[30].

Computational Details

Potential-energy surface

We have chosen to employ the model potential-energy surface constructed by Hutchinson.[249] Although the barrier on this potential-energy surface probably overestimates the actual value by a few kcal/mol,[247] and the geometric parameters are not in exceptionally good agreement with the known values,[243] it does posses some properties that are essential to reaching a qualitatively correct conclusion concerning mode-specific effects in the tunneling splitting. Foremost among these is the fact that the minimum-energy path requires both bending and stretching displacements, as pointed out by Hutchinson (see Fig. 120). Moreover, Hutchinson found that the

Fig. 120. Contour plot of the model potential-energy surface for the hydrogen-transfer process in malonaldehyde. The surface is taken directly from Ref. 429. The transition state is 10.26 kcal/mol higher in energy than the equilibrium geometry. The solid line is the path of steepest descent obtained from a damped trajectory.

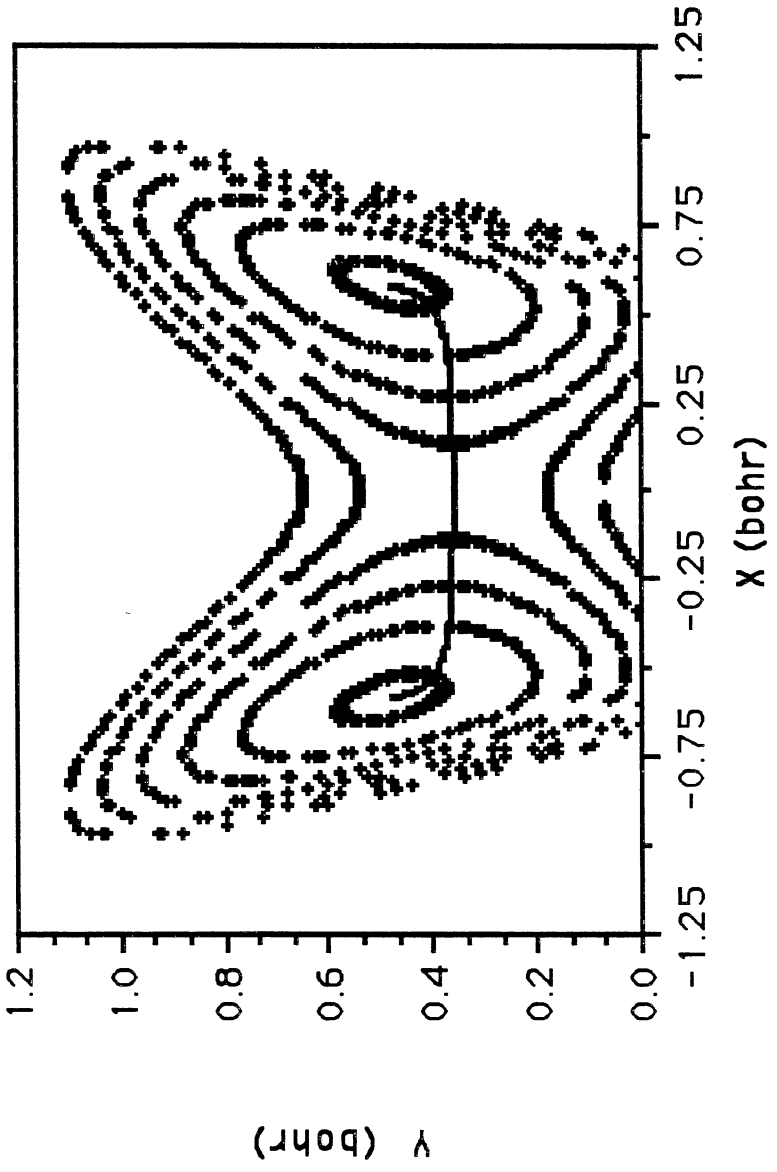
1.2
1.0
0.8
0.6
0.4
0.2
0.0
Y (bohr)
-1.25
-0.75
-0.25
0.25
0.75
1.25
X (bohr)

classical dynamics are relatively insensitive to reasonable variation of the potential-energy surface parameters.

A contour plot of the potential-energy surface is shown in Fig. 120. The barrier is 10.26 kcal/mol. The solid line connecting the three stationary points corresponds to the path of steepest descent. It was obtained by running a "damped trajectory" initialized at the transition state with a small component of momentum in the ± x direction. The damping was accomplished by zeroing the momenta after each integration step.

Trajectory Calculations

Ensembles of 2500 trajectories were computed at three energies and for four qualitatively different kinds of excitation schemes. The energy for which calculations were performed correspond to zero-point energy in both modes (6.6 kcal/mol). Trajectories were integrated in Cartesian coordinates using a fixed stepsize of 2.69×10^{-17} s. Individual trajectories were followed for 100 fs.

Initial Conditions

Initial conditions were obtained by partitioning the energy either i) randomly (by random selection of coordinates and momenta), ii) according to the quasiclassical prescription given in Chapter II, or by assigning all of the energy to either iii) the zeroth-order stretch or iv) the zeroth-order bending mode. For the three cases where "quasiclassical" initial conditions were selected, the phases were selected from the standard distributions.[34] The bend and stretch modes were fit to harmonic and Morse oscillator functions, respectively, in order to allow for selection of initial conditions as described above. The parameters used are given in Table XXXII. The resulting zero-point energy is in quite good agreement with the quantum eigenvalues reported by Hutchinson (6.8 kcal/mol).[249]

Table XXXII. Parameters Used for Initial Conditions Selection.

Bond stretching mode:	$r^o = 0.956$ Å	$D_e = 33.44$ kcal/mol	$\alpha = 3.785$ Å^{-1}
Angle bending mode:	$\theta^o = 114.1^o$	$k_\theta = 146.2$ kcal mol^{-1} rad^{-2}	

Calculation of the Tunneling Splitting

The tunneling splitting was computed using the classical plus tunneling model of Waite and Miller[144-145] in conjunction with a more recent variant due to Makri and Miller[30]. The Waite and Miller model[144-145] computes the tunneling probability in terms of the WKB approximation[38] by assuming that the trajectory evolves classically until it experiences a turning point in the "tunneling direction" at time t_k, at which time a tunneling probability is computed for that turning point and a cumulative tunneling probability due to all times up to and including t_k is augmented. In the model of Waite and Miller, the tunneling direction is taken to be one of the internal coordinates,[145,323] for instance a bond angle or dihedral angle. Since the other coordinates are held fixed during the calculation of the tunneling probability, this constitutes a sudden approximation. Mathematical details of the model are given in Refs. 30, 144, and 145. Expressions pertaining to calculations of the tunneling splitting within the framework of the classical plus tunneling model are given in Ref. 30.

Makri and Miller[30] modified the model of Waite and Miller by assuming a more general tunneling coordinate. The calculation of the tunneling probability was not affected directly. However, rather than tunneling in a direction corresponding to a sudden displacement of one of the internal coordinates, the tunneling coordinate is taken to be the shortest straight-line distance connecting the caustics of the (assumed quasiperiodic and quantized) trajectories in the reactant and product wells.[30] Thus, in general, the tunneling direction will correspond to motion of all the atoms in the system.

For two-dimensional systems (the only cases which Miller and Makri considered[30]), the method is easy to implement; this is evidently not the case for higher dimensional systems. Inspection of Fig. 120 reveals that a tunneling coordinate defined in terms of a single internal coordinate (a bond distance or angle) will not be adequate; passage from the equilibrium geometry to the transition state corresponds to

displacement of both the bond and the angle. Thus, the more general tunneling direction described by Makri and Miller is required. However, given the symmetry of the system and the symmetry of the model, the tunneling direction simply corresponds to the x axis. Thus, for a trajectory evolving in the "left-hand" well in Fig. 120, the cumulative tunneling probability is augmented[144-145] each time the x component of the momentum changes sign (positive to negative).

Rigorously, Miller and Makri[30] require that the classical trajectories be quasiperiodic and correspond to a semiclassical state of the system.[30] This can be accomplished using adiabatic switching (if the trajectories are quasiperiodic).[28] In the calculations described here, we did not attempt a semiclassical quantization of the system (see the section above initial conditions selection) but, rather, chose to investigate the influence of various *ad hoc* distributions of energy on the tunneling splitting.

Results and Discussion

We present in Table XXXIII the calculated tunneling splittings obtained for the various initial distributions of energy. The results clearly show a dependence on the nature of the initial conditions. The calculated splittings vary by roughly a factor of three, depending on how the energy is distributed. Interestingly, the calculated splittings are in fairly close agreement with experimental values.[243,248] Undoubtedly, this agreement is coincidental, given the highly approximate potential-energy surface we have used. The highest splitting, 50.9 cm^{-1}, corresponds to quasiclassical selection of initial conditions with zero-point energy in both the stretch and bend modes. The lowest splitting, 16.2 cm^{-1}, is obtained when all of the energy is initially projected onto the angle-bending coordinate. Pure bond-stretching excitation and random excitation yield splittings of 41.5 and 38.3 cm^{-1}, respectively. Plots of the net tunneling amplitude (from which the splittings are extracted[30]) are given in Fig. 121. Panels a, b, c, and d

Table XXXIII. Calculated Tunneling Splittings in Model Malonaldehyde Molecule.

Excitation Scheme	Calculated Splitting (cm^{-1})
Pure angle	16.2
Pure stretch	41.5
Random	38.8
Quasiclassical	50.9

Fig. 121. Plots of the tunneling amplitude versus time for the model malonaldehyde system. The time unit is 1 au = $0.53871469 \times 10^{-14}$ s.

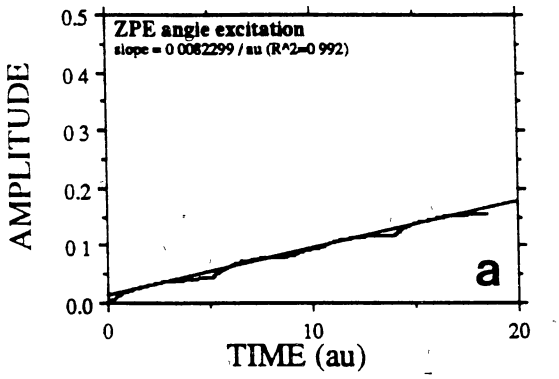
ZPE angle excitation
slope = 0 0082299 / au (R^2=0 992)
AMPLITUDE
TIME (au)
a

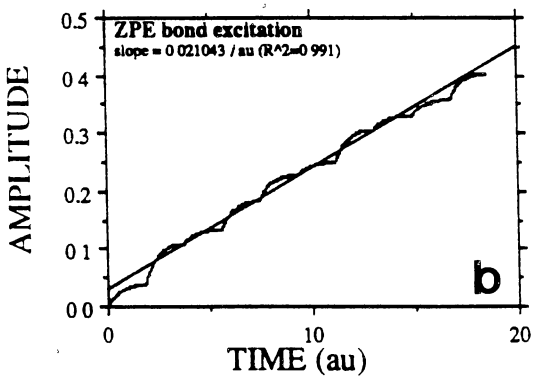
ZPE bond excitation
slope = 0 021043 / au (R^2=0 991)
AMPLITUDE
TIME (au)
b

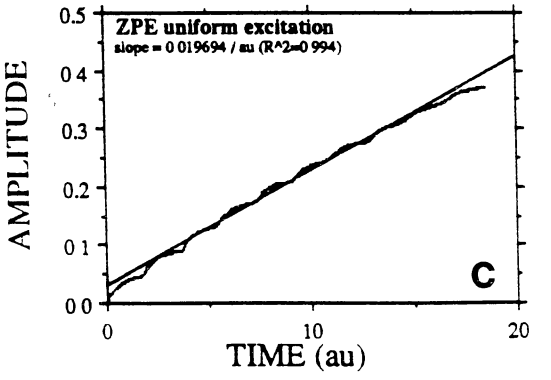
ZPE uniform excitation
slope = 0 019694 / au (R^2=0 994)
AMPLITUDE
TIME (au)
c

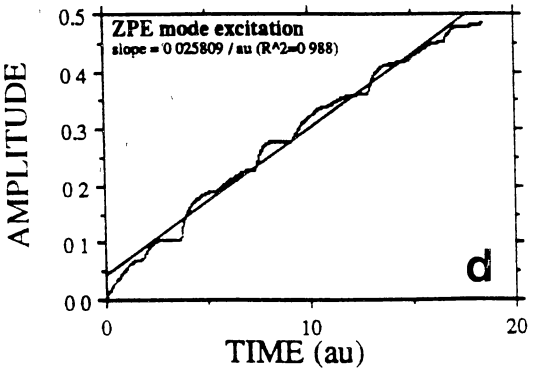
ZPE mode excitation
slope = 0 025809 / au (R^2=0 988)
AMPLITUDE
TIME (au)
d

correspond to pure angle stretching, pure angle bending, random partitioning of the energy, and quasiclassical distribution of the energy, respectively. The quality of the calculated results are such that the numbers are fairly reliable within the framework of the model we have employed.

The results shown in Table XXXIII are qualitatively reasonable. Trajectories computed on this potential-energy surface at the zero-point energy are quasiperiodic. Projection of all of the energy onto the bending coordinate results in a stable, highly excited bending motion; very little energy tends to leak into the stretching mode. Thus, even though the bend is undergoing large amplitude motion, the locus of points corresponding to turning points in the +x direction will dictate that the tunneling occurs through a wide, relatively high barrier. By contrast, localized excitation of the stretching will lead to a set of turning points that are closer to x=0 (compared to the previous case), which means that the domain over which the integral must be solved is decreased; and height of the barrier through which tunneling must occur is decreased as well. These two factors lead to a much increased splitting for the case of pure stretching excitation.

Random distribution of energy results in excitation of both the stretching and bending degrees of freedom but does so (on average) with a larger amount of energy in the bend (on average) than does the quasiclassical distribution. Quasiclassical excitation places energy in both the bending and stretching modes; the ratio of stretch to bend energy is roughly two to one. It is obvious that there is a relative distribution of energy that maximizes the tunneling splitting and, evidently, this distribution corresponds to having between $0 < E_{bend} < \langle E_b \rangle$, where $\langle E_b \rangle$ is the average energy in the bend when random selection of initial conditions is used.

Conclusions

The model calculation of the splitting in a prototypical malonaldehyde "molecule" indicates the presence of significant mode-specific effects. The mode specificity is understandable in terms of the simple dynamics that occur on the potential-energy surface. The calculations corroborate the intuitive expectation that a combination of bending and stretching motion is required in order to maximize the splitting. The calculated splittings bracket the experimental values, however, the agreement is almost surely fortuitous.

The results suggest that it may be possible to observe mode-specific effects in the tunneling splitting of real molecules. Since tunneling is a sensitive function of the dynamics and the energy, low-energy excitations could perhaps be designed to preferentially excite selected modes (i.e., C-O-H bends or skeletal modes) in the hopes of observing specificity in the splitting. Since the principal interest would be on low energies, the description could probably be couched in terms of normal modes and, moreover, the lifetime of the states might be long enough to be chemically significant.

Such speculations must be regarded with extreme caution, however, as extension of the simple model we have used here to the real malonaldehyde molecule is not a simple matter (either theoretically or experimentally). For instance, there are a number of difficulties that would be encountered in attempting a more realistic trajectory calculation. The problem of constructing a suitable potential-energy surface would be a time-and-labor intensive undertaking; since we are interested in a low-energy process, much attention would need to be given to details that might reasonably be neglected in studies of classical reaction dynamics. (There is, however, an experimentally derived force field in the literature,[428] which would provide a useful starting point.) A potentially more serious problem is the large dimensionality of malonaldehyde (twenty-one vibrational degrees of freedom) which would presumably make rigorous application

of the Miller and Makri[30] ansatz extremely difficult. Also, there are four high-frequency X-H modes in the molecule, which might lead to problems with zero-point energy effects. None of the published methods[46-47] for constraining zero-point energy will be useful here since the relevant energies are at or slightly above the zero-point level. Finally, the tunneling motion in malonaldehyde may involve heavy-atom motion due to the significant electronic rearrangement that occurs upon hydrogen transfer..[38,274,425-427] The are references to this phenomenon in the literature, and some of the examples are in systems similar to malonaldehyde.[425-427] These factors, when combined, would make the execution of a "realistic" trajectory-based semiclassical calculation of the splitting in malonaldehyde an extremely difficult problem.

CHAPTER X

CONCLUSIONS

We have investigated a number of interesting aspects of the reactive and nonreactive dynamics of chemical systems. The studies address: i) mode specificity (and the more general question of statistical behavior) in polyatomic molecules; ii) the applicability of standard classical trajectory methods to full-dimensional treatments of the multichannel reaction dynamics of very large molecules; iii) the extent that the vibrational dynamics of realistic polyatomic molecules are influenced by chaos; iv) how best (or perhaps, whether) to enforce constraints on the zero-point energy flow in classical trajectories; and iv) what degree of mode specificity might be expected in the tunneling splitting of symmetric, double-well molecules.

Unimolecular Dissociation of 2-chloroethyl Radical

Our studies indicate that 2-chloroethyl radical is a statistical system. There is no evidence for mode-specific effects and, based on comparison of our classical trajectory results to the those obtained by Schranz, Raff, and Thompson using Monte Carlo transition-state theory, the radical behaves statistically. The main reasons for the observed behavior appear to be: i) the large energetic changes associated with bond cleavage in the radical, which results in significant coupling between the reaction coordinate and the remaining modes; ii) the relatively high energies at which the calculations were performed, the upper end of which may be above the chaotic threshold in 2-chloroethyl radical; and iii) the lack of strong or preferential coupling between the activation coordinate (in the case of initial ·C-H bond excitations) and the reaction

coordinates. The three factors are essentially diametrically opposed to the conditions which we think will promote nonstatistical behavior.

Some interesting calculations dealing with potentially mode-specific processes were suggested in Chapter III. The ones of particular interest with regard to the preceding paragraph are the isomerization reactions of cyclobutene and 2-methylcyclopentadiene, reactions (R9) and (R10), respectively. Construction of a reasonable potential-energy surface for the ring opening of cyclobutene (R9) should be a manageable task. The hydrogen-transfer potential for the isomerization of 2-methylcyclopentadiene (R10) would probably be more difficult to formulate (although one might be able to borrow some ideas from the work of Hase *et al.*[270] on the ethyl radical potential-energy surface).

Unimolecular Reaction Dynamics of RDX

Our calculations of the reaction dynamics of RDX have convinced us that it is possible to treat the reaction dynamics of large molecules using classical mechanics. In spite of the paucity of data for the equilibrium potential-energy surfaces, and a complete lack of information concerning the saddle points, we were able to construct a simple potential that nominally describes the N-N bond fission and triple dissociation reactions in RDX. Due to the lack of data, development of the potential was largely based on "chemical intuition." The results were found to be in reasonable accord with the experiments of Zhao, Hintsa, and Lee,[222] although closer agreement could probably be achieved with further refinement of the potential-energy surface. In particular, the barrier to ring fission must be too low, based on visual extrapolation of the computed branching ratios back to the experimental energy. Therefore, careful consideration should be given to performing parametric studies in order to determine the sensitivity of the results to this particular aspect of the potential-energy surface. If this Author were to

specify the course taken in subsequent (and more detailed) investigations of RDX reaction dynamics, such a parametric study would be the next step taken. Another flaw that should be remedied prior to subsequent reaction dynamics studies of RDX is the total neglect of attenuation of force-field parameters (other than diminution of five angle-bending force constants per channel) along the N-N bond-fission reaction coordinates. "Improving the potential-energy surface" may be regarded by some as a trite suggestion for further work. However, if continuing studies of the RDX system are to be performed in the laboratory where this work was done, then improvements on this "first attempt" are definitely indicated.

It would be interesting (although perhaps prohibitively complicated) to attempt to explicitly treat the secondary reactions such as the isomerization / dissociation of $CH_2N_2O_2$ and the ultimate decomposition of the large cyclic radical produced by N-N bond fission. There would be myriad difficulties associated with writing down a general form for such a comprehensive potential; however, this would be a prerequisite to simulating the solid-phase reaction dynamics of RDX.

An equally interesting and less ambitious undertaking would be to examine the reaction dynamics of RDX in a rare-gas environment. (This is currently being done by E. P. Wallis and D. L. Thompson for the case of boat-to-chair and boat-to-twist-boat *conformational* changes in RDX.) It should be possible to incorporate the potential-energy surface we have constructed and place it in a bath of, say, argon atoms to study the effects of an inert solvent on the unimolecular decomposition.

Nonchaotic Dynamics in Highly Excited Polyatomic Molecules

The calculations on 2-chloroethyl radical and RDX allow for fairly straightforward conclusions, i.e., 2-chloroethyl radical decomposiyion is statistical (and

we think we know why); and, yes, it is feasible to treat the multichannel reaction dynamics of large molecules in a fairly realistic manner and without introducing overly restrictive approximations into the potential-energy surface. By contrast, the work that questions whether excited polyatomic molecules are chaotic is not as readily evaluated. With the exception of the spectra for SiF_4 and C_2H_4, the results are hard to interpret. Although we can almost certainly state that SiF_4 is not globally chaotic at 143 kcal/mol, and that C_2H_4 is largely chaotic at 155 kcal/mol (but probably not completely so[233-238]), the results for the other three systems are less clear cut. The spectra for CH_3ONO, $\cdot C_2H_4Cl$, and RDX are broadened when appreciable amounts of energy are placed in the molecules. Moreover, spectra for individual trajectories are rather "grassy" which, based on the results of two and three degree-of-freedom systems,[260] is an indication of chaos. (However, as Dumont and Brumer[407] have noted, the appearance of grassiness in the spectrum should not be regarded as unequivocal evidence of chaotic motion.) On the other hand, the spectra show definite structure; and the spectrum computed from one trajectory is usually quite similar to that computed from another. This would imply that we are either observing the "long-time limiting behavior"[307] of the power spectra or that the systems are not really chaotic. It would be interesting indeed if the long-time limiting behavior of the spectra for three arbitrarily chosen molecules was essentially independent of energy. Thus, while freely admitting the difficulties associated with applying the power spectrum method to the dynamics of large molecules, we are led to conclude that the dynamics of many polyatomic systems are not chaotic at and above the dissociation energy. If this is the case for molecules consisting of five to twenty-one atoms, it is almost surely the case for larger systems.

Zero-point Energy Constraints in Classical Trajectories

There are two (published) methods for constraining the zero-point energy in classical trajectory calculations.[46,47] Unfortunately, based on our studies using the Hénon-Heiles Hamiltonian, the use of either of the methods introduces serious aphysical behavior into the dynamics. This is particularly true for low-energy studies. The work we have done using the method of Bowman *et al.*[46] and the (equivalent) "simple" method of Miller *et al.*[47] clearly indicates that they are not suitable for use in practical applications. Although it does not appear in this Dissertation, we have just completed calculations on the Hénon-Heiles system using the "general" version of Miller *et al.*[47] to constrain the dynamics.[61] The results, while somewhat different from those shown in Chapter VIII, are similarly disappointing.

We have suggested a method for constraining the energy in harmonic modes to have constant values. The method borrows heavily from work published by Haile and Gupta[419], using nonholonomic constraints that act at each step of the trajectory integration. The method suffers from several deficiencies. First, the original system Hamiltonian is not conserved. Second, the present formulation is restricted to simple model systems. Third (and most seriously), the method is not stable with respect to numerical integration due to singularities in the equations of motion.

The zero-point energy problem in classical trajectories is just that -- a problem. Our results lead us to question whether it is possible to constrain the zero-point energy without destroying the dynamics of the system. Work on this problem should continue, although it is not clear to this Author how to proceed. If the problem can be solved in a practically useful manner, it will substantially expand the range of utility and reliability of the classical trajectory method.

Mode Specificity in the Tunneling Splitting in a Model of Malonaldehyde

The calculations of the tunneling splitting on the model "malonaldehyde" system indicate the presence of mode specificity. However, the calculation is so rudimentary as to be of little practical utility. The role of quasiperiodic dynamics on mode specificity is clearly illustrated by the calculation, however, and is therefore of some interest. It would be very interesting to attempt a full-dimensional calculation of the tunneling process in malonaldehyde. If the problems noted at the conclusion of Chapter IX could be dealt with or overcome, the calculation would provide some insight into mode specificity in the tunneling processes of a large molecule. Simply accomplishing the technical aspects of the calculation (in the full spirit of Makri and Miller[30]) would be worthwhile.

REFERENCES

1. L. R. Khundkar and A. H. Zewail, Annu. Rev. Phys. Chem. **41**, 15 (1990).

2. *Advances in Gas-Phase Photochemistry and Kinetics: Molecular Photodissociation Dynamics,* edited by M. N. R. Ashfold and J. E. Baggott (The Royal Society of Chemistry, London, 1987).

3. *Advances in Gas-Phase Photochemistry and Kinetics: Bimolecular Collisions,* edited by M. N. R. Ashfold and J. E. Baggott (The Royal Society of Chemistry, London, 1989).

4. F. F. Crim, Annu. Rev. Phys. Chem. **35**, 657 (1984).

5. W. H. Miller and J. Z. H. Zhang, J. Phys. Chem. **95**, 12 (1991).

6. T. Uzer, Physics Reports **199**, 73 (1991).

7. S. Mukamel, Annu. Rev. Phys. Chem. **41**, 647 (1990).

8. G. S. Ezra, in *Intramolecular and Nonlinear Dynamics* , edited by W. L. Hase (JAI press, 1991), preprint.

9. J. J. Valentini and D. L. Phillips, in *Advances in Gas-Phase Photochemistry and Kinetics: Bimolecular Collisions,* edited by M. N. R. Ashfold and J. E. Baggott (The Royal Society of Chemistry, London, 1987).

10. R. E. Continetti, B. A. Balko, and Y. T. Lee, J. Chem. Phys. **93**, 5719 (1990).

11. D. V. Kliner, D. E. Adelman, and R. N. Zare, J. Chem. Phys. **94**, 1069 (1991).

12. W. H. Miller, Annu. Rev. Phys. Chem. **41**, 245 (1990).

13. K. Nishikawa and S. H. Lin, Chem Phys. Lett. **149**, 243 (1988).

14. K. T. Marshall and J. S. Hutchinson, J. Phys. Chem. **91**, 3219 (1987).

15. J. S. Hutchinson, J. T. Hynes, and W. P. Reinhardt, Chem. Phys. Lett. **108**, 353 (1984).

16. E. L. Sibert III, W. P. Reinhardt, and J. T. Hynes, Chem. Phy. Lett. **92**, 455 (1982).

17. P. R. Stannard and W. M. Gelbart, J. Phys. Chem. **85**, 3592 (1981).

18. W. H. Miller, N. C. Handy, and J. E. Adams, J. Chem. Phys. **72**, 99 (1980).

19. T. Carrington, Jr. and W. H. Miller, J. Chem. Phys. **81**, 3942 (1984).

20. T. Carrington, Jr. and W. H. Miller, J. Chem. Phys. **84**, 4364 (1986).

21. M. Page and J. W. McIver, Jr., J. Chem. Phys. **88**, 922 (1988).

22. E. Bosch, M. Moreno, J. M. Lluch, and J. Bertran, J. Chem. Phys. **93**, 5685 (1990).

23. D. G. Truhlar, A. D. Isaacson, and B. C. Garrett, in *Theory of Chemical Reaction Dynamics*, edited by M. Baer (CRC Press, Boca Raton, 1985), Vol. 4.

24. W. H. Miller, in *Advances In Chemical Physics*, edited by I. Prigogine and S. A Rice (John Wiley and Sons, New York, 1974), Vol.25.

25. S. Shi and W. H. Miller, Theor. Chim. Acta. **68**, 1 (1985).

26. E. J. Heller, Faraday Discuss. Chem. Soc. **75**, 141 (1983).

27. E. J. Heller and R. C. Brown, J. Chem. Phys. **79**, 3336 (1983).

28. W. P. Reinhardt, in *Advances in Chemical Physics*, edited by J. O. Hirschfelder, R. E. Wyatt, and R. D. Coalson (John Wiley and Sons, New York, 1989), Vol.73.

29. J. R. Reimers and E. J. Heller, J. Phys. Chem. **92**, 3225 (1988).

30. N. Makri and W. H. Miller, J. Chem. Phys. **91**, 4026 (1989).

31. A. Miklavc, Mol. Phys. **39**, 855 (1980).

32. A. J. Cruz and B. Jackson, J. Chem. Phys. **94**, 5715 (1991).

33. J. I. Steinfeld, J. S. Francisco, and W. L. Hase, *Chemical Kinetics and Dynamics* (Prentice Hall, New Jersey, 1989).

34. L. M. Raff and D. L. Thompson, in *Theory of Chemical Reaction Dynamics*, edited by M. Baer (CRC Press, Boca Raton, 1985), Vol. 3.

35. R. N. Porter and L. M. Raff, in *Dynamics of Molecular Collisions*, Part B, edited by W. H. Miller (Plenum Press, New York, 1976).

36. D. L. Bunker, Method Comput. Phys. **10**, 287 (1971).

37. E. Merzbacher, *Quantum Mechanics*, second ed.(John Wiley and Sons, New York, 1970).

38. R. P. Bell, *The Tunnel Effect in Chemistry* (Chapman and Hall, New York,1980).

39. W. H. Miller, Chem. Rev. **87**, 19 (1987).

40. G. C. Schatz, Chem. Rev. **87**, 81 (1987).

41. J. C. Tully, in *Dynamics of Molecular Collisions*, Part B, edited by W. H. Miller (Plenum Press, New York, 1976).

42. J. C. Lorquet and B. Leyh-Nihant, J. Phys. Chem. **92**, 4778 (1988).

43. D-h. Lu and W. L. Hase, J. Chem. Phys. **91**, 7490 (1989).

44. G. Nyman and J. Davidsson, J. Chem. Phys. **92**, 2415 (1990).

45. Y. Guan, T. Uzer, B. D. MacDonald, and D. L. Thompson, in *Advances in Molecular Vibrations and Collision Dynamics*, edited by J. M. Bowman and M. Ratner (1991), in Press.

46. J. M. Bowman, B. Gazdy, and Q. Sun, J. Chem. Phys. **91**, 2859 (1989).

47. W. H. Miller, W. L Hase and C. L. Darling, J. Chem. Phys. **91**, 2863 (1989).

48. M. Perisco, I. Cacelli, and A.Ferretti, J. Chem. Phys. 94, 5508 (1991).

49. D. Poppe, Chem. Phys. **45**, 371 (1980).

50. M. González, A. Aguilar, and M. Gilbert, Chem. Phys. **131**, 347 (1989).

51. J. C. Tully and R. K. Preston, J. Chem. Phys. **55**, 562 (1971).

52. J. A. McCammon and S. C. Harvey, *Dynamics of Proteins and Nucleic Acids*, (Cambridge University Press, New York, 1988).

53. M. P. Allen and D. J. Tildesley, Computer Simulation of Liquids, (Oxford University Press, New York, 1990).

54. M. L. Klein, Ann. Rev. Phys. Chem. **36**, 525 (1985).

55. A. Cheng and M. L. Klein, J. Phys. Chem. **95**, 6750 (1991).

56. T. D. Sewell and D. L. Thompson, J. Chem. Phys. **93**, 4077 (1990).

57. T. D. Sewell , H. W. Schranz, D. L. Thompson, and L. M. Raff, J. Chem. Phys. (accepted).

58. T. D. Sewell and D. L. Thompson, J. Phys. Chem. **95**, 6228 (1991).

59. T. D. Sewell and D. L Thompson (manuscript in preparation).

60. T. D. Sewell, D. L. Thompson, and R. D. Levine (manuscript in preparation).

61. T. D. Sewell, D. L. Thompson, D. Gezelter, and W. H. Miller (manuscript in preparation).

62. T. D. Sewell, Ph. D. dissertation, Oklahoma State University, 1991.

63. J. D. Rynbrandt and B. S. Rabinovitch, J. Chem. Phys. **54**, 2275 (1971).

64. J. D. Rynbrandt and B. S. Rabinovitch, J. Phys. Chem. **75**, 2164 (1971).

65. J. F. Meagher, K. J. Chao, J. R. Barker, and B. S. Rabinovitch, J. Phys. Chem. **78**, 2535 (1974).

66. F.-M.Wang and B. S. Rabinovitch, Can. J. Chem. **54**, 943 (1976).

67. A. N. Ko, B. S. Rabinovitch, and K. J. Chao, J. Chem. Phys. **66**, 1374 (1977).

68. A. N. Ko and B. S. Rabinovitch, Chem. Phys. **30**, 361 (1978).

69. I. Oref and B. S. Rabinovitch, Acc. Chem. Res. **12**, 166 (1979).

70. A. B. Trenwith and B. S. Rabinovitch, J. Phys. Chem. **86**, 3447 (1982).

71. A. B. Trenwith, D. A. Oswald, B. S. Rabinovitch, and M. C. Flowers, J. Phys. Chem. **91**, 4398 (1987),

72. J. M. Farrar and Y. T. Lee, J. Chem. Phys. **65**, 1414 (1976).

73. R. Naaman, D. M. Lubman, and R. N. Zare, in *Spectroscopy in Chemistry and Physics: Modern Trends*, edited by F. J. Comes, A. Muller, and W. J. Orville-Thomas (Elsevier Scientific Publishing Company, New York, 1980).

74. J. M. Jasinski, J. K. Frisoli, and C. B. Moore, J. Phys. Chem. **87**, 2209 (1983).

75. J. M. Jasinski, J. K. Frisoli, and C. B. Moore, J. Phys. Chem. **87**, 3826 (1983).

76. J. M. Jasinski, J. K. Frisoli, and C. B. Moore, J. Chem. Phys. **79**, 1312 (1983).

77. J. M. Jasinski, J. K. Frisoli, and C. B. Moore, Faraday Discuss. Chem. Soc., **75**, 289 (1983).

78. M-C. Chuang and R. N. Zare, J. Chem. Phys. **82**, 4791 (1985).

79. E. S. McGinlely and F. F. Crim, J. Chem. Phys. **85**, 5741 (1986).

80. J. E. Baggott and D. W. Law, J. Chem. Phys. **88**, 900 (1988).

81. P. G. Wang and L. D. Ziegler, J. Chem. Phys. **95**, 288 (1991).

82. K. V. Reddy and M. J. Berry, Chem. Phys. Lett. **52**, 111 (1977).

83. K. V. Reddy and M. J. Berry, Faraday Disc. Chem. Soc. **67**, 188 (1979).

84. K. V. Reddy, R. G. Bray, and M. J. Berry, in *Advances in Laser Chemistry*, edited by A. H. Zewail (Springer, Berlin, 1978).

85. H. H. Harris and D. L. Bunker, Chem. Phys. Lett. **11**, 433 (1971).

86. D. L. Bunker, J. Chem. Phys. **57**, 332 (1972).

87. D. L. Bunker and W. L. Hase, J. Chem. Phys. **59**, 4621 (1973).

88. W. L. Hase, J. Chem. Phys. **69**, 4711 (1978).

89. B. G. Sumpter and D. L. Thompson, J. Chem. Phys. **87**, 5809 (1987).

90. K. V. Reddy and M. J. Berry, Chem. Phys. Lett. **66**, 223 (1979).

91. J. Segall and R. N. Zare, J. Chem. Phys. **89**, 5704 (1988).

92. M. D. Likar, J. E. Baggott, and F. F. Crim, J. Chem. Phys. **90**, 6266 (1989).

93. T. R. Rizzo and F. F. Crim, J. Chem. Phys. **76**, 2754 (1982).

94. P. R. Fleming and T. R Rizzo, J. Chem. Phys. **95**, 1461 (1991).

95. D. W. Chandler, W. E. Farneth, and R. N. Zare, J. Chem. Phys. **77**, 4447 (1982).

96. M-C. Chuang, J. E. Baggott, D. W. Chandler, W. E. Farneth, and R. N. Zare, Faraday Discuss. Chem. Soc. **75**, 301 (1983).

97. J. H. Gutow, D. Klenerman, and R. N. Zare, J. Phys. Chem. **92**, 172 (1988).

98. H. Gai, D. L. Thompson, and G. A. Fisk, J. Chem. Phys. **90**, 7055 (1989).

99. S. Chapman and T. Uzer, in *Intramolecular and Nonlinear Dynamics*, edited by W. L. Hase (JAI Press, 1991), preprint.

100. P. A. McDonald and J. S. Shirk, J. Chem. Phys. **77**, 2355 (1982).

101. A. E. Shirk and J. S. Shirk, Chem. Phys. Lett. **97**, 549 (1983).

102. Y. Guan, G. C. Lynch, and D. L. Thompson, J. Chem. Phys. **87**, 6957 (1987).

103. Y. Guan and D. L. Thompson, Chem. Phys. **139**, 147 (1989).

104. B. K. Carpenter, J. Am. Chem. Soc. **107**, 5730 (1985).

105. W. von E. Doering and W. J. Ehlhardt, J. Am. Chem. Soc. **109**, 2697 (1987).

106. R. H. Newman-Evans, R. J. Simon, and B. K. Carpenter, J. Org. Chem. **55**, 695 (1990).

107. K. I. Lazaar and S. H. Bauer, J. Phys. Chem. **88**, 3052 (1984).

108. S. H. Bauer, D. B. Borchardt, and N.-S. Chiu, Ber. Bunsenges. Phys. Chem. **92**, 407 (1988).

109. D. B. Borchardt and S. H. Bauer, J. Chem. Phys. **85**, 4980 (1986).

110. H. Gai and D. L. Thompson, Chem. Phys. Lett. **168**, 119 (1990).

111. J. P. Chauvel, Jr., B. R. Friedman, and N. S. True, J. Chem. Phys. **84**, 6218 (1986).

112. S. H. Bauer, J. Chem. Phys. **87**, 6209 (1987).

113. S. H. Bauer and N. S. True, J. Phys. Chem. **84**, 2507 (1980).

114. A. Preiskorn and D. L. Thompson, J. Chem. Phys. **91**, 2299 (1989).

115. E. D. Potter, M. Gruebele, L. R. Khundkar, and A. H. Zewail, Chem. Phys. Lett. **164**, 463 (1989).

116. S. Ruhman, Y. Haas, J. Laukemper, M. Preuss, H. Stein, D. Feldmann, and K. H. Welge, J. Phys. Chem. **88**, 5162 (1984).

117. P. Rogers, D. C. Montague, J. P. Frank, S. C. Tyler, and F. S. Rowland, Chem. Phys. Lett. **89**, 9 (1982).

118. P. J. Rogers, J. I. Selco, and F. S. Rowland, Chem. Phys. Lett. **97**, 313 (1983).

119. S. P. Wrigley and B. S. Rabinovitch, Chem. Phys. Lett. **98**, 386 (1983).

120. S. P Wrigley, D. A. Oswald, and B. S. Rabinovitch, Chem. Phys. Lett. **104**, 521 (1984).

121. V. López and R A. Marcus, Chem. Phys. Lett. **93**, 232 (1982).

122. K. N. Swamy and W. L. Hase, J. Chem. Phys. **82**, 123 (1985).

123. H. W. Schranz, S. Nordholm, and B. C. Freasier, Chem. Phys. **108**, 69 (1986).

124. H. W. Schranz, S. Nordholm, and B. C. Freasier, Chem. Phys. **108**, 93 (1986).

125. H. W. Schranz, S. Nordholm, and B. C. Freasier, Chem. Phys. **108**, 105 (1986).

126. T. Uzer and J. T. Hynes, J. Phys. Chem. **90**, 3524 (1986).

127. T. Uzer and J. T. Hynes, Chem. Phys. **139**, 163 (1989).

128. S. M. Lederman, V. López, V. Fairén, G. A. Voth, and R. A. Marcus, Chem. Phys. **139**, 171 (1989).

129. D. L. Thompson, in *Mode Selective Chemistry (Proceedings of the 24th Jerusalem Symposium on Quantum Chemistry)*, edited by B. Pullman, J. Jortner,

and R. D. Levine (Reidel, Dordrecht, 1991).

130. R. D. Levine and J. Jortner, in *Mode Selective Chemistry (Proceedings of the 24th Jerusalem Symposium on Quantum Chemistry)*, edited by B. Pullman, J. Jortner and R. D. Levine (Reidel, Dordrecht, 1991).

131. F. Remacle and R. D. Levine, J. Phys. Chem. **95**, 7124 (1991).

132. E. W. Schlag and R. D. Levine, Chem. Phys. Lett. **163**, 523 (1989).

133. J. Jortner and R. D. Levine, Isr. J. Chem. **30**, 207 (1990).

134. R. D. Levine, "Intramolecular Dynamics," Lecture at the 6'th International Congress of Quatum Chemistry.

135. W. L. Hase and K. N. Swamy, Chem. Phys. **139**, 1 (1989).

136. S. A. Rice and P. Gaspard, Isr. J. Chem. **30**, 23 (1990).

137. P. Brumer and M. Shapiro, Chem. Phys. **139**, 221 (1989).

138. P. Brumer and M. Shapiro, Acc. Chem. Res. **22**, 407 (1989).

139. R. Kosloff, S. A. Rice, P. Gaspard, S. Tersigni, and D. J. Tannor, Chem. Phys. **139**, 210 (1989).

140. I. Levy, M. Shapiro, and P. Brumer, J. Chem. Phys. **93**, 2493 (1990).

141. R. D. Levine, Ber. Bunsenger. Phys. Chem. **92**, 222 (1988).

142. D-h. Lu and W. L. Hase, J. Phys. Chem. **93**, 1681 (1989).

143. D-h. Lu and W. L. Hase, J. Chem. Phys. **90**, 1557 (1989).

144. B. A. Waite and W. H. Miller, J. Chem. Phys. **73**, 3713 (1980).

145. B. A. Waite, J. Phys. Chem. **88,** 5076 (1984).

146. B. A. Waite and W. H. Miller, J. Chem. Phys. **76**, 2412 (1982).

147. B. A. Waite, S. K. Gray, and W. H. Miller, J. Chem. Phys. **78**, 259 (1983).

148. W. H. Miller, J. Am. Chem. Soc. **105**, 216 (1983).

149. Y. Y. Bai, G. Hose, C. W. McCurdy, and H. S. Taylor, Chem. Phys. Lett. **99**, 342 (1983).

150. S. K. Gray, S. A. Rice, and M. J. Davis, J. Phys. Chem. **90**, 3470 (1986).

151. M. J. Davis and S. K. Gray, J. Chem. Phys. **84**, 5389 (1986).

152. S. K. Gray and S. A. Rice, J. Chem. Phys. **86**, 2020 (1987).

153. D. L. Bunker, J. Chem. Phys. **37**, 393 (1962).

154. D. L. Bunker, J. Chem. Phys. **40**, 1946 (1964).

155. C. A. Parr, A. Kuppermann, and R.N Porter, J. Chem. Phys. **66**, 2914 (1977).

156. R. J. Wolf and W. L. Hase, J. Chem. Phys. **73**, 3779 (1980).

157. R. J. Wolf and W. L. Hase, J. Chem. Phys. **72**, 316 (1980).

158. W. L. Hase and R. J. Wolf, J. Chem. Phys. **75**, 3809 (1981).

159. W. L. Hase, R. J. Duchovic, and K. N. Swamy, J. Chem. Phys. **80**, 714 (1984).

160. K. N. Swamy, W. L. Hase, B. C. Garrett, C. W. McCurdy, and J. F. McNutt, J. Phys. Chem. **90**, 3517 (1986).

161. W. L. Hase and D-F. Feng, J. Chem. Phys. **61**, 4690 (1974).

162. C. S. Sloane and W. L. Hase, J. Chem. Phys. **66**, 1523 (1977).

163. T. Uzer and J. T. Hynes, Chem. Phys. Lett. **113**, 483 (1985).

164. T. A. Holme and J. S. Hutchinson, J. Chem. Phys. **83**, 2860 (1985).

165. R. S. Smith, R. B. Shirts, and C. W. Patterson, J. Chem. Phys. 86, 4452 (1987).

166. R. S. Smith and R. B. Shirts, J. Chem. Phys. **89**, 2948 (1988).

167. E. R. Grant and D. L. Bunker, J. Chem. Phys. **68**, 628 (1978).

168. W. L. Hase, R. J. Wolf, and C. S. Sloane, J. Chem. Phys. **71**, 2911 (1979).

169. W. L. Hase, D. G. Buckowski, and K. N. Swamy, J. Phys. Chem. **87**, 2754 (1983).

170. I. NoorBatcha, L. M. Raff, D. L. Thompson, and R. Viswanathan, J. Chem. Phys. **84**, 4341 (1986).

171. L. M. Raff, J. Chem. Phys. **90**, 6313 (1989).

172. H. W. Schranz, L. M. Raff, and D. L. Thompson, J. Chem. Phys. **94**, 4219 (1991).

173. H. W. Schranz, L. M. Raff, and D. L. Thompson, J. Chem. Phys. **95**, 106 (1991).

174. G. Nyman, K. Rynefors, and W. L. Hase, Chem. Phys. **110**, 27 (1986).

175. B. G. Sumpter and D. L. Thompson, J. Chem. Phys. **88**, 6889 (1988).

176. A. J. Marks and D. L. Thompson, "*A Trajectory Surface-hopping Study of Mode Specificity in the Predissociation of N_2O*," J. Chem. Phys. (in press).

177. A. J. Marks and D. L. Thompson, "*A Phase-space Theory and Monte Carlo Sampling Method for Studying Nonadiabatic Unimolecular Reactions*," J. Chem. Phys. (in press).

178. P. Pechukas, Ann. Rev. Phys. Chem. 32, 159 (1981).

179. E. E. Aubanel, D. M. Wardlaw, L. Zhu, and W. L. Hase, "*Role Of Angular Momentum In Statistical Unimolecular Rate Theory*," (preprint).

180. P. J. Robinson and K. A. Holbrook, *Unimoleculat Reactions*, (John Wiley and Sons, New York, 1972).

181. S. J. Klippenstein, Chem. Phys. Lett. **170**, 71 (1990).

182. J. D. Doll, Chem. Phys. Lett. **72**, 139 (1980).

183. J. D. Doll, J. Chem. Phys. **74**, 1074 (1981).

184. R. Viswanathan, L. M. Raff, and D. L. Thompson, J. Chem. Phys. 82, 3083 (1985).

185. M. Karplus, R. N. Porter, and R. D. Sharma, J. Chem. Phys. **42**, 3259 (1965).

186. S. B. Woodruff and D. L. Thompson, J. Chem. Phys. **71** 376 (1979).

187. H. Gai, D. L. Thompson, and L. M. Raff, J. Chem. Phys. **88**, 156 (1988).

188. P. M. Agrawal, D. L. Thompson, and L. M. Raff, J. Chem. Phys. **89**, 741 (1988).

189. J. A. Miller and N. J. Brown, J. Phys. Chem. **86**, 772 (1982).

190. B. M. Rice, L. M. Raff, and D. L. Thompson, J. Chem. Phys. **85**, 4392 (1986).

191. R. Viswanathan, D. L. Thompson, and L. M. Raff, J. Chem. Phys. **80**, 4230 (1984).

192. L. M. Raff, R. Viswanathan, and D. L. Thompson, J. Chem. Phys. **80**, 6141 (1984).

193. T. Uzer, J. T. Hynes, and W. P. Reinhardt, J. Chem. Phys. **85**, 5791 (1986).

194. K. Nishikawa and S. H. Lin, Chem. Phys. Lett. **149**, 243 (1988).

195 T. Uzer, B. D. MacDonald, Y. Guan, and D. L. Thompson, Chem. Phys. Lett. **152**, 405 (1988).

196. B. G. Sumpter and D. L. Thompson, Chem. Phys. Lett. **153**, 243 (1988).

197. C. Getino, B. G. Sumpter, J. Santamaria, and G. S. Ezra, J. Phys. Chem. **93**, 3877 (1989).

198. C. Getino, B. G. Sumpter, and J. Santamaria, and G. S. Ezra (preprint).

199. C. Gentino, B. G. Sumpter, and J. Santamaria (preprint).

200. L. G. Spears, Jr., and J. S. Hutchinson, J. Chem. Phys. **88**, 240 (1988).

201. L. G. Spears, Jr., and J. S. Hutchinson, J. Chem. Phys. **88**, 250 (1988).

202. L. M. Raff, J. Chem. Phys. **60**, 2220 (1974).

203. W. L. Hase and D. G. Buckowski , J. Compu. Chem.**3**, 335 (1982).

204. W. L. Hase, D. M. Ludlow, R. J. Wolf, and T. Schlick, J. Phys. Chem. **85**, 958 (1981).

205. K. N. Swamy and W. L. Hase, J. Phys. Chem. **87**, 4715 (1983).

206. M. Nonella, J. R. Huber, A. Untch, and R. Schinke, J. Chem. Phys. **91**, 194 (1989).

207. B. M. Rice and D. L. Thompson, J. Chem. Phys. **93**, 7986 (1990).

208. R. M. Benito and J. Santamaria, J. Phys. Chem. **92**, 5028 (1988).

209. L. M. Raff and R. W. Graham, J. Phys. Chem. **92**, 5111 (1988).

210. L. M. Raff, J. Phys. Chem. **92**, 141 (1988).

211. P. M. Agrawal, D. L. Thompson, and L.M. Raff, J. Chem. Phys. **92**, 1069 (1990).

212. C. S. Choi and E. Prince, Acta. Cryst. **B28**, 2857 (1972).

213. R. Wood, Proc. Intern. Meet. Mol. Spectroscopy (4th Meeting), Bologna **2**, 955 (1959).

214. T. M. Haller, T. B. Brill, and A. L. Rheinhold, Acta Cryst. **C40**, 517 (1984).

215. Z. Iqbal, K. Suryanarayanan, S. Bulusu, and J. R. Autera, Army Technical Report 4401 (1972).

216. R. J. Karpowicz and T. B. Brill, J. Phys. Chem. **88**, 348 (1984).

217. A. Filhol, C. Clement, M-T. Forel, J. Paviot, M. Rey-Lafon, G. Richoux, C. Trinquecoste, and J. Cherville, J. Phys. Chem. 75, 2056 (1971).

218. C. F. Melius and J. S. Binkley, Twenty-First Symp (Int.) Combust. Flame, 1953 (1986).

219. R. C. Mowrey, M. Page, G. F. Adams, and B. H. Lengsfield, III, J. Chem. Phys. **93**, 1857 (1990).

220. M. K. Orloff, P. A. Mullen, and F. C. Rauch, J. Phys. Chem. **74**, 2189 (1970).

221. R. Shaw and R. E. Walker, J. Phys. Chem. **81**, 2572 (1977).

222. X. Zhao, E. J. Hintsa, and Y. T. Lee, J. Chem. Phys. **88**, 801 (1988).

223. D. W. Oxtoby and S. A. Rice, J. Chem. Phys. **65**, 1676 (1976).

224. P. Brumer and J. W. Duff, J. Chem. Phys. **65**, 3566 (1976).

225. T. Matushita, A. Narita, and T. Terasaka, Chem. Phys. Lett. **95**, 129 (1983).

226. N. Moiseyev, J. Phys. Chem. **87**, 3420 (1983).

227. D. Carter and P. Brumer, J. Chem. Phys. **77**, 4208 (1982).

228. M. J. Davis and A. F. Wagner, in *Resonances in Electron-Molecule Scattering, van der Waals Complexes, and Reactive Chemical Dynamics*, edited by D. G. Truhlar (ACS, Washington DC, 1984).

229. M. J. Davis, Chem. Phys. Lett. **110**, 491 (1984).

230. S. Kato, J. Chem. Phys. **82**, 3020 (1985).

231. J. H. Frederick and G. M. McClelland, J. Chem. Phys. **84**, 4347 (1986).

232. G. S. Ezra, Chem. Phys. Lett. **127**, 492 (1986).

233. S. C. Farantos, J. Chem. Phys. **85**, 641 (1986).

234. J. M. G. Llorente and E. Pollak, J. Chem. Phys. **89**, 1195 (1988).

235. J. M. G. Llorente, J. Zakrzewski, H. S. Taylor, and K. C. Kulander, J. Chem. Phys. **89**, 5959 (1988).

236. J. M. G. Llorente, J. Zakrzewski, H. S. Taylor, and K. C. Kulander, J. Chem. Phys. **90**, 1505 (1989).

237. J. M. G. Llorente and E. Pollak, J. Chem. Phys. **90**, 5406 (1989).

238. J. M. G. Llorente and H. S. Taylor, J. Chem. Phys. **91**, 953 (1989).

239. W. F. Polik, D. R. Guyer, W. H. Miller, and C. B. Moore, J. Chem. Phys. **92**, 3471 (1990).

240. R. A. Marcus, Faraday Discuss. Chem. Soc. **75**, 103 (1983).

241. J. S. Hutchinson, E. L. Sibert III, and J. T. Hynes, J. Chem. Phys. **81**, 1314 (1984).

242. M. Hénon and C. Heiles, Astron. J. **69**, 73 (1964).

243. S. L. Baughcum, R. W. Duerst, W. F. Rowe, Z. Smith, and E. B. Wilson, J. Am. Chem. Soc. **103**, 6296 (1981).

244. C. J. Seliskar and R. E. Hoffmann, J. Mol. Spectrosc. **96**, 146, (1982).

245. J. Bicerano, H. F. Schaeffer III, and W. H. Miller, J. Am. Chem. Soc. **105**, 2550, (1983).

246. S. L. Baughcum, Z. Smith, E. B. Wilson, and R. W. Duerst, J. Am. Chem. Soc. **106**, 2260, (1984).

247. N. Shida, P. F. Barbara, and J. E. Almlöf, J. Chem. Phys. **91**, 4061 (1989).

248. D. W. Firth, K. Beyer, M. A. Dvorak, S. W. Reeve, A. Grushow, and L. R. Leopold, J. Chem. Phys. **94**, 1812 (1991).

249. J. S. Hutchinson, J. Phys. Chem. **91**, 4495 (1987).

250. K. L. Bintz, D. L. Thompson, and J. W. Brady, J. Chem. Phys. **85**, 1848 (1986).

251. K. L. Bintz, D. L. Thompson, and J. W. Brady, J. Chem. Phys. **86**, 4411 (1987).

252. Y. Guan and D. L. Thompson, J. Chem. Phys. **88**, 2355 (1988).

253. N. Metropolis, A. W. Rosenbluth, M. N. Rosenbluth, A. H. Teller, and E. Teller, J. Chem. Phys. **21**, 1087 (1953).

254. J. W. Brady, J. D. Doll, and D. L. Thompson, J. Chem. Phys. **74**, 1026 (1981).

255. H. W. Schranz, S. Nordholm, and G. Nyman, *J. Chem. Phys.* **94**, 1487 (1991).

256. G. Nyman, S. Nordholm, and H. W. Schranz, *J. Chem. Phys.* **93**, 6767 (1990).

257. E. B. Wilson, J. C. Decius, and P. C. Cross, *Molecular Vibrations*, (Dover, New York, 1955).

258. J. S. Bendat and A. G. Piersol, *Engineering Applications of Correlation and Spectral Analysis*, (John Wiley & Sons, New York, 1980).

259. J. D. Cryer, *Time Series Analysis*, Duxbury Press, Boston, 1986).

260. D. W. Noid, M. L. Kozydowski, and R. A. Marcus, in *Quantum Mechanics in Mathematics, Chemistry, and Physics*, edited by K. E. Gustafson and W. P. Reinhardt, (Plenum Publishing Corporation, 1981).

261. GenDyn is a general classical dynamics program written at Oklahoma State University. For a detailed description of the core components of the code see: K. L. Bintz, M.S. Thesis, Oklahoma State University (1986).

262. J. N. Murrell, S. Carter, S. C. Farantos, P. Huxley, and A. J. C. Varandas, *Molecular Potential Energy Functions* (John Wiley & Sons, New York, 1984).

263. *Potential Energy Surfaces and Dynamics Calculations,* edited by D. G. Truhlar, (Plenum Press, New York, 1981).

264. A recent review of polyatomic potential-energy surfaces is given in: D. G. Truhlar, R. Steckler, and M. S. Gordon, Chem. Rev. **87**, 217 (1987).

265. D. R. McLaughlin and D. L. Thompson, J. Chem. Phys. **59**, 4393 (1973).

266. D. W. Noid, S. K. Knudson, M. L. Kozykowski, and R. J. Renka, J. Phys. Chem. **90**, 6135 (1986).

267. For instance, the MOPAC program; available from QCPE.

268. S. Dasgupta and W. A. Goddard III, J. Chem. Phys. **90**, 7207 (1989).

269. K. L. Bintz (private communication).

270. W. L. Hase, G. Mrowka, R. Brudzynski, and C. S. Sloane, J. Chem. Phys. **69**, 3548 (1978).

271. R. J. Duchovic, W. L. Hase, and H. B. Schlegel, J. Phys. Chem. **88**, 1339 (1984).

272. W. J. Lemon and W. L. Hase, J. Phys. Chem. **91**, 1596 (1987).

273. S. R. Vande Linde and W. L. Hase, J. Phys. Chem. **94**, 2778 (1990).

274. S. C. Tucker and D. G. Truhlar, J. Am. Chem. Soc. **112**, 3338 (1990).

275. L. M. Raff, J. Phys. Chem. **91**, 3266 (1987).

276. G. Herzberg, *Molecular Spectra and Molecular Structure. II. Infrared and Raman Spectra of Polyatomic Molecules* (Van Nostrand and Reinhold, New York, 1945).

277. H. Goldstein, *Classical Mechanics,* 2nd ed. (Addison-Wesley, Reading Massachusetts, 1980).

278. P. Carsky and R. Zahradnik, J. Mol. Struct. **54,** 247 (1979).

279. P. Pulay, G. Fogarasi, and J.E. Boggs, J. Chem. Phys. **74**, 3999 (1981).

280. K. Fan and J.E. Boggs, J. Mol. Struct. (Theochem) **138**, 401 (1986).

281. C. S. Sloane and W. L. Hase, Faraday Discuss. Chem. Soc. **62**, 210 (1977).

282. T. L. Windus, M. S. Gordon, K. L. Bintz, and D. L. Thompson, work in progress.

283. P. K. Pearson and H. F. Schaeffer III, J. Chem. Phys. **62**, 350 (1975).

284. R. J. Wolf, D. S. Bhata, and W. L. Hase, Chem. Phys. Lett.**132**, 493 (1986).

285. H. J. Oelichmann, D. Bougeard, and B. Schrader, J. Mol. Struct. **77**, 49 (1981).

286. J. Overend and J. R. Scherer, J. Chem. Phys. **33**, 446 (1960).

287. K. N. Swamy and W. L. Hase, J. Chem. Phys. **84**, 361 (1985).

288. D-h Lu, W. L. Hase, and R. J. Wolf, J. Chem. Phys. **85**, 4422 (1986).

289. A. García-Ayllón, J. Santamaría, and G. S. Ezra, J. Chem. Phys. **89**, 801 (1988).

290. A. García-Ayllón and J. Santamaría, Chem. Phys. **141**, 197 (1990).

291. W. L. Hase and D. G. Buckowski, Chem. Phys. Lett. **74**, 284 (1980).

292. E. A. Solov'ev, Sov. Phys. JETP **48**, 635 (1978).

293. R. T. Skodje, F. Borondo, and W. P. Reinhardt, J. Chem. Phys. **82**, 461 (1985).

294. B. R. Johnson, J. Chem. Phys. **83**, 1204 (1985).

295. R. T. Skodje and F. Borondo, Chem. Phys. Lett. **118**, 409 (1985).

296. T. P. Grozdanov, S. Saini, and H. S. Taylor, Phys. Rev. A **33**, 55, (1986).

297. R. T. Skodje and F. Borondo, J. Chem. Phys. **84**, 1533 (1986).

298. P. Diaconis and B. Efron, *Sci. Am.* **248**, 116 (1983).

299. L. M. Raff, J. Chem. Phys. **89**, 5680 (1988).

300. B. R. Henry, Acc. Chem. Res. **10**, 207 (1977).

301. M. E. Kellman and L. Xiao, Chem. Phys. Lett. **162**, 486 (1989).

302. Gendyn[261] has been modified so that the local-mode kinetic energy is now calculated in terms of the projection of the relative velocities of the two atoms

defining the bond onto a unit vector directed along the bond. This increases the accuracy of the approximation.

303. R. T. Seeley, *Calculus of One Variable* (Scott, Foresman, Glenview, Ill., 1968).

304. W. P. Reinhardt and C. Duneczky, J. Chem. Soc. Faraday Trans. 2 **84**, 1511 (1988).

305. F. F. Crim, in*Advances in Gas-Phase Photochemistry and Kinetics: Molecular Photodissociation Dynamics,* edited by M. N. R. Ashfold and J. E. Baggott (The Royal Society of Chemistry, London, 1987).

306. B. G. Sumpter and D. L. Thompson, J. Chem. Phys. **82**, 4557 (1985).

307. R. L. Swofford, M. E. Long, and A. C. Albrecht, J. Chem. Phys. **65**, 179 (1976).

308. R. J. Hayward and B. R. Henry, J. Mol. Spectrosc. **50**, 58 (1974).

309. R. J. Hayward and B. R. Henry, Chem. Phys. **12**, 387 (1976).

310. B. R. Henry, J. Phys. Chem. **80**, 2160 (1976).

311. Matthew Cote and James Myers (personal communication).

312. H. B. Schlegel and C. Sosa, J. Phys. Chem. **88**, 1141 (1984).

313. T. A. Holme and R. D. Levine, Chem. Phys. Lett. **150**, 393 (1988).

314. T. A. Holme and R. D. Levine, Chem. Phys. **131**, 169 (1989).

315. T. R. Rizzo, C. C. Hayden, and F. F. Crim, Faraday Disscuss. Chem. Soc. **75**, 223 (1983).

316. T. R. Rizzo, C. C. Hayden, and F. F. Crim, J. Chem. Phys. **81**, 4501 (1984).

317. H. R. Dübal and F. F. Crim, J. Chem. Phys. **83**, 3863 (1985).

318. T. M. Tichich, T. R. Rizzo, H. R. Dübal, and F. F. Crim, J. Chem. Phys. **84**, 1508 (1986).

319. B. G. Sumpter and D. L. Thompson, J. Chem. Phys. **86**, 2805 (1987).

320. B. G. Sumpter and D. L. Thompson, J. Chem. Phys. **86**, 3301 (1987).

321. B. Engels, S. D. Peyerimoff, and P. Skell, J. Phys. Chem. **94**, 1267 (1990).

322. F. E. Budenholzer, C. Chen, C. M. Huang, and K. C. Leong, J. Phys. Chem. **95**, 4213 (1991).

323. Qin Yue and D. L. Thompson, manuscript in preparation.

324. Qin Yue and D. L. Thompson, submitted for publication.

325. J. D. Baldeschwieler and G. C. Pimentel, J. Chem. Phys. **33**, 1008 (1960).

326. R. A. Marcus Commemorative Issue, J. Phys. Chem. **90**, 3467-3656 (1986).

327. J. S. Hutchinson, W. P. Reinhardt, and J. T. Hynes, J. Chem .Phys. **79**, 4247 (1983).

328. J. S. Hutchinson, L. T. Hynes, and W. P. Reinhardt, J. Phys. Chem. **90**, 3528 (1986).

329. S. Kato, J. Chem. Phys. **83**, 1085 (1985).

330. T. A. Holme and R. D. Levine, J. Chem. Phys. **89**, 3379 (1988).

331. P. Hofmann, R. B. Gerber, M. A. Ratner, L. C. Baylor, and E. Weitz, J. Chem. Phys. **88**, 7434 (1988).

332. The December 1, 1989 issue of Chem. Phys. is dedicated to mode selectivity: Chem. Phys. **139**, 1-238 (1989).

333. Y. Guan and D. L. Thompson, J. Chem. Phys. **92**, 313 (1990).

334. A. J. Bowles, A. Hudson, and R. A. Jackson, Chem. Phys. Lett. **5**, 552 (1979).

335. J. Cooper, A. Hudson, and R. A. Jackson, Tetrahedron Lett. **11**, 831 (1973).

336. A. R. Rossi and D. E. Wood, J. Am. Chem. Soc. **98**, 3452 (1976).

337. T. K. Minton, G. M. Nathanson, and Y. T. Lee, Laser Chem. **7**, 297 (1987).

338. I. Biddles and A. Hudson, Chem. Phys. Lett. **18**, 45 (1973).

339. A. C. Hopkinson, M. H. Lien, and I. G. Csizmadia, Chem. Phys. Lett. **71**, 557, (1980).

340. J. L. Holmes and F. P. Lossing, J. Am. Chem. Soc. **110**, 7343, (1988).

341. F. Bernardi and J. Fossey, J. Mol. Struct. (Theochem), **180**, 79, (1988).

342. T. Hoz, M. Sprecher, and H. Basch, J. Phys. Chem. **89**, 1664 (1985).

343. T. Hoz, M. Sprecher, and H. Basch, Isr. J. Chem. **23**, 109 (1983).

344. J. A. Franklin and G. H. Huybrechts, Int. J. Kin. Kinet. **1**, 3 (1969).

345. J. L. Duncan, D. C. McKean, and P. D. Mallinson, J. Mol. Spectrosc. **45**, 221 (1973).

346. C. W. Gullikson and J. R. Nielsen, J. Mol. Spectrosc. **1**, 158 (1957).

347. D. Kivelson and E. B. Wilson, Jr., J. Chem. Phys. **32**, 205 (1960).

348. J. E. Douglas, B. S. Rabinovitch, and F. S. Looney, J. Chem. Phys. **23**, 315 (1955).

349. V. Staemmler, Theoret. Chim. Acta (Berl.) **45**, 89 (1977).

350. M. Said, D. Maynau, J. P. Malrieu, and M. A. G. Bach, J. Am. Chem. Soc. **106**, 571 (1984).

351. H. Ichikawa, Y. Erisawa, and A. Shigihara, Bull. Chem. Soc. Jpn. **58**, 3619 (1985).

352. P. L. Muller-Remmers and K. Jug, Int. J. Quant. Chem. **28**, 703 (1985).

353. S. Kato and K. Morokuma, J. Chem. Phys. **72**, 206 (1980).

354. L. S. Kassel, J. Phys. Chem. **32**, 225 (1928).

355. J. P. Chauvel, B. R. Friedman, N. S. True, and E. D. Winegar, Chem. Phys. Lett. **122**, 175 (1985).

356. B. D. Ross and N. S. True, J. Amer. Chem. Soc. , **105**, 4871 (1983).

357. P. S. Chiu and N. S. True, J. Phys. Chem. **89**, 2625 (1985).

358. C. A. Spring and N. S. True, J. Amer. Chem. Soc. **105**, 7231 (1983).

359. B. K. Carpenter, private communication to professor L. M. Raff.

360. H. W. Schranz, L. M. Raff, and D. L. Thompson, Chem. Phys. Lett., accepted for publication.

361. H. W. Schranz, L. M. Raff, and D. L. Thompson, Chem. Phys. Lett. **171**, 68 (1990).

362. W. H. Miller, J. Chem. Phys. **61**, 1622 (1974).

363. W. H. Miller, J. Chem. Phys. **65**, 2216 (1976).

364. B. C. Garrett and D. G. Truhlar, J. Phys. Chem. **83**, 1052 (1979).

365. D. G. Truhlar and B. C. Garrett, Acc. Chem. Res. **13**, 440 (1980).

366. STEPIT is a function minimization program written by J. P. Chandler of Oklahoma State University. It was incorporated into GenDyn[261] by E. P. Wallis.

367. The statistical calculations were performed by Dr. H. W. Schranz, currently working at the Research School of Chemistry at the Australian National University in Canberra. They are included here for completeness and do *not* constitute work done by this Author.

368. R. Viswanathan, L. M. Raff, and D. L. Thompson, J. Chem. Phys. **81**, 828 (1984).

369. R. Viswanathan, L. M. Raff, and D. L. Thompson, J. Chem. Phys. **81**, 3118 (1984).

370. P. M. Agrawal, D. L. Thompson, and L. M. Raff, J. Chem. Phys. **88**, 5948 (1988).

371. W. L. Hase and K. C. Bhalla, J. Chem. Phys. **75**, 2807 (1981).

372. M. A. Schroeder, USARO Technical Report BRL-TR-2673, September 1985.

373. M. A. Schroeder, USARO Technical Report BRL-TR-2659, June 1985.

374. T. L. Boggs, Prog. Aero. Astron. **90**, 121 (1984).

375. R. A. Fifer, Prog. Aero. Astron. **90**, 177 (1984).

376. F. I. Dubovitskii and B. L. Korsunskii, Russ. Chem. Rev. **50**, 958 (1981).

377. J. D. Cosgrove and A. J. Owen, Chem. Comm., 286 (1968).

378. F. C. Rauch and A. J. Fanelli, J. Phys. Chem. **73**, 1604 (1969).

379. J. J. Batten, Aust. J. Chem. **24**, 945 (1974).

380. J. D. Cosgrove and A. J. Owen, Combust. Flame 22, 13 (1974).

381. J. D. Cosgrove and A. J. Owen, Combust. Flame 22, 19 (1974).

382. M. Farber and R. D. Srivastava, Chem. Phys. Lett. **64**, 307 (1979).

383. R. J. Doyle, Jr. and J. E. Campana, J. Phys. Chem. **89**, 4251 (1985).

384. J. J. Batten, Int. J. Chem. Kinet. 17, 1085 (1985).

385. J. C. Hoffsommer and D. J. Glover, Combust. Flame **59**, 303 (1985).

386. R. Behrens, Jr., Int. J. Chem. Kinet. **22**, 135 (1990).

387. R. Behrens, Jr., Int. J. Chem. Kinet. **22**, 159 (1990).

388. R. Behrens, Jr., J. Phys. Chem. **94**, 6706 (1990).

389. F. J. Owens and J. Sharma, J. App. Phys. **51**, 1494 (1980).

390. S. Bulusu, D. I. Weinstein, J. R. Autera, and R. W. Velicky, J. Phys. Chem. **90**, 4121 (1986).

391. R. N. Rogers and G. W. Daub, Anal. Chem. 45, 596 (1973).

392. C. Capellos, P. Papagiannakopuolos, and Y-L Liang, Chem. Phys. Lett. **164,** 533 (1989).

393. H. Zuckermann, G. D. Greenblatt and Y. Haas, J. Phys. Chem. **91,** 5159 (1987).

394. G. Edwards, Trans Faraday Soc. **49,** 152 (1953).

395. J. M. Rosen and C. Dickinson, J. Chem. and Eng. Data, **14,** 120 (1969).

396. E. P. Wallis and D. L. Thompson (in preparation).

397. *Thermochemical Data of Organic Compounds*, edited by J. B. Pedley, R. D. Naylor, and S. P. Kirby (Chapman and Hall, New York, 1986).

398. *The Chemical Thermodynamics of Organic Compounds*, edited by D. R. Stull, E. F. Westrum Jr., and G. C. Sinke (John Wiley and Sons, New York, 1969).

399. M. E. Zandler (private communication).

400. T. Vladimiroff (private communication).

401. J. E. Huheey, Inorganic Chemistry: Principles of Structure and Reactivity 3ed. (Harper and Row, New York, 1983).

402. J. W. Brady, J. D. Doll, and D. L. Thompson, J. Chem. Phys. **73,** 2767 (1980).

403. E. A. Gislason and E. M. Goldfield, J. Chem. Phys. **80,** 701 (1984).

404. A. M. Wodtke and Y. T. Lee, in *Advances in Gas-Phase Photochemistry and Kinetics: Molecular Photodissociation Dynamics*, edited by M.N.R. Ashfold and J.E. Baggot (Royal Society of Chemistry, London, 1987).

405. D. W. Noid and B. G. Sumpter, Chem. Phys. Lett. **121,** 187 (1985).

406. S. K.Knudson and D. W. Noid, Chem. Phys. Lett. **145,** 16 (1987).

407. R. S. Dumont and P. Brumer, J. Chem. Phys. **88,** 1481 (1988).

408. B. Eckhardt, J. M. G. Llorente, and E. Pollak, Chem. Phys. Lett. **174,** 325 (1990).

409. S. C. Farantos, J. M. G. Llorente, O. Hahn, and H. S. Taylor, Chem. Phys. Lett. **166,** 71 (1990).

410. C. C. Martens, M. J. Davis, and G. S. Ezra, Chem. Phys. Lett. **142,** 519 (1987).

411. M. L. Kozykowski, D. W. Noid, M. Tabor, and R. A. Marcus, J. Chem. Phys. **74,** 2530 (1981).

412. J. T. Muckerman, D. W. Noid, and M. S. Child, J. Chem. Phys. **78**, 3981 (1983).

413. Y. J. Cho, P. R. Winter, H. H. Harris, E. D. Fleishmann, and J. E. Adams, J. Phys. Chem. **94**, 1847 (1990).

414. D. W. Noid, M. L. Kozykowski, and R. A. Marcus, J. Chem. Phys. **67**, 404 (1977).

415. P. N. Ghosh and Hs. H. Günthard, Spectrochim. Acta **37**, 1055 (1981).

416. M. S. Gordon, private communication.

417. M. Dupuis, D. Spangler, J. J. Wendoloski, Natl. Res. Comput. Chem. Software Cat. 1980, 1, Q601.

418. We have neglected the 1.6 kcal/mol zero-point energy correction and used the value of D_0 for a typical Si-F bond as given by J. E. Huheey, *Inorganic Chemistry*, 3rd ed. (Harper and Row, New York, 1983).

419. J. M. Haile and S. Gupta, J. Chem. Phys. **79**, 3067 (1983).

420. D-h. Lu and W. L. Hase, J. Chem. Phys. **89**, 6723 (1988).

421. W. H Miller, J. Phys. Chem. **83**, 960 (979).

422. F. B. Brown, S. C. Tucker, and D. G. Truhlar, J. Chem. Phys. **83**, 4451 (1985).

423. S. Okuyama and D. W. Oxtoby, J. Chem. Phys. **88**, 2405 (1988).

424. E. Bosch, M. Moreno, J. M. Lluch, and J. Bertrán, Chem. Phys. **148**, 77 (1990).

425. R. L. Redington, J. Chem. Phys. **92**, 6447 (1990).

426. R. L. Redington, T. E. Redington, M. A. Hunter, and R. W. Field, J. Chem. Phys. **92**, 6456 (1990).

427. T. Tsuji, H. Sekiya, Y. Nishimura, A. Mori, and H. Takeshita, J. Chem. Phys. **95**, 4802 (1991).

428. Z. Smith, E. B. Wilson, and R. W. Duerst, Spectrochim. Acta **39A**, 1117 (1983).

429. J. E. Del Bene and W. L Kochenour, J. Am. Chem. Soc. **98**, 2041, (1976).

430. G. Karlström, B. Jönsson, B. Roos, and H. Wennerström, J. Am. Chem. Soc. **98**, 6851 (1976).

VITA

Thomas Dan Sewell

Candidate for the Degree of

Doctor of Philosophy

Thesis: UNIMOLECULAR REACTION DYNAMICS OF LARGE POLYATOMIC MOLECULES

Major Field: Chemistry

Biographical:

Personal Data: Born in Altus, Oklahoma, October 17, 1963, the son of Edward H. and Phyllis R. Sewell.

Education: Graduated from Abilene High School, Abilene, Texas in May 1982; attended University of Texas at Austin from August 1982 until May 1983; received Bachelor of Science Degree in Chemistry and Physics from Hardin-Simmons University, Abilene, Texas in December, 1986; completed requirements for Doctor of Philosophy Degree at Oklahoma State University in October, 1991.

Professional Experience: vice president, Phi Lambda Upsilon (honorary chemical society), 1988-1989; Teaching Assistant, Department of Chemistry, Oklahoma State University, January, 1987 to May, 1989; Graduate Research Assistant, Oklahoma State University, May,1989 to December, 1991; Postdoctoral Research Scientist, Department of Physical Chemistry, University of Göteborg, Göteborg, SWEDEN (current position).